CARBON BLACK

Second Edition, Revised and Expanded

edited by

Jean-Baptiste Donnet

Roop Chand Bansal

Meng-Jiao Wang

Science and Technology

Carbon Black

Science and Technology Second Edition, Revised and Expanded

Edited by
Jean-Baptiste Donnet

Centre de Recherches sur la Physico-Chimie
des Surfaces Solides, CNRS
Mulhouse, France

Roop Chand Bansal

Panjab University
Chandigarh, India

Meng-Jiao Wang

Degussa AG
Hürth, Germany

The publisher offers discounts on this book when ordered in bulk quantities. For more information, write to Special Sales/Professional Marketing at the address below.

This book is printed on acid-free paper.

10 9 8 7 6 5 4
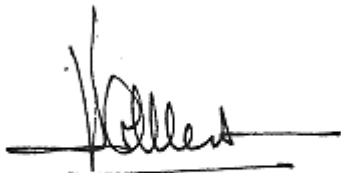
Foreword

Carbon Black, published in 1976 and written with Andy Voet and the help of my coworkers, has been sold out for many years and from many sides, academic and industrial, I was urged to prepare a second, updated edition.

I decided to prepare an edited book, with chapters by several colleagues and friends, most being authorities in this field, who accepted the task of writing separate, well documented chapters which make the new Carbon Black, I believe, a comprehensive reference book. I express my thanks to every coworker.

It was not easy to succeed in collecting the chapters, editing and preparing the book, and I wish to express my deepest gratitude to Roop C. Bansal and Meng-Jiao Wang, colleagues, friends and working as co-editors; without them the present edition would never have reached completion.

It is my hope that this work will serve the scientific and industrial Carbon Black community.

Jean-Baptiste Donnet

Preface

Carbon black is a fascinating material which has not only engaged the attention of those who are concerned with the technology and applications of this material but has also inspired a large number of fundamental investigations in scientific laboratories of universities and research institutes around the world.

Carbon black is widely used as a filler to modify the mechanical, electrical and optical properties of the medium in which it is dispersed. These applications play a major role in elastomers, plastics and in paints and inks. It is, therefore, hardly surprising that the literature on carbon black and its applications is extensive and is scattered in rubber, paint and printing ink trade journals, in general scientific and technical journals, and in periodicals covering such specialised subjects as Colloid Chemistry, Rheology, Polymer Chemistry, Material Science, Carbon, etc.

Since publication of the first edition in 1976, a huge amount of research work has been carried out using latest innovations such as FTIR, ESCA, inverse gas chromatography and STM. The examination of carbon black surfaces by these methods has led to a better understanding of the processing and the applications of this material as a filler. The discovery of fullerenes has given a new twist to the mechanism of carbon black formation, while STM has enabled scientists to have a look at carbon black structure on the atomic scale.

The literature on carbon blacks is so diverse that it appears beyond the capacity of a single author to justify all the subjects that need to

be discussed in a book on carbon blacks. Consequently, an attempt has been made to collect chapters for the book from experts in their own fields and arrange them in one cover after suitable editing. Many of the theories and concepts presented in the first edition have been reviewed only briefly and more emphasis has been focussed on more recent investigations.

The book comprises 14 chapters discussing carbon black manufacture, the mechanism of its formation, its microstructure, morphology, physical and

other properties, the chemical structure of carbon black surface, its fractal geometry and the role of carbon black in elastomers, plastics and xerographic toners. There are separate chapters on STM, surface energy, conductivity and health effect of carbon blacks while the role of carbon black in elastomers has been discussed in three different chapters. The book, thus, is expected to initiate scientists and technologists working in research centres and industry to take full advantage of the recent innovations and to have access to the relevant literature.

The manufacture of carbon blacks which include furnace, thermal, channel and acetylene blacks is discussed in the first chapter. Furnace blacks are made in a furnace by partial combustion of hydrocarbons. Channel blacks, which are now a very small part of the market, are manufactured by impingement of natural gas flames on channel irons. Thermal blacks are produced by thermal decomposition of natural gas, while acetylene black, a special type of thermal black, is made by exothermal decomposition of acetylene. The chapter describes the various processes along with the latest developments in the choice of the source materials and the factors influencing the optimum yield of carbon blacks. The mechanism of carbon black formation based on recent developments including the discovery of fullerenes is discussed in chapter 2.

The next four chapters deal with the microstructure, physical and other properties as well as the porous and chemical structure of the carbon black surface; the microstructure, morphological and other physical properties of carbon blacks are discussed in chapter 3, while chapter 5 provides a look at the atomic scale microstructure

of carbon blacks by scanning tunnelling microscopy. The modification of carbon black surface by the formation of different types of surface chemical groups, their estimation and their influence on the physico-chemical behaviour of carbon blacks is the subject matter of chapter 4 and the influence of these chemical surface groups and microstructure on the basis of surface energetics is discussed in chapter 6.

There is a separate chapter each on fractal geometry and conducting carbon blacks. The concept of fractal geometry, as applied to agglomerate morphology and the interaction of carbon black with polymer, is dealt with in chapter 7. Chapter 8 discusses the influence of carbon black properties such as particle size and aggregate size on the conductivity of polymer-carbon black compounds. The mechanism of conductance in these compounds is also discussed.

The following five chapters are devoted to the applications of carbon blacks in elastomers (chapter 911), plastics (chapter 12) and xerographic toners (chapter 13). Chapter 9 discusses in detail the parameters of carbon black which govern their reinforcing ability in rubber. The factors such as interfacial interaction between rubber and carbon black, occlusion of the polymer in the internal voids of the aggregate and the agglomeration of the

carbon black aggregates in the polymer matrix which determine their reinforcing behaviour are outlined, while chapter 10 discusses the fracture of carbon black filled vulcanizates at high temperature and under swollen conditions. Chapter 11 deals with the dynamic viscoelastic properties of carbon black loaded elastomers. The influence of carbon black properties on its applications in plastics to obtain compounds with excellent UV protection, SMI and antistatic shielding are discussed in chapter 12 while the influence of surface acidity and dispersion properties of carbon blacks on its performance in copiers and printers is considered in chapter 13.

Finally, the health effects of carbon black, a very important topic, are dealt with in chapter 14.

We express our thanks to the authors of different chapters who, at no small inconvenience, agreed to our request to write for the book. Professor Roop C. Bansal acknowledges his thanks to the CNRS Centre Mulhouse for the financial support and to Professor Schultz and Dr. Derai for making his stay comfortable. Professor Bansal also appreciates the patience and understanding of his wife Rajesh and daughters Meenakshi and Nidhi, who stayed in India during the several months that he spent in Mulhouse for the preparation of the book.

JEAN-BAPTISTE DONNET
ROOP CHAND BANSAL
MENG-JIAO WANG

Contents

Carbon Black Surface Studied by Scanning Tunneling
Microscopy
Jean-Baptiste Donnet and Emmanuel Custodéro

Chapter 6   229
Surface Energy of Carbon Black
Meng-Jiao Wang and Siegfried Wolff

Chapter 7   245
Fractal Geometry
Alain Le Méhauté, Michel Gerspacher and Claude Tricot

Chapter 8   271
Conducting Carbon Black
Nicolas Probst

Chapter 12   389
Carbon Black in Plastics
John M. Funt, William L. Sifleet and Marcel Tommé

Chapter 13   409
Carbon Black in Xerographic Toners

Contributors

Roop Chand Bansal

Department of Chemical Engineering and Technology, Panjab University, Chandigarh, India.

Anil K. Bhowmick

Rubber Technology Centre, Indian Institute of Technology, Kharagpur, India.

Emmanuel Custodéro

Ecole Nationale Supérieure de Chimie de Mulhouse, Mulhouse, France.

Jean-Baptiste Donnet

Centre de Recherches sur la Physico-Chimie des Surfaces Solides, CNRS, Mulhouse, France.

John M. Funt

Billerica Technical Center, Cabot Corporation, Billerica, Massachusetts, U.S.A.

Michel Gerspacher

Fort Worth Research Center, Sid Richardson Carbon & Gasoline Co., Fort Worth, Texas, U.S.A.

Charles R. Herd

Operations and Technology Center, Columbian Chemicals

Company, Swartz, Louisiana, U.S.A.

William M. Hess

Operations and Technology Center, Columbian Chemicals
Company, Swartz, Louisiana, U.S.A.

Paul C. Julien

Webster Research Center, Xerox Corporation, Webster, New York,
U.S.A.

Gerhard Kühner

Inorganic Chemical Products Division, Degussa AG, Frankfurt (Main), Germany.

Alain Le Méhauté

Département Matériaux et Procédés, Alcatel Alsthom Recherche, Marcoussis, France.

Nicolas Probst

Chemical Products Division, M. M. M., Brussels, Belgium.

Donald Rivin

Department of the Army, Natick Research, Development and Engineering Center, Natick, Massachusetts, U.S.A.

William L. Sifleet

Billerica Technical Center, Cabot Corporation, Billerica, Massachusetts, U.S.A.

Marcel Tommé

Billerica Technical Center, Cabot Corporation, Billerica, Massachusetts, U.S.A.

Claude Tricot

Département de Mathématique, Ecole Polytechnique, Montreal, Quebec, Canada.

Manfred Voll

Inorganic Chemical Products Division, Werk Kalcheuren, Degussa

AG, Hürth, Germany.

Meng-Jiao Wang

Department of Applied Technology, Fillers and Rubber Chemicals, Inorganic Chemical Products Division, Degussa AG, Hürth, Germany.

Siegfried Wolff

Department of Applied Technology, Fillers and Rubber Chemicals, Inorganic Chemical Products Division, Degussa AG, Hürth, Germany.

Introduction

The term carbon black refers to a group of industrial products involving thermal, furnace, channel and acetylene blacks. They essentially consist of elemental carbon in the form of near spherical particles of colloidal size, coalesced into particle aggregates and agglomerates, and are obtained by the partial combustion or thermal decomposition of hydrocarbons. The use of carbon blacks dates back many centuries to when the Chinese and Indians used them as pigment in black ink in the third century B.C.

Carbon black is widely used as a filler in elastomers, plastics and paints to modify the mechanical, electrical and the optical properties of the materials in which they are dispersed and consequently determine their applications in a given market segment. Carbon black when compounded with plastics imparts unique properties such as UV protection, electrical conductance, range of darkness (jetness), opacity and reinforcement; when used in rubber these fillers change its fracture behaviour and improve abrasion and failure properties. About 90% of the worldwide production of carbon black is used by the tire industry where the carbon black enhances tear strength and improves modulus and wear characteristics of the tires.

Carbon black is an important pigment for use in xerographic toners as it plays a significant role in maintaining a suitable level of electric charge on the toner which is essential for proper operation of the electrographic copiers and printers. In 1992 in the USA alone, the copier industry consumed over 2000 metric tons of

carbon black. This is relatively a small market compared to the industry. However, it is a significant portion of the market for speciality blacks.

The primary carbon black characteristics that influence the properties of carbon black compounds with elastomers are the particle size, aggregate size, the morphology of the carbon black aggregates and its microstructure. In addition, the nature of the carbon black surface and its characteristics with respect to its structural organization, porous structure, surface area and its chemical composition are of vital importance. A more precise knowledge

of the chemistry of the carbon black surface is also essential for the proper development and improvement of carbon black for specific applications. The surface acidity and the dispersion properties of the various colour blacks have a great influence on their performance in xerographic toners.

Carbon blacks are electrically conductive and impart good conductivity to thermoplastic polymers. Consequently they are used in the manufacture of conducting compounds. The electrical and dielectric behaviour of a polymer-carbon black compound depends upon the concentration, the nature and the characteristics of the carbon black, the nature and the molecular weight of the polymer and the mixing and finishing conditions.

Chapter 1
Manufacture of Carbon Black

Gerhard Kühner and Manfred Voll
Degussa AG,
Frankfurt (Main)/Hürth, Germany

Carbon black can be ranked as being one of the oldest manufactured products and its usage as a pigment for the production of India inks and mural paints can be traced back to the ancient Chinese and Egyptians. However, it was after the invention of movable type in the fifteenth century that the printed book became the most important means of communicating information, and as a consequence the demand for a strong black pigment increased steadily.

The most important event which was to have the greatest influence on the usage of carbon black occurred at the turn of the century and involved the discovery of the reinforcing effect of carbon blacks when added to natural rubber, a discovery that was destined to become the most significant milestone in the rubber and automotive industry. By using carbon black as a reinforcing filler the service life of a tire was greatly increased, ultimately making it possible to achieve durabilities of several ten thousand kilometers. Today carbon blacks play an important role, not only as a reinforcing filler for tires and other rubber goods but also as a pigment for printing inks, coatings, plastics, and a variety of other applications.

For several thousand years the use of carbon blacks was only

possible after a suitable production process became available. It is a well-known fact that restricting the access of oxygen to the flames of burning oils or resins results in the formation of carbonaceous materials, an effect which was the basis of all historic production processes.

The majority of industrial carbon blacks produced today is also based on the process of incomplete combustion of hydrocarbons. However, a second process is also used, namely that of thermal decomposition, during which the carbon black is formed in the absence of oxygen. These two process definitions may serve as a preliminary classification which subsequently will be subdivided further.

For the manufacture of industrial blacks the only processes used today are those which can be precisely controlled by appropriate measuring and control techniques, thus allowing the production of carbon blacks with clearly defined properties. They are therefore different from those processes in which soot is released as a contaminated byproduct, such as occurs in poorly adjusted heating ovens or during the uncontrolled burning of carbonaceous materials like wood, coal or oil. This chapter deals only with processes which yield clearly defined end products and for which the English term carbon black has been adopted in many countries.

1.1. The Carbon Black Industry

As a member of the carbon family, carbon black differs from other carbon-based materials in many respects, an important one being that of bulk density. This property has prompted carbon black production facilities to be sited as close as possible to consumers since, when compared with carbon black feedstock, the transportation costs for carbon black are considerably higher. As a consequence carbon black plants are concentrated in those parts of the world where major portions of the industry requiring this material are located (Table 1).

The most important regions are North America, West and East Europe, and Asia, while South America, Africa, and Australia are at the lower end

Table 1. Distribution of World Carbon Black Production Capacity

Region	Number of plants	Estimated capacity, 1000 tons/year	Capacity share, %
North America	25	1925	27
West Europe	20	1420	20
East Europe	20	1485	21
Asia	69	1750	24
South America	8	410	6
Africa/Australia	4	165	2
World total	146	7155	100

of the scale. Today the global installed capacity is in excess of seven million tons per annum, with a worldwide demand for carbon blacks currently in the order of six million tons per annum. This quantity is produced by more than 140 carbon black plants situated in 35 countries.

Since carbon black is predominantly used as a rubber reinforcing material and mainly in tires, most of the carbon black production facilities are located in those countries possessing major tire and automotive industries.

Table 2 shows the 10 major carbon black producing countries. The top ten have each capacity of over 200,000 tons per annum, sharing together 77% of the total world capacity.

Following the rationalization and concentration of the automotive and tire industries, a consolidation of the carbon black industry also took place with the result that, of five major U.S.-based producers having worldwide activities in 1980 only two, Cabot and Columbian, survived - with the German-based company, Degussa, becoming a third major producer. These three companies operating globally, together with those local producers having capacities in excess of 200,000 tons per annum, are listed in Table 3.

This table shows that the seven major producers listed account for 57%

Table 2. Major Carbon Black Producing Countries

Country	Number of plants	Estimated capacity, 1000 tons/year	Capacity share, %
1. USA	20	1570	22
2. CISa	20	1200	17

3. Japan	12	780	11
4. Germany	5	405	6
5. China	40	300	4
6. France	3	280	4
7. Brazil	3	255	4
8. South Korea	3	250	3
9. Italy	3	210	3
10. India	7	210	3
Total 1 10	116	5460	77
Other countries	30	1695	23
World total	146	7155	100

aCommonwealth of Independent States (former USSR).

Table 3. Major Carbon Black Producers

Countrya	Number of plants	Estimated capacity, 1000 tons/year	Capacity share, %
1. Cabot/USA	26	1725	24
2. Degussa/Germany	10	830	12
3. Columbian/USA	10	595	8
Total global producers	46	3150	44
4. Huber/USA	3	270	4
5. Sid Richardson/USA	3	245	3
6. Tokai Carbon/Japan	3	230	3
7. Witco/USA	3	200	3
Total Big Seven	58	4095	57
Others	88	3060	43
World total	146	7155	100

aPlants and their capacities are included if at least 50% of the shares are controlled by the company.

of the total world capacity with the three top global producers sharing between them 44%. The three companies - Cabot, Degussa, and Columbian - are not only the leading manufacturers of rubber grades but also of pigment and specialty blacks on a worldwide basis.

The rubber industry is by far the largest consumer of carbon blacks, accounting for approximately 90% of total carbon black sales, the major portion being concerned with sales to the tire industry. However, not only tires but also mechanical rubber goods and

carbon black filled plastics are major component materials used in automotive production. Consequently, growth and development of the automotive industry, combined with changes in driving behavior, are key factors having the most significant influence on carbon black production.

The remaining 10% is sold to the non-rubber industry. Their uses as pigment blacks in printing inks and in the plastic industry are by far the most important. Both of these sectors are estimated as consuming roughly one-third each of total pigment black sales. The next important application, especially for the higher-priced, fine-particle-size blacks, is in the production of black paints and coatings taking about 9% of production. This is followed by the paper industry, consuming about 4%.

Table 4. Breakdown of Total Carbon Black Sales According to the Fields of Application (Estimated)

Rubber/non-rubber,	%	Non-rubber,	%
Tires	65		
MRGa	25		
Total Rubber	90		
Non-rubber	10	Printing inks	30
		Plastics	36
		Coatings	9
		Paper	4
		Others	21
		Total pigment	100
Total	100		

aMechanical rubber goods.

Other areas, not based on the pigmentation characteristics of carbon blacks but which, nevertheless, are classified as applications for pigment blacks are manufacture of electrodes and reduction of metal oxides, etc. These applications altogether have a share of about 21% of total pigment black sales (Table 4).

The overall growth rate of carbon black production is between 1 and 2% per annum. This surprisingly low percentage, compared with the production records of the automotive industry, is due to the fact that the service life of tires has been continuously improving. The first major step in this field was made with the introduction of the so-called improved blacks which provided superior performance in treadwear at little or no extra cost. This development has been continued with the introduction of high-performance carbon blacks which are making a substantial contribution to continued performance improvement.

Additionally, the switch from bias to radial-belted tires was a major advancement in tire performance, significantly increasing the tire's service life. These are the main reasons why overall sales of carbon black have more or less been in a state of stagnation for the last 15 years.

With detailed examination it is possible to highlight growth rates for the main sectors of application, and it can be seen that pigment grades show a more pronounced growth rate compared with that of rubber grades, particularly those used in tire production.

1.2. Carbon Black Manufacturing Processes

Considered on a worldwide basis the average plant capacity is approximately about 50,000 tons per annum. In practice, however, the individual annual production capacities may vary between 15,000 and 150,000 tons. One plant usually comprises several production lines allowing different carbon black grades to be produced simultaneously. Such a carbon black plant having three production lines is shown in Fig. 1. This plant is located in the Netherlands, close to Rotterdam. Another one, with a capacity of more than 150,000 tons per annum is located in Germany, near Cologne (Fig. 2). The latter plant is the largest one in Europe and produces carbon black according to three different processes.

In principle a large-scale industrial plant for the production of carbon blacks consists of the following sections:

I. storage facilities for feedstocks,

II. carbon black production units,

III. equipment for the separation of carbon black from the process off-gas (tail gas),

IV. final processing of the carbon black,

V. storage facilities for the end product,

VI. utilization of waste gases.

The individual sections are interconnected by transport and conveying facilities which are completely closed systems in modern carbon black plants avoiding the release of carbon black dust into the surroundings. Industrial carbon blacks constitute no

health hazard [32]. However because of its considerable coloring strength the product is regarded as a nuisance dust. Therefore, emission controls are an important aspect of carbon black production.

1.2.1. Classification of Carbon Black Manufacturing Processes

From a chemical point of view, it is essential to classify carbon black manufacturing processes into two categories of incomplete combustion and thermal decomposition of hydrocarbons, depending upon the presence or absence of oxygen [31]. The process of incomplete combustion, termed thermal-oxidative decomposition, is by far the most important one. In terms of quantity, the second process, i.e., the thermal decomposition of hydrocarbons in the absence of oxygen, plays only a very limited role.

The thermal-oxidative processes can be further subdivided according to certain flow criteria. The formation of carbon black in a turbulent flow is different from that in diffusion flames. An oil-fired domestic central heating boiler may serve as an example of a turbulent flame, whereas a well known example of a diffusion flame is a burning candle, at which we will take a closer look. The flame of a candle consists of several zones layered like skins of an onion. In the outer zone, where sufficient oxygen is available from the sur-
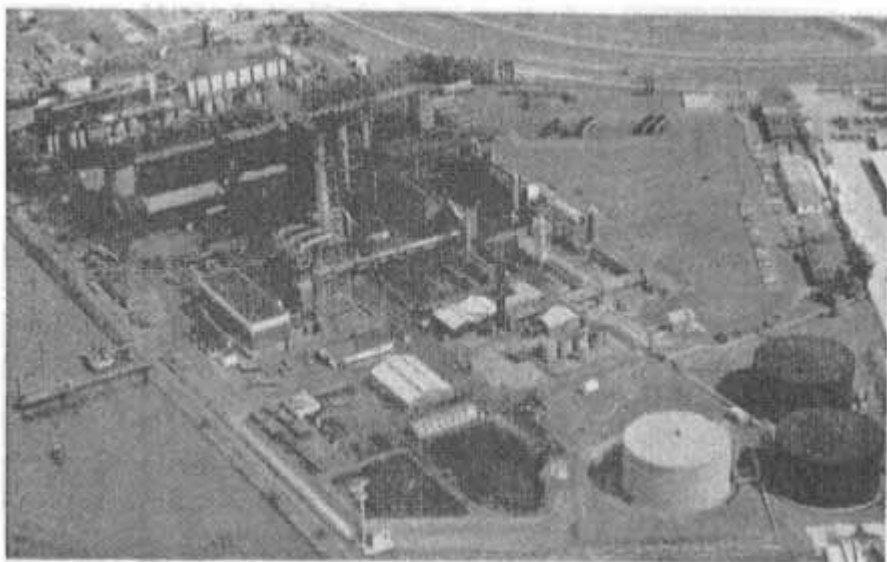
Fig. 1.
Carbon Black Nederland B. V., Botlek, a Degussa AG affiliate.
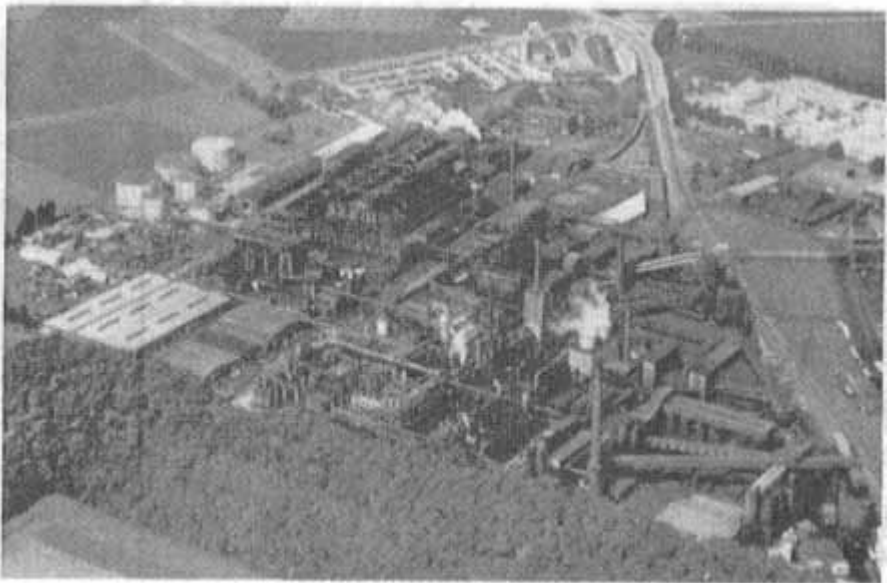
Fig. 2.
Carbon black plant, Degussa AG, Kalscheuren, Germany.

rounding air, the carbonaceous material burns almost completely. Simultaneously, heat is generated which melts and vaporizes the wax. The next inner zone is characterized by a deficiency of oxygen. Since the diffusion rate of oxygen is lower than the rate of the decomposition reaction, carbon is formed which causes the flame to glow. Normally, the decomposition products are burned as soon as they reach the outer zone containing sufficient oxygen, but if a cold object is held in the flame the reaction temperature will decrease and the combustion will be reduced to the extent that the carbon particles are no longer burned, but deposited on the surface of the cold object.

This process represents an open system, since oxygen from the surrounding air has free access to the diffusion flames and any lack of oxygen is only local and temporary. Carbon black formation in a turbulent-flow environment requires a closed system with an appropriately designed flow reactor. The advantages of a closed system are clearly apparent. The reaction components can be introduced in accurately controlled quantities and also independent of each other, giving the process considerable flexibility. In addition, a closed system prevents loss of carbon black from the production unit into the surroundings, avoiding unwelcome pollution.

In practice, the methods used to produce carbon black can be classified according to the above criteria as shown in Table 5.

As previously stated, the thermal-oxydative process is by far the most important for the production of carbon black and accounts for more than 98% of carbon black consumed worldwide. The reaction takes place at high

Table 5. Classification of Manufacturing Processes and Feedstocks

Chemical process	Production process	Feedstock
Thermal-oxidative decomposition		
Closed system (turbulent flow)	Furnace black process	Aromatic oils based on coal tar or crude oil, natural gas
	Lampblack process	Aromatic oils based on caol tar or crude oil
Open system (diffusion flames)	Degussa gas black process	Coal tar distillates
	(Channel black processa)	Natural gas
Thermal decomposition		
Discontinuous	Thermal black process	Natural gas (oils)
Continuous	Acetylene black process	Acetylene

aHistoric.

temperatures in a refractory-lined reactor or furnace - from which the term furnace black process is derived. The lampblack process also falls into the category of thermal-oxidative decomposition taking place in a closed system. Today carbon black production by this process is limited to one grade only. The processes constituting thermal-oxidation in open systems are the gas black process and the historic channel black process.

The thermal decomposition of hydrocarbons is carried out in closed systems, and two major processes belong to this category, namely those of thermal black and acetylene black. The thermal black process is cyclic, and the energy required to decompose the hydrocarbons is generated separately without production of any carbon black. In the acetylene black process, acetylene is decomposed in an exothermic reaction, permitting the process to become continuous once the reaction has been initiated.

1.2.2. Individual Sections of a Carbon Black Production Plant

The diagram in Fig. 3 shows the individual process steps in carbon black manufacture. The heart of the process is the carbon black production unit (1) which, depending on the process, may consist of reactor(s) or apparatus. The initial product of the unit is a mixture of process gas and carbon black suspended in the form of an aerosol. This aerosol is cooled and directed into collecting systems (2), where the solids are separated from the process gas. The carbon black thus obtained has a fluffy appearance, hence the designation fluffy black. Due to its low bulk density and its tendency to dust, the black cannot be handled in this form and, therefore, must to be subjected to some form of densification (35). The fluffy black is either densified to powder black (5) or

pelletized and, depending on the pelletizing process, dry- (4) or wet-pelletized (3) carbon black is obtained. The carbon black is then conveyed to the storage and packaging sections (67). Powder black is always packed in bags (8), whereas pelletized black is shipped either in bags, usually shrinkor stretch-wrapped on pallets (710), or as bulk or semibulk material (11) in road or rail tankers or in containers.

1.3. Feedstocks

As mentioned initially, hydrocarbons are the raw materials on which the production of all carbon blacks is based, and from the shape of the carbon black particles it can be concluded that they are formed in the gas phase. The carbon black particles and aggregates resemble those of other products obtained by pyrogenic processes, such as those found in fumed silica. One major prerequisite, therefore, is that the carbon black feedstock must be capable of being completely converted into the gaseous state. Consequently, the feedstocks used are either gases or liquids which can be vaporized under the given reaction conditions. In the case of the thermal-oxidative processes, non-vaporized hydrocarbon molecules can be broken into smaller fragments
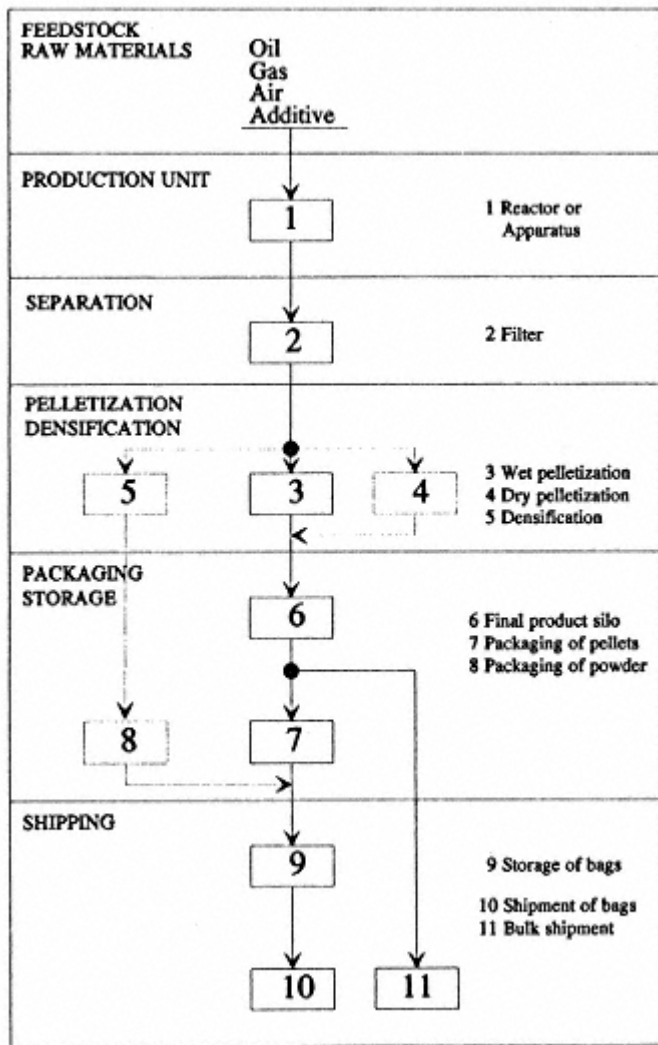
Fig. 3.
Schematic diagram of the individual process steps
in a carbon black production unit.

by the attack of oxygen, thus converting them into the gaseous phase. Larger polymeric hydrocarbons such as certain asphaltenes cause the carbon black to be contaminated with grit, i.e., products similar to coke, the particles of which are much coarser than carbon black and have a completely different shape.

On account of its availability, natural gas is the most frequently used raw material among the gaseous hydrocarbons. Only the acetylene black process constitutes a special case, since, as the name suggests, it uses only acetylene as the feedstock.

The preferred raw materials for other production processes of carbon black, besides natural gas, are oils which have a high content of aromatic hydrocarbons. Aromatics containing a number of condensed rings are particularly advantageous in terms of production yield, since the carbon/hydrogen ratio increases with the number of rings. The absence of side chains also improves the C/H ratio, and aromatics without them are therefore preferred. Since the feedstock has to be vaporized, the boiling point of feedstock oils must not be too high. More suitable feedstocks consist mainly of aromatics with three- or four-membered rings. Some important components of carbon black feedstocks are listed in Table 6.

In practice, both carbochemical and petrochemical oils are used as feedstock sources (Table 7).

Carbochemical oils are fractions obtained during coal tar distillation. Depending on the conditions of the distillation, coal tars contain up to 18% highly aromatic fractions which can be used as carbon black feedstocks. Besides other materials such as naphthalene and washing oils, electrode pitch is one of the main products obtained from tar. The sulfur content of these oils can vary between 0.5 and 0.7%, depending on the origin of the coal. The availability of carbochemical oils obtained from coal tar is largely dependent on the production of coke used in the manufacture of steel. The quantities available today are not sufficient to satisfy all the demand for carbon black feedstocks. Also, in highly industrialized countries, production of carbochemical oils is declining.

Although carbochemical oils are preferred in terms of efficiency,

petrochemical oils are more important in terms of quantities available, particularly in the production of furnace blacks. These are residual oils resulting either from catalytic cracking processes (catcracker decant oils) or from the production of olefins in steam crackers using naphtha or gas oil as a raw material.

Table 6. Aromatic Hydrocarbons Contained in Carbon Black Feedstocks

Aromatic hydrocarbons	Formula	C/H-ratio, weight %	Carbon content, weight %	Factor, fc[a]
Benzene	C_6H_6	11.9	92.3	1.08
Naphthalene	$C_{10}H_8$	14.9	93.7	1.07
Methyl naphthalene	$C_{11}H_{10}$	13.1	92.9	1.08
Dimethyl naphthalene	$C_{12}H_{12}$	11.9	92.3	1.08
Trimethyl naphthalene	$C_{13}H_{14}$	10.1	91.7	1.09
Anthracene	$C_{14}H_{10}$	16.7	94.3	1.06
Phenanthrene	$C_{14}H_{10}$	16.7	94.3	1.06
Pyrene	$C_{16}H_{10}$	19.1	95.0	1.05

[a]Factor c = 100/carbon content.

Table 7. Processes Yielding Carbon Black Feedstocks

Type of feedstock	Raw material/Source	Manufacturing process
Carbochemical oils		
Coal tar oils	Unrefined coal tar	Distillation to obtain washing oils, electrode pitch and other valuable carbonaceous materials
Petrochemical oils		
Steam cracker oils	Naphtha, gas oil	Steam cracking to produce ethylene, propylene, and other olefins
Catcracker oils	Heavy petroleum fraction	Fluid catcracking processes to produce gasoline
Aromatic concentrates	Distillation residues from oil refineries	Extraction with furfural to obtain greases and lubricating oils
Mixed oils	Mixtures of different oils of various origins	

In Europe, mainly steam cracker oils are available, which can be low in sulfur content (< 0.2%), particularly, when naphtha is used as a raw material. In the United States, where catalytic cracking units are favored by the petroleum industry for production of gasoline, catcracker oils tend to predominate. These types of oils may contain up to 2.5% sulfur, sometimes even more.

The availability of aromatic concentrates extracted during the production of lubricating oils and greases is no longer significant

these days.

It is apparent from the above that carbon black feedstocks are exclusively byproducts of processes used for the production of special chemical products such as electrode pitch, ethylene and gasoline [1]. Nevertheless, the choice of carbon black feedstocks is not merely determined by price and efficiency, but also by specific quality criteria. However, due to their origin, the feedstocks are mixtures of a large number of individual substances and are, therefore, not easy to characterize. More than 200 different components have been recorded in the range able to be detected by gas chromatography.

An important parameter for the evaluation of carbon black feedstocks is the density, since it increases with increasing aromaticity. It is also used for determination of the Bureau of Mines Correlation Index (BMCI) [2], which is obtained either from density and midboiling point or from density and viscosity for those feedstocks which cannot be distilled completely. This index is used by the carbon black industry as an important criterion for feedstock

evaluation. An economically viable feedstock should have an index above 110. The BMCI and some other data describing the quality of the three most important types of carbon black feedstocks are listed in Table 8.

More detailed information than that provided by the density or the BMCI is obtained from distillation curves or gas chromatograms, which provide information concerning the chemical composition, the density, the boiling behavior and the C/H ratio of the feedstock. The C/H ratio can also be determined by elemental analysis which, in addition to carbon and hydrogen, gives the nitrogen, oxygen, and sulfur contents. The relevance of the C/H ratio is that it provides an indication of the aromaticity of the feedstock (Table 6). The aromaticity can be estimated more precisely by means of NMR spectroscopy by determining the ratio between aromatic and aliphatic C-H bonds, but this analysis is not performed on a routine basis.

Additional information can be gained from the distillation residue or from liquid chromatography. Asphaltenes, determined as pentane-insoluble matter, provide indications concerning the possibility of grit formation. Further analyses are carried out to determine the content of foreign elements such as halogens, alkali, alkaline earth and heavy metals. The alkali metals, in

Table 8. Data of Typical Feedstock Grades Produced by Different Processes

	Steamcracker process	Catcracker process	Coal tar distillation
BMCI	127	132	161
Density at 15°C, g/cm3	1.07	1.101	1.136

API gravity at 15°C	n.a.	-3.04	n.a.
Viscosity, SSU at 100°C	120	82	80
Midboiling point, °C	n.a.	n.a.	355
Flash point, °C	70	130	90
Pour point, °C	30	30	60
Distillation residue, wt%	21.8	n.a.	2.7
Asphalthenes, wt%	19	8	1.65
Toluene insolubles, wt%	0.1	0.01	0.04
Water, wt%	0.1	0.1	0.1
Ash, wt%	0.02	0.05	0.04
Carbon content, wt%	92.0	90.6	92.1
Hydrogen content, wt%	7.11	7.05	6.4
C/H ratio, p.wt	12.9	12.9	14.3
Sulfur, wt%	0.2	2.1	0.6
Sodium, ppm	0.8	1.2	1.6
Potassium, ppm	0.3	0.1	0.2

particular, are subjected to tight specifications due to their influence on the structure formation of carbon blacks produced by the furnace black process. Oxygen in the feedstock has an adverse effect on yield and is therefore not desired. The sulfur content is restricted in many countries due to environmental laws limiting the emission of sulfur compounds in the waste gases. The viscosity, the pour point, and, for safety reasons, the flash point determine the handling properties and storage conditions of the feedstock. Specific details of carbon black feedstocks which are relevant for the manufacturing process will be discussed in corresponding sections which follow.

Until the mid-19th century, vegetable oils, fats, waxes and resins were used in the manufacture of carbon black, and in this class of products pine resin was of particular importance as a feedstock. With the onset of largescale production of steel, which uses coke as a source of carbon, coal tar oils became available and were used in the production of lampblacks. In the U.S.A., natural gas has become the most important feedstock and was used in the production of channel and gas furnace blacks. However, emergence in 1941 of the oil furnace process led to a continuous shift towards petrochemical feedstocks.

1.4. Production by the Furnace Black Process

The furnace black process is the most modern process for the manufacture of carbon black, and is particularly flexible and economical. By the criteria described above, this process uses the principle of oxidative decomposition. The process is continuous, and is operated in closed reactors where highly turbulent flows prevail due to high flow velocities. Because of its importance for

large-scale industrial carbon black production this process will be described in detail. Except for the actual carbon black production unit, i.e., the furnace black reactor, other plant sections such as the conveying, filtering and pelletizing installations, are very similar to those used in other carbon black manufacturing processes. These will, therefore, be discussed in detail only in the section dealing with the furnace black process. Specific differences regarding other processes will be pointed out in the appropriate sections.

1.4.1. Description of the Process

Following the general flowsheet in Fig. 3, Fig. 4 provides a schematic illustration of a production unit for the industrial-scale manufacture of wetpelletized carbon blacks by the furnace black process.

The carbon black feedstock is pumped from the storage tank to the reactor (1) via an oil preheater. Gas and preheated process air are also fed into the reactor. At a certain distance from the feedstock injection the thermal-oxidative reaction is arrested by injection of water, whereby the carbon black formed and the reactor off-gas are cooled. After further cooling in heat ex-
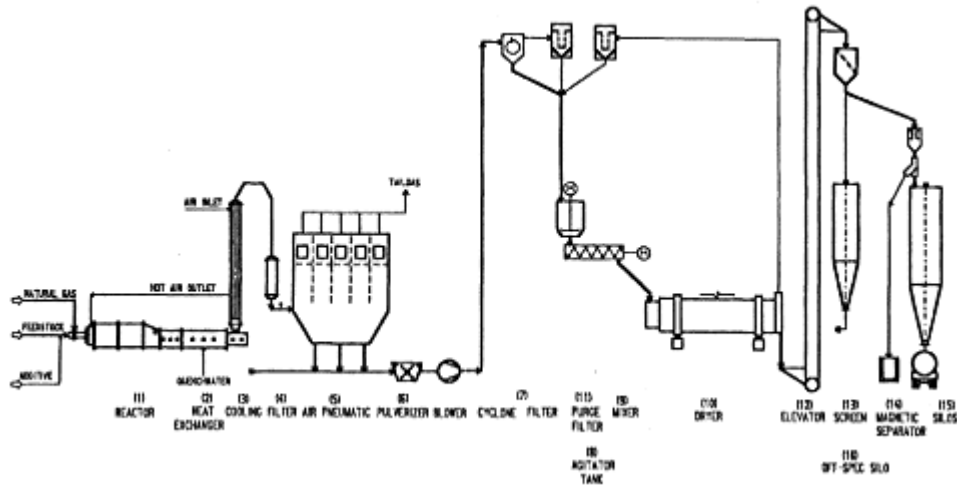
Fig. 4.
Illustration of a furnace black plant.

changers (2,3), the mixture of carbon black and off-gas is directed into filters (4) where the carbon black is separated from the tail gas. The filtered carbon black is then conveyed pneumatically (5) to the pelletizing section. Grit that may be present in the form of coarse particles is usually reduced to an acceptable size by the use of a hammer mill (6). After separation (7) and prior to the pelletizing unit, the carbon black enters a surge bin or agitator tank (8), which acts as a material buffer for the pelletizing unit and where some initial densification of the black takes place. Controlled amounts of black are then fed from the surge bin into a pelletizer or pin mixer (9) and mixed with approximately the same amount of water. The wet pellets formed are subsequently dried in a rotary kiln dryer (10) which is heated by hot gases preferably from the combustion of tail gas. Carbon black dust carried off by the dryer exhaust gases is collected in a filter (11) and recycled into the process. After leaving the dryer and before entering the storage silo, the carbon black pellets pass through screens (13) which act as classifiers for

the pellet sizes, and through powerful magnetic separators (14) to remove any ferrous metal and rust contamination. The carbon black is conveyed to the storage silos (15) by means of bucket elevators (12), conveyer belts, and/or screw coveyors. From there it is discharged into the packaging units or directly to the bulk loading station. A separate storage facility serves as an off-spec silo and receives carbon black which does not meet the specifications. This may occur upon starting a production line or upon switching to a different grade. Depending on the type and extent of deviation, carefully controlled quanti-

ties of the off-spec black may be blended with material from subsequent production or eventually be used for applications not critical with respect to the quality deviation.

As previously mentioned, the tail gas is burned, and the generated heat is utilized in the dryers. Any excess gas can also be employed for generation of steam.

Fig. 5 depicts a plant for the production of furnace blacks.

This general survey of the manufacturing process is now followed by a description of the individual process steps.

Feedstocks and Additives

The necessary raw materials consist of gaseous or liquid hydrocarbons. For a better understanding of the process, one can differentiate between fuel and feedstock, although the limits between both materials are not clearly defined. Natural gas is the most frequently used fuel due to its ease of handling, whereas the feedstocks are comprised of the various types of oils described previously.

The distinction between fuel and feedstock is a simplification, since the two types of hydrocarbons cannot be varied independently. The ratio of the two materials depends on the carbon black's quality requirements and economic efficiency. Changes in the ratio between the natural gas fuel and the carbon black feedstock affect carbon black properties and are therefore
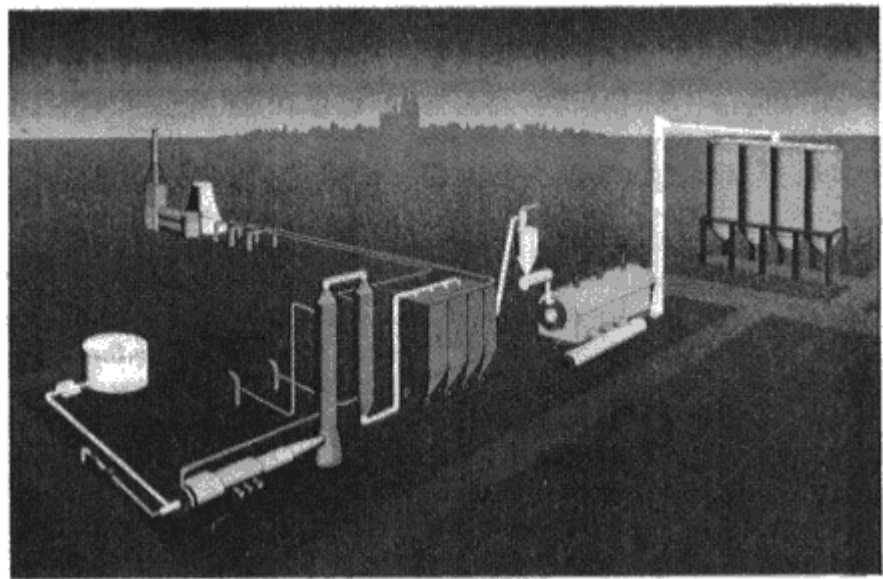
Fig. 5.
Production plant for furnace blacks.
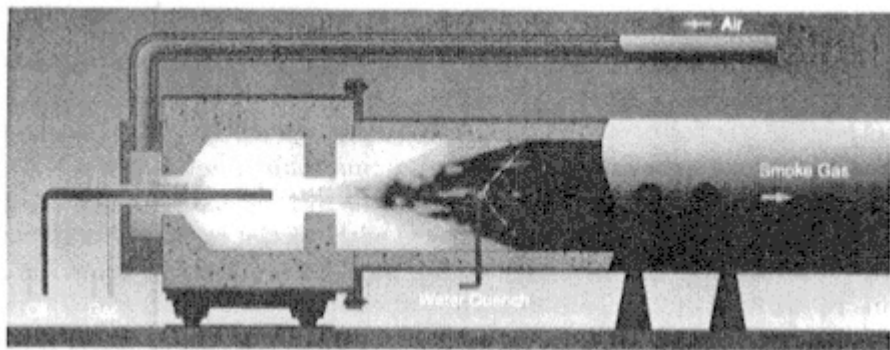
Fig. 6.
Schematic representation of a furnace black reactor.

means of adjusting quality parameters (see *Structure*). Fig. 6 provides a schematic representation of a furnace black reactor.

The first section of the reactor comprises of the combustion zone, where the fuel is burned in an excess of process air. In the subsequent section, the mixing zone, the carbon black feedstock is added and mixed as homogeneously as possible with the hot gases from the combustion chamber. In the third section, the reaction zone, a minor portion of the feedstock reacts with the remaining oxygen from the combustion chamber, but the major portion of the feedstock is pyrolyzed and decomposed into carbon black and off-gas. In the final section, the quench zone, the mixture resulting from this reaction is cooled by injection of water.

Although the most commonly used fuel is natural gas, propane or butane, synthetic gas or tail gas may also be used if natural gas is not available. If the calorific value of the gas is too low, the air may be enriched with oxygen in order to reach the required temperatures. Liquid fuels such as light or heavy fuel oils may also be used in place of gaseous fuels. In contrast to the carbon black

feedstock, the requirement for fuels with respect to their chemical nature is simpler. In the case of commercial natural gas, the material is so inherently clean that no special requirements are needed. However, when, due to local conditions, the fuel is oil, some restrictions are necessary particularly with regard to sulfur content and trace elements. The decisive criteria of handling, air requirements and calorific values would apply for all fuel forms.

Carbon black feedstocks are usually stored in tanks capable of holding several thousand cubic meters of oil. Since most feedstocks are highly viscous at room temperature or may undergo partial crystallization, they are stored at elevated temperatures ranging from 70 to 120°C, depending on the feedstock type. The contents of the tanks are homogenized by stirring or by cycling. The feedstock oil is pumped from the storage tanks to the reactors either

directly or via smaller day tanks which are used for intermediate storage and possible oil blending. The pipes are heated to maintain a desired viscosity and to prevent partial crystallization or solidification of the oil. In addition, the feed to the reactors is in the form of a ring main, thus keeping the oil in circulation even if none is fed into the reactor. Multistage centrifugal pumps are used. These pumps are equipped with special seals due to the low lubricating effect of these oils. Depending on the injection and atomization systems of the reactor, the pressures applied can vary between 8 and 40 bars.

Atmospheric air is commonly used as an oxidizing agent. If necessary the process air passes through a filter for cleaning, and is then compressed to approximately 1.5 bars by rotary-piston blowers, or onestage or multistage centrifugal blowers. Special reactor types are prepared to use oxygen-enriched air, partly in combination with higher pressures. Depending on the technique employed to atomize the oil, additional pressurized air or steam may be used to facilitate the atomization.

Alkali metal salt additives are employed to control carbon black structure. The ions of these additives influence the degree of aggregation of primary particles in the flame [3]. Their effectiveness is solely determined by the cation of the alkali metal, a few ppm in relation to the carbon black feedstock, producing a considerable effect. Potassium salts are usually preferred which are commonly used in the form of aqueous solutions. Amounts of 10 2000 ppm of potassium in relation to the oil are applied, depending upon the extent of the desired reduction in structure and on the composition of feedstock used. To be effective, the salts have to be

available in vaporized form during carbon black formation and hence are introduced either into the combustion chamber or together with the feedstock into the mixing zone.

To arrest the carbon black forming reactions and to avoid secondary reactions between the freshly formed carbon black and components of the reactor off-gas, water is injected into the reactor in the quench zone. This also acts to cool the mixture of carbon black and off-gas to a temperature suitable for the heat exchanger. Depending on the quality of the water available and the required purity of the carbon black, untreated, partially or totally deionized water can be used. In some cases, the total amount of quench water is split between a pre-quench and a main quench.

General Construction of Furnace Black Reactors

A feature common to all furnace black reactors is that they are enclosed in a gas-tight steel jacket. This is a major prerequisite permitting flows of all material to be closely controlled. This steel jacket is usually refractory-lined with highly heat-resistant material consisting of several layers of different types of ceramics. For the innermost layer, gas-tight material possessing the greatest heat resistance is used. It usually consists of alumina with very small amounts of silica, in order to improve the resistance against changes

in temperature. Towards the outside are several layers having increasing silica contents and increasing porosity. This provides a gradually increasing insulating effect and a decreasing heat resistance. Instead of alumina/silica, chrome/aluminum oxides may also be used. Both materials provide refractory linings which allow reaction temperatures of up to, and sometimes above, 1900°C. When zirconia is used, the temperatures may even exceed 2000°C, but the use of this material is limited to oxidizing atmospheres found in the combustion chamber. The refractory lining may be constructed of bricks or from material which is cast and compacted. The use of bricks ensures the longest service life but is the most time-consuming and expensive method of producing shaped refractory sections. A relatively fast and easy way of preparing refractory linings, especially for intricately shaped reactors, is the use of material which is cast and compacted in situ. However, since the compaction is less than that of bricks and since it can only be sintered inside the reactor, cast refractories are less resistant to wear and have a shorter life cycle. Depending on the use of the reactor, the material employed and its location within the reactor, the life span of the refractory lining may be anything between a few months and several years.

The individual ceramic layers are chosen in such a way as to ensure that each layer offers the maximum insulating effect and the required heat resistance at the moment when the adjoining inner layer is at its maximum temperature. It is usually not possible to insulate the steel jacket, since a certain flow of heat is necessary to maintain the required temperature profile within the refractory lining. To avoid condensation, the outer steel jacket temperature should be approx. 130 to 150°C. If the lining is designed correctly,

the heat loss from the reactor shell is in the order of 1 to 2% of the energy input. In special cases, when extremely high energy densities and temperatures are to be generated, particularly with oxygen enrichment, parts of the reactor may be provided with water cooling, sometimes without the refractory lining or with only a thin layer of refractory material.

Reactor geometries differ not only between the manufacturers (see Section 1.4.3), but are also dependent on the product range and the available fuels and feedstocks. In general, two main types of reactors are used to produce rubber-grade blacks. The reactors referred to as hard black or tread black reactors are used for the production of fine-particle carbon blacks of the ASTM 100, 200, and 300 series while those commonly referred to as soft black or carcass black reactors manufacture the coarser carbon blacks of the 500, 600, and 700 series. Carbon blacks having fine primary particles are obtained at higher reaction temperatures than the blacks with coarser particles. Hence the reaction is faster and the reactors are therefore designed for higher reaction velocities and shorter residence times. For the production of coarser carbon blacks, the reaction takes place at comparatively low temperatures

and longer residence times are required, which can be accomplished in large volume reactors.

The functions of the individual elements of a furnace black reactor (Fig. 6), namely the combustion, mixing, reaction and quench zones, is now described in detail.

Energy is generated in the combustion chamber by reacting an oxidizing agent, usually air, sometimes enriched with oxygen, with the gaseous or liquid fuel. It is particularly important that air and fuel are mixed thoroughly, since the degree of the combustion and the volume of the combustion chamber are determined mainly by the mixing time. A complete conversion of the fuel into carbon dioxide and water in the combustion zone is required for optimum utilization of the energy input. High conversion rates are obtained by a through premixing of the fuel and process air, for instance by injecting the fuel transversely to the air stream at high pressure. By suitable choice of the size and number of gas nozzles, optimum premixing of the process air with the fuel is achieved at the location, where the gas is injected. Shear forces are utilized to achieve further mixing. They are generated by either injecting the gas transversely to the flow of air or by changing the cross section of the combustion chamber using chokes, venturis, restrictors or baffles. High flow velocities lead to increased turbulence and improve the combustion of the fuel. In some types of combustion chambers, the turbulence is further increased by creating a vortex in the flow, but care has to be exercised as this may cause a considerable back flow. All elements comprising the combustion chamber have to be carefully matched to obtain stable flames at the

highest possible reaction rates. Modern combustion chambers allow energy densities of up to 100 MJ/m3 to be achieved.

The process air is preheated by the waste heat generated by the process. Air temperatures of up to approximately 800°C are quite common. Compared to the stoichiometric air requirement of the fuel, the process air is usually in excess. This excess is necessary to limit the combustion temperature since the conventional refractory-lined combustion chambers are only able to withstand temperatures of up to 1900°C. In addition, the excess of air promotes the complete conversion of the fuel, especially at very high temperatures where the products carbon dioxide and water begin to undergo dissociation reactions.

The reaction in the combustion chamber is determined by the mass flows of process air and fuel, as well as by the process air temperature and the composition of the fuel. These are important parameters since they determine temperature, amount and composition of the gas leaving the combustion chamber. The fuel-to-air ratio is a key component and is best characterized by the air consumption factor. This consumption factor k, given in percent, defines the fraction of the total oxygen content of the process air consumed

by complete combustion of the fuel. For gaseous fuel, k is given by:

$$k = 100 \times fs \times gas/air \text{ \% (1)}$$

where gas = fuel gas rate (Nm3/h), air = the air rate (Nm3/h) and fs = the stoichiometric factor (Nm3 air/Nm3 gas).

In practice the air consumption factors lie between 30 and 80%. In refractory-lined combustion chambers, the air consumption factor has to remain below 80% when using high process air temperatures to avoid overheating, whereas air consumption factors below 30% are problematic due to reduced ignition velocity.

When different kinds of fuels are used, the air consumption factor is especially useful for comparing the states of the combustion zone and of the carbon black forming zone. The amount of gas leaving the combustion chamber, its temperature and composition, and especially the excess of oxygen can be easily calculated with this factor.

The energy input is estimated from the tangible heat introduced with the process air and the heat of combustion of the fuel. As a first approximation, the energy input Hi is:

$$Hi = 1.357 \times air \times Tair + gas \times Hu \text{ (2)}$$

where $Tair$ = process air temperature (°C) and Hu = net heat of combustion of the gas (kJ/Nm3).

Fig. 7 shows the temperature of the gas leaving the combustion chamber as a function of the air consumption factor and the air temperature, and it is apparent from the diagram that temperatures

may easily exceed 2000°C. Since the upper limit for the commonly used alumina ceramic is 1900°C, unless special precautions are taken to dissipate the heat, the process air temperature and air consumption factor have to be adjusted.

As indicated above, the type of fuel may also vary. As long as the fuel contains only aliphatic hydrocarbons, there is a good correlation between the net heat of combustion of the hydrocarbons and the stoichiometric air requirement, as shown in Table 9. This relation is given by a regression analysis ($r = 0.9999$):

$$Hu = 4085 \times fs - 3567 \quad (3)$$

where Hu = net heat of combustion of the fuel (kJ/Nm3). Combining Equations 1, 2 and 3 allows the calculation of the energy input into the combustion chamber for any given fuel:

$$Hi = (1.357 \times Tair + 40.85 \times k - 35.67 \times k/fs) \times air \quad (4)$$

In the mixing zone, the feedstock is introduced into the hot gases leaving the combustion chamber. This area is characterized by high shear forces
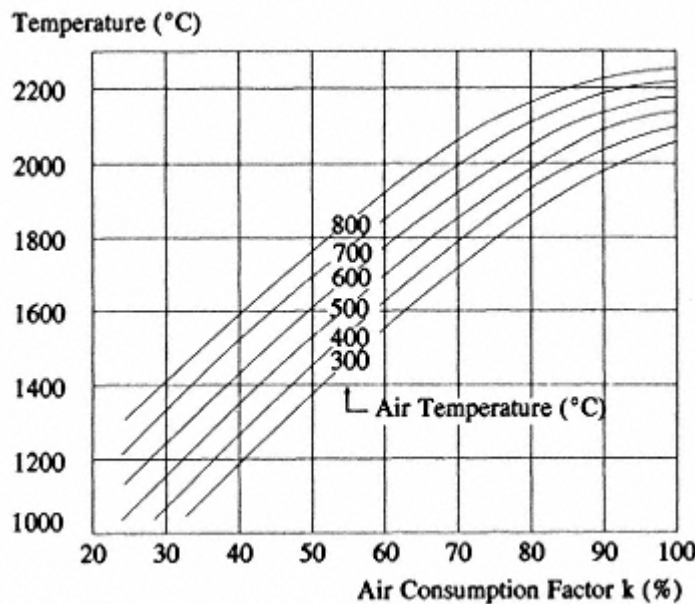
Fig. 7.
Temperature of gases leaving the combustion
chamber as a function of the air consumption factor
and air temperature.

created by varying crosssections and high turbulences due to very
high flow velocities, both of which can be increased by the action
of a vortex. Gas velocities of 0.3 to 0.8 Mach are typical for most
modern reactors. The carbon black feedstock is injected into the
highly turbulent gases usually through nozzles designed to achieve
optimum atomization and distribution in the flowing gases. Both
single- and bi-fluid nozzles are in use. Bi-fluid nozzles have the
advantage of providing better atomization in terms of smaller mean
droplet sizes and are more flexible with respect to variations in
throughput and atomizing energy. The disadvantage is that
additional energy in the form of an atomizing medium is required,
usually pressurized air or steam. The

Table 9. Stoichiometric Air Consumption and Net Heat of Combustion of Hydrocarbons

Hydrocarbons	H/C ratio	Stoichiometric air consumption, f_s, Nm^3/Nm^3	Net heat of combustion, H_u, kJ/Nm^3
CH_4	4.0	9.55	35797
C_2H_6	3.0	16.71	64351
C_3H_8	2.7	23.87	93575
C_4H_{10}	2.5	31.03	123552

use of air entails the danger of coke formation at nozzles, whereas steam may adversely affect the yield due to partial gasification of the feedstock. Good atomization is achieved at gas pressures of 6 bar to 8 bars and gas loads of approximately 100 Nm3/t of feedstock. Single-fluid nozzles are operated at pressures ranging from 6 bar to 40 bars. However, there are also other reactors in which the carbon black feedstock is not atomized but injected directly into the mixing zone in the form of coherent streams. In this case the atomization is obtained mainly by the shear forces of the gas stream. Consequently, such reactors require very high gas velocities (up to 1 Mach).

The throughput of a reactor is usually determined by the cross section of the mixing zone since the process air representing the largest volume determines the pressure drop in the reactor. Modern industrial scale reactors have production capacities of up to 4 t/h of carbon black. In principle it is possible to build even larger reactors, but this would not be economical. Due to production volumes in terms of carbon black output of large reactors the individual production runs would become too short.

The mixing zone is the most sensitive part of a furnace black reactor since its geometry has immediate consequences on the properties of the carbon black. There is a large variety of possible configurations (see Section 1.4.3). A glance at the various locations of feedstock injection shows that in some reactors the oil is injected through centrally located axial sprays, while some other reactors use sprays which are directed radially inwards. There are others which have a combination of both axial and radial sprays. The carbon black feedstock can be introduced downstream or upstream

of, or directly at the site of highest flow velocity, or at a combination of these sites simultaneously. Any of the above-mentioned different nozzle types may be used at the various locations. Finally, there are different designs for the mixing zone in which its inlet and outlet may be either conical or stepped.

In the reaction zone which follows the mixing zone, the atomization and vaporization of carbon black feedstock is completed. The gas leaving the combustion chamber still contains some oxygen which reacts with part of the feedstock vapor. The temperature in the reaction zone is of particular importance, since it is largely responsible for the primary particle size of the carbon black. In refractory-lined reactors, the maximum temperature and thus the fineness of the particles are limited by the temperature resistance of the refractory material.

It is important for the production of carbon blacks that the feedstock is completely vaporized before the onset of pyrolysis, since carbon black can only be formed by the decomposition of hydrocarbons which are in a gaseous phase. If, due to process parameters or feedstock properties, droplets of oil are decomposed before they have been vaporized, spherical coke particles are formed which contaminate the final product. Coke grit can also be formed

when liquid feedstock impinges upon the reactor walls.

The size of the reaction zone is mainly dependent on the throughput and the residence time required for the carbon black formation to be completed. To obtain the desired flexibility by controlling the residence time, the size of the reaction zone is not rigidly fixed, but must be capable of being adjusted depending on the carbon black grade which has to be produced. This is achieved by varying the positions along the reaction zone where the reaction mixture can be quenched by the injection of water. In this quench zone all major reactions are arrested or slowed down to such an extent that no further measurable conversion can take place.

One single quench may be sufficient and may serve as well to arrest the reaction as to adjust the reactor outlet temperature. However, several quench positions may also be used, one upstream to arrest the reaction and one downstream to control the reactor outlet temperature. Conventional atomizing nozzles with different spray characteristics (hollow- and full-cone nozzles, flat sprays) are used for the injection of water. Both axial co- or contra-flow or radial configurations are possible. Apart from the choice between different quench positions, the type and number of nozzle positions as well as the amount of water injected by the different nozzles offer additional means of a fine adjustment of quality parameters. If two quench positions are used, the quench temperature usually ranges from 900 to 1200°C, while the reactor outlet temperatures lie between 700 and 1000°C depending on the type and materials of construction of the heat exchanger.

During the process by which carbon black is manufactured different gases are produced, the composition of which depends on

the stage of the process involved. Therefore, for correct understanding it should be appropriate to give a nomenclature to identify each of the gases.

There are four basic off-gases:

I. The combustion off-gas is the gas leaving the combustion chamber and becomes mixed with the feedstock before entering the reaction zone.

II. The reactor off-gas or smoke gas is the gas formed after the conversion of the feedstock into carbon black which acts as the gas carrier for the fluffy black entering the separation zone such as filtration.

III. The tail gas is the gas remaining after the filtration of the black and which, due to its calorific value, is used to produce heat for dryers in the wet pellet process, and for the steam boiler.

IV. The waste gas, as its name suggests, is the final product after all the combustibles have been burned and used for drying, power generation, etc.

Heat Exchanger

The reactor connects directly to a heat exchanger in which the reactor

off-gas containing the carbon black is cooled and the process air is preheated. It is usually constructed as a tubular heat exchanger through which the process air passes in counterflow to the reactor off-gas. The reactor off-gas with the carbon black passes through a bundle of tubes which, depending on the size of the installation, may consist of between 50 and 200 tubes with diameters of 50 to 100 mm. The flow velocities are sufficiently high to prevent the carbon black from being deposited on the heat exchanger walls. In addition, special cleaning systems are employed to remove such deposits and to prevent plugging.

With reactor off-gas temperature between 700 and 1000°C at the inlet of the heat exchanger, and 400 to 600°C at the outlet, process air temperatures range between 400 and 800°C, with the most common air temperature lying between 600 and 750°C. Higher preheat temperatures are possible, but they would require the heat exchanger to be constructed from specialized and usually very expensive materials. In terms of energy, it would seem appropriate to always achieve the highest possible air preheat temperature. However, this is not always possible due to the temperature limitations of the combustion chamber, the possibility of fowling in the heat exchanger, and restrictions with respect to carbon black properties.

The mixture of carbon black and reactor off-gas leaving the heat exchanger at a temperature of at least 400°C has to be further cooled to 260280°C before it may enter the carbon black separation units. This may be achieved by a second heat exchanger in the form of air or feedstock preheater, a waste heat boiler, or simply by the injection of water. With the second heat exchanger, also of a

tubular type, air may be preheated for use in other processes. The steam obtained from a waste heat boiler may be utilized to preheat the feedstock or for other heating purposes. If the installation has an integrated oil preheater, additional cooling by injection of water is necessary.

Separation

The carbon black is separated from the tail gas by means of bag filters. Two different filter systems are in use, repress bag filters and pulse-jet filters. In repress-type filters, the deposited carbon black is removed from the filter bags in sequence by repressurization with filtered tail gas. Typical filter loads are in the range of 0.2-0.4 $m^3m^{-2}min^{-1}$. In pulse-jet filters, pulses of pressurized air or steam are applied to clean the filters bags. The advantage of pulse-jet filters is the higher specific load of the filter surfaces, so that compared to the repress type, these filters may be built smaller for the same filter capacity. A disadvantage is the greater mechanical strain on the filter bags. If air is used as a cleaning medium, the amount of air has to be limited so as to prevent the formation of flammable mixtures with the combustible tail gas. In all types of carbon black filters the carbon black is discharged from the filter bags into the filter cone or hopper, from which it is conveyed

by means of a screw conveyor and rotary star valves.

In the past, the carbon black was separated from the tail gas by means of cyclones. Today, cyclones are only used infrequently as pre-separators or as agglomeration cyclones where a large part of the carbon black is first separated and then taken up again by the tail gas. The purpose of this technique is to achieve a limited agglomeration of the carbon black and thus facilitate the ensuing separation in the filters.

The filter inlet temperatures are in the range of 260 to 280°C, these comparatively high inlet temperatures being necessary to prevent condensation. Since the tail gas contains approximately 3040% water, the dew point lies at least in the range of 7080°C. The actual dew point may be much higher, depending on the sulfur content of the tail gases. In addition, the temperature of the walls of the filter housing may be far lower than that of the gas in the filter due to the excellent insulating capacity of the carbon black which becomes deposited on the filter walls.

The filter bags are usually made of special surface-treated glass fiber cloth. The service life of these filters may be up to two years depending on operating conditions and the sulfur content of the feedstock. The residual carbon black content of the purified tail gas varies slightly according to the carbon black grade. Values of 10 to 20 mg/m3 can be achieved.

Due to the presence of combustible substances such as hydrogen, carbon monoxide, and some low molecular weight hydrocarbons, the filtered tail gas in most cases is utilized to generate heat for drying of the carbon black (see *Densification and Pelletization*)

and for generation of steam. Some of the steam is consumed internally, but the largest part can be sold or used to generate electricity. A modern carbon black plant is capable of generating approximately three times the amount of electricity it consumes, the excess usually being sold to the local distribution network.

Conveying (Loose Black)

The carbon black discharged from the filter is conveyed pneumatically to other sections for further processing. Conventionally, tail gas or air are used as carriers. Both systems have their advantages and disadvantages. In the case of tail gas, it is less important that the seals at the discharge of the filters are absolutely gas-tight. Furthermore, since the tail gas is recirculated into the main filter, additional filters are not required. On the other hand, the high dew point necessitates higher temperatures than in the case of air, and corrosion may be a major problem. A considerable advantage when using air as a carrier is the fact that flammable gas is prevented from entering the pelletizing section. Any reaction between the freshly produced carbon black and air occurs already in the pneumatic system. Pneumatic systems for conveying powder blacks are usually operated at elevated temperatures, with conveying rates of 1520 m/sec.

The carbon black is normally separated from the pneumatic system by means of cyclones which, in the case of an open air pneumatic system, are followed by a filter for cleaning. In the case of pneumatic systems using tail gas, the filter can be omitted since the tail gas is recirculated back into the process filter.

Purification

The carbon black may contain small amounts of solid contaminants such as coke particles, abraded particles from the refractory lining of the furnace or rust particles. These have to be removed prior to further processing. In many cases, it is sufficient to reduce such contaminants to acceptable particle sizes in micropulverizers.

Magnetic contaminations in the form of rust or metal abrasions can be removed by magnetic separators. The most simple method is to insert rodshaped permanent magnets into the carbon black conveying pipe. They are taken out from time to time and cleaned. More sophisticated systems use electromagnets which are cleaned automatically at fixed intervals. However, in order to minimize the possibility of rust formation, most carbon black plants are increasingly using stainless steel and other corrosion resistant metals.

The most efficient elimination of solid contaminants is achieved by the use of grit separators. A simple variant is the gravity separator in which the carbon black and contaminants are separated by their different fall velocities. Better results are obtained with centrifugal separators, but these are technically more complicated and more expensive. They use rotors to generate high centrifugal forces. The

separator conditions can be varied over a wide range by adjusting the rotor speed and the amount of auxiliary air.

Densification and Pelletization

The fluffy black separated from the pneumatic system still contains considerable amounts of air or gas and has a very low bulk density. Therefore it has to be further densified before it can be used commercially. The extent and the means of densification depend on the intended use of the carbon black.

An initial densification is achieved in the loose black surge bin, where the black is stirred slowly. The loose black surge bin is, therefore, also termed agitator tank. It not only ensures the initial densification of the black, but also acts as a buffer. Sensors allow its product level to be monitored and kept at a constant level so as to maintain a certain flow of carbon black through the screw conveyors or rotary star valves into subsequent densification processes.

The most controlled form of densification of the powder black is vacuum densification. It is achieved by passing the carbon black over porous rollers, the insides of which are under vacuum. The effect can be enhanced by gently pressing the carbon black against the vacuum roller by means of a second

roller. This form of densification is adopted mainly for pigment blacks which are used in the powder form and must be very easy to disperse. It is self-evident that such blacks require special care during packaging, storage and transport to avoid any further densification.

Higher densification of the carbon black is achieved by pelletization. It is the preferred method, if the application system and mixing equipment of the customer develops high shear forces for a more intensive dispersion of the black into the active media. With few exceptions, rubber-grade blacks are always pelletized, since only in this form can they be handled and incorporated into the various polymers using standard industrial equipment. Other advantages of pelletized blacks are smaller transport volumes, more favorable free-flow properties, and reduced dusting.

Because of their different characteristics it is necessary to differentiate between the two pelletizing methods commonly used, namely wet pelletization and dry pelletization. The process of dry pelletization makes use of the fact that densified carbon black particles can be formed into small round pellets in a rotating drum (dry mill). This process is continuous, but limited in its application. The higher the carbon black structure, the more difficult is dry pelletization. In order to achieve the desired throughput, a certain proportion of pelletized carbon black is recycled to act as seeds for new pellets.

In the wet pelletization process, the carbon black is mixed with water in special pin mixers, in which the amount of carbon black and water has to be closely monitored. The pelletizer, or pin mixer, is a cylinder which is 0.5 to 0.7 m in diameter and approximately 3

m long. It has a rotating shaft along its axis on which are fitted steel pins in the form of a helix, the pins extending almost to the cylinder wall. The shaft rotates at 300700 rpm and the pelletization water is injected towards the mixer axis through nozzles situated at different locations along the pelletizer. The water/carbon black ratio used is approximately 1:1 for most blacks. By the mechanical action of the pins wet pellets with a diameter of 0.52.0 mm are formed. If necessary, pelletizing agents or binders, such as molasses, lignin sulfonates, or sugar are added to influence pellet hardness. In principle, wet pelletization can be performed on all carbon black grades, but is rarely used in the case of pigment blacks because the densification is too high.

Since the ratio between carbon black and pelletizing water affects the pellet size, the degree of densification and hence the DBP number of the pelletized black, it is particularly important that this ratio is kept constant. Modern pelletizers are therefore fitted with a control device which uses the power demand of the mixer motor drive to keep this ratio constant since this power demand is very sensitive to the carbon-black-to-water ratio.

After leaving the pelletizer, the wet pellets have to be dried. This is achieved by rotary-kiln dryers heated externally, which may also be supple-

mented by hot gases passing through the dryer. Dryers with a throughput of 24 t/h have a diameter of 23 m and a length of 1520 m. They rotate at a rate of about 6 rpm. Heat transfer and the motion of the carbon black may be improved by fitting additional components such as lifters in the dryer.

The bed depth of wet pellets and thus the residence time in the dryer can be varied by means of adjustable weirs. The dryer outlet temperature of the carbon black is 150250°C. Since a certain oxidation of the carbon black surface may already occur at this temperature, selected carbon black properties which may be relevant to later applications can be influenced in this process stage by changing the bed depth and the temperature in the dryer. It is therefore important that the required temperature profile in the dryer is carefully controlled. This, however, can only be achieved with specific control devices. A problem may arise if the temperature of carbon black is too high when leaving the dryer. Due to its insulating property, its temperature will decrease slowly, and the carbon black may be too hot for loading and delivery to the consumer.

A special variant of carbon black pelletization is oil pelletization. It can be performed both as a dry or wet pelletizing process. During pelletization, 110% of oil is added to the carbon black which wets the carbon black surface, facilitating dispersion in later applications.

Storage and Packaging

Powder Black: The densified fluffy black is collected in a silo from which it is transported to turbo or screw packing machines that are

automated and make use of appropriate robotics to eliminate the former manual operations. The level of the product in the silo is kept low to prevent additional uncontrolled densification. Most carbon blacks are packed in multilayered paper sacks, but polyethylene bags are also used for products which are sensitive to moisture. The bags are stacked on pallets and shipped as such. In the case of powdered blacks the pallets may not be stacked.

Pelletized Black: From the pelletizing section, the pelletized black is transported by bucket elevators, conveyor belts and screw conveyors to single-or multiple-compartment storage silos with capacities between 100 and 1000 t. The pelletized black is stored in these silos from where it is discharged directly into road or rail tankers, intermediate bulk containers, or into automatic packaging lines.

The majority of rubber-grade blacks in Europe is shipped by road and through some rail tankers with a capacity of about 20 and 45 tons, respectively. In the U.S.A., rail tankers are preferred. Some carbon black is also packed and shipped in big bags of 500 or 1000 kg capacities. Smaller sacks containing 1530 kg are packaged by automated high-speed packaging lines and stacked on pallets ready for shipment.
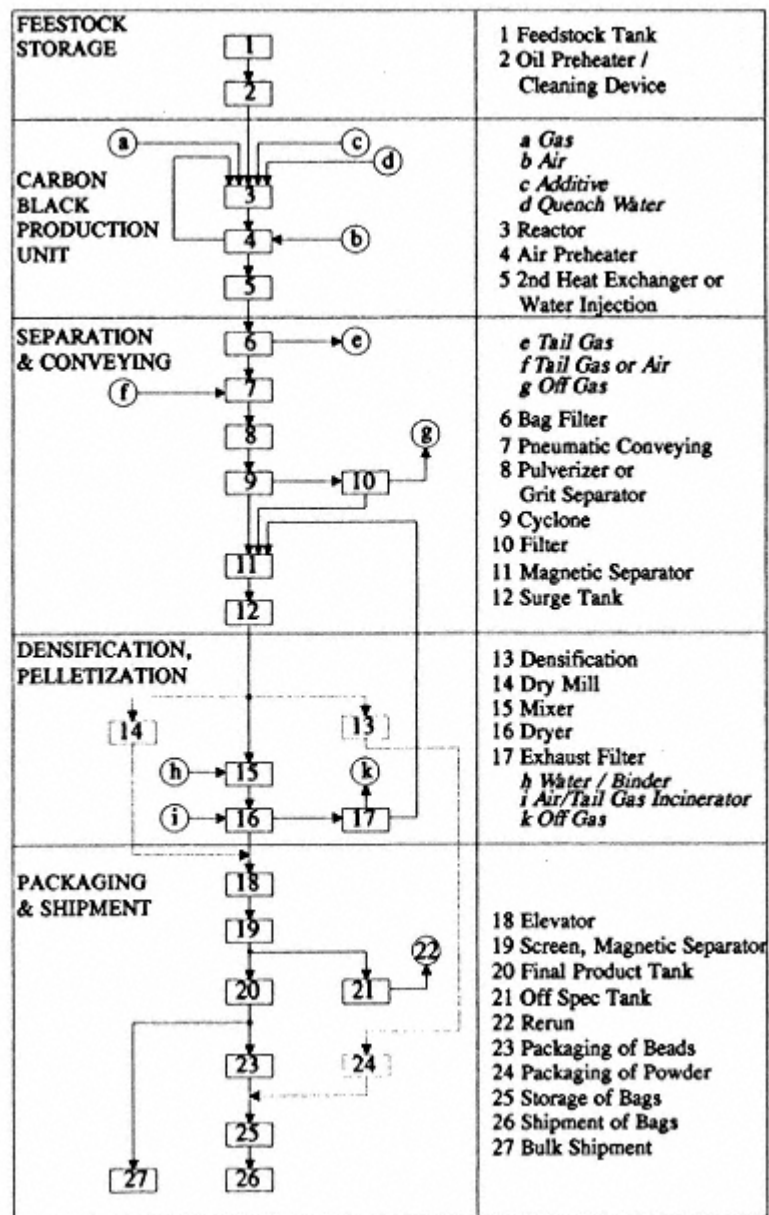
Fig. 8.
Schematic illustration of a furnace black plant including the
alternatives of powder blacks (13/24), dry pelletized blacks
(14), and wet pelletized blacks (15/16).

Summary

In contrast to Fig. 3, Fig. 8 shows a much more detailed illustration of the individual process steps involved in a furnace black production unit.

It shows the individual components of such a plant, starting with storage and preheating facilities for the feedstock (1,2), followed by the furnace black reactors with equipment to preheat the process air and cool the reactor off-gas (35), separation, conveying and purification stages (611), and finally the surge bin (12). After this bin, also known as agitator tank, several steps for further processing are possible: dry pelletization in the dry pelletizing drum (14), wet pelletization in the pin mixer (15) followed by the dryer (16), or preparation of a powder black in the densifier (13). A bucket elevator (18) transports the pelletized black via a screen and purifying equipment (19) to the final product tank (20) or the off-spec tank (21). The product is either shipped in bulk or semi-bulk (27), or both pelletized (23) and powder blacks (24) may be packed in bags, stacked on pallets, shrink-wrapped, and stored in the warehouse (25) until they are shipped to customers (26).

1.4.2. Control of Quality and Economic Efficiency

The furnace black process is today the most important process for the production of carbon black and has to produce materials which are able to fulfill a broad range of application requirements. For example, in rubber compounds for tires they should improve treadwear and traction, reduce rolling resistance and keep heat generation at a minimum, while in non-tire rubber applications they need to confer properties such as high resilience and dimensional stability in extruded goods. In pigment applications, they are to
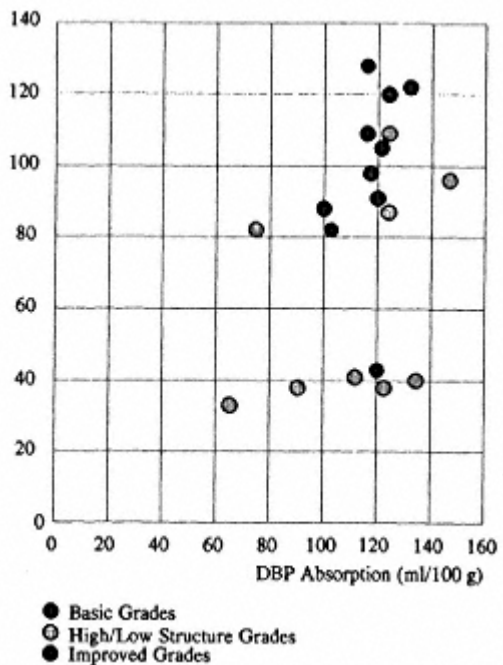
Fig. 9.
Range of rubber-grade furnace
blacks.

Table 10. Range of Variation of Furnace Black Properties

Properties	Variation	Properties	Variation
N2 surface area, m2/g	15 450	Blackness, My	210 270
Iodine adsorption, mg/g	15 450	Tinting strength	60 130
CTAB, m2/g	15 350	Volatiles, %	0.5 6
Mean particle size, nm	10 80	Toluene extract, %	max.0.5
DBP, ml/100g	40 200	pHa	6 10

aAfter-treated blacks: 26.

confer high coloring depths and strengths in the most varied systems, exhibit particular color tones, enhance the stability against UV light, etc. Other specialized blacks are also used to promote electrical conductivity. It goes without saying that such a wealth of demands cannot be met by a single carbon black grade. Rubber-grade blacks alone account for more than 40 different types of carbon black. The product variety is even greater in the case of pigment blacks. The diagram in Fig. 9 shows the rubber blacks with their respective specific surface area (CTAB) and structure (DBP absorption).

Fig. 9 comprises different generations of furnace blacks. Initially, it was only possible to produce the basic grades but gradually, as means of influencing structure became known, the range of furnace blacks was extended, and low- and high-structure blacks were developed. Another generation of furnace blacks owes its existence to process improvements which made it possible to produce carbon blacks with a narrow particle size distribution. In particular, these carbon black grades, known as improved blacks [4], exhibited improved abrasion properties at the same level of surface area as the older conventional grades.

This variety means that carbon black manufacturers have the ability to specifically influence individual carbon black properties, which if possible, should be without affecting other properties. Table 10 may provide an idea of the width of the range within which furnace black properties can be varied, and the following section will discuss the possibilities the furnace process offers by which the variation in the properties may be achieved.

Of course, specific properties in the final applications cannot be achieved directly by adjusting manufacturing conditions, since these properties are determined by the interaction of the carbon black with other ingredients of the system. The properties of the carbon black itself, however, can be adjusted.

There are two catagories of carbon black properties, one related to morphology, the other to surface chemistry. The morphological properties include primary particle size, porosity, aggregate shape and aggregate size. These are considered to be primary carbon black properties. From these, secondary

properties such as specific surface area can be deduced. Properties related to surface chemistry are determined primarily by the chemical compounds and functional groups which are present on the carbon black surface. This includes active sites which can be detected on account of their influence on surface energy.

The most important process stages which are able to influence carbon black properties are the atomization and vaporization of the oil droplets in the reactor, the partial combustion and pyrolysis of the atomized feedstock, and the secondary reactions between the carbon black particles and the components of the reactor off-gas. These stages are followed by the reaction of the carbon black with oxygen upon its first contact with air, mechanical treatment during the densification stage, by further chemical modification depending on the conditions during drying and sometimes by the addition of additives. If the desired extent of the modification cannot be achieved during the process itself, specific chemical after-treatment may also be carried out in a separate step following the actual manufacturing process.

The primary morphological properties are determined in the reactor and can only be changed to a very minor degree later in the process. Surface chemistry, on the other hand, can be influenced in the reactor, in the pneumatic handling system, during pelletization, and during drying. Additional specific changes in chemical surface properties may also be accomplished in separate chemical after-treatment stages.

Influence of Reactor Operating Conditions on Carbon Black Properties

Particle Size, Surface Area, Porosity: The carbon black is formed and its morphological properties are determined after injection of the feedstock into the reaction zone. Major parameters which can be adjusted are the volume of combustion off gas, the amount of feedstock used, and their chemical composition.

In the reaction zone, the gasified carbon black feedstock is subjected to very high temperatures. This causes the molecules to be decomposed into fragments. On losing hydrogen these fragments combine with other fragments until they have reached a size where they are spontaneously precipitated from the gas phase as nuclei. The higher the temperature, the higher is the rate of pyrolysis and the more frequently are such nuclei formed. As the pyrolysis proceeds, the molecular fragments precipitate onto existing nuclei [5] which then continue to grow until all of the feedstock has been consumed. The higher the number of nuclei at any given amount of feedstock, the earlier the particles will stop growing since the amount of starting material is limited.

The temperature in the reaction zone [6] is of fundamental significance, since it determines the most important primary property of the carbon black, namely its primary particle size. The temperature can be adjusted by means of the ratio between the input parameters of process air rate, gas (fuel) rate,

and oil (feedstock) rate. These parameters will be discussed separately for greater clarity.

The temperature in the reaction zone is influenced by the feedstock rate and by the combustion off-gas, the composition and the temperature of which depend on the air consumption factor (fuel/air ratio) and the process air temperature. According to Equation 4 these parameters are responsible for the heat input and therefore also for the process temperature.

The air consumption factor largely determines the course of the reactions in the reaction zone, hence, among other things, it affects the oxygen content of the combustion off gas. A certain amount of feedstock reacts with the residual oxygen and is no longer available for carbon black formation. The higher the air consumption factor, the less feedstock is withdrawn from carbon black formation and vice versa. The energy generated has the primary purpose of vaporizing the feedstock and heating it to the required reaction temperature. The amount of energy required for pyrolysis is so small that it can be neglected in the total energy balance.

The amount of carbon black feedstock (oil rate) is therefore the second important parameter determining the reaction temperature. Increasing the oil rate at a given air consumption factor k reduces the reaction temperature and yields a carbon black with a coarser primary particle size. Furthermore, the increased oil rate increases the amount of carbon black produced. Inversely, fine-particle blacks are formed at higher temperatures which, at constant air consumption factor k can only be reached by reducing the amount of feedstock available for pyrolysis. Consequently, yield and output per hour are at a lower level. This is illustrated by Table 11, which

compares different oil rates, reaction temperatures and mean particle sizes of the carbon blacks produced. These values are based on a fixed air rate of 10,000 m3/h, natural gas as a fuel, and an air consumption factor of 65%.

In practice, the desired carbon black particle size is obtained by appropriate adjustments of the oil rate at constant fuel and process air rates. This method of control is preferred since it has the least effect on other process

Table 11. Oil Rate, Reaction Temperature, and Primary Particle Size

Oil rate, kg/h	Reaction temperature, °Ca	Primary particle size, nm
4060	1450	44
3660	1500	35
3170	1570	26
3060	1580	24
2740	1630	21
2370	1680	19

aTemperature of the reactor wall.

parameters. When using oxygen-enriched air, the rate of oxygen may also be used for adjustments.

The relationship between reaction temperature and particle size does not only apply for the reaction zone as a whole but also for other specific locations within that zone, thus offering another interesting aspect. If conditions are chosen such that the temperature profile is inhomogeneous, both fine- and large-particle blacks can be formed simultaneously. The resulting carbon black thus has a broader primary particle size distribution than if it were produced in a homogeneous temperature field. The homogeneity of the temperature field is largely determined by the characteristics of the reaction chamber. The faster and the more evenly the feèdstock is dispersed in the mixing zone and the faster its vaporization, the more homogeneous is the local temperature distribution in the reaction zone. Inhomogeneous temperature fields are obtained by poor mixing, delayed vaporization of part of the feedstock, or by injection of the feedstock at several locations with different flow patterns.

The temperature in the reaction zone not only determines the rate of formation of carbon black and thus the primary particle size, but also affects any secondary reaction. Carbon black formation is followed immediately by secondary reactions. The longer the carbon black remains in contact with the hot reactor off-gas and the higher the temperature in the reactor, the more pronounced is the effect of the secondary reactions. This involves the homogeneous gas phase reaction (e.g., $CH_4 + H_2O \rightarrow CO + 3H_2$) as well as the freshly formed carbon black which is oxidized by carbon dioxide and water present in the reactor off-gas. Water-gas and Boudouard

reactions cause carbon to be gasified from the carbon black surface, leaving pores. The earlier the freshly formed carbon black is quenched, the lower its porosity. The reaction times for the formation of very fine particle blacks which are produced at temperatures up to 1900°C and high reaction rates are in the order of 10 to 100 msec. Large particle furnace blacks which are formed at reaction temperatures starting at 1200°C require much longer reaction times of up to 10 sec. Fine-particle blacks, therefore, have to be precisely short-quenched to suppress secondary reactions.

Since methods for the determination of mean primary particle sizes require considerable time and money, measurements of specific surface area have become a standard procedure. It is known that there is a geometric relationship between the size of a particle and the extension of its surface. If the density of a carbon black is assumed to be 1.8 g/cm3, the following equation applies for spherical particles:

$$Fg = 3333/d \text{ (5)}$$

where Fg=geometric surface area in m2, and d=particle diameter in nm.

Since aggregation of the particles reduces the specific surface area, the degree of aggregation also has to be taken into account.

The first method for the determination of specific surface area to be considered is the BET surface area [7]. This is based on the adsorption of nitrogen and measures the total surface area of carbon blacks including any pores. The determination of BET surface area is mainly for the verification of selected reactor operating conditions and for fundamental investigations. Iodine adsorption was found to be a fast and reliable method for routine analysis. However, the iodine adsorption not only reflects the surface area of the carbon black, but also is affected by surface chemistry. Increases in the toluene extractibles or increases in the number of oxygen groups on the surface will have the effect of depressing the iodine adsorption. This method is therefore not suitable for oxidized blacks or blacks having high levels of extractable matter. Similar to the BET method, iodine adsorption also includes a major portion of the pores.

CTAB surface area [8] gives the best correlation with primary particle size, since this test method determines only the accessible external surface area of the carbon black particles and for all practical purposes can be regarded as being unaffected by porosity or surface chemistry.

The ratio between BET surface area or iodine adsorption and the CTAB surface area may be used as a measure of porosity. In the case of blacks with fine-particle size, this ratio is equal to or slightly less than unity for very short-quenched carbon blacks (no porosity) and greater than unity for those produced with a longer quench distance. There are, however, limits to which porosity may

be adjusted in the reactor. In the case of large-particle carbon blacks, the formation of any significant porosity is limited by the comparatively low temperatures which, for porosity to form, would require long residence times and very large reactor volumes. Residence time has therefore little effect on the porosity of these blacks since all secondary reactions take place with similar slowness and the exact quench position is less critical. Very fine-particle blacks, on the other hand, always exhibit a certain amount of porosity. Since the quench can only be placed at fixed locations along the reactor, the optimum position may not always be available. As a consequence the reaction may not be arrested at the precise moment at which the carbon black formation has just been completed. In addition, the residence time of the individual particles in the reactor varies so that some carbon black particles may already have become porous while others have only just been formed.

The influence of the secondary reactions is illustrated in Fig. 10, which shows a plot of CTAB surface area versus iodine adsorption. For a medium quench position, the iodine/CTAB ratio of large-particle blacks is unity and
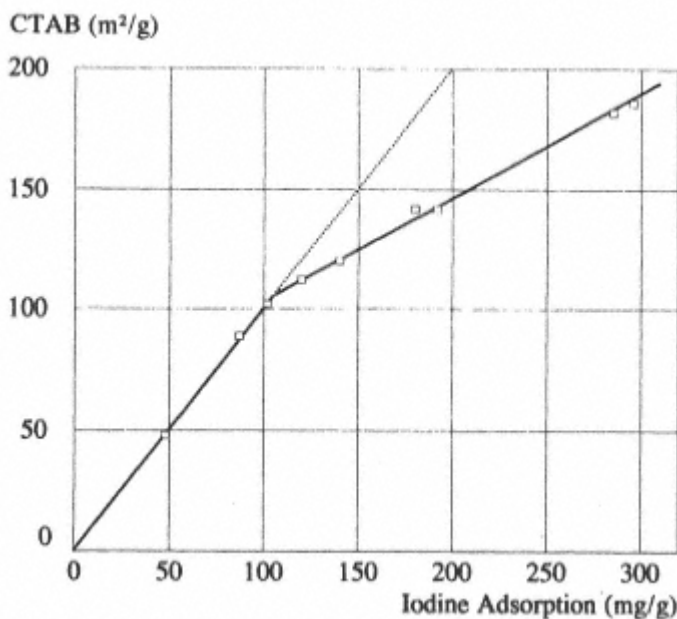
Fig. 10.
CTAB surface area as a function of iodine
adsorption.

increases beyond unity for fine-particle blacks. The limit in this illustration is approximately 100 m2/g.

An iodine/CTAB ratio of less than unity indicates that the carbon black has been extremely short-quenched and that its surface still contains toluene-extractible matter. This consists of small amounts of organic material from feedstock which has not been totally pyrolyzed.

Different residence times not only affect porosity, but also the surface chemistry of the blacks. The surfaces of very short-quenched blacks are rich in hydrogen from CH groups or those groups which act similar to olefinic double bonds. This is regarded as being one of the reasons for the high treadwear index of tread

blacks or for blacks quenched in this way. The longer the residence time in the reaction zone, the lower is the hydrogen content and the higher is the exposed carbon at the surface and under these conditions porosity may also develop. Subsequently some basic surface oxides are always formed when the carbon black comes into contact with air.

Structure: The primary particles formed during carbon black production hardly ever exist in an isolated form. Instead, they fuse together building aggregates of various sizes. These aggregates, in turn, may form loose agglomerates. Size and bulkiness of the aggregates and agglomerates are described by the somewhat imprecise term of carbon black structure.

Aggregates develop during the carbon black forming stage as individual particles which adhere to others of a similar size and which subsequently become fused together by the deposition of further carbon from the gas stream.

The large aggregates are formed under those conditions which promote the frequency of particle collision. The size and shape of the aggregates are important primary carbon black properties. Like particle size, they have a fundamental influence on the properties of carbon blacks in practical applications.

Aggregate size distribution and aggregate shape can be determined by electron microscopy. However, this is costly and time-consuming and so simple methods have been used for routine determinations, although they cover collective properties. These include DBP absorption and Crushed DBP absorption (CDBP), the latter being determined after controlled compression of the carbon black [8]. It is assumed that the DBP absorption reflects the total carbon black structure which comprises both aggregates and agglomerates, whereas the mechanical treatment in the Crushed DBP absorption test eliminates loose agglomerates and easily destroyable aggregates. This method records the permanent or primary structure formed by the stable aggregates.

The carbon black structure formed in the reactor is largely dependent on the formation and concentration of solid particles, both being determined by the concentration of feedstock vapor. High feedstock/air ratios reduce the concentration of feedstock vapor and lead to lower carbon black structures. The use of steam for feedstock atomization will enhance dilution as a consequence of gasification of the oil, and hence will also reduce the structure. Inversely, very high structure is obtained with oxygen or oxygen-enriched air. Restricting the reaction zone by injecting the feedstock upstream of the reactor throat or increasing local concentrations by poor atomization or dispersion of the feedstock

are other means by which the concentration of solid particles may be affected.

A process commonly applied to reduce structure is the use of alkaline and alkaline-earth metal salts in vaporized form which are able to supress the aggregation of the carbon black particles. The exact mechanism is unknown, but it is assumed that the positive metal ions add on to the carbon black nuclei, causing electrostatic repulsion and thus preventing the fusion of carbon black particles. The effect seems to be related to the ionization energy. Alkaline metal salts are most effective, and their effect increases with atomic weight from lithium to caesium. The best compromise economically is the use of potassium salts, aqueous solutions of potassium carbonate, potassium nitrate, and potassium hydroxide being preferred. Oil-compatible forms are alkali metal salts of fatty acids. The nature of the anion is virtually of no importance. The additive can be sprayed into the combustion chamber or injected together with the carbon black feedstock. It is important that the salts are present in the carbon black forming zone in vaporized form. The quantities of potassium vary considerably. Medium- or high-structure blacks

DBP-Absorption
(ml/100g)
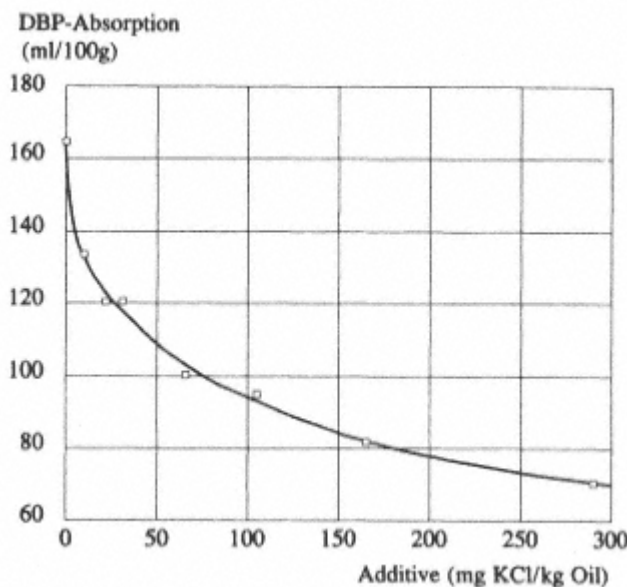
Fig. 11.
DBP absorption as a function of the amount
of additive used.

having DBP numbers greater than 100 cm3/100 g usually require between 10 and 100 ppm of potassium, depending on the type and quality of the feedstock. For specialyty blacks with extremely low structures, such as carbon blacks consisting almost exclusively of small aggregates, the amount can be as high as 1000 to 2000 ppm (Fig. 11).

The above measures affect both DBP and Crushed DBP absorption. How and to what extent the ratio between the two parameters can be influenced depends on the specific reactor configuration, its operating conditions, and on the subsequent carbon black processing.

Size Distribution Curves: The primary particles and aggregates of blacks are by no means uniform in size, but are characterized by a

certain particle and aggregate size distribution [9]. The distribution curves for primary particle and aggregate sizes can be obtained by electron microscopy. In addition, aggregate size distribution can also be determined by light scattering (Photon Correlation Spectroscopy) and disc centrifuge photosedimentometry measurements. The width of the aggregate size distribution may also be reflected in the tint measurements.

The width of primary particle size and aggregate size distribution can be adjusted, but the one cannot be changed independent of the other. It is generally true that the more homogeneous the conditions of temperature, feedstock concentration, residence time, and flow throughout the reaction zone, the narrower are the distribution curves. High flow velocities, steep shear gradients in the mixing zone as well as optimum atomization and mixing of the carbon black feedstock promote narrow primary particle and aggregate

size distributions.

Broad to bimodal distributions are obtained as a result of low flow velocities, reverse flow areas in the reaction zone, inhomogeneous shear gradients in the mixing zone, and inhomogeneous distribution of the feedstock. The latter may be achieved by injecting feedstock simultaneously at different positions in terms of flow pattern and by the use of different types of injector nozzles.

Fig. 12 shows the primary particle size distribution curves of different furnace blacks.

Influence of Reactor Operating Parameters on Economic Efficiency

To start with, the nomenclature of the reactor operating conditions already described should be presented in a comprehensible form.

There are six basic parameters or input data at the reactor:

I. process air rate,

II. process air temperature,

III. fuel gas rate or air consumption factor according to Equation 1,

IV. oil rate,

V. amount of additive,

VI. quench water rate and quench position.

Considering the sequence of reactions in the furnace black process, process air and fuel are fed into the reactor first. Once these two process parameters are fixed, the other parameters depend on the properties of the carbon black grade to be produced: The amount of

feedstock is determined by the desired primary particle size, the quench position by the desired porosity and
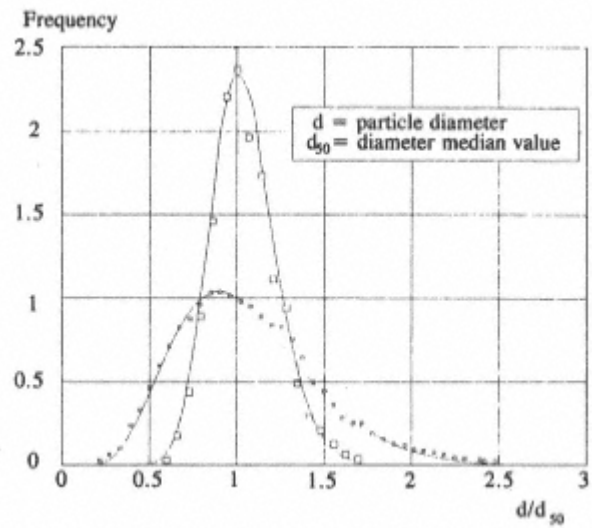
Fig. 12.
Primary particle size distribution curves.

the amount of additive by the desired level of structure.

In a given reactor, the flow velocity and hence the process air rate may be varied within certain limits. For any given grade, the process air rate determines the feedstock rate and therefore the amount of carbon black produced. Once specific reactor conditions have been set, the output can be raised or lowered by changing the input parameters of fuel rate, oil rate, additive and quench water in direct proportion to the process air rate. Temperature, yield and quality of the carbon black thus remain constant within the normal process fluctuations. The process air rate is, therefore, the first parameter to be fixed.

The fuel rate may also be varied within a certain range, the upper limit being set by the temperature resistance of the combustion chamber, the lower limit by the flame propagation velocity. The fuel rate at a given air rate, i.e., the heat input, within certain limits may be chosen on the basis of economic considerations. The relationship between oil rate, reaction temperature, carbon black output, and carbon black properties is vital to all carbon black manufacturing processes. Only few publications [6] have dealt with this subject.

We will now take a closer look at the interdependence of reactor input parameters and their effect on economic efficiency.

Oil Rate, Carbon Black Output, Consumption Factor: As described in *Particle Size, Surface Area, Porosity,* at a given air consumption factor *k,* it is the amount of feedstock alone which determines the temperature in the reaction chamber and consequently certain quality characteristics of the carbon black such as primary particle

size or specific surface area. Examples are given in Table 11. The relationship between the oil rate, M, and carbon black output, CB, at constant process air and fuel rates, that is a constant air consumption factor k, can be determined quantitatively. Fig. 13 shows a plot of feedstock input (oil rate) versus the carbon black produced. An empirical relationship can be deduced from this plot which fulfills the linear equation

$$M = 1.06 \times CB + 990 \quad (6)$$

for a process air rate of 10,000 Nm3/h and $k = 65\%$ using natural gas as fuel. The measured points in Fig. 13 carry a reference to the respective mean primary particle size of the carbon blacks. It is obvious that, as indicated above, primary particle size increases with the oil rate.

The relationship expressed by Equation 6 is illustrated by means of the plot in Fig. 13. If, following the diagram, one starts with an oil rate $M = 0$ and increases it steadily, the oil burns with the excess oxygen left from the combustion chamber until all the oxygen has been consumed. In the diagram, this point is reached at $M = 990$. At this oil rate, no carbon black is formed
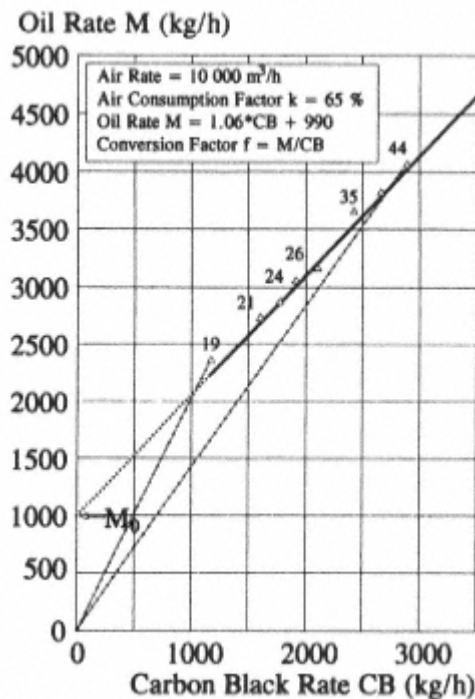
Fig. 13.
The relation between oil rate and
carbon black output.

yet, and it is referred to as the non-carbon-black-producing oil rate *M°. The graph in Fig. 13 thus offers the possibility of determining the carbon black point, the conditions under which carbon black formation starts. Evidently M°* is dependent on the amount of combustion air consumed in the combustion chamber. Equation 6 can therefore take the following general form to apply for any given air consumption factor:

$$M = 1.06 \times CB + M° \quad (7)$$

According to Equation 7, the total amount of feedstock introduced into the reactor is divided in two parts: A carbon-black-producing and a non-carbon-black-producing oil rate.

The gradient of the straigth line in this equation indicates that at oil rates higher than $M°$, the amount of 1.06 kg carbon black feedstock is required to produce 1 kg of carbon black. In other words, the carbon contained in the carbon-black-producing amount of feedstock is quantitatively converted to carbon black (see also Table 6). It goes without saying that the factor 1.06 applies only to one specific carbon black feedstock. The poorer the quality of the feedstock, the higher the factor.

Besides the yield, which reflects the percentage of the carbon black produced to the total oil input, the conversion factor is also often used. It is

calculated by forming the quotient of oil rate and carbon black output and indicates the total amount of feedstock required to produce 1 kg of carbon black. The higher the conversion factor, the higher are the production costs. The conversion factors of different blacks can be deduced directly from the gradients of the straight lines passing through the origin (Fig. 13). Only the two lines for the highest and the lowest value, respectively, were plotted in this diagram. The plot shows that large-particle blacks can be manufactured at lower, i.e., more favorable, conversion factors than fine-particle blacks. Carbon black output under the specific conditions of constant air rate and constant air consumption factor is higher if the carbon black has large particles than if it has fine particles. This is so because, with constant air and fuel rates but increasing oil rate, the temperature in the reaction zone decreases, primary particle size increases, and the part of the feedstock exceeding the oil rate of $M°$ is quantitatively converted to carbon black. At constant air and fuel rates, only a limited but fixed amount of oxygen remains to react with the feedstock and hence, $M°$ is constant.

Fuel Rate, Feedstock Equivalent: If, however, the fuel rate changes, $M°$ also changes as a consequence of the changing amounts of remaining oxygen. Fig. 14 shows a plot of the non-carbon-black-producing oil rate $M°$ versus the fuel rate G.

An empirical linear relationship can be deduced from the graph:

$$M° = -1.16 \times G + 1900 \quad (8)$$
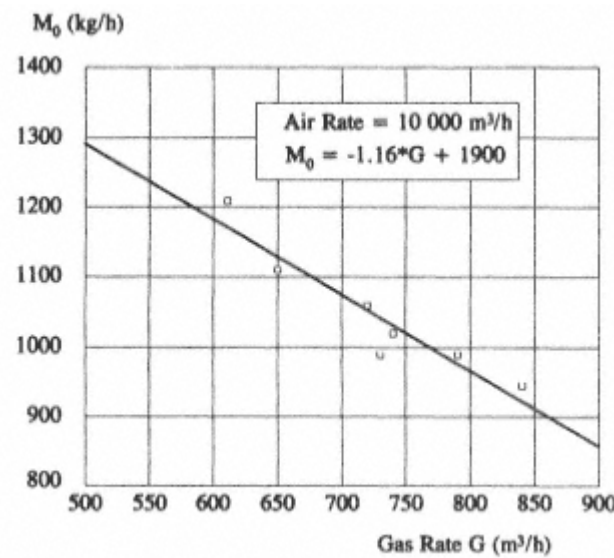
Fig. 14.
Non-carbon-black-producing oil rate as a
function of the fuel rate.

As expected, $M°$ decreases with increasing fuel rate. If the fuel gas rate increases by 1 m3/h, the oil rate has to be reduced by 1.16 kg/h. Hence, the feedstock equivalent at a given fuel rate is 1.16 kg/m3. Of course, the factors of this relationship are again only valid for the specific materials used in the example.

Inserting Equation 8 into Equation 7 yields a formula which incorporates both feedstock (oil) and fuel (gas). Using Equation 1, the fuel rate can be replaced by the air consumption factor k, giving the following relationship:

$$M = 1.06 \times CB - 116 \times k/fs + 1900 \ (9)$$

This equation encompasses a family of parallel straight lines in the M/CB diagram where each straight line is characterized by a specific fuel rate or a specific air consumption factor. It can also be used to calculate and optimize raw material costs on the basis of oil and gas prices within the limits allowed by the carbon black quality.

Quench Position, Amount of Quench Water: It was shown that the quenching of the reaction by injection of water is important and determines product quality. Carbon black reactors possess a number of different quench positions and the reaction time can be increased or reduced by changing the quench position. The water quench furthermore serves a second purpose in determining the reactor outlet temperature. The higher the reactor outlet temperature, the higher is the process air temperature which can be achieved in the heat exchanger. The reactor outlet temperature and, hence, the process air temperature, are determined by the amount of quench water used. In many cases, a secondary quench is

adopted, one upstream quench to adjust product quality and further downstream a second quench at a fixed position to control the temperature at the inlet to the air preheater.

However, the required amount of quench water depends not only on the reactor outlet temperature but also on the reaction temperature. Fine-particle blacks are formed at higher temperatures and therefore require greater amounts of quench water than large-particle blacks. It was shown that the reaction temperature is predominantly a function of the oil rate. At constant reactor outlet temperature and combustion air temperature, the amount of quench water required can be expected to correlate with the oil rate. The more the off gas leaving the combustion chamber is quenched by feedstock, the less quench water is required. By rule of thumb, the amount of quench water has to be reduced by 0.5 kg if the oil rate increases by 1 kg.

Tail Gas: Furnace black production yields not only the solid carbon black with its respective properties, but also a tail gas, the amount and composition of which depend on the input parameters for the grade being produced.

The main components of the tail gas, besides nitrogen, are hydrogen, carbon monoxide, some carbon dioxide and small quantities of light hydrocarbons such as methane and acetylene. Sulfur compounds are also present, these depending on the sulfur content of the feedstock. The same applies for nitrogen compounds.

An analysis of the dried waste gas yields information concerning its composition and also, by drawing up a nitrogen balance, permits the individual components to be determined quantitatively and thus calculation of the carbon black output. Table 12 shows the typical ranges of the tail gas components. The figures refer to the dried tail gas. In addition, the tail gas contains between 35 and 45 vol.% of water vapor.

If the air consumption factor and the process air rate are constant, the amount of residual oxygen leaving the combustion chamber is also constant. The oxygen-containing components are therefore barely affected by changes in the oil rate. However, with increasing oil rate, the amount of hydrogen released increases in direct proportion to carbon black output, as does the content of low hydrocarbons. Changes in the fuel rate alter the ratio between carbon- and hydrogen-containing components due to the higher H/C ratio of natural gas in comparison to oil.

To a first approximation, the amount of tail gas is independent of the fuel rate and affected only by the oil rate. Since the amount of hydrogen available increases with increasing oil rate, the amount of tail gas must also rise. However, this applies only for the dried tail gas. At an air rate of 10,000 m3/h, the following relationship exists between the amount of dried tail gas, *TG(dr),* and the oil rate *M:*

$$TG(dr) = 0.69M + 10350 \ (10)$$

It has been seen that the amount of quench water decreases with increasing oil rate, which balances the higher hydrogen content of the tail gas. The amount of wet tail gas is therefore not affected by input parameters other than the process air rate. The following rule of thumb is adopted to calculate the amount of wet tail gas, $TG(w)$:

$$TG(w) = 2 \times air \ (11)$$

This equation applies only for the off-gas leaving the heat exchanger, and any additional water injected for cooling purposes must also be taken into account.

The tail gas is combustible due to its hydrogen and carbon monoxide content. Its net calorific value ranges from 2000 to 3000 kJ/Nm3, and is therefore considered to be a lean gas. Tail gas is combusted to provide heat for drying wet pelletized carbon black and, when economic, for the generation of steam and electricity.

Table 12. Composition of the Dried Tail Gas

Tail gas components	vol.%
N_2	61 67
CO_2	3 5
CO	11 15
H_2	12 24
CH_4	0.02 0.5
C_2H_2	0.02 0.5

The tail gas analysis is an important tool for controlling the carbon black production process. A carbon balance permits the amounts of carbon black produced to be monitored continuously. This provides important data permitting control not only of the reactor but of the entire plant, including the steam boilers, as well as optimization of the process.

Means of Control Downstream of the Reactor

Densification: As described above, freshly produced carbon black is densified after separation in the process filters either by stirring the fluffy black in the surge bin or by means of vacuum rollers. The bulk weight of the fresh carbon black, which may be 1060 g/l depending on its structure, can thus be raised to 100300 g/l. This densification is necessary to improve the handling properties. However, the treatment has to be careful and reproducible since excessive densification has adverse effects on dispersibility, and the best method for powder blacks as final product is, therefore, vacuum densification.

Dry Pelletization: Dry pelletization is usually performed on

pigment blacks which are required to be largely non-dusting. With regard to dispersibility, the dry-pelletized blacks range between powder black and the wet-pelletized products. The resulting bulk densities lie between 300 and 500 g/l, depending on the structure of the carbon black. A dry-pelletized carbon black is characterized by particularly small pellets and usually contains a relatively high proportion of micro-pellets which are less than 0.1 mm in diameter. The influence of process parameters on pellet size and pellet size distribution is comparatively small. Not all carbon black grades lend themselves to dry pelletization. Low-structure carbon blacks are particularly suited for dry pelletization. Large-particle high-structure blacks, however, are problematic. Pellet hardness can be increased by increasing the residence time in the drum, e.g., by increased bed depth in the pelletizing drum or by recycling of pelletized material into the drum. However, since the pellet hardness is still low, attrition of the pellets may occur in certain conveying systems.

Dry-pelletized blacks are nevertheless preferred in certain applications which require ease of dispersion.

Wet Pelletization and Drying: In the case of wet pelletization, the pellet size is affected by the carbon black/water ratio. High-structure blacks require more water than low-structure blacks. On average, the ratio between water and carbon black is approximately 1 litre per kg, yielding pellets with a diameter of 0.52.0 mm. This ratio can only be varied within very narrow limits for each carbon black grade. If the amount of water during wet pelletization tends towards the lower limit, smaller pellets are obtained. The addition of small amounts of light hydrocarbons also enhances the formation of small pellets with a narrow pellet size distribution. Pellet hardness can, to a certain extent, be influenced by the speed of the spiked helix in the pin mixer. It is more common, however, to use pelletizing agents or binders such as molasses or ligninsulfonates. Depending on the dosage, single pellet crush strengths between 20 and 80 g and mass strengths of 10 to 50 kg can be obtained.

The mechanical energy applied by the rotating mixer shaft reduces the amount of secondary structure, the extent of which depends on the speed of rotation. The speed of the helix and the residence time in the pin mixer can, therefore, be employed to adjust the ratio between DBP and the Crushed DBP absorption. This difference is regarded as being a measure of the densification history of the carbon black and the value is referred to as the ΔDBP.

Drying of the wet pellets is another process step in which carbon black properties can be varied. If the carbon black is dried at comparatively low temperature and in contact with as little oxygen

as possible, carbon black surface properties remain virtually unchanged. On the other hand, elevated temperatures of 250400°C and a sufficient supply of oxygen in the air cause the carbon black surface to become oxidized. In addition to the basic surface oxides which always exist on the carbon black surface, acidic oxides are formed which may reduce the pH from originally 910 to 68 and even lower. If the carbon black contains noticeable quantities of sulfur from the feedstock, sulfuric acid and sulfonic-acid groups are also formed.

The influence of the drying process on carbon black properties can be controlled with appropriate process instrumentation.

After-Treatment: After-treatment of carbon blacks constitutes a drastic intervention in the chemical and physical properties of the carbon black surface and will be described in detail in Section 1.6.

Control of the Carbon Black Process, Quality Assurance, Safety

Consumer requirements regarding carbon black quality are very stringent since deviations affect the end product performance. The process re-

quires exact and reproducible operating conditions, not only to produce the multitude of carbon black grades required but also to maintain the individual properties at a constant level. Carbon black manufacturers, therefore, implemented sophisticated quality assurance systems which enable them to meet and guarantee the parameters laid down in the specifications.

This task is aggravated by two factors. Firstly, there is the feedstock. As explained earlier, carbon black feedstocks are byproducts of large-scale industrial processes and in spite of agreed specifications may be subject to some unavoidable deviations. These deviations are not influencing the quality of the carbon black produced since the furnace black process is very flexible enabling the operator to adjust the process parameters to feedstock variations. Mixing and blending facilities at the plant are also tools to level out possible feedstock deviations. These corrective actions are taken on basis of the feedstock tests carried out on samples of each feedstock shipment. The second factor is connected with the formation of the carbon black. It is important that all parameters affecting carbon black formation can be controlled and adjusted with high precision. The amount of measurement and control equipment required is thus considerable.

In contrast to chemical processes taking place in homogeneous gaseous or liquid phases, product properties and output in the case of carbon blacks can only be determined with a time lag. Numerous investigations have been carried out in the search for on-line measurements which yield correlations with specific carbon black properties. Such measurements, in addition to recording the exact input data and indicating the conditions in the reaction zone, are

temperature measurements and tail gas analysis. The significance of the reaction temperature for adjusting primary particle size should be borne in mind. The measurement of the temperature, more accurately of the temperature profile, in the reactor is an important source of information for reactor control. Based on tail gas analysis, the amount of carbon black formed can be calculated, thus providing a basis for control of the drying and pelletization processes. A good correlation was observed between the methane content of the tail gas and iodine adsorption [10]. Structure and bulk density are also closely related. That is, the bulk density decreases with increasing DBP absorption. Such correlations can be used for on-line process control.

Of course, these correlations cannot replace the determination of surface area and structure. Carbon black samples, both fluffy and pelletized, therefore, have to be tested at regular intervals, and here automatic titrating equipment and robots may replace some of the manual work. Quality checks performed at specific intervals help to ensure that quality remains constant and that deviating material is directed to the off-spec tank instead of the product silo. The data obtained from these checks are processed by computer.

From these data the operating staff is made aware of the trends and can take corrective action when required, following the principles of Statistical Process Control (SPC). Modern furnace black plants are operated by process control systems which are able to correct small variations in quality automatically, or to calculate the required changes in process parameters essential to the operating personnel.

These facilities are also important for safety reasons since, in the case of plant failure, the entire unit has to be shut down in a controlled operation to prevent the formation of explosive mixtures which can cause severe damages to the plant. Not only the actual carbon black production unit has to be taken out of operation, but also the boilers, turbines and power generators connected to it. All these different installations can be monitored from a central control room which receives and processes all data gathered in the various plant sections. This also includes emissions control which have to meet legal regulations concerning NO_x, SO_2 and particulate matter. In addition, video cameras may be used to constantly monitor the combustion chambers of reactors and boilers for intermediate action to be taken if required.

1.4.3. Process Variants and Patents

Since the oil furnace black process replaced most of the other manufacturing processes during the 1950s and 1960s, the majority of patents and publications refer to this process. They mostly describe designs or procedures related to the reactor, since this is what determines the most important carbon black properties. This short survey of the technology of different manufacturers will therefore be limited to reactors and their operation.
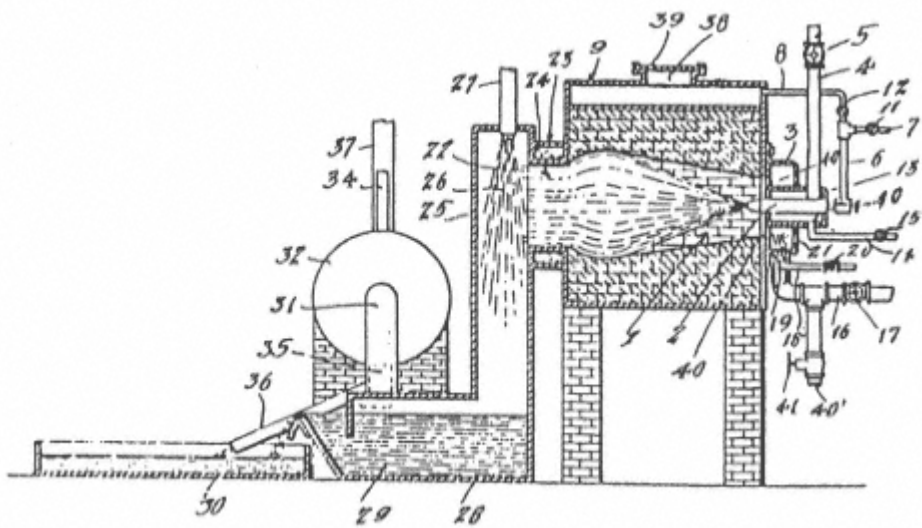
Fig. 15.
Furnace black reactor (U.S. Patent 1,438,032).

Carbon black production in a closed system was the subject of research as early as the late 19th century (DRP 50,606 from 1899) [20]. Performance of the method at the time was not satisfactory, as was the process published [11] in U.S. Patent 1,438,032 (Fig. 15).

Having spent several years on the gas furnace process, the restrictions imposed by the Second World War caused the industry to switch over to the oil furnace process.

The breakthrough was achieved by Phillips Petroleum in the U.S.A. In the early 1940s, the first semi-reinforcing black FEF (N 550) was manufactured by the oil furnace process [7]. The first technically viable version of the Phillips Tangential Reactor for high reinforcing blacks is described [12] in U.S. Patent 2,564,700 of 1956 (Fig. 16).

The Phillips reactor triggered off a development which was then pursued by all major carbon black manufacturers [31,33]. They began to experiment with the oil furnace process, developed and constantly improved their own, company-specific reactor configurations. The most important milestones of this development are selected and discussed below in greater detail.

Two of the patents concerning the furnace process which indicate ways of influencing the morphological properties of furnace blacks were granted to Cabot [3]. These patents show the influence of small quantities of alkalis on aggregate formation (see also *Structure*). After primary particle size, it was now also possible to adjust the second important parameter, the carbon black structure. In addition to the basic grades, carbon blacks with different levels of structure could be produced, and the range set by specific

surface area and structure was filled with a variety of new carbon black grades (see also Fig. 9).
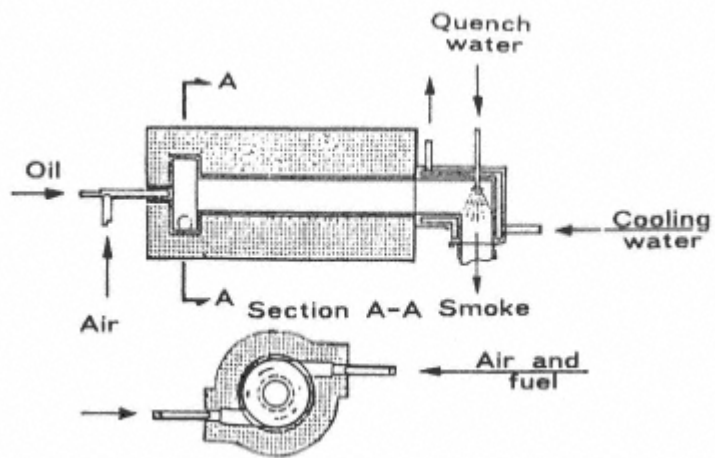
Fig. 16.
Phillips tangential reactor.
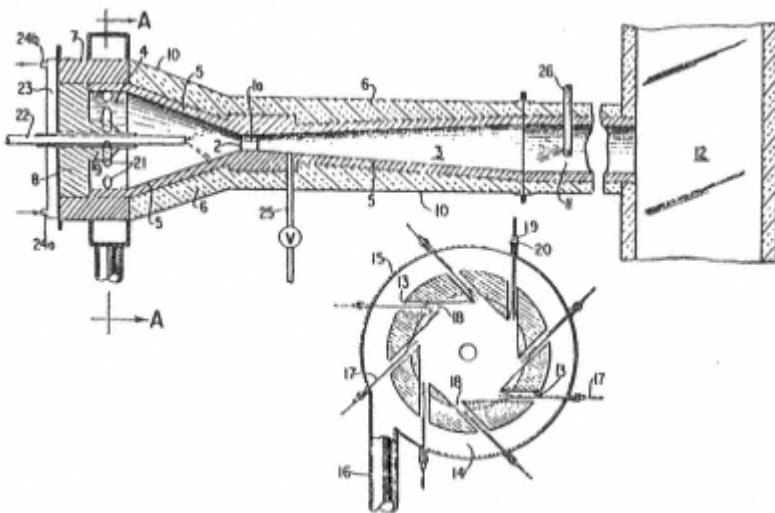
Fig. 17.
Venturi-type reactor (Columbian).

Experiments with oil atomization [13] and residence time yielded a new category of carbon blacks whose most outstanding feature was that they imparted good abrasion resistance to tire treads. These blacks were termed Improved Blacks and had basically the same structure and surface area as the conventional carbon black grades [4]. The new procedures allowed the carbon black to be quenched immediately upon completion of the pyrolysis to suppress secondary reactions.

One of the first versions of second-generation furnace black reactors for the production of Improved Blacks was the Venturi reactor developed by Columbian Carbon (U.S. Patent 3,490,869) [14]. In this reactor, the oil is injected into a converging zone where the oil droplets receive considerable acceleration (Fig. 17).

Another technique to disperse the feedstock is described in U.S. Patent
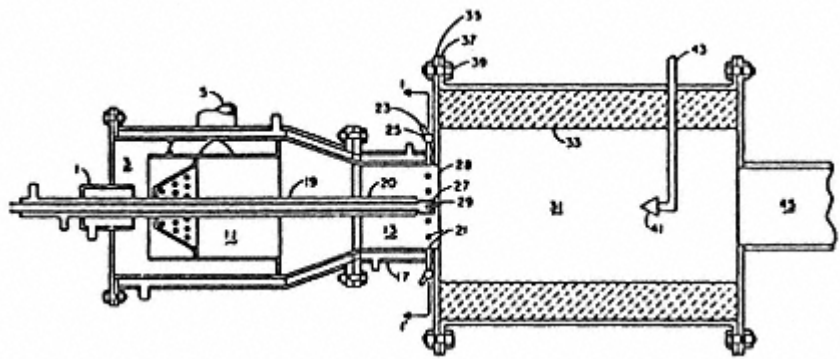
Fig. 18.
Furnace black reactor (Cabot).

3,922,335 from Cabot [15]. The required shear forces which have to break up a compact jet of oil are obtained by high flow velocities and high energy densities of the combustion off gas leaving the water-cooled combustion chamber (Fig. 18).

Other carbon black manufacturers developed similar reactor geometries serving the same purpose.

The sharp rise in energy prices in the 1970s provided the incentive for new investigations aimed at saving feedstock and energy. U.S. Patent 4,393,034 granted to Ashland [16] provided for the tail gas released during carbon black production to be recycled into the reactor to replace natural gas. This required that the process air be enriched with oxygen to increase the low heating value of the tail gas. Although the process works in principle, it was unable gain ground in practice.

The purpose of U.S. Patent 3,256,065 by Continental Carbon [17] was also to make optimum use of the available energy. In this version, the thick ceramic insulation of the reactor head was replaced by a jacket through which the process air was passed. The combustion chamber wall is cooled by the process air and the energy thus recovered.

The German patent DP 2,944,855 held by Degussa [18] falls into the same category. It describes how the preheated process air is heated further to reach temperatures of up to 1100°C.

Since the beginning of the 1980s, tire development has no longer been focused on treadwear alone. Other properties such as rolling resistance, heat build-up, and wet traction are gaining increasing importance. Consequently, present-day reactors are expected to be

highly versatile and able to produce carbon blacks having a wide range of properties such as primary particle size and distribution, aggregate size and distribution, structure stability and controlled porosity. If possible, this is to be achieved by a single, universal reactor type. The PIER-type reactor (Fig. 19) developed by Phillips Petroleum [19] (U.S. Patent 4,540,560) can be considered to be a prototype of such a third-
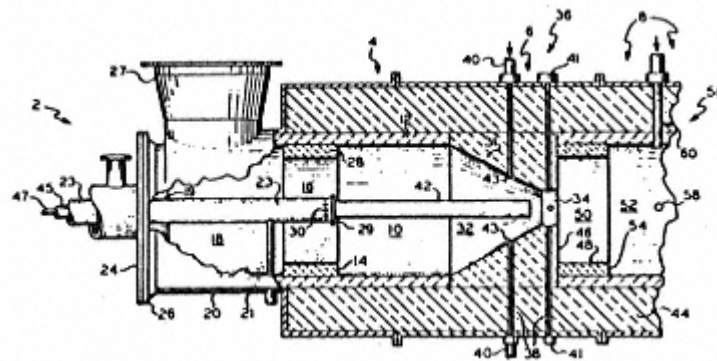
Fig. 19.
PIER-type reactor (Phillips/Degussa).

Table 13. Latest patents on furnace black reactors and furnace processes

Company	Patent	Year
Cabot Corp.	US 4,879,104	1987
	DE-OS 3,841,285	1988
	DE-OS 4,016,475	1990
	DE-OS 4,028,578	1990
	DE-OS 4,928,586	1990
	DE-PS 3,443,978	1985
Columbian Carbon Co.	EP 0,360,379	1989
	EP 0,384,080	1989
	US 5,009,854	1988
Degussa AG/Phillips Petroleum Co.	EP 0,102,072	1983
	EP 0,206,315	1986
	US 4,540,560	1983
	US 4,765,964	1985
	US 4,822,588	1985
	US 4,824,643	1987
Mitsubishi Kasei Corp.	EP 0,412,265	1990
Witco Corp.	US 4,988,493	1987
	EP 0,315,442	1988

generation reactor. A notable feature of this latest generation of carbon black reactors is the fact that the feedstock is no longer injected only at the position of highest flow velocity. Depending on the desired carbon black properties, the feedstock may be injected upstream or downstream of the choke or in a combination of both. Preferentially, the feedstock is injected from the outside radially into the reactor, however additional axial oil injectors may be used. A further variation of carbon black properties can be achieved by non-symmetrical arrangement of the injector nozzles at the various

positions. It is interesting to note that this development has not led to further diversification, but to greater similarities between the reactor configurations of different carbon black manufacturers. This is shown by several patent applications filed in recent years (Table 13).

1.5. Other Manufacturing Processes

1.5.1 Lampblack Process

One of the oldest processes for carbon black production is the lampblack process [20]. Since antiquity, significant quantities of carbon black have been required for the preparation of inks, but also of paints for mural paintings. These were produced mainly by the lampblack process. The Roman architect Vitrivius already described the preparation of lampblacks [21] from the resin of pine trees:

First, a vaulted chamber is built in the form of a (Roman) steam bath, lined carefully on the inside with marble stucco, and smoothed. In front of this chamber a small combustion chamber is set up, the discharge openings from which lead into the (separation) chamber, and with the inlet opening closed exactly far enough so that the flame does not shoot out. Pine resin is now placed in the furnace. During burning, carbon black develops from the resin because of the great heat. This carbon black passes through the outlet openings into the separation chamber, and is precipitated on the rounded sections of the chamber and of the vaulted ceiling. The carbon black is then collected, with the largest amount of it incorporated into gum arabic in order
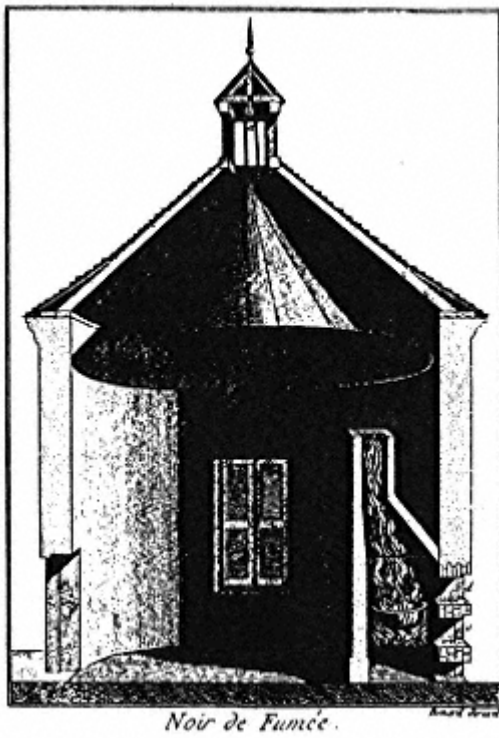
Fig. 20.
Historic lampblack process
(Encyclopedia Diderot, Paris, 1770/80).

to produce writing inks. The remainder is mixed with glue by stucco workers, and is used for mural paintings.

The main characteristics of this process, such as heating of the resin, the limited air supply, and recovery of the carbon black in depositing chambers remained unchanged for centuries. After the invention of letterpress printing in the 16th century, the requirements for carbon blacks increased more and more because now it became necessary to replace the writing inks by printing inks providing a higher viscosity. In Europe, many small and medium sized carbon black production shops arose, which operated according to the lampblack process. Such a production plant is shown in Fig. 20. Only as late as in the nineteenth century carbon black production was turned from a craft to an industrial production process which was operated in large-scale plants and used coal tar oils as feedstocks. The depositing chambers were arranged as a maze in which the majority, but not all, of the carbon black was deposited. In the mid-20th century, the depositing chambers were finally replaced by modern filtering equipment in which the carbon black could be completely separated. Since carbon black was required for printing inks, electrodes, and - after the discovery of its reinforcing effect in rubber - also in tires and mechanical goods, production grew steadily. Until the mid-1930s, carbon blacks were produced in Europe almost exclusively according to the lampblack process, but were then gradually replaced by the more reinforcing gas and furnace blacks.

The lampblack process belongs to the processes of thermal-oxidative decomposition and is characterized by great simplicity.

The only feedstock required is an aromatic oil mainly based on coal tar.

The lampblack apparatus (Fig. 21) consists of a flat cast-iron pan which contains the liquid feedstock, the level of which has to be kept as constant as possible. A refractory-lined hood is installed above the pan in such a way that a ring-shaped gap is left between the edge of the pan and the hood. The
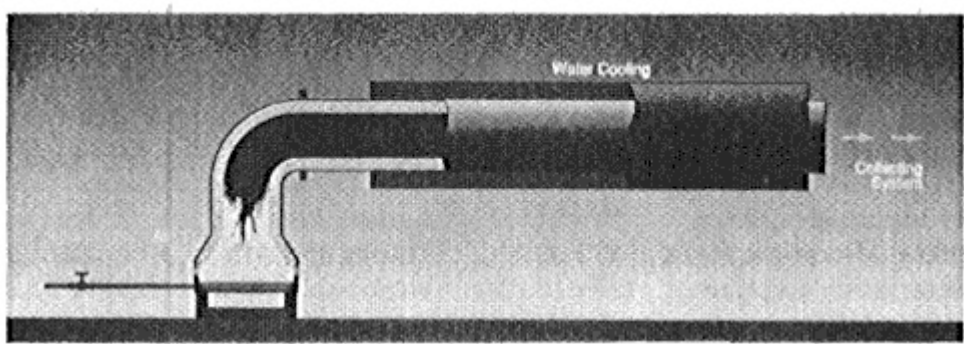
Fig. 21.
Lampblack plant.

process air is fed into the system through this gap. A water-cooled tube which is connected to the hood cools the carbon black smoke. The carbon black is then separated in filters and pelletized as in the furnace black process (see Section 1.4.1).

The lampblack process has only one variable input parameter: the process air rate. The size of the gap and the vacuum generated by the suction created by the filter fan determine the amount of air drawn in and hence the reaction temperature. At increased air rates, a greater portion of the feedstock is burned, leading to higher temperatures. These result in the formation of smaller primary particles and higher specific surface areas. However, the process is not very flexible with a given set of equipment. For fine-particle blacks the pans have to be small, and inversely, large-particle blacks require feedstock pans with large diameters.

The input of air from the periphery creates areas where different conditions prevail. A shell of very hot flames forms around a cooler core and the temperature gradient decreases from the edge of the pan to its center. In the outer regions of the shell, the feedstock predominantly undergoes combustion, whereas cracking reactions increase towards the center. This temperature gradient leads to the formation of carbon blacks with very broad particle size distributions which are a typical feature of lampblacks.

The conical shape of the hood is required by the process. The function of the ceramic material heated by the flames is to radiate the heat and vaporize the feedstock similar to a surface vaporizer. Easily vaporized oils lead to higher concentrations of hydrocarbons and thus to larger-particle blacks. Since the feedstock has to be vaporized before it can react and since the vaporized portion of the

oil is constantly replaced by fresh preheated oil, non-vaporizable, partly polymerized substances remain in the feedstock dish. These are drawn off from time to time and replaced by fresh oil.

Before the development of the furnace process, a wide range of lampblack grades was produced, both large- and fine-particle blacks. By now, most of these earlier blacks have been replaced by furnace blacks, and only carbon blacks with comparatively large particles are still manufactured by this process. Due to its broad primary particle size distribution and resulting ease of dispersion, lampblack is highly suitable for use in mechanical rubber goods.

Table 14. Lampblack Properties

N_2 surface area, m_2/g	16 24	Jetness, My	200 220
Iodine adsorption, mg/g	23 33	Tinting strength	25 35
Mean particle size, nm	110 120	Volatiles, %	1 2.5
DBP, ml/100g	100 200	Toluene extractables, %	max. 0.3
pH	6 9		
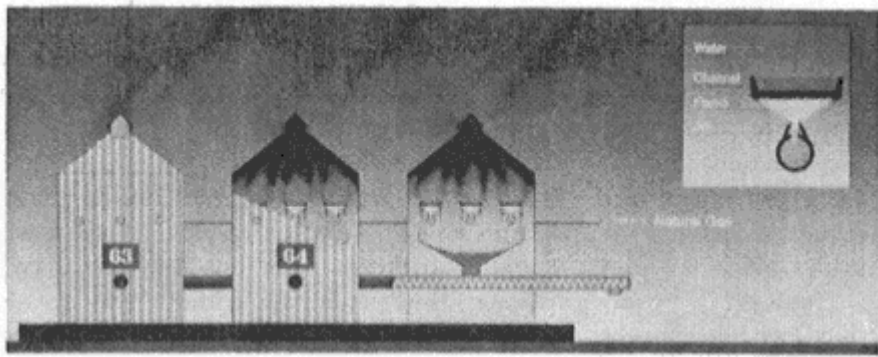
Fig. 22.
Channel black plant.

Other applications are electrodes and carbon brushes. The indications in Table 14 refer to the lampblack manufactured by Degussa.

1.5.2. Gas Black Process/Channel Black Process

A common feature of both processes is that they are operated in open systems where a multitude of small diffusion flames burn in air and the carbon black is deposited on cooled surfaces. The development of the older channel black or impingement process goes back to 1872 and, after a history of more than one hundred years, was completely discontinued in the U.S. in 1976. The process used natural gas as a raw material. Its name was derived from the fact that thousands of small flames fed by natural gas from ceramic openings impinged upon the underside of water-cooled iron channels [22]. The deposited carbon black was scraped off into a funnel-shaped trough (Fig. 22) and collected in screw conveyers. However, since not all of the carbon black was deposited on the iron channels and since no filters were used at the time, a large part of the carbon black was released into the

atmosphere together with the waste gas. The so-called hot houses which contained these production plants could be recognized from miles away by the carbon black cloud hanging overhead. This drawback and a yield of only 5% made this process uneconomical and forced it out of operation.

Historically, the channel process played an important role. It was on channel blacks that the reinforcing effect of carbon black in rubber was discovered early this century. In the decades that followed, channel blacks were used mainly in tire treads where they were far superior to lampblacks. During the first half of the 20th century, channel blacks were produced predominantly in the U.S.A. and exported worldwide, since its feedstock, natural gas, was cheap there and available in sufficient quantities. This was not the case in Europe, which resulted in the investigation of different procedures, and in

1935 Degussa successfully developed the gas black process. The properties of these blacks were similar to the U.S. channel blacks, and they quickly gained significance in Europe as reinforcing blacks, and a number of gas black plants were constructed [23].

Like the channel process, the gas black process is based on the principle of thermal-oxidative decomposition and operates as an open system where the carbon black is formed in diffusion flames. Air has free access to the system resulting in surface oxidation, thus producing acidic blacks.

The gas black process uses vaporized oil instead of natural gas, with coal tar distillates being the preferred feedstock. These oils are heated in a vaporizer, and the resultant vapors are carried by a hydrogen-rich gas to the burners, the flames from which are allowed to impinge on water-cooled rollers. Most of the carbon black formed is deposited on these rollers, the remainder being collected in filters (Fig. 23). Both carbon black streams are combined and processed further, as described in Section 1.4.1. The impingement process is much more flexible than the lampblack process. Although the access of air is free and is only controlled by diffusion, the process of charging the carrier gas with vaporized oil provides a means of achieving the desired primary particle size or specific surface area. Primary particle size ranges from 10 to 30 nm. Extremely fine particles can thus be obtained with the gas black process. It is not possible, however, to influence carbon black structure. The range of gas black properties is illustrated in Table 15.

Having lost their significance as reinforcing blacks, gas blacks are now mainly used as pigment blacks. It is an application for which

they are particularly suited because of their acidic surface oxides. In many cases, this acidity is increased by oxidative after-treatment (Section 1.6.1).

The impingement process has its origins far back in history. In ancient China special carbon blacks were needed for the preparation of inks, and their production from the flames of oil lamps was highly important. The carbon black was obtained by allowing the flames to impinge on water-cooled porcelain dishes, and the carbon black which was deposited on the surface was carefully removed. Produced from vegetable oils, these carbon blacks were of a fine particle size and were preferred to the coarser lampblacks in color applications.

Table 15. Range of Gas Black Properties

N_2 surface area, m^2/g	90 500	Jetness, My	230 300
Iodine adsorption, mg/g	n.a.	Tinting strength	90 130
Mean particle size, nm	10 30	Volatiles, %	4 24
Oil absorption, ml/100g	220 1100	pH	4 6a

aAfter-treated Blacks: min. 2.
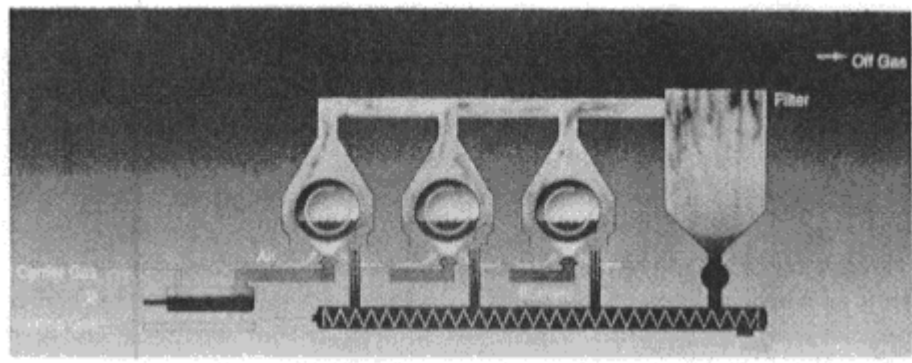
Fig. 23.
Gas black plant.

1.5.3. Thermal Black Process

The thermal black process is based on thermal decomposition in the absence of oxygen and operates in a closed system. Its special feature is that it is a cyclic process. The reactor is vertical and consists of a refractory-lined furnace which is fitted with a grid structure of fire bricks to increase the interior surface area. In the process, reactor heating and decomposition cycles alternate every 5 to 8 min.

During the heating cycle, fuel is burned with air in the reaction chamber until a predetermined temperature level is reached. The air feed is then stopped, the waste gas vents closed, the feedstock introduced, and the decomposition cycle begins. On the hot internal reactor surfaces, the feedstock decomposes into carbon black and hydrogen. Separation of the carbon black from the gas stream and subsequent processing take place as described pre-
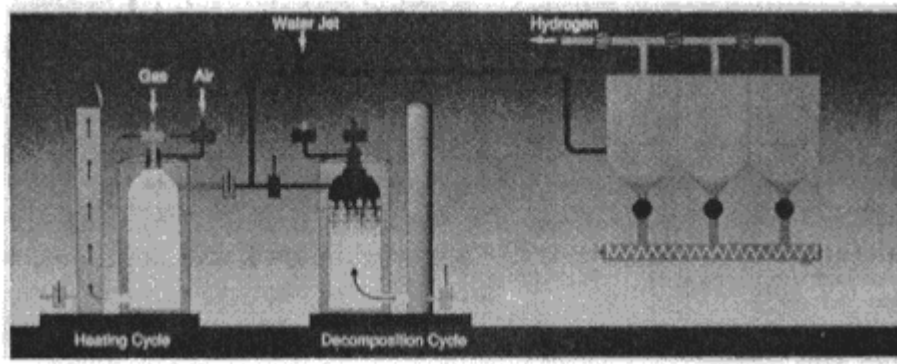
Fig. 24.
Thermal black plant.

viously for furnace black. The most economical process configuration is when the reactors are coupled in tandem operation (Fig. 24).

While Reactor 1 is on the heating cycle, Reactor 2 is on the decomposition cycle. In the case of a gas feedstock, the hydrogen gas produced in Reactor 2 can be used to heat Reactor 1. As Reactor 1 starts the decomposition cycle, Reactor 2 is reheated. Then as the Reactor 1 temperaure falls in the make cycle and increases in Reactor 2 during the heat cycle, at set points the cycles are reversed. The use of the hydrogen in the heat cycle allows a gaseous hydrocarbon feedstock to be utilized to optimum since most of the hydrogen produced is burned to preheat the reactor, and most of the carbon is converted to carbon black. If oil is used as feedstock, the hydrogen produced is often too contaminated to be used in the heat cycle and is burned for other processes which are heat intensive. In order to differentiate, it is common practice to refer to the product from the two feedstock types as either gas thermal or oil thermal.

Since the thermal black process is carried out at comparatively low temperatures and long residence times, thermal blacks differ from carbon blacks produced by thermal-oxidative decomposition. The particles grow very slowly and can become very large and have a tendency to form filamentous structures.

The significance of thermal blacks lies in their physicochemical properties. The process yields carbon blacks having the largest possible primary particles of up to 500 nm, thus allowing the achievement of high degrees of filler loading in rubber and plastics, imparting specific property profiles to these polymers. Originally

two different gas thermal grades were produced, depending on the concentration of the feedstock which is adjusted by diluting with recycled hydrogen. However, in the case of oil thermal blacks, only one grade was produced.

Medium Thermal (MT, N990) was produced from either gas or oil feedstocks having particle diameters up to 500 nm giving surface areas of 6 to 8 m2/g.

Fine Thermal (FT, N880) was produced only from gas feedstock having particle sizes ranging between 150 and 200 nm with surface areas of 8 to 11 m2/g.

However, today the production of fine thermals has ceased, and the N880 nomenclature no longer appears on the ASTM listing.

The thermal black process was developed in the U.S.A. in the early 20th century. The first patents [24] appeared in 1916, and production was first started in the 1920s. Initially, thermal blacks were used not only because of their compounded properties but also because of their low cost as high-quality bulk fillers. The effects of the first oil crisis in the 1970s dealt a blow to thermal black consumption from which it could never fully recover. Due

to increased production costs it could no longer be regarded as being a low-cost material. These days the use of thermal blacks is limited to speciality applications in which their unique compounding properties cannot be matched with other fillers or filler combinations.

1.5.4. Acetylene Black Process

Acetylene blacks are produced in closed reactors by thermal decomposition in the absence of oxygen. Whereas the feedstocks for thermal blacks can only be decomposed in an overall endothermal reaction, acetylene is thermally unstable and, after a start-up phase, can be split into hydrogen and carbon black in a highly exothermal reaction. The heat released has to be dissipated, which is achieved by the water-cooled cylindrical reactors. After the reactor has been heated briefly by burning acetylene, the air input is stopped permitting the formation of carbon black. This reaction continues until the flow of feedstock is interrupted.

Due to its reaction conditions and the unique feedstock properties, acetylene black differs from other carbon black grades. The comparatively long residence time, the homogeneous hydrocarbon feedstock, and the considerable heat generated by the reaction yield very pure carbon blacks which exhibit a greater degree of crystallization than blacks obtained by the other methods previously mentioned. The shape of the primary particles is definitely not spherical and because aggregation of the particles is promoted by the high reactor feedstock concentrations, acetylene blacks are characterized by high structure. It is, therefore, difficult to densify acetylene blacks and impossible to pelletize them.

With these inherent physical limitations and because of their electrical properties, acetylene blacks are used primarily as conductive blacks in electric cells and conductive and antistatic rubber and plastic applications.

1.5.5. Gas Furnace Black Process (Historic)

Before the oil furnace black process became the most important production method for carbon blacks, the gas furnace black process was practiced in countries where low-priced natural gas was available. Gas furnace blacks were mainly produced in the U.S.A. The process is described in a fundamental patent by Matlock [25]. Gaseous hydrocarbons, particularly natural gas, were used as feedstock to be transferred into carbon black by the oxidative decomposition process executed in large ceramic-lined reactors. The first blacks produced according to this method were large-particle blacks supplementary to the fine-particle channel blacks. In the early 1940s also fine-particle gas furnace blacks were developed which, compared to channel blacks, achieved higher yields and therefore better economics. Since 1960 the gas furnace black process which had a lifetime of about 40 years was replaced by the more effective oil furnace black process [26].

1.5.6. Carbon Black Formed as Byproduct

Besides the already described processes whose intended purpose is to produce carbon blacks, blacks are also obtained as a byproduct in several other processes. If the production parameters can be kept constant, it can be expected that they should yield a uniform product. As carbon black production is not their main purpose, there is no flexibility in producing different grades or in changing the properties of the blacks, therefore these processes are only to be described briefly.

Hüls Electric Arc Process: The electric arc process produces acetylene from hydrocarbons and by this thermal process carbon black is obtained as a byproduct. These carbon blacks have primary particles of a special flake-like shape with a mean particle size of about 35 nm. In former times this black was used for rubber and pigment applications. But due to its high contamination with hydrocarbons the black obtained by this process is no longer of any practical use and therefore burned as a waste product.

Production of Synthesis Gas: Synthesis gas is produced in large scale industrial process based on the incomplete combustion of hydrocarbons, in particular of heavy oil fractions. Small amounts of carbon blacks are obtained as a byproduct.

The oil feedstock is preheated and mixed with air or oxygen enriched air in order to achieve high reaction temperatures. In this thermal-oxidative process water is also introduced to optimize the production of hydrogen. The carbon black is separated from the synthesis gas by wet scrubbers: Different process steps are used to free the carbon black from catalyst contamination and water. In

some cases it is separated by filtration, in others by extraction with light hydrocarbons. Since the separation and purification methods require expensive installations there are only a few cases where the carbon black is separated. In most cases this product is internally recycled and used as feedstock.

The carbon black has a high surface area of 1000 m2/g or greater, which is combined with high level of porosity and aggregation. Due to these properties the carbon blacks exhibit high electrical conductivity in plastics and elastomers. Therefore, they are used in conductive compounds where only low carbon black concentrations are required.

1.6. After-Treatment of Carbon Black

Not all properties relevant for practical applications can be affected in the desired way or to the desired extent by adjustments in the manufacturing process. Carbon blacks used for coloring high-quality coatings have to possess highly polar surfaces for optimum wetting by the binder. Toners require carbon blacks with sufficient coloring strength which impart both either low or high electrical conductivity to the resin at relatively high levels of loading. Conductive blacks need clean carbon black surfaces free from oxides and

organic materials. The desired surface properties are achieved by subjecting the carbon blacks to a specific after-treatment processes.

1.6.1. Oxidative After-Treatment

Carbon blacks of different origin behave differently during oxidation. Due to the specific manufacturing processes, furnace blacks contain only small quantities of oxygen in the form of basic surface oxides, whereas gas blacks are always slightly oxidized and contain predominantly acidic surface oxides. Treatment with strong oxidizing agents in a gas phase or an aqueous medium can raise the concentration of acidic oxides considerably. In large-scale industrial processes, oxygen contents of up to 15 weight% can be achieved. Common oxidizing agents are ozone, air, nitric oxide/air mixtures and nitric acid. Surface oxides are intermediate states during oxidation of the carbon to carbon dioxide. The composition of the oxides and their concentration on the surface therefore depend on the conditions of the oxidation. The chemistry of these surface oxides is discussed in detail in Chapter 4.

Oxidation by ozone is carried out at room temperature by passing a gas produced in an ozonizer through a layer of carbon black. In order to ensure a uniform reaction with all carbon black particles, the carbon black has to be kept in motion. Fluidized-bed reactors where the carbon black is fluidized with the ozone-containing gas are particularly suited for this purpose. However, this procedure is only applicable to fine-particle, high-structure blacks. Large-particle blacks with very low structure cannot be fluidized and are oxidized in stirred stationary-bed reactors or rotary kilns.

The most simple form of oxidation is after-treatment by air at

temperatures between 350 and 700°C. Due to the thermal stability of the surface oxides, the extent of the oxidation is limited. The formation of a sufficient number of oxygen groups can only be achieved at temperatures below 400°C.

Much higher contents of surface oxides are obtained by treatment with nitrogen dioxide and air. The nitrogen dioxide acts as a catalyst in oxidizing the carbon surface, being itself reduced to NO which is oxidized to NO_2 by the oxygen in the air. The reaction temperature ranges between 200 and 300°C, and the reaction may last up to several hours, depending on the carbon black grade and the desired degree of oxidation. This type of after-treatment is carried out preferentially in fluidized-bed reactors (Fig. 25).

The process comprises two steps. First, the carbon black is oxidized with nitrogen dioxide/air. In the second step, the nitrogen dioxide adsorbed on the carbon black surface is desorbed by treatment with hot air [27].

A second oxidizing agent employed on an industrial scale is nitric acid. A very simple procedure is to add the nitric acid to the pelletizing water. The carbon black is then oxidized at elevated temperatures during drying. Another method is oxidation with nitric acid in a tubular kiln. HNO_3 is sprayed onto the carbon black as it is being fed into the kiln. In a second
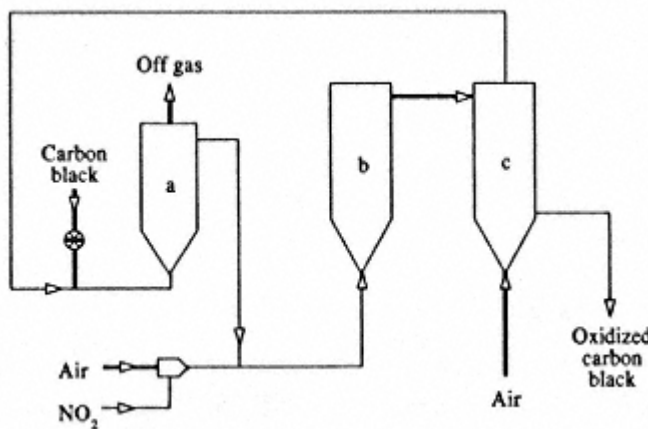
Fig. 25.
Fluidized-bed reactor for carbon black
after-treatment.

pass through the kiln, the mixture is heated and the nitrogen oxides formed as a byproduct are purged with air in reverse flow. The advantages offered by the simplicity of this method are offset by problems of corrosion and possible environmental hazards. The major advantage of oxidation by gas (ozone, NO_2/air) is that the carbon black retains its powder form and remains easily dispersible due to the absence of any densification [28].

1.6.2. Other Methods of After-Treatment

After-treatment for purposes other than oxidation is achieved with water vapor. If the after-treatment is carried out at relatively low temperatures (300500°C), it primarily removes extractable matter from the carbon black surface. At higher reaction temperatures (9001100°C) not only the oxygen groups and organic matter are removed, but also carbon is attacked, thus yielding porosity.

Removal of Extractable Matter

Certain applications require carbon blacks with extremely low levels of extractable matter. Extractable matter sometimes exhibits a strong color. In black-and-white or black-and-colored plastics staining may occur due to migration from black parts of the article where the color of the extract is invisible. In these cases and for applications which come into contact with foodstuffs, the level of extractables has to meet very stringent limits [29]. Some carbon blacks have to undergo special after-treatment, advantageously by steam distillation at a temperature of 300350°C, whereby the steam may also contain some air. Like oxidation, this procedure may take place either in a fluidized-bed reactor or rotary kiln [30].

Production of Porous Blacks

Porous blacks are obtained directly by the furnace black process if sufficient volumes, and hence sufficient residence times, are available. Again, the temperature plays an important role. Nevertheless, porosity is better achieved in a separate after-treatment step by means of steam since the reaction conditions are then independent of the carbon black production process. The temperature is in the range of 9001000°C to permit the porous blacks to be obtained within acceptable residence times. The reaction can be catalyzed, e.g., by potassium salts. Since steam preferentially attacks the less ordered regions of the carbon located inside the carbon black particles, a considerable number of pores is formed which may lead to the complete erosion of the inside of the particles. Such treatment may yield specific surface areas of 1000 m2/g and more. Carbon blacks with such high specific surface areas are of special interest for imparting electrical conductivity to plastics. Depending on the ability of the carbon black to sustain fluidization and on its densification, the after-treatment may be carried out in fluidized-bed reactors, stationary-bed reactors or rotary kilns.

References

1. Stokes, C. A. Guerico, V. J., *Erdöl und Kohle - Erdgas -,* 38, 31 (1985).

2. Bur. Mines Technical Paper 610 (1940).

3. Cabot Corp, U. S. Patent 3,010,794, U. S. Patent 3,010,795, 1958.

4. Medalia, A. I., Dannenberg, E. M., Heckmann, F. A. and Cotten, G. R., *Rubber Chem. Technol.,* 46, 1239 (1973).

5. Ulrich, G. D., *C&EN,* Aug. 22 (1984).

6. Kühner, G. and Dittrich, G., *Chemie Ing. Technol.,* 44, 717 (1972).

7. Kirk-Othmer, *Encyclopedia of Chemical Technology,* 3rd Edition, Vol.4, 631, 1978.

8. *What is Carbon Black?,* Brochure of Degussa AG, 1992.

9. Seibold, K. and Voll, M., *Chemiker-Zeitung,* 102, (4), 131 (1978).

10. Degussa AG, D. P. 2,113,425, 1975.

11. Frost, W. H., U. S. Patent 1,438,032, Dec. 5, 1922.

12. Phillips Petroleum Co., U. S. Patent 2,564,700, Aug. 21, 1956.

13. Degussa AG, D. P. 2,608,417, 1976.

14. Columbian Carbon Co., U. S. Patent 3,490,869, Jan. 20, 1970.

15. Cabot Co., U. S. Patent 3,922,335, Nov. 25, 1975.

16. Ashland Oil Inc., U. S. Patent 4,393,034, 1980.

17. Continental Carbon Co., U. S. Patent 3,256,065, 1962.

18. Degussa AG, D. P. 2,944,855, 1986.

19. Phillips Petroleum Co., U. S. Patent 4,540,560, Sept. 10, 1985.

20. Köhler, H., *Die Fabrikation des Russes und der Schwärze,* Verlag Vieweg & Sohn, Braunschweig, 1912.

21. Vitruv, De Architectura, ed., Valentin Rose, Verlag B.G. Teubner, Leipzig, 1899.

22. McNutt, L. J., U. S. Patent 481,240, 1892.

23. Flasskamp, W., *Technische Mitteilungen,* 49, (7) 329 (1956).

24. Brownlee, R. H. and Uhlinger, R. H., U. S. Patent 1,168,931, 1916.

25. General Atlas, U. S. Patent 1,738,716, 1926.

26. Dannenberg, E. M., The carbon black industry: over a century of progress, Rubber Division 75th Anniversary, 3540, (19091984).

27. Degussa AG, GB 895,990, 1958.

28. Cabot Co., U. S. Patent 2,439,442, 1943.

29. ECBECB Bulletin No. 6, Legislation concerning carbon black.

30. Degussa AG, D. P. 3,118,907, 1982.

31. Ullmann's Encyclopedia of Industrial Chemistry, VCH Verlags Gesellschaft mbH, Vol. A5, 140, 1986.

32. Rivin, D. and Smith, R. G., *Rubber Chem. Technol.,* 55, 707 (1982).

33. Davidson, H. W. et al., *Manufactured Carbon,* Pergamon press, New York, 1968.

Chapter 2
Mechanism of Carbon Black Formation

Roop Chand Bansal
Department of Chemical Engineering and Technology,
Panjab University,
Chandigarh, India

Jean-Baptiste Donnet
Centre de Recherches sur la Physico-Chimie des Surfaces Solides,
CNRS,
Mulhouse, France

Carbon particulate can be obtained form hydrocarbons either by pyrolysis or by incomplete combustion. In the former case the hydrocarbon and air are mixed before leaving the burner (premixed flames) while in the latter, oxygen diffuses into the gaseous hydrocarbon stream after leaving the burner (diffusion flames). The hydrocarbons produce two types of carbons. The first type is formed by the deposition on the walls of the reactor and is known as pyrocarbon while the second type is formed in the bulk of the gaseous phase. The gaseous phase particulate matter could be termed carbon black or soot. The former is an industrially manufactured carbon material and is characterized by spherical or nearly spherical fused aggregate particles with a range of sizes between 100 and 1000 nm. Soot, on the other hand, is a randomly formed particulate carbon which in addition to carbon contains a large variety of inorganic and organic impurities.

Pyrolysis and combustion has been the field of study by a large

number of investigators for almost a century but still no clear picture for the conversion of a hydrocarbon into more or less spherical particles has emerged although the process appears to be quite well understood. This lack of understanding is due to the fact that earlier workers were more interested in

the combustion phenomenon as a generator of free radicals. The formation of carbon particles for them was of secondary importance.

Several theories have been proposed for the formation of particulate carbon but no one mechanism could explain the formation from all flames regardless of their nature or the type of fuel. However, it is now agreed that the formation of carbon black involves three different stages:

* Nucleation or formation of soot precursors and soot inception which involved the transformation of a molecular system to a particulate system.

* Aggregation of particles which involves collisions between the large number of tiny particles with dimension in the order 12 nm produced by nucleation. This results in the formation of larger spherical particles with dimensions in the order 1050 nm or so.

* Aggregation or agglomeration of these spherical particles into chains approximately up to 1mm in length.

Out of these three stages of carbon black formation, the nucleation stage is the most interesting chemically and probably the least well understood stage of the whole process. Thus before discussing the theories of carbon black formation, a review of the important work done in the nucleation process will be presented.
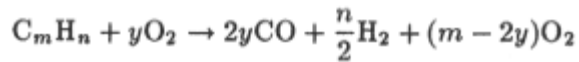
2.1. Formation of Soot Precursors

The formation of soot particles is a logical consequence of the growth of molecules through collisions. The process involves the conversion of primary molecular species which include free

radicals and ions into relatively larger particles containing many tens of thousands of atoms and a far greater C/H ratio. The process takes place in only a few milliseconds in a premixed flame and may be somewhat slower in diffusion flames. The overall process can be represented as in Fig. 1.

In its simplest form the process is assumed to take place by dehydrogenation to atomic carbon or perhaps to C_2 radicals, which then condense to solid carbon [1]. Alternatively a large hydrocarbon molecule is first formed which then is dehydrogenated to give soot. However, a mechanism intermediate between these two extremes involving simultaneous polymerization and hydrogenation is more feasible (Fig. 2).

The thermodynamic equation for the formation of soot can be written as

$$C_m H_n + y O_2 \rightarrow 2y CO + \frac{n}{2} H_2 + (m - 2y) O_2$$

According to this equation soot should be formed only when $m > 2y$, i.e., when the C/O ratio is greater than unity. The results of such calculation for some oxy-acetylene flames are given in Table 1. It is seen that if equilibrium
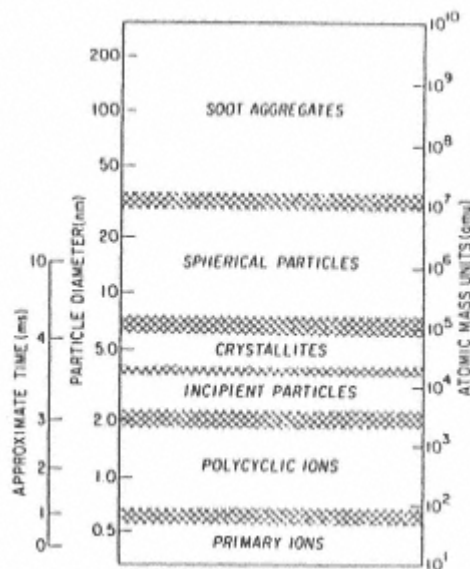
Fig. 1.
Growth from primary molecular
species to soot aggregation,
assuming ions as the nucleating
agent (from ref. [5])

is attained, solid carbon should only be present in mixtures with a
C/O ratio greater than 1.03. However, soot formation has long been
recognized as a non-equilibrium process. The carbon formation in
oxyacetylene mixtures has been observed with a C/O ratio of 0.8
while in many other fuels in premixed flames a C/O ratio of 0.5 or
even lower has been observed [2,3]. An increase in temperature
shifts the ratio to higher values while the fuel pressure and
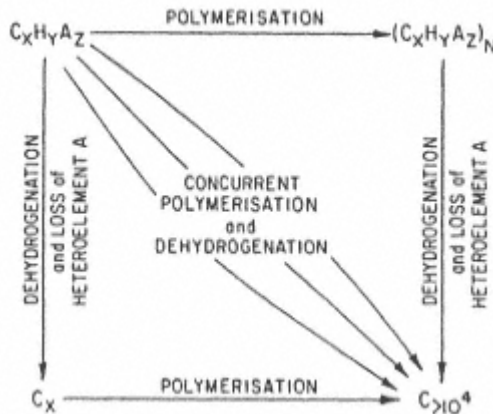
Fig. 2.
Possible pathways for carbon
formation (from ref. [36]).

Table 1. Equilibrium Temperature and Partial Pressures, in Atm, of Some Carbon Species and Major Constituents of Acetylene/Oxygen Fames at 1 Atm.

C/O	0.67	0.91	1.00	1.03	1.08	1.11	1.25	2.00
T(K)	3435	3383	3325	3304	3275	3266	3233	3122
C(gas)	$4.9\times10-9$	$2,2\times10-8$	$1.9\times10-3$	$3.8\times10-4$	$4.8\times10-4$	$4.5\times10-4$	$3.5\times10-4$	$1.3\times10-4$
C2	$1.3\times10-14$	$3.8\times10-13$	$3.8\times10-7$	$1.8\times10-4$	$3.6\times10-4$	$3,2\times10-4$	$2.4\times10-4$	$8.2\times10-5$
C3	0	$2.5\times10-17$	$3.1\times10-8$	$4.5\times10-4$	$9.5\times10-4$	$1.1\times10-4$	$7.4\times10-4$	$2.7\times10-4$
C(solid)a	0	0	0	0	0.0009	0.0197	0.0945	0.414
CH	$3.1\times10-10$	$2.1\times10-9$	$2.1\times10-6$	$4.5\times10-5$	$6.1\times10-5$	$5.8\times10-5$	$4.9\times10-5$	$2.8\times10-5$
C2H2	$1.2\times10-13$	$9\times10-12$	$1.6\times10-5$	$9\times10-3$	0.025	0.0226	0.0234	0.0257
CO	0.50	0.58	0.61	0.60	0.60	0.59	0.57	0.47
CO2	0.49	0.011	$1.0\times10-5$	$4.3\times10-7$	$2.7\times10-7$	$2.7\times10-7$	$2.6\times10-7$	$2.1\times10-7$
H2	0.092	0.17	0.21	0.22	0.22	0.23	0.25	0.37
H	0.15	0.19	0.18	0.17	0.16	0.16	0.15	0.14
H2 O	0.075	0.027	$2.8\times10-5$	$1.2\times10-6$	$8.0\times10-7$	$8.3\times10-7$	$9.3\times10-7$	$1.3\times10-6$
OH	0.059	0.013	$1.1\times10-5$	$4.3\times10-7$	$2.5\times10-7$	$2.5\times10-7$	$2.4\times10-7$	$1.9\times10-7$

aThe solid carbon is expressed as moles of carbon per mole of gaseous products. (After Gaydon and Wolfhard, 1979).

the type of reactor do not greatly affect the ratio [3,4].

Calcote [5] compared the thermodynamic or equilibrium critical equivalence ratios with the experimental values for soot formation in the case of acetylene, benzene and *n*-hexane flames and observed larger ratios in the case of benzene and *n*-hexane. This indicates that benzene and *n*-hexane have a larger tendency to produce soot compared to acetylene. This has been attributed to the higher temperature of acetylene flames as the increase in flame temperature generally reduces tendency to produce soot [5].

Mass spectrometric analysis of the samples drawn from different flames through a probe before and after soot formation indicates the presence of a large number of molecular compounds, radicals and ions [4,5,7-13]. Simple species and free radicals such as C_2, CH, C_2H, CHO, OH, ON, CO, CO_2, H_2O [1417] and small hydrocarbons such as CH_4, C_2H_4, C_3H_4, C_4H_4, C_4H_2, C_4H_3 [18,19], polycyclic aromatic hydrocarbons [20] with molecular weights upto 300 amu or more and some with up to 21 rings [21], and conjugated species such as 1,3-butadiene [22], or vinyl acetylene [23] have been identified. Polycyclic aromatic hydrocarbons (PAH) ranging from benzene to coronene have been identified more commonly. The larger the polycondensed species, the more stable they are and thus less likely to be converted into soot particles. In addition to these PAH, ions varying from H+ upwards such as $C_{13}H_9^+$ $C_{17}H_{11}^+$ and $C_{19}H_{11}^+$ have been identified [1]. Thus many of these different molecular compounds, radicals or ions with molecular mass intermediate between a small ion (10100 amu) and soot particle (1,000,000 amu) could be precursors for the inception of soot particles. It may, however, be mentioned that the
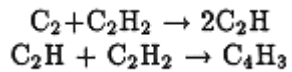
presence of a particular species is not a sufficient proof that it is involved in soot formation. A species may be present because it is not reactive.
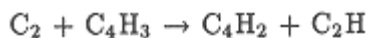
2.1.1. Nucleation or Soot Particle Inception

Several different theories have been proposed for the mechanism of soot particle inception and many of those have been extensively reviewed [2426]. Thus a detailed discussion of all the view points is not essential. In this chapter only more accepted points of view will be discussed although a brief mention may be made of the classical approaches as well.
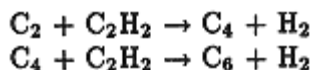
2.1.2. C2 Condensation Theory

According to this view point the fuel is dissociated into C2 or C3 species which polymerise to give solid carbon [18,19,24,27,28,29]. Palmer and Cullis [24] have suggested the following mechanism for the formation of polyacetylene by C2 initiation,

$$C_2 + C_2H_2 \rightarrow 2C_2H$$
$$C_2H + C_2H_2 \rightarrow C_4H_3$$

$$C_2 + C_4H_3 \rightarrow C_4H_2 + C_2H$$

while Gaydon and Fairbain [30] suggested the following reaction scheme for the formation of solid carbon

$$C_2 + C_2H_2 \rightarrow C_4 + H_2$$
$$C_4 + C_2H_2 \rightarrow C_6 + H_2$$
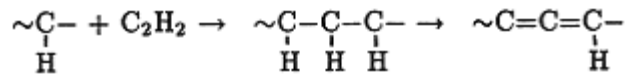
However, there are several shortcomings of the above mechanism. For example, if solid carbon results from the condensation of C_2 radicals, then the cynogen-oxygen (C_2N_2-O_2) flame which contains large amounts of C_2 should be expected to deposit soot but it does not [31]. Furthermore the solid material obtained from C_2 condensation should be pure carbon while soot always has a certain amount of hydrogen. The view that soot may be obtained by the condensation of C_3 never received any support. Thus although the condensation of C_2 can deposit some solid carbon, it appears that this process could only be important in very hot mixed flames.

2.1.3. The Acetylene Theory

As acetylene is formed in all rich premixed hydrocarbon flames and as it is also formed in a large number of pyrolysis reactions under a wide range of conditions, it was suggested by Berthelot [32] and Abadzheh et al [33] that acetylene is the main intermediate in the formation of solid carbon. Porter [34,35], during his flash photolysis studies using ketene and some other molecules, observed that considerable amounts of acetylene were formed and there was deposition of soot but there was no formation of either C_2 or benzene. He suggested that acetylene is the essential building block in soot formation and that the soot was formed by

the simultaneous polymerization and dehydrogenation of acetylene and gave the following mechanism

$$\sim\!\underset{\underset{H}{|}}{C}\!- \;+\; C_2H_2 \;\rightarrow\; \sim\!\underset{\underset{H}{|}}{C}\!-\!\underset{\underset{H}{|}}{C}\!-\!\underset{\underset{H}{|}}{C}\!- \;\rightarrow\; \sim\!C\!=\!C\!=\!\underset{\underset{H}{|}}{C}\!-$$

Cullis and Coworkers [3640], however, are of the view that the actual soot formation mechanism is not as simple as suggested by Porter [34,35]. For example, on a C/O ratio basis, premixed acetylene-oxygen flames do not soot nearly as readily as the flames from many other fuels. Ferguson [41], on the basis of his tracer studies using propane with 13C labelled in the 2 position, observed that the deposited carbon was not obtained directly from 12C or 13C but that 13C was distributed randomly in the soot.

The acetylene theory also does not explain the remarkable ease by which carbon is formed from benzene or from certain unsaturated hydrocarbons such as diacetylene or butadiene [42]. According to Cole and Minkoff [42,43], the strong tendency of benzene to form carbon is certainly due to the presence of diacetylene while Ray and Long [44] as well as Thomas [45] were convinced that butadiene is an important intermediate in the formation of carbon.

It appears that the role of acetylene, as intermediate in soot formation, is not as important as indicated by some of the proponents of the acetylene theory.

2.1.4. The Polyacetylene Theory

This theory is an extension of the acetylene theory and was proposed by Bonne, Homann and Wagner [14,17,46,47]. It is based on their work on the study of intermediates from premixed flat flames at reduced pressure for mixtures of fuels of C_2H_2 or C_2H_4 or C_6H_6 or C_2H_5OH with oxygen. Mass spectrometric analysis of the flames for various mixture compositions showed that the polyacetylene formed in the reaction zone play an important role in the formation and growth of the soot particles. The concentration of the polyacetylene goes through a maximum early in the reaction zone and reaches a constant final value in the burnt gas (Fig. 3).

The carbon paticales become detectable (~4 nm) a short distance behind the oxidation zone. In the region where the polyacetylene concentration decreases, the size of the particles increases by agglomeration of small particles and by addition of higher polyacetylenes and polyacetylene radicals. Consequently the number density of carbon particles goes down. Finally a stage is reached where the particle diameter, particle number and the total amount of carbon formed attain a constant value, although the concentration of acetylene and of polyacetylene is comparatively high. Apparently the production and disappearance of acetylene and specially of its homologues is strongly related to the process of carbon formation. These workers have suggested the following mechanism for the formation of polyacetylenes:
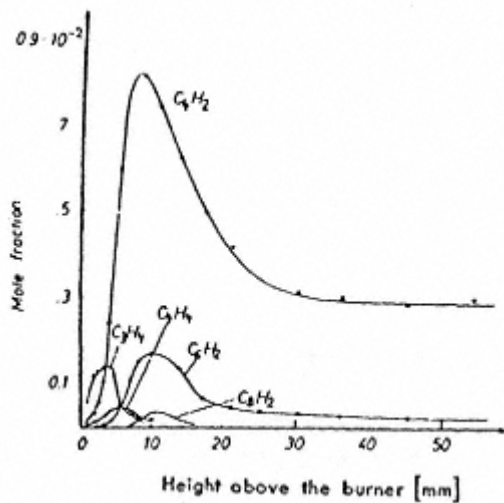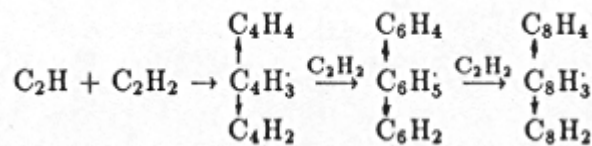
Fig. 3.
Concentration profiles in a flat
acetylene-oxygen flame (C2H2:O2=0.95)
at 20 mm Hg pressure and unburnt gas
flow density 50 cm/sec.

$$C_2H + C_2H_2 \rightarrow \begin{matrix} C_4H_4 \\ \uparrow \\ C_4H_3 \\ \downarrow \\ C_4H_2 \end{matrix} \xrightarrow{C_2H_2} \begin{matrix} C_6H_4 \\ \uparrow \\ C_6H_5 \\ \downarrow \\ C_6H_2 \end{matrix} \xrightarrow{C_2H_2} \begin{matrix} C_8H_4 \\ \uparrow \\ C_8H_3 \\ \downarrow \\ C_8H_2 \end{matrix}$$

The polyacetylenes attain a steady state value and are apparently in equilibrium with acetylene and hydrogen. These workers also observed the formation of polycyclic aromatic hydrocarbons (PAHs) which are formed later than polyacetylenes. But their concentration continues to increase down the flame even after the rate of carbon particle formation has fallen to zero [17,44]. Several other workers [4649] have observed that the concentrations of these PAHs do not increase down the flame but that they peak within the flame for premixed flames of acetylene [4649], ethene [46], butadiene [49] and benzene [50]. This has been attributed by Hirschler as due to the fact that individual concentrations of PAHs increase since these hydrocarbons continue to add carbon [11,50].

It may, however, be mentioned that these processes alone may not lead to soot formation since soot does not contain giant linear molecules [16,42,44,51] and polyacetylenes are rigid molecules which do not cyclise readily or sufficiently fast.

2.2. Soot Formation Involving Ions

All flames contain ions but their concentration is usually greater than that of soot particles but very much less than that of polyacetylenes and radicals. As ion-molecule interactions are usually faster than the molecule-molecule or radical-molecule interactions, it is possible that the ions may play an important role in soot formation [5,10,5056]. According to Hirschler [1], the most

dominant ion in flames often is $C_3H_3^+$ which is produced by the reaction

$$CH^{\cdot} + C_2H_2 \rightarrow C_3H_3^+ + e^-$$

At the critical equivalent ratio for soot formation, the concentration of this ion $C_3H_3^+$ has been found to decrease rapidly (Fig. 4) resulting in the formation of bigger ions such as $C_5H_3^+$, $C_7H_5^+$, $C_9H_5^+$, $C_4H_3^+$, $C_6H_3^+$, $C_{13}H_9^+$, $C_{19}H_{11}^+$, etc., by reaction with acetylene or polyacetylenes although the concentration of $C_{13}H_9^+$ and $C_{19}H_{11}^+$ have been found to be larger. Mass spectrometric studies have shown that these ions rearrange very rapidly into more stable polynuclear or aromatic structures (Fig. 5) which are the precursors for soot formation. These reactions continue to produce larger and larger ions with the increasing C/H ratio. As these ions and neutral molecules grow in size, their properties gradually approach those of particles rather than molecules, the transition occurring around 104 amu and diameters of about 3 nm. As these ions are formed by chemiionisation processes in the flame front itself and since the concentration decreases in the burnt gas as a
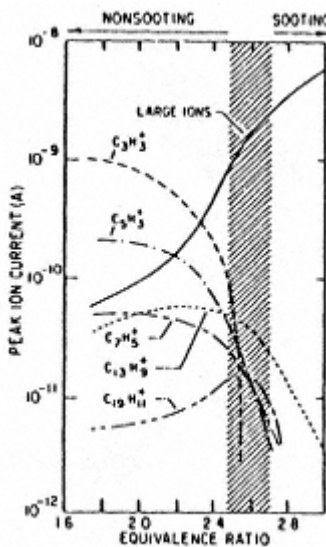
Fig. 4.
Effect of equivalence ratio
on peak ion currents for
2.0 kPa acetylene-oxygen
flames. The shaded area
indicates the minimum
equivalence ratio for
soot formation
(from ref. [5]).

result of the recombination reactions, the rate of soot formation will also fall.

Bertrand and Delfau [57] have observed more recently that at a low rate of thermal ionisation, the presence or absence of an electric field made no difference to the amount of soot formed. This indicates that the ions are a result of the thermal ionisation of the larger hydrocarbon molecules with low ionisation potentials. Thus an ionic soot nucleation is of much less importance than a purely radical mechanism. However, further work by Calcote [58] has

shown that the decay in the total ion concentration occurs simultaneously with the increase in the soot concentration, which is consistent with the view that neutral soot particles are produced by ion combination. However, this aspect can be resolved only by calculating rates of formation of ions from neutral species and the rate of formation of soot particles rather than concentrations, and both measurements must be made in the same flame.
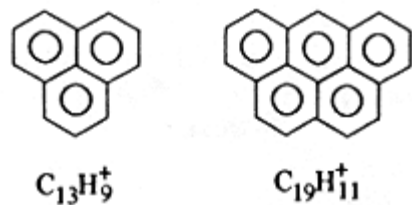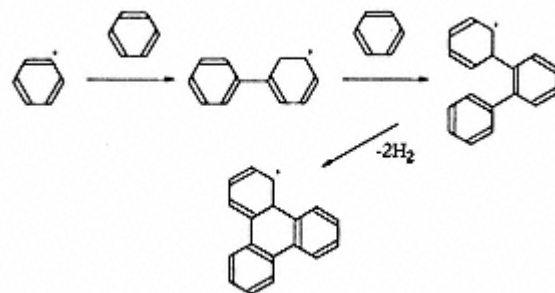
Fig. 5.
Structure of two abundant
hydrocarbon ions, masses 165
and 239.

Hayhurst and Jones [13] have suggested an intermediate mechanism according to which the ionic nucleation is probably accompanied by the formation of neutral PAHs until these larger fragments can ionize forming heavy charged particles. This will result in very fast molecule-ion interactions which can explain the very rapid rate of formation of soot.

2.2.1. The Polyaromatisation Theory
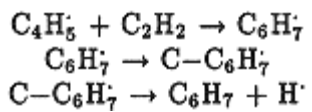
All sooting flames contain aromatic hydrocarbons; consequently it has been strongly felt that the condensation of these aromatic species may be an important route to the formation of soot in flames [4,1417,21,24,4650]. One such scheme given by Palmer and Cullis [24] is reproduced below:

Polyaromatization scheme for carbon formation. Some possible condensation reactions involving phenyl radicals and benzene (after Palmer and Cullis, 1965, reprinted from ref. [24]).

Delfau and Vovelle [50] in their molecular beam and mass spectrometric studies of premixed acetylene-oxygen flames have shown that polyacetylenes are not very reactive in the zone where soot formation takes place. PAHs, on the other hand, are strongly

reactive at the boundary between the oxidation and the soot formation zones. This indicates that the PAHs play an important role in the formation of soot. This is not in disagreement with the polyacetylene theory because polyacetylenic structures eventually lead to polyaromatic structures by ring closure. Howard et al [11,52], during their studies of aliphatic fuel flames observed that 1,3 butadienyl radical $(C_4H_5^{\cdot})$ adds to acetylenic species forming aromatic compounds in aliphatic flames. These workers have given the following free radical mechanism for the reaction:

$$C_4H_5^{\cdot} + C_2H_2 \rightarrow C_6H_7^{\cdot}$$
$$C_6H_7^{\cdot} \rightarrow C\!-\!C_6H_7^{\cdot}$$
$$C\!-\!C_6H_7^{\cdot} \rightarrow C_6H_7 + H^{\cdot}$$
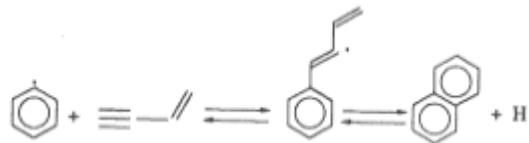
as suggested by Bittner [59]. Similar mechanisms have been proposed for the formation of toluene, phenyl acetylene and styrene. In the case of aromatic flames, the aromatic rings do not, generally, survive intact. Thus though some polyaromatic hydrocarbons may be formed in side-reactions, the soot itself probably comes mainly through non-aromatic intermediates [51].

Prado et al [60] determined intensity profiles of laser scattering and fluorescence along the axis of the flame for a methane diffusion flame and observed that the fluorescence signal given by PAH goes through a maximum and then decreases sharply at the inception of soot (Fig. 6).

Harris and Weiner [61], from absorption at a series of wavelengths between 488 and 1100 nu in the case of a premixed flat sooting $C_2H_4/O_2/Ar$ flame, found that in the intermediate post-inception zone the growth kinetics follow the profile of high molecular weight hydrocarbons (>500 amu). In a later study using the same flame these workers measured the fluorescence and scattered light from an ionized argon laser and observed that heavy aromatic precursors (mol. wt.~1000 amu) contribute significantly to the formation of soot and the formation ceases when they are depleted.

Bittner [59] measured the fluxes of different species and studied the kinetics and thermodynamics of species formation and consumption in fuel rich and sooting benzene/oxygen/argon premixed flame and observed that a part of the aromatics were destroyed to form unsaturated aliphatic species indicating that the formation of polyaromatic hydrocarbons proceeds through reactions between aromatics and acetylene species.

Formation of polyaromatics from
reaction between aromatic and
acetylene species.

Subsequently reactions involving the formation of benzyl type radicals by substitution of a methyl radical at the a position of naphthalene and by the release of a hydrogen atom may take place. C_2H_2 addition to this radical may lead to cyclisation.

In the case of nonaromatic carbonaceous materials, the formation of aromatic radicals is a rate determining step in the kinetics of PAH formation. Shock tube pyrolysis of acetylene-1,3-butadiene and benzene-ethylene flames [6064] has suggested a reaction sequence for the formation of the first aromatic ring, the molecular structure of the fuel influencing the growth process only in its early stages. These results agreed with those of Kent and Wagner
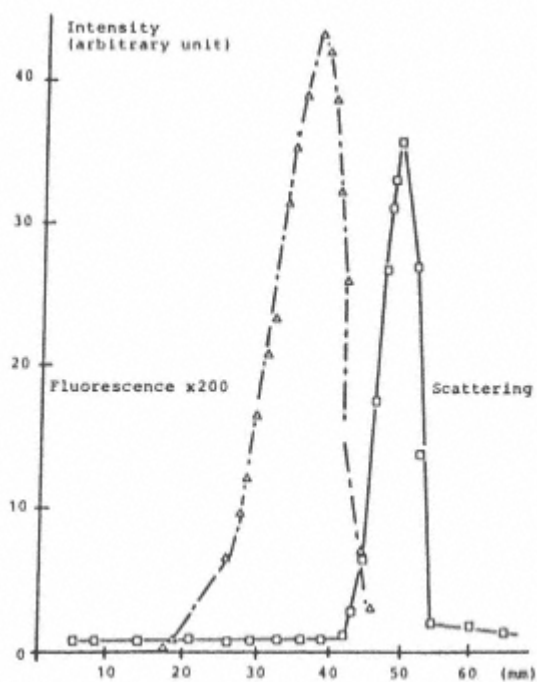
Fig. 6.
Axial profiles of intensities of scattering
and fluorescence at 90°C for a laminar
diffusion flame of methane
(from ref. [62]).

[65] and Gomej et al [66], who observed that for laminar diffusion flames the residence time in the initial region of the flame is one of the controlling factors for soot formation. Homann [67] also is of the view that soot is formed from polyaromatic hydrocarbons since these soot precursors appear as one or more groups of species which have their mass, size and structures and C/H ratio distributed over a certain range. However, the conversion of these soot precursors into soot will depend upon the burning conditions, the local composition and the temperature of the combustion flame.

Thus it is evident that the formation of soot takes place through

aromatic hydrocarbons present in all flames. These aromatic structures may lead to molecular growth resulting in the formation of PAH and soot formation through its ability to stabilize radicals formed from additions of aromatic radicals to unsaturated aliphatics such as acetylenic species. Accordingly, both aliphatic and unsaturated aliphatics would be important for growth processes. Indeed both types of species are present in flame zones where growth takes place. Gerhardt et al [86] have found that C_{60}^+ is indeed a dominant ion in a sooting flame, although it is not clear where it is because there is lot of hydrogen in soot. Kroto [87] has also indicated that the discovery that C_{60} appears to form spontaneously and this has particularly important implications for formation in combustion as well as for the formation of PAH.

In summarizing the above discussion of the different theories of soot formation it appears that each of the mechanism shows some shortcomings. Polyacetylene formation is very slow and presents difficulties with rearrangement to a polycyclic structure. Polycyclics have been rejected because they continue to increase in concentration even when the rate of soot formation has fallen to zero. Combination of free radicals which are decaying through the flame front with acetylene, polyacetylenes, or polycyclics may be the key to nucleation or soot inception mechanism but none of these various concepts have been developed to the point of being a final word. There are many difficulties in the formation of cyclic structures without extensive molecular rearrangement and hence large entropy changes. In case of ionic mechanism it has been suggested that ions were the result of soot formation and not the cause.

Thus much more is needed to be done because the difference in properties between the largest precursor and the first soot particle themselves is not very clear. Moreover, the processes leading to soot formation take place at high temperatures and at very high speeds (a few tenths of a microsecond). The observation of Lahaye there is no true nucleation so that there is no continuity between polyaromatic hydrocarbons and soot nuclei. Polyaromatic hydrocarbons grow in size during dehydrogenation and progressively develop the properties that characterise soot is worth consideration.

2.3. Aggregation of Soot Particles (Particle Growth)

In all systems, soot is constituted by large number of particles which collide to produce larger spherical particles which further

agglomerate into final aggregates of soot. The final number density of agglomerates is much the same, typically 10_{16}/m3 irrespective of the conditions of the pyrolysis or combustion.

Whatever be the mechanism of the nucleation process, the particle growth involves two processes, namely deposition of carbonaceous material on the particle surface and coalescence of small particles into larger ones [25]. It has been suggested [68] that this coalescence takes place at certain growth centers present in individual carbon particles. Wersborg and Howard [69,70] made theoretical calculations of particle growth by taking into account deposition on the particle surface and of coalescence. According to Wersborg [69], later restated by Lahaye [62], during a sticking collision process, the rate of change of particle number density, N with time t can be expressed as

$$\frac{dN}{dt} = \dot{N}_n + \dot{N}_c$$

(1)

where $\dot{N}_n$ is the nucleation rate and $\dot{N}_c$ is the coagulation rate. The nucleation rate is important only in the earlier stages of the process and is taken over

very rapidly by the coagulation rate. The rate of increase of total particle volume V_p is given by

$$\frac{dV_p}{dt} = \frac{4}{3}\pi a_0^3 N_n^{\cdot} + 4\pi \sum_i n_i a_i^2 S_i^*$$ (2)

in which a_0 is the initial particle radius and S_i^* is the surface growth rate of particles of radius a_i and concentration $n_i \cdot S_i^*$ here includes the contribution of surface reactions and the deposition of particles of radius less than a_0. The summation accounts for the particle size distribution and possible dependence of surface reactions upon particle size.

The coagulation rate constants were experimentally obtained by assuming a monodispesse system and expressing the coagulation rate in the form of Smoluchovski's [71] equation

$$N_c^{\cdot} = \frac{K}{2}n^2$$ (3)

combination of equations (1) and (2) gives

$$\frac{d(1/n)}{dt} = \frac{K}{2} - \frac{N_n^{\cdot}}{n^2}$$ (4)

which was verified for a flat premixed acetylene-oxygen flame and a fairly good agreement was observed [25].

Considering the system to be in the free molecular region (Knudson number>10), it has been shown by Lahaye [62], that at constant volume fraction and temperature

$$N = N_0(1 + 9.03 \cdot 10^{-13} N_0^{5/6} T^{1/2} f_v^{1/6} t)^{-5/6} \quad \text{(SI Units)}$$ (SI Units) (5)

where N_0 is the initial particle number density, N is the particle number density at time t, T is the temperature in degree Kelvin and f_V is the volume fraction of the particles (which is volume of particles per unit volume and hence a nondimensional quantity).

For large enough volumes of N_0 (typically $N_0 > 10_{18}/m_3$), this equation can be reduced to

$$N = 2.84 \cdot 10^{14}(T^{1/2} f_v^{1/6} t)^{-6/5} \quad (6)$$

This theoretical expression shows that the final number density N is independent of the initial particle number density N_0. Lahaye and coworkers [72,73] measured the particle number density in a premixed propane/oxygen flame using absorption/scattering of a laser beam. A plot of experimental and computed number densities versus height above the burner (H.A.B.) (Fig. 7) shows good agreement except near the end of the process where the number of the particles measured optically might be inaccurate due to the non-sphericity of the aggregates.
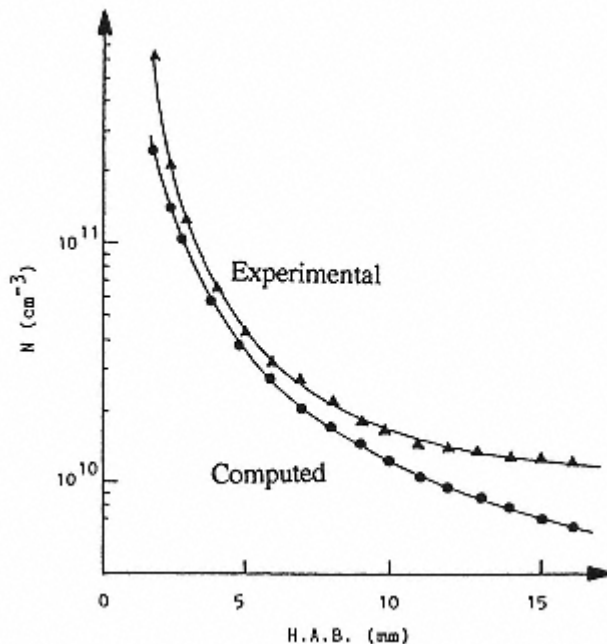
Fig. 7.
Experimental and computed number density of
agglomerates (N/cm3) (propane/oxygen
premixed flame, fuel equivalence ratio 2.5, cold
gas velocity 5.5cm/sec) (from ref. [62]).

2.4. Surface Growth

Inception of nucleation of soot particles is the most important process in soot formation. However, it is important to know that only 10% of the soot mass is produced during the inception process, while the remaining 90% of the total carbon yield comes as a result of the surface growth processes both for premixed and for diffusion flames [72,7480]. This surface growth corresponds to the attachment to, and incorporation in, existing particles of species smaller than the first observable soot particle. These species can be gaseous hydrocarbons or small nuclei. Subsequent to this formation and growth, the soot and mass usually decreases as a result of the

oxidation processes [77,81]. The rates of surface growth and the kinetics of formation of gaseous species in the flame have indicated that acetylene and not the PAH is the major hydrocarbon which is responsible for soot growth. The concentration of PAH is not high enough to made a significant contribution.

The increase in soot volume fraction fv has been described by the expression

$$\frac{d(f_v)}{dt} = K_E(f_v^* - f_v) \qquad (7)$$

where KE is a constant and f_v^* is an empirical value which can be identified

with a depletion reservoir for soot growth. Its value depends strongly upon the nature of the flame. Although KE and f_v^* have no clear kinetic meaning, the expression is convenient for modelling.

According to Harris and Weiner [7880], the increase in soot volume fraction fv can be described by the surface growth expression

$$\frac{d(f_v)}{dt} = K_s \cdot S \quad (8)$$

where S is the total soot surface area concentration and Ks is the specific rate constant which is first order with respect to the partial pressure of acetylene and given by

$$Ks = KC2H2 \cdot PC2H2 \quad (9)$$

$KC2H2$ decays with time as fv approaches an asymptotic value. Dash [82] introduced the decay term of soot surface reactivity of Haynes et al [83] in the above surface growth expression of Harris and Weiner and found that Wagner and Harris kinetic expressions were equivalent, provided $PC2H2$ and S do not vary very much in the region of final surface growth. The empirical rate constant KE is not a surface growth rate constant but rather the decay rate of the surface reactivity.

It has been mentioned earlier that surface growth represents about 90% of the total soot yield. In order to know whether this surface growth occurs in individual particles or on aggregates or on both, Lahaye [62] carried out phase contrast electron microscopy which visualizes carbon layers through interference patterns. A schematic of one such micrograph of a soot aggregate (Fig. 8) shows that the surface growth occurs on individual particles. The surface growth

of aggregates is responsible for the stability of soot aggregates as they are not stabilized by weak short distance forces but by a continuous carbon network.
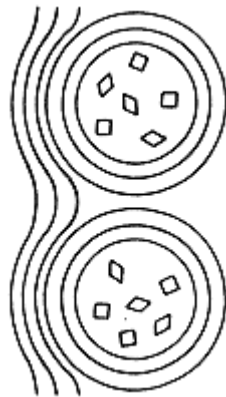
Fig. 8.
Schematic of phase contrast electron micrograph of soot aggregate (from ref. [62]).

2.5. Soot Oxidation

After its formation and growth, the soot concentration often decreases as a result of the oxidation processes. Whether the particles survive or are burnt depends on local flame conditions such as the temperature, the oxygen concentration, the flow rates and the fuel species (or fuel C/H and C/O ratios). Garo et al [84] observed that in a laminar methane diffusion flame, the oxidative destruction of soot had already begun before the aggregations had attained the maximum diameter.

In the soot producing zone both soot formation and its oxidation go side by side and it is difficult to decouple them. However, in the lean part of the flame only oxidation of the soot can take place and, therefore, it is easier to explain the processes involved. A large variety of species such as molecular and atomic oxygen or the hydroxyl radical (OH·) can oxidize soot particle. Neoh et al [85], using a two-stage burner system, and Lahaye [62], using a methane diffusion flame, have shown that OH· radical is responsible for soot oxidation. This was based on the calculations of the apparent collision efficiency (probability of oxidizing one carbon atom by collision between a soot particle and one OH· radical) of OH· radical and soot which was found to be quite high (0.10.3). The value agreed well with the other investigators. Thus Lahaye suggested that there is random oxidation of the entire surface of the soot particle. The oxidation front moves progressively towards the centre of the aggregate and a high weight loss of about 80% is required for the aggregate to collapse. In the case of molecular oxygen, the collision efficiency is much lower so that oxygen molecules preferentially attack soot particle defects, and penetrate

the aggregate. This results in the development of porosity which is followed by fractures causing a collapse of the aggregates for a low weight burn off (~10%).

A new family of carbon molecules known as fullerenes has been recently discovered. A general review about the work on fullerenes has been performed by Kroto, Allaf and Balm [88]. The fullerenes C_{60} and C_{70} were first detected in 1985 by Kroto, Heath, O'Brien, Curl and Smalley [89] in carbon vapor produced by laser evaporation of graphite. They were recently produced in larger quantities by vaporization of graphite with resistive heating under inert atmosphere [90]. In July 1991, Howard [91] showed that fullerenes can be synthesized in a premixed laminar flame of benzene and oxygen with argon diluent. The largest yield was 3 g of fullerenes C_{60} and C_{70} per kg of fuel carbon burnet.

A carbon vapor nucleation model was proposed by Zhang et al [92] and Kroto and Mckay [93] to explain the spontaneous creation of C_{60}. A modified form of this scheme was proposed to explain both the mechanism of fullerenes formation and the spheroidal nature of soot. During the soot formation by the spiral nucleation process, carbon networks grow, leading to embryos capable

of closing to form fullerenes as a by-product of soot formation [92,93]. These fullerenes, particularly C_{60} and its spherical closed cage, preclude further growth. On the contrary, incomplete closure of fullerenes would play a role in soot formation. This new scheme for the soot formation mechanism appears in good agreement with observations made on soot and its formation process. This view point is criticized by Frenklach and Ebert [94,95], who affirm that fullerenes have nothing to do with the soot formation process. Frenklach has modeled the growth of PAH in a flame environment and this model is also to predict the growth of closed curved carbon clusters. But the computed kinetics are not high enough compared to observed kinetics of soot formation.

Despite differences between the formation processes of fullerenes and soot, their comparison is useful for the understanding of these processes.

References

1. Hirschler, M. M., *J. Fire Sci,* 3, 380 (1985).

2. Street, J. and Thomas, S., *Fuel,* 34, 4 (1955).

3. Takahashi, F. and Glassman, I., *Combustion Sci. Technol.,* 37, 1 (1984).

4. Wagner, H. G., *17th Symposium (Int.) on Combustion,* The Combustion Inst., Pittsburgh, p. 3, 1979.

5. Calcote, H. F., *Combustion and Flame,* 42, 215 (1981).

6. Millikan, R. C., *J. Phys. chem.,* 66, 794 (1962).

7. Gaydon, A. G. and Wolfhard, H. G., *Flames, Their Structure,*

Radiation and Temperature, Chapman and Hall, London, (4th Edit), 1979.

8. Prado, G., Lee, M. L, Hites, R. A., Hoult, D. P. and Howard, J. B., *16th Symposium (Int) on Combustion,* The Combustion Inst., Pittsburgh, p. 649, 1977.

9. Delfau, J. L., Michaud, P. and Barassin, A., *Combustion Sci. Technol.,* 20, 165 (1979).

10. Olson, D. B. and Calcote, H. F., *18th Symposium (Int.) on Combustion,* The Combustion Inst., Pittsburgh, p. 453, 1981.

11. Bittner, J. D., Howard, J. B. and Palmer, H. B., in *Soot in Combustion Systems and Its Toxic Properties,* p. 95, J. Lahaye and G. Prado eds, Plenum, New York, 1983.

12. Homann, K. H., *12th Symposium (Int.) on Combustion,* The Combustion Inst., Pittsburgh, p. 857, 1985.

13. Hayhurst, A. N. and Jones, H. R. N., *12th Symposium (Int.) on Combustion,* The Combustion Inst., Pittsburgh, p. 1121, 1985.

14. Bonne, U., Homann, K. H. and Wagner, H. G., *10th Symposium (Int.) on Combustion,* The Combustion Inst., Pittsburgh, p. 503, 1965.

15. Homann, K. H. and Wagner, H. G., *Bur. Bunsenger Phys. Chem.,* 69, 20 (1965).

16. Homann, K. H., *Combustion and Flame,* 11, 265 (1967).

17. Homann, K. H. and Wagner, H. G., *11th Symposium (Int.) on Combustion,* The Combustion Inst., Pittsburgh, p. 371, 1967.

18. Parker, W. G. and Wolfhard, H. G., *J. Chem. Soc.,* p. 2038 (1950).

19. Parker, W. G. and Wolfhard, H. G., *Fuel,* 35, 323 (1956).

20. Cullis, C. F., Read, I. A. and Trimm, D. L., *11th Symposium (Int.) on Combustion,* The Combustion Inst., Pittsburgh, p. 391, 1967.

21. Prado, G. and Howard, J. B., *Adv. Chem. Sci.,* 166, 153 (1978).

22. Glassman, I., 1980 Meeting, Eastern Section of the Combustion Inst., Princeton Univ., Princeton, N. J., Nov. 1214, 1980.

23. Bittner, J. D. and Howard, J. B., *18th Symposium (Int.) on Combustion,* The Combustion Inst., Pittsburgh, p. 1105, 1981.

24. Plamer, H. B. and Cullis, C. F., *Chemistry and Physics of Carbon,* P. L. Walker, Jr. ed., Marcel Dekker, New York, Vol. 1, p. 266, 1965.

25. Lahaye, J. and Prado, G., *Chemistry and Physics of Carbon,* P. L. Walker, Jr. and P. Thrower eds., Marcel Dekker, New York, Vol. 14, p. 168, 1978.

25a. Donnet, J. -B. and Voet, A., *Carbon Black,* Marcel Dekker, New York, 1976.

26. Lahaye, J. and Prado, G., in *Soot in Combustion Systems and Its Toxic Properties,* J. Lahaye and G. Prado eds., Plenum, New

York, p. 95, 1983.

27. Smith, S. R., *Proc. Roy. Soc., Landon,* A174, 122 (1940).

28. Parker, W. G. and Wolfhard, H. G., *4th Symp. (Int.) on Combustion,* Williams and wilkins Baltimore, p. 420, 1953.

29. Jensen, D. E., *Proc. Roy. Soc., London,* A338, 375 (1974).

30. Gaydon, A. G. and Fairbain, R., *5th Symp. (Int.) on Combustion,* The Combustion Institute, Pittsburgh, p. 324, 1954.

31. Jessen P. F. and Gaydon A. G., *12th Symp. (Int.) on Combustion,* The Combustion Inst., Pittsbergh, p. 481, 1969.

32. Berthelot, M. C. R., *Acad. Sci., Paris,* 62, 947 (1866).

33. Abadzheh, S. S., Tesner, P. A. and Shevchuk, V. V., *Gozov. Prom.,* 14, 36 (1969).

34. Porter, G., *4th Combustion Symp.,* Cambridge Mass., p. 248, 1953.

35. Porter, G., *Combustion Researches and Reviews,* Butterwouth, London, p. 108, 1955.

36. Cullis, C. F., in *Petroleum Derived Carbons,* p. 348, M. L. Deviney and T. M. O'Grady eds., Am. Chem. Soc., Washington, 1976.

37. Cullis, C. F. and Franklin, N. H. *Proc. Roy. Soc., London,* A280, 139 (1964).

38. Cullis, C. F., Read, I. A. and Trimm, D. L., *11th Symp. (Int.) on Combustion,* The Combustion Inst., Pittsburgh, p. 391, 1967.

39. Cullis, C. F. and Read, I. A., *Trans. Faraday Soc.,* 66, 920 (1970).

40. Cullis, C. F. and Hirschler, M. M., *The Combustion of Organic Polymers,* Oxford University Press, Oxford, 1981.

41. Ferguson, R. E., *Combustion and Flame,* 1, 431 (1957).

42. Cole, D. J. and Minkoff, G. J., *Fuel,* 35, 135 (1956).

43. Cole, D. J. and Minkoff, G. J., *Proc. Roy. Soc., London,* A239, 280 (1957).

44. Ray, S. K. and Long, R., *Combustion and Flame,* 8, 139 (1964.)

45. Thomas, A., *Combustion and Flame,* 6, 46 (1962).

46. Wagner, H. G., *Proc. Roy. Soc., London,* A370, 141 (1968).

47. Wagner, H. G., in *Particulate Formation During Combustion,* D. C. Siegela, and G. W. Smitter eds., Plenum, New York, p. 1, 1981.

48. Crittendon, B. D. and Long, R., *Combustion and Flame,* 20, 359 (1973).

49. Bittner, J. D. and Howard, J. B. in *Particulate Formation During Combustion,* D. C. Siegela and G. W. Smith eds., Plenum, New York, p. 98, 1981.

50. Delfau, J. L. and Vovelle, C., *Combustion Sci. Technol.,* 41, 1 (1984).

51. Cole, J. A., Bittner, J. D., Longwell, J. P. and Howard, J. B., *Combustion and Flame,* 56, 51 (1984).

52. Bittner, J. D. and Howard, J. B., *18th Symp. (Int.) on Combustion,* The Combustion Inst., Pittsburgh, p. 1105, 1981.

53. Lahaye J., Prado, G. and Donnet, J. B., *Carbon,* 12, 27 (1974).

54. Lahaye, J. and Prado, G., in *Petroleum Derived Carbons,* M. L. Deviney and T. M. O'Grady eds., ACS Symp. Seriers, 21, 335, 1976.

55. Thomas, A., *12th Symp. (Int.) on Combustion,* The Combustion Inst., Pittsburgh, p. 511, 1965.

56. Weinberg, F. J., *Proc. Roy. Soc., London,* A307, 195 (1968).

57. Bertrand, C. and Delfau J. L., *Combustion Sci. Technol.,* 44, 29 (1985).

58. Keil, D. G., Gill, R. J., Olson, D. B. and Calcote, H. F., *20th Symp. (Int.) on Combustion,* The Combustion Inst., Pittsburgh, p. 1129, 1985.

59. Bittner, J. D., D. Sc. Thesis, Dept. of Chem. Engg., Massachussetts Inst. Technol., Cambridge, MA., 1981.

60. Prado, G., Garo, A., Koofn, A. and Sarofim, A., *20th Symp. (Int.) on Combustion,* The Combustion Inst., Pittsburgh, p. 989, 1984.

61. Harris, S. J. and Weiner, A. M., *22nd Symp. (Int.) on Combustion,* The Combustion Inst., Pittsburgh, p. 333, 1989.

62. Lahaye, J., *Polymer Degradation and Stability,* 30, 111 (1990).

63. Frenklach, M., Clary, D. W., Gardiner, Jr, W. C. and Stein, S. E., *20th Symp. (Int.) on Combustion,* The Combustion Inst., Pittsburgh, p.

887, 1984.

64. Frenklach, M., Clary, D. W., Gardiner Jr, W. C. and Stein, S. E., *21st Symp. (Int.) on Combustion,* The Combustion Inst., Pittsburgh, p. 1067, 1986.

65. Kent, J. H. and Wagner, H. G., *Combust. Sci. Technol.,* 41, 245 (1984).

66. Gomej, A., Littman, M. G. and Glassman, I., Joint Central Wester States Sections Meeting of the Combustion Inst., San Antonio, Texas, 1985.

67. Homann, K. H., Some Remarks on Precursors Formation, Guttingen/Reinhausen (Germany), March 2930, 1989.

68. Gordon, A. S., Smith, S. R. and McNesby, J. R., *7th Symp. (Int.) on Combustion,* London Oxford. p. 317, 1959.

69. Wersborg, B. L., Howard, J. B. and Williams, G. C., *14th Symp. (Int.) on Combustion,* The Combustion Inst., Pittsburgh, p. 929, 1973.

70. Ball, R. J. and Howard, J. B., *13th Symp. (Int.) on Combustion,* The Combustion Inst., Pittsburgh, p. 353, 1971.

71. Smoluchovski, Z., *Phys. Chem.,* 92, 129 (1917).

72. Prado, G., Jagoda, I. J., Neoh, K. and Lahaye, J., *13th Symp. (Int.) on Combustion,* The Combustion Inst., Pittsburgh, p. 1127, 1981.

73. Prado, G., Lahaye, J. and Haynes, G. H., in *Soot in Combustion Systems and Its Toxic Properties,* p. 145, J. Lahaye and G. Prado

eds., Plenum, New York, 1983.

74. Tanner, S. D., Goodings, S. M. and Bohme, D. K., *Can. J. Chem.,* 59, 760 (1981)

75. Beretta, F., Cavaliere, A., Ciajole, A., D'Alessio, A., Langella, C. and Dilorenzo, A., *18th Symp. (Int.) on Combustion,* The Combustion Inst., Pittsburgh, p. 1091, 1981.

76. Kent, J. H., Jander, H. and Wagner, H. G., *18th Symp. (Int.) on Combustion,* The Combustion Inst., Pittsburgh, p. 1117, 1981.

77. Santoro, R. J., Semerjian, H. C. and Dubbins, R. A., *Combust. Flame,* 51, 203 (1983).

78. Harris, S. J. and Weiner, A. M., *Combust. Sci. Technol.,* 32, 15 (1983).

79. Harris, S. J. and Weiner, A. M., *Combust. Sci. Technol.,* 32, 26 (1983).

80. Harris, S. J. and Weiner, A. M., *Combust. Sci. Technol.,* 38, 75 (1984).

81. Glassman, I. and Yaccarino, P., *Combust. Sci. Technol.,* 24, 107 (1980).

82. Dash, C. J., *Combustion and Flame,* 61, 219 (1985).

83. Haynes, B. S. and Wagner, H. G., *J. Phys. Chem.,* Neue Folge, 133, 201 (1983).

84. Garo, A., Lahaye, J. and Prado, G., *21st Symp. (Int.) on Combu-*

stion, The Combustion Inst., Pittsburgh, p. 1023, 1986.

85. Neoh, K. G., Howard, J. B. and Sarofrin, A. F., *20th Symp. (Int.) on Combustion,* The Combustion Inst., Pittsburgh, p. 951, 1984.

86. Gerhardt, P. H., Loffer, S. and Homann, K. H., *Chem. Phys. Lett.,* 137, 306 (1987).

87. Kroto, H., *Science,* 242, 1139 (1988).

88. Kroto, H. W., Allaf, A. W. and Balm, S. C., *Chemical Reviews,* 91, 1213 1991.

89. Kroto, H. W., Heath, J. R., O'Brien, S. C., Curl, R. F. and Smalley, R. E., *Nature (London),* 318, 162 (1985).

90. Kratschmer, W., Lamb, L. D., Postiropoulos, K., Huffman, D. R., *Nature (London),* 347, 354 (1990).

91. Howard, J. B., McKinnon, J. T., Makarovsky, Y., Lafleur, A. L. and Johnson, M. E., *Nature (London),* 352, 139 (1991).

92. Zhang, Q. L., O'Brien, S. C., Heath, J. R., Liu, Y., Curl, R. F., Kroto, H. W. and Smalley, R. E., *J. Phys. Chem.,* 90, 525 (1986).

93. Kroto, H. W. and HcKey, K. G., *Nature (London),* 331, 1988.

94. Frenklach, M. and Eberrt, L. B., *J. Phys. Chem.,* 92, 561 (1988).

95. Ebert, L. B., *Science,* 247, 1968 (1990).

Chapter 3
Microstructure, Morphology And General Physical Properties

William M. Hess and Charles R. Herd
Columbian Chemicals Company,
Swartz, Louisiana, U. S. A.

The physical properties of carbon black have received the attention of a large number of authors over the past 70 years or more. This is not unexpected since the reinforcement of elastomers, the protection of plastics from ultraviolet degradation, and the blackness and tint properties of paint and ink coatings are all highly dependent on particle size and other aspects of carbon black morphology and microstructure. All of these properties have been the subject of extensive reviews, the most notable being included in the previous book on carbon black by Donnet and Voet [1]. Other comprehensive reviews which include pertinent information on carbon black physical properties are those by Dannenberg [2] and Medalia and Rivin [3] on general properties; Kraus [4] and Gessler, Hess and Medalia [5] on properties relating to elastomer reinforcement; Heckman [6], and Ban and Hess [7] on microstructure; Studebaker [8] and Riven [9] on surface properties; Schubert, Ford and Lyon [10] on analytical testing; and Janzen [11] on physiochemical characterization. Each of these reviews will provide the reader with additional information in the specific areas cited.

3.1. Background

Early attempts to characterize the morphological properties of carbon black were largely limited to optical microscopy studies. During the 1920's a number of researchers employed ultramicroscopy techniques to determine the particle size of the channel (gas) blacks which were available at that time [1217]. The ultramicroscope provided better resolution than conventional optical microscopes through the scattering of light by the carbon black particles in dark field. However, the early estimates of carbon black particle size varied widely from about 15 to 200 nm and no reliable information was obtained on the degree of aggregation and shape of carbon black aggregates.

The first transmission electron microscope was developed by Knoll and Ruska [18,19] in 1932. This invention revolutionized the field of microscopy and later had a particular impact on characterizing carbon black morphology and microstructure.

Prebus and Hillier [20] constructed a 2-stage electron microscope in 1938 which was employed to take the first electron micrographs of a commercial carbon black [21]. These studies led to the first actual measurements on particle diameter which was found to average in the range of 26 to 29 nm for an EPC channel black.

Other early electron micrographs of carbon black were taken by Von Ardenne and Beischer [22]. They showed differences in particle size between a channel black and a lampblack and also were the first to show electron micrographs of carbon black in rubber. The first comprehensive studies on particle size variations among different commercial carbon blacks were carried out by W.

A. Ladd in the early 1940's [23]. Ladd and Wiegand [24] also introduced the concept of structure for carbon blacks, referring to the tendency of the particles to be linked together in chains or clusters. Electron microscope measurements on the length/width ratio of carbon black aggregates were first reported by Cohan and Watson in 1951 [25]. More commonly, the structure of carbon black has been measured as a function of vehicle absorption. Sweitzer and Goodrich [26] developed the first oil absorption test in 1944. This type of analysis measures the amount of oil required to change a unit weight of carbon black from a crumbly powder to a cohesive plastic mass. The early test, called stiff paste oil absorption, was carried out manually by spatulating the oil/black mixture as the oil was added dropwise until the end point (solid ball of black and oil) was reached.

The first significant study on carbon black microstructure was carried out by Warren in 1934 [27] using X-ray diffraction. His work indicated that carbon black was composed of small crystallites which were made up of parallel graphitic layers with a spacing of approximately 0.350 to 0.380 nm in contrast to graphite at 0.335 nm. He concluded that carbon black represented a structure form that was intermediate between graphite and a truly

amorphous material.

3.2. Microstructure

Because of early resolution limitations in the field of electron microscopy, detailed knowledge of carbon black microstructure was not obtained until well after the compilation of very comprehensive information pertaining to particle size and structure. Nevertheless, microstructure will be discussed first because of its importance in accurately defining the morphological properties of carbon black.

3.2.1. X-ray Diffraction

Based on X-ray diffraction studies, Warren [27] proposed that carbon blacks were composed of small layers with the same atomic positions as graphite within the layers. Warren [28] further developed a theory for the diffraction of X-rays by random layer lattices which was subsequently applied to a detailed study of different carbon blacks [29]. These studies showed that the X-ray diffraction patterns for carbon blacks are composed of *(001)* three-dimensional and *(hk)* two-dimensional reflections, a type of structure that was defined as turbostratic, i.e., the layers are parallel but rotated around the *c*-axis. The positions of the *(001)* reflections also indicated that the layers were spaced further apart than in graphite. Crystallite size along the *c*-axis, *Lc,* was determined from the *(002)* and *(004)* reflections, using the Scherrer equation [30]. The size of the layer planes, *La,* was derived from the *(hk)* reflections, assuming a 60° rhombus. *Lc* represents a measure of the average stacking height of the layers and *La* is indicative of their average diameter.

Others who contributed significantly to the study of carbon blacks by X-ray diffraction were Franklin [3133], Alexander et al [34,35], Austin [36], Mering et al [3739] and Ergun et al [4042]. The work of Franklin was particularly important in that she showed that the various types of carbon differ only in the magnitude of their variation from graphite rather than representing different crystallographic structures. Franklin further separated carbons into graphitizing and non-graphitizing, depending on whether they achieved the crystalline order of graphite when heated at very high temperatures (~3000°C).

X-ray diffraction data for a range of different commercial carbon blacks are listed in Table 1, as determined by Austin [36]. These represent carbon blacks made by the acetylene, thermal, channel, and oil furnace processes, the latter being in greatest number. Listed in this table are the L_a and L_c values, the calculated percentages of unorganized carbon and carbon existing in parallel or single planes, and the probabilities for 3 or 4 layer plane stacking. For the rubber grade carbon blacks designated with an ASTM N Number [43], there is a significant variation in particle size. The first digit in the number represents the particle size range which increases as the numbers become

Table 1. Structural Properties of Carbon Blacks as Determined by X-Ray Diffraction

Carbon black	ASTM No.	Dimensions, Å			Carbon, %			Probability of number of parallel layers	
		La		*Lc*					
		(10)	(11)	(002)	random	parallel layers	single layers	3	4
Acetylene	-	26	26	25	4	96	0		-a
Vulcan SC	N294	20	16	10.6	8	90	2	1.0	0
Sterling SO	N550	16	14	11.3	11	83	5	0.8	0.2
Philblack A	N550	20	15	12.4	5	70	25	0.5	0.5
Kosmos 50	N550	18	14	12.4	11	79	10	0.5	0.5
Philblack O	N330	20	16	11.7	15	83	2	0.7	0.3
Philblack I	N220	19	16	11.3	16	80	4	0.8	0.2
Philblack E	N110	17	16	11.3	15	79	6	0.8	0.2
Sterling V	N660	20	15	12.4	13	74	13	0.5	0.5
Statex B	N440	20	16	11.7	5	89	6	0.7	0.3
Kosmos 40	N601	22	22	13.4	7	63	30	0.2	0.8
Pelletex	N770	20	16	13.4	8	83	9	0.2	0.8
Thermax	N990	24	17	13.8	4	90	6	0.1	0.9
P-33	N880	28	19	13.4	8	82	10	0.2	0.8
Spheron 3	-	16	16	11.2	9	67	24	0.9	0.1
Spheron 6	S301	20	16	11.7	6	80	14	0.7	0.3

| Spheron 9 | S300 | 16 | 14 | 11.7 | 15 | 81 | 4 | 0.7 | 0.3 |
| Carbolac[b] | HCC | 16 | 15 | 11.2 | 26 | 74 | 0 | 0.85 | 0.15 |

a Acetylene black has between 6 and 7 parallel layers.
b High color channel.
From ref [36].
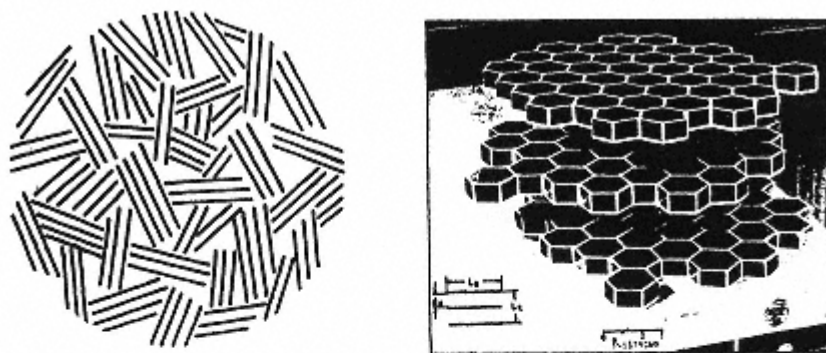
higher. Overall, it can be seen that L_c also increases in the direction of increasing particle size, a trend that appears related to the greater radius of curvature, as well as longer residence times in the reactor. There is also a tendency toward a reduction in unorganized carbon for the larger particle size blacks, along with a greater probability for 4 parallel planes.

Acetylene carbon black exhibits notably higher L_c values relative to all of the other carbons, indicating a much higher level of crystalline development. This is to be expected since acetylene black formation is exothermic in nature [44].

The differences in the values of L_a from the *(10)* and *(11)* reflections were attributed by Austin [36] to be related to lattice imperfections or to a distortion of the graphitic layers by impurities. It is apparent that L_a is less sensitive to the particle size and other variations among the different carbon
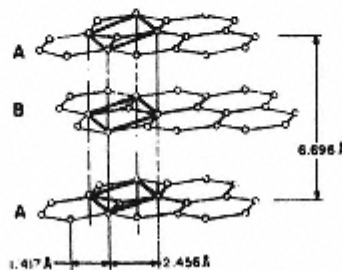
black grades, except for acetylene black and some of the very large particle size grades which give higher values.

Microstructural models based on the X-ray diffraction work are illustrated in Fig. 1 in comparison to hexagonal graphite. Fig. 1a depicts the random orientation of crystallites within a single carbon black particle and a typical crystallite is illustrated in Fig. 1b [45]. The schematic for the unit cell of graphite is illustrated in Fig. 1c [46]. The carbon atoms in every other layer are aligned (aba stacking). The graphite structure may be described as a neatly stacked deck of cards in contrast to the turbostratic structure of carbon black in which the cards are rotated or shifted horizontally in the same plane.

a. Carbon Particle Showing Random Crystallite Orientation (From Ref. 45).

b. Typical Crystallite Showing Turbostratic Structure (From Ref. 45).

c. Graphite Unit Cell (From Ref. 46).

Fig. 1.
Early models for carbon black microstructure in comparison to graphite.

3.2.2. Dark Field Electron Microscopy

The concept of a generally random crystallite orientation in carbon blacks as shown in Figures 1a and 1b was the most widely accepted microstructural model for many years. The electron microscope analyses of Hall [47,48] were among the first studies to suggest that this type of orientation might not be valid. Hall employed the technique of dark field transmission electron microscopy to compare crystallite orientation in thermal and other large particle size blacks. Dark field imaging eliminates the bulk of the electrons that are scattered inelastically by the sample and enables better resolution of structural variations relating to crystallinity. Hall's work indicated that the parallel layer groups were oriented with the graphitic planes approximately parallel to the surface rather than in a random configuration. Because of limited resolving power, however, he was unable to determine if this type of orientation existed in the smaller particle size carbon blacks.

3.2.3. Oxidation Studies

A number of researchers employed transmission electron microscopy to study the oxidative patterns of carbon blacks. Ladd and Ladd [49] employed both thermal and acid oxidation to study the microstructure of different types of carbon blacks. With acid oxidation of a thermal black (N990) they reported that once penetration into the particle is made, the center is removed completely, leaving the outer shell intact. They also reported onion skin type peeling of ball milled N990 particles which indicated a layered structure that is in agreement with that reported by Hall [47,48]. The oxidative hollo-wing effect is illustrated for a large

particle size carbon black in Fig. 2. This electron micrograph indicates a well defined hollow shell structure.

More comprehensive oxidative studies were carried out by Donnet and Bouland [50] and by Heckman and Harling [6,51]. These studies clearly indicated selective internal hollowing by oxidation, thereby confirming the concept of a more ordered graphitic layer structure at the surface of the particles where the layer planes are aligned parallel to the surface. It should be noted that a random layer structure would tend to produce multiple oxidation entry points with no well defined shell. Heckman and Harling [51] reported this type of orientation for a small particle size channel black in that no shell structure was resolved. For other carbon blacks, the model shown in Fig. 3 [58] applies. This model shows small crystallites and a diminishing tendency toward alignment toward the center core of the particle.

Heckman [6] also employed high temperature heat treatments (partial graphitization in an inert atmosphere) to further verify the proposed orientation of layer groups at the surface. The carbon blacks heated at very high temperature exhibited a capsular structure analogous to the hollowing by oxidation. The graphitization process proceeds outwardly toward the more ordered layer groupings at the surface, leaving behind hollow centers.
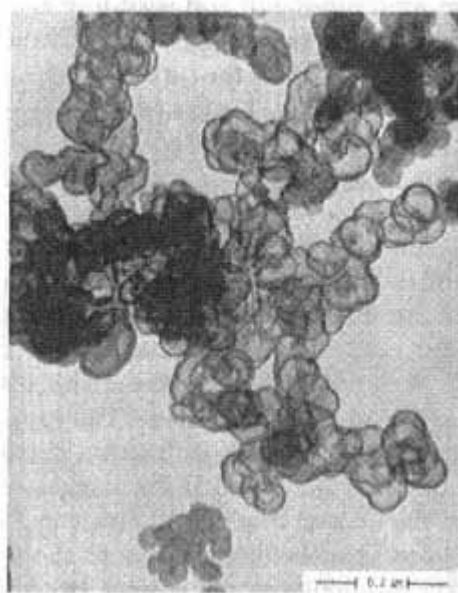
Fig. 2.
Transmission electron micrograph
showing hollow particles of carbon
black following severe thermal
oxidation.

3.2.4. Diffracted Beam Electron Microscopy

The first high resolution diffracted beam transmission electron micrographs of carbon black were published by Hess and Ban [52]. Diffracted beam microscopy differs from the simple dark field technique because specific parts
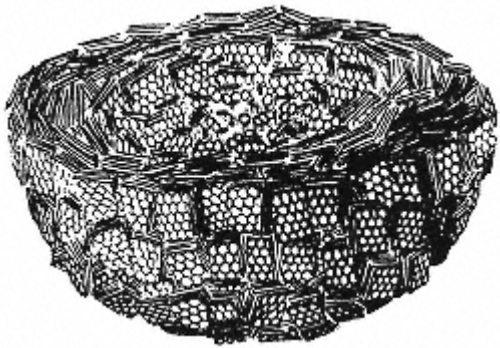
Fig.
3. Model showing cutaway view of single carbon black particle with concentric surface parallel orientation of ordered layer groupings and diminishing graphitic order near the particle center (from ref. [58]).

of the diffraction pattern are isolated and used to form the image. This provides more precise information pertaining to microstructure and orientation effects. The two strongest reflections for carbon black are the *(002)* and *(10)*. To satisfy the diffraction conditions for the *(002)* images, the graphitic layers must be approximately parallel to the incident electron beam while the *(10)* images are formed from layers that are almost perpendicular to the beam.

Imaging by the diffracted beam technique is accomplished through tilting of the electron beam by means of properly placed magnetic coils [52,53]. The desired portion of the diffraction pattern is centered in this manner and then isolated with an aperture so that only that part of the beam contributes to the image. This procedure is illustrated for the diffraction pattern of acetylene black in Fig. 4. The white spot shows the placement of the aperture for imaging a portion of the *(002)* reflection. The *(10)* and *(11)* reflections, although weaker, are also visible in the diffraction pattern.

Typical *(002)* and *(10)* diffracted beam images of acetylene black are illustrated along with the normal bright field image in Fig. 5 [52]. The bright spots in the dark field images are attributable to the diffracted beams from ordered graphitic layer groupings at the correct Bragg angle for diffraction. Note that the *(002)* images tend to be seen starting at the edges of the particles in wedges or streaks that taper off near the center. For spheroidal particles with concentrically oriented graphitic layers, the peripheral regions are most likely to give the correct angle for diffraction. The fact that the images tend to appear as wedges is attributable to two factors: 1.) only a small portion of the diffraction pattern is being imaged

and 2.) the circumference of the concentrically oriented layers becomes smaller toward the center of the
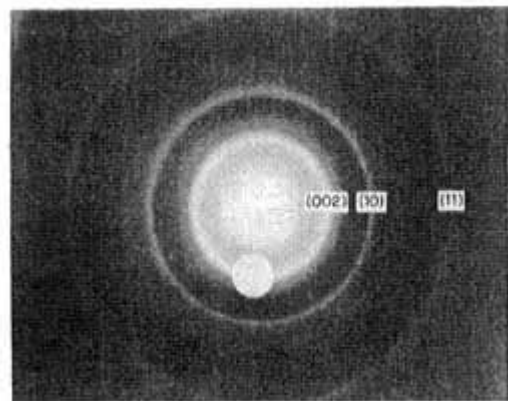
Fig. 4.
Electron diffraction pattern of acetylene carbon black showing (002), (10) and (11) reflections. Aperture (white spot) is placed for (002) diffracted beam imaging (from ref. [52]).
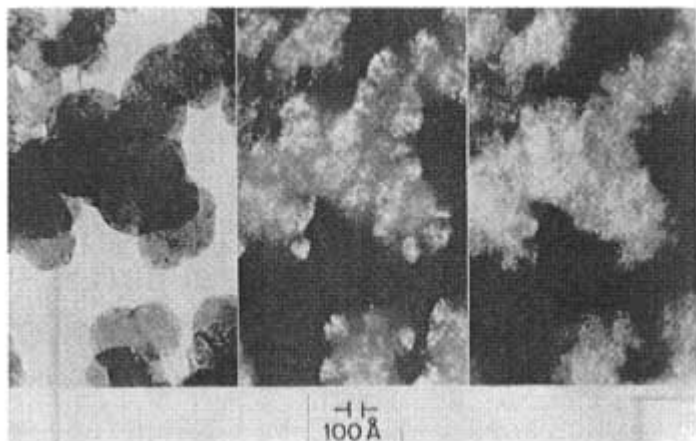
Fig. 5.
TEM imaging of acetylene black (from ref. [52]).

particles and the diffracted beam images are emitted across a diminishing arc. The effect is analogous to the appearance of spherulites under crossed polarizers in an optical microscope. The absence of detail at the centers of well defined particles supports the observations pertaining to hollowness or absence of order in these regions. As would be expected, the *(10)* images in Fig. 5 tend to be strongest in the central areas, particularly in the regions that are devoid of *(002)* images.

A further example of the concentric, surface parallel orientation of the graphitic layers in carbon blacks is illustrated for the *(002)* images of a thermal type black in Fig. 6 [54]. The particles for this grade are more spheroidal and the wedge shaped patterns are better defined. Again, there is an absence of detail in the center regions of the particles which indicates either hollowness or a lack of ordered graphitic layer segments.

Carbon blacks made by four different processes are compared in Fig. 7 [54]. These micrographs show that all carbon blacks,

including the channel types, have essentially the same graphitic layer orientation, i.e., surface parallel layers with larger, more ordered groupings near the surface. Acetylene black contains larger layer groupings than the other three types.

The effect of post heat treatment is shown for a series of partially graphitized N220 carbon blacks in Fig. 8. The samples labeled as HT were induction heated in an inert atmosphere (nitrogen) at various temperatures up to approximately 2000°C [52,54]. The listed Lc values were determined by X-ray diffraction [29]. The relative sizes of the spots in the *(002)* diffracted beam images correlate well with the Lc values.
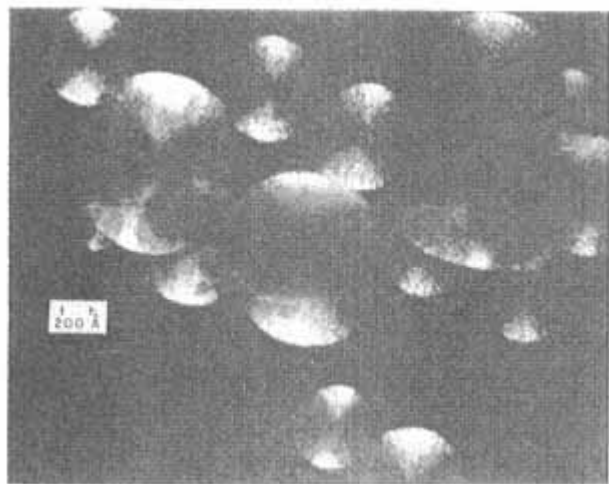
Fig. 6.
TEM (002) diffracted beam image of thermal black. Wedge shaped zones (white) indicate concentric ordering of surface parallel graphitic layers (from ref. [54]).
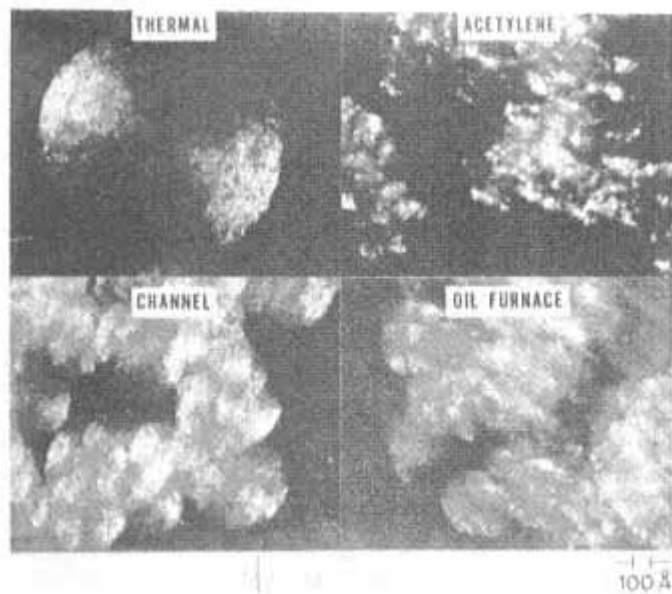
Fig. 7.
TEM (002) diffracted beam images for different

carbon black manufacturing processes (from ref. [54]).
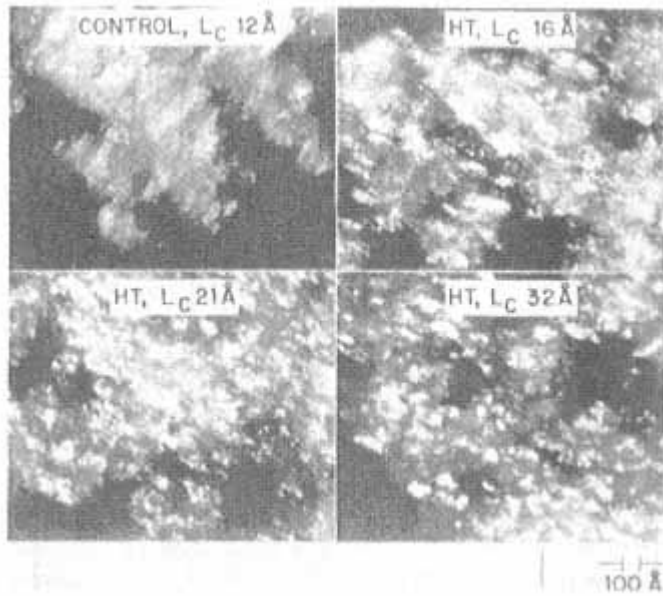
Fig. 8.
TEM (002) diffracted beam images for an N220
carbon black heated in an inert atmosphere at
different temperatures. The changes in the size of
the images from ordered layer segments correspond
to the Lc measurements from X-ray diffraction
(from ref. [54]).

Plots of Lc vs. induction furnace heat treatment temperature (9001500°C) are shown in Fig. 9 for N121 and N650 rubber grade carbon blacks. Ordering of the layers is initiated in the range of 9001000°C, the point at which the carbon-bound hydrogen starts to be released. However, the effects on Lc are quite insignificant in this range. From 1100 to 1500°C (and higher) there is sharp increase in Lc up to a limiting value that is dependent on particle size. Thus, the changes are much greater for the larger particle size N650 sample relative to N121.

While the relationships shown in Fig. 9 are typical, some degree of

caution should be used in directly relating heat treatment temperature to carbon black properties or end-use performance characteristics. The effects of heat treatment vary appreciably as a function of furnace type, size and overall efficiency. For example, resistively heated carbon black samples have required treatments at 200 to 300°C higher in temperature than induction heating to achieve the same Lc level. A near maximum reduction in the surface reactivity of carbon blacks (in polymeric systems) has been observed with induction heat treatments in the range of 14001500°C [54]. This is
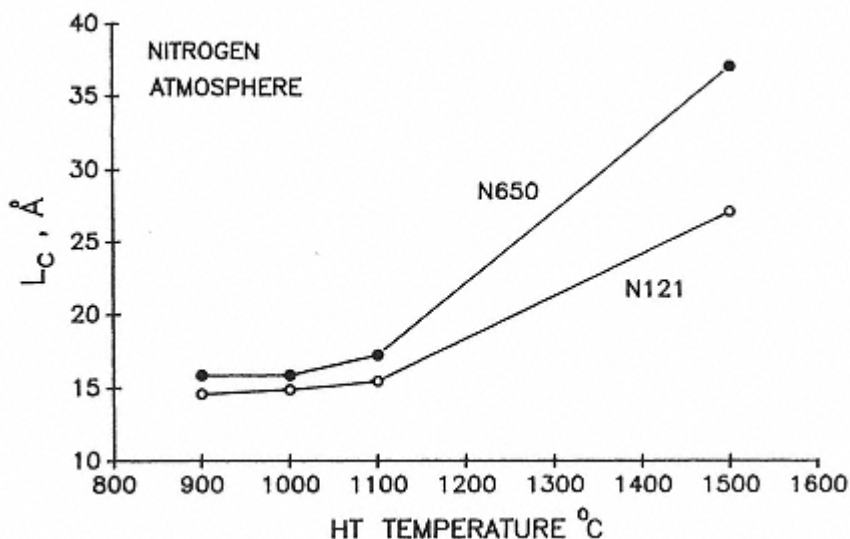
Fig. 9.
Plot showing the changes in Lc for N121 and N650 carbon black
as a function of heating in an induction furnace (nitrogen
atmosphere).

related to the removal of chemically bound hydrogen from typical
levels of 25004000 ppm down to about 100 ppm or less [55]. The
importance of chemically bound hydrogen has been emphasized by
Studebaker [8] and Donnet and coworkers [56,57]. The specific
role of hydrogen in carbon black surface reactivity will be
discussed in another chapter.

3.2.5. Phase Contrast TEM Imaging

The first high resolution phase contrast electron micrographs of
carbon black were taken by Heidenreich and coworkers in 1967
[58]. This type of image is formed by interference of the main (0
order) beam with a specific diffracted beam relating to a periodic
spacing in the sample. The control of phase contrast is achieved
through the extent of defocus of the image, ΔL, which depends

primarily on the spacing, *d,* and wavelength of the electron beam, λ. To determine the best focus for spacing, *d,* increments of $\Delta L = d^2/\lambda$ are employed. At these increments, maximum interference occurs and the periodic spacings are most clearly visible. Other considerations for contrast and coherency pertain to the electron source. Preferably, this should be a pointed single crystal filament in the Schottky-emission mode [59]. Additional important factors are the minimization of astigmatism and sample contamination, the latter generally being accomplished by means of a liquid nitrogen cold trap in the vicinity of the specimen.

The first high resolution phase contrast images of carbon black were obtained on the more ordered heat treated samples. An N220 carbon black heated to approximately 3000°C is illustrated in Fig. 10a. This sample has a

(a)

(b)

Fig. 10.
TEM high resolution phase contrast
images of an N220 carbon black.
a: Induction heated at 2700°C.

b: Untreated. The light and dark lines correspond to the graphitic layers (from ref. [58]).

d(002) of 0.344 nm as measured by X-ray diffraction. Each graphitic layer spacing in the phase contrast image is represented as the distance from the start of one dark or light line to the beginning of another. The capsular structure reported by Heckman [6] is readily evident in these images. The outer shells are clearly indicated by the bands of continuous layers surrounding the clear central regions which represent large voids within the particles. The layers also bend continuously around the particles which raises some interesting considerations pertaining to the X-ray diffraction analyses. The X-ray measurements do not compensate for layer bending; therefore, the actual La values are much larger than the X-ray measurements. The high resolution images of the heat treated carbon black indicate continuous layers around the circumference of particles or even entire aggregates. This is shown by the model in Fig. 11 [58] which is a cutaway view of a single highly graphitized carbon black particle. Additional support for this structure is based on the inert nature of the surface of heat treated blacks, as well as their impermeability to helium. Helium densities on carbon blacks often diminish significantly with heat treatment and are much lower than would be expected because of the sealed-off internal voids.

The Paracrystalline Model for Carbon Black Microstructure

Phase contrast images of untreated carbon blacks were obtained in 1968 by Hess and Ban [60,61] and by Harling and Heckman [62]. For carbon blacks made by the oil furnace, channel, thermal and acetylene processes, phase contrast images clearly showed that the graphitic layers in all commercial carbon blacks tend to be

continuous (Fig. 10b), which is in agreement with the hypothesis of Ergun [40]. His X-ray diffraction studies supported the
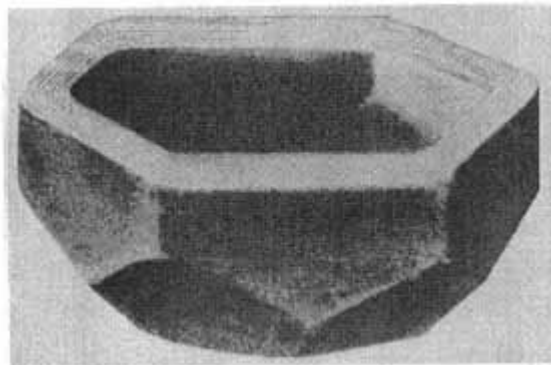
Fig. 11.
Model showing cutaway of highly graphitized carbon black particle. The graphitic layers bend continuously around the circumference of the particle which exhibits a polyhedron shape (from ref. [58]).

concept that the individual graphitic layers, not crystallites, were the basic building block of carbon black particles. Ergun defined this as a paracrystalline structure, i.e., parallel layers but no discrete 3-dimensional groupings forming crystallites. The high resolution phase contrast images clearly support this hypothesis for all types of commercial carbon blacks.

The paracrystalline structure model and the surface model of a carbon black particle are shown in Fig. 12a [62] and 12b. This model represents a small surface segment, with the mesh depicting the hexagonal nets of carbon atoms in the graphite layers. The layers exhibit numerous distortions and discontinuities.

Phase contrast imaging has also enabled direct measurements on the distribution of layer spacings in carbon blacks. Marsh and coworkers [63,64] used micrographs to measure the *(002)* d-spacing distributions of several carbon black grades ranging from N220 to N990. A fairly broad distribution
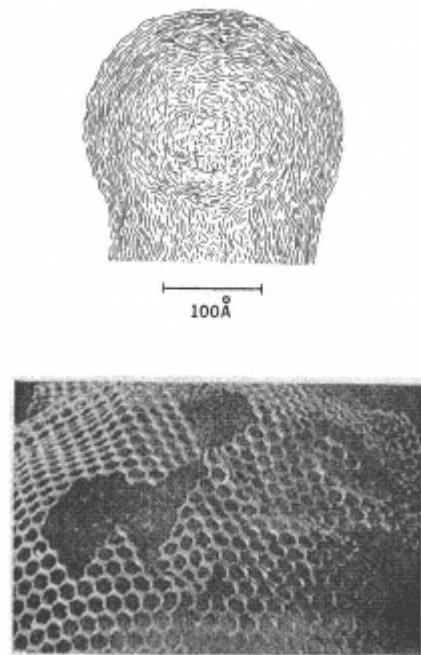
Fig. 12.
Model illustrating paracrystalline
layer structure for carbon blacks.

of d-spacings (~0.35 to 0.41 nm) was indicated for the furnace grades, regardless re-gardless of particle size and structure. The average EM measured d-spacings for the furnace blacks varied from about 0.383 to 0.392 nm and were significantly larger than the X-ray spacings (0.352 to 0.356 nm). Overall, however, the EM d-spacings were in good relative agreement with the X-ray results. For commercial blacks, only N990 (0.363 nm) and acetylene black (0.355 nm) indicated lower average d-spacings than the furnace or channel (MPC) types. A significantly narrower distribution of d-spacings was reported for highly graphitized (heat treated) carbon black particles relative to normal particles.

Ban and coworkers [65,66] employed optical diffraction of high resolution photographic plates to measure d-spacing distributions in N990 and N220 carbon blacks heated to a range of different temperatures (900 to 1400°C) in an induction furnace. The spots in the optical diffraction patterns represent spacings between single layers as well as groups of layers which can also diffract to single spots. The measured spacings varied from about 0.309 to 0.824 nm, with the very large spacings being attributable to distortions in the graphitic layer structure. These large spacings were also prevalent in the heat treated samples despite the increase in more ordered layer groupings. The N990 sample exhibited a narrower distribution of spacings and lower average values relative to N220, as previously reported by Marsh et al [63,64]. These differences persisted with the heat treatments. Lattice distortions in the 0.380 to 0.824 nm range remained greater for N220 even at 1400°C [65]. However, when these samples were heated at 3000°C, a more perfect polyhedron structure was indicated for N990. This type of structure was shown in the early TEM studies of Kmetco [67], who

examined metal shadowed replicas of N990 particles which had been heated at 3000°C. Direct imaging to show this type of particle geometry is now possible with a scanning electron microscope, as illustrated in Fig. 13. The micrographs shown here represent SEM images of untreated N990 particles and a sample heat treated at 3000°C. The specimens were platinum/gold sputtered to enhance conductivity for improved imaging. The change from the initial spheroidal to a polyhedron shape at 3000°C is evident.

3.2.6. High Resolution SEM, STEM, STM, SFM and AFM Imaging

The scanning transmission electron microscope (STEM) provides scanning images using transmitted electrons. Crewe and Wall [68] showed the first high resolution STEM images of carbon black in 1969. By using a field emission electron gun, they were able to resolve the 0.344 nm *(002)* spacing in the same partially graphitized carbon black sample illustrated in Fig. 10. Nomura et al [69] and Ray et al [70] published improved STEM micrographs of this type of carbon black in 1976. Crewe has summarized the advantages
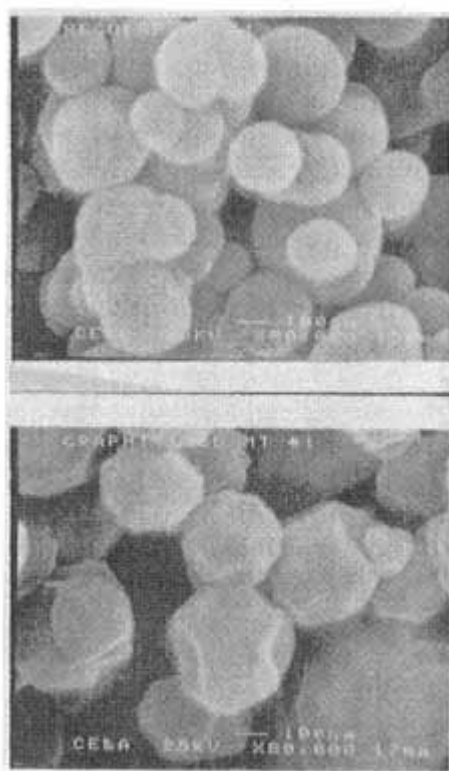
Fig. 13.
Scanning electron microscope
images of N990 carbon black
(micrographs taken by Charles
Evans and associates).

of STEM over TEM in terms of improved image contrast, the ability to utilize and interact different forms of contrast and better elimination of the various types of image aberration which limit resolving power. In subsequent studies, Crewe and coworkers were able to resolve single metallic atoms on substrates [72] and also obtain high resolution images of DNA [73].

The field emission gun (FEG) also enables high resolution SEM images (0.51.0 nm) through the ability to operate at low voltages

with uncoated specimens. This is an area of possible future potential for resolving the surface microstructure of carbon blacks.

Scanning Tunneling Microscopy

The scanning tunneling microscope (STM) was developed by Binnig et

al [74]. This revolutionary new type of microscope has the capability to analyze surfaces with the resolution of single atoms. Basically, the surface of the sample is scanned at close proximity (<1.0 nm) with a sharp tungsten tip which is biased at the appropriate tunneling voltage. The current for electrons tunneling from the surface of the sample to the probe is exponentially proportional (inverse) to the gap spacing. Therefore, it is very sensitive to changes in gap spacing and can be employed to determine surface topography on an atomic scale. A variation as small as 0.1 nm in gap spacing causes about a 10-fold change in tunneling current. The STM may be operated at variable or constant tunneling current. In the latter instance, the raster scans (x, y) on the sample cause the vertical z-axis of the scanner to adjust accordingly. A computer records the vertical displacement in conjunction with each x, y position and is then subsequently employed to reconstruct the topography of the surface. Since the method is based on electron tunneling, it is limited to conductive materials. Many different versions of STM are commercially available in a very rapidly expanding field. Graphite is one of the more commonly analyzed materials and represents an ideal specimen because it is inert and atomically flat over large areas. Many micrographs showing the atomic structure of the graphite surface have been published [75,76]. More detailed applications of STM to carbon black microstructure are discussed in a separate chapter in this book.

Scanning (or Atomic) Force Microscope

The scanning force microscope (SFM) or atomic force microscope (AFM) was also developed by Binning et al [77]. The resolution of

the SFM is near that of STM [78] with atomic resolution possible on certain samples. However, the SFM can be used to image both conductive and insulating surfaces at ambient conditions.

The SFM has been described as a miniature surface profilometer that works by measuring the deflection of a small cantilever as a result of interatomic forces as it scans the surface. Forces as small as 10^{-9} N are detected with the resulting cantilever movement sensed by either a laser or a tunneling tip behind the conducting cantilever [78]. Again, the displacement is recorded on a computer from which the 3-dimensional topography of the examined surface is reconstructed.

3.3. Morphological Properties

3.3.1. Terminology

Based on very early electron micrographs, carbon black particles were thought to be discrete, spheroidal units which tended to be joined together in chains or clusters. As instrument resolution improved, it became clear that the particles of most carbon blacks were fused together in a continuous solid carbon structure. In an early review, Hess and Ford [79] published

micrographs comparing a high structure furnace carbon black to a thermal black. These clearly showed complete particle boundaries for the overlaying thermal black particles while the internal particle boundaries were not visible in the furnace black.

The concept of carbon black structure was first defined by Ladd and Wiegand [24]. Unfortunately, this is an ambiguous term because it implies microstructure. The term aggregate is more suitable to describe the chaining and clustering of carbon black particles. Hess and Ford [79] referred to aggregates in terms of the discrete units of carbon black that exist in elastomer vulcanizates. However, this terminology was not widely used until the work of Medalia [80].

In view of the findings of high resolution electron microscope analyses on carbon blacks, Burgess et al [81] redefined the carbon black aggregate as a paracrystalline unit. The particles were defined as domains of rotational graphitic layer orientation. While this terminology was actually more descriptive of the true nature of carbon blacks, it was not widely accepted. This also applies to the term nodule which was used by Janzen and Kraus [82] to describe carbon black particles.

Today, the terms particle and aggregate remain as the primary descriptors of carbon black morphology and are defined below [83].

Carbon Black Aggregate - a discrete, rigid colloidal entity that is the smallest dispersible unit; it is composed of extensively coalesced particles.
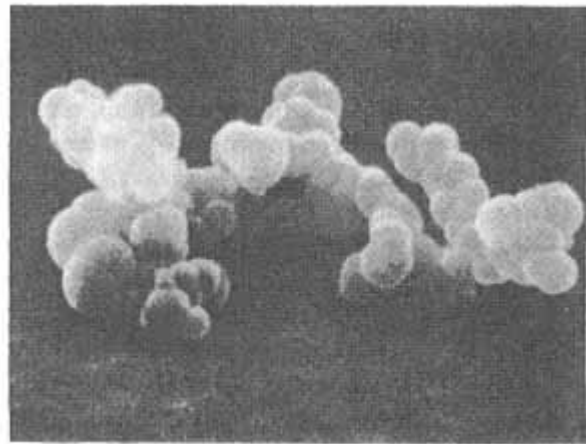
Fig. 14.
Scanning electron micrograph of a carbon
black aggregate.

Carbon Black Particle - a small spheroidally shaped, paracrystalline, non-discrete component of an aggregate; it is separable from the aggregate only by fracturing.

A scanning electron micrograph of a carbon black aggregate is illustrated in Fig. 14. The fusion of the spheroidal particles is evident in this image. It should be noted that the morphological properties of carbon blacks are all distributive in nature; i.e., particle size, aggregate size and aggregate shape vary over a broad range within and between the different grades. Sometimes the term agglomerate is also confused with aggregate. An agglomerate is actually comprised of a large number of aggregates which are physically held together as opposed to the continuous graphitic structure which links the particles in aggregates

Particle size and its distribution are probably the most important physical properties of carbon black in terms of end-use applications, even though particles do not exist as discrete entities except for thermal blacks. Therefore, the methods employed to measure particle size directly and indirectly will be described first, followed by those for surface area, porosity and aggregate size and shape.

3.3.2. Particle Size

Electron Microscope Measurements

The electron microscope remains the most accurate means of measuring the particle size distributions of carbon blacks, despite the obvious problem of defining particle boundaries. The first extensive measurements on commercial grade carbon blacks were carried out by Ladd [23]. The diameters of particles (at least 50%

of their circumference visible) were measured manually on suitably enlarged micrographs. The dispersions used in these early studies were typically based on a high frequency discharge [84] to scatter the carbon black onto thin plastic films of nitrocellulose or polyvinyl formal (Formvar). It was later found that the discharge method actually altered some of the carbon black particles through oxidation or partial graphitization. In addition, the plastic films were prone to tearing and drifting in the microscope and added to the contamination of the specimen in the electron beam.

The use of evaporated carbon films [85] eliminated the instability problems associated with the plastic films and produced a significant improvement in the yield of high quality TEM micrographs for carbon black particle size analysis. Another major advance was the development of a semiautomatic measuring device by Endter and Gebauer [86] which was later marketed by the Zeiss Optical Co. This instrument utilizes a variable light spot to measure the particle diameters on micrographs, and the values are recorded automatically. The application of the Zeiss Particle Size Analyzer for carbon black particle size measurements has been described in detail by

Schubert et al [10] along with procedures for estimating particle size from micrographs. The estimation technique is a comparative system based on standard reference micrographs showing known variations in particle size. Marsh [87] further refined and simplified the estimation method by recording and storing the micrographs of standards and unknowns on a video disk. In the playback mode, the unknown fields were displayed simultaneously along with the standards which were alternated to obtain the best match for particle size.

Automated Image Analysis

The first transmission electron microscope/automated image analyses (TEM/AIA) on carbon black were carried out by Hess et al [88] employing a Quantimet B Image Analyzer [89] for the measurement of aggregate images on photographic prints. These images were measured by means of a television type scanner, the output of which was then analyzed in a computer. Particle size was not specifically measured in this early work but the average values for the mean chord (aggregate area÷projected length) were found to be proportional to the values for particle diameter measured on the Zeiss Particle Size Analyzer.

One of the important aspects of TEM/AIA is the fact that discrete images in a large field are measured separately; therefore, good dispersions are of the utmost importance. Ultrasonic agitation (~40 kHz, 100 watts) in a highly polar liquid such as chloroform was found to be an excellent means of dispersing carbon black for deposition as a layer of well separated aggregates on a carbon substrate [88]. This dispersion procedure was subsequently refined by employing an AC glow discharge treatment with air to activate

the carbon substrate [90]. The glow discharge treatment both cleans and oxidizes the surface of the carbon film, thereby making it highly receptive for interaction with carbon black aggregates that are dispersed in highly polar liquids with low hydrogen bonding. Either chloroform or tetrahydrofuran (THF) are excellent media for dispersing the standard rubber grade carbon blacks. Acid-base relationships [91] appear to affect carbon black dispersions in liquid media. Since THF is a weak Lewis base and chloroform is a weak Lewis acid, THF is preferred for oxidized blacks which have surface oxygen functionalities that are acidic in nature.

Most of the early automated image analysis systems were operated off-line using micrographs. In addition, they were field specific; i.e., different measurements on the same feature could not be linked together to provide multivariate functions for shape analysis. A feature specific Quantimet 720 System [92] was introduced in 1972 and subsequently developed into an on-line TEM/AIA System for carbon black analyses [9395]. For this type of system, the television camera was linked directly by a fiber optics coupling to a high resolution transmission electron microscope. In addition to the ob-

vious advantage of reducing the time and cost of photographic printing, there was an additional improvement for obtaining densitometric information on images. Controlling optical density is a considerable problem when working with photographic prints or plates.

Particle size information by on-line TEM/AIA was reported by Hess and McDonald [94] using the mean chord model [88] which was further modified with aggregate shape measurements. Dispersion techniques were expanded from the simple analyses on dry carbon blacks to include samples removed from unvulcanized elastomers through ultrasonic breakdown of carbon-polymer gel [95] and thin layer pyrolysis [90].

Improved particle size measurements were achieved through cellulose acetate butyrate (CAB) paint chip dispersions [96]. The CAB procedure, now part of the ASTM D 3849 Method [83], causes extensive breakdown of the carbon black aggregates, essentially reducing aggregate irregularity (or the number of particles per aggregate) to a similar level for the different grades. Therefore, particle size becomes more directly proportional to aggregate size. For each individual aggregate, an average particle diameter, d is derived as:

$$d = \alpha(\pi A/P) \quad (1)$$

where A is the projected aggregate area, P is the perimeter and α is a shape related aggregation factor. The $\pi A/P$ function represents the mean chord or average width of the aggregate. The α function is self determined from the circularity factor, P^2/A, and is employed to correct for the fact that the mean chord is a measure

across multiple rather than individual carbon black particles. Janzen and Goodarz-Nia [97] employed a similar area/perimeter relationship to derive specific surface areas from TEM/AIA measurements on carbon black aggregates.

The success of Equation 1 is largely attributable to the uniformity of particle size within any given carbon black aggregate [98]. Therefore, the number of particles n in each aggregate may be approximated as:

$$n = VA/VP \text{ (2)}$$

where VA is the calculated aggregate volume and VP is the particle volume, assuming a spherical shape. Knowing both d and n for each aggregate, the full particle size distribution may be determined.

The particle size histograms (obtained from TEM/AIA) illustrating particle size differences among commercial furnace grade carbon blacks (N100 to N700) are shown in Fig. 15. These histograms are plotted as frequency % vs. particle diameter over specific range intervals: 5 nm for N110 and N351, and 20 nm for N650 and N762. It can be seen that a much smaller range of particle size exists for N110 and N351 relative to the other blacks. The distributions all tend to be positively skewed, i.e., they contain a higher population of par-
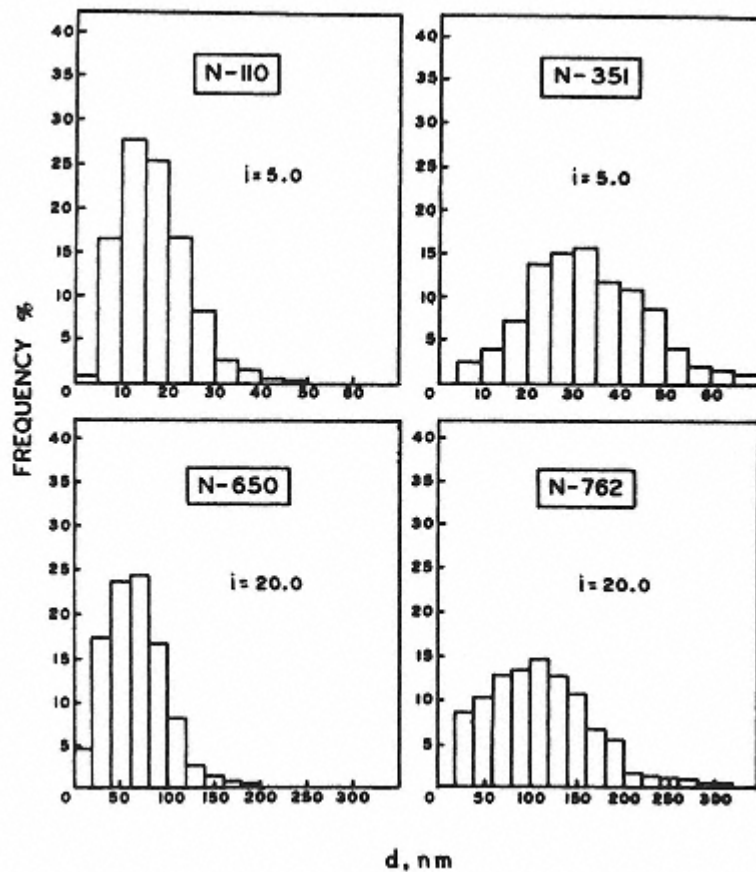
Fig. 15.
Particle size histograms for different oil furnace carbon blacks (CAB dispersions) shown in Fig. 18 (from ref. [96]).

ticles in the smaller diameter range than at the larger end of the distribution.

Particle size data on a broad range of current rubber grade carbon blacks are listed in Table 2 and include the mean particle diameter, M (nm), the heterogeneity index, HI (a measure of the breadth of the distribution) and the specific surface area (m2/g) as determined by the electron microscope (EMSA), BET nitrogen adsorption and

the CTAB adsorption (see Section 3.3 for details on the BET and CTAB methods). The various statistical parameters used to define particle size have been defined by Cadle [99].

A non-dimensional statistic which has been applied to define the breath of a distribution is the heterogeneity index, HI, a measurement which was originally utilized by Janzen and Kraus [82]. The HI values in Table 2 are the ratio of the weight mean to arithmetic mean diameter. The higher the number, the broader the size distribution. For most commercial carbon blacks, HI values for particle size range from about 1.4 to 1.8. The conductive N472

grade is much broader in distribution with a value of approximately 2.3. The larger particle size carbon blacks (N550N990) have higher HI values than the finer, more reinforcing grades (N110N358), as would be expected from the histograms illustrated in Fig. 14. The heterogeneity index or the coefficient-of-variation (C.O.V.) are dimensionless numbers, however, and are not directly dependent on the size level.

The specific surface area (EMSA) is derived directly from the surface mean diameter, *dsm,* using the following expression:

$$S \ (m2/g) = 6000/pdsm \ (3)$$

where ρ is the density of the carbon black in g/cm3 and *dsm* is in nanometers. It should be noted that the electron microscope surface area model [83] assumes unattached, spheroidal particles. The values are a useful means of comparing different carbon blacks because they are based on the full particle size distribution. However, the method is not a true surface area measurement and will give low values if applied to highly porous samples.

The typical commercial rubber grade furnace carbon blacks listed in Table 2 range in mean particle diameter from about 17 nm (N110) up to 107 nm (N762). N990 is considerably larger (285 nm). The full range of specific surface areas based on particle size (EMSA, m2/g) varies from about 9 to 138.

The average particle size and EMSA for several non-rubber grade carbon blacks are listed in Table 3. These are listed in terms of their level of blackness or color, i.e., high color furnace (HCF), medium color furnace (MCF) and low color furnace (LCF) as described by Schubert et al [10]. The HCF grades are much smaller in average

particle size (~9 to 16 nm) in comparison to the rubber grades and range in EMSA from 148 to 295 m2/g.

Colloidal Techniques

Colloidal methods are frequently employed to estimate carbon black particle size. One of the earliest techniques is the estimation of masstone, also referred to as blackness or color. Sweitzer and Goodrich [26] developed a quantitative visual method for assessing the blackness of carbon blacks dispersed in mineral oil and examined under the illumination of a carbon arc. An arbitrary blackness index scale was established with the grayest carbon (N990 type) assumed to be 0. About 260 different shades can be detected with the human eye for carbon blacks ranging from an average particle diameter of 300 to 400 nm down to approximately 10 nm. Fig. 16 [10] illustrates the changes in the blackness index for a broad range of carbon blacks as a function of their electron microscope surface area. The carbon black sampling is divided into three structure levels. It is apparent that increasing structure (larger aggregate size) reduces blackness index which, otherwise, increases proportionately with diminishing particle size. The plots in Fig. 16 are rea-

Table 2. Typical Particle Size and Surface Area Values for Rubber Grade Carbon Blacks

ASTM number	Mean[a] particle dia., nm	HI[a]	EMSA[a] m2/g	BET[b] N2SA m2/g	CTAB[c] m2/g	Tinting[d] strength
N110	18	1.59	138	138	127	124
N121	19	1.58	131	132	123	122
N220	21	1.51	121	116	111	116
N234	20	1.57	124	125	118	120
N299	24	1.44	107	106	101	112
N326	27	1.44	87	85	84	114
N330	30	1.59	80	83	84	102
N339	26	1.56	96	95	94	109
N351	32	1.44	77	74	74	100
N358	30	1.49	84	85	82	97
N472	21	2.32	91	230	129	93
N550	56	1.67	41	41	43	61
N630	58	1.76	35	36	37	62
N650	61	1.65	39	38	38	56
N660	67	1.65	35	36	35	58
N762	107	1.57	24	26	28	49
N774	79	1.68	29	29	30	52
N990	285	1.63	9	9	9	24

aASTM D 3849, Dispersion Procedure D (CAB).
bASTM D 3037.
cASTM D 3765.
dASTM D 3265.

sonably linear above a specific surface area of 100 m2/g. It should be noted that blackness index also diminishes with a broadening of the particle size distribution and, therefore, a more discerning

comparison of different carbon blacks can be made by TEM/AIA relative to any of the colloidal or adsorptive measurements.

The color differences in matter are largely based on the interaction of light with electrons [100]. The electrons in the graphitic layers of carbon black are free to vibrate at practically any frequency and thereby absorb all wavelengths of visible light ranging from infrared to ultraviolet. Carbon black is a semiconductor and has a gap of forbidden energies separating the filled valence band from the empty conduction band. If the minimum energy required to transfer an electron from the valence band to the conduction band is below the energy for the longest wavelength of the incident light (infrared),
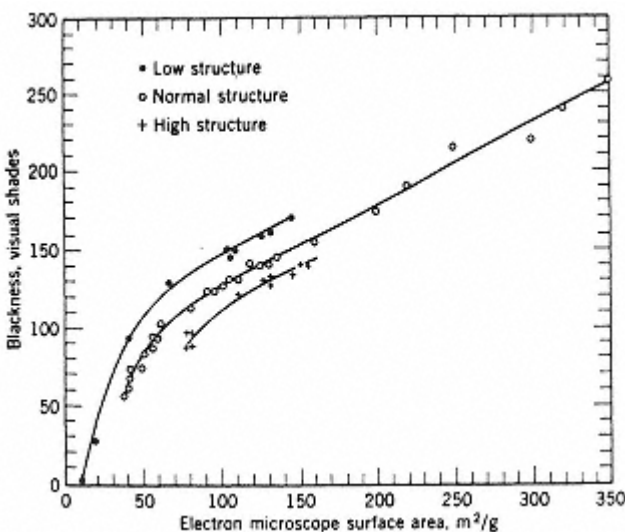
Fig. 16.
The effects of varied particle size and
structure on the blackness index of carbon black
(from ref. [10]).

then all visible wavelengths are absorbed and the material appears black. On the other hand, if the energy gap is higher than the energy for the shortest wavelength of the incident light (ultraviolet), then the material appears colorless. The latter applies to diamond which is also a semiconductor. The degree of blackness in carbon blacks is dependent on the efficiency of re-emission of the light. The smaller particle size carbons are less efficient in re-emission because of more forward scattering, thereby leading to greater absorption. The tone of the reflected light also changes with particle size. All carbon blacks tend to selectively absorb the shorter wavelengths at the blue end of the spectrum [101]. Therefore, since the smaller particle size carbon blacks are more absorbing, the light that they reflect tends to have a browner tone. The larger particle size carbon blacks tend to reflect more of the entire spectrum and, therefore, appear bluer in tone. These factors

are important in paint and ink applications in which carbon blacks are used as a colorant.

Spectrophotometry has been employed for less subjective measurements on the masstone of carbon blacks, although the human eye is actually more sensitive to small differences. The nigrometer [102,103] was one of the earliest instruments employed to measure blackness differences among carbon blacks. This technique utilizes carbon black dispersions in linseed oil [10]. Reflectivity measurements for particle size estimates on dry carbon blacks have also been reported [104]. Nabors and Studebaker [105] used compressed samples (15,000 psi) of carbon blacks for these studies to minimize prior handling effects. They employed a Densichron Reflectometer (W. M. Welch Scientific Co., Chicago) for these measurements and emphasized the need for uniform, smooth, carbon

surfaces to obtain reliable values.

Tinting Strength

This method is based on the reflectance of mixtures of carbon black with a white pigment (zinc oxide) in oil. Typically, the zinc oxide is at a very high weight ratio relative to the carbon black, e.g., ~38 to 1 for the smaller particle size carbon blacks and ~19 to 1 for the larger particle size N500 to N700 grades. The smaller the particle size of the black, the greater their ability to cover the typically larger size zinc oxide particles. Therefore, carbon black tinting strength increases with diminishing particle size.

Voet [106] developed a method for determining the relative tinting strength of carbon blacks used in printing inks. This is based on the Densichron Reflectometer mentioned previously. No. 1 pale litho varnish is employed as the vehicle and mixing is done on a Hoover Muller. All tinting strength values are reported relative to a standard. The ASTM tinting strength test [107] is similar in nature but utilizes a soybean oil epoxide as the vehicle.

The ASTM tinting strength values for the different rubber and non-rubber grade carbon blacks are listed in Tables 2 and 3, respectively. Across all of the carbon black grades, tint varies from about 41 to 135. These values are calculated by dividing the measured reflectance by that of an industry standard (ITRB, D 3265) and then multiplying by 100. The tint test is insensitive at the smaller particle size levels and it can be seen that the values for the finer samples (9 to 20 nm mean particle diameter) are all quite similar (130135). This is caused by the inability to adequately disperse the finer carbon blacks in the tint paste, a problem that is

further compounded by the greater disparity in particle size relative to the much coarser zinc oxide pigment.

The values for tinting strength are significantly reduced with increasing carbon black structure [108110], the magnitude of the effect being somewhat greater than that observed for masstone. Medalia and Richards [109] and others [108] have reported a strong inverse relationship between tint and aggregate size as measured by TEM/AIA. McDonald and Hess [90] showed an inverse correlation between tint and aggregate width (mean chord). Their studies were based on a series of ten carbon blacks varying in ASTM tinting strength from 109 to 130. A significantly improved correlation of aggregate size with tint was obtained when the TEM/AIA analyses were carried out on carbon black specimens extracted from the actual tint strength pastes. These results showed that tinting strength tends to increase with breakdown of the carbon black aggregates and decrease with micro-agglomeration, both effects taking place as a result of the mixing of the black into the paste. In addition, tint values also diminish with broader particle size distribution.

In summary, tinting strength and masstone are both indirect methods for assessing the overall level of carbon black particle size. They are use-

ful screening methods because of their simplicity but are not capable of the accuracy of electron microscope procedures and do not provide any direct information on particle size distribution. The tinting strength values for carbon blacks that are below 20 nm in average particle size also reach a maximum. Therefore, this method is not well suited for the very small particle size grades which are employed in many paint and ink applications.

3.3.3. Surface Area

Surface area is an important property in carbon black grade classification and production control. For non-porous carbon blacks the values exhibit an overall inverse correlation with particle size. As mentioned previously in Section 3.2, however, it is inadvisable to try to forecast either property from the other. Furthermore, surface areas provide no distributional information.

Many procedures are available for determining surface area and usually involve the adsorption of specified molecules on the carbon black surface. Three of the most widely used adsorption methods are based on nitrogen, ASTM D 3037 [111], cetyltrimethyl ammonium bromide (CTAB), ASTM D 3765 [112]; and iodine, ASTM D 1510 [113]. Other gaseous adsorption techniques are also available. The surface areas derived from each of the above methods can be affected in different ways by the amount and type of porosity, as well as the chemical nature of the surface of the carbon black being analyzed. It is important, therefore, to keep these possible effects in mind when interpreting the surface area data from each specific test.

Langmuir and BET Theories of Adsorption

The surface area for almost all solids can be determined from the volume *(Vm)* or weight *(Wm)* of molecules that are adsorbed as a monolayer on their surface. Once this volume has been determined, the surface area, *S,* can be calculated by simply multiplying the number of adsorbed molecules or atoms by the cross-sectional area of the adsorbent. Thus the surface areas can be calculated as follows:

$$S\ (m^2) = W_m N A / M \quad (4)$$

where *Wm* = weight of monolayer (g), N = Avogadro's number (6.024×10^{23} mol^{-1}), A = cross sectional area of adsorbate (m^2), and M = molecular weight of adsorbate (g mol^{-1}). The specific surface area (m^2/g) can then be calculated by simply dividing S by the actual weight of the sample in grams. It is obvious that the accuracy of the nitrogen surface area values is dependent upon the accuracy of the measurements for *Wm* and the cross-sectional area of the adsorbate.

The determination of the volume or weight of the adsorbed monolayer is achieved through consideration of kinetic theories, which attempt to model the adsorption of gases as observed in adsorption isotherms. Several books [114116] are available that fully describe adsorption theories and isotherms.

The Langmuir model [117] assumed that adsorption was limited to a monolayer and, as this is rarely the case, a better model was needed. In 1938, Brunauer, Emmett and Teller [119] developed a model which took into account multilayer adsorption, but could still determine the number of molecules or atoms of the adsorbate that formed a monolayer. This model is now well known as the BET theory and is the accepted method for carbon black surface area determination via multipoint gas (usually nitrogen) adsorption [120].

The BET equation has found great utility because it is simple to use and can generally model the five basic isotherms normally observed [118,121] and yields the most accurate results for surface area determination compared to other adsorption theories.

Nitrogen Surface Area

Nitrogen is the most widely used adsorbate for BET surface area determinations on carbon blacks. Studies on the use of other gases such as argon [122], krypton [123], and xenon [124] have been performed, but nitrogen remains the industrywide standard.

The BET nitrogen adsorption surface area can be determined using a single point or multipoint BET plot. The main advantages of the single point plot are speed of operation and reduced testing cost. However, this type of measurement is not as accurate as a multipoint BET plot. In spite of this, the single point method has and continues to yield reasonably accurate values for use as a quality control procedure.

The most common single point technique used in the carbon black industry is called continuous flow chromatography. With this

method a nitrogen/helium mixture is passed through the carbon black in a sample cell that is immersed in liquid nitrogen. Once adsorption is complete (as determined by a flat baseline on the GC recorder), the liquid nitrogen reservoir is quickly removed and the cell is placed in a heating mantle. The adsorbed nitrogen then desorbs which is detected using a thermal conductivity detector on the gas chromatograph. The resulting peak area yields the volume of nitrogen adsorbed. Since the amount of surface area that each cm^3 of nitrogen represents can be calculated [111], the surface area of the sample is easily determined. Commercial instruments based on this principle are available, e.g., Quantachrome Monosorb (Syosset, NY) and Micromeritics Flowsorb (Norcross, GA). These instruments have a counter that reads out the surface area directly in increments of 0.1 m^2 thus eliminating the need for the reference tables.

Typically a 5 point BET plot is used for a multipoint analysis and can take up to one hour to complete and is taken over the relative pressure range of 0.1 to 0.3 in increments of 0.05. The acquisition of a full nitrogen adsorption/desorption isotherm can take up to 24 hours. Commercial multi-

point instruments are available (Quantachrome, Autosorb and Micromeritics ASAP 2400) which are computer controlled and less operator, labor intensive.

Multipoint continuous flow instruments are also available commercially but these must utilize numerous nitrogen/helium gas mixtures (7.5 to 30 volume % N2) to obtain the BET multipoint plot. Thus, an accurate determination of the gas mixtures must be known for reliable measurements.

The BET (nitrogen) surface areas for the rubber and non-rubber grade carbon blacks are listed in Tables 2 and 3, respectively. For the non-porous rubber grade carbon blacks, the values are in good agreement with EMSA. The exception is N472 which contains considerable porosity that is available to the nitrogen molecule. This also applies to the three HCF and one of the MCF carbon blacks (Table 3). The N2SA values for the HCF samples range up to more than three times the EMSA measurements.

CTAB Surface Area

The adsorption of cetyltrimethyl ammonium bromide (CTAB) by carbon black in an aqueous solution is another method for surface area determination. Janzen and Kraus [125] have pointed out that the three requirements for accurate surface area measurements by adsorption of surfactants in an aqueous medium are: (1) the adsorption isotherm should have a long horizontal region at monolayer coverage, (2) enough of the surfactant should

Table 3. Typical Physical Properties of Some Non-Rubber Carbon Black Grades

Carbon	Mean part.	HI	EMSA	N2SA	CTAB	DBPA	Tinting

black type	diam. nm		m2/g	m2/g	m2/g	cm3/100g	strength
HCF*a*	8.9	1.47	295	430	300	95	133
HCF	11.3	1.40	235	575	330	95	135
HCF	16.4	1.58	148	525	270	98	135
MCF*b*	16.0	1.48	161	190	175	65	130
MCF	20.0	1.51	126	125	131	56	133
MCF	24.2	1.54	103	95	102	55	121
MCF	29.7	1.95	71	65	66	50	97
LCF*c*	73.5	1.51	34	33	33	63	64
LCF	85.7	1.56	28	25	29	75	48

*a*High color furnace.
*b*Medium color furnace.
*c*Low color furnace.

be adsorbed to yield accurate and precise values, and (3) analysis of the surfactant should be straightforward and reliable. The use of CTAB with sodium di(2-ethylhexyl) sulfosuccinate (Aerosol OT) meets the above criteria. CTAB was first used for carbon black analysis by Saleeb and Kitchener [126] and Aerosol OT was first used by Abram and Bennett [127]. The test method for CTAB surface area determination of carbon black is well described in the ASTM procedure [112].

Recently, Sanders et al [128] have modified the ASTM CTAB procedure by making the filtration and filtrate (CTAB) analysis automated. High pressure liquid chromatography was used to analyze the filtrate instead of a volumetric titration with Aerosol OT. This new method was shown to have a higher sample throughput and to be more precise compared to the current ASTM procedure.

The CTAB molecule is much larger than the nitrogen molecule. Thus, this test finds its utility in the fact that any contributions to the surface area from external porosity are basically eliminated. The CTAB method measures the so called smooth surface area of the carbon black that is accessible to elastomers and other vehicle systems. Janzen and Kraus [125] have shown a good correlation for the difference between nitrogen and CTAB surface area versus known pore area. Finally, another advantage of the CTAB method is that it, like nitrogen adsorption, is relatively unaffected by normal surface chemical groups, but may be influenced if severe chemical treatment of the surface has occurred.

CTAB surface areas for the rubber and non-rubber grades are listed in Tables 2 and 3, respectively. For the larger particle size rubber

blacks (e.g. >24 nm mean diameter), CTAB shows good agreement with N2SA and the values are in line with the changes in particle size. For the finer N220, N234, N121 and N110 samples, however, the CTAB values are all notably lower than the N2SA values because of microporosity. The differences are much more apparent for N472 and the highly porous HCF carbon blacks in Table 3. Here, the corresonding CTAB values are 130 to 250 m2/g lower than the N2SA measurements, and neither method is indicative of the large differences in particle size.

Iodine Adsorption Number

The adsorption of iodine by carbon black is also used as a measure of the surface area and is probably the most commonly used procedure for manufacturing quality control of furnace blacks. The iodine number is expressed in milligrams of iodine adsorbed per gram (mg/g) of carbon black and is not a true surface area. However, the concentration of the iodine solution has been adjusted so that the values are generally in good agreement with the nitrogen surface area for nonporous and nonoxidized carbon blacks.

It should be noted that the iodine number is affected by porosity, surface

impurities and surface oxidation. Iodine adsorption can be increased by the presence of porosity although not as much as nitrogen due to the larger size of the iodine molecule. Surface impurities such as residual oil or oil used for beading will depress the iodine number. The presence of these hydrocarbon extractables can be determined via the light transmission of a toluene extract of the carbon black [129]. The presence of high levels of surface oxygen functionality, which is typical of many carbon blacks used in paint and ink applications, will also cause a severe reduction in the iodine number by as much as 40%. The oxygen groups on the surface of the carbon black actually react with the potassium iodide in the test solution, thereby causing a release of free iodine which makes the surface area appear to be lower. Thus, care must be exercised when testing unknown carbon black samples for iodine number. However, for routine production control or quality assurance testing of known grades, the iodine test is widely used.

Other Surface Area Methods

Other adsorption methods [130132] have been used for the surface area determination of carbon blacks. However, none of these methods have found widespread use throughout the industry on a routine basis as have the nitrogen, CTAB and iodine surface area tests.

One of these techniques is similar to the nitrogen adsorption method, but the amount of gas adsorbed is determined by gas chromatography and not by pressure measurements. This is the headspace gas chromatographic (HS-GC) method and was developed by Pauseh and McKallen [132]. The technique utilizes the adsorption of a hydrocarbon with a high boiling point near

room temperature. It was determined that n-octane was a suitable adsorbate. The procedure involves the injection of 1 mm3 doses of n-octane into a headspace vial containing a 0.1 gram sample of vacuum dried carbon. The amount of unadsorbed n-octane is then determined by GC analysis of the hydrocarbon concentration in the headspace. Finally, the value of $1/CW$ (where the term C is the vapor phase concentration of the adsorbate and W is the weight of the sample) is determined, and from calibration plots of $1/CW$ versus the surface area, S, for known surface area blacks (from N2SA measurements) the surface area of the unknown can be determined.

The HS-GC method requires larger doses for high surface area carbon blacks (140 m2/g) and is less precise in this range. It also measures the smooth surface area, as the n-octane molecule is sufficiently large so that microporosity is not detected. The headspace method is rapid with little labor involved and thus could be suitable as a routine method of surface area determination.

3.3.4. Porosity

The characterization of porosity in carbon blacks is important from a practical and theoretical standpoint. As already mentioned, porosity can affect surface area measurements and other tests. It can also influence certain applications and properties by increasing the effective loading of the carbon black. Theoretically, porosity is also of fundamental importance in understanding the microstructure and formation of carbon blacks. Several books [114,115] are available that contain information on the analysis of porosity in materials.

The porosity in carbon blacks can be divided into two categories, open and closed porosity. The open porosity can be in the form of small pores of the order of nanometers of an undefined shape on the surface which may or may not provide access to internal voids. If the internal voids are not accessible to the surface, they represent closed porosity. Internal porosity may occur as a result of oxidative hollowing-out of the centers of individual particles within an aggregate [6,4951]. This type of porosity is accessible to small gas molecules and will affect surface area measurements in two ways: (1) additional internal surface is measured, and (2) the total number of aggregates per unit weight increases from the oxidative carbon removal. A second type of internal porosity which exists in the more disordered core of the carbon black particles [52,54], is generally closed to the surface, particularly after heat treatment of the carbon black at high temperatures [6,51].

The primary methods for determining the degree of porosity in carbon blacks are based on density and gas adsorption techniques. Mercury porosimetry is not considered a viable method, especially

for small particle size carbon blacks, because the very high pressures that are required can result in compression of the sample. The determination of the density can be done in several ways and will be discussed in Section 3.4.1. It should be noted, however, that density measurements do not provide direct information on pore sizes and their distributions. Density provides information on the total closed and open porosity through the comparison of measurements made in different media. For gas adsorption techniques, models or theories have been derived which can yield information on pore sizes, their distribution, total volume, and total surface area contributions.

Pores are typically categorized into three size ranges: (1) pores >50 nm are termed macropores, (2) pores >2 nm and <50 nm are termed mesopores, and (3) pores <2 nm are termed micropores. Many porous materials with meso and macropores will exhibit hysteresis in a full adsorption-desorption isotherm. The observed hysteresis is a result of the gas desorbing from inside the pores in a different way than it was originally adsorbed into them [114]. Most hysteresis loops become closed at relative pressures of approximately 0.3 [114], which, according to the Kelvin equation [133], corresponds to a

pore radius of approximately 1.5 nm. The form of the hysteresis loop has been shown by deBoer [134] to depend on the pore shape. He has identified five different hysteresis loops representative of five different type pores which include slit shaped, wedged shaped, wedged shaped with narrow necks, and bottleneck pores. However, in most studies on the porosity of carbon blacks via gas adsorption, including highly oxidized carbon blacks, the hysteresis has not been observed. This includes the highly porous HCF samples listed in Table 3. For most carbon blacks, therefore, the open porosity is predominantly in the micropore range (<2 nm).

One of the first methods developed for pore size analysis of carbon blacks and other reinforcing pigments was proposed by Voet [135, 136]. His method was based on comparing the reduction in the amount of nitrogen adsorption for a porous material to that of a non-porous surface. The value compared was *n,* the statistical average number of gas molecule layers adsorbed on the surface at various relative pressures. The value of *n* is calculated by dividing the amount of nitrogen adsorbed at various relative pressures by *VM,* the volume of a monolayer. Voet was able to calculate the percent pore area for a given *P/Po* range and, employing the theory of Barrett, Joyner and Halenda [137], obtained plots of percent pore area versus pore diameter.

The data of Voet [135, 136] showed the effects of oxidation on carbon blacks. An EPC (Easy Processing Channel) black with no post treatment had essentially 0% pore area while an MPC (Medium Processing Channel) black with some further thermal oxidation had an 18% pore area. Monarch 74 indicated a 25% pore area while the highly oxidized Carbolac I had a total pore area of

55%. It was noted that as oxidation was increased, more and smaller pores were produced.

In another study on five different carbon blacks, Walker and Kotlensky [138] utilized a method by Pierce [139,140] to determine the volume of nitrogen required to completely fill the micropores. Again, it was shown that the more highly oxidized carbon blacks contained significantly greater pore volumes compared to those that were not oxidized.

Atkins [141] calculated a cumulative surface area for several carbon blacks using the improved BJH method developed by Cranston and Inkley [142]. For graphitized carbon blacks with no porosity, the agreement between the BET nitrogen surface area and the cumulative surface area was good. However, for a highly air-oxidized carbon black with pores <1.0 nm in diameter, the BET nitrogen surface area was higher than the true value (i.e., the smooth surface area value) while the cumulative surface area was lower. This work demonstrated that the lower limit for pore size determination using the BJH [137] and Cranston and Inkley [142] methods is of the order of 1 nanometer.

A method of micropore analysis termed the *t-* method was developed in

1964 by Lippens, Linsen, and deBoer [143149]. This method is viable for pore size analysis down to 0.7 nm and yields information on pore shape, size, distribution and the sample's surface area. The method is based on plots of the volume of nitrogen adsorbed, *VA,* versus the statistical layer thickness of nitrogen, *t,* for a nonporous reference standard. The term, *t,* is called the statistical layer thickness due to the fact that the adsorbed gas molecules do not actually cover the entire surface of a pore wall in monolayer increments. Rather the adsorbed molecules exist in stacks of various heights and thus the *t* layer thickness is termed a statistical thickness. It has been shown that the value of *t* can be calculated as follows [143]:

$$t \ (nm) = 0.354(Va/Vm) \ (5)$$

where 0.354 is the thickness of a single layer of nitrogen molecules (assumes $N2$ has a density of 0.81 g/cm3 at -196°C with spherical geometry and hexagonal close packing). There are, however, differences in the literature [143,149,150] on the exact values of *t* for nitrogen at various relative pressures which are partly due to differences in the assumptions made about the nature of the packing of the nitrogen molecules adsorbed on surfaces. For carbon black though, the t values of deBoer [143] generally have been used and were confirmed to be applicable to carbon black by Voet and Aboytes [151]. They used a fine thermal carbon black treated with methane at 1050°C to essentially seal off all porosity.

A *VA - t* plot for a flat, nonporous surface yields a straight line that passes through the origin. If pores are present, a break in the *VA - t* curve will occur. A sharp break indicates a narrow pore size distribution, while a broad bend indicates a wide size distribution.

An increase of the slope in the V_A - t plot indicates pores filling by capillary condensation, while a decrease in the slope indicates pores filling by multilayer adsorption (for $P/P_o < 0.75$) since a net reduction in available surface area occurs once these pores are filled.

There have been several studies [149,151154] on the porosity of carbon blacks utilizing the t-method or improved versions of this procedure. deBoer, Linsen, Plas and Zondervan [149] analyzed five carbon blacks and found that only very small pores on the order of 0.7 to 1.5 nm were present. They assumed slit shaped pores because of the downward break in the V_A - t plot and also suggested that pores <0.7 nm were present for oxidized channel blacks because the intercept of the V_A - t plot did not pass through the origin. However, due to the limitations of the t-method, they were unable to quantify the size of these pores.

Voet, Lamond, and Sweigart [155] carried out a thorough study on a variety of carbon blacks that included normal furnace, channel and acetylene, along with oxidized carbon black and partially graphitized samples which

were heat treated in an inert atmosphere at 1400°C for three hours. Their measurements on oxidized carbon blacks agreed with deBoer et al [149] in that they had non-zero intercepts, but they also found non-zero intercepts for normal furnace blacks of low porosity with low BET C values of 200400. They suggested that this was caused by a residual surface homogeneity in the form of microcrystalline sites on the surfaces. The influence of these sites was no longer apparent at $t = 0.450$ nm, at which point a normal VA - t plot through the origin resulted. This idea was supported by the fact that the surface areas obtained from VA - t lines beginning at $t = 0.450$ nm agreed very well with the surface area values obtained from BET plots. This surface homogeneity extended out to $t = 0.60$ nm for the graphitized carbon blacks which showed a significant decrease in VA with a resulting non-zero intercept up to $t = 0.60$ nm. Porosity was not found in the graphitized carbon blacks but, as expected, a larger amount of porosity was observed in the oxidized samples versus the untreated furnace types. This is seen in Table 4 in which porosity data is listed for four standard furnace grades (N110, N220, N330, N700) and four oxidized carbon blacks. The St column is the total BET nitrogen surface area and Sx is the external surface area or the total surface area, St, minus the total pore surface area, Sp. As can be seen, the total amount of porosity and pores <0.9 nm in width increases with oxidation.

Table 4. Surface Area and Porosity Data for Normal and Oxidized Carbon Blacks

Carbon black	St m2/g	Sx m2/g	Percent surface area of pores of width (nm)a				Percent total pore area,	BET C value
			0.55	0.90	1.25	1.60		

							m2/g	
N110	133.0	99.3	0	13.9	4.4	7.0	25.3	-
N220	116.9	91.0	0	0	16.9	5.3	22.2	-
N330	88.7	70.2	0	8.6	10.7	3.5	22.8	290
N330 (oxidized)b	97.6	44.1	19.6	10.7	13.1	11.9	55.3	2650
SRF(N700)	22.5	18.6	0	0	9.3	8.3	17.6	260
SRF(N700) (oxidized)b	39.3	24.8	11.5	7.1	10.4	7.9	36.9	700
Mogul Ac	275.4	107.4	52.4	1.0	0	7.6	61.0	3950
Carbolac 1c	942.0	375.0	48.8	3.2	0	8.2	60.2	2000

aAssumed slit shaped pores with a width of 2t.

bOxidized with air at 300°C.

cHighly oxidized, high color channel black.

Reprinted with permission from ref. [151], Pergamon Press plc.
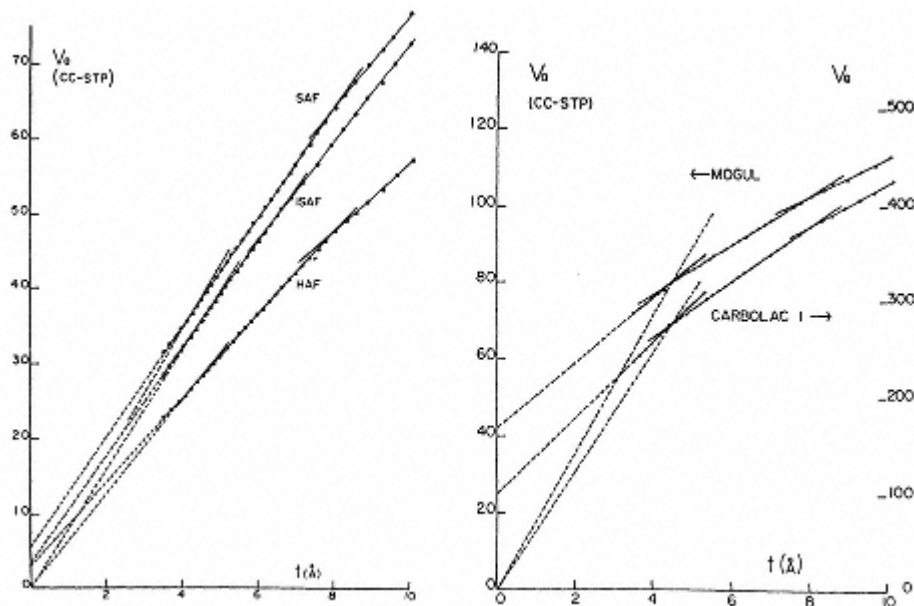
Fig. 17.
V_a-t plots for normal carbon blacks (N110, SAF; N220, ISAF; N330, HAF) and two highly oxidized HCF carbon blacks (Mogul and Carbolac 1). V_a is the volume adsorbed and t is the statistical layer thickness. Reprinted with permission from ref. [151], Pergamon Press plc.

The BET C constant increases with oxidation due to the increased adsorbate/adsorbent interaction in the pores where two surfaces are available for interaction instead of only one.

Also, as seen in Fig. 17, all the V_A - t plots in this study contained sharp breaks indicating pores of discrete widths, which again suggested slit-like pores as reported by deBoer [149]. However, Voet et al [155] noted that the pores present were in increments of 0.35 nm which is the approximate average spacing of the graphitic layers in carbon blacks. Therefore, they postulated that the pores most likely resulted from the removal of graphitic layers by oxidation.

It should be pointed out that Smith and Kasten [152] also analyzed several oil furnace blacks (N110, N220, N330, N347, N550) using t vlaues they obtained on a fine thermal (FT) carbon black. They did not observe any breaks or non-zero intercepts in the VA - t plots for these oil furnace samples. However, they did observe non-zero intercepts for these samples when they used the t values of deBoer [143] that Voet et al [155] used and later were confirmed to be applicable to carbon black [151]. This demonstrates the importance of accurate t values when attempting to analyze porosity using the t-method.

Other studies on graphitized and non-graphitized carbon blacks have been carried out by Salinas-Martinez de Lecea et al [153] and Carrot, Roberts,

and Sing [156]. These workers used the t-method, the Dubinin-Radushkevick method [157] and the α_s method [156] to analyze the microporosity in the various carbon blacks samples that were studied. Carrot, Roberts, and Sing [156] showed that the BET surface area, *ABET,* and the α_s surface area value, *As,* agreed quite well for the non-graphitized blacks, while the *ABET* value for the graphitized blacks was lower than *As*. This was in agreement with previous findings [158].

Lastly, Kuwabara et al [159] have used the adsorption of He at 4.2°K to analyze for what they termed ultramicropores (<0.7 nm) and supermicropores (0.7 nm<w<2.0 nm) in activated carbon fibers. Because of the smaller size of the He atom compared to the N_2 molecule they detected up to 50% more pore volume in the carbon fibers.

Donnet and Voet [1] pointed out that the analysis of pore sizes and pore size distributions is a complex topic that does not at this time have any one complete solution. Also, the various models contain many assumptions that are not necessarily valid, e.g., the Kelvin equation assumes that all pores are cylindrical and the *t*-method depends on accurate values of *t* that are derived from a flat non-porous surface, for which there is disagreement in the literature. However, notwithstanding these shortcomings, much has been learned about porosity in carbon blacks utilizing the various pore size analysis models. Typical oil furnace carbon blacks, which comprise the vast majority of grades currently produced, contain very little porosity. The porosity that is present in these furnace grades, as well as those oxidized at high temperatures, is basically confined to the micropore range (<2 nm). Also, the *VA - t* plots for

porous carbon blacks typically show a decrease in the slope indicating that the pores are possibly slit-like in shape. Finally, the V_A - t and s methods both show that there is a reduced adsorption of nitrogen at 77°K for graphitized blacks from a P/P_o 0.05 to 0.30, which is also present as a knee on the adsorption isotherm. Thus, a multipoint BET calculated in this relative pressure range is actually too low compared to the true value, which can subsequently be calculated at higher relative pressures using the V_A - t or α_s plots.

3.3.5. Aggregate Size

Aggregates represent the true primary units of carbon black. However, unlike particle size which is not affected by mechanical handling, aggregate size is system dependent. High shear mixing in polymeric systems causes significant aggregate breakdown relative to the dry state.

Electron Microscope Measurements

The first studies directed at quantifying carbon black aggregate size distribution were carried out by Medalia and Heckman [80,98,160162]. Using transmission electron micrographs, these authors carried out the first image

analyses on carbon black. This was accomplished by manually digitizing the boundary of each aggregate silhouette and storing this information in a computer for computation of size (projected area) and other properties. A radius-equivalent ellipse was defined for each aggregate in order to determine anisometry (ratio of long and short axes of ellipse) and bulkiness (area of ellipse/area of silhouette).

To reconstruct the 2-dimensional aggregate images on micrographs to 3-dimensional structures, Medalia [80] employed the floc simulation techniques used by Vold [163] and Sutherland [164]. The number of particles per aggregate *(Np)* was derived as:

$$Np = (A/Ap)1.15 \ (6)$$

N110   N351

N650 ——|0.34 µm|—— N762
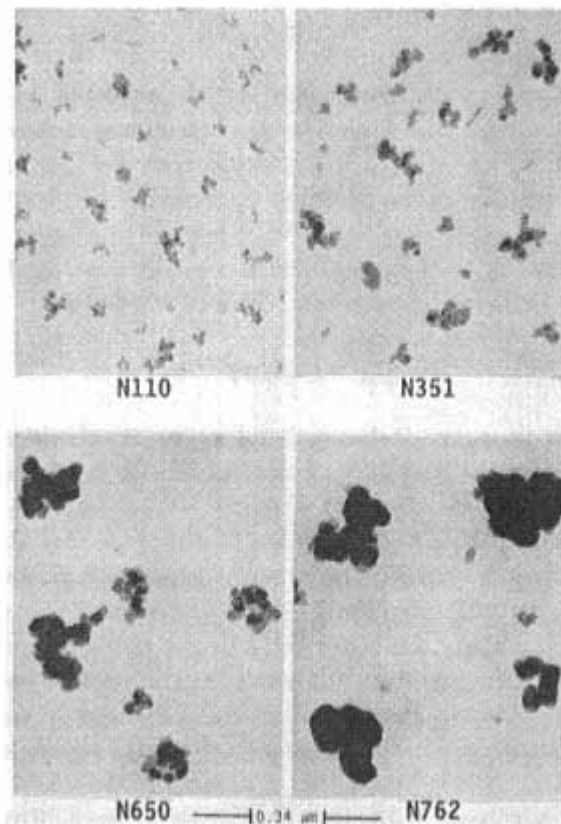
Fig. 18.
TEM of CAB dispersion showing particle
size differences among oil furnace
blacks (from ref. [96]).

where A is the projected area of the aggregate and A_p is the area of a particle. The latter value assumes that all particles are of the same size and density. The assumption of similar particle size within each aggregate is a reasonable approximation and can be seen visually in Fig. 18.

The development of TEM/AIA procedures [83,88,90,9396] enabled automated measurement of the various parameters defined by Medalia and Heckman, along with many other functions. Hess and McDonald [90,93,94] measured the volume of carbon black aggregates by means of microdensitometry. As a size function, volume has the advantage of not having to assume any particular aggregate shape. In carrying out this type of analysis it was found to be desirable to calibrate the densitometer using carbon black aggregates of known volume, i.e., single spheroidal particles found in thermal or other very low structure types. It was later determined that the volume, V, of carbon black aggregates could be derived more simply from the projected area, A, and perimeter, P.

$$V = 8/3(A^2/P) \quad (7)$$

This expression applies specifically to the projected images of spheres. Nevertheless, this model was found to give comparable results to the densitometer derived values when applied extensively to the full size range of non-porous rubber grade carbon blacks. A constant density was assumed in either case.

A more commonly used aggregate size classifier is an aggregate diameter, D_A, based on the projected area alone. This is derived as:

$$D_A = (4A/\pi)^{1/2} \quad (8)$$

and is determined from the 2-dimensional aggregate projection as a circle. Typical D_A values for the current commercial rubber grade carbon blacks are listed in Table 5. The measurements were carried out on these samples in the dry (as manufactured) state and are based on the same statistical parameters shown earlier for particle size. The average aggregate diameters vary from 68 nm (N110) up to 483 nm (N990). The differences are related to both particle size and structure, the latter reflecting a greater number of particles in the aggregate for any give size. For example, the smaller particle size N299 sample exhibits larger aggregate size than N326 because of its more complex structure. This also applies to the comparable average aggregate size for N660 versus N762.

It can be seen that the size distributions are much broader (higher HI values) for the aggregate diameters (Table 5) relative to the respective particle diameters (Table 2). This is further illustrated for D_A histograms in Fig. 19 which show the same four carbon black grades illustrated for particle size
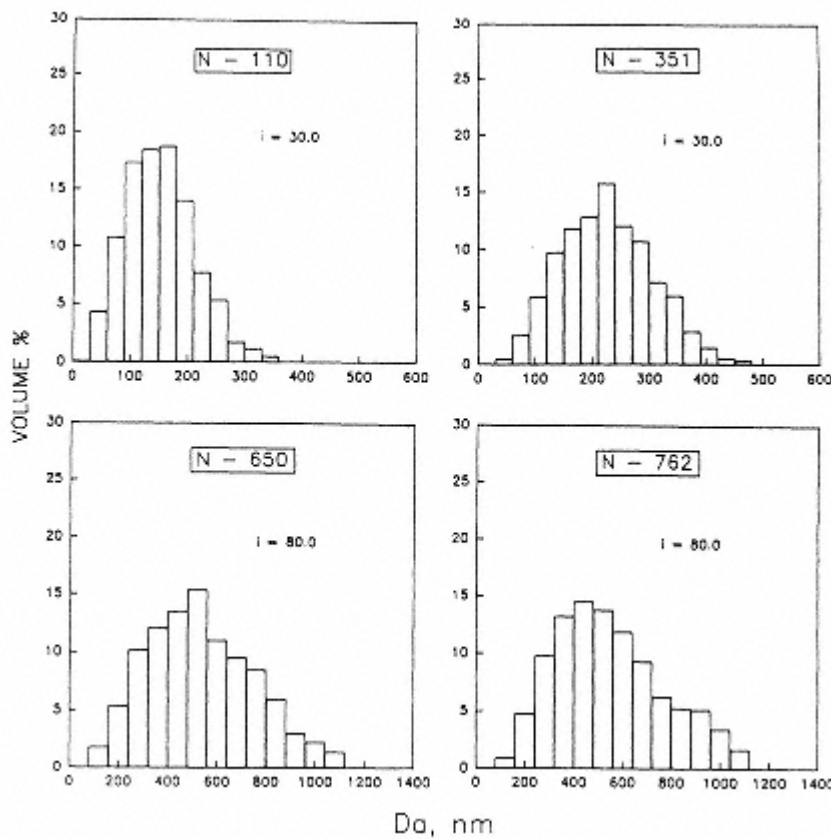
Fig. 19.
Aggregate diameter histograms for oil furnace carbon blacks in
the dry state.

distribution in Fig. 15. The aggregate diameter histograms are plotted as volume percent vs. D_A. Volume or weighted distributions provide better representation of the coarse tail of the distribution which tends to be low in number but high in volume. The weight mean aggregate diameter is near the peak value for these histograms. Since carbon blacks are normally compounded on a weight basis, the weight mean diameter is probably the best single value for comparing the different grades for aggregate size. However, distributional properties are important in how the aggregates will pack, both in the dry state and in different vehicles

(e.g. polymers and oils). Maximum packing density is achieved with a very broad aggregate size distribution [165]. Medalia and Sawyer [166] carried out studies on blends of different grades of carbon black which varied widely in particle size. They demonstrated that a blend of 60% MT and 40% of a small particle size black (Elftex 5) would actually occupy only 89% of the combined volumes for the same amounts of each black measured alone. Therefore, broad size distributions reduce the total packing volume by enabling the smaller aggregates to fit into the voids

Table 5. Typical Aggregate Morphological Properties of Rubber Grade Carbon Blacks

| ASTM number | Aggregate diameter[a] | | | | | DBPA[b] cm3/100g | Compressed DBPA[c] cm3/100g |
	Dwd, nm	M, nm	Wm,, nm	HI	V'/V		
N110	85	68	135	1.98	2.23	113	101
N121	-	77	151	1.96	2.50	133	110
N220	-	78	158	2.03	2.21	114	99
N234	97	80	164	2.05	2.48	125	109
N299	-	93	181	1.95	2.43	124	104
N326	98	87	177	2.03	1.64	71	68
N330	133	105	225	2.14	1.96	101	85
N339	104	103	211	2.05	2.41	121	104
N351	126	129	253	1.96	2.43	120	92
N358	153	136	275	2.02	2.92	155	110
N550	240	234	482	2.06	2.45	122	81
N630	-	220	440	2.00	1.40	77	69
N650	-	271	566	2.09	2.63	126	83
N660	283	252	535	2.12	2.15	91	73
N762	-	255	482	1.89	1.33	65	62
N774	261	228	470	2.06	1.45	77	67
N990	436	483	811	1.68	0.46	38	34

aASTM D 3849-89 (Dispersion Procedure A, Dry State).
bASTM D 2414-90.
cASTM D 3493-90.
dStokes diameter, from DCP [173].

within and between the larger aggregates.

Liquid and Aerosol Measurements

Other methods available for carbon black aggregate size

determination include: disc centrifuge photosedimentometry (DCP), sedimentation field flow fractionation (SF3), capillary hydrodynamic fractionation (CHDF), dynamic light scattering (DLS), and differential mobility (DM). An extensive review describing these and other particle size analysis techniques in terms of their general principles of operation and size measurement limits has been written by Barth and Sun [167]. Typically the liquid and aerosol techniques measure carbon black aggregate size using an aqueous dispersion with a small (<0.05%) amount of surfactant.

The disc centrifuge photosedimentometry (DCP) technique has probably been the most commonly utilized non-microscopic method for carbon black aggregate size determination. However, relatively few papers have been

published [168174]. A thorough description of centrifugal sedimentation has been given by Kaye [172]. The aggregate size distribution is determined using Stokes' law, modified for centrifugal sedimentation. The concentration of aggregates in a certain size range is measured by the degree of attenuation of a light beam as the aggregates settle. The measured aggregate diameter is termed the equivalent Stokes diameter, DST, and is defined as the diameter of a sphere of equal specific gravity which settles in a centrifugal field at the same rate in the same fluid as the aggregate. The accuracy of the method depends upon the quality of the carbon black dispersion and the values used for the light absorption coefficients of the carbon black aggregates of various size ranges, which are not well known.

Patel and Lee [173] have published the most comprehensive range of carbon black Stokes diameters to date, which are included in Table 5 (listed as Dw). These values are typically between the mean (m) and weight mean (Wm) TEM/AIA DA values for those same grades listed in this table.

Comparisons between TEM/AIA aggregate size data and DCP aggregate size data are difficult, but it is generally thought that for a given aggregate the TEM/AIA data would be larger than DCP data. This is due to the extra drag experienced by the higher structure aggregates in the DCP which shows their sedimentation rate and results in a smaller Stokes diameter. This type of behavior has been cited by Shieh et al [174] to explain the apparent bimodality observed in DCP curves of certain high structure carbon blacks. However, the situation may be much more complex due to the distribution of aggregate shapes present in a grade of carbon

black and the relative orientations they assume upon sedimentation in the disc centrifuge.

The main advantages of using the DCP technique (relative to TEM/AIA) for carbon black analysis pertain to lower equipment cost, simplicity of operation, the very large sampling of aggregates and the applicability to very broad distributions. The major disadvantages of DCP relate to the fact that it can provide no specific information on aggregate shape or particle size because of the assumption that the discrete entities in the dispersion are spheres. Therefore, without data from other test procedures, a precise interpretation of the DCP test results on different carbon blacks is not possible, i.e., in determining whether the observed differences are particle size or structure related. In addition, there is no good method for precisely monitoring the quality of the carbon black dispersions.

The scattering and absorption of light by carbon blacks in dilute suspensions has also been applied to measure carbon black aggregate size [110,175]. Stacy, Johnson and Kraus [110] measured the changes in the optical extinction coefficient for dilute suspensions of carbon blacks which were passed through cylindrical pore filters of precisely known diameters. Retention diameters for aggregate size were derived from the distribution curves.

Janzen [175] applied Mie theory to the absorption and scattering of light by dilute carbon black suspensions employing spectrophotometric determinations. Two aggregate diameters (nm) were derived for a wide range of carbon blacks: Xg (geometric mean) and $X606$, a higher moment of the distribution which was related to its breadth. The $X606$ values indicate a reasonably good correlation with TEM/AIA DA values for comparable carbon black grades.

3.3.6. Aggregate Shape

Carbon black aggregates vary in shape from the individual spheroidal particles that are found in thermal carbon blacks to the more clustered and fibrous types that are common in all other grades. The presence of these more complex shapes creates internal voids within any given bulk sampling of carbon black which are much greater than those that occur in a simple packing of spheres. It is not surprising then that the most commonly used techniques for measuring carbon black structure have been based on internal void volume using absorptive measurements or volumetric measurements under specific pressure conditions.

Absorptive Properties

The absorptive capacity of a carbon black for liquids is predominantly related to aggregate shape, i.e., aggregates with a highly open, branched structure are capable of absorbing more vehicle both internally and in the voids between them and other aggregates in comparison to closely packed particle aggregations or individual spheres. In the latter instance (e.g. thermal blacks) internal aggregate occlusion of vehicle is essentially zero. High

absorption can be achieved with either large particle size (very large voids) or small particle size (greater number of smaller voids).

A method for measuring the oil absorption of carbon black was described by Sweitzer and Goodrich in 1944 [26]. Linseed oil was added dropwise to a one gram sample of carbon black and mixed with a spatula using moderate pressure. During this process tiny pellets are formed which gradually increase in size and diminish in number as additional oil is added. An end point is reached when a single ball of stiff paste is formed, indicating that the voids within the carbon black have been filled with oil. The higher the oil absorption per unit weight of black, the greater the extent of the aggregate structure. Absorption occurs both within the aggregate branches and between contacting aggregates in a 3-dimensional network.

A less subjective, automated oil absorption test was developed by Eaton and Middleton [176]. This is based on the use of a torque measuring absorptometer (Brabender Instruments, Inc., Hackensack, N.J.). The oil, di(*n*-dibutyl) phthalate (DBP), is added continuously to the carbon black using a constant rate buret and incorporated by means of high shear mixing. There is a sharp increase in the viscosity of the mixture when it changes from

a free flowing powder to a semiplastic continuous mass. This sharp viscosity increase is accompanied by a rapid rise in torque. The instrument stops automatically at this point of torque increase and the amount of DBP absorbed is registered on the buret digital counter.

The DBP absorption test (DBPA) is now one of the most widely used methods for measuring the level of aggregate absorptivity in carbon blacks and is an ASTM Standard Method [177]. A second version of this test was developed by Dollinger and coworkers [178]. In this test the black is compressed in a cylinder at 165 MPa (24000 psi). This operation is repeated a total of four times, breaking up the compressed lump of carbon black after each individual compression. The final sample is then measured for DBPA in the absorptometer in the same manner as the regular test. The compressed DBPA procedure is also an ASTM standard method [179]. Its major purpose is to approximate the level of aggregate structure that may exist after a carbon black is mechanically mixed into a vehicle system. Comparison of the standard and compressed DBPA values also provides an approximation of the stability of the carbon black aggregate structure. Typically, the higher structure carbon blacks show a greater drop in DBPA with compression than low structure types. This is apparent in Table 5, which lists the DBPA and compressed DBPA values for the rubber grade carbon blacks. Low DBPA carbon blacks such as N326 and N990 exhibit very little difference between their regular and compressed values. The level of breakdown increases with increasing particle size, however, and it is apparent that blacks such as N550 and N650 exhibit much greater breakdown than comparable DBPA carbon blacks in the

tread black particle size range. One possible reason for this is the higher percentage of linear type aggregates in the coarser grades. This will be discussed further in the section on electron microscope measurement of aggregate shape.

The usefulness of the compressed DBPA test cannot be questioned. However, some caution should be exercised in the interpretation of this test in terms of forecasting carbon black aggregate breakdown in different vehicles. Breakdown may vary considerably according to vehicle type and mixing procedure. Furthermore, the breakdown of carbon black during compression may also be influenced by inter-aggregate surface attraction, or by the breadth of the aggregate size distribution. A broad distribution carbon black will compress into less volume because the smaller aggregates collect between the larger ones. This causes greater compaction of the sample, while at the same time preventing the larger aggregates from undergoing further distortion and breakage.

Specific Volume Measurements

A second procedure for determining the void volume within the carbon black aggregate structure is based on the volume of a given weight of carbon

black at a specified level of pressure. Studebaker [8] measured the specific volume of rubber grade carbon blacks at a fixed pressure of 5.06 MPa (734 psi) and the values showed a good correlation with mineral oil absorption. Mrozowski [180] carried out more comprehensive studies on a limited sampling of carbon blacks and other type carbons. His studies were performed at the much higher pressure of 35.2 MPa (5100 psi). Mrozowski emphasized the importance of the smoothness and hardness of the cylinder walls in carrying out this type of study. He used relatively small samples of black (1 g) in a glazed porcelain cylinder (with copper plungers) to minimize wall effects in his compression studies. He also showed the effects of heat treating (inert atmosphere) the carbon blacks at temperatures ranging up to 2800°C. At very high temperatures most samples showed a reduction in void volume. Carbon blacks containing high surface oxygen functionality showed a sharp increase in specific volume at heat treatment temperatures in the range of 10001200°C. It is likely that this was attributable to inter-particle sintering following removal of the chemisorbed oxygen. These results demonstrate that variations in surface properties can also influence the compressibility of carbon blacks.

Voet and Whitten [181,182] applied the Mrozowski technique to a broad range of rubber grade and other types of carbon blacks using a wide range of pressures. Specific volume exhibited a linear relationship to the logarithm of pressure except at very low pressures below 0.07 MPa (10 psi) or very high pressures above 69 MPa (10000 psi). This relationship is illustrated in Fig. 20 [182] for eight different rubber grade carbon blacks ranging from the N200 to N700 particle size levels. The higher structure carbon blacks

clearly show the highest specific volume at any given pressure and also the sharpest drop-
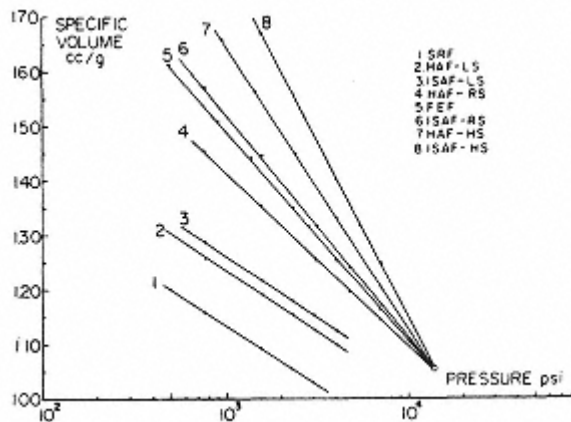
Fig. 20.
Specific volume-pressure relationship for
carbon blacks (from ref. [182]).

off in volume with increasing pressure. Voet and Whitten reported that the plots could be extrapolated to a common point at about 90 MPa (13000 psi). At this point, the void volumes are approaching the calculated value for a random packing of contacting spheres of the same size.

From the typical plots shown in Fig. 20, Voet and Whitten concluded that a pressure of about 9.79 MPa (1420 psi) was a good single point measurement for comparing specific volumes among different grades of carbon black. Medalia and Sawyer [166] preferred multipoint measurements which were carried out at pressures up to 51.7 MPa (7,500 psi) on carbon blacks compressed in a stainless steel cylinder. The void ratio, σ, for each carbon black was expressed as:

$$\sigma = A - B(log\ P)\ (9)$$

where P is the pressure and A and B are constants representing the intercept and slope, respectively, of the linear plot. The values for the slopes, B, gave the best correlation with oil absorption while the intercept, A, equals the void ratio at about 0.007 MPa (1 psi) and is indicative of the void ratio in a pellet of the uncompressed carbon black.

More recent application of the specific volume technique has been reported by Patel [183,184]. A capillary rheometer was modified for these measurements by substituting a steel plug for the extrusion die.

Electron Microscope Measurements

The first direct measurements on carbon black aggregate shape

were reported by Cohan and Watson [25]. They derived a shape factor for different carbon blacks based on the ratio of the average chain length to average width. This type of anisometry factor was also reported by Hess and coworkers [88,93] using TEM/AIA. Aggregate form factors were derived from the total projected length divided by the average width (mean chord) as well as the ratio of longest dimension (longest Feret diameter) to the average width.

Medalia and Heckman [160162] reported an aggregate anisometry factor based on the radius equivalent ellipse defined for each aggregate. This factor represents the ratio of the long and short axes of the ellipse. They also described a bulkiness factor from the area of the ellipse divided by the projected area of the carbon black aggregate. Bulkiness was found to correlate more directly with known variations in absorptive properties in comparison to anisometry. However, the best relationship to DBP absorption was indicated for the number of particles per aggregate.

In a later publication, Medalia [185] carried out a more detailed treatment on aggregate absorptivity from electron microscope images. For each aggregate he defined an equivalent sphere based on the measured projected area as a circle. The Volume, V', of liquid which could be absorbed within a given aggregate was defined as the volume of the equivalent sphere, V_{es},

less the volume, *V,* of the solid carbon in the aggregate. From the estimated packing of the equivalent spheres for the full carbon black aggregate size distribution, Medalia was able to derive absorption values for different carbon blacks which were in reasonably good agreement with the respective DBPA values. The following relationship was reported:

$$V'/V = (DBPA - 21.5)/68.26 \quad (10)$$

Despite the empirical nature of this equation, which includes certain assumptions and corrections for aggregate packing and alignment, it is an extremely useful relationship to account for the occlusion of polymer when carbon black is mixed into elastomers and other vehicles [185187].

McDonald and Hess [90] and more recently Herd et al [188] used Medalia's equivalent sphere concept to measure *V'/V* for a broad range of carbon blacks using TEM/AIA. In the recent work, the diameter of the equivalent sphere was measured as an average of that for the Medalia model (area) and a sphere based on the average Feret diameter. The Feret diameter is a measure of the distance between parallel tangents to the aggregate boundaries in a specific direction. Earlier TEM/AIA [93,94] measurements were limited to four Ferets at 45° angular increments. Current image analysis equipment is capable of a much larger number of measurements to more accurately define the values for longest, shortest and average Feret diameter.

The *V'/V* values for the rubber grade carbon blacks are listed in Table 5. These data, along with values for a few additional carbon blacks, were plotted against DBPA, and show a good correlation

[188]. But it should be noted that the major advantages of the TEM/AIA measurements pertain to their ability to provide distributional information and to measure the absorptivity of carbon blacks as they may exist in specific vehicle systems.

Transmission electron micrographs and V'/V distribution curves (dry state) are shown for four N300 carbon blacks of varied DBPA in Figs. 21 and 22, respectively [188]. The V'/V curves are plotted over a range interval of 0.50. The distributions broaden markedly with increasing DBPA with individual aggregate void volume ratios as high as 7 to 10× existing for very high DBPA carbon blacks [189]. Considerable breakdown of the larger, more irregular aggregates occurs in rubber and other high viscosity vehicle systems. It was observed that when these four N300 carbon blacks were subjected to the ASTM D3849 dispersion procedure in cellulose acetate butyrate (CAB), most of the highly irregular aggregates were broken down in the high shear (2-roll mill) CAB mix and the four carbon blacks were now quite similar in appearance. Fig. 23 compares the V'/V distribution curves for N358 in the dry state and in CAB, the latter showing that most of the aggregates with V'/V greater than 2.0 have been broken down.

Hess and coworkers [190] measured the changes in aggregate length, width and length/width ratio in rubber compounds relative to the dry state
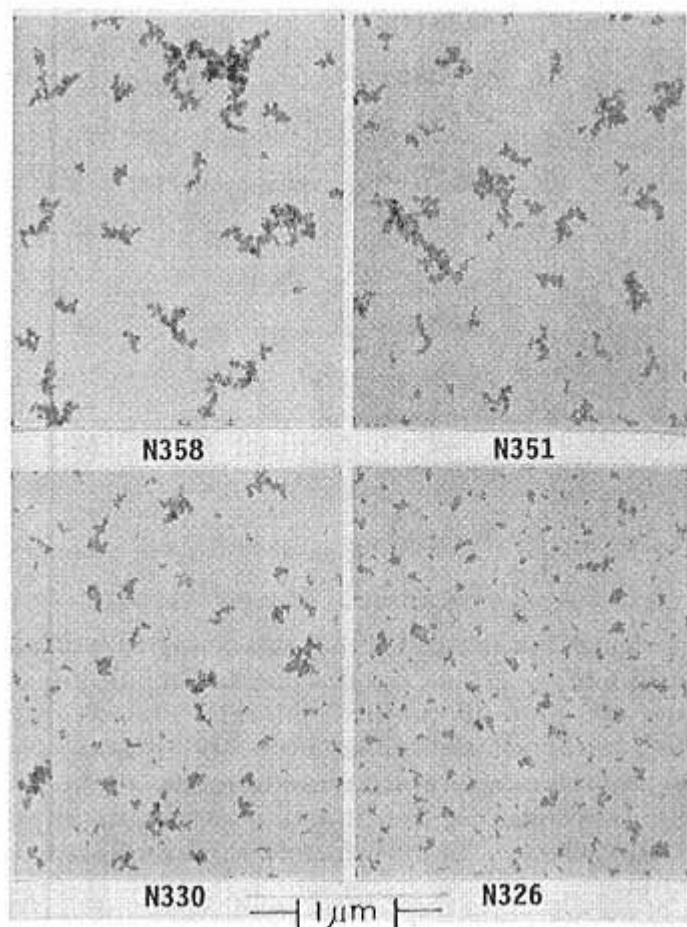
Fig. 21.
TEM of N300 carbon blacks (dry state) of varied
DBPA (from ref. [188]).

for a number of different carbon blacks. Typically, aggregate
breakdown was greater for the large particle size, higher DBPA
type carbon blacks. Breakdown was also studied by compressing
the carbon blacks at 165.5 MPa (24,000 psi) and by ball milling.
The latter was carried out in a vibratory ball mill operating at a
frequency of about 100,000 Hz and an amplitude of about 6.4 mm
using steel balls which were about 1.6 cm in diameter. A 50/1
weight ratio of steel balls to carbon black was employed and the

samples were treated at varying times ranging from 4 to 120 minutes. Under these treatment con-
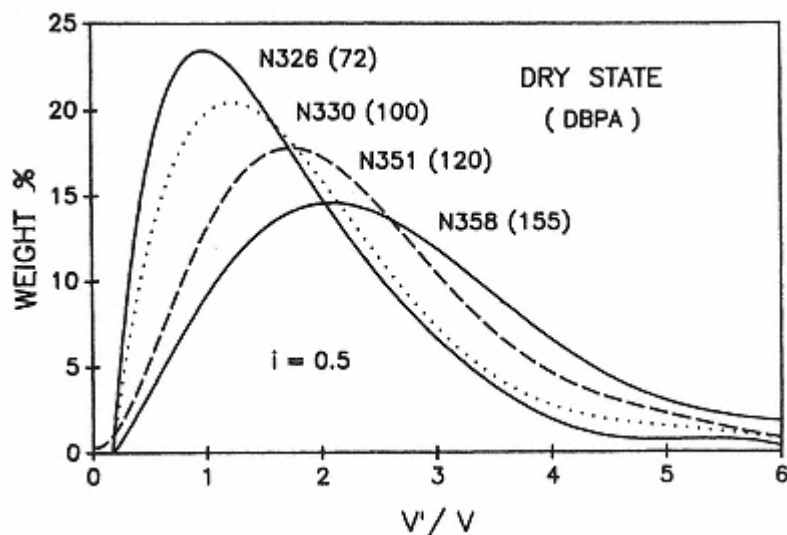
Fig. 22.
Distribution of V'/V for N300 carbon blacks of varied
DBPA (from ref. [188]).

ditions, it was found that all carbon blacks achieved a maximum level of breakdown in 15 minutes or less, and that further ball milling then tended to compact the aggregates into microagglomerates. At the maximum level of breakdown (4 to 15 min.) by ball milling in the dry state, the measured morphological properties for a broad range of rubber grade carbon blacks (N200N700) showed good agreement with respective values for the same samples in natural rubber. The correlation for the carbon blacks compressed
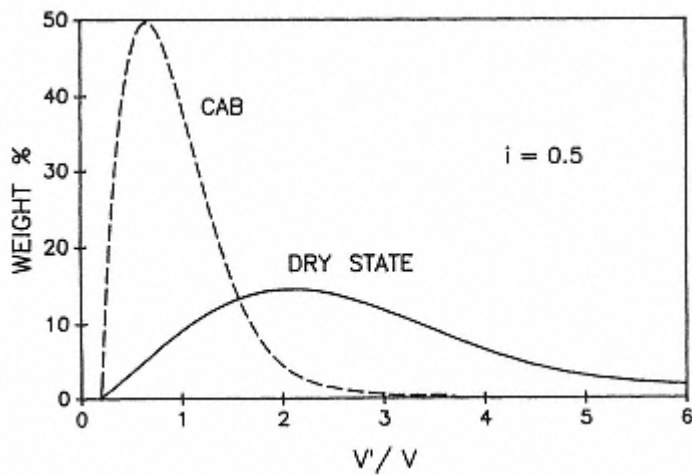
Fig. 23.
Distribution of V'/V for N358 in CAB chip relative
to the dry state (from ref. [188]).

four times at 165.5 MPa (24,000 psi) was considerably poorer. This appears to have been due, at least in part, to the difficulty in achieving satisfactory dispersions of the compressed blacks for TEM/AIA. The compression step highly compacts the carbon blacks and makes it difficult to disperse them ultrasonically. As mentioned previously, compaction is a possible factor influencing the compressed DBPA values. Insufficient breakup of the compressed lump of black prior to mixing with the dibutyl phthalate would tend to produce low values.

Specific Shape

Carbon black aggregates vary considerably in their actual shape, ranging from some near perfect spheres in thermal types to the grapelike clusters and chains that exist in other grades. The electron microscope undoubtedly remains as the best instrument for resolving shape differences among the individual aggregates of carbon black. These studies can be enhanced by viewing the aggregates 3-dimensionally, which has been accomplished almost from the very onset of transmission electron microscopy [22,23]. Stereo imaging is accomplished simply by rotating the specimen within the microscope to produce images at two slightly different angles (e.g. ~ 6° separation). TEM stereo pairs of different shaped individual carbon black aggregates have been published by Hess and coworkers [93]. Mercer et al [191] went a step further and actually measured TEM and SEM images of individual carbon black aggregates using a stereoscope. This type of analysis is not practical at the present time, but may be at a later date when some form of holographic imaging technique can be directly linked to an image analysis system.

Despite the obvious limitation of 2-dimensional imaging, the analysis of large samplings of aggregate projections can provide useful information pertaining to the shape difference existing among carbon blacks. A 1970 review by Medalia and Hornik [192] discussed the problems and the general progress made in the use of pattern recognition techniques to classify the various properties of carbon black. They cited the improvements made in determining aggregate shape factors but, at that time, fully automatic feature specific image analysis systems were not available commercially. The introduction of such systems about two years later [92,193] greatly enhanced this type of analysis and a number of non-dimensional shape discriminators then became available for routine analyses. Hess, McDonald and Urban [93] published a listing of 10 such discriminators which they employed to classify carbon black aggregates into nine shape categories. Among the most important of these shape classifiers were the aggregate length/width ratio and Feret standard deviation which both measure anisometry, and the perimeter squared/area ratio which provides a measurement of irregularity. The ellipsoidal model of Medalia and Heckman [160162] also provided good discriminators for irregularity. The most useful of these functions were the ratios of the ellipse/aggregate

perimeters and areas, the latter representing the bulkiness factor reported in those publications.

In a recent paper, Herd and coworkers [188] have classified carbon blacks into four easily discernible aggregate shape categories which are described below and illustrated in Fig. 24.

1.) Spheroidal

2.) Ellipsoidal

3.) Linear

4.) Branched

These studies were carried out using discrimination analysis techniques [194, 195] on data obtained with an on-line Quantimet 970 image analysis system (Leica Corp., Deerfield, Ill.) coupled to a computerized Philips CM-12 Transmission Electron Microscope [196]. Non-dimensional image shape classifiers similar to those reported earlier [93] were employed in these studies, along with additional functions based on the number of branches in the aggregate and how branching relates to some of the other shape parameters.

The use of discriminatory mathematical analyses to both classify and test the significance of the shape differences produced a great improvement over the earlier pattern recognition techniques. Based on rigorous analysis of the shape classifiers for a large sampling of aggregates, a set of descriptor equations was established to define the different shape categories. These equations are solved simultaneously for each unknown aggregate and the best
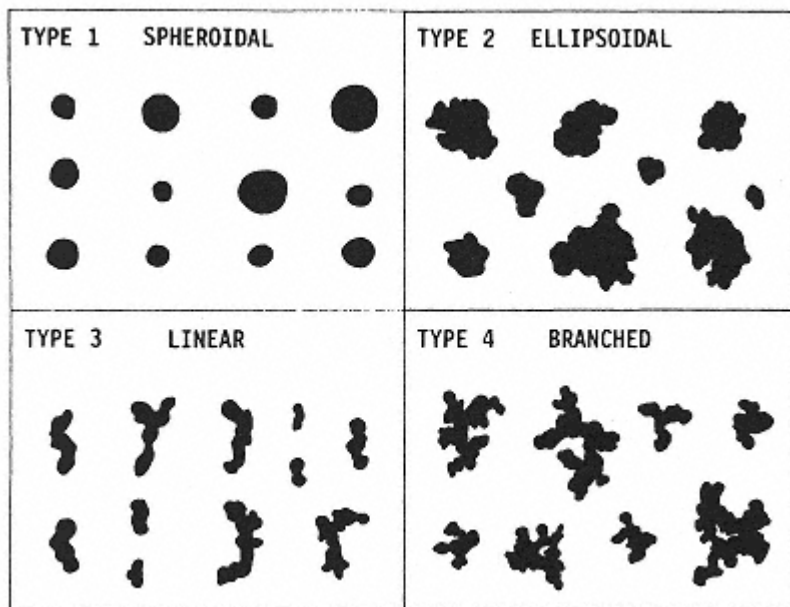
Fig. 24.
Shape categories for carbon black aggregates (from ref. [188]).

fit is employed to make the classification. Based on Hotellings T test [197], all of the four shape categories were found to be mathematically different at a high level of significance.

The shape classifications for 19 rubber grade carbon blacks of varied particle size and DBPA are listed in Table 6 [188]. The spheroidal category actually represents discrete particles rather than aggregates and only becomes significant for thermal blacks or very low DBPA types. The Type 4 (branched) aggregates tend to increase in the direction of increasing DBPA and diminishing particle size while Type 3 (Linear) shows the opposite pattern. Type 2 (ellipsoidal) aggregates increase with diminishing DBPA.

Aside from the known importance of carbon black aggregate shape to applications properties, the classification into specific shape categories may also provide useful information on the kinetics of aggregate growth in the reactor. There are obviously different conditions associated with the formation of linear chains of particles as opposed to the highly branched aggregates

Table 6. Weight Percent of Aggregates in Four Shape Categories for Various Carbon Black Grades (Dry State)

Carbon black	DBPA, cm3/100g	Weight, %			
		1	2	3	4
CD-2005	174	0.1	4.8	17.8	77.3
N358	155	0.1	7.9	34.9	57.1
HV-3396	138	0.2	4.2	33.4	62.2
N121	134	0.4	8.8	28.7	62.1
N650	129	0.2	9.2	47.0	43.6
N234	124	0.3	9.0	32.5	58.3
N299	124	0.4	10.0	33.2	56.4
N351	120	0.1	9.2	46.9	43.8

N550	120	0.6	13.8	45.3	40.3
N339	118	0.2	9.5	36.6	53.7
N110	115	0.3	8.7	31.1	59.9
N220	115	0.6	11.9	34.0	53.5
N330	100	0.2	10.2	44.1	45.5
N660	91	0.4	15.4	52.5	31.7
N630	78	0.4	21.4	49.0	29.2
N774	77	1.3	20.8	46.3	31.6
N326	72	1.6	23.4	35.2	39.8
N762	67	2.5	22.4	47.7	27.4
N990	35	44.9	34.8	14.4	5.9

that exist in current high DBPA furnace grades. The small ellipsoidal aggregates or single particles found in low structure carbon blacks are favored by reducing particle collisions either through charging (alkali metal addition) or dilution. Schaefer [198] has classified the growth mechanisms of silica aggregates into three basic groups: ballistic, reaction and diffusion limited. Fractal analyses of the resulting aggregates from each of these models were used to characterize the growth mechanisms of real systems.

The use of fractal geometry has currently seen wide acceptance in the characterization of irregular objects, both in terms of growth processes and end-use applications. The use of fractals to classify carbon blacks will be discussed in the next section.

3.3.7. Fractal Models

Most of the TEM/AIA methods described above for aggregate size and shape classification involve models based on geometrical objects such as spheres or ellipsoids, which are amenable to the laws of Euclidean geometry. This is done because of the complexity encountered in trying to fully describe the highly irregular nature of carbon black aggregates. Fractal geometry has emerged fairly recently as a means of quantifying the irregularity of non-Euclidean objects. There are many different types of fractals and the exact meaning of the fractal dimension, *D,* can vary depending on the model used. The use of fractal geometry has also allowed investigators to better understand a variety of phenomena ranging from aggregation kinetics to salary distributions [199]. Many books have been written on the subject [199203], with the actual concept of fractal geometry first being presented by Mandelbrot [200].

The first fractal analyses on carbon blacks aggregates were based on the irregularity of the profiles of two dimensional electron microscope images. This work was done by Kaye [204] and Flook [205] using the methods of Mandelbrot [206]. Basically, this method involved determining the perimeter of the aggregate profile using a smaller and smaller yardstick and has been termed the structured walk technique by Kaye [203]. The length of the perimeter *(P)* increases as the length of the measuring stick (λ) decreases and the slope of a plot of log *P* versus log λ yields the perimeter fractal, *Dp*. The value of *Dp* lies between 1 and 2 and the more irregular the profile, the larger the value of *Dp;* however, the values of *Dp* do not yield any information on the specific shape of the aggregates.

Recently, Gerspacher and O'Farrell [207] and Herd et al [188] have utilized the perimeter-area relationship of Mandelbrot [201] to determine a perimeter fractal for a broad range of carbon blacks. The perimeter-area relation is as follows:

$$P \sim A^{D/2} \quad (11)$$

where P is the perimeter, A is the area, and D is the perimeter fractal dimension. The slope of a plot of log P versus log A for a group of carbon black aggregates yields Dp. This perimeter fractal increases with increasing irregularity of the two-dimensional profile, but highly acicular type particles with a smooth perimeter can also give a high Dp. Therefore, some caution must be used in interpreting values of Dp.

Fig. 25 [188] is a plot of log P versus log A for 1000 aggregates of an N121 carbon black in the dry state and is representative of the data obtained for all grades analyzed. All data were obtained using a transmission electron microscope/automated image analysis (TEM/AIA) system and total analysis time was approximately 1.5 hours per grade. Table 7 lists the values of Dp obtained for 19 grades of carbon black ranging in surface area from 9 to 174 m2/g and DBPA from 35 to 174 cm3/100g. Across this broad range of carbon blacks, the values of Dp range from 1.05 to 1.35 and there appears to be a general correlation of Dp with DBPA. The increase in Dp with higher DBPA reflects the greater aggregate irregularity.

Other studies utilizing fractal analysis of TEM images of carbon black aggregates were performed by Bourrat and Oberlin [208] and by Ehrburger-Dolle and Tence [209]. These investigations utilized the mass fractal which yields information on how an aggregate's mass scales with its size. The general relation is

$$M \sim R^{Dm} \quad (12)$$
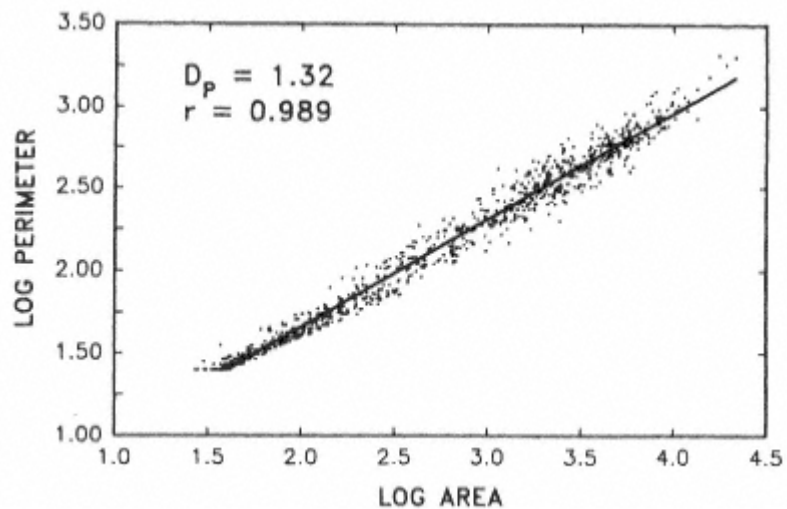
Fig. 25.
Perimeter-area plot for 1000 N121 aggregates in the dry
state (from ref. [188]).

where M is the mass of the object and R is its size. Open, branched aggregates have lower mass fractals than clustered, bulky types. The mass fractal model has also been applied extensively on such colloidal aggregates such as gold clusters [210], silica [198], and soot aggregates [211213]. Finally Clearly, Samson and Genky [214] have described in depth the terminology and methodology of both the perimeter fractal and the cluster or mass fractal.

Bourrat and Oberlin [208] showed that the mass fractal for three conductive carbon blacks increased as the conductivity decreased. The slope of plots of log M vs. log R yielded Dm. The values of M were taken as the measured surface area of the aggregate inside a group of circles of an increasing linear diameter, R. This procedure is referred to as the mass in the box method. The lowest Dm corresponded to the carbon black with the most open structure and highest specific surface area.

Ehrburger-Dolle and Tence [209] used the mass in the box or nested squares method as they called it, as well as the mass-size method. They determined the actual mass of the aggregates from digital annular dark field images using scanning transmission electron microscopy. In the mass-size method the slope of a plot of log M versus log (size) of many individual aggregates yields Dm. These workers analyzed a fine thermal black, an acetylene black, and two oil furnace grades. They compared the mean values of Dm obtained by the nested squares method to that of Dm obtained by the mass-size method. In both methods, 50 aggregates were analyzed to obtain the values of Dm. The Dm values were lower using the nested squares method for the fine thermal and acetylene black and higher for the two furnace blacks in comparison to the

values from the mass-size method. These differences were explained by the fact that the low scale values of the nested squares method are most likely probing the mass of primary particles which could strongly influence the value of Dm. They also suggested that the value of Dm of 1.99 for the acetylene black, compared to approximately 1.8 for the two furnace blacks, might indicate a different mechanism of aggregation. A Dm of 1.8 has been obtained from a group of aggregates created via computer simulation of cluster-cluster aggregation processes [209].

Herd, McDonald and Hess [188] have used the mass-size method to determine values of Dm for the 19 grades listed in Table 7. Fig. 25 is a plot of log M versus log $(L \times W)1/2$ for 1000 aggregates of N121 in the dry state and is representative of the data obtained for all grades. The mass of the aggregates was determined by first calculating the volume of each aggregate using Equation 7. The size was taken as the geometric mean or $(L \times W)1/2$, where L is the longest Feret and W is the shortest Feret. The values of Dm range from 2.28 up to 2.84. Again, there is a general correlation of Dm with DBPA, i.e., as Dm increases, DBPA decreases. The increases in Dm with decreasing DBPA reflect the fact that the aggregates for the lower structure

Table 7. Perimeter and Mass Fractal Values for Various Carbon Black Grades (Dry State)

Carbon black	N2SA, m2/g	DBPA, cm3/100g	*Dp*	*Dm*
CD-2005	120	174	1.34	2.35
N358	82	155	1.33	2.35
HV-3396	174	138	1.35	2.33
N121	132	134	1.32	2.39
N650	38	129	1.33	2.28
N234	123	124	1.30	2.42
N299	107	124	1.29	2.42
N351	74	120	1.30	2.38
N550	39	120	1.26	2.42
N339	94	118	1.30	2.40
N110	133	115	1.30	2.41
N220	113	115	1.28	2.43
N330	83	100	1.28	2.40
N660	36	91	1.22	2.50
N630	34	78	1.18	2.57
N774	29	77	1.16	2.56
N326	85	72	1.22	2.52
N762	26	67	1.16	2.59
N990	9	35	1.05	2.84

From ref. [188].
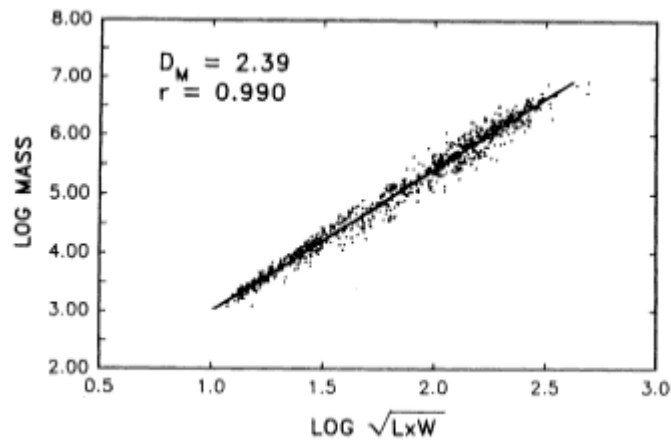
Fig. 26.
Mass-size plot for 1000 aggregates in the dry state
(from ref. [188]).

grades are becoming more compact in nature and thus yield a larger D_m. The value of 2.85 obtained for the N990 on thermal black is in good agreement with the values of 2.96 ± 0.11 (mass-in-the-box method) obtained by Ehrburger-Dolle and Tence [209] for this grade. However, for two furnace grades of unknown DBPA, they obtained values of 1.76 ± 0.12 and 1.83 ± 0.13 (mass-size method) and 1.92 ± 0.21 and 2.14 ± 0.20 (mass-in-the-box method) which are below the range of values obtained in Table 7.

Using the aggregate shape classifications shown in Table 6, it was possible to determine the perimeter and mass fractals for each of the four shape categories shown in Fig. 23. These data are listed in Table 8 which includes the D_p values for the same 19 grades of carbon black. Within a category, the values of D_p are fairly constant at similar particle size levels but the categories are distinctly different from each other. The range of D_p values observed from the type 1 to type 4 shape categories is actually wider than the full distribution across all the grades (Table 7). It is also seen that the values of

Table 8. Perimeter Fractal Values for Each Shape Category (Dry State)

			D_p		
Carbon black	DBPA, cm3/100g	1*a*	2	3	4
CD-2005	174		1.15	1.30	1.43
N358	155		1.21	1.32	1.44
HV-3396	138		1.17	1.33	1.43
N121	134		1.18	1.32	1.40
N650	129		1.12	1.30	1.44
N234	124		1.19	1.27	1.37
N299	124		1.17	1.29	1.36
N351	120		1.20	1.28	1.38

N550	120		1.14	1.26	1.27
N339	118		1.19	1.28	1.37
N110	115		1.20	1.29	1.33
N220	115		1.15	1.29	1.32
N330	100		1.14	1.28	1.31
N660	91		1.10	1.23	1.18
N630	78		1.11	1.16	1.13
N774	77	1.08	1.10	1.16	1.17
N326	72	1.05	1.14	1.23	1.23
N762	67	1.02	1.09	1.17	1.15
N990	35	1.04	1.04	1.07	1.13

a Listed only for > 1% by weight.

Dp increase progressively from the spheroidal-ellipsoidal-linear-branched types in the direction of increasing aggregate irregularity. By combining the shape classification program with fractal analyses, more sensitivity is obtained in characterizing the different carbon black grades. This approach may ultimately prove useful in relating to the kinetic growth mechanisms of carbon black aggregates in the reactor.

True fractal objects are self-similar in that at any level of observation the material is similar in form or topography. Materials such as carbon black and other colloidal type aggregates are not completely self-similar and exhibit different types of fractal behavior over various ranges of magnification or observation. Schaefer and Hurd [198] gave an excellent description of this phenomenon. The structured walk method of Kaye [203] is done at a magnification in which the actual surface roughness of the particles that makeup the aggregates is not resolved. Two techniques have been used to characterize surface roughness: adsorbed gas phase molecular probes and small angle X-ray or neutron scattering (SAXS or SANS).

Avnir and Farin [216] determined the surface fractal dimension of various adsorbents (graphite, various charcoals, fumed silica, crushed glass, a zeolite) and of carbon black (grade not specified). The surface fractal of 2.25±0.09 was determined from the following equation that relates the mole number, *n,* of monolayered adsorbate to various adsorbate cross section area, σ,

$$log \ n = (-D/2)log \ \sigma + constant \ (13)$$

The slope of a plot of log *n* vs log σ of various adsorbates yields

the surface fractal dimension, *D*. A value of 2.0 is considered a smooth surface and was the value obtained for graphite. The rougher the surface the larger the value of *D*, with 3.0 being the upper limit. A value of 2.25 for this carbon black sample indicates a surface of moderate irregularity.

The SAXS and SANS techniques have also been used to obtain surface fractal values for fumed silica [198], various carbonaceous materials [215], and carbon black [207,217]. For fifteen different grades of carbon black Gerspacher and O'Farrell [207] found that *Ds* was nearly constant for all grades at a value of ~2.4. The SAXS measurements of Hurd et al [218] gave values in the same range of 2.26 to 2.43±0.15 for four different grades. For two of the grades studied, SANS gave lower values and the authors were unable to explain the discrepancy. Regardless of the method employed, however, the surfaces of most carbon black grades appear to be similar in their degree of irregularity.

3.4. Other Physical Properties

3.4.1. Density

The density of carbon blacks and other materials can have a number of different meanings. Values based on microcrystallinity are usually accepted

as the true material density. Other commonly used procedures are based on pycnometer measurements using helium or different liquids. In addition, there is bulk density which typically refers to the packing density of the carbon black as it is supplied for commercial usage. All of these various aspects of density are important and certain measurements, when combined, also provide information pertaining to the type of porosity (open vs. closed) that exists in a carbon black.

X-ray Measurements

Densities based on X-ray diffraction are derived from the atomic spacings within the unit cell of a material and are, therefore, independent of porosity and other effects. X-ray density measurements on carbon blacks have been carried out by Rossman and Smith [219], Austin and Hedden [220] and Kotlensky and Walker [221]. The densities for carbon blacks are inverse to the lattice parameter, C_o, which is the dimension of the unit cell along the C axis, perpendicular to the layers. C_o is usually derived from $d(002)$ and is equal to twice the measured d-spacing from this peak.

Kotlensky and Walker [221] calculated X-ray densities for a broad range of carbon blacks along with graphite. All of the carbon blacks were analyzed before and after heating them in an inert atmosphere at temperatures ranging up to 2500 or 2800°C. Fig. 27 is based on the Kotlensky and Walker results and shows a plot of X-ray density vs. $d(002)$ for 11 carbon blacks before and
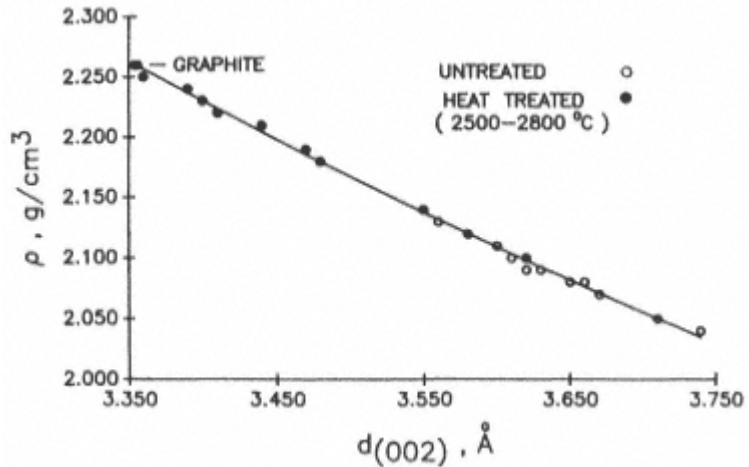
Fig. 27.
Density of carbon black as a function of the average layer spacing, d(002) from X-ray diffraction (from ref. [221]).

after the heat treatment. Also included are samples of spectrographic and ceylon graphite which gave densities of 2.26 g/cm3. The untreated carbon blacks varied in density from 2.04 to 2.11 g/cm3, with some tendency toward higher values for the larger particle size carbon blacks. This tendency was also apparent following the heat treatments which produced the greatest increase in the density for large particle size oil furnace and thermal blacks. Heat treated samples of FT (2700°C) and MT (2800°C) gave density values of 2.24 and 2.25 g/cm3, respectively, and were quite close to the values for the graphite samples.

Pycnometer Measurements

For this type of measurement the volume of a known weight of a material is determined by its displacement in a gas or liquid. However, for porous materials such as carbon blacks the degree of penetration of the liquid or gas into the sample will affect the values. Therefore, pycnometer measurements are generally described as the apparent density; if the gas or liquid does penetrate all pores of the sample, however, its true density can be determined.

Helium provides the smallest molecule for density measurements and is also the least adsorptive. Smith and Howard [222] developed a helium density procedure for carbonaceous materials which was subsequently employed by Rossman and Smith [219] for carbon blacks. Kotlensky and Walker [221] compared helium densities to the X-ray values and to particle densities based on mercury porosimetry. For any given carbon black, the values increase from mercury to helium to the X-ray method because of the influence of porosity.

Pycnometer measurements based on benzene or other liquid hydrocarbons have also been commonly employed to measure carbon black density. Procedures for the benzene method, as well as the helium technique, have been published by Shubert, Ford and Lyon [8]. A general procedure for pycnometer density measurements using liquids is also described in ASTM D 1817 [223]. The use of hydrocarbons has been considered to be more realistic for measuring the effective carbon black densities that exist in rubber and other polymers which are unable to penetrate the finer pores that exist on the black surface. Benzene densities have been used to define tread grade carbon blacks in a recent patent [224], with lower values being cited as advantageous for higher reinforcement. It should be noted that lower pycnometer values for carbons can be attributable either to a less developed graphitic structure or a large volume of inaccessible pores.

Although benzene pycnometer values may be more realistic in terms of the specific gravities of carbon black-polymer composites, the method is quite tedious and time consuming. New auto-pycnometer techniques based on helium are considerably more accurate and precise [225]. Extensive measurements on a broad range of carbon blacks have been carried out using the

Micromeritics Autopycnometer 1330 (Micromeritics Co., Norcross, Georgia). Following drying (2 hours at 125°C), a known weight of carbon black (2.5 g) is inserted into a cell of known volume and then sealed off and purged with helium to eliminate any air in the system. From this point on, the operation is fully automatic and is not operator intensive. The density of the unknown is determined by the displaced volume of helium from the calibrated cell containing the sample to a second cell of known volume. Displacement occurs when the ambient pressure of the sample cell is increased to a higher value and the cell is then opened to permit flow of helium into the second cell. The volume of the sample is derived from the differences in the initial and final pressure (relative to the ambient level), in conjunction with the known cell values. During any single analysis the density measurements can be repeated automatically and sequentially. Typical standard deviations for carbon blacks are in the range of 0.001 to 0.003 g/cm3. A single five repeat analysis requires about 30 minutes.

Kotlensky and Walker [221] carried out comprehensive density studies on a broad range of carbon blacks (N2SA from 9 to 980 m2/g) by means of X-ray diffraction, helium pycnometry and mercury porosimetry. In addition, the samples were analyzed after heating in an inert atmosphere at temperatures up to 2800°C. For the untreated carbon blacks, it was observed that the helium densities diminished in the direction of increasing particle size, this being in line with diminishing porosity for the coarser blacks. A generally opposite trend, although not as consistent, was indicated for the mercury porosimeter results which the authors regarded as a measure of particle density. Following very high temperature

treatments (~2500 to 2800°C), the helium densities dropped significantly for the smaller particle size carbon blacks while showing the opposite trend for the coarser samples. Thus, the relationship to surface area was completely reversed. Kotlensky and Walker related this behavior to the variations in the levels of open and closed pores which they derived from the X-ray, helium and mercury measurements as shown below:

$$\text{Total porosity (\%)} = 100(1 - \rho_{part}/\rho_{X\text{-}ray}) \quad (14)$$

$$\text{Closed porosity (\%)} = 100(1 - \rho_{He}/\rho_{X\text{-}ray}) \quad (15)$$

For the untreated carbon blacks, the level of open porosity ranged from as little as 1% for the MT sample up to about 30 to 38% for the highly porous channel blacks. Following the heat treatment, however, much of the internal porosity was sealed off and there was a significant increase in closed porosity, particularly for the small particle size channel blacks. For example, a Carbolac 1 sample went from a helium density of 2.02 g/cm3 down to 1.52 g/cm3 after heating at 2800°C. In contrast, the MT sample increased from its untreated value of 1.84 g/cm3 up to 2.13 g/cm3 after being heated to the same temperature.

Table 9. Pycnometer Density Measurements on Different Carbon Blacks

Carbon black type	N2SA, m2/g	Apparent density, g/cm3	
		Helium	Benzene
HCC	900	2.02	2.00
HCF	430	2.03	-
N110	133	2.02	1.78
N121	132	1.97	-
N121 (HT 1500°C)	128	1.81	-
N220	113	2.01	1.79
N330	83	1.97	1.80
N330 (HT 1500°C)	80	1.88	-
N550	39	1.94	1.82
N650	38	1.92	-
N650 (HT 1500°C)	36	1.94	-
N990	9	1.85	1.8

The helium densities (autopycnometer measurements) on several carbon blacks are listed in Table 9 along with benzene measurements on some of the samples. The helium values on the untreated samples indicate the same surface area related pattern of increase shown by Walker and Kotlensky [221]. The benzene values show the opposite trend, except for the high color channel black (HCC) which is comparable for both measurements due to the presence of relatively large open pores. At the other extreme (N990), the two values are also quite close due to the lack of porosity.

Three of the carbon blacks (N121, N330 and N650) listed in Table 10 were also analyzed for helium density after induction heating (nitrogen atmosphere) at 1500°C. Following heat treatment, the

densities are now directionally in line with the benzene values and the pattern of change is similar to that observed by Kotlensky and Walker [221], i.e., greater change (lower values) for the higher surface area carbon blacks. A simple comparison of the helium densities for untreated and heat treated carbon blacks, in conjunction with BET measurements, should provide a means of assessing the relative levels of surface microporosity and internal (closed) porosity for many types of commercial carbon blacks. The results using the highly functional helium autopycnometer are considerably more meaningful when applied in this manner.

3.4.2. Electronic Properties

Electrical Resistivity

Carbon black is a semiconductor and is used in many products in which electrical conductivity (or its inverse, resistivity) is important. Medalia [226] and Aminabhavi and Cassidy [227] have reviewed the electrical properties of carbon blacks in polymeric composites. While this is not the subject of this particular chapter, some of the information presented by these authors is also pertinent to electrical conduction in the dry state. Medalia has summarized the most important mechanisms of electrical conductivity in carbon black composites, which include:

* Electron tunneling

* Dielectric breakdown and internal field emission

* Capacitance

* Graphitic conduction (throughgoing chains)

Graphitic conduction (contacting carbon black aggregates) is most prevalent at high carbon black loadings. This type of conduction is ohmic in nature and would be expected to be the most prevalent in compressed dry carbon blacks. Dielectric breakdown and internal field emission both exhibit non-ohmic behavior, as does electron tunneling at high field strengths.

Since carbon blacks are composed of graphitic layers, a brief mention of the conductive properties of graphite is necessary. These have been reviewed by Spain [228] and Woolam [229]. Natural graphite single crystals (NSC) or highly oriented pyrolytic

graphite (HOPG) behave as semi-metals, i.e., the energy gap between the valence and conduction electron bands is very low (less than 0.04 electron volt). There is, however, considerable anisometry in electrical behavior in terms of the graphitic layer orientation. For example, the specific resistance of graphite single crystals is about 5×10^{-5} ohm-cm in the a-axis direction and is about 10^4 higher in the c-axis direction perpendicular to the layers ($\sim 5 \times 10^{-1}$ ohm-cm). As pointed out by Medalia [226], this is an important consideration pertaining to touching carbon black aggregates. Most of the contacts are along the c-axis due to the concentric nature of the graphitic layer orientation.

A number of authors [8,180,230234] have studied the conductive properties of different carbon blacks under compression. Schaefer, Smith and Polley [230] compared different carbon blacks at a pressure of 150 psi before and after heat treatment in an inert atmosphere over a range of temperatures up to 2400°C. All blacks exhibited an initial drop in resistivity with heat treatment, which is in line with the graphitic layer growth and subsequent reduction in the energy gap [235]. However, a minimum in resistivity was indicated at about 1200°C and then a progressive increase up to a maximum at 2400°C. The 1200°C resistivity minimum for heat treated carbon blacks was confirmed by Mrozowski et al [231]. At the higher pressure (5100 psi) which

they employed, however, the increase in resistivity above 1200°C was much smaller and the maximum typically occurred in the lower temperature range of 0600°C. It is possible that the minimum in electrical resistivity at 1200°C is related to the graphitic layer orientation in the individual carbon black aggregates. Above this temperature, the layers show an increased tendency to form a continuous encapsulating shell around the aggregates as illustrated in Figure 10a. Hence, there is a diminishing possibility for conductive paths along the a-axis between aggregates.

The studies of Mrozowski and coworkers [231] included a comparison of carbon blacks which varied widely in particle size, structure and surface chemistry. A small particle size channel black (oxidized surface) and a fine thermal black (high hydrocarbon content) gave the largest drops in resistivity from the untreated sample to 1200°C. This is attributable to removal of the insulating material at the surface. In the case of the fine thermal (FT, N880) carbon black, its minimum resistivity was not too different than that of an MT (N990) which was initially at a much lower level. The resistivity of the fine channel blacks remained the highest after heat treatment followed by a high structure furnace black, acetylene black, FT, lampblack and MT in that order, the latter three being relatively close. These differences appear to be related predominantly to compressibility and graphitic layer growth, both of which are highest for the large particle size, lower structure carbon blacks. For the fine channel blacks there are the additional factors of particle expansion during heat treatment and aggregate sintering following the removal of chemisorbed oxygen.

Mrozowski [180] and Voet et al [233,234] have both shown that the

resistivity of carbon blacks diminishes with increasing pressure. Mrozowski attributed this to increased interaggregate contact area through elastic and yielding deformation. Voet and coworkers considered carbon black powders to be dispersions in air with very high void volumes. They measured electrical resistance over a broad range of pressures from about 0.07 to 55.2 MPa (10 to 8000 psi) and related the changes in resistance to the cube root of the specific volume of the carbon black. This was done for 10 different rubber grade carbon blacks which varied in DBPA over a particle size range from N100 to N500. The plots of the log resistance versus the cube root of specific volume were all linear and intersected at a single point which corresponds to an open packing at the resistance of solid carbon. From these studies, it was concluded that the resistivity of carbon black is an exponential function of the average particle distance at the prevailing pressure and that the predominant mechanism is electron tunneling. This is certainly the case for moderate loadings in polymer composites in which carbon blacks with a highly open pore structure (more aggregates per unit weight) give the highest electrical conductivity [236]. At very high loadings, however, most carbon blacks tend

to approach the same limiting level of conductivity. Medalia [226] has related this to a reduction in contact resistance as a result of the aggregates becoming more tightly packed and pressed against each other. This would certainly also apply to dry carbon blacks under pressure and, at very low contact resistance, the conductivity mechanism would tend to be graphitic in nature. Evidence for throughgoing chains conduction at high loadings in composites has been based on less dependence on frequency (which normally increases conductivity) [237] and temperature [238].

In summary, the electrical conductivity of dry carbon blacks increases with:

* Higher Pressure (higher effective volume fraction)

* Greater Compressibility (low DBPA)

* Clean Surface (low oxygen and hydrocarbons)

* Higher Graphitic Layer Ordering (up to a limiting level)

* Lower Porosity

From considerations on aggregate packing under compression [166] it also follows that broad distribution carbon blacks would give higher electrical conductivity.

Magnetic properties

The volume magnetic susceptibility, κ, of a material is based on the following expression [239]:

$$M = \kappa H \quad (16)$$

where H is the magnetic field strength and M is the induced

magnetic moment. A closely related quantity is the mass magnetic susceptibility χ which is generally expressed as:

$$\chi = 1000\,\kappa/(\rho/gcm\text{-}3) \quad (17)$$

where ρ is the density of the material.

Materials for which κ or χ are positive are called paramagnetic. Those for which susceptibility is negative are called diamagnetic.

The mass susceptibilities of carbon blacks are diamagnetic and become increasingly more diamagnetic with higher graphitic order [240243]. There is also a paramagnetic component of the mass susceptibility which is proportional to the concentration of unpaired electrons in the carbon black. The technique of electron paramagnetic resonance (electron spin resonance) has been applied extensively to the study of unpaired electrons in carbon blacks [240252]. The electron spin resonance technique enables the study of molecules containing unpaired electrons by observing the magnetic fields at which they come into resonance with monochromatic electromagnetic radiation.

Marchand and coworkers [240242] and Uebersfeld et al [244] established the existence of unpaired electrons in carbon blacks at the surface, or with the

ability to move to the surface. Pacault et al [242] showed that the intensity of the signal did not obey Curie's law for the behavior of free radicals, and it was proposed that a large proportion of the spins were related to electron deficiencies (holes) in the π band. These findings were supported by the subsequent studies of Mrozowski [251] and Marchand and Amiell [252].

Kraus and Collins [245] measured the magnetic susceptibilities and spin concentrations for a wide range of different type carbon blacks. Their data are shown in Table 10. They also broke down the mass susceptibility values into their respective diamagnetic and paramagnetic components, the latter being derived from the spin concentration and susceptibility of free electrons. The results for the furnace carbon blacks (N110, N220, N330, N550) are quite similar although the coarser N550 black has somewhat higher diamagnetic (larger graphitic layers) and paramagnetic (higher spin concentration) components. The FT sample is similar in this respect in terms of the diamagnetic component but has a markedly lower spin concentration. The reduced spin concentration is more pronounced for the highly graphitic acetylene black and Graphon (Spheron 6 Channel Black Heat Treated at 3000°C) samples which are considerably more diamagnetic than any of the other carbon blacks.

Surface oxygen increases the paramagnetic response which accounts for the much higher paramagnetic susceptibilities for the EPC and MPC channel blacks.

3.4.3. Thermal Conductivity

The thermal conductivity of a material is typically derived at steady

state from the quantity of heat flow per unit area (or length) across a temperature gradient. There are a number of ASTM test methods or practices

Table 10. Carbon Black Electron Spin Concentrations

Carbon black	Mole% carbon	Spin conc.$\times 10^{19}$ spins/g	Mass susceptibility $\times 10^{6}$		
			Net	Paramagnetic	Diamagnetic
N550	95.77	10.0	-0.82	0.21	-1.03
N330	95.75	8.0	-0.79	0.17	-0.96
N220	-	9.2	-0.76	0.19	-0.95
N110	94.78	8.1	-0.73	0.17	-0.90
S300 (EPC)	89.70	15.0	-0.59	0.32	-0.91
S301 (MPC)	92.00	13.9	-0.66	0.29	-0.95
N880	94.39	5.9	-0.95	0.13	-0.08
Acetylene	99.12	3.8	-2.6	0.08	-2.68
Graphon	99.66	1.1	-2.8	0.02	-2.82

From ref. [245].

for measuring this property which include C 177 [253] and E 1225 [254]. The ASTM E 1225 procedure represents a guarded-comparative-longitudial heat flow technique and the thermal conductivity values are expressed in watts/(meter)(K).

Jamieson and Mrozowski [255] employed molded cylindrical rods as specimens in measuring the thermal conductivities of polycrystalline carbons and graphite. They reported that the thermal conductivity (λ) of carbons is due to lattice vibrations and not electrons as is the case for metals. Therefore, the Debye equation applies:

$$\lambda = \gamma \rho C v l \ (18)$$

where ρ is the density of the material, C is its specific heat, v is the velocity of the lattice waves, l is the mean free path for the scattering of the waves and γ is a numerical factor usually taken to be 1/3. The thermal conductivity variations among different carbons were found to be most dependent on the size of the graphitic layers L_a. For heat treated carbons (1200 to 3100°C), L_a varied from 3.7 to 105.0 nm. The corresponding values of λ (watt/cm·°C) at an ambient temperature of 295°K ranged from about 0.057 to 1.75. The maximum values for the most highly graphitized sample occurred at 205°K. All of the other carbons showed a progressive rise in λ from 115 to 385°K, the magnitude of the change being inverse to L_a.

A maximum for λ near room temperature was also indicated for graphite in the studies of Castle [256], who measured the thermal conductivity both parallel and perpendicular to the graphitic layers. From 100 to 300 K he found λ to be on the order of 3 times greater

along the a-axis relative to the c-axis. At very high temperatures (up to 2500°C) thermal conductivity drops off sharply due to acoustic interference. Resistance to heat flow is also caused by voids and interparticle junctions which can cause scattering of the lattice waves.

Published data on the thermal conductivity of carbon blacks is very limited. Voet [1] compared several different carbon blacks which were measured for thermal conductivity in the dry state at constant pressure. These represent N300 carbons varying in oil absorption (OA, g/100g) from 76 to 276 as well as an N242 (OA=212) and N472 (OA=257). For the N300 blacks, the thermal conductivity increased progressively by a factor of more than two from the lowest to highest oil absorption. However, the finer N242 and higher structure N472 samples were well below where they would be expected in terms of the N300 oil absorption relationship. Voet related the lower value for N472 to porosity which would be in line with a loss of thermal conduction due to scattering of the lattice waves at the intraparticle voids. The studies of the present authors on carbon blacks dispersed in a butyl rubber bladder formulation (50 phr loading) tend to support this contention. We also found the porous conductive carbon black grades such as N472 to give lower thermal

conductivity values and observed the highest values for partially graphitized furnace blacks or acetylene black. The degree of graphitic order was found to be the dominant factor among all of the different carbon blacks measured, which is in agreement with the results of Jamieson and Mrozowski [255]. Also exhibiting some positive influence λ was the average aggregate longest dimension, which increases as a function of both structure and particle size. It should be noted, howevever, that the values measured at 50 phr carbon black in butyl were on the order of 10 times lower than those reported by Voet on dry carbon blacks and conductivity increased by only 41% from the lowest to the highest value.

Atkins and Sullivan [257] measured the thermal conductivity of butyl compounds containing carbon blacks ranging in particle size from N100 to N900. A pattern of somewhat higher thermal conductivity with increasing carbon black structure was indicated, with MT being the lowest and N472 the highest. For the full range of carbon blacks, however, λ varied by only about 18% from lowest to highest. Among the standard furnace grades (N100 to N700) the range of variation was only about 8%.

Sircar and Wells [258] employed scanning microcalorimetry to measure the thermal conductivity of different elastomeric compounds as a function of both carbon black type and loading. Their work also indicated rather small differences among commercial carbon blacks but did show very significant changes in thermal conductivity as a function of black loading. For example, the thermal conductivity of a butyl bladder compound increased from about

Table 11. Aggregate Structure and Particle Size Effects on

Thermal Conductivity of Natural Rubber (NR) Compounds at 40°C

Carbon black	EMSA, m2/g	DBPA, cm3/100g	λ, W/mK
None (Pure NR)	-	-	0.155
N220	133	114	0.365
N219	127	79	0.357
N293	135	102	0.386
N242	129	123	0.392
N285	119	123	0.387
N234	135	125	0.373
N330	103	103	0.418
N550	68	123	0.425
N660	47	90	0.425
N762	35	62	0.399
N990	7.8	43	0.375

From ref. [258].

0.28 to 0.59 watts/meter·K (W/MK) when the volume fraction of N299 carbon black was increased from 0.02 to about 0.17. Their results on different carbon blacks in NR (50 phr loading in AMA-7 with dicumyl peroxide cure) are shown in Table 11. The values for the different carbon blacks range from 0.365 0.425 (~16% increase from lowest to highest) relative to the unpigmented gum stock at 0.155 W/MK. The authors concluded that carbon black particle size has very little effect on thermal conductivity and that there is a slight increase with structure.

The results of Hands and Horsfall [259] on carbon black filled natural rubber compounds (60 phr loading) also indicated minimal differences among the furnace grades but showed significantly higher values for MT (N990), particularly at elevated test temperatures. From room temperature to about 200°C, the furnace carbon blacks (N110, N220, N330, N550) all dropped to about the thermal conductivity level of the gum stock which indicated no significant change. The MT compound showed a lower overall drop in thermal conductivity with temperature and remained well above the gum stock, even at 200°C.

3.4.4. Bulk Properties

The physical form of carbon black as it is shipped is extremely important, although it does not generally have a bearing on the final applications properties. Typically, all rubber grade carbon blacks are shipped in pelleted (beaded) form. Many non-rubber grades, however, are shipped as powders because they are often incorporated into vehicles using low energy mixing procedures.

Pelletized Carbon Blacks

The bulk density of carbon black pellets can be measured by the Pour Density Test, ASTM D 151389 [260]. The pour density is derived from the weight of carbon black pellets that fill a 624 cm3 capacity cylindrical container.

$$D = (W/10) \times 16 \quad (19)$$

where D is the pour density in kg/m3 and W is the mass of the carbon black in grams.

Janzen [11] has related the pour density to the inverse of DBP absorption.

$$D = 610/(\rho_{-1} + v2414) \quad (20)$$

where ρ is the density of the carbon black in g/cm3 and $v2414$ is the DBPA value in cm3/g. Thus, the higher the DBPA value, the lower the bulk density of the carbon black. For the commercial rubber grade carbon blacks, pour density typically varies from about 190 to 510 kg/m3.

Other important pellet properties are the size distribution and the pellet strength or hardness. Size distribution is measured with sieves of different sizes using ASTM D 1511 [261]. A stack of 5 sieves (No. 10, 18, 35, 60 and 120) are employed with a shaker to fractionate the carbon black sample (2 minute time period). These standard sieves have respective openings of 2000, 1000, 500, 250 and 125 μm. The final pellet size distribution is based on the weight % of carbon black in the five sieves and that remaining in the pan below the bottom (finest) sieve.

During handling, carbon black pellets may break and be reduced to powder. This component of the beads is referred to as fines and can cause a problem with bulk flowability and dustiness. The fines content of pelleted blacks is measured by ASTM D 1508-89 [262]. In this test 25g of the carbon black are placed on a 125 μm sieve in a mechanical shaker of 5 minutes. All material passing through the screen is defined as carbon black fines which are expressed as weight percent. On occasion, more severe treatments (e.g., 20 minutes of shaking) are employed to determine the % fines, based on a higher degree of expected attrition during shipping and bulk handling.

Another means of assessing the bulk handling properties of pelletized carbon blacks is to measure the actual strength of the pellets. Two tests are employed for this purpose, ASTM D 1937-89 [263] for mass strength and ASTM D 3313-88 [264] for the strength of individual pellets. Mass strength provides a measure of flowability and is important in determining the ability to unload bulk (e.g., railroad hopper cars) shipments of carbon black. In the D 1937 test a sample of carbon black is compressed in a cylinder

until a packed endpoint is reached, i.e., the carbon black bridges across the cylinder and will not drop out when the bottom is opened. The mass strength is defined as the minimum force (in Newtons) required to compact the carbon black in this manner.

In the D 3313 test, the force (milliNewtons) required to fracture individual pellets (12 to 14 mesh size) is measured. A total of 20 pellets are measured to determine the average crushing strength, and the minimum and maximum values are also typically reported. This type of testing can now be carried out quite effectively using automated equipment (Concarb/Titan Pellet Tester, Titan Specialties, Inc., Pampa, Texas) which measures the full sampling of pellets without the operator in attendance.

The pellet mass strength of commercial carbon blacks typically varies from about 40 to 70 newtons and the average individual pellet crushing strength ranges from about 1050 milliNewtons. Low crushing strengths are required for mixing into relative low viscosity vehicles (e.g., butyl rubber). Higher values are required for blacks entering bulk storage and transport systems. Everything else being equal, crushing strength tends to be inverse to the DBPA of the carbon black, i.e., more dense packing for low struc-

ture aggregates. The level is also controlled, however, by binders used in the pelletization process, which is discussed in another chapter.

Powders

Carbon blacks in powdered form exhibit much lower bulk densities in the range of about 48159 kg/m3. To improve shipping flowability and incorporation into different vehicles, powdered carbon blacks are generally densified by compression which produces bulk densities in the range of about 151367 kg/m3.

The method for measuring the bulk density of unpelleted carbon blacks is often referred to as tap density and has been described by Schubert, Ford and Lyon [10]. The carbon black is added up to the 100-ml mark in a preweighed 100-ml graduated cylinder without tapping. The bottom of the hand held cylinder is then tapped gently on a table top at the rate of approximately 2 taps/sec until the level of the carbon black reaches an equilibrium volume. This volume is then recorded and the tap density, d (kg/m3), is measured from the weight of carbon black in the cylinder divided by its volume.

The flowability or relative stickiness of carbon black powders may be measured from the angle of repose, which is analogous to a contact angle when the powder has been deposited on a particular surface. This property may be measured by pouring a given amount of carbon black onto a glass plate through a funnel at a fixed height above the surface. The angle defined by the resulting pile of black from its center to periphery is the angle of repose. The wider the angle, the less cohesive and more free flowing the powder. An alternate procedure is to fill an open cylinder with carbon black on

the center of the glass plate and then lift it up, thereby permitting the sample to flow out until it reaches its angle of repose.

3.4.5. Impurities

The non-carbonaceous components of carbon blacks include moisture, residual hydrocarbons and chemically bound hydrogen, sulfur and oxygen, as well as various inorganic species. The solid particulate contaminants in carbon black may be metallic, carbon or inorganic salts and are often referred to as grit or residue. Only these particulate impurities, rather than the chemically bound or surface adsorbed constituents, will be discussed in this section.

The most common types of particulate residue found in carbon blacks are listed in Table 12. Coke represents carbonaceous residue which is formed when the oil feedstock directly converts to carbon without going through the vapor phase. Ball coke is typically found in the large particle size carbon blacks which are made at lower temperatures. The particles of ball coke are formed from individual hydrocarbon droplets and range from <5 μm to >200

Table 12. Most Common Types of Particulate Residue Found in Carbon Blacks

Material	Typical source
Ball coke	Oil feedstock (poor atomization)
Refractory (impingement) coke	Oil feedstock (deposition on refractory)
Catalyst residue	Oil feedstock (residual zeolite cracking catalyst)
Inorganic salts	Water (cooling or beading) or alkali metal salts used in structure control
Refractory	Alumina/aluminum silicate from refractory brick in reactor
Metals, rust	Iron or steel components of collection/beading system

µm in size. The particles tend to be hollow with holes in the surface from the passage of internal gaseous materials, during carbonization.

Refractory (or impingement) coke is formed as a layer on the refractory walls of the reactor. It appears in the carbon black as irregular chunks and also may be intermixed with fused agglomerations of the carbon black.

The presence of catalyst residue depends on the nature of the carbon black feedstock. This material is typically a zeolite (potassium aluminum silicate) and exists as spheroidal particles of varied size which can sometimes be mistaken for ball coke. Actually, the two types of contaminant are often intermixed. It is not unusual for a ball coke particle to contain a high concentration of aluminum/silicon from the catalyst. However, the most typical

coke and catalyst particles can readily be distinguished from one another employing EDX [265].

The most common additional source of inorganic materials in carbon blacks comes from salts contained in the water that is used to either quench the carbon black after it is formed in the reactor or to pelletize it in the final stages of the operation. In addition, alkali metals (typically a potassium salt) are employed to control the DBPA of carbon blacks. These contribute to the ash of a carbon black but are generally in very finely divided from rather than discrete residual particulates. Furnace refractory is a less common source of inorganic residue but can exist as fairly large particles. These tend to be irregular in nature and generally exhibit a much higher aluminum/silicon ratio relative to silicates from the cooling water or cracking catalyst.

Finally, there are contaminants from the erosion/corrosion of the carbon black collection or handling systems, generally bits of iron, steel or rust. Any large pieces of metallic iron residue are typically removed magnetically from the carbon black prior to shipment. In addition, many modern carbon

blacks plants now utilize stainless steel processing equipment which greatly minimizes the presence of any iron containing residue.

Despite the large variety of possible contaminants in carbon blacks, it should be noted that the actual quantities of such materials are usually quite small (e.g.<5 to ~300 ppm). The amount of residue is most frequently measured using ASTM Procedure D 1514 [266]. This is a water-wash procedure in which a flow of filtered water at a pressure of 207 Pa (30 psi) is used to force 100g of carbon black through a funnel containing a sieve (or sieves) of appropriate size (most typically 35 and 325 mesh). The percentage of residue above a certain size is determined from the weight of materials trapped on the screen relative to the total weight of the carbon black.

The D 1514 method is obviously not applicable for determining the amounts of any water soluble contaminants. This shortcoming can be overcome by employing the screenpack plugging technique developed by Topcik [267,265]. With this method a 40% weight loading of the carbon black is mixed into low density polyethylene and then extruded through a screenpack containing the appropriate size mesh (e.g. 325 mesh). Smaller mesh sizes can be employed for more critical applications. For a well dispersed mix, the amount of particulate residue in the carbon black has a significant effect on the relative screen life, i.e., the time required for a specific pressure buildup, or the incremental change in pressure over a specific time interval. A high screen life value (e.g. 40 to 60 min. for a pressure increase to about 20.7 MPa with a 325 mesh screen) is indicative of very low residue. However, a low screen life does not necessarily mean high residue because the test is also influenced by carbon

black dispersion. Qualitative information pertaining to the type of material causing plugging of the screen can be obtained through X-radiography of the screenpack, which can isolate inorganic contaminants, in combination with EDX which can be employed to analyze the plugged interface of the screenpack [265]. The latter technique is accomplished by peeling away the black-polyethylene composite on the plugged side of the screen and then analyzing the exposed surface by SEM/EDAX. This procedure is most effective for the detection of inorganic materials that are causing plugging, but can also identify particles of carbonaceous contaminants such as coke.

Ash

The inorganic content of carbon blacks can also be approximated by ashing the sample in air using ASTM D 1506 [268]. A 2g sample of the dried carbon black is placed in a crucible which is heated overnight (16 hours) in a muffle furnace at 550°C. The ash residue is then weighed and expressed as a weight % of the carbon black sample. The ash values for furnace grade carbon blacks typically range from about <0.1 to 2%. The inorganic content of the ash can be classified quantitatively by plasma emission spectrometry [269]. However, for a good materials balance relative to the amount of ash,

anion analysis is also necessary. The anions present in carbon black ash are most typically sulfates and oxides. The relative levels of each are dependent on the amount of sulfur present in the carbon black.

Very low ash (as well as low residue) is particularly important for conductive carbon blacks which are used in plastics for electrical cables. Most critical is the semiconductor strand shield compound that is employed to reduce electrical stress as a thin layer between the metal conductor and insulator. The presence of metallic ions or particulate impurities at the strand shield-insulator interface can promote premature cable failure.

References

1. Donnet, J. B. and Voet, A., *Carbon Black, Physics, Chemistry, and Elastomer Reinforcement,* Marcel Dekker, Inc., New York and Basel, 1976.

2. Dannenberg, E. M., Carbon Blacks, in *Kirk-Othmer Encyclopedia,* Vol.4, John Wiley and Sons, New York, p. 631, 1978.

3. Medalia, A. I, and Rivin, D., *Carbon Black, Characterization of Powder Surfaces,* G. D. Parfitt and K. S. W. Sing eds., Academic Press, New York, New York, p. 279, 1976.

4. Kraus, G., ed., *Reinforcement of Elastomers,* Interscience, New York, 1965.

5. Gessler, A. M., Hess, W. M. and Medalia, A. I., *Plastics and Rubber Processing,* 3, 1 (1978).

6. Heckman, F. A., *Rubber Chem. Technol.,* 37, 1245 (1964).

7. Ban, L. L. and Hess, W. M., *Interactions Entre Les Elastomeres et les Surfaces Solides Ayant Une Action Renforcante,* Colloques Internationaux Du CNRS, France, September 2426, p. 81, 1973.

8. Studebaker, M. L., *Rubber Chem. Technol.,* 30, 1400 (1957).

9. Riven, D., *Rubber Chem. Technol.,* 44, 307 (1971).

10. Schubert, B., Ford, F. P. and Lyon, F., *Encyclopedia of Industrial Chemical Analysis,* Vol.8, John Wiley and Sons, Inc., p.179, 1969.

11. Janzen, J., *Rubber Chem. Technol.,* 55, 669 (1982).

12. Wiegand, W. B., *Canadian Chemical Journal,* 4, 160 (1920).

13. Green, H., *Chem. and Met. Eng.,* 28, 53 (1923).

14. Spear, E. B., *Colloid Symposium Monographs,* 1, 321 (1923).

15. Goodwin, N. and Park, C. R., *Ind. Eng. Chem.,* 20, 621 (1928).

16. Grenquist, E. A.,*Ind. Eng. Chem.,* 21, 665 (1929).

17. Parkinson, D. N., *Trans. Inst. Rubber Ind.,* 5, 263 (1930).

18. Knoll, M. and Ruska, E., *Ann. der Physik,* 12, 607 (1932).

19. Knoll, M. and Ruska, E., *Z. Physik,* 78, 318 (1932).

20. Prebus, A. F. and Hillier, J., *Can. J. Research,* 17, 49 (1939).

21. *Columbian Colloidal Carbons* Vol. II; *Rubber Chem. Technol,* 14, 52 (1940).

22. Von Ardenne, M. and Beischer, D., *Kautschuk,* 16, 55 (1940); *Rubber Chem. Technol.,* 14, 15 (1941).

23. Ladd, W. A., *Columbian Colloidal Carbons,* Vol. III, 1942.

24. Ladd, W. A. and Wiegand, W. B., *Rubber Age,* 57, 299 (1945).

25. Cohan, L. H. and Watson, J. H. L., *Rubber Age,* 68, 687 (1951).

26. Sweitzer, C. W. and Goodrich, W. C., *Rubber Age,* 55, 469 (1944).

27. Warren, B. E., *J. Chem. Phys.,* 2, 551 (1934).

28. Warren, B. E., *Phys. Review,* 59, 693 (1936).

29. Biscoe, J. and Warren, B. E., *J. Appl. Phys.,* 13, 364 (1942).

30. Short, M. A. and Walker, P. L., Jr., *Carbon,* 1, 3 (1963).

31. Franklin, R. E., *Acta Cryst,* 3, 107 (1950).

32. Franklin, R. E., *Proc. Royal Soc.,* A209, 196 (1950).

33. Franklin, R. E., *Acta Cryst.,* 4, 253 (1951).

34. Alexander, L. E. and Darin, S. R., *J. Chem. Phys.,* 23, 594 (1955).

35. Alexander, L. E. and Sommer, E. C., *J. Chem. Phys.,* 24, 1646 (1956).

36. Austin, A. E., *Proc. of 3rd. Conf. on Carbon,* University of Buffalo, New York, p. 389, 1958.

37. Maire, J. and Mering, J., *Proc. of 4th Conf. on Carbon,* University of Buffalo, New York, p. 345, 1960.

38. Bouraoui, A. and Mering, J., *Carbon,* 1, 465 (1963).

39. Mering, J. and Maire, J., *Les Carbones,* 1, 129 (1965).

40. Bayer, J. and Ergun, S., *Carbon,* 5, 107 (1967).

41. Ergun, S., *Carbon,* 6, 7 (1968).

42. Ergun, S., *Carbon,* 6, 141 (1968).

43. ASTM D 1765, *Annual Book of ASTM Standards,* Vol.9.01, p. 315 (1990).

44. Schwob, Y., *Physics and Chemistry of Carbon,* 15, p. 109 (1980).

45. Sweitzer, C. W. and Heller, G. L., *Rubber World,* 134, 855 (1956).

46. Warren, B. E., *Proc. of 1st Conf. on Carbon,* University of Buffalo, New York, p. 49, 1956.

47. Hall, C. E., *J. Appl. Phys.,* 18, 588 (1947).

48. Hall, C. E., *J. Appl. Phys.,* 19, 198 (1948).

49. Ladd, W. A. and Ladd, M. W., *Rubber Chem. Technol.,* 34, 697 (1961).

50. Donnet, J. B. and Bouland, J. C., *Rev. Gen. Caout.,* 41, 407 (1964).

51. Heckman, F. A. and Harling, D. E., *Rubber Chem. Technol.,* 39, 1 (1966).

52. Hess, W. M. and Ban, L. L., *Proceedings of 6th International Congress for Electron Microscopy,* Kyoto Japan, Norelco Reporter, 13, 102, 1966.

53. Moon, D. M. and Robinson, W. H. presented at Electron Microscopy Society of America Annual Meeting, Detroit, Michigan, 1964.

54. Hess, W. M., Ban, L. L., Eckert, F. J. and Chirico, V. E., *Rubber*

Chem. Technol., 41, 356 (1968).

55. Ayala, J. A., Hess, W. M., Dotson, A. O. and Joyce, G. A., *Rubber Chem. Technol.,* 63, (5), 747 (1990).

56. Papirer, E., Donnet, J. B. and Heinkele, J., *J. Chim. Phys.,* Phys. - Chim. Biol., 68, 58C (1971).

57. Donnet, J. B., *Carbon,* 20, 267 (1982).

58. Heidenreich, R. D., Hess, W. M. and Ban, L. L., *J. Appl. Cryst.,* 1, 1 (1968).

59. Everhart, T. E., *J. Appl. Phys.,* 38, 4944 (1967).

60. Hess, W. M., Burgess, K. A., Lyon, F. and Chirico, V. E., *Kauts. Gummi Kunstst.,* 21, 689 (1968).

61. Ban, L. L. and Hess, W. M., *Proc. of 26th Annual EMSA Meeting,* New Orleans, Louisiana, p. 256, 1968.

62. Harling, D. F. and Heckman, F. A., *Mater. Plast. Elastomeric,* 35, 80 (1969).

63. Marsh, P. A., Voet, A., Mullens, T. J. and Price, L. D., *Rubber Chem. Technol.,* 43, 470 (1970).

64. Marsh, P. A., Voet, A., Mullens, T. J. and Price, L. D., *Carbon,* 9, 797 (1971).

65. Ban, L. L., *Surface and Defect Properties of Solids,* Vol. 1, The Chemical Society of London, p. 54, 1972.

66. Ban, L. L., Vegvari, P. C. and Hess, W. M., *Norelco Reporter,* 20, (1), 1 (1972).

67. Kmetco, E. A., *Proc. of 1st Conf. on Carbon,* Univ. of Buffalo, New York, p. 21, 1953.

68. Crewe, A. V. and Wall, J., *Proc. of Electron Microscopy Society of America,* 27th Annual Meeting, St. Paul, Minnesota, p. 172, 1969.

69. Nomura, S., Todekoro, H. and Komoda, T., *Proc. of Electron Microscopy Society of America,* 34th Annual Meeting, Miami Beach, Florida, p. 524, 1976.

70. Ray, I. L. F., Drummond, I. W. and Banbury, J. R., *Developments in Electron Microscopy and Analysis,* Academic Press, London, New York, San Francisco, p. 11, 1976.

71. Crewe, A. V., *Developments in Electron Microscopy and Analysis,* Academic Press, London, New York and San Francisco, p. 1, 1976.

72. Crewe, A. V., *Proc. of 5th European Congress on Electron Microscopy,* p. 640, 1972.

73. Crewe, A. V., *Chem. Sci.,* 14, 17 (1979).

74. Binning, G., Rehren, H., Gerber, C. and Weibel, E., *Phys. Rev. Lett.,* 49, 57 (1982).

75. Mizes, H. H., Park, S. and Harrison, W. A., *Phys. Rev.* B, 36, 4491 (1987).

76. Park, S., Nogami, J. and Quate, C. F., *SPIE,* Vol. 897, p. 8 (1988).

77. Binning, G., Quate, C. F. and Gerber, C., *Phys. Rev. Lett.,* 56, 930 (1986).

78. Tang. S. L., *Chemtech,* 21, (3), 182 (1991).

79. Hess, W. M. and Ford, F. P., *Rubber Chem. Technol.,* 36, 1175 (1963).

80. Medalia, A. I., *J. Colloid Interface Sci.,* 24, 393 (1967).

81. Burgess, K. A., Scott, C. E. and Hess, W. M., *Rubber Chem. Technol.,* 44, 230 (1971).

82. Janzen, J. and Kraus, G., *Proc. of International Rubber Conference,* Brighton, U. K., p. G7-1, 1972.

83. ASTM D 3849, *Annual Book of ASTM Standards,* Vol.09.01, p. 630 (1990).

84. Prebus, A. F., Ohio State University, Unpublished work, 1940 1941.

85. Bradley, D. E., *Brit. J. Appli. Phys.,* 10, 198 (1959).

86. Endter, F. and Gebauer, H., *Elektronenmikroskopischen Aufnahmen, Optik,* 13, 97 (1956).

87. Marsh, P. A., J. M. Huber Company, Private Communication.

88. Hess, W. M., Ban, L. L. and McDonald, G. C., *Rubber Chem. Technol.,* 42, 1209 (1969).

89. Fisher, C. and Cole, M., *The Microscope,* 162, (2), 81 (1968).

90. McDonald, G. C. and Hess, W. M., *Rubber Chem. Technol.,* 50, 842 (1977).

91. Fowkes, F. M., *Rubber Chem. Technol.,* 57, 328 (1984).

92. Gibbard, D. W., Smith, D. J. and Wells, A., *The Microscope,* 20, (1), 37 (1972).

93. Hess, W. M., McDonald, G. C. and Urban, E., *Rubber Chem. Technol.,* 46, 204 (1973).

94. Hess, W. M. and McDonald, G. C., *ASTM STP,* 553, p. 3, 1974.

95. Ban, L. L., Hess, W. M. and Papazian, L. A., *Rubber Chem. Technol.,* 47, 858 (1974).

96. Hess, W. M. and McDonald, G. C., *Rubber Chem. Technol.,* 56, 892 (1983).

97. Janzen, J. and Goodarz - Nia, *J. Colloid Interf. Sci.,* 69, 476 (1979).

98. Medalia, A. I., Heckman, F. A. and Harling, D. F., *Proc. Nat. Rubber Res. Conf.,* Kuala Lumpur, p. 1, 1968.

99. Cadle, R. D., *Particle Size Determination,* Interscience Publishers, New York, 1955.

100. Nassau, K., *Scientific Am.,* 243, (4), 124 (1980).

101. Voet, A., *Rubber Age,* 82, (4), 656 (1958).

102. Johnson, C. R., *Indian Rubber World,* 77, 65 (1927).

103. Smith, W. R., Thornhill, F. S. and Bray, R. I., *Ind. Eng. Chem.,* 33, 1303 (1941).

104. Rose, H. E., *J. Appl. Chem.,* 7, 244 (1957).

105. Nabors, L. G. and Studebaker, M. L., *Rubber Chem. Technol.,* 40, 1323 (1967).

106. Voet, A., *Am. Ink Maker,* 34, (5), 63 (1956).

107. ASTM D 3265, *Annual Book of ASTM Standards,* Vol. 09.01, p. 530 (1990).

108. Hess, W. M. and Chirico, V. E., *Proc. of Akron Rubber Group Symposia,* 1970 1971.

109. Medalia, A. I. and Richards, L. W., *J. Coll. Interf. Sci.,* 40, 233 (1972).

110. Stacy, C. J., Johnson, P. H. and Kraus, G., *Rubber Chem. Technol.,* 48, 535 (1975).

111. ASTM D 3037, *Annual Book of ASTM Standards,* Vol. 9.01, p. 465 (1990).

112. ASTM D 3765, *Annual Book of ASTM Standards,* Vol. 9.01, p. 614 (1990).

113. ASTM D 1510, *Annual Book of ASTM Standards,* Vol. 9.01, p. 269 (1990).

114. Lowell, S. and Shields, J. E., *Powder Surface Area and Porosity,* Chapman and Hall, London and New York, Chapter 4, 1984.

115. Gregg, S. J. and Sing, K. S. W., *Adsorption, Surface Area and Porosity,* Academic Press, New York, 1982.

116. Adamson, A. W., *Physical Chemistry of Surfaces,* Chapter XIII, John Wiley and Sons, New York, 1967.

117. Langmuir, I., *J. Am. Chem. Soc.,* 40, 1361 (1918).

118. Brunauer, S., Deming, L. S., Deming, W. E. and Teller, E., *J. Am. Chem. Soc.,* 40, 1723 (1940).

119. Brunauer, S., Emmett, P. H. and Teller, E., *J. Am. Chem. Soc.,* 60, 309 (1938).

120. ASTM D 4820, *ASTM Annual Book of Standards,* Vol. 9.01, p. 764 (1990).

121. Magee, R., Columbian Chemicals Company, Private Communication.

122. Corrin, M. L., *J. Am. Chem. Soc.,* 73, 4061 (1951).

123. Haul, R. A. W., *Angew. Chem.,* 68, 238 (1956).

124. Cochrane, H., Walker, P. L. Jr., Diethorn, W. S., and Friedman, H. C., *J. Coll. Interf. Sci.,* 24, 405 (1967).

125. Janzen, J. and Kraus, G., *Rubber Chem. Technol.,* 44, 1287 (1971).

126. Saleeb, F. Z. and Kitchener, J. A., *J. Chem. Soc.,* 911 (1965).

127. Abram, J. C. and Bennett, M. C., *J. Colloid. and Interface Sci.,* 27, 1 (1968).

128. Sanders, D. R., Murphy, L. J., Creeden, D. R. and Davis, G., presented at a meeting of the Rubber Division, ACS, Toronto, Canada, May 21-

24, 1991.

129. ASTM D 1618, *Annual Book of ASTM Standards,* Vol. 9.01, p. 297 (1990).

130. Harkins, W. D. and Jura, G., *J. Am. Chem. Soc.,* 66, 919 (1944).

131. Kraus, G. and Rollmann, K. W., *Rubber Chem. Technol.,* 40, 1305 (1967).

132. Pauseh, J. B. and McKallen, C. A., *Rubber Chem. Technol.,* 56, 440 (1983).

133. Thompson, W. T., *Philos. Mag.,* 42, 448 (1871).

134. deBoer, J. H., *The Structure and Properties of Porous Materials,* Butterworth, London, p. 68, 1958.

135. Voet, A., *Rubber World,* 139, (1), 63 (1958).

136. Voet, A., *Rubber World,* 139, (2), 232 (1958).

137. Barrett, E. P., Joyner, L. G., and Halenda, P. P., *J. Am. Chem. Soc.,* 73, 373 (1951).

138. Walker, P. L. and Kotlensky, W. V., *Can. J. Chem.,* 40, 184 (1962).

139. Pierce, C., *J. Phys. Chem.,* 63, 1076 (1959).

140. Pierce, C., *J. Phys. Chem.,* 1184 (1960).

141. Atkins, J. H., *Carbon,* 3, 299 (1965).

142. Cranston, R. W. and Inkley, F. A., *Advances in Catalysis,* 9, 143 (1957).

143. Lippens, B. C., Linsen, B. G. and deBoer, J. H., *J. Catalysis,* 3, 32 (1964).

144. deBoer, J. H. and Lippens, B. C., *J. Catalysis,* 3, 38 (1964).

145. Lippens, B. C. and deBoer, J. H., *J. Catalysis,* 37, 44 (1964).

146. deBoer, J. H., Van Den Henvel, A. and Linsey, B. G. *J. Catalysis,* 3, 268 (1964).

147. Lippens, B. C. and deBoer, J. H., *J. Catalysis,* 4, 319 (1965).

148. deBoer, J. H., Linsen, B. G., and Osinger, J. T., *J. Catalysis,* 4, 643 (1965).

149. deBoer, J. H., Linsen, B. G., van der Plas, Th. and Zandervan, G. J. *J. Catalysis,* 4, 649 (1965).

150. Carruthers, J. D., Cutting, P. A., Day, R. E., Harris, M. R., Mitchell, S. A. and Sing, K. S. W., *Chem. Ind.,* 50, 1772 (1968).

151. Voet, A. and Aboytes, P., *Carbon,* 9, 135 (1971).

152. Smith, W. R. and Kasten, G. A., *Rubber Chem. Technol.,* 43, 960 (1970).

153. Salinas - Martinez de Lecea, C., Linares - Solano, A., de D. Lopez - Gonzalez, J. and Rodriguez - Reinoso, F., *Carbon,* 19, 65 (1981).

154. Van Aken, J. G. T., Ph.D. Thesis, Techn. Uni. Delft., Netherlands, 1969.

155. Voet, A., Lamond, T. G. and Sweigart, D., *Carbon,* 6, 707 (1968).

156. Carrot, P. J. M., Roberts, R. A. and Sing, K. S. W., *Carbon,* 25, 59 (1987).

157. Dubinin, M. M. and Radushkevick, L. V., *Dokl. Akad. Nauk. SSSR,* 55, 327 (1947).

158. Pierce, C. and Ewing, B., *J. Phys. Chem.,* 68, 2562 (1964).

159. Kuwabara, H., Suzuki, T. and Kaneko, K., *Proc. of the 20th Biennial Conference on Carbon,* Santa Barbara, California, p. 48, 1991.

160. Medalia, A. I. and Heckman, F. A., *Carbon,* 7, 567 (1969).

161. Heckman, F. A., Medalia, A. I. and Harling, D. F., *Proc. of 25th Annual EMSA Meeting,* Chicago, Illinois, p. 358, 1967.

162. Heckman, F. A. and Medalia, A. I., *J. I. R. I.,* 3, (2), 66 (1969).

163. Vold, M. J., *J. Coll. Interf. Sci.,* 18, 684 (1963).

164. Sutherland, D. N., *J. Coll. Interf. Sci.,* 25, 373 (1967).

165. Ritter, *J., Appl. Polym. Symposia,* New York, 15, 239 (1970).

166. Medalia, A. I. and Sawyer, R. L., *Proc. of 5th Conf. on Carbon,* Vol. II, Penn State University, Pennsylvania, p. 563, 1962.

167. Barth, G. and Sun, S., *Anal. Chem.,* 57, 151R (1985).

168. Florenza, A., *Rubber Age,* 84, (6), 945 (1959).

169. Medalia, A. I., Dannenberg, E. M. and Heckman, F. A., *Rubber Chem. Technol.,* 46, 1239 (1973).

170. Redman, E., Heckman, F. A. and Connally, J. E., *Rubber Chem. Technol.,* 50, 1000 (1977).

171. Probst, N. and Berote, G., Paper No.31, presented at a meeting of the Rubber Division, ACS, Mexico City, 1989.

172. Kaye, B. H., *Direct Characterization of Fineparticles,* John Wiley and Sons, New York, p. 189, 1981.

173. Patel, A. C. and Lee, K. W., *Elastomerics,* 122, (3), 14 (1990).

174. Shieh, C. H., Mace, M. L., Ouyang, G. B., Branan, J. M., Funt, J. M., Juengel, R. R. and Patterson, W. J., Paper No. 56, presented at a meeting of the Rubber Division, ACS, Toronto, Canada, 1991.

175. Janzen, J., *Appl. Optics,* 19, 2977 (1980).

176. Eaton, E. R. and Middleton, J. S., *Rubber World,* 152, 94 (1962).

177. D 2414-90, *Annual Book of ASTM Standards,* Vol. 09.01, p. 434 (1990).

178. Dollinger, R. E., Kallenberger, R. H. and Studebaker, M. L., *Rubber Chem. Technol.,* 40, 1311 (1967).

179. D 3493, *Annual Book of ASTM Standards,* Vol. 09.01, p. 566 (1990).

180. Mrozowski, S., *Proc. of 3rd Conf. on Carbon,* University of Buffalo, New York, p. 495, 1959.

181. Voet, A. and Whitten, W. N., *Rubber World,* 146, (3), 77 (1962).

182. Voet, A. and Whitten, W. N., *Rubber World,* 148, (5), 33 (1963).

183. Patel, A. C., *Elastomerics,* 110, (9), 69 (1978).

184. Patel, A. C. and Brown, W. A., *Rubber World,* 194, (1), 20 (1986).

185. Medalia, A. I., *J. Coll. Interf. Sci.,* 32, 115 (1970).

186. Medalia, A. I., *Rubber Chem. Technol.,* 45, 1171 (1972).

187. Kraus, G., *Rubber Chem. Technol.,* 44, 199 (1971)..

188. Herd, C. R., McDonald, G. C. and Hess, W. M., *Rubber Chem. Technol.,* 65, 1 (1991).

189. Swor, R. A., Hess, W. M. and Micek, E. J., *Elastomerics,* 123, (3), 30 and 123, (4), 18 (1991).

190. Hess, W. M., Chirico, V. E. and Burgess, K. A., *Kauts. Gummi Kunsts.,* 26, 344 (1973).

191. Mercer, H. N., Bayer, A. H., Brusk, P. L. and Deviney, M. L., *Rubber Chem. Technol.,* 49, 1968 (1976).

192. Medalia, A. I. and Hornic, G. J., *Pattern Recognition,* 4, 155 (1972).

193. Fisher, C. and Bond, C. D., *The Microscope,* 20, 37 (1972).

194. Anderson, T. W., *Introduction to Multivariate Statistical Analysis,* John Wiley and Sons, New York, 1958.

195. Morrison, D. F., *Multivariate Statistical Methods,* McGraw-Hill Book Co., p. 130 (1968).

196. Gross, U., Mescher, F. J. M. and Tiemeijer, J. C., *Philips Tech. Rev.,* 43, (10), 273 (1987).

197. Kshirsager, A. M., *Multivariate Analysis,* Marcel Dekker, Inc.,

New York, p. 187 (1972).

198. Schaefer, D. W. and Hurd, A. J., *Aerosol Sci. Technol.,* 12, 876 (1990).

199. Feder, J., *Fractals,* Plenum Press, New York, p. 2, 1988.

200. Mandelbrot, B. B., *Les Objects Fractals: Forme, Hasard et Dimension,* Flammarion, Paris, 1975.

201. Mandelbrot, B. B., *Fractal: Form, Chance, and Dimension,* W. M. Feeman, San Francisco, 1977.

202. Mandelbrot, B. B., *The Fractal Geometry of Nature,* W. H. Freeman, New York, 1982.

203. Kaye, B. H., *A Random Walk Through Fractal Dimensions,* VCH Publishers, New York, 1989.

204. Kaye, B. H., *Powder Technol.,* 21, 1 (1978).

205. Flook, A. G., *Powder Technol.,* 21, 295 (1978).

206. Mandelbrot, B. B., *Science,* 156, 636 (1967).

207. Gerspacher, M. and O'Farrell, C. P., *Elastomerics,* 123, (4), 35 (1991).

208. Bourrat, X. and Oberlin, A., *Carbon,* 26, (1), 100 (1988).

209. Ehrburger -Dolle, F. and Tence, M., *Carbon,* 28, 448 (1990).

210. Weitz, D. A. and Oliveria, M., *Phys. Rev. Lett.,* 52, 1433 (1984).

211. Forrest, S. R. and Witten, T. A., Jr., *J. Phys. A: Math. Gen.,* 12, (5), L 109 (1979).

212. Samson, R. J., Mulholland, G. W., and Gentry, J. W.,

272 (1987).

213. Megaridis, C. M. and Dobbins, R. A., *Combust. Sci., and Technol.,* 71, 95 (1990).

214. Cleary, T., Samson, R., and Gentry, J. W., *Aerosol Science and Technology,* 12, 518 (1990).

215. Jullien, R. and Bufet, R., *Aggregation and Fractal Aggregates,* World Scientific, Singapore (1987).

216. Avnir, D., Farin, D. and Pfeifer, P., *J. Chem. Phys.,* 79, (7), 3566 (1983).

217. Reich, M. H., Russo, S. P., Snook, J. K. and Wagenfold, H. K., *J. Colloid. Interface Sci.,* 135, 353 (1990).

218. Hurd, A. J., Schaefer, D. W., Smith, D. M., Ross, S. B., Le Méhauté, A. L. and Spooner, S., *Phys. Rev. B: Condensed Matter,* 39, (13), 9742 (1989).

219. Rossman, R. P. and Smith, W.R., *Ind. Eng. Chem.,* 35, 972 (1943).

220. Austin, A. E. and Hedden, W. A., *Ind. Eng. Chem.,* 46, 1520 (1954).

221. Kotlensky, W. V. and Walker, P. L., Jr., *Proc. 4th Conf. on Carbon,* University of Buffalo, New York, p. 423, 1960.

222. Smith, R. C., Jr. and Howard, H. C., *Ind. Eng. Chem.,* 34, 438 (1942).

223. ASTM D 1817, *ASTM Annual Book of Standards,* Vol. 9.01, p. 323 (1990).

224. Misono, S. and Suzuki, H., U. S. Patent No. 4 478 973, 1984.

225. Lowell, S. and Shields, J. S., *Powder Surface Area and Porosity,* Chapman and Hall, London, New York, p. 217, 1984.

226. Medalia, A. I., *Rubber Chem. Technol.,* 59, 432 (1986).

227. Aminabhavi, T. M. and Cassidy P. E., *Rubber Chem. Technol.,* 63, 451 (1990).

228. Spain, I., *Chemistry and Physics of Carbon,* Vol. 8, Marcel Dekker, Inc., N. Y., p. 1, 1973.

229. Woolam, J. A., *Petroleum Based Carbons,* M. L. Deviney and T. M. O'Grady eds., *ACS Symposium Series,* 21, Chapt. 27, p. 378, 1976.

230. Shaefer, W. D., Smith, W. R. and Polley, M. H., *Ind. Eng. Chem.,* 45, 1721 (1953).

231. Mrozowski, S., Chaberski, A., Loebner, E. E. and Pinnick, H. T., *Proc. of 3rd Conf. on Carbon,* Buffalo, New York, p. 211, 1959.

232. Adelman, E. and A. E. Austin, *Proc. of 6th Conf. on Carbon,* 1963.

233. Voet, A., *Rubber Age,* 95, 746 (1964).

234. Voet, A., Whitten, W. N. and Cook, F. R., *Kolloid Z Polymere,* 201, (1), 39 (1965).

235. Pinnick, H. T., *Proc. of 1st and 2nd Conf. on Carbon,* University of Buffalo, New York, p. 3, 1956.

236. Verhelst, W. K., Wolthuis, K. G., Voet, A., Ehrburger, P. and Donnet, J. B., *Rubber Chem. Technol.,* 50, 735 (1977).

237. Kawamoto, H., *Carbon Black-Polymer Composites,* E. K. Sichel, ed., Marcel Dekker, N. Y., Chapter 5, 1982.

238. Sichel, E. K., Gittleman, J. I. and Sheng, P., *Carbon Black-Polymer Composites,* E. K. Sichel, ed., Marcel Dekker, N. Y., Chapter 2, 1982.

239. Atkins, P. W., *Physical Chemistry,* W. H. Freeman and Co., N. Y., p. 597, 1986.

240. Marchand, A., *Comp. Rend.,* 238, 1645 (1954).

241. Marchand, A., *C. R. Acad. Sci. Paris,* 239, 1609 (1954).

242. Pacault, A. and Marchand, A., *Proc. of 3rd Conf. on Carbon,* University of Buffalo, New York, p. 37, 1959.

243. Kiive, P. and Mrozowski, S., *Proc. of 3rd Conf. on Carbon,* University of Buffalo, New York, p. 165, 1959.

244. Uebersfeld, J., Etienne, A. and Combrisson, J., *Nature,* 174, 614 (1954).

245. Kraus, G. and Collins, R. L., *Rubber World,* 139, 219 (1958).

246. Collins, R. L., Bell, M. D. and Kraus, G., *J. Appl. Phys.,* 30, 56 (1959).

247. Kraus, G. and Collins, R. L., *Rubber Chem. Technol.,* 32, 107 (1959).

248. Castle, J. G. and Wobschall, D. C., *Proc. of 3rd Conf. on*

Carbon, University of Buffalo, New York, p. 129, 1959.

249. Pacault, A., Marchand, A., Botherel, P., Zanchetta, J., Boy, F., Cherville, J. and Oberlin, M. C., *J. Chim. Phys.,* 57, 892 (1960),

250. Spackman, J. W. C., *Rev. Gen. Caout.,* 41, 417 (1964).

251. Mrozowski, S., *Carbon,* 3, 305 (1965).

252. Marchand, A. and Amiell, J., *Carbon,* 8, 707 (1970).

253. ASTM C 177, *Annual Book of ASTM Standards,* Vol. 04.06, (1990).

254. ASTM C 1225, *Annual Book of the ASTM Standards,* Vol. 14.02, p. 701 (1990).

255. Jamieson, C. P. and Mrozowski, S., *Proc. of 1st and 2nd Conf. on Carbon,* University of Buffalo, New York, p. 155, 1956.

256. Castle, J. G. Jr., *Proc. of 1st and 2nd Conf. on Carbon,* University of Buffalo, New York, p. 13, 1956.

257. Atkins, J. H. and Sullivan, J. E., Jr., *Rubber Chem. Technol.,* 42, 1314 (1969).

258. Sircar, A. K. and Wells, J. L. *Rubber Chem. Technol.,* 55, 191 (1982).

259. Hands, D. and Horsfall, F., *Rubber Chem. Technol.,* 50, 253 (1977).

260. ASTM D 1513, *Annual Book of ASTM Standards,* Vol. 09.01, p. 280 (1990).

261. ASTM D 1511, *Annual Book of ASTM Standards,* Vol. 9.01, p. 275 (1990).

262. ASTM D 1508, *Annual Book of ASTM Standards,* Vol. 9.01, p. 265(1990).

263. ASTM D 193, *Annual Book of ASTM Standards,* Vol. 9.01, p. 344 (1990).

264. ASTM D 3313, *Annual Book of ASTM Standards,* Vol. 9.01, p.535 (1990).

265. Hess, W. M., *Rubber Chem. Technol.,* 64, 386 (1991).

266. ASTM D 1514, *Annual Book of ASTM Standards,* Vol. 9.01, p. 282 (1990).

267. Topcik, B., *Mod. Plast.,* 51, (4), 94 (1974).

268. ASTM D 1506, *Annual Book of ASTM Standards,* Vol. 9.01, p. 263 (1990).

269. Skoog, D. A., *Principles of Instrumental Analysis,* CBS College Publishing, U.S.A., p. 292, 1985.

Chapter 4
Surface Groups on Carbon Blacks

Roop Chand Bansal
Department of Chemical Engineering and Technology,
Panjab University,
Chandigarh, India

Jean-Baptiste Donnet
Centre de Recherches sur la Physico-Chimie des Surfaces Solides,
CNRS,
Mulhouse, France

4.1. Carbon Black Surface Compounds

Carbon blacks are invariably associated with varying amounts of oxygen and hydrogen. In addition they may be associated with atoms of chlorine, nitrogen and sulphur. These atoms are introduced into the carbon black sample during the manufacturing process because of their presence in the feedstock, reactor furnace, postreactor chamber and become a part of the chemical structure. They may also become chemically bonded to the surface during subsequent treatments or during storage. Carbon blacks tpically contain about 9099% elemental carbon with oxygen and hydrogen as the other major constituents. In general, channel blacks contain the largest amount of oxygen (varying between 38%) and hydrogen (less than 1%) and the thermal blacks contain the smallest amounts of both oxygen and hydrogen (Table 1). The sulphur in carbon blacks originates from the feedstock. Sulphur contents of 0.6% are

common in furnace blacks while thermal black are nearly sulphur free. The larger content of oxygen in color blacks is due to the fact that they are exposed to air at about 400°C, the temperature which is optimum for the formation of oxygen surface groups.

X-ray diffraction studies have shown that these oxygen heteroatoms are retained or bonded at the edges and corners of the aromatic sheets or to carbon atoms in defect positions of the aromatic sheets or they can be incorporated within carbon layers forming heterocyclic ring systems. These carbon atoms have unsaturated valencies and have a tendency to reduce their potential energy by forming bonds with these heteroatoms. Since these edges constitute the main adsorbing surface, the presence of heteroatoms is expected to modify the surface characteristics and surface behaviour of these carbons. The presence of these surface compounds in carbon blacks determines their applications in rubber, plastics and paint industries and they determine the lubricating properties in graphite as well as their use as moderator in atomic reactor. In the case of carbon fibers these surface compounds determine their adhesion to plastic matrices and consequently their use in composites.

Table 1. Hydrogen and Oxygen Contents of Different Carbon Blacks

Trade name	Hydrogen by ultimate analysis	Oxygen by ultimate analysis
Furnace blacks		
Pelletex	0.38	0.22
Kosmos-40	0.35	0.23
Statex-B	0.36	0.43
Philblack-A	0.35	0.58
Philblack-O	0.30	0.79
Philblack-I	0.29	1.17
Philblack-E	0.31	1.01
Vulcan-SC	0.17	1.18

Channel blacks		
Spheron-9	0.62	3.49
Spheron-6	0.55	3.10
Spheron-4	0.47	3.28
Spheron-C	0.33	3.14
Colour blacks		
ELF-O	0.47	4.89
Mogul-A	0.51	7.63
Mogul	0.48	8.22

4.1.1. Carbon-Oxygen Surface Groups

Carbon-oxygen surface structures are by far the most important surface groups which influence the physico-chemical properties such as wettability, catalytic, electrical and chemical reactivity of carbon blacks. In fact, these surface compounds have been found to be the source of the property by which a carbon black becomes useful or effective in certain respects. Carbon blacks have a tendency to extend this layer of chemisorbed oxygen by decomposing certain oxidizing gases such as ozone [14], oxides of nitrogen [5,6], or by decomposing aqueous solutions of silver salts [7], halogens [810], ferric chloride [11], potassium and ammonium persulphate [1213], sodium hypochlorite [14,15], potassium permanganate [16,17], potassium dichromate [17], sodium thiosulphate [18], hydrogen peroxide [19,20] and nitric acid [17,21,22]. In each case there is chemisorption of oxygen and a buildup of the oxide layer on the carbon surface. However, the nature and the amount of the surface oxide formed depends upon the nature of the carbon black surface and the history of its formation, its surface area and the temperature of treatment. The reaction of carbon blacks with oxygen at temperatures below 400°C predominantly results in the chemisorption of oxygen and the formation of carbon-oxygen surface compounds whereas at temperatures above 400°C, the decomposition of the surface compounds and the gasification of the carbon are the predominating reactions. In the case of oxidative reactions in solution phase, the major reaction is the formation of the surface compounds although some gasification may also take place depending upon the strength of the oxidative treatment and the severity of the experimental conditions. The formation of these

surface oxygen compounds using several different types of oxidative treatments in gaseous and liquid phases has been very well reviewed [23,24,25].

Three types of surface oxides, acidic, basic and neutral, have been proposed. The acidic surface oxides are formed when carbon is treated with oxygen at temperatures up to 400°C or by reaction with oxidizing solutions at room temperature. These surface groups are less stable and decompose on heat treatment under vacuum or in an inert atmosphere in the temperature range 300800°C evolving CO_2. These surface oxides have been suggested to be acidic functional groups such as carboxylic, lactonic, phenolic or a frozen layer of CO_2 and are known to render the carbon surface polar in character.

The basic surface oxides are obtained when a carbon surface, freed from all surface compounds by heat treatment in vacuum or inert atmosphere at 1000°C, and after cooling to room temperature, is contacted with oxygen gas. Garten and Weiss [24] proposed a pyrone type structure for basic surface oxides which has also been referred to as a chromene structure. This structure has a heterocyclic oxygen-containing ring with an activated $=CH_2$ or $=CHR$ group (R is an alkyl group). Boehm and Voll [26] has suggested that these

basic surface oxides can be represented by pyron-like structure with the oxygen atoms, in general, located in two different rings of a graphite layer, the positive charge being stabilized by resonance. Out of the two differently bonded oxygen atoms present on the basic surface site, one was decomposed into CO and CO_2 at 900°C and the other at 1200°C.

The neutral surface oxides are formed by the irreversible adsorption of oxygen at the unsaturated sites (ethylenic type) present on the carbon surface [23]. The oxygen atoms form aCCOOC bond that decomposes into CO_2 on heat treatment in vacuum. The neutral surface oxide is more stable than the acidic surface oxide, and begins to decompose in the temperature range 500600°C.

4.1.2. Carbon-Hydrogen Surface Groups

Hydrogen is the second hetero atom which is invariably present in carbon blacks. An accurate analysis of various types of commercial grade carbon blacks carried out by Studebaker and Puri et al (Table 1) indicates that the hydrogen contents vary between 0.01 and 0.7% by weight with a trend towards increase of hydrogen content with decrease in surface area, in furnace blacks. In general, a carbon hydrogen ratio (C:H) varying between 5 and 35 has been observed.

The chemisorption of hydrogen on carbon and graphite surface and on graphitized carbon black Spheron-6 (Graphon) surface has been extensively studied [2730]. It has been observed that the hydrogen is adsorbed as atoms and even at as low as room temperature although the rate of chemisorption is measurable around 200°C. Bansal et al [30] have shown that the chemisorption of hydrogen

takes place at carbon atoms situated at the edges and corners of the graphitic crystallites and that the chemisorption of hydrogen interstitially between the basal planes does not occur significantly [31]. Puri and Bansal [32] and Bansal et al [30] have shown conclusively that the chemisorption of hydrogen involves different sites associated with varying activation energies (Fig. 1).

The carbon-hydrogen surface compounds, though more stable than the carbon-oxygen surface compounds, are given out as water and elementary hydrogen on high temperature treatment in vacuum or in inert atmosphere. Thermal desorption studies of carbon blacks [89a] have shown that the evaluation of elementary hydrogen commences in small amounts around 700°C although it is desorbed in larger amounts and at higher rates between 1000 and 1200°C. An appreciable proportion of the chemisorbed hydrogen is retained even after evacuation at 1200°C, the last traces being removed at ~1600°C.

According to Redmond and Walker [27] the hydrogen in carbons is located predominantly on the surface with only a small amount being located in the crystal lattices. Snow et al [32a], while working on EPC carbon black,
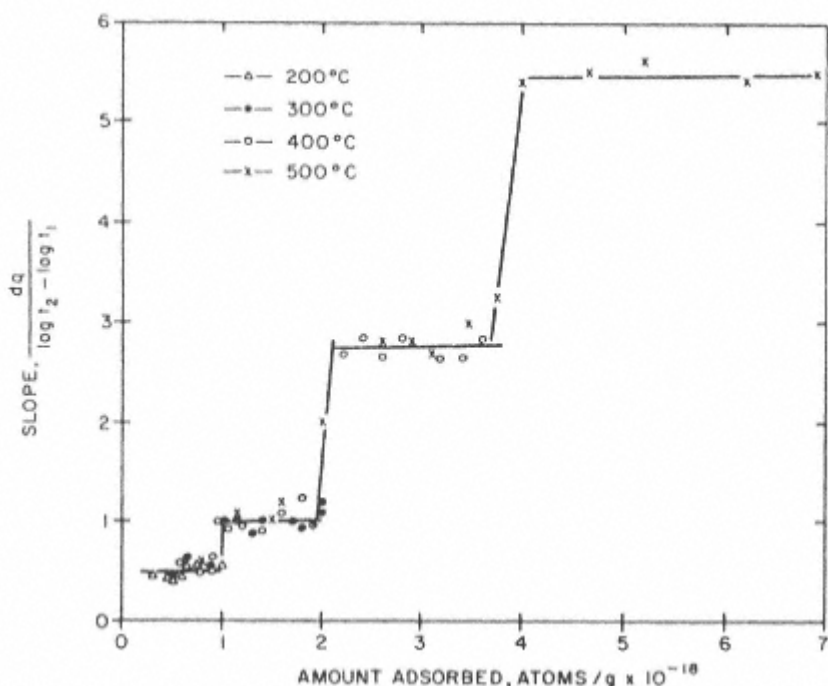
Fig. 1.
Slopes of Elovich plots as a function of amount of hydrogen adsorption at 200, 300, 400 and 500°C. Hydrogen pressure, 0.10 Torr (from ref. [30]).

observed that considerably more hydrogen was present in the outer 12 nm of the carbon particles than in the interior. The analysis of Studebaker [34] indicated that the surface hydrogen constituted about one hydrogen atom for each 3.2 carbon atoms at the edges of the layer planes in the case of channel blacks. However, Smith et al [35], on the basis of their experiments with Graphon, suggested that the hydrogen was distributed throughout the carbon particles and is not bound to the surface alone. Furthermore, on the basis of their stepwise oxidation of Graphon and the amount of hydrogen evolved, these workers reported that the hydrogen content in the interior of the graphon particles was more than on the surface.

However, they also suggested that the distributions of hydrogen in carbon blacks could be different since graphon, being a graphitized carbon black, has more homogeneous surface consisting primarily of basal planes.

Bansal et al [32,36,89a] while evacuating charcoal and carbon blacks observed that the amount of hydrogen desorbed as water and as free hydrogen was less than the value obtained by ultimate analysis. The balance of the hydrogen, which constitutes about 30% of the total, is retained by the carbons even on evacuation at 1200°C. These results led these workers [36] to suggest that a part of the hydrogen is associated with carbon atoms in the interior of the carbon particles.

The hydrogen in carbons is present as chemisorbed water and as part of the hydroxyl, phenol and hydroquinone groups. In addition it is also bonded to carbon atoms as C-H bonds.

4.1.3. Carbon-Nitrogen Surface Complexes

As received, carbon blacks do not contain significant amounts of nitrogen complexes. However, gas phase reactions of carbons with dimethylamine [34] at 150°C for about one hour or with dry ammonia [23,37,38] at 300°C introduce substantial amounts of carbon-nitrogen surface complexes. For example, Boehm et al [39] and Hofmann and Ohlerich [40] observed that when an oxidized charcoal was heated with dry ammonia, nitrogen was fixed on the surface. At low temperature, the fixation of nitrogen was equivalent to the number of acidic oxygen groups and was attributed to formation of ammonium salts. However, at high temperature treatment, a substitution of the hydroxyl group by amino group was postulated. Puri and Mahajan [41] observed that the interaction involved neutralization of the surface acidic complexes and fixation of some additional amounts in non-hydrolyzable form. But they could not attribute this fixtion of ammonia to any particular group on the carbon surface. Puri and Bansal [42] found that the treatment of chlorinated sugar charcoal with ammonia at 300°C resulted in the substitution of a part of the chlorine by amino groups. The resulting carbons were basic in character and showed enhanced adsorption for acids. The increase in the acid adsorption corresponded to nitrogen fixed, indicating an exchange of C-Cl bond by C-NH$_2$ bond. The interaction of ammonia gas with carbon fibers [43] before and after oxidation

showed that ammonia reacted with cyclic anhydrides and lactone structures resulting in the formation of imide structures.

Liquid phase reactions of diazomethane [44,45] or ammonia in methanol [46] with carbon blacks resulted in an uptake of nitrogen which is believed to occur by the formation of C-N bonds. The amount of nitrogen fixed by reaction with dimethylamine increases with the initial oxygen content of the sample [37] and the amount of bonded nitrogen was approximately equal to the amount of oxygen present in 1,4-quinone-type groups. Thus the reactions are attributed to occur at the 1,4-quinone and lactone groups on the carbon black surface. The carbon nitrogen surface complex is stable to thermal desorption. Heat treatment in the range 9001200°C is essential to desorb nitrogen which is evolved mostly as free nitrogen with small amounts of HCN, cyanogen and ammonia [23].

4.1.4. Carbon-Sulphur Surface Complexes

Sulphur is present in carbon blacks to the extent of 1% and in many different forms such as elemental sulphur, inorganic sulphate and as organosulphur compounds. The elemental sulphur can be removed by extraction

with various solvents and constitutes about 10% of the total sulphur [47]. The free elemental sulphur contributes to crosslinking during vulcanizations of rubber compounds while the chemically combined sulphur generally appears to be inert. The chemisorbed sulphur is present in the form of carbonsulphur surface compounds which are formed either during or subsequent to the formation of the carbon. However, their formation, their high thermal stability, the manner and the form in which they can be decomposed and their influence on the surface behavior of carbons are some of the factors which have been the source of investigations by different groups of scientists.

These sulphur surface compounds are non-stoichiometric, falling within a wide range of composition, depending on the nature of the carbon, the experimental conditions of their formation and the magnitude of the surface of the carbon. They frequently contain appreciable amounts of sulphur varying sometimes between 40 and 50%, even when the contribution due to sulphur contents of inorganic impurities is excluded. These surface compounds can be neither extracted with solvents, nor decomposed completely on heat treatment in vacuum at 1000°C but they can be removed completely as H_2S on heat treatment in hydrogen between 500 and 700°C. They are generally formed by heating a carbon in the presence of sulphur vapor [48,54,39,40,37], or sulphurous gases such as H_2S [37,5659,9296], SO_2 [53,54,6063] and carbon disulfide [64,53,54], or during carbonization of organic compounds containing sulphur [50] or during the carbonization of organic materials in the presence of elementary sulphur materials [65], yielding sulphurous pyrolytic products [66]. The solid sulphur surface compounds so obtained by different processes show many

similarities with regard to their non-stoichiometric character and chemical behavior although their formation by the different methods offers different possibilities of sulphur addition to, or substitution in, the carbon lattice.

The sulphur surface compounds are formed by the interactions of charcoal and carbon blacks with sulphur between 100 and 1000°C [4851,39,40]. The amount of sulphur fixed varies between 20 and 40%, only a part of which could be washed with solvents. The interaction of sulphur and H2S with carbon blacks [37] in the temperature range 150600°C involves two reactions: a rapid reaction which was directly proportional to the amount of oxygen present as 1,4-quinone groups indicating addition of one sulphur atom for each quinone type oxygen atom and a slow reaction which was retarded by the presence of oxygen atoms. The amount of oxygen fixed in the slow reaction was related to the hydrogen content of the carbon indicating an exchange for hydrogen.
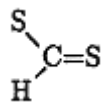
ESR studies of the carbon-sulphur surface compounds formed by interacting PVC, PVDC and cellulose chars with sulphur vapors and hydrogen sulphide gas indicated a decrease in the spin concentration progressively with

increasing sulphur content in low temperature carbons sulphurized with sulphur vapors. There was little change in spin concentration in case of PVC charcoal carbonized at 1000°C. It was suggested that the sulphur is fixed by chemisorption including spin pairing of sulphur with spin centers and by exchange with combined hydrogen. Although no definite structure was arrived at for the surface compound, it was suggested that surface thioethers and disulphids were the possible surface groups which formed peripheral heterocyclic structures on the layer lattice in the carbon surface or sulphur bridges between the adjacent layer. The presence of sulphide groups was based on the reaction of sodium azide with iodine and on certain reduction reactions.

The interaction of charcoal and carbon blacks with H_2S [5259,9296,102105] and SO_2 [5962,5255,57] indicated that the fixation of sulphur occurs partly by addition at the unsaturated sites, and partly by substitution in place of that part of oxygen which is evolved as CO on evacuation [58]. As carbon monoxide was evolved by the decomposition of phenolic and quinonic structures, it was suggested [5254,57] that the exchange with these groups leads to the formation of sulphide and hydrosulphide groups. Puri and coworkers [53], on the bases of their interactions of the carbon-sulphur compounds with oxidizing solutions such as aqueous chlorine, acidified potassium chlorate and concentrated nitric acid, suggested that different types of sulphur groups were formed by treatment with different sulphurizing agents. These workers speculated that the treatment with SO_2 produced readily oxidizable sulphoxides and sulphone structures as well as sulphide and hydrosulphide groups. The formation of sulfone and sulfoxide groups was evidenced by the chemisorption of appreciable amounts

of oxygen during the reaction of carbon with SO_2. The treatment with H_2S produced sulphide and hydrosulphide groups whereas the treatment with sulphur vapors produced highly stable sulphur containing aromatic ring structures. The presence of sulphide groups was evidenced by the sodium azide-iodine reaction.

Chang [66] prepared carbon-sulphur surface compounds by heating active carbons, carbon blacks, graphon, polymer chars, and petroleum pitches with carbon disulfide, H_2S, SO_2 and $SOCl_2$ (thionyl chloride) in the temperature range 800900°C. X-ray diffractometry and electron microscopy of the surface compound showed that it had a disordered structure. XPS spectra (Fig. 2) showed a carbon 1s binding energy of 284.3 eV and a sulphur $2p_{3/2}$ binding energy of 163.7 eV. On the basis of these binding energies and the FTIR absorption bonds at 1180 and 1150 cm-1, Chang suggested that these surface compounds were thiocarbonyls (=C=S) and thiolactons

$$\begin{array}{c} S \\ \diagdown \\ C{=}S \\ \diagup \\ H \end{array}$$

analogous to carbonyls and lactones existing on the surface of carbons. X-ray
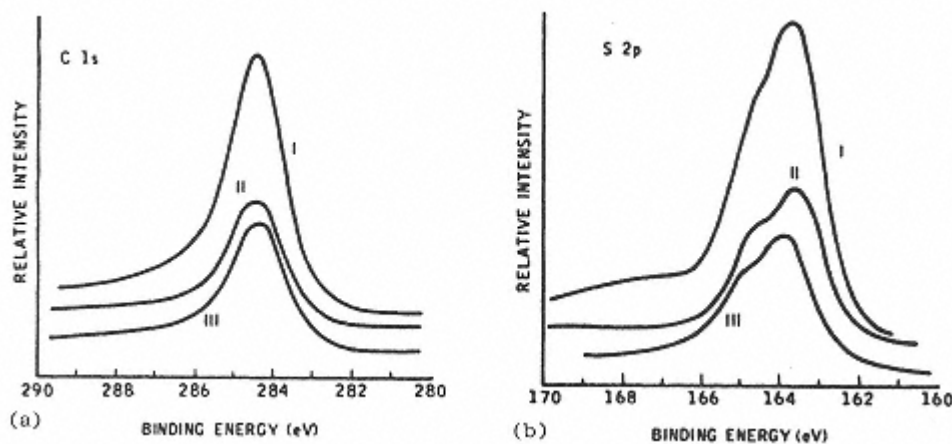
Fig. 2.
(a) XPS spectra of carbon 1s: (I) C_2S (PVDF); (II) mixture of PVDF charcoal and 24% sulfur; (III) C_2S (sucrose). (b) XPS spectra of sulfur 2p: (I) C_2S (sucrose); (II) mixture of PVDF charcoal and 24% sulfur; (III) C_2S (PVDF). From ref. [66].

photoelectron spectroscopy (XPS) analysis of a carbon black EC-A-sulphur compound containing 1.7% sulphur indicates that sulphur is present in two different chemical states. A sulphur 2p peak with a binding energy of ~164 eV, the one similar to the one obtained by Chang [66], was interpreted as originating from sulphur bonded directly to the graphitic ring structure or as an inclusion in the ring structure. The sulphur 2p peak observed at a binding energy of ~169 eV is attributed to the presence of sulphur in the +6 state such as in a sulphate-like group (S^{6+}). On heat treatment at 800°C, the sulphate-like group is converted to SO_2, H_2S or S.

The carbon-sulphur surface compounds are extremely stable and are not decomposed on refluxing with strong alkalis or on degassing at 1000°C in vacuum or in an inert atmosphere. They,

however, can be desorbed as H2S completely on heat treatment with hydrogen between 500 and 700°C.

4.1.5. Carbon-Halogen Surface Compounds

The treatment of activated carbons, charcoal and carbon blacks with halogens in the gaseous and aqueous phase results in the adsorption of appreciable amounts of the halogen to form stable carbon-halogen surface compounds. The amount adsorbed depends upon the nature of the carbon surface, the oxygen and hydrogen contents of the carbon, the experimental conditions and the nature of the halogenating species. The adsorption is both physical [67,78] and chemical and proceeds through one or several mechanisms which include addition at the unsaturated sites [33,6975], exchange

with chemisorbed hydrogen [7075] and surface oxidation of the carbon when the reaction is in the aqueous phase [71,73,76]. In addition, the interaction in the gaseous phase may involve dehydrogenation of the carbon surface. The carbon-halogen surface compounds are highly stable and cannot be desorbed on heat treatment in vacuum up to 1000°C if the carbon has no residual hydrogen. However, a part of the halogen could be exchanged with -OH groups on treatment with alkali hydroxides [69] and with -NH$_2$ groups on treatment with gaseous ammonia.

The reactivity of halogens toward carbon decreases in the order chlorine > bromine > iodine and the stability of the corresponding carbon-halogen surface compounds also varies in the same order. Thus while all of the adsorbed iodine could be dissociated from the carbon black surface, only 80% of bromine and 60% of chlorine could be dissociated in the presence of suitable neucleophiles [77]. Puri and Bansal [69] and Puri et al [33,70,78,79] while studying the interaction of charcoal and carbon blacks with chlorine observed that the fixation of chlorine on charcoal occurs partly by addition at the unsaturated sites vacated by the associated oxygen [70,79] and partly by substitution for hydrogen in the case of charcoal while the carbon blacks fixed almost all of their chlorine by exchange with hydrogen (Table 2). These views were substantiated by the chlorination of anthracites by Walker et al [80] and by Puri et al in their reactions of charcoal with chlorine water [71], a mixture of HCI and H$_2$O$_2$ [81], and a mixture of oxygen and chlorine at 400°C [82].

Tobias and Soffer [83], through a study of the stepwise chlorination of carbon cloth (TCM128), a carbon black (Continex N-110) and a

graphitized carbon black (Carbopak B), after outgassing them at 1000°C to eliminate the influence of associated oxygen, observed that the interaction involved addition, exchange and dehydrogenation. The addition was the first to occur both in carbon cloth and carbon black while the exchange reactions were more predominant in the case of carbon blacks [69]. There was little dehydrogenation in carbon blacks but high in active carbon. The exchange reactions involved an exchange of C-H bond by C-Cl bond during chlorination and an exchange of C-Cl bond by C-H bond during hydrogenation.

The interaction of carbon with bromine involved the same mechanism as the interaction with chlorine. The fixation of bromine occurred by addition at the ethylenic double bond sites which were created by the elimination of that part of the associated oxygen which was evolved as CO_2 on evacuation [79,70]. Puri et al [70,79], Bansal et al [76] and Stearns and Johnson [84] thus suggested that the adsorption of bromine from its aqueous solutions is a measure of the unsaturation in a given sample of charcoal or carbon black. Brooks and Spotwood, working with bituminous coal, observed three different types of adsorbed bromine. A part of bromine which could be removed

Table 2. Fixation of Bromine by Various Samples of Charcoal and Carbon Black before and after Fixation of Chlorine (Values in m.eq/g)

Sample	(a) H_2 present in sample	(b) Cl_2 fixed at 450°C	(c) before chlorination	(d) after chlorination	(e) Cl_2 fixed by addition [(cd)]	(f) Cl_2 fixed by substitution [(b) (e)]
			Unsaturation as determined by Br_2 uptake from aqueous solution			
Coconut charcoal						
degassed at 400°C	20.10	10.28	2.40	0.65	1.75	8.53
degassed at 700°C	10.10	5.63	3.16	0.93	2.23	3.4
degassed at 1000°C	6.40	3.39	3.14	1.14	2.00	1.39
degassed at 1200°C	6.10	2.31	3.16	1.24	1.92	0.39
Carbon black						
Philblack-A	3.50	3.57	0.30	nil	0.30	3.27
Spheron-9	5.30	3.31	0.43	nil	0.43	2.88
Spheron-6	4.90	3.97	0.62	nil	0.62	3.35
Spheron-4	3.80	3.14	0.45	nil	0.45	2.69
Spheron-C	2.50	2.65	0.70	nil	0.70	1.95
ELF-O	3.80	4.48	0.12	nil	0.12	4.34
Mogul	3.00	3.15	nil	nil	nil	3.15

From ref. [46].

with boiling water or alcohol was attributed to addition compounds of phenanthrene or anthracene type; another part which could be recovered by hydrolysis with sodium hydroxide was ascribed to residual aliphatic or alicyclic structures, while the third part which could not be removed except under strongly alkaline conditions was considered to be exchanged for hydrogen in polycyclic ring systems. The interaction of charcoal and carbon blacks with bromine dissolved in carbon tetrachloride solutions was partly reversible and partly irreversible (Tables 3 and 4) [72,85]. The irreversible adsorbed bromine involved both addition at the unsaturated sites and exchange for hydrogens. The interaction with bromine vapors, like chlorine, involved addition and exchange and caused dehydrogenation in charcoal but only exchange reactions in carbon blacks [74]. The amount of bromine fixed was as high as 38% in charcoal and about 31% in Spheron-9 carbon black.

The interaction with iodine from aqueous or nonaqueous solutions does not involve chemisorption of iodine of formation of carbon-iodine surface compounds. The adsorption of iodine was purely physical and has been used as a measure of surface area [8689], although opinions differ as to the way iodine is adsorbed on carbons. While Hill and Marsh [89] view it as a process of micropore filling and multilayer adsorption, Puri and Bansal [86] and Juhula [87] view it as a monolayer adsorption from both aqueous and nonaqueous solutions. The reaction of iodine vapors with carbons involved addition at the unsaturated sites with maximum uptake observed around 300°C [23].

4.2. Characterization of Surface Groups

Carbon-oxygen surface groups are by far the most important

surface groups which influence the surface characteristics and surface behavior of carbons. Consequently attempts have been made to identify and estimate them using several physical, chemical, and physico-chemical techniques which include desorption of the oxygen groups, neutralization by bases, potentiometric, thermometric and radiometric titrations, direct analysis by specific chemical reactions, polarography, infrared spectroscopy and X-ray photoelectron spectroscopy. On the basis of these investigations the existence of such functional groups as carboxyl, phenols, lactones, aldehydes, ketones, quinones and hydroquinones, anhydrides and ethereal structures have been postulated. However, these methods have not yielded comparable results and the entire amount of combined oxygen has not been accounted for. Thus Puri [23] has suggested caution in the interpretation of the results as the surface groups on carbon are unlikely to behave exactly in the same way as those in simple organic compounds.

Table 3. Reversible and Irreversible Adsorption of Bromine by Carbon Blacks and Sug Charcoal of Different Specific Areas, Surface Unsaturations, and Hydrogen Contents

	(a)	(b)	(c)	(d)	(e)	(f)	(g)
Carbon	Surface area, m2/g	Hydrogen content	Bromine adsorbed reversibly	Bromine adsorbed irreversibly	HBr formed (bromine fixed by substitution)	Surface unsaturation (bromine fixed by addition at unsaturated sites)	Bromine unaccounted for [d-(e+f)]
Mogul	308	480	171	132	23	16	93
Mogal-A	228	510	132	131	18	14	99
Elf-0	171	471	105	124	25	13	86
Spheron-C	253	332	144	148	19	70	59
Spheron-4	153	472	86	117	21	41	55
Spheron-9	116	620	65	118	23	42	53
Philblack-A	46	350	26	32	11	11	10
Philblack-I	116	242	68	57	16	21	20
Philblack-E	135	310	72	61	13	22	26
Vulcan-SC	194	140	111	122	11	64	48
Philblack-O	80	310	38	45	12	18	15
Kosmos-40	31	350	11	24	8	9	7
Carbolac	839	470	226	183	32	96	55
Sugar	412	1984	210	393	140	46	207

From ref. [72].

Table 4. Effect of Outgassing Carbon Blacks and Sugar Charcoal on Reversible and Irreversible Adsorption of Bromine[a]

Carbon	(a) Surface area, m2/g	(b) Bromine adsorbed reversibly	(c) Bromine adsorbed irreversibly	(d) HBr formed (bromine fixed in substitution for hydrogen)	(e) Surface unsaturated (bromine fixed by addition at unsaturated sites)	(f) Bromine unaccounted for [c−d(d+e)]
Mogul						
original	308	171	132	23	16	93
outgassed at 600°C	335	183	267	13	76	178
outgassed at 1000°C	828	173	221	0	74	147
Carbolac						
original	839	226	183	32	96	55
outgassed at 600°C	815	232	291	20	168	103
outgassed at 1000°C	760	201	272	11	170	91
Spheron-C						
original	253	144	148	19	70	59
outgassed at 600°C	290	173	183	15	88	80
outgassed at 1000°C	281	160	174	10	82	82
Vulcan-SC						
original	194	111	122	11	64	47
outgassed at 600°C	202	118	154	0	80	74
outgassed at 1000°C	198	104	152	0	76	76
Sugar charcoal						
original	412	210	393	140	46	207
outgassed at 600°C	637	282	557	119	380	58

| outgassed at 1000°C | 388 | 201 | 433 | 0 | 375 | 58 |

a Columns (b) - (f) expressed in milliequivalents per 100 grams.
From ref. [72].

4.2.1. Thermal Desorption

The surface groups present on received carbon blacks or formed as a result of interaction with oxygen or oxidizing gases or oxidizing solutions are generally quite stable even under vacuum at temperatures below 200°C irrespective of the temperature at which they are formed. However, when they are heated at higher temperature they decompose, producing CO_2 and H_2O vapor at lower temperatures and CO and H_2 at higher temperatures. They are desorbed almost completely at 1000°C.

Puri and Bansal [89a] evacuated 15 samples of carbon blacks representing furnace, channel and color blacks at temperatures up to 1200°C. The total oxygen evolved as CO_2, CO and H_2O vapor is in fairly good agreement (Table 5) with the total oxygen obtained by ultimate analysis. The total hydrogen evolved as water vapor and free hydrogen is significantly less, by ~30%, than the hydrogen content obtained by ultimate analysis, indicating that the hydrogen was held much more firmly. The surface groups evolving CO_2 are much less stable than the surface groups evolving CO. The evolution of CO_2 commences around 200300°C and ends at about 600700°C while that of CO begins at ~500700°C and finishes in the 10001200°C temperature range (Table 6). Free hydrogen was evolved in the 500700°C range and continued even at 1200°C. However, there was no correlation between total oxygen (or any part thereof) and total hydrogen (or any part thereof).

The total oxygen content remains below 1.5% in the case of furnace blacks (Table 5), between 3 and 4% in channel and between 4 and 8% in color blacks. The higher oxygen content of color blacks is consistent with the observation [90,91] that 400°C

(the temperature around which the color blacks are exposed to air) is the optimum temperature for the fixation of oxygen on exposure of carbons to air. The oxygen present as CO_2-complex constitutes about 14–17% and 30% of the total oxygen in channel and color blacks, respectively. The total oxygen content in most of the furnace blacks was too low for a satisfactory proportion of oxygen evolved as CO_2. The greater proportion of the CO_2-complex in color blacks appears to be due to their exposure to air at 400°C. The channel blacks which are exposed to air at the higher temperature of the order of 600°C contain a much smaller proportion of this complex on account of the instability of the complex at this temperature. The oxygen present as CO-complex constitutes nearly 50–60% of the total oxygen in most of the carbon black samples. Broadly speaking, the furnace, channel and color blacks contain 9, 25 and 30 mg oxygen per 100 m^2 of the surface. The channel blacks rank with furnace blacks in having a lower value (3 mg/100m^2) of oxygen disposed of as CO_2 complex (Fig. 3) but with color blacks in having a higher value (~16 mg/100m^2) of oxygen disposed of as CO-complex per unit surface (Fig. 4). This is due to the fact that the air treatment at ~600°C to which channel blacks are subjected

Table 5. Surface Area and Surface Oxygen and Hydrogen Complexes of Various Carbon Blacks

Trade name	Type	Nitrogen surface area, m2/g	Oxygen evolved on outgassing at 1200°C, g/100g				Oxygen by ultimate analysis, %	Hydrogen evolved on outgassing at 1200°C, g/100g			Hydrogen by ultimate analysis, %
			CO2	CO	H2O	total		H2O	H2	total	
Pelletex	Furnace	27.1	0.051	0.331	0.133	0.52	0.22	0.016	0.238	0.25	0.38
Kosmos-40	"	31.2	0.088	0.320	0.017	0.48	0.23	0.009	0.209	0.22	0.35
Statex-B	"	48.3	0.115	0.400	0.089	0.60	0.43	0.011	0.248	0.26	0.36
Philblack-A	"	45.8	0.187	0.343	0.000	0.53	0.58	0.000	0.209	0.21	0.35
Philblack-O	"	79.6	0.209	0.428	0.107	0.74	0.79	0.013	0.207	0.22	0.30
Philblack-I	"	116.8	0.348	0.628	0.355	1.33	1.17	0.042	0.139	0.18	0.29
Philblack-E	"	135.1	0.401	0.411	0.435	1.26	1.01	0.054	0.137	0.19	0.31
Vulcan-SC	"	194.4	0.428	0.800	0.133	1.36	1.18	0.016	0.094	0.11	0.17
Spheron-9	Channel	115.8	0.536	1.928	0.710	3.17	3.49	0.089	0.321	0.41	0.62
Spheron-6	"	120.0	0.500	2.122	0.462	3.08	3.10	0.058	0.284	0.34	0.55
Spheron-4	"	152.7	0.547	2.829	0.689	4.06	3.28	0.086	0.232	0.32	0.47
Spheron-C	"	253.7	0.575	2.000	0.600	3.17	3.14	0.075	0.152	0.23	0.33
ELF-O	Colour	171.0	1.176	2.171	0.710	4.05	4.89	0.089	0.247	0.34	0.47
Mogul-A	"	228.4	1.894	4.228	0.979	7.10	7.63	0.122	0.236	0.36	0.51
Mogul	"	308.0	2.205	4.180	1.440	7.82	8.22	0.180	0.132	0.31	0.48

Table 6. Analysis of the Gas Evolved on Evacuating Mogul and Mogul-A at Different Temperatures

Temperature, °C	Weight percent oxygen evolved as:				Weight percent hydrogen evolved as:		
	CO_2	CO	H_2O	total	H_2O	H_2	total
				Mogul			
30200	nil	nil	nil	nil	nil	nil	nil
200300	0.220	nil	0.178	0.398	0.022	nil	0.022
300400	0.661	nil	0.417	1.078	0.052	nil	0.052
400500	0.655	nil	0.791	1.446	0.099	nil	0.099
700800	0.269	2.000	0.019	2.288	0.002	0.085	0.087
8001000	0.008	0.612	0.026	0.646	0.003	0.082	0.085
10001200	0.014	0.251	0.009	0.274	0.001	0.007	0.008
				Mogul-A			
30200	nil	nil	nil	nil	nil	nil	nil
200300	0.356	nil	0.196	0.552	0.024	nil	0.024
300400	0.579	nil	0.160	0.739	0.020	nil	0.020
400500	0.519	nil	0.533	1.052	0.067	nil	0.067
500700	0.417	1.071	0.044	0.532	0.005	0.035	0.040
700800	0.004	0.739	0.045	1.788	0.006	0.092	0.098
7001000	0.010	0.830	0.000	0.840	0.000	0.084	0.084
10001200	0.000	0.590	nil	0.590	nil	0.025	0.025
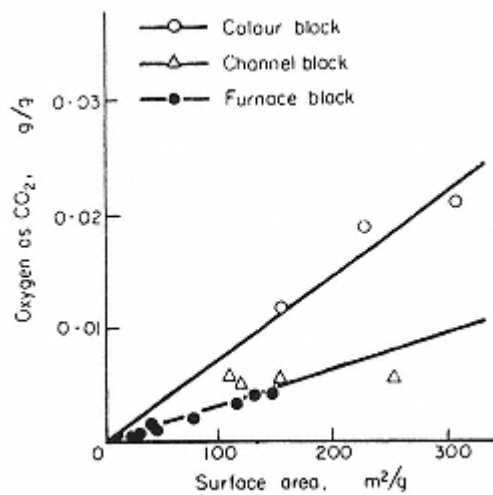
Fig. 3.
Relation between oxygen evolved as
carbon dioxide and surface area
(from ref. [89a]).

during their formation eliminates most of the CO2-complex without appreciably affecting the CO-complex (Table 6).

Similar thermal desorption of Spheron-6 at heat treatment temperatures up to 1000°C [92] showed that the order of thermal stability for desorption is H2>CO>CO2 (Fig. 5). Several similar desorption studies using different types of carbons have been carried out by several workers [36,93102] using several different techniques. All these studies suggested that the chemisorbed
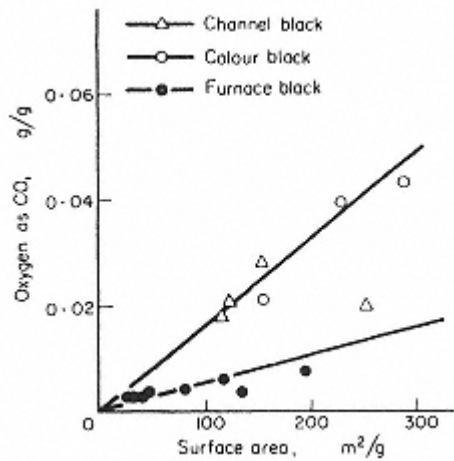
Fig. 4.
Relation between oxygen evolved
as carbon monoxide and surface
area (from ref. [89a]).
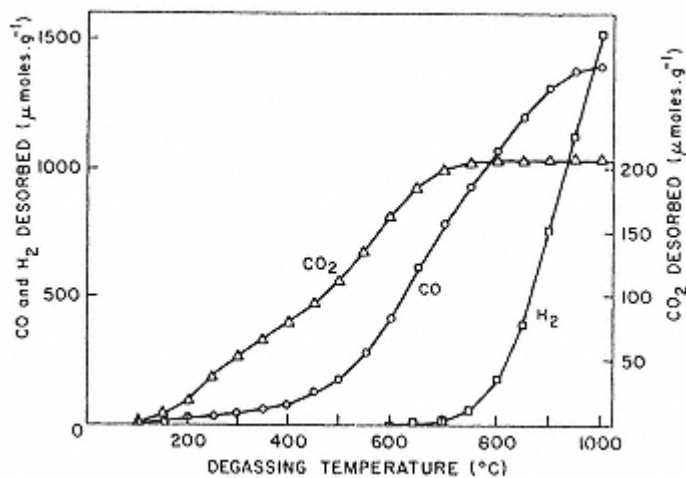
Fig. 5.
Amounts of CO, CO2, and H2 desorbed when
Spheron 6 is degassed at various temperatures
(from ref. [92]).

oxygen in carbons constitutes different surface structures which involve different sites associated with varying energies and that CO2 and CO are evolved from two different surface structures. The surface chemical structures that evolve CO2 are less stable and decompose at temperatures as low as 300°C and could be carboxylic or lactonic functions. The other chemical structures, which evolve CO, are fairly stable, and decompose only above 500°C, could be postulated as phenols or quinones.

4.2.2. Neutralization of Surface Groups

The nature and the amount of surface groups can be determined by titration with alkalies. However, the standard conditions under which reproducible and comparable results can be obtained have been realized only during the last two or three decades. Under these conditions the carbon sample is first outgassed at 150°C to remove

any physically adsorbed gases and then contacted with 0.10.2N alkali solution for times varying between 24 and 72 hrs. The contact time, however, can be reduced to a few hours if the carbon and the alkali solution are heated under reflux. These standard conditions are now being followed by most of the workers.

The titration of ink and channel blacks with alkalies led Schweitzer and Goodrich [103], Studebaker et al [45] and Hoffman and Ohlerich [40] to suggest the presence of carboxylic groups on the carbon black surface. Garten and Weiss [24], on the hasis of their titration curves on sugar carbons, and Villars [104], on ink and other carbon blacks, attributed the acidity of both types of carbons to phenolic hydroxyl groups attached to the edges of the layer planes. Garten and Weiss in their work on the reaction of carbons with

diazomethane and subsequent hydrolysis postulated the existence of flourescein type lactones (-lactone) which behaved as weak acids, were methylated with diazomethane and subsequently hydrolysed by a mineral acid. The difference in the surface acidity measured by alkali neutralization and that due to lactone and phenols was explained by postulating yet another lactone (*n*-lactone) which reacted with alkalies but not with diazomethane. The presence of these two types of lactones was deduced on the basis of their IR absorption bands at 1760 and 1210 cm-1. However, Van der Plas [46], on the basis of his reaction of carbon blacks with hydrochromic acid dissolved in glacial acetic acid, indicated the absence of lactone groups in carbon blacks.

Rivin [102,105,106] combined acidimetry and vacuum pyrolysis technique to determine the distribution of functional groups on several carbon blacks and attributed surface acidity to carboxylic, phenolic, neutral lactone and to quinone groups (Table 7). These results are based upon determination of total acidity by titration with lithium aluminum hydride, selective neutralization techniques using bases of different strengths [25], reduction of neutral groups to acidic groups, and analysis of vacuum pyrolysis products of the surface oxide layer. Rivin also determined the influence of heat treatment up to 1500°C on the surface group distribution of as-received and oxidized HAF blacks. The heat treatment up to 450°C causes little or no change in the relative amounts of carbon-hydrogen (-H) or hydroxyl groups ($^{)}$OH) while amounts of carboxyl ($^{)}$COOH), lactonic ($^{)}$CO2) and the quinonic groups decrease considerably. In general, carboxylic and lactonic groups start decomposing at much lower temperatures while the phenolic and quinonic structures decompose almost completely in the

temperature range 500900°C. The carbon-hydrogen groups are the most stable and are decomposed completely on heat treatment at 1500°C.

Puri and coworkers [107,108] examined a large number of sugar and coconut charcoals before and after outgassing and after extensive oxidation treatments in oxygen, as well as oxidizing solutions [20,71,90], and tried to correlate the base neutralization capacity of these carbons with the oxygen evolved as CO_2 on evacuation at 1200°C (termed CO_2-complex). Puri and Bansal [12] extended this work to carbon blacks. The surface acidity of carbon blacks was determined by neutralization with sodium and barium hydroxides and was observed to be close to each other as well as to the amount of CO_2-complex (Table 8) contained in each sample. The base neutralization of a carbon black decreased gradually with outgassing of the samples at gradually increasing temperatures and the decrease at any temperature corresponded with the decrease in the CO_2-complex at that temperature (Table 9). When the entire amount of the complex was eliminated on outgassing around 750°C the carbon blacks lose the capacity to react with alkalies altogether even though they still retain appreciable amounts of oxygen which is evol-

Table 7. Chemical and Thermal Analysis of Surface Groups on Carbon Blacks[a]

Carbon	Type	Surface area, m2/g	Volatile content, %	H2, mmol/g	CO2, mmol/g	CO, mmol/g	>-COOH, meq/g	>-OH, meq/g	>=O, meq/g	>-CO2 meq/g	>-H meq/g
Black Pearls2	C[b]	744	15.8	0.47	4.74	1.46	0.45	2.00	2.81	0.02	0.47
Black Pearls A	C	299	12.6	0.52	3.53	1.80	0.28	1.30	2.29	0.24	2.02
Black Pearls 74	C[c]	322	4.85	0.18	1.31	1.32	0.06	0.89	0.49	0.12	1.69
Vulcan 6	F[d]	114	2.47	0.18	0.51	0.70	0.02	0.56	0.00	0.16	0.82
Regal 600	F	108	2.19	0.13	0.51	0.50	0.02	0.54	0.02	0.00	0.46
Sterling S	F	23	1.09	0.05	0.17	0.68	0.00	0.18	0.02	0.05	3.18
Regal SRF	F	30	1.46	0.07	0.28	1.47	0.00	0.21	0.11	0.07	2.73
Sterling MT	T	6	0.54	0.02	0.07	1.12	0.00	0.10	0.00	0.02	2.14

[a]From ref. [102].
[b]Channel black.
[c]Furnace black.
[d]Thermal black.

Table 8. Alkalis Neutralized by Various Samples of Carbon Blacks in Relation to CO2 Evolved on Outgassing Them

| Trade name | Type | Barium hydroxide neutralized, meq/100g | | Sodium hydroxide neutralized, meq/100g | | CO2 evolved on outgassing at 1200°C, meq/100g |
		by shaking for 60 hr	by heating for 6 hr	by shaking for 60 hr	by heating for 6 hr	
Pelletex	Furnace	27	3-3	5-1	4-3	3-2
Kosmos-40	"	5-3	58	5-2	5-1	5-5
Statex-B	"	7-5	6-3	6-5	7-6	7-2
Philblack-A	"	10-6	9-5	9-1	9-6	11-7
Philblack-O	"	15-9	15-8	12-8	14-4	13-1
Philblack-I	"	21-2	20-7	19-5	19-2	21-8
Philblack-E	"	23-9	25-2	22-7	26-9	25-1
Vulcan-SC	"	26-6	28-4	23-7	27-9	26-8
Sterling-V	"	17-1	18-9	16-9	18-5	18-8
Spheron-9	Channel	29-9	28-2	28-5	28-9	33-5
Spheron-6	"	31-9	29-4	26-6	28-9	31-2
Spheron-4	"	31-5	33-5	31-1	32-9	34-2
Spheron-C	"	37-7	37-8	38-8	35-7	35-9
ELF-O	Color	70-5	69-3	68-2	72-2	73-5
Mogul-A	"	113-2	115-2	114-8	134-7	137-8
Ck-4	Germen	28-2	31-2	29-9	30-5	30-3

From ref. [12].

Table 9. Decrease in the Amount of Barium Hydroxide Neutralized By Mogul-A and Mogul after Outgassing at Various Temperatures in Relation to the Amount of CO_2 Evolved at Each Temperature

Temperature of outgassing (°C)	Barium hydroxide neutralized (meq/100g)	Decrease in barium hydroxide neutralized (meq/100g)	CO_2 evolved on outgassing (meq/100g)
Mogul-A			
30	115.2	nil	nil
200	115.2	nil	nil
300	93.7	21.5	22.2
400	58.6	56.6	58.4
500	23.6	91.6	90.9
700	0.4	114.8	117.0
800	nil	115.2	117.2
1000	nil	115.2	117.8
1200	nil	115.2	117.8
Mogul			
30	138.5	nil	nil
200	138.5	nil	nil
300	127.4	11.1	13.8
400	81.7	56.8	55.1
500	45.2	93.3	96.6
700	21.7	116.8	119.2
800	1.6	136.9	136.0
1000	nil	138.5	136.5
1200	nil	138.5	137.4

ved as CO.

The oxidation of carbon blacks with nitric acid resulted in a considerable loss of carbon and in the fixing of considerable

amounts of oxygen, most of which was desorbed as CO_2 on evacuation. The base neutralization capacity of the oxidized samples in each case increased in proportion to the amount of CO_2-complex formed (Table 10). The removal of CO_2-complex on evacuation, once again, caused a corresponding decrease in the base adsorption capacity. Puri and Mahajan [41], Anderson and Emmett [109], and Puri, Talwar and Sandle [110] studied the adsorption of ammonia and several amines on several charcoals and carbon blacks and observed that the amount adsorbed was close to the amount of CO_2-complex present on the carbon surface.

Table 10. Treatment of Carbon Blacks with Nitric Acid

Trade name	Type	Loss of carbon due to oxidation, g/100g	Total oxygen present on the sample, g/100g		Barium hydroxide neutralize, meq/100g	CO_2 evolved on outgassing at 1200°C, meq/100g
			Before treatment	After treatment		
Pelletex	Furnace	17.4	0.52	1.92	75.6	78.1
Spheron-6	Channel	26.5	3.08	6.95	252.6	256.5
Mogul	Color	42.5	7.82	14.34	529.2	524.2

Thus Puri and coworkers are of the view that in charcoal as well as in carbon blacks, the same surface group which is involved in the liberation of CO_2 on evacuation is also involved in the neutralization of alkalies. This cannot be a carboxylic group since there is no significant correlation between CO_2 evolved and active (Grignard) hydrogen. This cannot be a lactone group as suggested by Garten and Weiss [24] because it did not show equivalence between CO_2 evolved and alkali neutralized. However, Puri and his coworkers did not rule out the possibility of the existence of certain types of lactone structures which would hydrolyse to give a carboxylic group and a phenolic hydroxylic group, each capable of stoichiometric ionic adsorption.

Boehm [25] differentiated the acidic surface groups on oxidized charcoal and carbon black by selective neutralization technique using bases of different strengths, namely $NaHCO_3$, Na_2CO_3, NaOH and C_2H_5ONa. The strongly acidic groups, neutralized by $NaHCO_3$ but not by Na_2CO_3, were believed to be lactone. The weakly acidic groups, neutralized by NaOH but not by sodium carbonate, were postulated as phenols. The reaction with sodium ethoxide was not considered a true neutralization reaction since it did not involve exchange of $H+$ by $Na+$ ions. The groups reacting with sodium ethoxide but not with sodium hydroxide were suggested to be carbonyls which were created by the oxidation of the disorganized aliphatic carbon [25]. Puri [23], however, questioned the validity of the selective neutralization technique in determining the acidic groups of varying strengths. According to him, the same acid group will neutralize different amounts of alkalies of varying strengths. For example, a weak acid like acetic acid can be neutralized only partially when titrated against

$NaHCO_3$ or Na_2CO_3, while the same acid can be neutralized completely by NaOH.

Barton and coworkers [92,111,112] investigated acidic surface oxygen groups on a sample of graphite and a carbon black Spheron-6, by degassing these samples at different temperatures and determining quantitatively the amount of CO_2 evolved at each temperature using a mass spectrometer and measuring the base neutralisation capacity of the degassed samples. In the case of Spheron-6, they observed the presence of two types of acidic oxygen groups both of which decompose to give CO_2, one decomposing at about 250°C and the other at 600°C. A plot of base uptake against CO_2 (Fig. 6) on the surface shows two intersecting stright lines. The first linear region which corresponded to the desorption of CO_2 at temperatures around 600°C showed a slope of 2 indicating that the acidic group being desorbed is dibasic. The second linear region had a slope of 1 indicating that the acidic oxide was monobasic in character. Combining these studies with the change in the surface acid groups on reaction with methyl magnesium iodide and diazomethane, these workers suggested the presence of two type of acidic groups in Spheron-6. Both these groups are lactones but only one of them has active
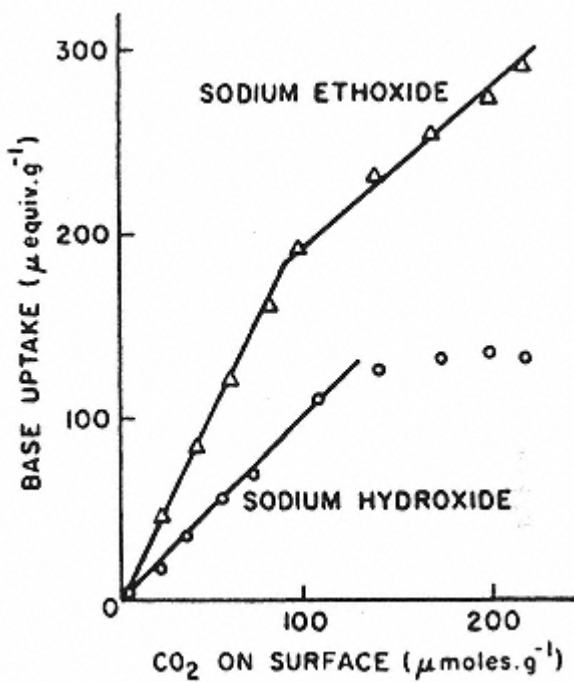
Fig. 6.
Relationship between base neutralization
capacity of a carbon and CO_2 desorbing
complex on its surface from Spheron-6
(from ref. [92]).

hydrogen associated with it.

Bansal et al [114] extended their earlier work on surface acidic groups on carbon blacks [12] to acidic surface groups on polymer charcoals. The base neutralisation with sodium hydroxide was almost exactly equivalent to the amount of CO_2 evolved on evacuation in case of PVDC, PVC and saran charcoals but was almost half of the amount of CO_2 evolved in case of PF (polyfurfural) and UF (urea formaldehyde) charcoals. The base neutralization capacity decreased on evacuation at gradually increasing temperatures and the decrease at any temperature

corresponded to the amount of CO_2 evolved at that temperature. Futhermore, the temperature interval over which the drop in base neutralization capacity occurred appeared to be the same as the temperature interval over which CO_2 was eliminated from the charcoal sample. The relationship between the associated oxygen desorbing as CO_2 on evacuation and the base neutralization capacity (Fig. 7) indicates that for every millimole of CO_2 evolved the base neutralization capacity decreased by 1 milliequivalent in PF charcoal and by 2 milliequivalent in PVDC charcoal. Thise showed that the acidic groups were monobasic in PF charcoal and dibasic in PVDC charcoal. This monobasic character of some carbons could be explained only if there is a phenolic group in conjunction with a carboxylic group. The phenolic group will neutralize the base but would not evolve
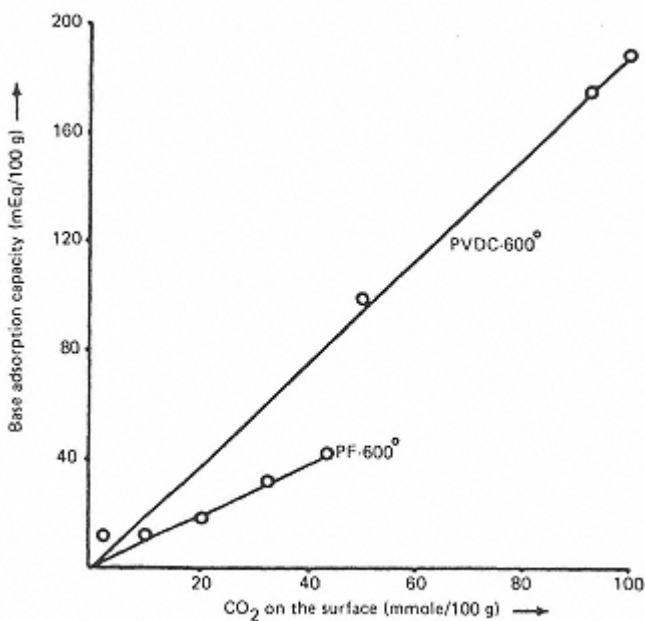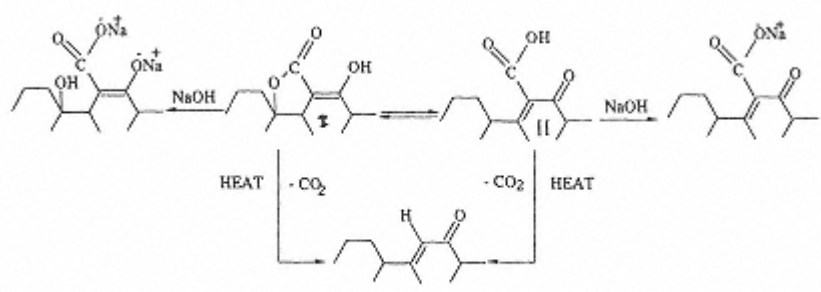
Fig. 7.
Relationship between base adsorption and
acidic oxide desorbing as CO_2 (from ref. [114]).

CO_2. Since the existence of phenolic groups is still under dispute, it could be present as part of a lactone. The possible structure for lactone which would explain most of the data on desorption and base neutralization could be an *f*-lactone suggested by Garten and Weiss [24] and later restated by Barton et al [111,112]. The lactone exists in two tantomeric forms. The keto form explains the base adsorption capacity of carbons with monobasic surface group whereas the enol form is applicable in the case of dibasic (see structure 1) surface group. The existence of these two forms is quite reasonable in the case of different carbons since the presence of individual oxygen-containing surface groups and their proportions are very much dependent on the starting material from which the carbons are obtained.

Structure 1 (from ref. [114]).

Structure 1
(from ref. [114]).

4.2.3. Electrochemical Methods

Several workers have used electrochemical methods for determining the acidic structures on carbon blacks since these methods are more precise and require small amounts of the black sample. The procedure essentially consists of preparing a suspension of the carbon black in CO_2-free distilled water and adding standard alkali solutions in small amounts and measuring the current using a precision instrument.

Wiegand [115] measured the *pH* of carbon blacks and observed a relationship between the *pH* and the volatile content of the carbon black which in turn was related to the carboxylic acid concentration. The *pH* of the carbon black decreased with an increase in the concentration of the carboxylic group. The heat treatment which removes the carbon-oxygen surface groups enhanced the *pH* of the carbon black, the heat treatment at 1000°C producing a carbon black with a basic *pH* of 10.8. Villars [104] used 0.5N KOH to carry out potentiometric titrations of several carbon blacks and observed no inflection points. However, Puri and Bansal [12], in their potentiometric titration with 0.1N barium hydroxide, observed that the end points, though not sharp (Fig. 8), could be located without much difficulty. The base neutralization values observed at the inflection points agreed fairly well with those obtained by direct titration. The shapes of the isotherms indicated the presence of weaker acid structures such as phenols because the *pK* values were between 9 and 10. However, when one of the sample, Mogul, was oxidized with nitric acid which extended its surface acidity from 115 to 530 meq/100g, the shape

of the titration curve indicated the presence of a much stronger group like carboxyl (Fig. 9), the pK value now being 5.5.

Studebaker [116] conducted potentiometric titration curves of a number of carbon blacks in ethylene diamine using 0.1N sodium aminoethoxide as the titrant. The titration curves of carbon blacks with high oxygen contents showed two inflections which were attributed to carboxylic and phenolic groups. The low oxygen content carbon blacks showed only one break which was ascribed to phenols. Garten and Weiss [24], however, on the basis of the shapes of titration curves questioned the presence of carboxylic acid groups.

Papirer and Guyon [117] titrated carbon blacks potentiometrically using bases of different strength such as $NaHCO_3$, Na_2CO_3, and $NaOH$. This selective neutralization technique indicated the presence of two different acidic surface groups with pK 5.8 and 9.89 which could be carboxylic and phenolic acid groups.

Matsumura and coworkers [118120] carried out potentiometric titration curves of several carbon blacks before and after oxidation with nitric acid and after reduction with excess of sodium borohydride. Oxidations for shorter periods enhanced both carboxylic and phenolic acidic groups whereas longer oxidation time enhanced only phenolic structures. The titration curves of
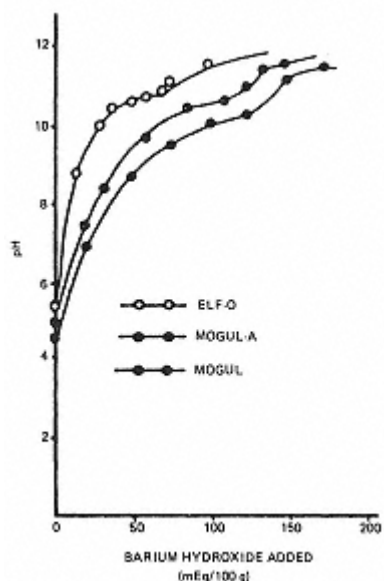
Fig. 8.
Titration curves of
Mogul with barium
hydroxide before and
after different treatment
(from ref. [12]).

the blacks after esterification with *n*-buthanol followed by
hydrolysis failed to show the existence of lactonic structure. The
titration curves of the reduced carbon blacks showed two types of
reducible structures. Those which were reduced reversibly were
attributed to quinonic groups while the others which
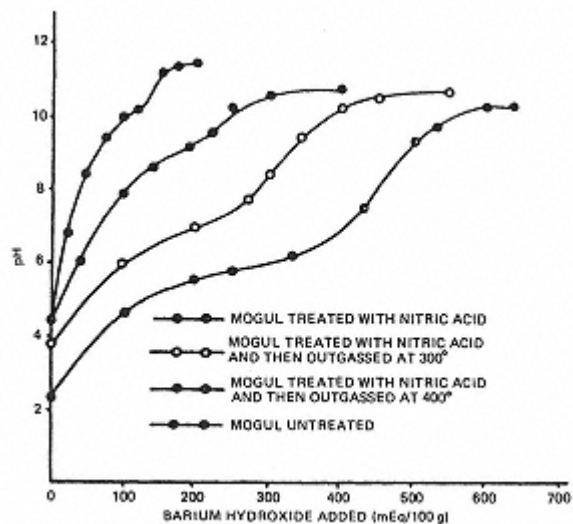
Fig. 9.
Titration curves of various carbon blacks
with barium hydroxide (from ref. [12]).

were reduced irreversibly were ascribed ketonic and aldehydic structures. However, the amounts of quinonic groups obtained by this reduction method were lower than the amounts found by Studebaker [34], Rivin [105,106] and Suzuki and Miyazaki [121].

It may be mentioned that the carbon blacks are associated with surface groups with varying acidities. This distribution of groups with varying acidities is likely to produce poor resolution in inflection points. Consequently it is difficult to compare the results obtained by different investigators.

4.2.4. Thermometric Titration

Given and Hill [122] used direct nonaqueous titrations of several carbon blacks with thermometric detection of the end points and using several combinations of titrant and dispersant. On the basis of the comparison of the titration results for different carbon blacks obtained by thermometry with their phenolic contents determined by acetylation with $C14$ labeled acetic anhydride, these workers suggested that phenolic hydroxyl structures contributed between 5 and 100% of the total carbon black acidity.

Papirer and Guyon [117] used thermometric titration in aqueous media using 0.05N NaOH as the titrant and observed that the surface acidity of the carbon black Carbolac 1 was smaller than the value obtained by direct titration. However, the two values agreed closely when the Greenhow and Spencer method [123] which involves an acrylonitrile polymerization to indicate the end point of the neutralization process was used.

4.2.5. Specific Chemical Analysis

Several workers have carried out a more direct analysis of the surface oxygen functional groups by studying specific chemical reactions of organic chemistry. Many of these reactions have been carried out in conjunction with base neutralization studies. The more important surface oxygen groups for which chemical analysis has been used are carboxyl, phenols, quinones and lactones. As the reactions used to identify and estimate these functional groups are discribed in most organic chemistry books and as the chemistry involved in this group analysis has been very nicely reviewed by several workers [23,25,124,137], we merely offer a very brief representation of the reactions and the chemical reagents used in Table 11. The results of some of these studies carried by different workers for carbon blacks and charcoal are given in Tables 12 and 13.

Surface group estimation using direct chemical methods has not been able to account for the chemisorbed oxygen. Thus Puri [23] has suggested caution in the interpretation of the results as the surface groups on carbons are unlikely to behave exactly in the same way as those in organic compounds. Papirer and Guyon [117], on the basis of their group determination using organic methods and spectroscopic analysis, have suggested that the surface

Table 11. *Analysis of Surface Groups on Carbon*

Reactant and/or technique	Identifying reaction[a,b]
	Carboxylic group
Alkali (KOH, NaOH, etc)	$R\text{-}COOH+NaOH\rightarrow RCOONa+H_2O$
Na_2CO_3	$2R\text{-}COOH+NaCO_3\rightarrow 2RCOONa+CO_2+H_2O$
$NaHCO_3$	$R\text{-}COOH+NaHCO_3\rightarrow RCOONa+CO_2+H_2O$
Sodium acetate	$R\text{-}COOH+CH_3COONa\rightarrow RCOONa+CH_3COOH$
Grignard reagent	$R\text{-}COOH+CH_3MgI\rightarrow RCOOMgI+CH_4$
Diazomethane	$R\text{-}COOH+CH_2N_2\rightarrow RCOOCH_3+N_2$
$LiAlH_4$	$4R\text{-}COOH+3LiAlH_4\rightarrow LiAl(CH_2OR)_4+2LiAlO_2+4H_2$
Acid chloride	$R\text{-}COOH+SOCl_2\rightarrow RCOCl+SO_2+HCl$
Dimethyl sulfate	$2R\text{-}COOH+SO_2(OCH_3)_2 \rightarrow 2RCOOCH_3+H_2SO_4$
Thermal	$R\text{-}COOH \xrightarrow{>600°C} RH+CO_2$
	Phenolic group
Grignard reagent	$R\text{-}OH+CH_3MgI\rightarrow ROMgI+CH_4$
Diazomethane	$R\text{-}OH + CH_2N_2\rightarrow ROCH_3+N_2$
$LiAlH_4$	$4R\text{-}OH+LiAlH_4\rightarrow LiAl(OR)_4+LiAlO_2+4H_2$
Benzoyl nitrochloride	$ROH+NO_2(C_6H_4)COCl\rightarrow RO(CO)(C_6H_4)NO_2+HCl$
Dimethyl sulfate	$R\text{-}OH+SO_2(OCH_3)_2\rightarrow ROCH_3 + SO_2(OH)OCH_3$
Thermal	$R\text{-}OH \xrightarrow{>600°C} RH + CO_2$
	Quinone group[c]
Diazomethane	$\rangle{=}O+CH_2N_2\rightarrow\rangle\text{-}OH$
Catalytic hydrogenation	$\rangle{=}O+H_2\rightarrow\rangle\text{-}OH$
$NaBH_4$	$\rangle{=}O+NaBH_4+H_2O\rightarrow\rangle\text{-}OH+NaBO_2$
$LiAlH_4$	$\rangle{=}O+LiAlH_4\rightarrow\rangle\text{-}OH+Li^++3Al^{3+}$
Ti^{3+}	$\rangle{=}O+Ti^{3+}\rightarrow\rangle\text{-}O^-+Ti^{4+}$
Sn^{2+}	$\rangle{=}O+Sn^{2+}\rightarrow\rangle\text{-}O^-+Sn^{4+}$
Hydroxylamine	$\rangle{=}O+NH_2OH\rightarrow\rangle{=}N\text{-}OH+H_2O$
Thermal	$\rangle{=}O\xrightarrow{>600°C}\rangle CO$
	Lactone group
Ammonia	$\rangle\text{-}\overset{\displaystyle}{C}{=}O+NH_3 \text{ (in methanol) }\rightarrow\rangle\text{-}C(O)NH_2$
	$\rangle\text{-}O\qquad\qquad\qquad\rangle\text{-}OH$
HBr	$\rangle\text{-}\overset{\displaystyle}{C}{=}O+HBr\rightarrow\rangle\text{-}C(O)OH$
	$\rangle\text{-}O\qquad\qquad\rangle\text{-}Br$
$LiAlH_4$	$\rangle\text{-}\overset{\displaystyle}{C}{=}O+LiAlH_4\rightarrow\rangle\text{-}C(O)OH$
	$\rangle\text{-}O\qquad\qquad\rangle\text{-}OH$
Thermal	$\rangle\text{-}\overset{\displaystyle}{C}{=}O\xrightarrow{>600°C}CO_2$
	$\rangle\text{-}O$

[a] *The identifying reactions are not necessarily presented as stoichiometric reactions.*

[b] *R is a representation for carbon surface atoms.*

[c] *Only the reaction of the $\rangle{=}O$ group is presented.*

Table 12. Surface Group Analysis by Reaction with Diazomethane

Carbon sample	Sodium hydroxide neutralization capacity (meq/100g)	-OCH$_3$ introduced		Non-hydrolyzable =phenolic groups (meq/100g)	Sodium hydroxide neutralized minus total -OCH$_3$ *n-*lactone groups (meq/100g)
		Total	Hydrolizable =COOH or lactone group (meq/100g)		
Carbolac-1	183	146	90	56	37
Mogul-A	118	54	33	21	64
ELF-O	58	24	14	10	34
Spheron-6	37	14	9	6	23
Spheron-9	46	10	5	5	36

structure on carbon should not be considered classical organic functional groups but rather combined structures which may present numerous forms largely favored by their location on the same polyaromatic frame.

4.2.6. Spectroscopic Methods

A considerable amount of effort has been devoted to the spectroscopic analysis of surface compounds of carbon. Consequently several spectroscopic techniques have been used to investigate the physico-chemical properties of these materials. Infra red (IR) and electron spin resonance (ESR) are the two most commonly used spectroscopic techniques. However, in more recent years X-ray photoelectron spectroscopy (XPS) and Raman spectroscopy have been increasingly applied for the examination of

carbon surfaces. Although a detailed description of the instruments and procedures used in these spectroscopic techniques is beyond the scope of the chapter, the results obtained on different types of carbons will be briefly discussed.

Infrared Spectroscopy

IR spectroscopy in its various forms is an important and forceful technique which can provide useful information about surface functional groups on carbon. These spectral studies can also provide useful information regarding the molecular forces involved in the absorption process. Carbon being black in color has a tendency to absorb most of the radiation, at least in the visible region. Even its thin sections are opaque. However, the carbon blacks, being in a very fine state of subdivision, can be examined in the form of thin halide

Table 13. Surface Group Analysis by Specific Organic Reactions

Carbon sample	Oxygen as phenol group by Grignard reagent (%)	Oxygen as phenol group by neutralization of barium hydroxide (%)	Oxygen as quinone group by reduction with sodium borohydride (%)	Oxygen ether group by difference (%)
Pelletex	0.02	0.08	0.16	0.35
Stirling-V	0.03	0.07	0.22	0.23
Kosmos-40	0.08	0.14	0.15	0
Statex-B	0.06	0.17	0.16	0.44
Philblack-A	0.08	0.16	0.24	0.24
Philblack-O	0.11	0.14	0.41	1.16
Philblack-E	0.19	0.33	0.66	1.15
Spheron-9	0.20	0.60	0.92	2.63
Spheron-6	0.18	0.45	0.67	1.82
Spheron-C	0.39	0.76	0.89	1.31
ELF	0.54	0.78	1.10	2.34
Mogul-A	0.52	1.98	1.71	2.84
Mogul	0.71	2.52	2.03	3.18
Carbolac-2	0.96	4.25	2.62	1.84

pellets in which the carbon black can be dispersed. The IR spectroscopy technique using halide pellets also presented difficulties because of the exposure of carbon materials to

atmospheric gases and vapors. However, the development of elaborate techniques and the enhancement of the sensitivity of IR measurements by using Fourier Transform (FTIR), photo accoustic (PAS), attenuated total reflectance (ATR-IRS) and photo thermal beam deflection (PDS) has given very good results pertaining to carbon surface functionality.

The first IR transmission spectrum of a carbon black with a high oxygen content was reported by Hallum and Drushel [125] using a Nujol mull of the black. A band at 1600 cm-1 (6.3 μm) was attributed to either condensed aromatic ring system or to hydrogen bonded conjugated carbonyl groups. The band shifted to normal carbonyl wavelengths 5.75.9 μm (1750-1200 cm-1) on treatment of carbon black with diazomethane. Another band at 1250 cm-1 which was observed after methylation was attributed to aromatic hydroxyl groups hydrogen bonded to conjugated carbonyl groups.

Studebaker and Rinehart [126] examined 20 samples of commercial grade carbon blacks by IR spectroscopy using a potassium bromide pellet technique and using integrated intensities rather than absorbance at characteristic

wavelengths. A comparison of the IR integrated intensities and the functional group analysis by direct chemical reactions indicated that a considerable reactivity of carbon blacks was due to the presence of quinones and lactones (Table 14) although absorption typical of phenols and others was also observed.

Papirer et al [127] and Donnet [128] examined surface groups on a carbon black, Carbolac 1, before and after methylation followed by hydrolysis using direct transmission with scale expansion and internal reflection IR spectroscopy. Bands were observed at 1250, 1600 and 1740 cm-1 (Fig. 10) whose intensity decreased when the black was heated at 1000°C in hydrogen or in argon. Another band at 32003400 cm-1 was attributed to deformation vibrations of the hydroxyl group of carboxylic structures. There was no noticeable difference in the IR spectra after methylation either with diazomethane or with methanol (Fig. 11) except that the intending ratio of the peaks at 1740 and 1600 cm-1 was reduced. This was attributed to the elimination of ketonic or aldehydic structures and to the formation of non-chelate carbonyl groups.

Table 14. IR Integrated Intensities

Carbon black (frequency, cm-1)	Lactone (1775-1675)	Quinone (1675-1550)	Ether (1275-1265)	Phenol (1205-1195)
Thermax	-	0.6	-	-
P-33	1.10	2.8	-	-
Pelletex	0.45	2.4	0	0.37
Sterling	0.41	2.5	0.30	0.68
Kosmos 40	0.38	7.5	0	0.53
Statex B	1.10	8.0	0.43	0.81
Philblack A	0.20	8.3	0.87	0.80
Philblack O	0.20	9.4	0.25	0.49

Philblack I	0.35	8.9	0.66	0.98
Philblack E	0.95	9.1	0.02	0.71
Vulcan SC	0.13	12	0.10	0.53
Spheron 9	0.53	20	0.46	0.53
Spheron 6	0.82	19	0.49	0.75
Spheron 4	0.60	15	0.21	0.53
Spheron C	1.04	13	0.44	1.01
CK-4	0.45	11	0.45	0.81
ELF-O	1.55	25	0.76	1.35
Mogul A	2.35	19	0.65	1.48
Mogul	2.77	26	1.22	1.87
Carbolac 2	5.13	43	1.68	2.57

From ref. [126].
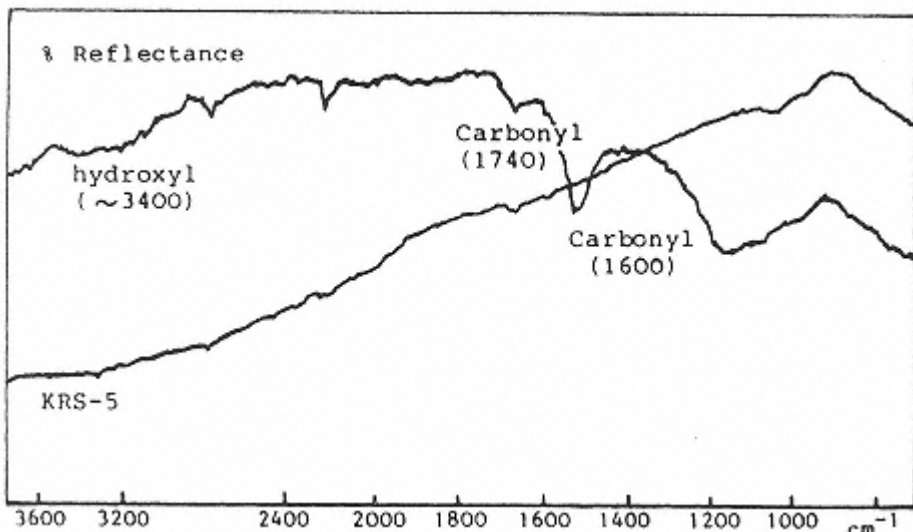
Fig. 10.
Internal reflectance IR spectra of Carbolac 1 (from ref. [127]).

The spectra of the methylated black after hydrolysis (Fig. 12) showed a new band at 1105 cm-1, which persisted even when the hydrolysed product was remethylated to get back the original structure on the carbon black.

The IR spectra for a carbon black and a soot obtained by FTIR, ATR-TRS, PAS and PDS are presented in Figs. 13 and 14. The FTIR spectrum obtained by O'Reilly and Mosher [129] for a low surface area (7 m2/g) thermal black Sterling MT (Cabot Corporation) with a violative content of 0.6%
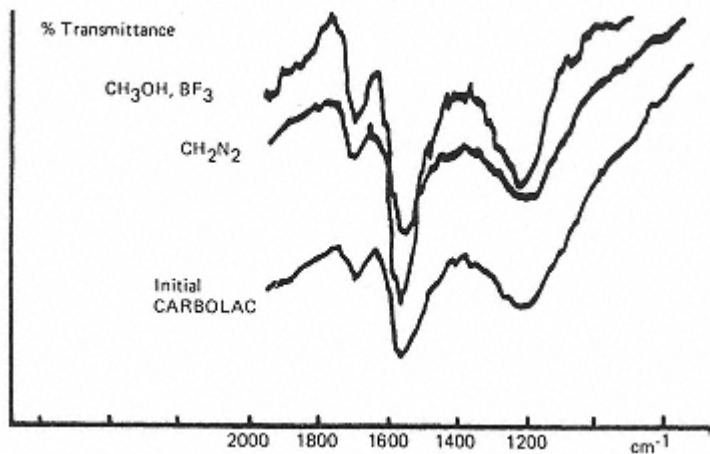
Fig. 11.
Internal reflectance IR spectra of Carbolac 1 after
methylation (from ref. [127]).
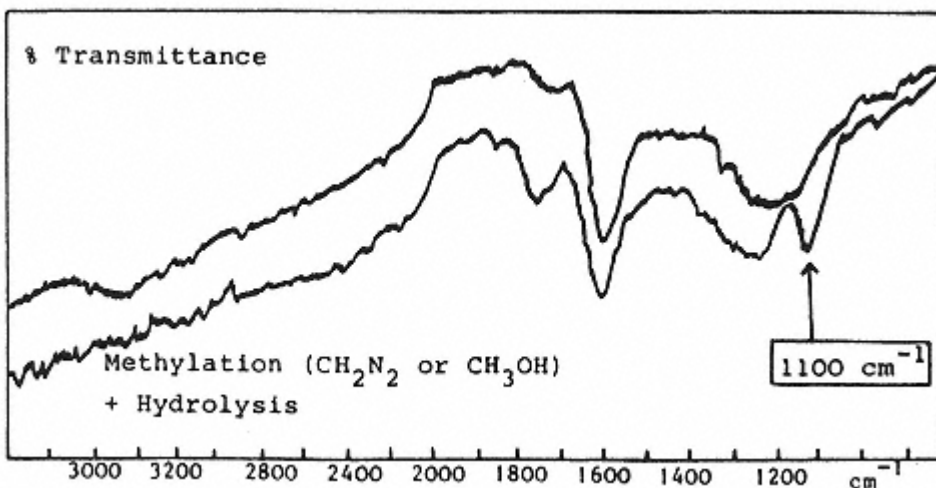
Fig. 12.
Internal reflectance IR spectra of Carbolac 1 after methylation and subsequent hydrolysis (from ref. [127]).

(Fig. 13) shows little evidence of surface group indicating that it is difficult to obtain a meaningful IR data from carbon blacks with low surface area and low volatile content. However, the spectrum for the high surface area (530 m2/g) and high volatile content (10.8%) carbon black Monarch 1300 clearly shows evidence for strong absorption peaks and bands which could be assigned to surface functional groups. The absorption band at 3430 cm-1 was attributed to adsorbed water and its intensity was reduced when the sample was dried. The absorption bands at 1720 and 1600 cm-1 were attributed to carbonyl
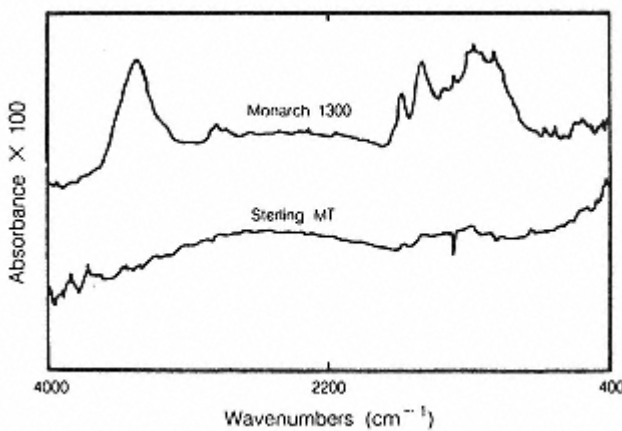
Fig. 13.
FTIR spectra of carbon blacks (0.01 to 0.1
wt% mixed with KBr) after baseline subtraction.
Monarch 1300 (furnace black) and Sterling
MT (thermal black) are products of Cabot Co.
(from ref. [129]).
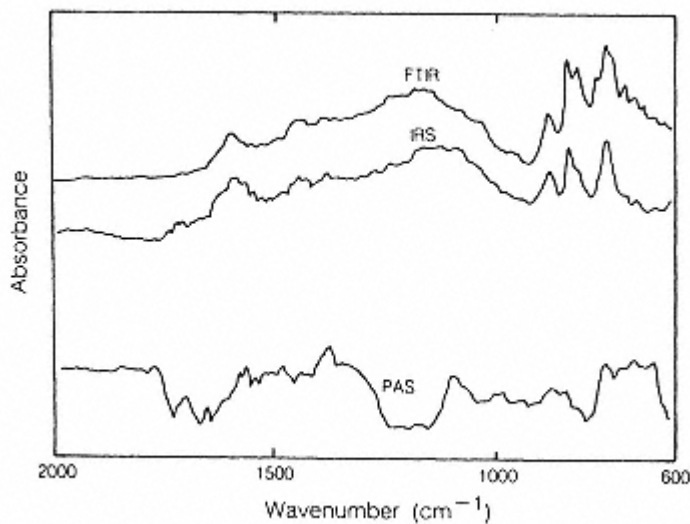
Fig. 14.
Absorbance spectra of hexane soot obtained by FTIR,
IRS, and PAS (from ref. [130]).

stretching frequencies for carboxylic and quinone groups, respectively. The intensities of two bands agreed reasonably well with the concentrations of carboxyl groups determined by titration with $NaHCO_3$ and of phenol groups determined by the difference between titration with NaOH and $NaHCO_3$.

Rockley and coworkers [130] compared the results obtained from IR spectroscopic techniques (such as FTIR, ATR-IRS and PAS) for a carbon black which was prepared by the combustion of spectra quality hexane in an open flame. The FTIR and ATR-IRS spectra (Fig. 14) are almost similar except for a small difference in intensity while the PDS spectra showed some different features. The negative absorbance bands with respect to the baseline indicate that the opaque carbon samples should be used with caution as photo accoustic reference standards [131].

Active carbons, charcoals and several types of carbon films before and after several treatments such as oxidation, degassing, sulfurisation and treatment with alkalies have been examined by different IR techniques. The results have been well reviewed [137].

Electron Spin Resonance (ESR) Spectra

The electron spins in carbons can provide information on the chemical and electrochemical processes taking place on carbon surface. The line widths and the line shapes are affected by chemical, mechanical and thermal treatment. For example in the case of graphite the ESR signal intensity increases as the particle size is reduced by grinding while the line shape of the derivative peak is more symmetrical when the sample is highly dispersed

[132]. But the amorphous carbons such as carbon blacks show only a broad line or no resonance at all. When the carbon blacks are heat treated, typical line shapes are obtained from ESR measurements. The data in the form of derivative of the ESR absorption signal for a carbon black heat treated at different temperatures (Fig. 15) indicate that the width of the ESR absorption signal is wide for the black heat treated at 1200°C and becomes narrower as the heat treatment temperature is increased.

The adsorption of oxygen by carbon enhances the line width considerably [133135] due to the perturbing influence of the magnetic moment of oxygen. ESR studies of carbon blacks heat treated at 18002200°C and then exposed to oxygen show an increase in line width which is greatest for carbons with the smallest particle size. The line width of the carbon black heat treated at 14002400°C also increases linearly when exposed to oxygen. However, this increase in line width is reversible probably because the oxygen was only physically adsorbed. However, when carbon blacks were heat treated in oxygen at 400°C, the intensity of the ESR signal was found to decrease with only a slight increase in the line width [136].

X-Ray Photoelectron Spectroscopy (XPS)

X-ray photoelectron spectroscopy is an ultra-high vacuum technique used for surface characterization of solids and powder samples. Essentially the technique measures the kinetic energy of electrons emitted from atoms under the influence of irradiation with X-rays. The kinetic energy of the
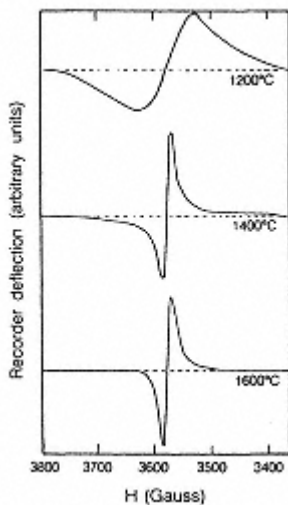
Fig. 15.
Typical line shapes
of heat-treated
channel black.
(Reprinted with
permission from
J. Appl. Phys., 30,
56 (1959).
Copyright 1959
American Institute
of Physics.)

emitted electron is related to the binding energy of the electrons which in turn depends upon the chemical environment of the atom emitting the electron. The variation of binding energy of the electrons with the environment of the atom gives rise to different peaks in the XPS spectrum with the varying intensity for the same atom depending upon the nature of the atoms to which the atom is attached. Furthermore the penetration depth from which the photoelectron emerges is seldom more than 1015 nm, i.e., about 1020 atomic layers from the surface which makes XPS ideal for surface chemical analysis as well as for the study of adsorbed species.

A major part of the XPS studies have been carried out using carbon fibre and graphite because of their easy manipulation although a few investigations have been reported on carbon blacks and activated carbons. Most of the XPS work on carbon fibre and carbons has been reviewed in our book [137]. Therefore, XPS work pertaining to carbon blacks will be mentioned in this chapter.

Donnet, Papirer and colleagues [127,128] applied XPS spectroscopy to the study of surface groups on a carbon black, Carbolic 1, before and after methylation followed by hydrolysis of the methylated product. The carbon black sample was spread on a double sided adhesive tape and the spectra for $C1s$ and $O1s$ were recorded at the rate of 0.05 V/sec. The $C1s$ spectra for all the three samples showed an asymmetric peak at about 284 eV tailing markedly to the high binding energy side. The asymmetry suggested the presence of carbon hydrogen bond (normally around 285 eV) and carbon-oxygen bonds (at about 288.5 eV). The $O1s$ peak also showed asymmetry suggesting the presence of two or

more forms of bonded oxygen. The deconvoluted $O1s$ spectrum showed constant positions of the four individual peaks, although their intensities showed a variation. The $O1s$ peaks in the original and methylated carbon black were almost similar but the methylated and hydrolysed samples showed a relatively larger concentration of the higher binding energy form of oxygen. But these workers did not draw definite conclusions regarding the nature of the surface oxygen structures on the basis of these studies alone.

The presence of surface functional groups and of chemisorbed species on carbons has been identified and estimated by the chemical shift for $C1s$ peak. Some examples from XPS studies on carbon fibre, carbons and carbon blacks are recorded in Table 15. The digital difference spectrum technique used by Ishitani and Takahagi [138,139] enables the analysis of surface groups on carbons. The difference spectra obtained by subtracting the $C1s$ spectra of control fibre from those of oxidized fibre (Fig. 16) using the appropriate weight factors showed three components with chemical shifts corresponding to hydroxyl groups $(\!)C\text{-}OH$, 286.6 eV), Carbonyl groups $(\!)C\!=\!O$, 287 eV) and carboxyl groups $(\!)C\text{-}OOH$, 288.6 eV). The curves resolving $C1s$ difference spectra gave the concentration of the three functions as carboxyl 17%, car-

Table 15. Phtoelectron-Spectroscopy (XPS)Studies of Carbon Materials

Carbon	Binding energy for $C1s$(eV)	Interpretation of spectra	Reference
Channel black	285.0	C bonded to H	93
	288.5	C bonded to O	93
Oxidized carbon fibre	286.0	Hydroxyl group	109
	287.0	Carbonyl group	109
	288.6	Carbonyl group	109
Carbon from PTFE reduced by Li	285.4285.9	C atoms in the basic C skeleton	124
	290.2290.8	C atom in surface COOH groups	124
Carbon fiber	285.0	Hydrocarbon group	125
	287.0	C singly bonded to O	125
	289.0	C doubly bonded to O	125
Graphite oxide	285.0	Carboxyl group	125
	287.2	Phenolic hydroxyl group	125
	289.0	Carbonyl and ether groups	125
Air-oxidized carbon fibre	$1.5a$	C-O- group	126
	$2.5a$	C=O group	126
	$4.0a$	Carboxyl group	126
Carbon fiber	$1.6a$	C-O- group	127
	$3.0a$	C=O group	127
	$4.5a$	Carboxyl or ester	127

		group	
Electrochemically oxidized carbon fibre	11.6[a]	C-O- group	128
	3.0[a]	C=O group	128
	4.5[a]	Carboxyl or ester-type group	128
Electrochemically oxidized carbon fiber	~2.1[a]	C=O and/or quinone-type group	104
	~4.0[a]	Ester-type group	104
	>6.0[a]	C_3^{2-} -type group	104
Fluorinated graphite	4.7[a]	CF group	53
	6.7[a]	CF2 group	53
	9.0[a]	CF3 group	53

[a]Chemical shift C1s peak (eV).
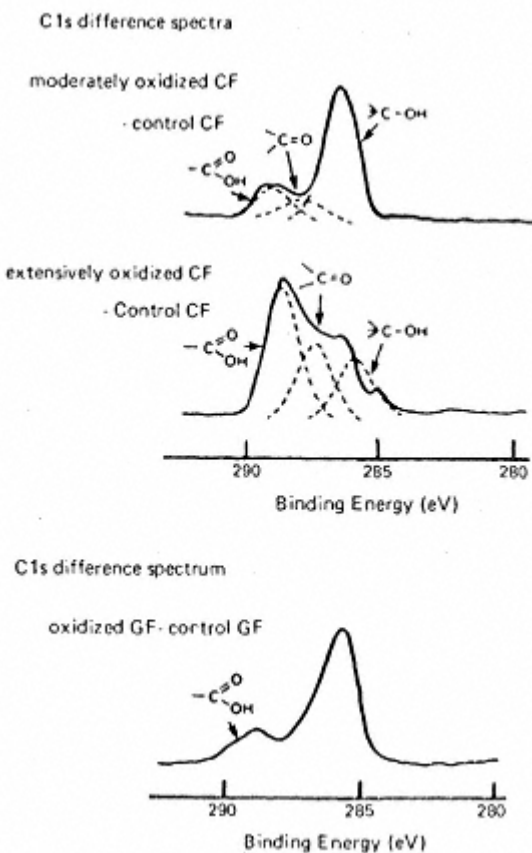
Fig. 16.
Carbon in digital difference spectra of
type II (CF) and type I (GF) carbon fibre
before and after oxidation (from ref.
[138]).

bonyl 10%, and phenolic 73% on moderate oxidation and carboxyl 54%, carbonyl 22% on extensive oxidation.

The preceding example illustrates the application of XPS in the identification and estimation of surface groups on carbon surface.

References

1. Donnet, J. B. and Papirer, E., *Rev. Gen. Caoutchouc Plastiques,*

42, 889 (1965).

2. Donnet, J. B. and Papirer, E., *Bull. Soc. Chim. France,* 1912 (1965).

3. Puri, B. R., Aggarwal, V. K., Bhardwaj, S. S. and Bansal, R. C., *Indian J. Chem.,* 11, 1020 (1973).

4. Dietz, V. R. and Bitner, S. L., *Carbon,* 11, 393 (1973).

5. Smith, R. N., Swinehard, J. and Lesssini, D., *J. Phys. Chem.,* 63, 544 (1959).

6. Puri, B. R., Bansal, R. C. and Bhardwaj, S. S., *Indian J. Chem.,* 11, 1168 (1973).

7. Puri, B. R., Singh, S. and Mahajan, O. P., *J. Indian Chem. Soc.,* 42, 427 (1965).

8. Behraman, A. S. and Gustafson, H., *Ind. Eng. Chem.,* 27, 426 (1935).

9. Puri, B. R., Mahajan, O. P. and Singh, D. D., *J. Indian Chem. Soc.,* 37, 171 (1960).

10. Puri, B. R., Singh, D. D., Sharma, L. R. and Chander, J., *J. Indian Chem. Soc.,* 35, 13 (1958).

11. Puri, B. R. and Mahajan, O. P., *J. Indian Chem. Soc.,* 39, 292 (1962).

12. Puri, B. R. and Bansal, R. C., *Carbon,* 1, 457 (1964).

13. Puri, B. R. and Sharma, S. K., *Chem. Ind.,* London, 160 (1966).

14. Donnet, J. B., Bouland, J. C. and Jeiger, J., *Compt. Reudu.,* 256, 5340 (1963).

15. Donnet, J. B., French patent 1 164 786, Oct. 14, 1958.

16. Puri, B. R., Sharma, A. K. and Mahajan, O. P., *Res. Bull.,* Panjab. University, Chandiginh, 15, 285 (1964).

17. Donnet, J. B., Heuber, F., Reitzer, C., Odoux, J. and Riess G., *Bull. Soc. Chim. France,* 1927 (1962).

18. Gandhi, D. L., Ph.D. Thesis, Paujab University, Chandigaih, 1976.

19. Puri, B. R. and Kalra, K. C., *Carbon,* 9, 313 (1971).

20. Puri, B. R., Sharma, L. R. and Singh, D. D., *J. Indian Chem. Soc.,* 35, 770 (1958).

21. Donnet, J. B. and Henrich G., *Bull. Soc. Chem. France,* 1609 (1960).

22. Puri, B. R. and Mahajan, O. P., *J. Indian Chem. Soc.,* 39, 292 (1962).

23. Puri, B. R., in *Chemistry and Physics of Carbon,* P. L. Walker, Jr. ed., Marcel Dekker, New York, p. 191, 1970.

24. Garten, V. A. and Weiss, D. E., *Rev. Pure Appl. Chem.,* 7, 69 (1957).

25. Boehm, H. P., in *Advances in Catalysis,* Vol.XVI, Acad. Press, New York, p. 179, 1966.

26. Boehm, H. P. and Voll, M., *Carbon,* 8, 227 (1970).

27. Redmond, J. P. and Walker, P. L. Jr., *J. Phys. Chem.,* 64, 1093 (1960).

28. Barrer, R. M., *J. Chem. Soc.,* 1256 (1937).

29. Kingman, F. E. T., *Trans. Faraday Soc.,* 28, 272 (1932).

30. Bansal, R. C., Vastola, F. J. and Walker, P. L. Jr., *Carbon,* 9, 185 (1971).

31. Baugham, D. H. and Stafford, J., *J. Chem. Soc.,* 127, 1985 (1925).

32. Puri, B. R. and Bansal, R. C., *Chem. Ind. (London),* 574, (1963).

32a. Snow, C. W., Wallace, D. R., Lyons, L. L. and Crocker, G. R.,

Proc. 4th Conf. on Carbon, Pergamon Press, New York, p. 79, 1960.

33. Puri, B. R., Malhotra, S. L. and Bansal, R. C., *J. Indian Chem. Soc.,* 40, 179 (1963).

34. Studebaker, M. L., *Rubber Chem. Technol.,* 30, 1401 (1957).

35. Smith, R. N., Duffield, J., Pierotti, R. A. and Mooi, J., *J. Phys. Chem.,* 60, 459 (1956).

36. Bansal, R. C., Dhami, T. L. and Parkash, S., *Carbon,* 15, 157 (1977).

37. Studebaker, M. L. and Nabors, L. G., *Rubber Age,* 80, 661 (1957).

38. Emmett, P. H., *Chem. Rev.,* 43, 69 (1948).

39. Boehm, H. P., Hoffmann, U. and Clauss, A., In *Proc. 3rd Conf. Carbon,* Pergamon Press, New York, p. 241, 1959.

40. Hoffmann, U. and Ohlrich, G., *Angew. Chem.,* 62, 16 (1950).

41. Puri, B. R. and Mahajan, O. P., *J. Indian Chem. Soc.,* 41, 586 (1964).

42. Puri, B. R. and Bansal, R. C., *Indian J. Chem.,* 5, 566 (1967).

43. Zawadski, J., *Carbon,* 19, 19 (1981).

44. Studebaker, M. L., *Rubber Age,* 77, 69 (1955).

45. Studebaker, M. L., Hoffman, E. W. D., Wolfe, A. C. and Nabors, L. G., *Ind. Eng. Chem.,* 48, 162 (1956).

46. de Bruin, W. J. and Van der Plas, T., *Rev. Gen. Caout.,* 41, 543 (1964).

47. Lewis, J. E., Deviney, M. L. and McNabb, C. F., *Rubber Chem. Technol.,* 43, 449 (1970).

48. Wibaut, J. P., *Proc. 3rd Int. Conf. Bituminous Coal,* p. 657,

1932.

49. Wibaut, J. P., *Rect. Trav. Chim.,* 41, 153 (1922).

50. Wibaut, J. P., Z. *Angew Chem.,* 40, 1136 (1927).

51. Juja, R. and Blanke, W. Z., *Anorg. Allgem. Chem.,* 210, 81 (1933).

52. Puri, B. R., Balwar, A. K. and Hazra, R. S., *J. Indian, Chem. Soc.,* 44, 975 (1967).

53. Puri, B. R., Kaistha, B. and Hazra, R. S., *J. Indian Chem. Soc.,* 45, 1001 (1968).

54. Puri, B. R. and Hazra, R. S., *Carbon,* 9, 123 (1971).

55. Karpinski, K. and Swinarski, A., *Chem. Stosow, Sci.,* A9, 307 (1965).

56. Karpinski, K. and Swinarski, A., *Pyzem. Chem.,* 43, 71 (1964).

57. Puri, B. R., Kaistha, B. C. and Hazra, R. S., *Chem. Ind. (London),* 2087, 1967.

58. Bansal, R. C. and Gupta, U., *Indian J. Technology,* 18, 131 (1980).

59. Blachand, L., in *C. R. 27th Conf. Int. Chim. Ind.,* p. 576, 1955.

60. Rossow, B. and Hoffmann, K., *J. Prokt Chem.,* 104, 207 (1922).

61. Siller, C. W., *Ind. Eng. Chem.,* 40, 1227 (1948).

62. Stacy, W. O., Vastola, F. J. and Walker, P. L. Jr., *Carbon,* 6, 917 (1968).

63. Puri, B. R., Jain, C. M. and Hazra, R. S., *J. Indian Chem. Soc.,*

43, 67 (1966).

64. Wibaut, J. P., *Pect. Trav. Chim.,* 38, 159 (1919).

65. Wibaut, J. P., and Stoffel, A., *Rect. Trav. Chim.,* 38, 132 (1919).

66. Chang, C. H., *Carbon,* 19, 175 (1981).

67. Gandhi, D. L., Sharma, S. K., Kumer, A. and Puri, B. R., *Indian J. Chem.,* 13, 1317 (1975).

68. Reyerson, L. H. and Wishart, A. W., *J. Phys. Chem.,* 42, 679 (1938).

69. Puri, B. R. and Bansal, R. C., *Indian J. Chem.,* 5, 381 (1967).

70. Puri, B. R. and Bansal, R. C., *Carbon,* 3, 533 (1966).

71. Puri, B. R., Mahajan, O. P. and Singh, D. D., *J. Indian Chem. Soc.,* 38, 943 (1961).

72. Puri, B. R., Gandhi, D. L., and Mahajan, O. P., *Carbon,* 15, 173 (1977).

73. Puri, B. R. and Bansal, R. C., *Carbon,* 5, 189 (1967).

74. Puri, B. R. and Sehgal, K. C., *Indian J. Chem.,* 4, 206 (1966).

75. Puri, B. R., Mahajan, O. P. and Gandhi, D. L., *Indian J. Chem.,* 10, 848 (1972).

76. Bansal, R. C., Dhami, T. L. and Parkash, S., *Carbon,* 18, 395 (1980).

77. Rivin, D. and Aron, J., *Proc. 7th Conf. Carbon,* Cleveland, Ohio, Abstracts, 1965.

78. Puri, B. R., Tulsi, S. S. and Bansal, R. C., *Indian J. Chem.,* 4, 7 (1966).

79. Puri, B. R., Sandle, N. K. and Mahajan, O. P., *J. Chem. Soc.,* 4880 (1963).

80. Stacy, W. O., Imperial, W. R. and Walker, P. L. Jr., *Carbon,* 4, 343 (1966).

81. Puri, B. R., Dhingra, A. K. and Sehgal, K. C., *Indian J. Chem.,* 7, 174 (1969).

82. Puri, B. R. and Sandle, N. K., *Indian J. Chem.,* 6, 267 (1968).

83. Tobias, H. and Soffer, A., *Carbon,* 23, 281 (1985).

84. Stearns, R. S. and Johnson, B. L., *Ind. Eng. Chem.,* 43, 146 (1951).

85. Watson, J. W. and Parkinson, D., *Ind. Eng. Chem.,* 47, 1053 (1955).

86. Puri, B. R. and Bansal, R. C., *Carbon,* 3, 227 (1965).

87. Juhola, A. J., *Carbon,* 13, 437 (1975).

88. Hassler, J. W. and McMinn, W. E., *Ind. Eng. Chem.,* 37, 645 (1945).

89. Hill, A. and Marsh, H., *Carbon,* 6, 31 (1966).

89a. Puri, B. R. and Bansal, R. C., *Carbon,* 1, 451 (1964).

90. Puri, B. R., Singh, D. D., Nath, J. and Sharma, L. R., *Ind. Eng. Chem.,* 50, 1071 (1958).

91. Weller, S. and Young, T. F., *J. Amer. Chem. Soc.,* 70, 4155 (1948).

92. Barton, S. S., Gillespie, D. and Harrison, B. H., *Carbon,* 11, 649 (1973).

93. Van Driel, J. in *Activated Carbon - A Fascinating Material,* A. Capelle and F. de Vooys eds., Norit W. V. Netherland, p. 40, 1983.

94. Lang, F. M. and Magnier, P., *Carbon,* 2, 7 (1964).

95. Bannetain, L., Duval, X. and Letort, M., in *Proc. 4th Conf. Carbon,*

Pergamon Press, Oxford, p. 107, 1962.

96. Bonnetain, L., *J. Chem. Phys.,* 58, 34 (1961).

97. Tucker, B. G. and Mulcahy, M. F. R., *Trans. Faraday Soc.,* 65, 247 (1969).

98. Matsumoto, S. and Setaka, N., *Carbon,* 17, 303 (1979).

99. Dollimore, J., Freedman, C. M., Harrison, B. H. and Quinn, D. F., *Carbon,* 8, 587 (1978).

100. Trembley, G., Vastola, F. J. and Walker, P. L. Jr., *Carbon,* 60, 35 (1978).

101. Matsumoto, S., Kanda, H., Suto, Y. and Setaka, N., *Carbon,* 15, 299 (1977).

102. Rivin, D., *Rubber Chem. Technol.,* 44, 307 (1971).

103. Schweitzer, C. W. and Goodrich, W. C., *Rubber Age,* 55, 469 (1944).

104. Villars, D. S., *J. Amer. Chem Soc.,* 69, 214 (1947).

105. Rivin, D., in *Proc. 4th Rubber Technol. Conf.,* London, p. 1, 1962.

106. Rivin, D., *Rubber Chem. Technol.,* 36, 729 (1963).

107. Puri, B. R., Meyer, Y. P. and Sharma, L. R., *Chem. Ind. (London), B. I. F. Rev. R.,* 30, 1956.

108. Puri, B. R., Meyer, Y. P. and Sharma, L. R., *J. Indian Chem. Soc.,* 33, 781 (1956).

109. Anderson, R. B. and Emmett, P. H., *J. Phys. Chem.,* 56, 753

(1952).

110. Puri, B. R., Talwar, C. and Sandle, N. K., *J. Indian Chem. Soc.,* 41, 581 (1964).

111. Barton, S. S. and Harrison, B. H., *Carbon,* 13, 283 (1975).

112. Barton, S. S., Gallispie, D. J., Harrison, B. H. and Kemp, W., *Carbon,* 16, 363 (1978).

113. Barton, S. S., Boulton, G. L. and Harrison, B. H., *Carbon,* 10, 395 (1972).

114. Bansal, R. C., Bhatia, N. and Dhami, T. L., *Carbon,* 16, 65 (1978).

115. Wiegand, W. B., *Ind. Eng. Chem.,* 29, 953 (1937).

116. Studebaker, M. L., in *Proc. 4th Carbon conf.,* Pergamon press, New York, p. 189, 1963.

117. Papirer, E. and Guyon, E., *Carbon,* 16, 127 (1978).

118. Matsumura, Y., Hagiwara, S. and Takahashi, H., *Carbon,* 14, 247 (1976).

119. Matsumura, Y., Hagiwara, S. and Takahashi, H., *Carbon,* 14, 163 (1976).

120. Matsumura, Y. and Takahashi, H., *Carbon,* 17, 109 (1979).

121. Suzuki, S. and Miyazaki, K., *Nippon Kagaku Zasshi,* 88, 299 (1967).

122. Given, P. H. and Hill, L. W., *Carbon,* 7, 649 (1969).

123. Greenhow, E. J. and Spencer, L. E., *Analyst,* 98, 90 (1973).

124. Matson, S. and Mark, H. B. Jr., *Activated Carbon - Surface*

Chemistry

and Adsorption, Marcel Dekker, New York, 1971.

125. Hallum, J. V. and Drushel, H. V., *J. Phys. Chem.,* 62, 110 (1958).

126. Studebaker, M. L. and Rinehart, R. W. Sr., *Rubber Chem. Technol.,* 45, 106 (1972).

127. Papirer, E., Guyon, E. and Perol, N., *Carbon,* 16, 133 (1978).

128. Donnet, J. B., *Carbon,* 20, 266 (1982).

129. O'Reilly, J. M. and Mosher, R. A., *Carbon,* 21, 47 (1983).

130. Rockley, M. G., Ratcliffe, A. E., Davis, D. M. and Woodard, M. K., *Appl. Spectrosc.,* 38, 553 (1984).

131. Bannett, C. A. and Patty, R. R., *J. Photoaccoustics,* 1, 237 (1982).

132. Singer, L. S. and Wagoner, G., in *Proc. 4th Conf. on Carbon,* Vol. 2, Pergamon Press, New York, p. 65, 1963.

133. Arnold, G. M., *Carbon,* 5, 33 (1967).

134. Antonowicz, K., *J. Chem. Phys.,* 36, 2046 (1962).

135. Seymour, R. C. and Wood, J. C., in *3rd Conf. Ind. Carbons and Graphite,* Soc. Chem. Ind., London, p. 264, 1971.

136. Harker, H., Jackson, C. and Wynne-Jones, W. F. K., *Proc. Royal Soc. London,* 262A, 328 (1961).

137. Bansal, R. C., Donnet, J. -B. and Stoeckli, F., *Active Carbon,* Marcel Dekker, New York, 1988.

138. Ishitani, A., *Carbon,* 19, 269 (1981).

139. Takahagi, T. and Ishitani, A., *Carbon,* 22, 43 (1984).

Chapter 5
Carbon Black Surface Studied by Scanning Tunneling Microscopy

Jean-Baptiste Donnet
Centre de Recherches sur la Physico-Chimie des Surfaces Solides, CNRS,
Mulhouse, France

Emmanuel Custodero
Ecole Nationale Supérieure de Chimie de Mulhouse,
Mulhouse, France

Scanning tunneling microscopy [1] appeared only ten years ago but is now recognized as a choice of technique for studying the surface of conductive solid materials, particularly at the atomic scale. Perfect graphite, such as highly oriented pyrolytic graphite (HOPG), which is a good electrical conductor and which shows flat surfaces at atomic scale, has rapidly become a reference material and is commonly used to calibrate scanning tunneling microscopes.

Many papers have been published on HOPG, but little has been published on the other carbonaceous materials, such as carbon black, carbon fibers, active carbon, whose industrial use is far more important than that of the nearly perfect graphites. Some studies of either carbon, amorphous carbon [25] or carbon fibers [68] surfaces have shown their actual atomic surface. Such rare studies emphasize how difficult it is to prepare STM-observable samples when a surface is not in the form of a macroscopic solid.

For several decades, our laboratory has studied the physicochemistry of carbon black. Recently, we have applied the STM to the systematic study of the carbon black surface [910]. Earlier, transmission electron microscopy had indicated that, morphologically, carbon black exists as aggregates of spherical particles. Generally, these particles are regarded as a concentric organization

Fig. 1.
Previous carbon black
model proposed by
Heckman and Hardling
in 1966.

of small graphitic crystallites (Fig. 1); the crystallographic dimensions were determined by X-ray diffraction. These studies allowed one to construct a surface pattern consisting of crystallites and amorphous areas. The functional groups bonded to carbon atoms were localized at the amorphous areas (Fig. 2). It is this generally accepted model that we wanted to check by STM.

5.1. STM Technique and Equipment

If there is a bias voltage between tip and sample, separated from one another, in the Z direction, by only a few tenths of a nanometer, some electrons can tunnel from the sample to the tip. The STM can be visuallized as a map of the tunnel current as a function of the position, obtained by scanning
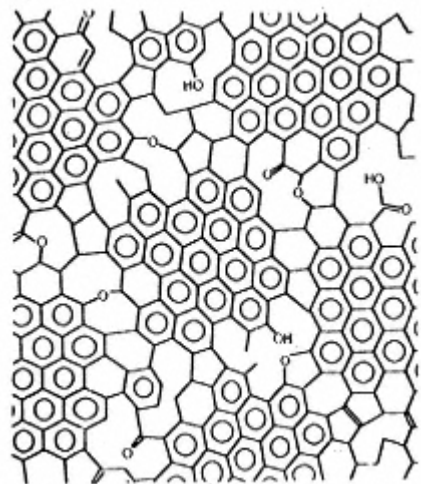
Fig. 2.
Surface model of carbon black
with graphitic crystallites and
amorphous areas with
functional groups.

the surface in X and Y-axis. The tunnel current intensity depends upon the gap between tip and surface as well as upon the electronical density of the observed atoms.

In practice, two different modes can be used:

* constant current scanning mode consists in moving the tip in the Z direction in order to keep the tunnel current constant. When the density of states is homogeneous, a tridimensional image of the solid surface is obtained. This mode is suitable for studying low enlarged images having significant features in a range of $75,000 \times 75,000$ nm2 to 1000×1000 nm2.

* constant height scanning mode consists in moving the tip in a quasi-constant height (in Z-axis) in order to measure the tunnel current value for each X,Y point. This mode has a higher resolution in the Z direction and is suitable to study the surface at the atomic scale.

A commercial scanning microscope, the Nanoscope II (Digital Instruments Inc.), was used (Software release 5.5) with commercial tips of 80/20 Pt/Ir (Nanotips). Standard observation conditions: bias voltage between the tip and the sample from 20 to 200 mV, tunnel current from 1 to 10 nA, scanning frequencies from 1 to 78 Hz were used. The feed-back parameters were adjusted in order to obtain as high resolution as possible. The resulting images 400×400 pixels were not filtered.

All the carbon blacks under examination were extracted in a Soxhlet for 48 hours using toluene. They were then dried in vacuum at 353 K. This extraction allows the elimination of the polyaromatic compounds that have been adsorbed and noticeably

improves the image quality. In order to observe the carbon black surface, 0.1 g of carbon black is ground in an agate mortar. The resulting powder is then compressed at high pressure to form a pellet (100 MPa, 1 min). The pellet was finally glued to a piece of glass. Before the microscopic observation, the sample is kept under vacuum for 24 hours. This technique has been applied successfully to different furnace carbon blacks (N110, N234, N330, N762) and also to thermal black (N990) and conductive black (XC 72).

5.2. Structure of Carbon Black Surface

5.2.1. Low Enlargement Images

At low magnification, the carbon black surface exhibits a very compact organization of small objects whose size is very much dependent upon the carbon black type (Fig. 3). It is possible to classify the carbon blacks and the STM classification follows: N110, N234, N330, N762 and N990. But it seems impossible to locate the precise frontier of the aggregates. Under observation carbon black surface appears as a macroscopic agglomerate of
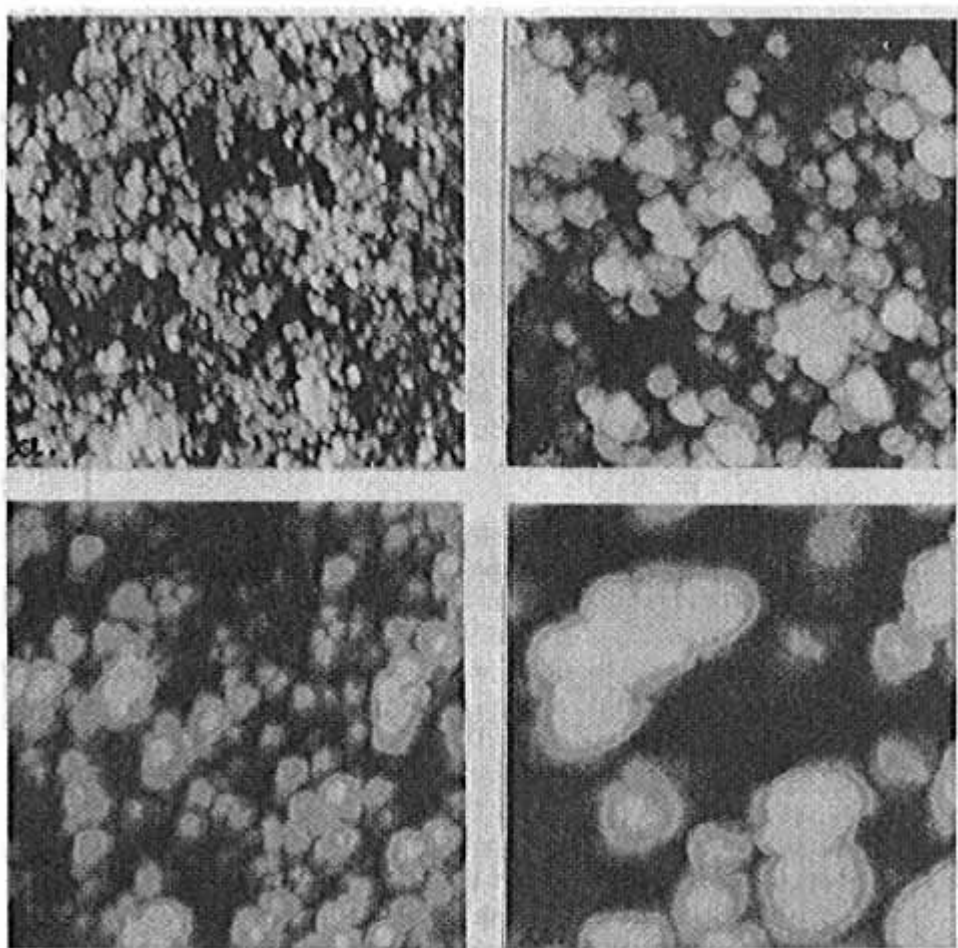
Fig. 3.
2500×2500 nm2 STM images of various carbon blacks showing aggregates. a: N110, b: N234, c: N762, and d: N990.

particles. At larger magnification it is possible to delimit the particles more sharply (Fig. 4). The particle joints are always sharp, and a large number of observations have shown that contiguous particles have generally close sizes. On the other hand, no contiguous particles that could be supposed to belong to two different aggregates can be very different in their size.

5.2.2. High Enlargement Images

At higher enlargement the particle surface can be finely observed and important deviations from flatness are noticed. The particle surface seems to be constituted of small V-shaped zones which are highly organized areas (Fig. 5). However, atomic resolution can be achieved. The atoms made visi-
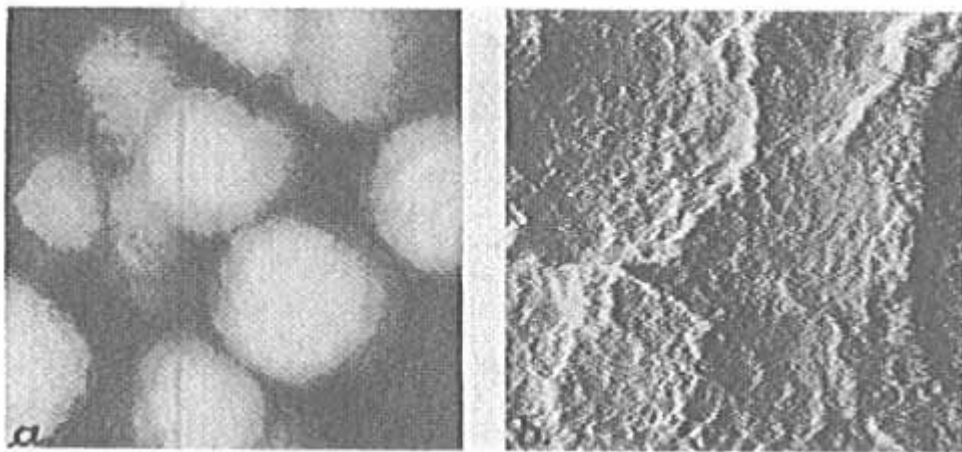
Fig. 4.
50×50 nm2 STM images showing particle surface roughness. a: N234
(constant current), b: N330 (constant height).

ble by STM appear generally in the form of 0.25×0.40nm2 rectangular arrangement. In some places the trigonal symmetry of graphitic layers is visible, but these organized areas show clean V-shaped borders which overlap each other on the particle surface. Because of their shape and organization, we will name them scales.

5.2.3. Modeling of Carbon Black Surface

The STM observations confirm that carbon blacks are constituted of small spherical particle as previously shown by TEM. However, the primary structure of the aggregate cannot be seen by STM, perhaps because of the
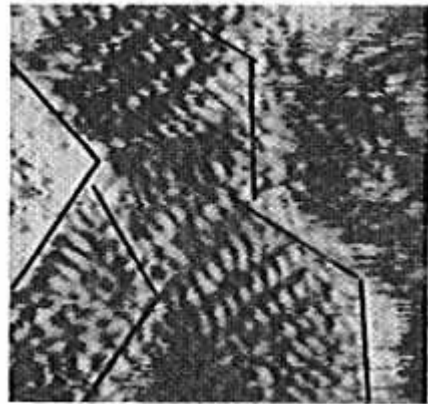
Fig. 5.
6×6 nm2 STM image of N330
carbon black showing graphitic
scales (constant height).

Fig. 6.
New surface model of carbon
black particle consisting of
overlapping graphitic scales.

high aggregation level induced by the pressure used to prepare the pellet. The atomic arrangement of carbon atoms seen at atomic resolution does not match strictly with the standard model (Fig. 2). The observed surface is more organized, and at a much larger scale.

The 0.25×0.40 nm2 rectangular arrangement made of visible atoms does not correspond to a crystallographic structure because STM does not make visible the atoms of the surface but their electronic density. Such an arrangement has never been described, but it has been shown in some recent publications concerning graphite [11]. On HOPG we have observed a continuous transition between the trigonal arrangement and the rectangular one, and it appears to us that this rectangular arrangement corresponds to a graphitic layer whose electronic states are perturbated. The rough V-shaped interruption of these rectangular arrangements probably corresponds to the end of a graphitic layer. The upper gaping of the

graphitic layers could explain the electronic state perturbation and lead to the observed STM image.

Thus, the surface structure of carbon black particles is made up of the overlapping of the end of many graphitic layers, which are organized in scales (Fig. 6). Therefore, the Lc values measured by X-ray diffraction must be considered as representing the average overlapping dimension of graphitic layers, but not as being the average size of independent crystallites. Since the atomic rectangular arrangement of independent scales has the same orientation we could suppose that their arrangement is not governed by chance.

It appears logical that if the particle surface is organized, it should be the same for the lower layers and consequently for the whole carbon black particle and this should involve a structuring element which would organize the particle growth. Recent studies have shown that fullerenes can be re-

garded as precursors in soot formation [1213]. We also think that fullerenes might give an organized nucleus for the growth of the carbon black particle and explain the unattempted order observed on particle surface.

More than fifty years ago, TEM had revealed the intimate structure of carbon black constituted of small spherical particles arranged in aggregates. This observation has induced many changes and discoveries in carbon black knowledge. The application of STM to carbon black has revealed that the particle surface is organized and exhibits graphitic scales. This organization at the atomic scale could explain many carbon black properties, and particularly its ability to reinforce elastomers. The study of chemically and physically modified carbon blacks should permit improvement in our knowledge of their structure and formation.

References

1. Binnig, G. and Rohrer, H., *Helv. Phys. Acta,* 55, 726 (1982).

2. Hu, C. Z., Feng, L. and Andrade, J. D., *Carbon,* 26 (4), 543 (1988).

3. Elings, V. B. and Wudl, F., *J. Vac. Sci. Technol. A,* 6 (2), 412 (1988).

4. Marchon, B., Salmeron, M. and Siekhaus, W., *Phys. Rev. B: Condens. Matter,* 39 (17), 12907 (1989).

5. Brown, N. D. M. and You, H. X., *J. Mater. Chem.,* 1 (3), 469 (1992).

6. Hoffman, W. P., Elings, V. B. and Gurley J. A., *Carbon,* 26 (5),

754 (1988).

7. Magonov, S. N., Cantow, H. -J. and Donnet, J. -B., *Polym. Bull.,* 23, 555 (1990).

8. Hofmann, W. P., *Carbon,* 30 (3), 315 (1992).

9. Donnet, J. -B. and Custodéro, E., *C. R. Acad. Sci. Paris Serie II,* 314, 579 (1992).

10. Donnet, J. -B. and Custodéro, E., *Carbon,* 30 (5), 813 (1992).

11. Chang, H. and Bard, A.J., *Langmuir,* 7 (6), 1143 (1991).

12. Kroto, H. W., Allaf, A. W. and Balm, S. P., *Chem. Rev.,* 91 (6), 1213 (1991).

13. Howard, J. B., McKinnon, J. T., Jonhson, M. E., Makarovsky, Y. and Lafleur, A. L., *J. Phys. Chem.,* 96 (16), 6657 (1992).

Chapter 6
Surface Energy of Carbon Black

Meng-Jiao Wang
and Siegfried Wolff
Degussa AG,
Hürth, Germany

It is now widely recognized that the primary carbon black parameters influencing elastomer reinforcement are particle size or specific surface area, structure, and surface activity. The surface activity dominates polymer-filler interaction, filler aggregate-aggregate interaction as well as filler-ingredient interactions. This factor can, in a chemical sense, be related to different chemical groups on the carbon black surface, such as carboxyl, quinonic, phenol and lactone groups. In a physical sense, variations in surface energy determine the adsorptive capacity of the filler and its energy of adsorption.

The chemical groups on the carbon black surface can, nowadays, easily be identified (see Chapter 4). It has been found that the surface chemistry of carbon blacks has a significant effect on the vulcanization of rubber compounds, although no direct correlation has been demonstrated between chemical groups on the carbon black surface and rubber-related properties [1]. It is generally believed that the surface energy of carbon blacks has much greater effect on the mechanical properties of filled elastomers than their chemical nature, particularly when general-purpose hydrocarbon rubbers are concerned.

The surface energy, γ, is defined as the work, *W,* necessary to create a unit new surface of liquid or solid. This energy is caused by different types of cohesive forces, such as dispersive, dipole-dipole, induced dipole-dipole, and hydrogen bond forces.

In the case of all these cohesive forces being involved in independent ways, the surface energy can be expressed as the sum of several components,

each corresponding to a special type of molecular interaction (dispersive, polar, hydrogen bond.). Since the effect of the dispersive force is universal, the dispersive component of the surface free energy is particularly important. If a solid substance can have only dispersion interaction with its environment, its surface energy, γ_s, is identical with its dispersive component, γ_s^d

$$\gamma_s = \gamma_s^d \quad (1)$$

For most of the substance, one has

$$\gamma_s = \gamma_s^d + \gamma_s^{sp} \quad (2)$$

where γ_s^{sp} is the sum of the other components of surface energy and is termed specific component.

The interaction between two materials, 1 and 2, is determined directly by their surface energy. When the interaction involves dispersion process only, then according to the Fowkes' model [24], the energy of adhesion, W_{d_a}, will correspond to the geometric mean of the dispersive components of their surface energies:

$$W_a^d = 2(\gamma_1^d \gamma_2^d)^{\frac{1}{2}} \quad (3)$$

Similarly, the polar components of adhesion energy, W_{p_a}, can be expressed by the polar components of surface free energies.

The total adhesion energy can, therefore, be given by:

$$W_a = W_a^d + W_a^p + W_a^h + \quad (4)$$

or

$$W_a = 2(\gamma_1^d \gamma_2^d)^{\frac{1}{2}} + W_a^p + W_a^h + \quad (5)$$

where W_a^h is the contribution of the hygrogen bond to adhesion.

So far, only a limited number of tools have been available to measure surface energy, and most of them are not accurate enough. However, inverse gas chromatography (IGC) has recently been shown to be one of the most sensitive and convenient methods for measuring filler surface energy [59]. With regard to the carbon blacks, the pioneer work has been done by Donnet and his co-workers [1013].

6.1. Determination of Surface Energy by IGC

In IGC, the filler to be characterized is used as the stationary phase and the solute injected is called a probe. When the probe is operated at infinite dilution, the adsorption energy, $\Delta G°$, of the probe on the filler surface and hence the adhesion energy, W_a, can be calculated from the net retention volume:

$$\Delta G° = NaW_a = -RTLn\frac{CV_N}{Sg}$$

(6)

where VN = net retention volume corrected for gas compressibility and temperature, S = specific surface area of the filler, g = mass of the filler packed in the column, R = gas constant, T = temperature in K, C = constant, N = Avogadro's number, and a = molecular surface area of the probe.

The retention volumes are related to the total surface area, A, of the filler in the column, which is the product of S and g, and also related to the surface partition coefficient, Ks, for the adsorbate between the adsorbed and the gaseous phase, i.e.,

$$VN = AKs \quad (7)$$

If, however, the surface is energetically heterogeneous, the statistical treatment of the chromatographic process leads to the same result as obtained by assuming an additive function of the elementary processes taking place in small patches within which adsorption is homogeneous but between which adsorption varies. Each patch is characterized by its surface partition coefficient, Ks,i. For n patches, the total retention volume VN can be given by [14]:

$$V_N = AK_s = \sum_{i=1}^{n} A_i K_{s,i} = A \left(\sum_{i=1}^{n} A_i K_{s,i} / \sum_{i=1}^{n} A_i \right) \quad (8)$$

with

$$A = \sum_{i=1}^{n} A_i \quad (9)$$

where A_i is the surface area of the ith surface patch. The surface partition coefficient Ks is, therefore, a mean value, and so are the adsorption free energy, $\Delta G°$, and the parameters calculated from it. However, these values are energy-weighted since Ks is related to

the adsorption energy. In other words, the high-energy patches (or high-energy sites) play a very important role in the determination of adsorption properties.

The value of γ_s^d is obtained from the free energy of adsorption per mole methylene group, ΔG_{CH_2} [6,7]. It can be derived from the slope of the linear plot of $\Delta G°$ of a series of n-alkanes which are only able to exchange interaction with the filler surface via dispersion forces, vs their carbon atom number:

$$\gamma_s^d = \frac{\Delta G_{CH_2}^2}{4N^2 a_{CH_2}^2 \gamma_{CH_2}} \quad (10)$$

where a_{CH_2} is the area covered by a $-CH_2-$ group, and γ_{CH_2} is the surface energy of a surface composed entirely of $-CH_2-$ groups.

Since γ_s^{sp} is extremely difficult to measure, Papirer et al [15], Schultz et al [16], and Donnet et al [1720] have proposed several approches to estimate γ_s^{sp} from the specific interaction, I_{sp}, which the filler is able to exchange with a polar probe. According to the method put forward by Wang and his co-
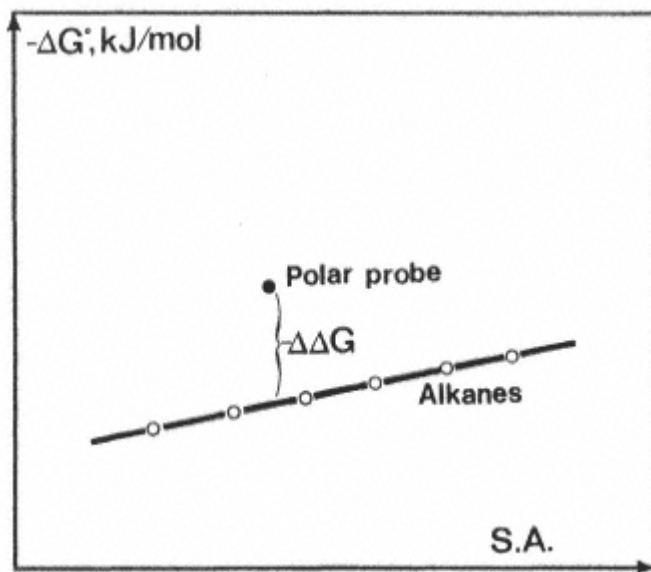
Fig. 1.
Schematic principle of estimating specific
interaction (from ref. [9]).

workers [9], the I_{sp} can be calculated from the difference between
the adsorption energies of polar probes and those of n-alkanes (real
or hypothetical) having the same molecular surface area. This
difference is termed $\Delta\Delta G$ (Fig. 1). One has

$$I^{sp} = \frac{-\Delta\Delta G}{N a_p} \qquad (11)$$

where a_p is the surface area of the polar probe.

Concerning filler/elastomer interaction, while fillers have polar
surfaces, hydrocarbon rubbers are usually non- (or very low-) polar
materials. The higher adsorption energy of nonpolar probes, such
as alkanes, resulting from a higher γ_s^d of the filler surface, should
indicate a greater ability of the filler to interact with hydrocarbon
rubber. On the other hand, the higher adsorption energy of a highly

polar probe, resulting from the high γ_s^{sp}, should be representative of a higher filler particle-particle interaction. It can be understood that when the dispersive component of the filler surface is constant, the increase of polarity of the filler surface would promote incompatibility of the filler with hydrocarbon rubber, thus enhancing aggregate agglomeration. On the contrary, at the same level of the polar component of the filler surface energy, the higher filler/polymer interaction would result in a lesser degree of association of the aggregates. Based on this consideration, a specific interaction factor, Sf, was introduced. This factor is related to both specific and dispersive components of the surface energy. It is defined as a ratio of the adsorption energy of a given probe, ΔG°, to that of an alkane (real or

hypothetical), the surface area of which is identical with that of the given probe, ΔG^o_{alk} (Fig. 2) [12]:

$$S_f = \frac{\Delta G^o}{\Delta G^o_{alk}} \quad (12)$$

In this definition, the reference state for the calculation of ΔG° is the ΔG° of a hypothetical alkane with zero surface area which was extrapolated from the ΔG° of a series of *n*-alkanes. For a highly polar probe, the higher the *Sf* of a filler, the more developed is its aggregate agglomeration in hydrocarbon rubbers.

With regard to surface energy, two parameters of fillers are, therefore, of relevance in hydrocarbon elastomer reinforcement: γ^d_s and *Sf*. The former determines polymer/filler interaction, whereas the latter determines interparticle or interaggregate interaction, i.e., the ability of the filler to form a secondary filler network.

6.2. γ^d_s of Carbon Black

The values of γ^d_s of a number of dry-pelletized carbon blacks are plotted as a function of carbon black surface area in Fig. 3. γ^d_s increases, almost linearly, with surface area. However, it has been demonstrated that the difference in γ^d_s between carbon blacks is associated with differences in their microstructure rather than their surface area or particle size [12]. The carbon atoms in carbon blacks are largely considered to be parts of quasi-graphitic crystallites consisting of several turbostratic layers at an interplanar distance,

$$S_f = \frac{-\Delta G_0^\circ}{-\Delta G_{Alk}^\circ}$$
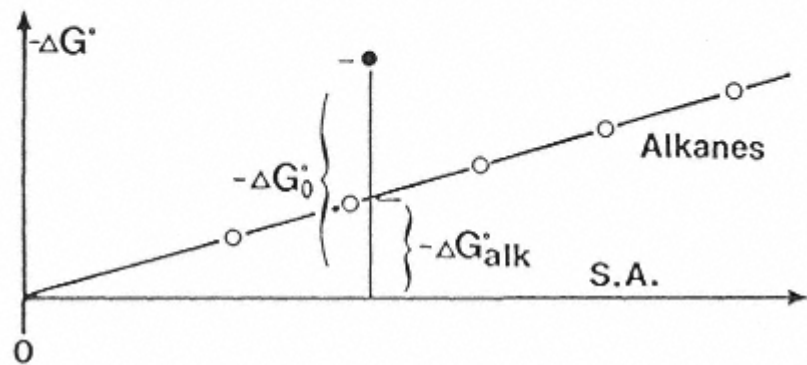
Fig. 2.
Definition of S^f factor (from ref. [12]).
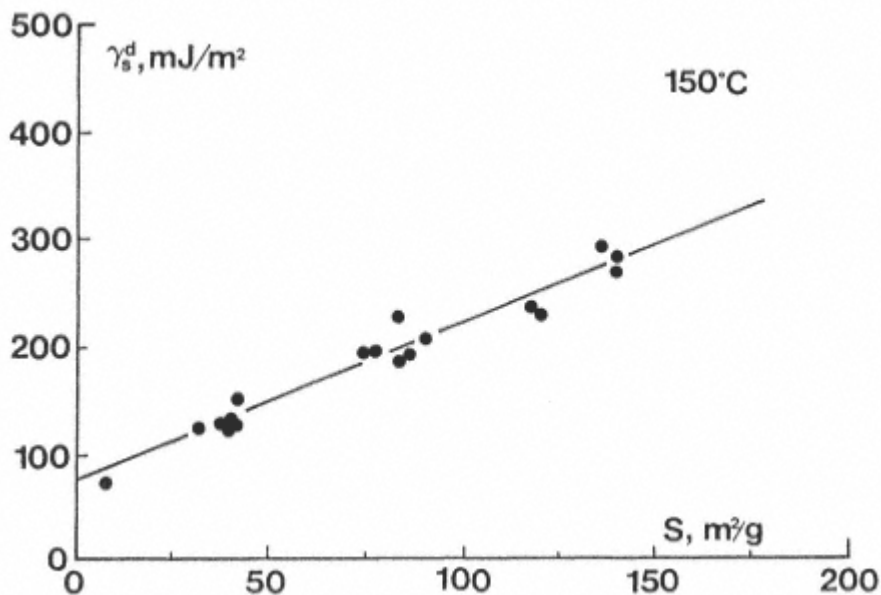
Fig. 3.
γ_s^d vs. nitrogen surface area for dry-pelletized carbon blacks at 150°C (from ref. [12]).

d, of 0.35 to 0.38 nm. The crystallite dimension is characterized by the average stacking height of the parallel planes in the c direction, Lc, and the average diameter of the parallel layers in the ab plane, La. The apparent surface area dependence of γ_s^d may reflect the particle size dependence of carbon black microstructure. Significant variations in the crystallographic parameters of carbon blacks have been reported [12,21,22], generally indicating a decrease in crystallite dimension with increasing surface area.

Fig. 4 presents γ_s^d as a function of Lc, suggesting that surface energy decreases with increasing crystallite dimensions. This is understandable since a greater number of crystal edges and a greater unsaturated charge, which can be considered as high-energy

sites, would be expected in the smaller crystallites observed in the small-particle products.

The effect of carbon black microstructure on γ_s^d has also been demonstrated by graphitization of carbon blacks. A drastic decrease in the γ_s^d of a wet-pelletized N375 carbon black from 257 to 189 mJ/m2 at 180°C upon graphitization is obviously due to the growth of crystallites. On the other hand, if the defects of the crystal structure are covered by chemical groups or strongly adsorbed impurities, the surface energy of carbon blacks should change. The post-treatment of carbon blacks, therefore, would have a considerable effect on carbon black surface energy.
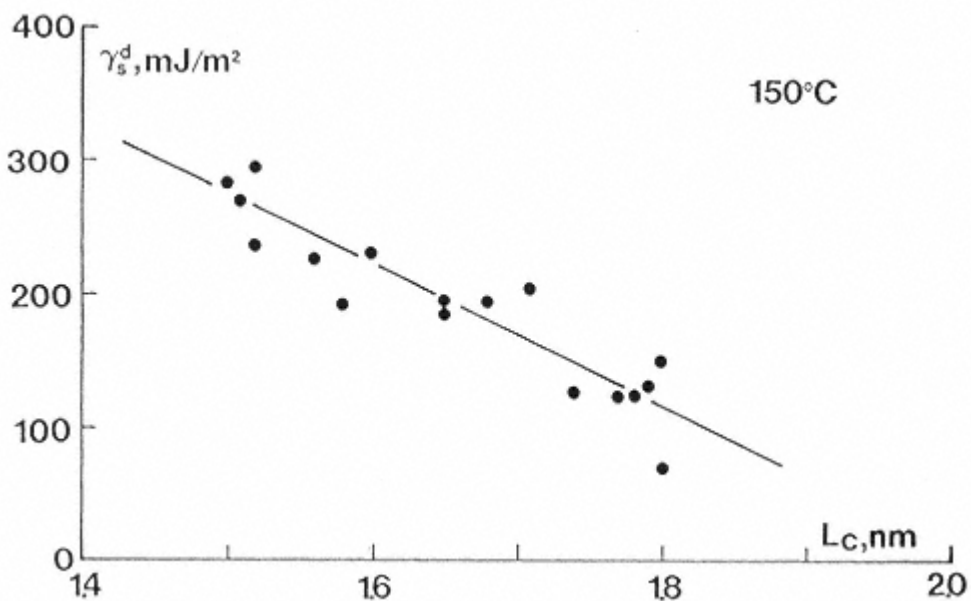
Fig. 4.
γ_s^d as a function of Lc for dry-pelletized carbon blacks at 150°C (from ref. [12]).

6.3. Specific Component of Surface Energy

The specific component of the surface energies of carbon blacks has been evaluated by the parameter I_{sp} of polar probes, such as benzene and acetonitrile (MeCN) [12]. Since benzene is capable of specific interaction with the carbon black surface via the electronic localization of a big π-bond system and since hydrogen bonding may be involved in the case of acetonitrile, the I_{sp} of benzene and MeCN should reflect the specific components of the surface free energies of carbon blacks.

A comparison of I_{sp} of carbon blacks is shown in Fig. 5 for acetonitrile adsorption. These values for I_{sp} suggest that the smaller-particle products exhibit higher specific interaction with

polar probes, even though the data are somewhat scattered. However, similar to the dispersive components of surface energy, the surface area dependence of the specific interactions is more representative of surface state rather than the surface area itself. This is indicated by the fact that the specific interaction of the channel black with polar probes is slightly, but definitely, higher than expected from the surface area dependence of I_{sp} of furnace blacks [12]. This is undoubtly related to its high concentration of oxygen groups which are polar sites by nature.

The Sf values for acetonitrile adsorption on carbon blacks are compared in Fig. 6, together with the data of the precipitated silicas Ultrasil VN 2 (P1) and Ultrasil VN 3 (P2). The values of Sf seem to be constant for all car-
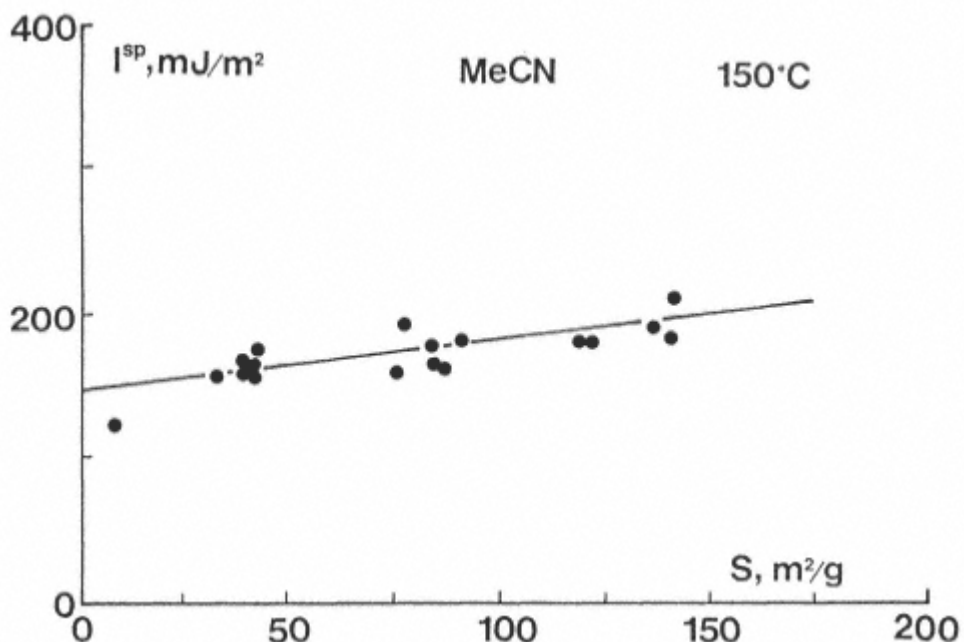
Fig. 5.
Isp of acetonitrile vs. nitrogen surface area for dry-pelletized carbon blacks at 150° C (from ref. [12]).

bon blacks, only slightly higher for the large-particle blacks. This suggests that, with regard to energy, the agglomeration tendency is the same for all carbon blacks in hydrocarbon elastomers. Hence, the agglomeration, i.e., the dispersion, of carbon blacks in a given polymer should only be determined by its particle size and structure, both of which determine the distance between carbon black aggregates (see Chapter 9). The very high Sf values of precipitated silicas suggest a very pronounced ability of these fillers to undergo networking in hydrocarbon elastomers. This has been demonstrated by the evaluation of compound viscosity and the strain dependence of natural rubber vulcanizates filled with N110 carbon black and Ultrasil VN 2, respectively, which both have approximately the same surface area and structure [23].

6.4. Estimation of Polymer-Carbon Black Interaction

Information on polymer-carbon black interaction has been estimated from the free energy of adsorption, $\Delta G°$, of low-molecular-weight analogs of rubber [9,12]. For this purpose, olefins were used as model compounds of unsaturated rubber such as NR and BR, and alkanes for those of saturated rubber such as EPR and butyl rubber. A series of alkylated benzenes and homologous nitriles were used to evaluate the contribution of an aromatic ring to interaction of SBR with carbon blacks and the contribution of the
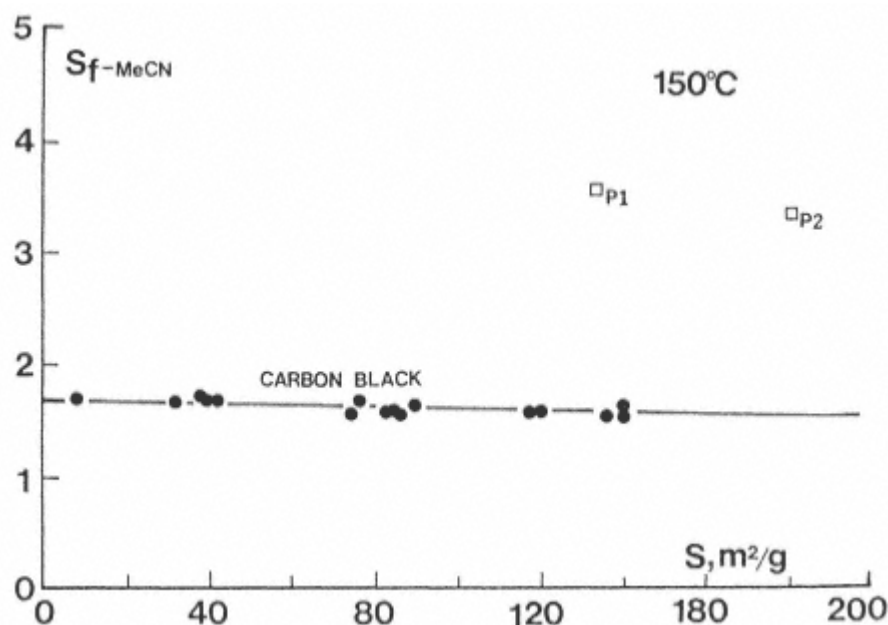
Fig. 6.
Sf of acetonitrile on carbon blacks and silicas at 150°C (from
ref. [12]).

-CN group to interaction of NBR with fillers, respectively. Fig. 7 illustrates the free energies of adsorption of a variety of rubber analogs on the carbon black N330 as a function of the surface area covered by the probe molecules. The plots of all homologous probes are straight lines which can be treated as family plots. The difference in the ordinate between the given family plot and the plot of *n*-alkanes is related to the contribution of the functional groups. It can, therefore, be concluded from the free energies of adsorption that NBR and SBR exhibit strong interaction with carbon blacks, followed by unsaturated rubbers, such as NR and BR. The saturated rubbers, particularly branched polymers, like butyl rubber, exhibit weak interaction with fillers. This observation is in good agreement with test results for bound rubbers, indicating

a higher activity for SBR, followed by polybutadiene, with butyl rubber giving the lowest bound rubber content [24].

6.5. Energetic Heterogeneity of Carbon Black Surface

Surface energy as measured by adsorption and wettability techniques is represented by a value which is averaged over the total filler surface. However, as mentioned previously, the thermodynamic parameters of adsorption and surface energies measured by means of IGC at infinite dilution are energy-weighted, i.e., the high-energy patches (or high-energy sites) play a very important role in the determination of the adsorption properties and surface
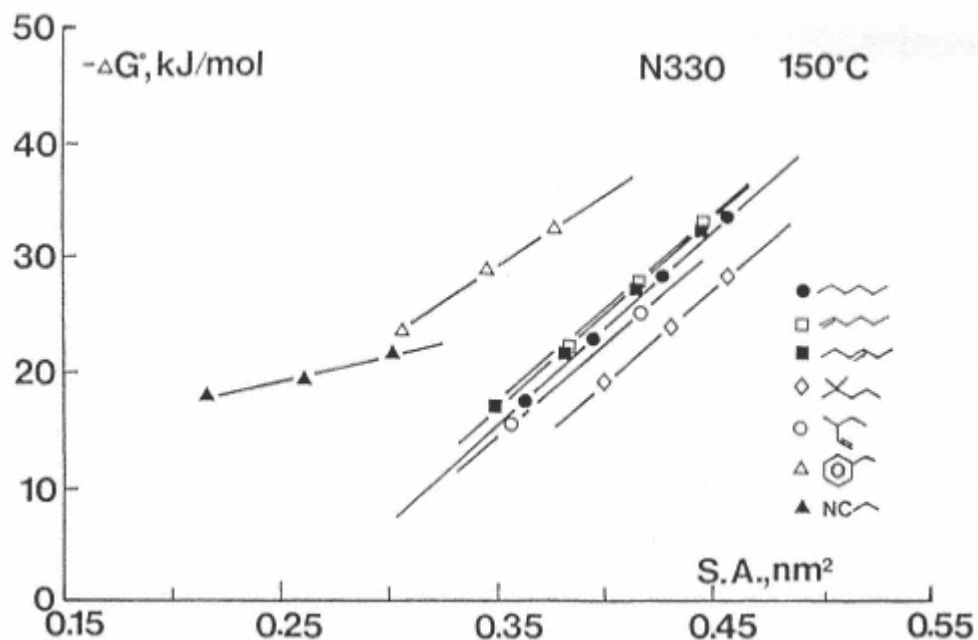
Fig. 7.
Energies of adsorption of various probes on N330 vs. their molecular
surface areas at 150°C (from ref. [12]).

energies of the fillers.

On the other hand, it has been recognized that a small percentage
of the carbon black surface with much higher energy has a
considerable influence on rubber reinforcement. This has been
confirmed by heat treatment and chemical treatment evaluations.
Loss of high-energy centers of the carbon black by graphitization
[2528] and alkylation [29] causes a profound change in its
reinforcing ability with regard to rubbers, leading to a low level of
bound rubber, a reduction in modulus and tensile strength, higher
tan δ, and lower abrasion resistance. It is, therefore, obvious that
the energy-weighted average surface energy measured
chromatographically at infinite dilution is a useful parameter for

characterizing the surface activity of the filler with regard to rubber reinforcement. Of course, the determination of the energetic heterogeneity of the carbon black surface could provide additional information concerning the nature of filler surface energies, which is desirable for a better understanding of the reinforcement of elastomers. This has been achieved by estimating the heats of adsorption and immersion at different levels of coverage of the surface. However, with IGC operated at finite concentration, the complete distribution function of adsorption energy of given adsorbates on rubber fillers, $\chi(\varepsilon)$, which is defined as the change in the number of energy sites with energy, ε, can be derived from isotherms of adsorption [13,30,31], or directly be calculated from the pressure dependence of the retention volume,

[14, 3234]:

$$\chi(\epsilon) = -\left(\frac{P}{RT}\right)^2 \frac{\partial V_N(P,T)}{\partial P} \qquad (13)$$

where P is the equilibrium pressure.

Besides the nature of the filler surface, this function is, of course, dependent on the adsorbed molecules. The energy distribution functions obtained by differentiation of the retention volume with respect to equilibrium pressure (Equation 13) are illustrated in Fig. 8 for cyclohexane adsorption [14] on various blacks. In this figure, $\chi(\varepsilon)$ per unit surface of the carbon blacks was plotted as a function of adsorption energy ε. The shape of the distribution curves is the same for all carbon blacks, i.e., they are skewed Gaussian-type distributions with very broad tails on the high-energy sides. This behavious is quite different from what was observed for the silicas. The energy distribution curves of benzene and n-hexane adsorption on silica at 40°C show several distinct peaks which were attributed to different types of silanols, siloxanes, and impurities [34]. The very broad distribution functions of the carbon blacks could be an indication of surfaces with highly heterogenous energies.

On the other hand, a comparison of the distribution functions of the different carbon blacks suggests that the peaks of the curves, i.e., the energy and the concentration of the most probable sites, are approximately the same for all carbon blacks. The energies of the sites with the highest concentration are about 31 kJ/mol for benzene adsorption as compared to 33 kJ/mol for
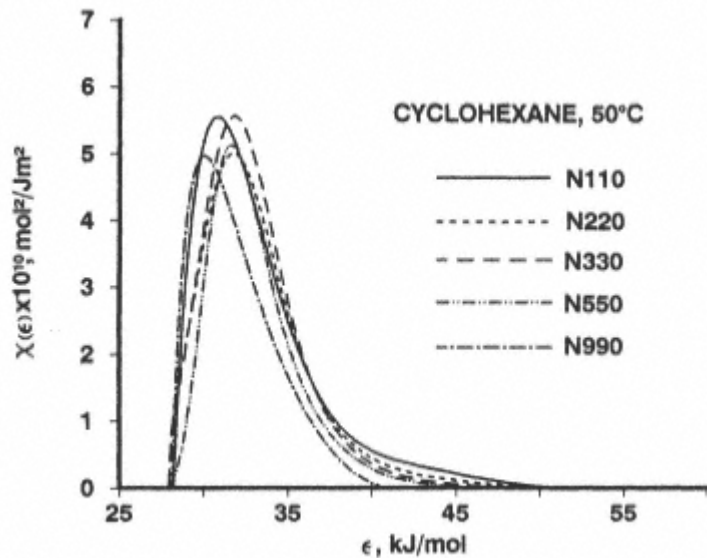
Fig. 8.
Energy distribution functions of cyclohexane
adsorption on a variety of carbon blacks at 50°C
(from ref. [14]).

cyclohexane [14]. The main difference in the distribution curves of the different carbon blacks is observed on the high-energy side. There is a consistent increase in the concentration of high-energy centers with increases in carbon black surface area. It is, therefore, reasonable to conclude that the higher surface energy measured by inverse gas chromatography at infinite dilution for hard carbon blacks is mainly caused by the greater concentration of high-energy centers.

The fact that the energies of the most likely occurring sites are comparable for furnace carbon blacks, gives rise to the assumption that the energetic sites, dominating the carbon black surface, are related to the basal planes of the graphitic crystallites. If this is so, the high-energy centers should constitute the edge and defects which occupy only a small percentage of the surface. It is therefore understandable that, as discussed above, the disordered part of the surface is more developed on small-particle carbon blacks which are characterized by smaller crystallites. On the other hand, if the surface is composed of these two parts with different energies, the distribution curve should have two distinct response peaks. The fact that only one broad peak is observed is not yet fully understood. One reason for this phenomenon may be that the chemical groups located on the edges of the graphitic basal planes, such as hydrogen, oxygen-containing groups and possibly hetero-atoms, as well as foreign matter adsorbed on the carbon black surface which cannot be removed by extraction, could change the energy of these two parts of the surface, thus broadening the distribution curves. On the other hand, the turbostratic structure under the first layer of the crystal lattice plane may also play a role in changing the surface energy.

A comparison of the energy distribution curves for benzene adsorption of the graphitized carbon black N110 and its nongraphitized counterpart is shown in Fig. 9. The same pattern was also observed for other carbon blacks. The distribution of adsorption energy is narrowed after graphitization, showing both high- and low-energy sites to have disappeared. While the loss of the high-energy centers can be attributed to the disappearance of the crystal edges, the decrease in the number of low-energy sites may be due to the removal of certain chemical groups and of substances which have a lower adsorption activity than the graphitic planes during graphitization at temperatures as high as 2700°C. This is in line with the result obtained at infinite dilution for carbon blacks treated in an inert atmosphere (helium stream) at relatively high temperature (e.g., 400°C) [12]. Surface energy increases considerably after heat treatment, which has been assumed to be the result of the removal of certain chemical groups from the surface. There is no reason to believe that any change in the crystallographic structure occurs at this temperature.

In comparison to the nongraphitized carbon blacks, the energy distribu-
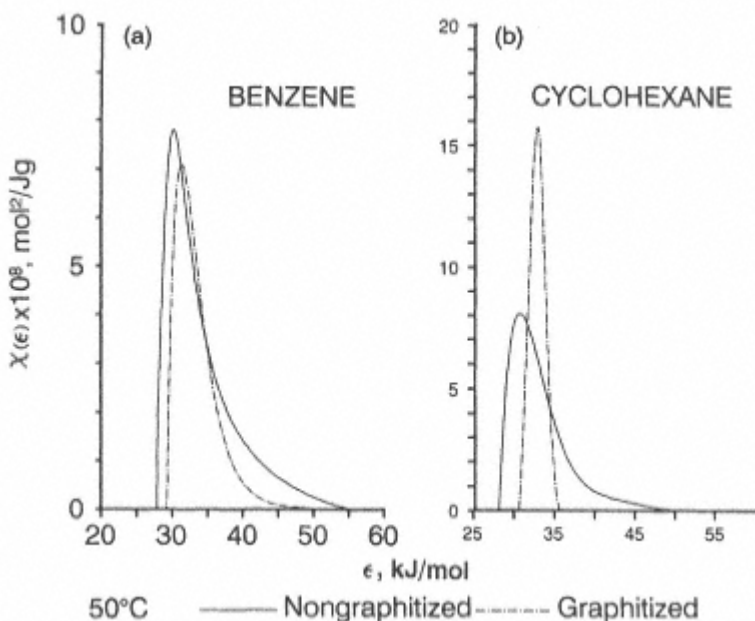
Fig. 9.
Comparison of energy distribution functions of adsorptions
on graphitized and nongraphitized N110 carbon black
- a: benzene adsorption; b: cyclohexane adsorption (from
ref. [14].

tion of cyclohexane on graphitized blacks is so narrow that almost all active sites are concentrated in an energy range from 30 to 35 kJ/mol [14] (Fig. 9). As in the case of benzene adsorption, both low- and high- energy sites for cyclohexane disappear during the heat treatment. The different patterns of the distribution functions for benzene and cyclohexane adsorption on graphitized carbon blacks, i.e., skewed *vs* symmetric peaks, may be explained by the different nature of the probes as well as the different configurations in adsorbed state of their molecules [14].

Since the surface energy measured at infinite dilution constitutes a mean value and is much higher for nongraphitized carbon blacks,

the removal of both high-and low-energy sites after graphitization supports the conclusion, drawn from the comparison of the energy distributions of adsorption on different grades of nongraphitized blacks, that the high-energy sites play a very important role with regard to surface energy. On the other hand, numerous studies have shown in the past that graphitization results in a drastic reduction in the capacity for elastomer reinforcement. With regard to surface activity, it can be concluded that the high-energy sites on carbon blacks are mainly responsible for the reinforcing capability of fillers in elastomers.

References

1. Donnet, J. -B. and Papirer, E., *Rev. Gen. Caout.,* 42, 729 (1965).

2. Fowkes, F. M., *J. Phys. Chem.,* 66, 382 (1960).

3. Fowkes, F. M., *Ind. Eng. Chem.,* 56, 40 (1964).

4. Fowkes, F. M., *J. Colloid Interface Sci.,* 28, 493 (1968).

5. Kiselev A. V. and Yashin, Y. I., *Gas-Adsorption Chromatography,* Plenum Press, New York, 1969.

6. Dorris G. M. and Gray, D. G., *J. Colloid Interface Sci.,* 71, 93 (1979).

7. Papirer, E., in *Composite Interfaces,* H. Ishida and J. L. Koenig, eds., Elsevier Science Publishers, New York, 1969.

8. Vidal, A., Wang, M. -J., Papirer, E. and Donnet, J. -B., *Chromatographia,* 23, 121 (1987).

9. Wang, M. -J., Wolff, S. and Donnet, J. -B., *Rubber Chem. Technol.,* 64, 559 (1991).

10. Vidal, A., Shi, Z. and Donnet, J. -B., presented at IRC'90, Paris, June 1214, 1990.

11. Donnet, J. -B. and Lansinger, C. M., presented at IRC'90, Paris, June 1214, 1990.

12. Wang, M. -J., Wolff, S. and Donnet, J. -B., *Rubber Chem. Technol.,* 64, 714 (1991)

13. Papirer, E., Li, S., Balard, H. and Jagiello, J., *Carbon,* 29, 1135 (1991).

14. Wang, M. -J. and Wolff, S., presented at a meeting of the Rubber Division, ACS, Detroit, Michigan, October 811, 1991; *Rubber Chem. Technol.,* in press.

15. Saint-Flour, C. and Papirer, E., *J. Colloid Interface Sci.,* 91, 69 (1983).

16. Schultz, J., Lavielle, L. and Martin, C., *J. Chim. Phys.,* 84, 231 (1987).

17. Dong, S., Brendle, M. and Donnet, J. -B., *Chromatographia,* 28, 469 (1989).

18. Donnet, J. -B., Park, S. J. and Balard, H., *Chromatographia,* 31, 434 (1991).

19. Donnet, J. -B. and Park, S. J., *Carbon,* 29, 955 (1991).

20. Donnet, J. -B. and Park, S. J., *Carbon,* 30, 263 (1992).

21. Austin, A. E., *Proc. 3rd Conf. on Carbon,* p. 389, 1958.

22. Gerspacher, M. and Lansinger, C. M., presented at a meeting of the Rubber Division, ACS, Dallas, Texas, April 1922, 1988.

23. Wolff, S. and Wang, M. -J., *Rubber Chem. Technol.,* in press.

24. Dannenberg, E. M., *Rubber Chem. Technol.,* 59, 512 (1986).

25. Brennan, J. J., Jermyn, T. E. and Boonstra, B. B., *J. Appl. Polym. Sci.,* 8, 2687 (1964).

26. Dannenberg, E. M., *Rubber Age,* 98, 9, 82; 10, 81 (1966).

27. Medalia, A., *Rubber Chem. Technol.,* 46, 877 (1973).

28. Degussa AG, unpublished work.

29. Vidal, A., Shi, Z. and Donnet, J. B., *Kautsch. Gummi Kunst.,* 44, 419 (1991).

30. Jagiello, J., Ligner, G. and Papirer, E., *J. Colloid Interface Sci.,* 137, 128 (1990).

31. Tijburg, I., Jagiello, J., Vidal, A. and Papirer, E., *Langmuir,* 7, 2242 (1991).

32. Rudzinski, W., Waksmundzki, A., Leboda, R., Suprynowicz, Z. and Lason, M., *J. Chromatogr.,* 92, 25 (1974).

33. Waksmundzki, A., Sokolowski, S., Rayss, J., Suprynowicz, Z. and Jaroniec, M., *Separ. Sci.,* 11, 29 (1976).

34. Wang, M. -J., Wolff, S. and Donnet, J. -B., *Kautsch. Gummi Kunst.,* 45, 11 (1992).

Chapter 7
Fractal Geometry

Alain Le Méhauté
Départment Matériaux et Procédés,
Alcatel Alsthom Recherche,
Marcoussis, France

Michel Gerspacher
Sid Richardson Carbon & Gasoline Co.,
Fort Worth, Texas, U. S. A.

Claude Tricot
Département de Mathématique,
Ecole Polytechnique,
Montreal, Quebec, Canada

The concept of fractal geometry was introduced in 1975 by B. Mandelbrot [1]. Initially this new way of looking at objects did not receive a lot of attention in the field of physics with the exception of some industrial sponsored research. In the late 1970's limited application of this mathematical concept was published especially from research teams working in the field of finely divided matter [2,3]. It is of interest to note that three initial industrial papers using this approach dealt with carbon black [46]. It is also interesting to note that the D.L.A (Diffusion Limited Aggregation) model, which is now widely used in numerous fundamental studies in physics and which attempts to address highly fragmented states of matter, was derived from an attempt to understand the formation of carbonaceous soots [6], a material similar to carbon black but

containing numerous impurities. The above mentioned works set the basis for a renewed interest in the geometrically complex object carbon black. The following section will review the application of fractal geometry of carbon blacks with emphasis on the most recent developments.

7.1 Fractal Geometry

In conventional Euclidean geometry, a surface measurement is expressed as the power two and a volume as a power three of a length. Therefore, lengths, areas and volumes are characterized by the respective dimensions 1, 2 and 3. Such measures are inadequate to take into account the complexity of many natural objects. It is known since the beginning of this century (H. Hausdorff, G. Bouligand) that finer measures exist, giving rise to non-integer dimensions, which are useful to describe irregular and broken *(fractus* in Latin) objects, defined as being *fractal.* It can be expected, therefore, that the dynamics and thermodynamics behaviors of such objects depend on their non-integer dimension.

As described above, the dimension in the Euclidean world is very intuitive and self explanatory; the fractal world characterized by non-integer dimension is not. A good example of this fractal world can be visualized as follows: a non-integer dimension can be derived from a mathematical object described in Greek antiquity and known as the *Apollonius* circles. This figure is composed of three circles tangent to each other (Fig. 1). These circles delimit a curvilinear triangle ABC whose area S_o can be expressed as a function of the radii of the initial circles. When the three circles have the same radii $R_o,$ the equation

$$S_o = (\sqrt{3} - \pi/2)R_o^2 \quad (1)$$

clearly indicating that if the radius R_o is finite, the area S_o is finite also. As it can be seen from Fig. 1a, an infinity of circles of radii R_i can be drawn in the curvilinear triangle ABC. This is known as the

Apollonian packing of circles. It can be proved that the sum of all radii R_i is infinite: in other words the series $\Omega_1 \approx \Sigma R_i^1$ is divergent.

On the other hand, it is also obvious that the sum of the area of all the circles of radius R_i is finite since it will always be inferior to the area S_o of the triangle ABC. Consequently the series $\Omega_2 = \Sigma R_i^2$ is convergent as i tends towards infinity.

$\Omega 1$ and $\Omega 2$ differ only by the value of the exponent of R_i. If this exponent is equal to 1 the series is divergent and if it is equal to 2 the series is convergent. Therefore, there must exist an exponent Δ, whose value lies between 1 and 2, for which the series stops diverging and starts to converge. This non-integer value is the *fractal dimension* of this mathematical object composed of all the circles R_i. It has to be noted that the sum of the perimeter of all these circles is infinite since $\Sigma \pi R_i = \Sigma \pi R_i = \pi \Omega 1$. This sum is the perimeter of the object defined above and this is a fundamental aspect of fractal objects which are characterized by an infinitely long boundary. This object is a *regular fractal,* like mathematical objects which look alike regardless of the scale (i.e., magnification) at which they are defined. In this context look alike means that every detail, multiplied by a proper constant (the scale), is
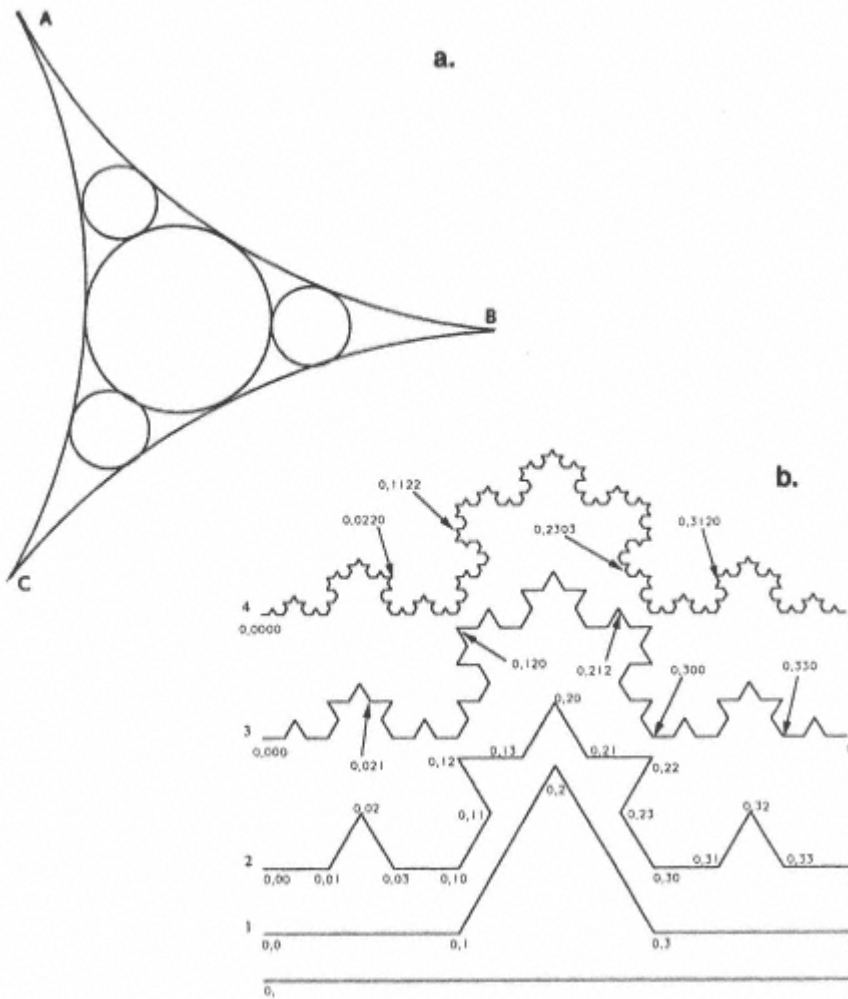
Fig. 1.
a: Apollonius circles, the oldest known artificial fractal
structure; b: von Kock curve and parametrisation of the curve.

the same as the whole set. The fractal is then said to be *self-similar*.
The above mentioned case of the Apollonian packing is slightly
more sophisticated, since as the magnification increases, some
small curvilinear triangles (those in the neighborhood of A, B and
C) become thinner and thinner. Nevertheless, they also look alike
as a whole, by the way of a well known geometrical transformation
called inversion. Mandelbrot's book [1,7] and the books of his

disciples [812] abound with many beautiful constructions of regular fractals. In $2D$ the fractal dimension is such as $0 < \Delta < 2$. The fractal dimension of an object in $3D$ is given by $D = \Delta + 1$ if Δ is the dimension of a $2D$ cross section and if the object is regular [11]. In addition the dimension

of the set in the vicinity of the fractal set is given by the codimension ξ:

$$\xi = 2 - \Delta = 3 - D = 4 - (D + 1) = (2)$$

In contrast to these mathematical fractal objects, shapes and patterns found in nature are usually *random fractals*. The reason is that they consist of random shapes or patterns that appear stochastically at a given length scale. That is to say that their self-similarity is only statistical. In practice, this phenomenon may be observed only over a finite range of scale lengths.

Most geometry textbooks deal only with the manner in which a fractal dimension can be determined. In contrast, Time in Fractal [11] addresses the question of the time dependence of performing a given measurement. This approach is absolutely necessary to understand the dynamics in fractal media. In order to consider the operational limitations of a human being, think of the mathematician Minkowski surveying a fractal Fig. 1b with a chain. How long does it take Minkowski to do this? It obviously depends on the shape of the interface to be measured, on the dimension of the link and the working frequency. Assume, for instance, the fractal in question is a von Kock curve. Given the frequency for surveying site to site is 4 Hertz if Minkowski wants to approximate a line of unit length (1 meter) in 1 second time. He should use a 1/3 meter long (η) yardstick which should be laid in a quarter of a second. Suppose now that our mathematician wants to approximate a length in the same lapse of time but with better resolution. He clearly has no choice: for instance, he must increase his measuring frequency up to $p = 16$ Hz and change the size of the yardstick ($\eta = 1/9$). The second test will give him a better approximation of the

length, but it will require a considerably greater effort, which can be measured by the frequency of the regular motion required to measure the surface. The higher the frequency p, the better the approximation η. In general, the working frequency and the size of the yardstick are interrelated. From our example we obtain:

$$p[\eta(p)]^\Delta = 1 \ (3)$$

with $\Delta = 1$ for the paving of a line, $\Delta = 2$ for the paving of a surface, and $\Delta = \ln 4/\ln 3$ for the von Koch curve. The number 1 in Equation 3 represents the unit length to the power, where Δ is the space dimension, this unit length being covered in one second. Of course, some other mathematician could possibly work faster, or slower, and also could have to cover a different length, let us say λ_0, if $\Delta = 1$, or a different area $(\lambda_0)2$, if $\Delta = 2$, in one second of time. A more general expression of (3) is therefore:

$$p[\eta(p)]^\Delta = \lambda_o^\Delta \quad [L^\Delta t^{-1}] \ (3')$$

where $[L^\Delta t$-1 represents the dimensional equation. The fractal expression (3') will stay accurate with any noninteger value as long as the mathematician

keeps his travelling frequency constant. This relation suggests that the total number of links needed, also called modes, in the framework of the motion on the fractal is given by $N(p) = p$. Then Equation 3' is no other than Mandelbrot's equation 4 [1,7] if the motion is assumed to be ergodic in the fractal meaning (the fractal average of the measure upon the space is equal to the fractal average of the measure upon the time, and is a constant):

$$N[\eta(p)]\Delta = constant \quad (4)$$

In the particular case where $\Delta = 1$, the quantity $\lambda_o^2[L^2 t^{-1}]$ simply represents the velocity of the oriented motion of the mathematician on the line. For $\Delta = 2$ the quantity λ_o^Δ represents the area covered per unit of time, the usual diffusion coefficient: *Diff*.

Obviously, if a fastidious mathematician wanted to work at a variable frequency or a variable characteristic length λo, this would cost him a large effort which he could not maintain for a long time without additional input of energy. Therefore we can be quite sure that under standard conditions he will work at a constant velocity: λ_o^Δ For any values of p the average on the fractal space of the expression $[\lambda_o^\Delta / p[\eta(p)]^\Delta$ is then equal to the general frequency of flight *[p]*.

The motion of any active molecule moving on the interface of aggregates where adsorption and chemical reaction occur is analogous to the regular motion of the mathematician measuring his surroundings. This motion is frozen at $T = 0$ but at T $\neq$ 0°C the mean path, covered on the interface by the species, must be referred to λ_o^Δ . Though totally ignored in physics textbooks, this constant controls the entropy production in fractal media which are

the thermodynamic and kinetic properties of the interface. This measure leads to an irreducible average amount of uncertainty over the exact location of the interface, so that Δ is related to the concept of entropy. If the speed is not a constant then

$$p[\eta(p)]\Delta = [l(p)]\Delta \quad (5)$$

The above point of view may easily be enlarged, as in a Fracton like analysis where $[l(p)]\Delta = p^{1-2d}$ which leads to the definition of spectral index: $ds = 2d/\Delta$ [1012].

The above concepts draw the major lines of fractal geometry needed to handle the physics of heterogeneous media, including carbon black.

7.2. Carbon Black

Carbon black, most commonly produced by an incomplete combustion of oil based feedstocks, is an object which, in spite of its generalized utilization for many years, is still being widely characterized by both academic and

industrial research laboratories. This material is constituted of carbon particles solidly fused together by covalent bonds to form aggregates which, in general, are considered as unbreakable during the normal processing of the materials.

Because of the nature of the carbon black surface the aggregates have a strong tendency to agglomerate. These agglomerates are characterized by weak bonding between the aggregates and, therefore, do not retain their integrity during processing. This does not imply that in the final product the aggregates are totally separated. Indeed it is well known from electron microscopy analysis, that varying concentrations of carbon black agglomerates [13] are present in the final product. Since these agglomerates are made up of aggregates loosely bonded together, it is impossible to know if the morphologies of the agglomerates present in the final product are the same as the one existing in the raw material [14,15].

Since agglomerate morphology is transient, additional structural definitions of the particle and the aggregate are mandatory. The particles are essentially geometric entities whose average dimension typically ranges from 50 to several 100 nm (Fig. 2). The aggregates composed of particles range from several nanometers to almost a micron in average size for the various grades of carbon black. Therefore, the scales at which the dimensions are measured for these two fundamental entities have to be chosen in accordance with the size of what has to be evaluated.
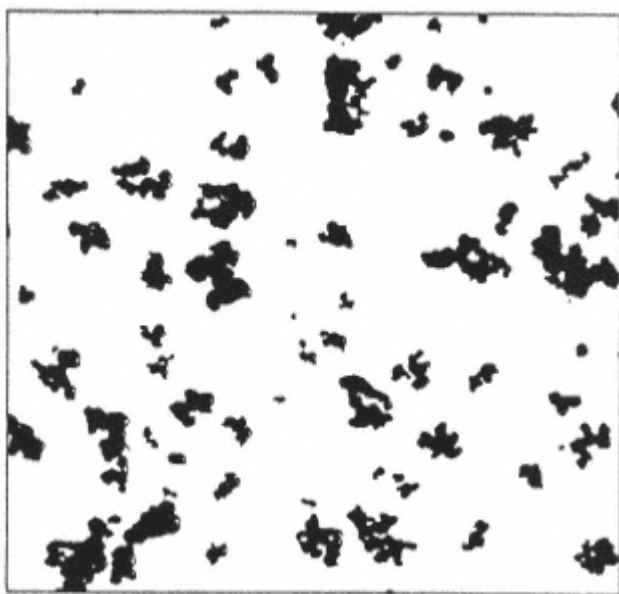
Fig. 2.
Typical picture of a cut of rubber loaded with
carbon black.

The carbon blacks, as mentioned, are widely used as a filler to modify the electrical properties of a composite structure and mainly, from a volume standpoint, the mechanical properties [1417] of a polymeric matrix. The physical properties depend on the average amount of carbon black but also on the morphology of the media at different scales [16]. Although non-universal behavior is observed in a few composites [18], it is now well accepted that the percolation scaling theory may be pertinent with regard to the threshold observed in conductivity above a critical volume fraction. However, the experimental behavior in electrical sciences and in mechanics is not only related to the percolation threshold but also to the structure of the carbon black. Electron microscopy, which can measure the aggregate lengthwise, has been used to characterize the morphology of carbon black in terms of bulkiness, anisotropy or shape factor, and more recently in terms of fractal dimension [1921].

The use of annular dark field imaging in scanning transmission electron microscopy leading to a $3D$ mass fractal analysis [22,23] can be considered, for instance, as a new power full method of carbon black aggregate characterization. Other experimental methods as diversified as neutron, light or X-ray scattering, surface adsorption techniques, thermoporometry, etc., can be used to obtain the fractal dimension of carbon black.

7.3. Scattering of Fractally Rough Surfaces

Small angle scattering by fractally rough surfaces has the potential to scale the surface geometry by the wavelength of the incident radiating source. By use of quantitative neutron and X-ray scattering, a direct analysis of the fractally rough carbon black

surface was made [24]. Depending on the nature of the scatterer, the scattering intensity is related to the scattering factor q by the following relationship:

$$\sim q^{-\Delta} \text{ for mass scattering} \quad (6)$$

or

$$\sim q^{2d-\Delta} \text{ for surface scattering} \quad (6')$$

From these expressions one calculates Δ equal to $D - 1$. D is the $3D$ fractal dimension, the Euclidean dimension d defines with Δ the codimension ξ of the space according to $2d - \Delta = d - \xi$. The results of experiments carried out by Hurd et al [24] clearly indicate that these techniques give access to the material properties of substances at the particle level (510 nm) and not at the aggregate level (larger yardstick required).

The scattering equation may be used to deduce the cross section of the electromagnetic interaction between waves and particle. For instance, Hurd et al [24] compared quantitatively small-angle X-ray scattering (SAXS) and small-angle neutron scattering (SANS) measurements on carbon and silica

powders with independent gas adsorption measurements by BET methods. In this paper the authors test the Bale-Schmidt and Wong-Bray amplitudes by comparing scattering and adsorption surface areas [25]. The data favor a recently proposed correction to the scattering formulas for fractal surface and provide an independent check on the much debated adsorbate molecular areas. It was shown that scattering measurements from fractally rough powders agree well with adsorption measurements when the Wong and Bray correction is used [25] with the Bale and Schmidt formula. This correction is related to the codimension ξ of the surface. Table 1 gives, among other data, fractal dimensions obtained by scattering and specific surface area for different class of carbons. Another scattering method utilizes Transmission Electron Microscopy (TEM) to assess the fractal dimension of the carbon black aggregate. TEM carbon black aggregate micrographs are contrasted

Table 1. Fractal Dimensions of Carbons from Electrochemical Tests (EC) and SAXS for Samples Used in Both Dry and Wet Forms

Sample	Surface area m2/g	Electro-chemistry $D1$(EC)	X-Ray scattering $D2$ (dry)	X-ray scattering $D3$ (wet)
Sterling MT	7	2.8±0.1	2.9	2.3b
Sterling R	25	2.21±0.005c	-	-
Graphite	10	2.1±0.1	2.7	2.6b
Elftex 12	45	2.18±0.005c	-	-
Acet. Black YS	52	2.1±0.1	2.6	2.6a
Shavinnigam	60	2.29±0.005c	-	-
Raven 400	70	2.50±0.1c	-	-
Regal 600 R	112	2.50±0.1c	-	-
Vulcan 6	115	2.4±0.1	2.6	2.2b

Raven 3500	138	2.60±0.1c	-	-
Vulcan XC72R	234	2.36±0.1c	-	-
Monach 1100	240	2.4±0.1	2.4	2.6
Conductex 950	245	2.32±0.1c	-	-
Super carbovar	400	2.5±0.2	2.3	2.6
Black Pearls	560	2.7±0.1	2.7	2.5
Pittsburg	825	2.7±0.2	3	2.7
Neospectra	900	2.60±0.1c	-	-
BRX	1300	2.4±0.2	2.4	2.6

aMass fractal.

bFit upon less than one decade.

cFractal dimension obtained from electrochemical analysis of the reduction of SOCl2.

using a binary technique (black and white). A laser probe is used to obtain the scattering pattern of this binary picture [26].

7.4. Fractal Dimension of the Aggregate Boundary

Medalia and Heckman [27,28] reported the first quantitative information on aggregate size and distribution using image analysis techniques based on digitized transmission electron micrographs. Later, automated electron microscope image analysis of carbon blacks was reported by Hess, McDonald and coworkers [2931]. The goal of these scientists is to relate the physical properties of the composite materials with the geometrical and the physico-chemical properties of the filler. Thus these workers characterized the interface between the polymer and the filler (Fig. 2). This interface is controlled by the aggregate boundary shape and geometrically related, even at the macroscopic level, to the local shape of the aggregate. It has been shown from the previously discussed experiments that in the range up to 10 nm, carbon black having a low surface area (10200 m2/g) exhibits roughly a quasi constant surface fractal dimension 2.3±0.1. In this range it represents a property of only a small number of particles. The next interesting step is to evaluate the aggregate, i.e., the primary mono-unit of carbon black. Since this entity is in general much larger than the range in which SAXS and SANS are practically applicable, other techniques must be used. An alternative method is to use a radiation source which provides a much longer wavelength. In fact, as explained above, this should be feasible using light scattering [26]. Another interesting approach is to determine the aggregate boundary dimension from appropriate images. These boundaries are accessible via transmission electron microscopy without any

additional physical treatment. The results described in this paper to evaluate the line fractal characteristic of the aggregates utilize TEM measurements; the method uses an area-perimeter relationship. Plane projections of carbon black aggregates are considered as growing objects, of characteristic size *R,* where *R* takes its values over a large range of real numbers. This parameter *R* may be measured by various geometric (diameter, perimeter of the convex hull, etc.) or analytic techniques. The area of the aggregate grows accordingly, as an increasing function of *R*. If *M(R)* denotes this area (the letter *M* is chosen here to refer to the mass of the area of the object), it follows typically in 2*D* a power law as

$$M(R) \sim R^{\Delta_1} \quad (7)$$

where $\Delta 1$ is a characteristic exponant, usually called the mass dimension. Since the elementary particles are quasi spherical rectifiable objects, every projected aggregate has a boundary of finite length. This length is called perimeter of the aggregate, and denoted by *P(R).* As for the area, or

mass, *P(R)* follows a power law:

$$P(R) \sim R^{\Delta_2} \quad (8)$$

It is possible to interprete the perimeter as the mass of the aggregate boundary. As such, $\Delta 2$ is nothing else than the mass dimension of the boundary. The inequalities $1 \leq \Delta 1 \leq \Delta 2 \leq 2$ between the two mass dimensions, are always true. By eliminating the variable R (Equations 7 and 8), it is possible to get the following direct relationship between area and perimeter:

$$M(R) \sim P(R)^{\Delta_1/\Delta_2} \quad (9)$$

The ratio $\rho = \Delta 1/\Delta 2$ lies between 1 and 2. Let us call it an area-perimeter exponant. It may characterize the fractal geometry of the aggregates. Indeed, very compact shapes have a ρ near 2. In the limit, euclidean objects such as squares or disks are such that all of their elementary particles lie close to the boundary: then $M \sim P$, giving $\rho = 1$. For example, this is the case of standard two-dimensionnal aggregates obtained by DLA techniques. For many other objects the boundary is fractal but the bulk looks like a disk. In this case the mass fractal dimension is close to two; that is why some scientists do not hesitate to use the approximation given by the equation.

$$M(R) \sim P(R)^{2/\Delta_{2'}} \quad (9')$$

Tables 2 and 3 give some examples concerning carbon blacks. Equation 9' with the hypothesis $\Delta 1 = 2$ has been used for carbon black aggregate analysis by Bourrat and Oberlin [20] and Ehrburger-Dolle and Tencé [21]. For instance, in spite of the lack of precision Bourrat and Oberlin used the mass in the box method

[1012] and correlated the value of the mass fractal dimension (1.46-180) with the conductivity of different carbon blacks. Ehrburger-Dolle and Tencé used both the mass-size and the mass in the box methods to evaluate the mass fractal dimension of different grade of carbon blacks. Their value range from 1.76 for furnace blacks to 2.96 for thermal blacks. With an original point of view Herd and coworkers [32] classified carbon blacks into four different aggregate shapes (spherical, ellipsoidal, linear, branched) and balanced the dimension by weigting the fractal dimension in each class independently (Table 3), so that they also relate DBP absorption test with linear fractal dimension of the perimeter $\Delta2'$ (Fig. 3).

For all carbon blacks studied the samples were prepared typically according to the ASTM test method D3849. Using a Philips EM 300, several pictures from different fields of each sample are taken. These pictures are digitized and analyzed.

The characteristic length used in this experimental method is in the range of 100 nm. As pointed out earlier, this scale length is much larger

Table 2. Fractal Dimension of Various Carbon Blacks

Carbon black	Linear fractal dimension Δ_2'	Area fractal dimension $\Delta 1$
N110	1.336	1.497
N121	1.319	1.516
N220	1.279	1.563
N299	1.247	1.604
N330	1.235	1.619
N339	1.225	1.633
N347	1.297	1.542
N351	1.218	1.642
N358	1.206	1.658
N550	1.164	1.718
N650	1.140	1.754
N660	1.158	1.723
N762	1.153	1.735
N765	1.150	1.734
N787	1.138	1.757

Data from Sid Richardson using the area-perimeter equation described in the text.

than the one used in both X-Ray and neutron scattering techniques. Table 2 is obtained using Equation 9 and the digitized image obtained from TEM micrographs; 250 individual aggregates were measured for each sample. The data obtained consists of sets of perimeter and area values of the aggregates. From these data the coefficient Δ was calculated. This table summarizes the data which clearly shows that between the different grades of carbon black there indeed exists a difference in linear fractal dimension of the aggregate boundaries.

It will be noted again that, following Mandelbrot's first proposal, Herd and coworkers suppose a priori $\Delta 1 = 2$. Table 3 is obtained under this particular hypothesis. It contains also information on the $3D$ mass fractal Dm obtained from mass versus size equation

$$[M_{3D}(R) \sim R^{D_m}]$$

To introduce the physical properties controled by the carbon black interface it is worth noting that the fractal character of the boundary can be seen as its intrinsic degree of transfer possibilities with the exterior when any flux of exchange of thermothynamic extensity is forced on the interface, at least under low power. The smaller the η, the closer the atoms of the objects are to the boundary, the easier the exchange will be. Obviously different values of the fractal dimensions and area-perimeter exponents indicate the ability of exchange of the interface and the grade dependence. Families of values representing subsets of the range of carbon black investigated certainly exist but the results cannot be understood if one does not take into account that

Table 3. Fractal Dimension of Various Carbon Blacks

Carbon black	Linear fractal dimension $\Delta 2'$	Volume fractal dimension *Dm*
CD-2005	1.341.39	2.35-2.19
N358	1.331.38	2.35-2.28
HV-3396	1.351.38	2.33-2.32
N121	1.34-1.32	2.39-2.37
N650	1.291.33	2.28-2.26
N234	1.301.31	2.42-2.40
N299	1.291.32	2.42-2.38
N351	1.301.31	2.38-2.36
N550	1.26-1.24	2.422.44
N339	1.301.32	2.40-2.39
N110	1.301.31	2.412.42
N220	1.281.29	2.432.44
N330	1.28-1.28	2.402.44
N660	1.22-1.20	2.502.53
N630	1.18-1.15	2.572.63
N774	1.16-1.15	2.562.59
N326	1.22-1.20	2.522.57
N762	1.16-1.14	2.592.63
N990	1.05-1.05	2.84-2.84

Data from Herd et al [32] using the area-perimeter M~P2/Δ2;

$$M(R) \sim R^{D_m}$$

All data are shape weighted (spheroidal, ellipsoidal, linear, branched).

the transfer ability is submitted to the control of the parametrisation of the interface at least at a high rate of exchange. This control is determined by the parameter Δ and λ_o^Δ (see 7.7). λ_o^Δ is cancelled at a low rate so that the first step for the physical caracterization of

the fractal interface requires a status close to equilibrium conditions.

7.5. Molecular Adsorption on Fractal Surfaces

One of the major studies reported on the fractal aspect in surface science, especially on carbon was done by Avnir's group [33]. Although their earlier studies were based on the adsorption methods, later these studies were diversified to using computerized image analysis techniques, analysis of photophysical processes, analysis of surface reactivity, etc.

In the adsorption method the surface is tiled with n moles/g of adsorbate molecules with cross sectional area σ. Assuming simple physisorption occurs, the material has a fractal surface and $n \sim \sigma^{-D/2}$ in a certain range of size. Typically, the range obtained by this technique covers one decade on molecular size scales (10100 square Angstrom). This analysis can be carried
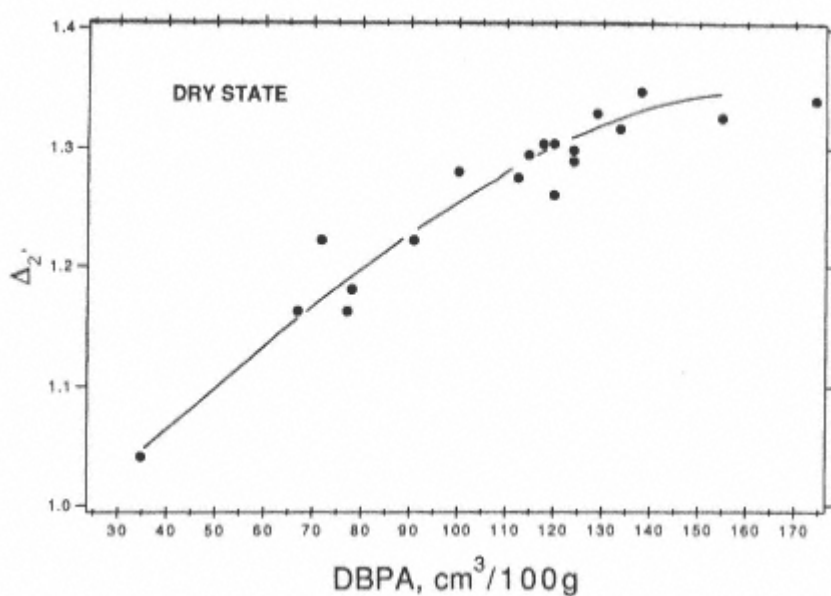
Fig. 3.
Correlation of linear fractal dimension Δ2' with
DBP absorption (from ref. [32]).

out alternatively by varying the radius and measuring the surface areas with *n* fixed probe-molecules.

The polyaromatic hydrocarbons were chosen and adsorbed flat on the surface. Such yardsticks offer an adsorbate series which are essentialy isotropic and comprise a considerable range of cross sections. In fact, the relevant cross section can then be estimated reliably from models. In ref. [3335] Avnir's group had determined the fractal dimension of different carbon blacks from adsorption of various aromatics, assuming a flat molecule position.

In addition, adsorption of polymers on charcoal and Graphon using a series of random copolymers of styrene and methyl acrylate has been used to probe surface irregularity [36]. The results gave a fractal dimensions of 2.78±0.21 and 2.13±0.16 for charcoal and

Graphon, respectively. These results reflect the difference in surface irregularity of the adsorbates on the macromolecular level [3740].

Multilayer adsorption techniques have been utilized to analyse the structure of the void inside the fractal structure. This is the major contribution of the Mulhouse group.

7.6. Characterization of the Aggregate Void Structure by Thermoporometry

This study has been mainly carried out by the Mulhouse Interface Group (MIG). The morphological characteristics of the carbon blacks characterized

by this group are given in Table 4 [41]. The principle of the method of thermoporometry is now well known and the methods used by the MIG have already been discussed in detail [42]. The upper limit of the pore size is dependent on the adsorbate, e.g., 330 nm in water and 170 nm in undecane.

To find the fractal dimension MIG starts from Pfeifer and Avnir [43] analysis that have shown that the surface fractal dimension D of a porous solid can be obtained from the pore size distribution curve by:

$$-\frac{dV}{dR} \sim R^{2-\Delta s} \quad (10)$$

that is

$$\Delta V min \Delta V max \sim [\Delta \eta min \Delta \eta max] \xi$$

where $\xi = 2 - \Delta = 3 - Ds$ is the codimension of the interface whatever the dimension of the embedding space [11], and $\Delta V min = V - Vmin$, etc. are the variables which introduce the cutoffs over V and characteristic length.

These relationships are obviously accurate for the aggregate porosity. Nevertheless to apply this equation one has to distinguish both dimensions, a surface fractal dimension $Ds > 2$, which gives a meaning to the right side of the curve, and the mass fractal dimension Dm, related to the properties of a set of singularity which shapes the fractal set. In fact the Equation 10 may apply only if the range of the pore size is large enough, i.e., the aggregates involve at least 500 elementary particules [41]. Tables 5 and 6 give the characteristics of the intra-aggregate voids as well as the fractal dimension for dispersion, respectively. The mean value

of $\Delta = 1.79 \pm 0.05$, in water and undecane, is in agreement with the fractal dimension measured on isolated aggregates (1.83±0.13).

Table 4. Morphological Characteristics of Carbon Black Aggregates

Sample	DBPA*a* cm3/g	DBPA (24M4)*b*cm3/g	V_o cm3/g	V_{ot} cm3/g
TB≠5500	1.55	1.17	20.6	12.1
TB≠4500	1.60	0.98	12.9	7.8
Acetylene black	2.15	1.23	21	12.1
Vulcan XC-72	1.74	1.14	3.4*c*	2.7*c*
Ketjen black	3.60	2.93	6.4*c*	4.8*c*

aASTM D 3493.
b ASTM D 3037.
cPelletized sample.

Table 5. Characteristics of Intra-Aggregate Voids of Carbon Blacks Dispersed in Water

Sample	Rmin, nm	Rmax, nm	Fractal dimension, Δ
TB≠5500	25	73	1.77±0.3
TB≠4500	32	120	1.82±0.3
Acetylene black	39	100	1.92±0.2
Vulcan XC-72	24	82	1.85±0.2
Ketjen black	23	65	1.84±0.3

The first point worth mentioning concerns the variance of the distribution of the fractal dimension. From the thermoporometry measurements it appears that, probably due to interpenetration of the aggregates dispersed in a liquid, the domain of fractality is narrow. This observation raises the question of the determination of the fractal dimension of an assembly of aggregates (dispersed either in liquid or in polymers) as achieved by scattering techniques or by electron microscopy of the isolated aggregates. In the first case due to the interpenetration of the aggregates, the fractal domain may be too narrow to be precisely evident. In addition, the problem of the spatial stability of the aggregates during the porosimetric test must be addressed. Also the question of the multifractal structure [9,11] of carbon black on which molecules are absorbed must be considered. Finally the surface or the mass fractal character of a given result must be taken into consideration.

Beyond thermodynamic considerations, how are dynamic properties influenced by fractal geometry? The opinion of the authors regarding this point is as follow.

As shown in Section 7.1 both Space and Time parametrization are essential and, therefore, the fractal dimension can be regarded as

the main universal parameter determining the thermodynamic and the dynamic behavior of heterogeneous materials. This opinion has to hold true for any materials based on carbon blacks. Let us illustrate this point of view through electrochemical and mechanical tests.

Table 6. Characteristics of Intra-Aggregate Voids of Carbon Blacks Dispersed in Undecane

Sample	*Rmin,* nm	*Rmax,* nm	Fractal dimension, Δ
TB≠5500	25	47	1.81±0.3
TB≠4500	34	65	1.84±0.3
Acetylene black	35	85	1.90±0.2
Vulcan XC-72	25	50	1.82±0.2
Ketjen black	25	44	1.81±0.3

7.7. The Electrochemical Characterization of Carbon Blacks

The carbon electrode is a key component in cells and batteries. For example, it constitutes the positive electrode in zinc/air batteries, and it is also one of the fractal electrodes of the power cells Li/SOCl2 [44]. The object of electrochemical study of carbons was to produce a low cost secondary air electrode of high performance for use in the KOH electrolyte. Intrinsic activity and structural characteristics were measured as a function of type of treatment for a wide range of carbonaceous materials, but no fractal characteristics were measured. This lack of measurement was simply due to the absence, at that time, of methodologies to characterize the fractal dimension. It was shown later that there exists a relationship between the yield of a battery and the fractal nature of carbon black electrodes. This finding was explicitly described for the first time in an internal report of the Alcatel Alsthom Recherche in 1980 [5] on carbon blacks for Li/SOCl2 batteries. This analysis leads to a generalization of the Faraday's law $(Q = I \cdot \tau)$ by coupling the discharge time of a battery τ to its discharge intensity I raised to the power of its fractal dimension Δ [45] such as:

$$I\Delta\tau = constant \quad (11)$$

This is the new invariance of charge in fractal electrodynamics. Obviously $\Delta=1$ gives the Faraday law but Equation 11 involves a definition of a new invariant. This important new relationship shows that the idea of electrical charge loses some of its conventional means in fractal media. The fundamental aspect of the relationship was initially perceived in 1980 with the creation of the

concept of fractance, which is a generalization of the concept of capacitance.

As is well known, the concept of charge is related to phase conservation in Euclidean geometry. But in practical terms the capacitor is the electrical response given by $Z(p) \sim [1/p]$ with $p = i\omega$, the generalized frequency. A fractal capacitor (fractance) is a generalization of a capacitor characterized by a pinning of the phase independent of the frequency. Its impedance is given by

$$Zdim(p) \sim [1/p]1/\Delta \text{ or } Zcodim(p) \sim [1/p]2\text{-}\Delta \quad (12)$$

depending on the self similarity or on the self affinity [11] of the interface, respectively [4655]. As for the capacitor, the constant required by these equations is related to the measure of the space properties involved in the physical process of extensity storage. The only difference is the fractal character of the dimensional equation of the constant of proportionality $(\lambda_o^\Delta : [L^\Delta t^{-1}])$. The above relation allows one to calculate the fractal dimension and a new constant using a simple frequency behavior analysis of the fractance. This

method was used to measure the fractal dimension of carbon via electrochemical tests [24,53]. Table 1 gives fractal dimensions of electrodes consisting mainly of carbon blacks compared with the dimension obtained by scattering on dry carbon. These results were obtained by electrochemical measurement of the fractal impedance (Equation 12) or by measuring the electrode's yield (Equation 11).

If, from a general point of view, an increase of the specific surface area of the material corresponds to an increase of the fractal dimension, this area can only be considered as a first approximation. For example, a carbon black with a specific surface area of 100 m2/g may have a fractal dimension $D = \Delta + 1$ ranging between 2.2 and 2.6. Thus, by itself, surface area cannot be a fundamental parameter. To describe the surface, an interesting question to be considered is the following: what length of yardstick should be used to measure the fractal dimension using electrochemistry: 1-10-100 nm? The answer can be given by comparing electrochemical methodologies with fractal results obtained using different approaches, i.e., small-angle scattering (SAXS or SANS), adsorption etc. To study the relationship of the fractal dimension of carbon black obtained from scattering experiments and Faradic impedance measurements, a joint research effort was undertaken between Alcatel Alsthom Recherche and Sandia Laboratory.

Fig. 4 shows that the correlation between the two types of experiments is rather good, which allows one to assign the characteristic yardstick length in electrochemical fractal determination which is of the order of magnitude
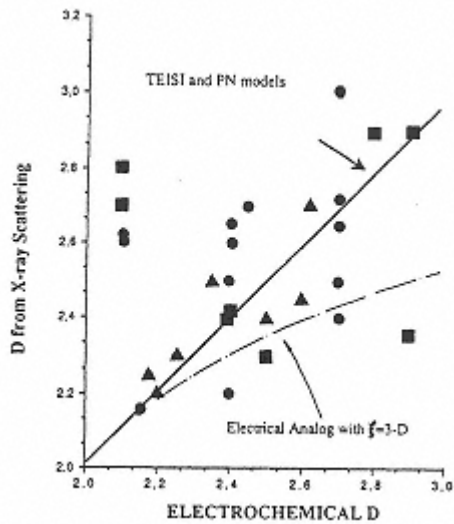
Fig. 4.
Experimental correlations between fractal dimensions of carbon for electrodes measured by X-ray scattering vs. fractal dimensions obtained from CPA like fractance behavior.

of 10 nm [24,53]. These results highlight the important distinction between the two types of fractance (self similarity and self affinity) based on fractal dimension Δ and fractal codimension ξ (Equation 12). Fig. 4, in addition, clearly indicates that there exists materials with inner porosity detected by SAXS but not by impedance spectroscopy.

These results are very important since they help to explain the size and shape and scaling properties of the curve of discharge of batteries [45]. The major parameter is not the high surface area but the relationship between the fractal properties of this surface and the rate of discharge (dynamics in fractal media). This relation is based on the constant λ_0^Δ previously described as the major parameter of the parametrisation of the interface [11]. This coefficient is proportional to the amplitude of movement of the adsorbed species at the interface. This characteristic was never checked before, in spite of its deterministic importance for the efficiency of any kinetic process requiring a fractal surface as a support.

$$Z1(p) \sim (\lambda_0/p)\Delta \quad (13)$$

This impedance is strictly equivalent to the equation giving the smallest yardstick (η) used to analyze the surface, in the Fourier space, at the generalized frequency

$$\eta(p)\Delta \sim \lambda_0/p \quad (14)$$

$\eta(p) < \lambda_0$. If the rate of discharge is too high, only a small part of the surface is accessible. Practically, the electrode yield is

determined by this parameter because it defines the cut-off between the two regimes $\psi=100\%$ and $\psi < 100\%$ [11,45].

The theoretical approach (TEISI model) constitutes a general model which does not specify the nature of the transfer at the fractal interface. Therefore this approach for the analysis of electrical as well as electromagnetical impedance should be applicable in the linear domain to the study of mechanical impedance

7.8. Mechanical Impedance Spectroscopy

Consider for instance how the mechanical properties of a polymer loaded with carbon black are controlled by the fractal dimension of the filler. Consider further that the momentum transfer in a mechanical system can be taken as equivalent to the electron transfer in an electrical circuit. Numerous viscoelastic studies on polymers and composites have pointed out the fractional nature of momentum transfers through its algebraic equivalence, the fractional derivative [5659]. To our knowledge this approach should be applicable to carbon black loaded elastomers. Let us consider two exemples.

An attempt to use the above-mentioned approach [60] was undertaken by considering that the mechanical impedance of rubbers loaded with carbon blacks can be represented by the complex modulus.

$$G = G' + iG'' \quad (15)$$

G' and G'' being respectively the elastic and loss modulus. This impedance is represented as a function of strain expressed as a % of deformation. Experiments are conducted using rotational shear mode with parallel plate geometry. Strain and stress results are obtained at $p = 1$ Hz and at room temperature. Since the deformation is different for different stresses, one can assign a velocity $v \sim \eta p,$ and also a characteristic frequency, at a given deformation. Taking the above into consideration one can understand that % of deformation plays the same role as the frequency in the electrical model and therefore the relationship G'' $= f(G'),$ can, in general, be expressed by the TEISI model (Fig. 5 [11]). The universal behavior observed is given by the complex plot:

$$G \sim 1/1 + (i.\ deformation)1/dw \quad (16)$$

According to this model, the power law is related to the fractal geometry of the set of dissipation of energy under transfer. However, a major difficulty is that dw cannot be reduced to the fractal dimension because the dimension calculated as described earlier is found equal to 4.5. This value is incompatible with the elementary TEISI model where Δ is the fractal dimension. To understand this high value one has to consider the notion of

Hyperscaling [11,47,48] which defines the equation of Fractance if the energy transfer in
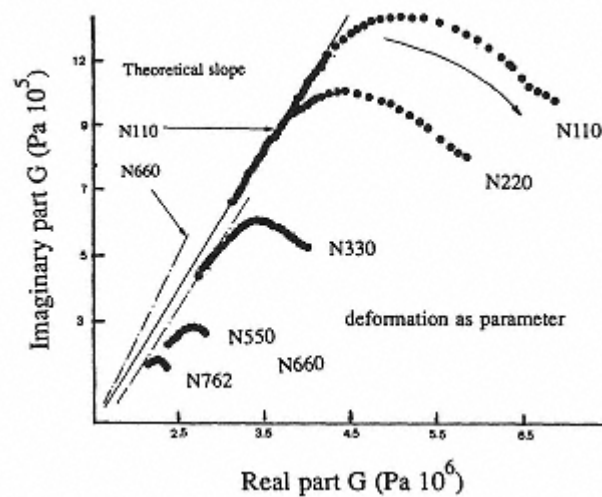
Fig. 5.
Cole-Cole analysis (TEISI model) applied on mechanical impedance G" /G'.
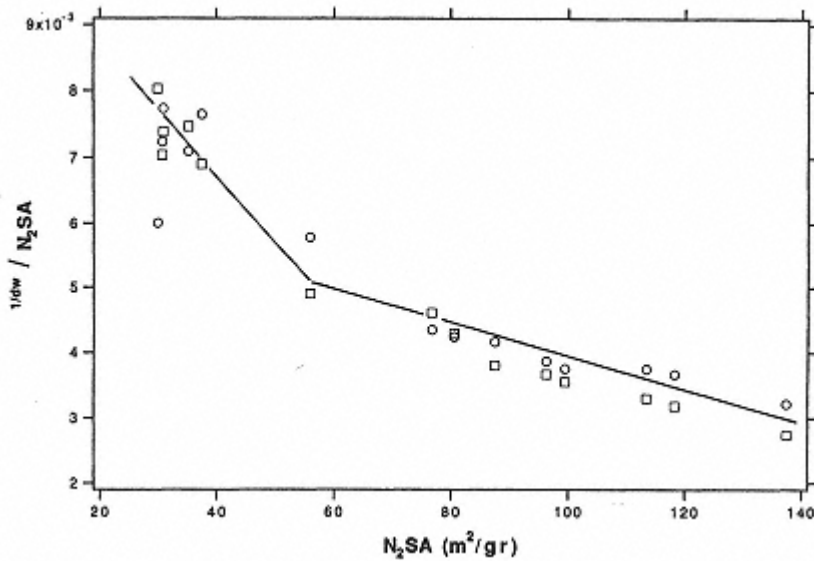
Fig. 6.
Correlation between the power law of the TEISI analysis
Hyperscaling behavior) and the surface area of carbon blacks
over a large range of grades.

the fractal media is controlled no more by δ-transfer elementary
TEISI model but either by a diffusion process $(\beta = 2)$ or by
fractional Brownian motion $(\beta \neq 2)$ inside the fractal media. The
result obtained employing Hyperscaling approach derived earlier
[11] gives:

$$1/dw = (1/\beta) + (1/\Delta) - 1 \quad (17)$$

where β is the dimension of the fractional Brownian motion. An
analysis of the power law with respect to the specific area of
carbon black shows a threshold in the behavior (Fig. 6). As the
carbon black surface is distributed over a large range of area, it is
reasonable to interpret the modification of the dynamic behavior,
from the nonreinforcing status to the reinforcing property of the
filler, as a threshold of β factor (modification of the fractional

Brownian random walk of the momentum in the complex structure).

Carbon blacks fractal properties *(β and Δ)* when employed as filler in SBR and in NR are obtained from image analysis (Tricot's works) and from Hyperscaling TEISI model (Equation 16). The values calculated indicate a threshold for *β*. Below A=40 m2/g, *β=4/3* and above *β=3/2*, these figures

Table 7. β Value According to Tricot Image Analysis and to Hyperscaling TEISI Model

	N110 → N358	N550 → N787
β (SBR)	1.35±0.1 (~4/3)	1.50±0.1(~3/2)
β (NR)	1.37±0.1 (~4/3)	1.50±0.1(~3/2)
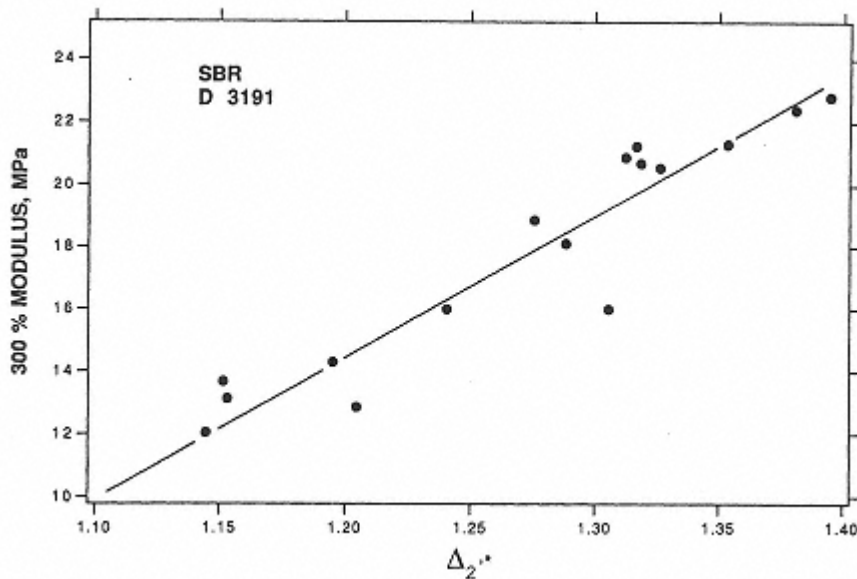
Fig. 7.
Correlation of 300% modulus in SBR with the weighted
composite perimeter dimension (from ref. [32]).

are probably related to universal behaviors (Table 7).

The relationship between mechanical properties of carbon black as filler and fractal dimension was also reported by the Columbian Chemical Company Research Group [32] which observes correlations of the fractal dimensions of filler with rubber mechanical properties without any notable influence of the polymer. Figs. 7 and 8 show their results. These results illustrate the relationship between surface fractal dimension and 300% modulus in SBR and OE-SBR/BR. Both correlations were highly significant over a broad range of modulus (12 to 23 MPa in SBR [ASTM D 3191] and 4 to 14 MPa in OE-SBR/BR [32]). The results obtained by the Columbian group are also obviously related to the entropy production in the fractal media under the exchange of mechanical momentum. Therefore, the TEISI model should be

applicable although no work has been reported to date using this model.

To characterize the behavior of a composite loaded with carbon black there exists another very promising advanced approach which consists of the electromagnetic transfer, or the electromagnetic flux accross the material. It considers the electromagnetic waves relationship with fractal media (see Section 7.3). In this approach the fractal geometry determines, according to the relativity and to universal behavior [11,62], the self similar structure of the space-time [61] and a new kind of propagation called propagation in the scales that is not only the modification of the boundary conditions applied to normal electromagnetic wave propagation (scattering). This analysis is currently in progress in Alcatel Alsthom Recherche in the frame of a scien-
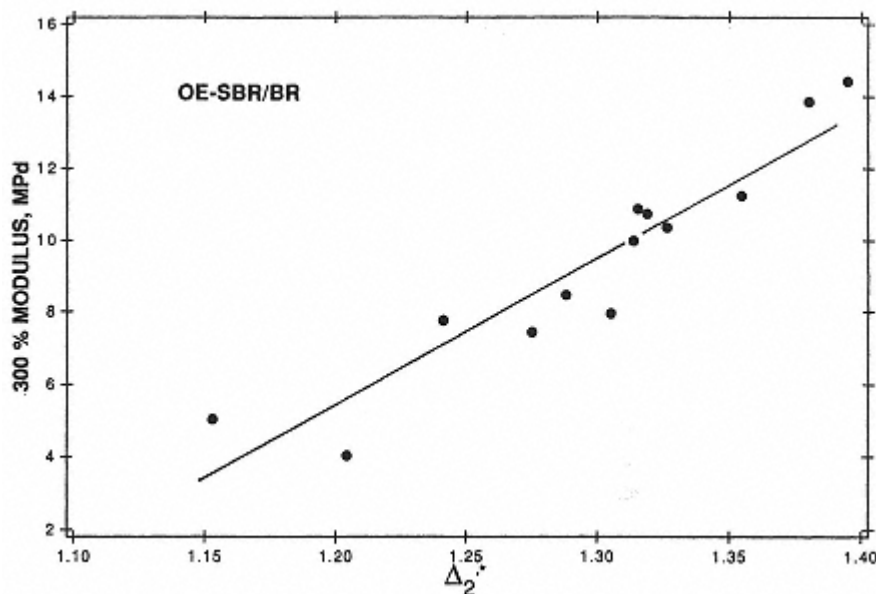
Fig. 8.
Correlation of 300% modulus in OE-SBR/BR weighted composite
perimeter dimension (from ref. [32]).

tific collaboration with L. Nottale for astrophysical applications
(fractal non-maxwellian approach) [6366].

7.9. Conclusion

The fractal geometry of surfaces has to be associated with either
the thermodynamic properties, especially the adsorption
phenomena, or the electrical or mechanical dynamics due to
momentum transfer. It appears then obvious that the dimension and
the codimension must play a central role in physical properties.
The application of fractal geometry has led, as referenced work
reflects, to a better understanding of the material carbon black and
its interaction with polymers.

Nevertheless, numerous questions are still pending. For instance if

one considers the relationship, already established, between thermodynamic potential and fractal dimension [11] a difficulty arises when one considers carbon black in distinguishing the entropic (i.e., geometric effects) from enthalpic contribution (i.e., physico-chemical effects). This could be a fruitful area for further research.

On the other hand, because it is simpler, the knowledge on forced kinetics studies applied to carbon black is greater than the one of thermodynamic properties, especially the electrochemical kinetics which for the first time shows an unequivocal relationship with other types of characterization (Faradic yield, impedance spectroscopy, X-ray scattering, etc.), but also the

mechanical kinetics analysis [32,60] which opens up large perspectives of advanced understanding. Meanwhile, in this particular domain many difficulties still remain mainly due to the complex behavior especially from the matrices standpoint. The above mentioned facts certainly will further delay the full understanding of carbon black polymer composites behavior even if the Hyperscaling TEISI model may be applied to distinguish the role of the filler from the role of the vicinity (polymers).

An important question is also brought up by the analysis using the TEISI model. The parameter λ_θ^Δ is the generalized species transport kinetics at the material surface which is the first physical concept which enlarged the primitive idea of diffusion. This parameter λ_θ^Δ which is neither velocity nor diffusion coefficient but just in between, is, as far as the authors are concerned, of extreme importance since it offers the first experimentally obtained example of a noninteger Brownian motion. Its future importance in the science of the dynamics of heterogeneous media should again be emphasized.

All the above has to be of the highest interest for any material scientist, since it has been shown that the fractal dimension is an important parameter related to entropic properties as different as electromagnetic wave scattering, relaxation dispersion, Faradic yield mechanical impedance, propagation of electromagnetic waves, etc.

To conclude it might be interesting to note that the approaches presented here can be expanded to understand fundamental entities like, for example, the meaning of electrical charge in such a media. As is well-known in conventional physics, the electrical charge is

associated with phase conservation. The concept of fractance and the generalized Faraday law brings up the question of the concept of electrical charges in a fractal media. This will be the subject of further studies, certainly very fundamental, which will address the propagation of electromagnetic waves in carbon black loading composites.

Once again, carbon black might be more than a black powder since it seems to open ways to better understand fundamental behaviors through physical science which might bring many more surprises in the future.

References

1. Mandelbrot, B., *Les Fractals,* Flammarion, 1975.

2. Kaye, B. H., *Powder Technologies,* 21, 1 (1978).

3. Flook, A. G., *Powder Technologies,* 21, 295 (1978).

4. Forrest, S. R. and Witten, T. A., *J. Phys.,* A12, L109 (1979).

5. Le Méhauté, A. and Crepy, G., *Reflexions sur le fonctionnement d'une électrode positive de pile Li/SOCl2,* Rapport N.1980/25177 and Salon de la Physique, Paris, 1981.

6. Witten, T. and Sander, L. M., *Phys. Rev. Lett.,* 47, 1400 (1981).

7. Mandelbrot, B., *The Fractal Geometry of Nature,* Freeman, San Francisco, 1982.

8. Barnsley, M .F., *Fractal Everywhere,* Academic Press Inc., Boston, 1988.

9. Fedder J., *Fractals,* Plenum Press, New York 1988.

10. Le Méhauté, A., in *The Fractal Approach to Heterogeneous Chemistry,* D. Avnir ed., John Wiley, New York, p. 311, 1989.

11. Le Méhauté, A., in *Les géométries Fractales,* Hermes ed., Paris, 1990, and in *Fractal Geometry,* Penton Press, London, 1991.

12. Takayasu, H., *Fractal in Physical Science,* Manchester University Press, New York, 1990.

13. Medalia, A. I., *J. Colloid Interface Sci.,* 32, 115 (1970).

14. Verhelst, W. F., Wolthuis, K. G., Voet, A., Ehrburger, P. and Donnet, J. -B., *Rubber Chem. Technol.,* 50, 735 (1977).

15. Medalia, A. I., *Rubber Chem Technol.,* 47, 411 (1974).

16. Reboul, J. P., in *Carbon Black-Polymer Composites,* E. K. Sichel ed., Marcel Dekker, New York, p. 79, 1982.

17. Fox, L. P., ibid, p. 163.

18. Balberg, I., *Phys. Rev. Lett.,* 59, 1305 (1987).

19. Samson, R. J., Mulholland, G. W. and Gentry, J. W., *Langmuir,* 3, 272 (1988).

20. Bourrat, X., Oberlin, A., van Damme, H., Gatineau, C. and Bachelar, R., *Carbon,* 26, 100 (1988).

21. Ehrburger-Dolle, F. and Tence M., *Carbon,* 28, 448 (1990).

22. Chevalier, J. P., Colliex, C. and Tencé, M. J., *Microsc. Spectrosc. Electron.,* 10, 417 (1985).

23. Tencé, M., Chevalier, J. P. and Julien R., *J. de Phys.,* 47, 1989 (1986).

24. Hurd, A. J., Schaefer, D. W., Smith, D. M., Ross B., Le Méhauté A. and Spooner, S., *Phys. Rev.,* B 39, 13, 9742 (1989).

25. Wong, P. Z. and Bray, A. J., *Phys. Rev. Lett.,* 60, 1344 (1988).

26. Chabassier, G., Angeli, B., Heliodore, F. and Le Méhauté, A., *Pure and Applied Optics,* 1, 41 (1992).

27. Medalia, A. I., *J. Colloid. Inter. Sci.,* 24, 393 (1967).

28. Heckman, F. A. and Medalia, A. I., *J. Inst. Rubber Ind.,* 3, (2), 6 (1969).

29. Hess, W. M., Ban, L. L. and Medalia, A. I., *Rubber Chem. Technol.,*

46, 204 (1969).

30. Hess, W. M., McDonald, G. C. and Urban, E. M., *Rubber Chem Technol.,* 46, 204 (1973).

31. Hess, W. M. and McDonald, G. C., *ASTM Special Tech. Publ.,* 553.3 (1973).

32. Herd, C. R., McDonald, G. C. and Hess, W. M., presented at a meeting of the Rubber Division , ACS, Toronto, Ontario (1991).

33. Avnir, D., Farin, D. and Pfeifer, P., *J. Chem. Phys.,* 79, 3567 (1983).

34. Farin, D., Avnir, D. and Pfeifer, P., *Nature,* 308, 261 (1984).

35. Farin, D., Ph. D. Thesis, The Hebrew Univ. Jerusalem, May, 1986.

36. Urano, K., Omori, S., Yamamoto, E., *Envir. Sci. Technol.,* 16, 10 (1982).

37. Rojanski, D., Huppert, D., Bale, H. B., Dacai, X., Schidt, P. W., Farin, D., Seri-Levy, A. and Avnir, D., *Proc. 2nd Int. Conf. Photoactive Solids,* H. Sher ed., Plenum Press, New York, 1986.

38. Avnir, D., *New Journal of Chemistry,* to be publiched.

39. Klafter, J. and Blumen, A., *J. Chem. Phys.,* 80, 875 (1984).

40. Farin, D., Volpert, A. and Avnir, D., *J. Am. Chem Soc.,* 107, 3368 (1986).

41. Ehrburger-Dolle, F., Shinji Misono, Lahaye, J., *J. Collid. Interf. Sci.,* 135, 468 (1990).

42. Ehrburger-Dolle, F. and Julien, R., in *Characterization of Porous Solid,* Unger, K. K. et al ed., Elsevier Sci. Publ. p. 441.

43. Pfeifer, P. and Avnir, D., *J. Chem. Phys.,* 79, 3558 (1983).

44. Appelby, J. A., Crépy, G. and Feuillade, G., *Proceedings of the 10th Power Sources Symposium,* Brigthon, p. 432, 1976.

45. Fruchter, L., Crépy, G. and Le Méhauté, A., *J. Power Sources,* 18, 51 (1986).

46. Le Méhauté, A., de Guibert, A., Delaye, M. and Fillipi, C., *C. R. Acad Sci.,* Paris t 294 , (II), 865 (1982).

47. Le Méhauté, A. and Crépy, G., *Solid State Ionics,* 9&10, 17 (1983).

48. Le Méhauté, A., *J. Stat. Phys.,* 36, (5&6), 665 (1984).

49. Swore, R. A., Hess, W. M., and Micek, E. J., *Elastomeric,* 123, (3), 18 and 123, (4), 30 (1991).

50. McDonald, G. C. and Hess, W. M. *Rubber Chem. Technol.,* 50, 842 (1977).

51. Le Méhauté, A. and Crepy, G., *C. R. Acad. Sci.,* 304, (II), 10 (1987).

52. Le Méhauté, A., *Electrochimic Acta,* 34, 591 (1989).

53. Le Méhauté, A., Crépy, G. and Hurd, A., *C. R. Acad. Sci.,* Paris t. 306, (II), 117 (1988).

54. Le Méhauté, A., Picard, L. and Fruchter, L., *Philosophical Magazine,* 52, 1071 (1985).

55. Le Méhauté, A. and Crépy, G., *J. Power Source,* 26, 179 (1989).

56. Bagley, R. L., *J. Rheology,* 27, 201 (1983).

57. Koeller, R. C., *J. Appl. Mechan.,* 51, 299 (1984).

58. Bagley, R. L. and Torvik, P. J., *AIAA J.,* 21, 741 (1983).

59. Caputo, M., *J. Acoust. Soc. Ame.,* 58, 897 (1976) and 60, 636 (1974).

60. Gespatcher, M. and O'Farrell, C. P., *Elastomeric,* 123, 35 (1991).

61. Jonscher, A. K., *Dielectric Relaxation in Solid,* Chelsea Dielectric Press ed., London, 1983.

62. Le Méhauté, A. and Héliodore, F., *Proceedings of Progress in Electromagnetic Research Symposium,* MIT Publ. Boston p. 755, 1991, and Héliodore, F., Cottevieille, D. and Le Mehauté, A., *Proceedings of MRS Meeting,* San Francisco, p. 453, 1990.

63. Heliodore, F., Riot, P. and Le Méhauté, A., *Fractal Space-Time: Propagation in Fractal Media,* Hermes ed., to be published.

64. Le Méhauté, A., Heliodore, F. and Cottevieille, D., in *Revue Technique et Scientifique de la Défense,* DGA, Paris, March, 1992.

65. Nottale, L., *Int. J. Mod. Phys.,* A4, 5047 (1989); A7, 4899 (1992).

66. Nottale, L., *The theory of scale relativity,* to be published.

Chapter 8
Conducting Carbon Black

Nicolas Probst
M. M. M.,
Brussels, Belgium

8.1. Electrical Conductivity

Carbon blacks are electrically conductive and their conductivity is in the range $10\text{-}1$ 10^2 $(Ohm\text{-}cm)\text{-}1$. They impart good conductivity to polymers and are consequently used at low concentrations in the manufacture of conducting compounds. However the use of a particular carbon black depends upon the following factors:

* the ability of the polymer to accept a certain carbon black concentration,

* the critical volume fraction at which the electrical percolation occurs,

* processability of the final composite,

* the overall mechanical property balance achieved at the desired conductivity level.

We will consider in this section the carbon black specificities in the frame of electrical conductivity.

8.1.1. Intrinsic Carbon Black Conductivity

Starting with the work done by Mrozowski [1] and Holm's [2]

contact theory, the investigations made by Blanchard [3], Chamberlin [4], Adelson and Austin [5], Voet et al [6,7] have shown that the logarithm of the resistivity is a function of the cubic root of specific volume, the limiting element being the interparticle distance. Donnet and Voet [8] conclude that the electrical conductivity is an exponential function of the average particle distance, while Studebaker [9] reported a linear relationship between the carbon content and
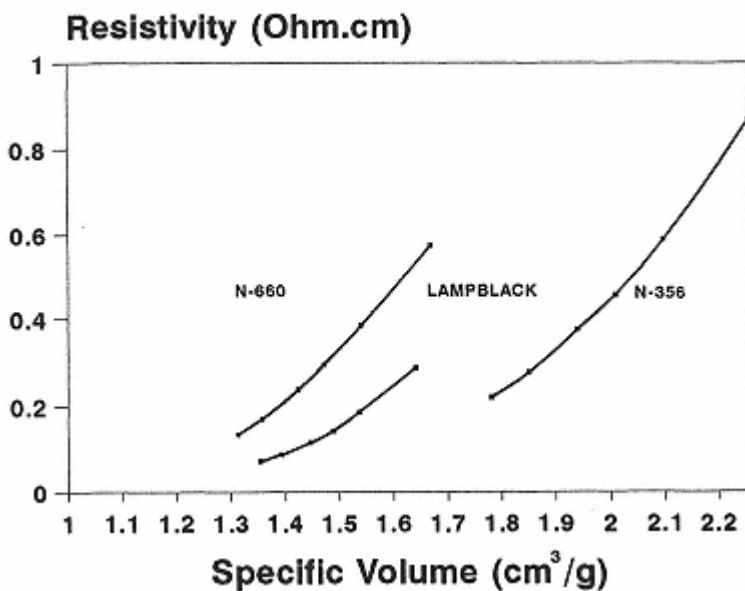
Fig. 1.
Relationship between carbon black resistivities and
specific volumes under pressure (from 0 MPa to 5.5 MPa)
[11].

the resistivity measured at a pressure of 50.7 bars. Ehrburger et al [10] studied the evolution of the resistivity under increasing pressure and observed that the percolation threshold is a function of the carbon black morphology, characterized by the exclusion radius and the fractal dimension D.

The intrinsic conductivity of carbon blacks, to a large extent, is a function of the level and the nature of impurities on the carbon surface as well as the presence of chemical groups [9]. The impurities and chemical groups modify the interparticle contact resistance and, therefore, interfere with the electrical measurement. It is not very easy to quantify the conductive character of a carbon black in a composite by its intrinsic conductivity determined on compressed carbon black.

Fig. 1 [11] shows a relationship between resistivity and the specific volume for three carbon blacks: N356, Lampblack Durex-O, and N660. It is seen that for the same specific volume (obtained by application of various pressures) the three carbon blacks show different resistivities and that the higher the specific volume, the less carbon black weight is required to achieve a certain resistivity within a given volume.

Under a pressure of 5.5 MPa, however, a good linear relationship between the specific volume and electrical resistivity [11] was observed for furnace blacks (Fig. 2). The Channel black and oxidized furnace black showed noticeably higher resistivities which is in consonance with the earlier observations of Voet [6,7] who attributed this higher resistivities at equal specific volume to the higher contact resistances due to the presence of oxygen atoms.
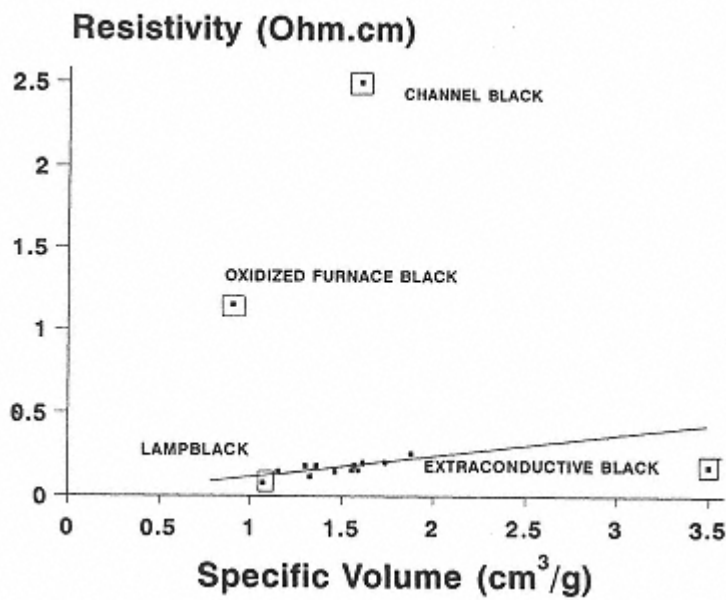
Fig. 2.
Resistivity vs. specific volume for high toluene
discolouration furnace blacks, oxidized furnace black,
lamp black, channel black and extraconductive black [11].

The influence of particle size on the intrinsic conductivity of carbon black does not seem to be established although porosity does play a role once the porosity level is very high. Highly conductive carbon blacks, composed of hollow particles, show a better intrinsic conductivity as could be expected from their specific volumes. Nelson and coworkers [12,13] and Probst and Bouquin [14] analyzed the influence of carbon black morphology on conductivity. It has been observed that most conductive carbon blacks have high porosity. One of the reasons is the very clean surface of these carbon blacks, having consequently smaller contact resistances.

Conductive carbon blacks are characterized by a high structure and a high porosity. The high porosity is, as seen above, in line with

good intrinsic conductivity, the high structure, however, gives high specific volume and consequently lower intrinsic conductivity. This is an apparent contradiction.

Special attention will have to be paid to this fact when discussing conductivity in a composite. No evidence could be discovered till now for an eventual influence of aggregate or primary particle size distribution on the intrinsic conductivity of carbon blacks.

8.1.2. Conductivity Imparted by Carbon Black to Composite

The incorporation of conductive particles into a polymer matrix modifies fundamentally the electrical and dielectrical behaviour. The typical curve of
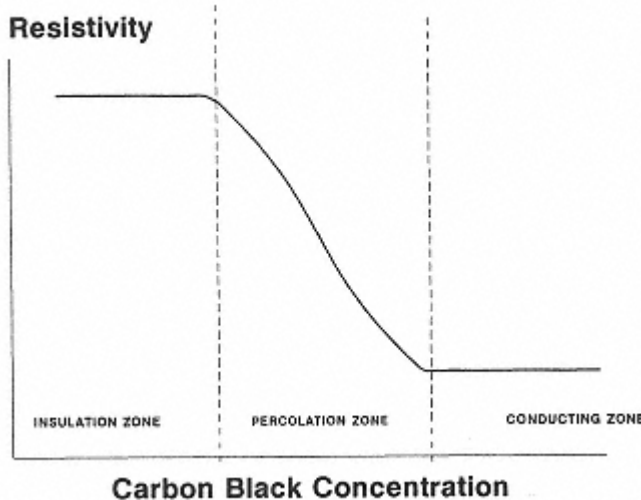
Fig. 3.
Schematic resistivity-concentration curve for
carbon black-polymer composite.

resistivity versus carbon black concentration is shown in Fig. 3.
Three distinct zones, i.e., insulating zone, percolation zone, and
conductive zone, can be observed. The percolation zone is the
transition between the insulating and the conductive zones.

The conductivity imparted to a compound by a carbon black is a
complex function of several parameters. The most important
parameters are:

* carbon black loading,

* carbon black properties,

* polymer, its chemical nature, molecular weight and viscosity,

* mixing and finishing process.

Fig. 4 shows the logarithm of resistivity as a function of carbon

black concentration for various carbon blacks [15] in high density polyethylene. All carbon blacks show a typical behaviour, each differing by the critical concentration at which the resistivity starts to drop. It is this critical concentration together with the evolution in the percolation zone and the conductivity level in the conductive zone which defines the electrical behaviour.

Table 1 [15] lists the critical weight concentrations for the same highly conducting carbon black Printex XE-2 for a number of thermo-plastic polymers. Fig. 4 and Table 1 illustrate clearly that both carbon black and polymer properties define the electrical properties of the compound.

Influence of Carbon Black Properties

The influence of carbon black parameters on compound conductivity has been discussed by many authors but the conclusions are not always concurrent with each other. This is at least the impression at a superficial examination.
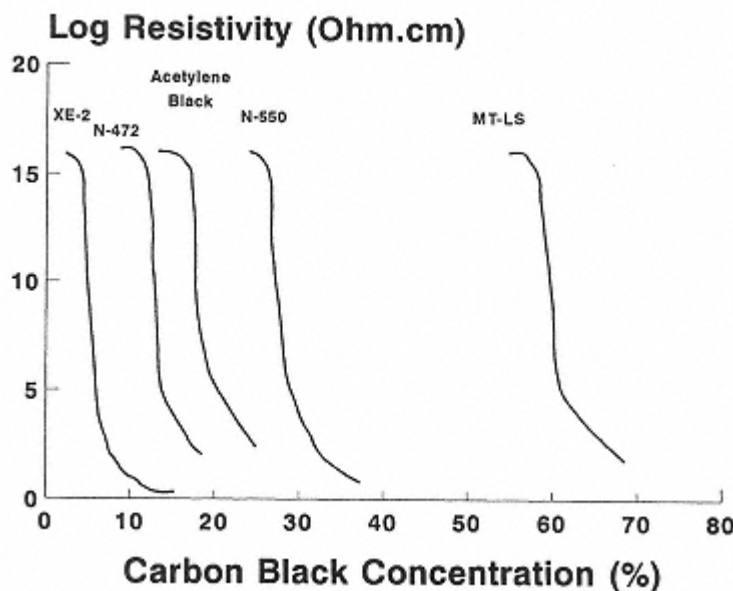
Fig. 4.
Resistivity-concentration curves for various carbon
blacks [15].

*Table 1. Threshold Concentrations for Highly Conductive
Carbon Black XE-2 in Various Polymers*

Polymer	Threshold concentration, wt%
High density polyethylene (MI=20)	4.0
High density polyethylene (MI=2)	2.6
Crosslinked high density polyethylene	1.8
Low density polyethylene	1.6
Polypropylene	1.6
Ethylvinylacetate (14%)	1.2
Ethylvinylacetate (28%)	3.2
High impact polystyrene	2.8
Transparent styrene butadiene copolymer	2.0
Polycarbonate	4.4

Polyphenyleneoxide	1.6
Polyphenylene sulphide	1.2
Polyacetal	1.0
Polyamide 66	1.4
Oilextended thermoplastic elastomer	2.4

Data from ref. [15].

Medalia [16] studied the influence of carbon black nature and morphology on the electrical properties of a composite and observed that some properties of the carbon black were modified in the composite. This is especially the case with the aggregate size.

Several authors [1721] have reported that particle size is the major carbon black property affecting conductivity. This has been attributed by Medalia [22] to the parallel evolution of particle and aggregate size. Medalia [22] further suggested that smaller particles have higher interaggregate attractive forces, resulting into a higher secondary structure, and an increased agglomerate size. This argument is supported by the flocculation theory.

The importance of aggregate size in the establishment of a conductive pathway throughout the compound has been recognized by many authors [2328] when reporting resistivity as a function of carbon black concentration. Aggregate size, usually indirectly expressed by DBP absorption, characterizes the number of particles making up the primary aggregate and its shape. This property describes the void volume, the interstitial and occluded volume of a carbon black [29]. A portion of the polymer enters the volume and reduces the critical volume fraction.

Carbon black structure and laoding play a comparable role in the compound. Kraus [30] introduced the structure-concentration equivalence principle, which, though originally defined for mechanical properties, is certainly valid for other structure dependent properties. Janzen [28] investigated the influence of carbon black structure and observed that the number of contacts of a particle with neighbouring particles governs the electrical

behaviour of the composite. The number of contacts, c, can be described by

$$c = p \times C \quad (1)$$

where p = the probability to have the contact, C = the maximum number of contacts a particle can have with its neighbours. At the percolation threshold

$$ccrit = pcrit \times C \quad (2)$$

where $ccrit$ and $pcrit$ are respectively the number of contacts and their probability at the percolation threshold.

Janzen, on the basis of a Monte Carlo type of calculation by Vissotsky [31], obtained a value $ccrit$=1.5 which was confirmed by Gurland [32] using the percolation theory and by experiment. Janzen [28] thus concluded that

$$c = \phi/(1 - \phi) \quad (3)$$

$$\phi crit = 1/[1 + \rho v(C/ccrit)] \quad (4)$$

where ϕ = the volume fraction of black, $\phi crit$ = the critical volume fraction, ρ = the density, and v = the DBP absorption on the crushed carbon black [33] expressed in cm3/g. For C = 6, equation (4) becomes:

$$\phi crit = 1/(1 + 4\rho v) \quad (5)$$

This equation predicts that $\phi crit$ decreases with increasing crushed DBP absorption. The crushed DBP-absorption is considered as the structure of carbon black in the compound. Janzen [28], Medalia [34] and Probst [15] have used this formula with noticeable success. Janzen's Equation 5, being developed on a general basis, should be applicable for all carbon blacks and all polymers. Although the general agreement is quite good, some deviations are observed for certain carbon blacks and for some polymers. Fig. 5 shows the critical weight fraction as a function of the crushed DBP absorption. The experimental results of loaded high density polyethylene are in an overall good agreement with the prediction from Janzen's Equation 5. It was observed that at low DBP absorption (very low structure carbon blacks), especially for thermal blacks, the experimental value is higher than predicted. For the carbon blacks with higher structures and smaller particle size, the experimental value is lower. This deviation could be attributed to the assumption that the crushed DBP absorption is describing the structure of the carbon black in the compound. Probst and Donnet [11] showed that with a more precise description of the carbon black structure in the compound the agreement of
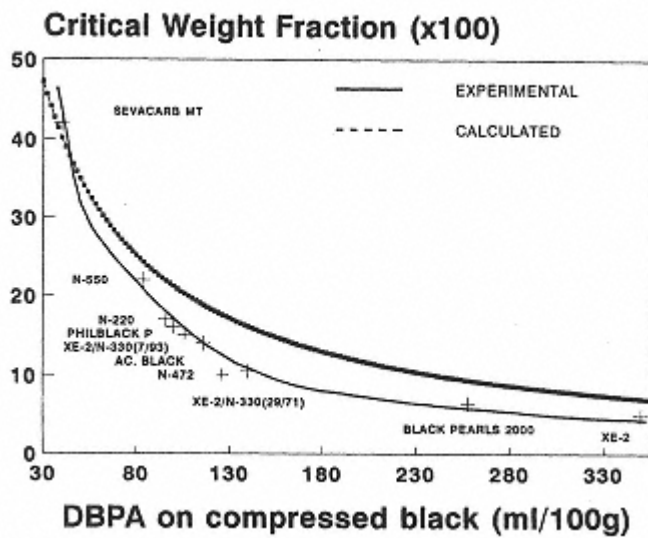
Fig. 5.
Critical weight fractions vs. compressed DBP
absorption for various carbon blacks and carbon
black blends. The calculated curve is obtained
from Janzen's equation [28]. From ref. [15].

Table 2. Volume Occupied by the Carbon Black, Including Carbon Black Volume and Void Volume, at the Percolation Threshold

Carbon black	Natural rubber	Styrene-butadiene rubber
N326	15	13
N356	15	14
N220	13	15
N115	13	13
N660	17	16
N550	17	17
MT	16	17
DUREX 0	12	20

Values calculated from Kraus' equation [30] using the structure in compound for natural rubber and SBR recipes [11].

the data calculated from Janzen's equation with the experimental results could be improved.

Probst and Donnet [11] applied Kraus' structure-concentration equivalence principle [30] to conductive compounds and observed that the total carbon black volume occupied in the compound at the percolation threshold is almost constant for all carbon blacks (see Table 2).

Thus the influence of carbon black structure and loading should be considered together with the other properties in the frame of the percolation theory. This same subject has been further discussed as suggested by Carmona [35] in view of the flocculation and coagulation theory [36,37].

Influence of Polymer Type

Miyasaka et al [38] have shown that viscosity and surface tension

of the polymer have a strong influence on the critical volume fraction which in turn affects on electrical conductivity of the compounds. Natural rubber shows a higher critical concentration than expected from its surface tension. This is probably due to its strong interaction with carbon black surface.

Blends of two or more polymers can produce extreme situations. Geuskens et al [39] have reported that the resistivity for extraconductive carbon black in blends of polyethylene and natural rubber shows a minima. However, high resistivity was observed in the blends of polymers where one of the components is present at low concentrations. This has been attributed to the exclusion of carbon black from the polyethylene phase. A very high carbon black concentration is thus initiated in the natural rubber phase which results in a conductive pathway. When natural rubber is present in larger quantities the carbon black is homogeneously distributed. This example shows the complex
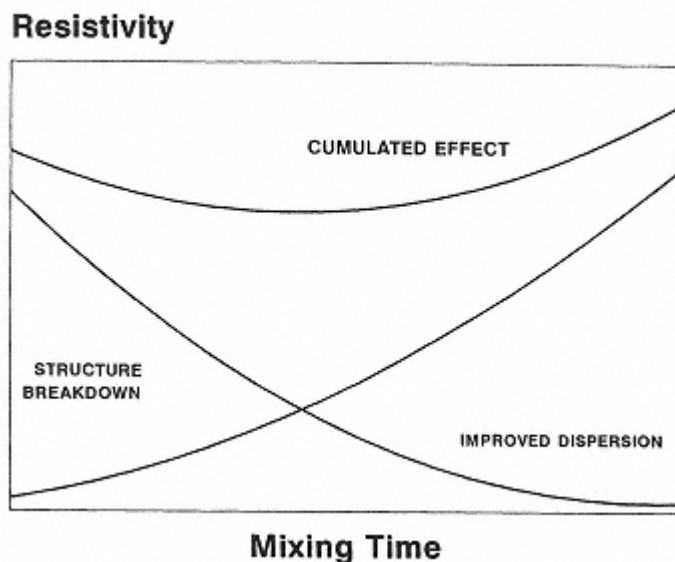
Fig. 6.
Schematic resistivity evolution vs. mixing time.

mechanism of electrical conductivity under the influence of carbon black distribution in a polymer blend.

Influence of Processing

Incorporation of carbon black and processing of the compound take a very important place in the production of conductive products. It is the interparticle or interaggregate distance which determines the electrical conductivity. Many authors [4042,16] have observed that a good dispersion of the carbon black reduces the conductivity. Fig. 6 shows schematically the evolution of the resistivity as a function of the mixing time. The resistivity of the compound is reduced when the carbon black is homogeneously distributed within the compound. On the other hand, when carbon black aggregates in the compound are submitted to mechanical shear, secondary aggregation is destroyed which increases with mixing time and

shear rate. The curve thus shows a minimum at a certain mixing time where homogenization and structure breakdown assures an optimum conductive pathway.

Similarly, any additional step, like the moulding process, generates lower conductivities. Fig. 7 depicts the difference in conductivity between an injection moulded (high shear) and a compression (low shear) moulding process for styrene-butadiene thermoplastic copolymer [15].

The increase in resistivity can be explained by the difference in carbon black structure resulting from the process. The effect of structure breakdown cannot always be overcome by higher concentration as the overall resistivity

Log Resistivity (Ohm.cm)
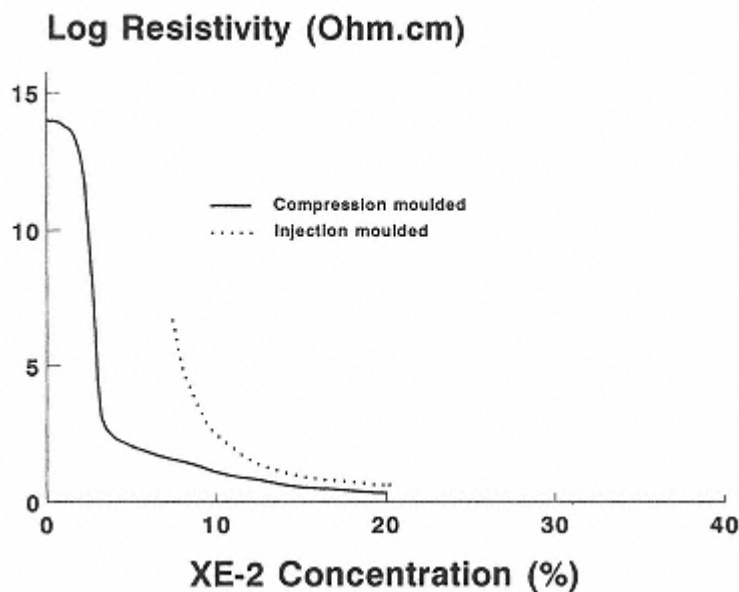
Fig. 7.
Resistivity-concentration curves for different molding
processing of styrene-butadiene thermoplastic
copolymer filled with extraconductive carbon black.

is the sum of all aggregate resistances and interaggregate resistances. This can be represented in a schematic way as shown in Fig. 8. The total resistance of a compound, R, can be expressed by

$$R = \Sigma Ra,i + \Sigma Re,i \quad (6)$$

where Ra = resistance of carbon black aggregate, and Re = resistance of the interaggregate space.
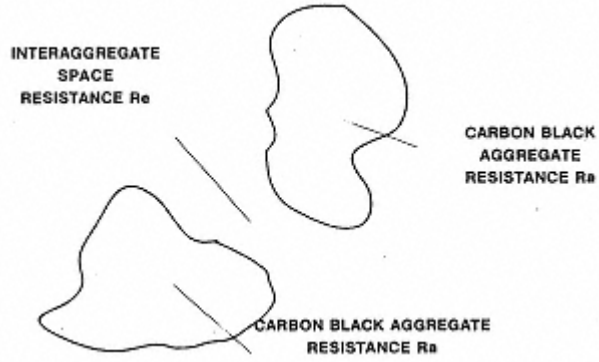
Fig. 8.
Resistance of black/polymer composite.
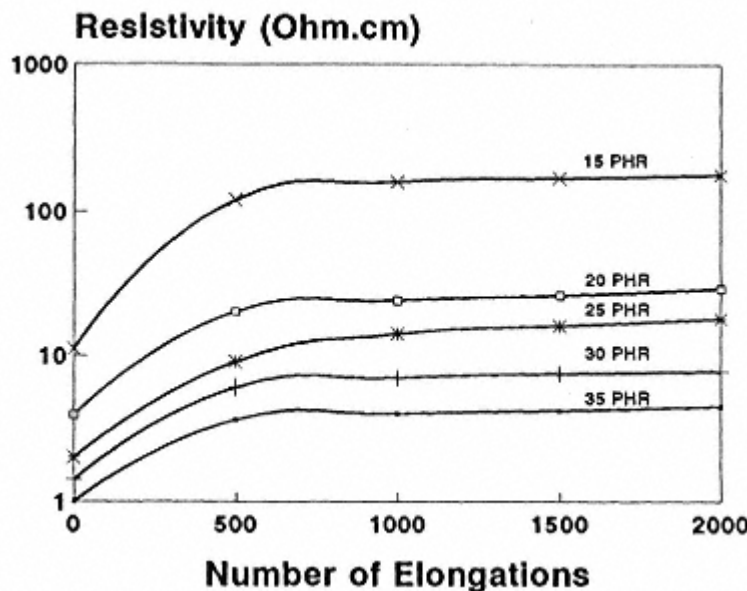
Fig. 9.
Resistivity vs. number of elongations for EPDM
compounds filled with different concentration of
extraconductive black.

Effect of Dynamic Deformation

Similar to the effect of processing, changes in resistivity are observed when an elastomer based compound is submitted to a deformation. Probst [15], based on the deformation of EPDM compounds, has shown that a plateau is reached after the first deformation series (Fig. 9). This plateau is due to the fact that we approach the maximum structure breakdown, which is expected to correspond to the crushed DBP absorption.

Parris et al [43] have shown that the recovery of electrical conductivity is quantitatively possible by thermally relieving the compound for a certain time at a higher temperature. Norman [23] reported experimental results of increase in compound conductivity

upon thermal treatment. Bulgin [24] also observed a decrease in resistivity during storage at room temperature.

8.1.3. Percolation Theory

The gradual addition of conductive carbon particles into an insulator polymer matrix leads to the critical concentration at which the percolation occurs. The transition from an insulator material to a conductor can be approached by the percolation theory (Broadent and Hammersley [44], Kirkpatrick [45]). Carmona [35] discusses the various evolution steps of the theory and its application to carbon black composites.

The percolation theory enables the calculation of the probability to have infinite connections between conducting particles and as such to predict the

critical concentration. The theory predicts for spherical and monodisperse particles, without interparticle interaction, a critical volume fraction of 0.16 to 0.18. In practice we have observed that many carbon blacks have higher or lower critical volume fractions. Carmona [35] attributes the deficiencies of the theory to the fact that the theory does not take into account either the aggregate-aggregate or aggregate-polymer interactions and the geometrical form.

The introduction of the coagulation and flocculation theory [36,37], allowed the development of a new approach [46,47].

Above the percolation point the behaviour of a conductive compound can be described by the equation

$$\sigma = \sigma_o (\phi - \phi_c)_t \quad (7)$$

where ϕ = the achieved volume fraction, ϕ_c = the volume fraction at the threshold, t = the conduction coefficient, σ = the compound conductivity, and σ_o = a prefactor corresponding to the compound conductivity at threshold. t has been calculated as 1.95 by several authors [4850], while Chen et al [51] and Carmona et al [52] report values noticeably higher than 2.0, both for carbon black and carbon fibres.

Carmona [35] attributes this non-conformity with the percolation theory to the difference between a perfect lattice of bends and the reality of a polymer carbon black composite, as such a first correction was required to take into account the non-sphericity of the carbon black aggregates, while a second one should take into account the interaction between the carbon black and the polymer matrix. Each polymer system has its specific rheological properties,

while each carbon black has its specific morphology and affinity to the polymer.

Although the application of the floculation and coagulation theory is still in a very early stage, a qualitative description of the mechanism can be made. The two processes taking place can be expressed as:

* those increasing the tendency of carbon black aggregates to agglomerate,

* those increasing the tendency of carbon black aggregates to be retained in the polymer lattice and as such separated from other carbon black aggregates.

The tendency of carbon black aggregates or particles to agglomerate can be summarized qualitatively by:

* the size of the aggregate or particle, determining the amplitude of the attractive or repulsive forces between two adjacent aggregates (Hamaker [53]),

* the surfaces tension of the polymer (Myasaka [38]),

* the tendency of the polymer to crystallise and as such to exclude

the carbon black,

* the creation of links between polymer and carbon black.

8.1.4. The Level of Conductivity in the Conductive Zone

Fig. 10 shows the resistivity-concentration curve for furnace, thermal and lampblacks in styrene-butadiene rubber. Different resistivities are observed in the conduction zone. Kawamoto [54] reported that at high loading (in the conductive zone) the compound resistance is equal to R_a, the resistance of the aggregate. Probst and Donnet [11] have shown that in natural rubber and in styrene-butadiene co-polymers important differences can be observed for the various carbon blacks studied. They observed that the classification of carbon blacks is different in natural rubber and styrene-butadiene rubber. This difference, as well as the apparent contradiction with Kawamoto's [54] statement, could be due to the different interactions between the carbon blacks and polymer or to a polymer specific arrangement in this interaggregate space.

The compound resistance has been indicated earlier as the sum of R_a and R_e. The aggregate resistance being the same for the same carbon black, the difference in resistivity has to be caused by R_e, the resistance of interaggregate space.

Differences in the behaviour of different carbon blacks can also be attributed to the difference in surface chemistry. Medalia [22] indicated that most studies in this field were carried out before the postulation of the modern
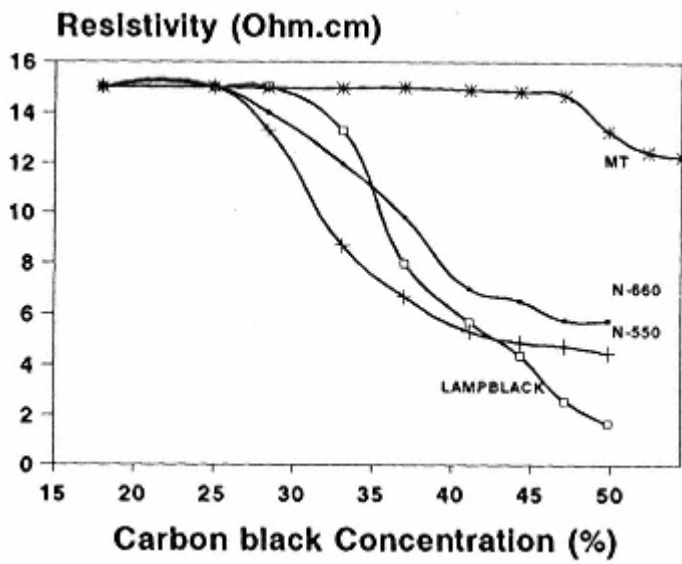
Fig. 10.
Resistivities vs. concentrations for various carbon
blacks in SBR compounds (from ref. [11]).

theories and consequently only qualitative results are available. Sichel et al [55] suggested that oxygen could, by producing an insulating barrier around the carbon black, reduce conductivity even at high loading.

8.1.5. Conducting Mechanism in the Polymer-Carbon Black Composite

It has been seen in the previous section that conduction occurs once a sufficiently high concentration of carbon black is present. This concentration is called critical concentration or percolation point. At this point a chain of conductive particles is present which has carbon black aggregates in sufficient content to allow electron passage. This quite general statement needs some clarification. Although we do not intend to discuss this subject in detail, some comments on the current acceptance of the theory are required.

The term contact used above has not to be understood as an indication of the value of the carbon black-carbon black interface. It might as well be a physical contact as a contact via an insulating interface. The interaggregate distance has to be small enough to allow an electron jump from one carbon black aggregate to another. Carmona [35] indicated that in the case of carbon black, the aggregates are usually separated by a thin polymer film and that a conduction mechanism by tunnelling has to be considered. Sheng et al [56,57] proposed a model describing the relationship between the resistance and the electric field, *E,* by a general equation as follows:

$$\sigma = \sigma_o' exp\left[-\frac{T_1}{T_1 + T_o}\left(1 - \frac{E}{E_o}\right)^2\right] \tag{8}$$

where σ_o' is carbon black concentration dependent, and $T1$, To and Eo are constants.

The influence of temperature is attributed to the thermal fluctuation as those fluctuations lower the interaggregate gap.

The fitting of the experimental points with the theory is confirmed by the view that in the case of carbon blacks the conduction takes place by fluctuation induced tunnelling. Fug et al [58] showed that in the case of very large carbon particles (>0.3 μm as thermal black) the conduction mechanism is through real physical contacts, similar to carbon fibres as shown by Carmona [52] and Mouney [46].

8.1.6. Conductive Carbon Blacks

A series of carbon blacks have been developed for specific conductive applications, the so-called conductive, superconductive and extraconductive carbon blacks. Although, as mentioned before, all carbon blacks can be used to produce conductive compounds, conductive blacks are designed to be used at low loading in most polymer types. Their major characteristics are:

Thermal Conductivity W/m K
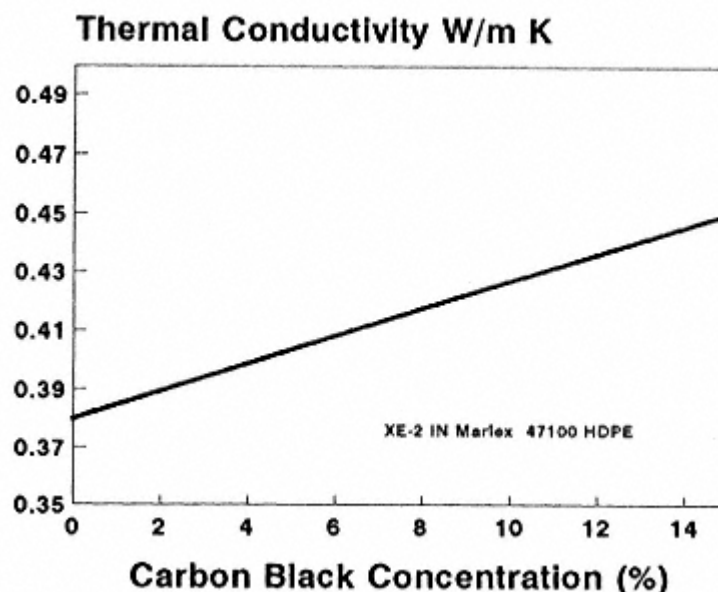
Fig. 11.
Thermal conductivity vs. concentration of
extraconductive black in polyethylene at room
temperature.

* high structure,

* high porosity,

* small module size,

* chemically clean surface.

8.2. Thermal Conductivity Of A Polymer-Carbon Black Compound

Thermal conduction is very often associated with electrical conduction. The parallelism with a metallic conductor is not valid. Issi et al [59], Berman [60], and Anderson [61] have analyzed different heat transportation mechanisms. In metals heat transport occurs by the electric charge carriers, in crystalline electrical insulators this transport is done by the lattice waves, while in the

case of amorphous materials, the transport mechanism is not fully understood. Thermal conductivity of a polymer-carbon black compound increases with carbon black concentration (Poulart and Probst [62]). The presence of a threshold, however, could not be observed. Fig. 11 shows a linear increase of thermal conductivity with increasing carbon black content in polyethylene. However, the influence of carbon black parameters is not clear. It is seen from Fig. 12 that extraconductive carbon black and acetylene black show higher thermal conductivities than furnace black. This may be due to the graphiticity level of these carbon blacks.
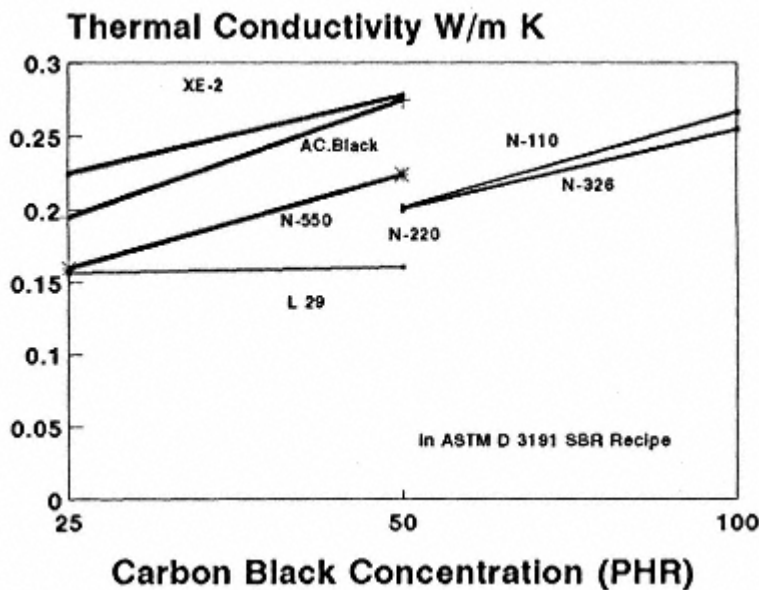
Fig. 12.
Thermal conductivity vs. concentration of various
carbon blacks in SBR vulcanizates.

References

1. Mrozowski, S., *3rd. Conf. on Carbon,* p. 211, 1959.

2. Holm, R., *Electrical Contacts,* Hugo Geben, Stockholm, 1946.

3. Blanchard, A. F., *Proc. Conf. Ind. Carbon Graphite,* Soc. Chem. Ind. London, p. 434, 1957.

4. Chamberlin, R. D., M. S. Thesis, Pennsylvania State University, 1959.

5. Adelson, E. and Austin, A. E., *Proc. 6th Bienn. Conf. on Carbon,* 1963.

6. Voet, A., *Rubber Age,* 95, 746 (1964).

7. Voet, A., Whitten, W. N., Jr. and Cook, R. F., *Koloid Z.*

Polymere, 201, (1), 39 (1965).

8. Donnet, J.-B. and Voet, A., *Carbon Black,* Marcel Dekker, 1976.

9. Studebaker, M. L., *Rubber, Chem., Technol.,* 30, 1401 (1957).

10. Ehrburger, F., Misono, S. and Lahaye, J., *Proc. Conf. Conducteurs Granulaires,* Paris, Oct. 10, 1990.

11. Probst, N. and Donnet, J.-B., *Proc. Conf. Conducteurs Granulaires,* Paris, Oct. 10, 1990.

12. Nelson, J. R., presented at 16th Carbon Conf., ACS, San Diego, 1983.

13. Nelson, J. R. and Wissing, W. K., *Carbon,* 24, 115 (1986).

14. Probst, N. and Bouquin, J. C., presented at a meeting of Rubber Division, ACS, spring meeting, Montreal, 1987.

15. Probst, N., *European Rubber J.,* Nov., (1984).

16. Medalia, A. I., in *Carbon Black-Polymer Composites,* E. K. Sichel ed., Marcel Dekker, p. 1, 1982.

17. Boonstra, B. B. and Dannenberg, E. M., *Ind. Eng. Chem.,* 46, 218 (1954).

18. Harris, E. V., Jones, F. E. and Church, F. C., Cabot Technical Report, Rg-130, Cabot Corporation.

19. Degussa Technical Report, Schriftenreihe Pigmente Heft 40, Degussa AG.

20. Garret, M. D., *Conductivity of Carbon Black Loaded Systems,* Cities Service Co, Cranbury, N. J.

21. Schaeffer W. D. and Smith, W. M., *Ind. Eng. Chem.,* 47, 1286 (1955).

22. Medalia, A. I., *Rubber Chem. Technol.,* 59, 432 (1986).

23. Norman, R. H., *Conductive Rubbers and Plastics,* Applied Science Publishers Ltd., London, 1970.

24. Bulgin, D., *Trans. IRI,* 21, (3), 188 (1945).

25. Verhelst, W. F., Wolthuis, K. G., Voet, A., Ehrburger, P. and Donnet, J. B., *Rubber Chem. Technol.,* 50, 735 (1977).

26. Medalia, A. I., *J. Colloid Interf. Sci.,* 32, 115 (1970).

27. Medalia, A. I., *Rubber Chem. Technol.,* 45, 1171 (1972).

28. Janzen, J., *J. Applied Phys.,* 46, 966 (1975).

29. Janzen, J. and Goodarz-Nia, I., *J. Colloid Interf. Sci.,* 69, 476 (1979).

30. Kraus, G., *J. Polymer Sci.,* 13, 601 (1970).

31. Vissotsky, V. A., Gordon, S. B., Frisch, H. L. and Hammersley, J. M., *Phys. Rev.,* 123, 1566 (1961).

32. Gurland, J., *Trans. Metall. Soc. Aime.,* 236, 642 (1966).

33. ASTM D-3493.

34. Medalia, A. I., *J. Coll. Interf. Sci.,* 32, 115 (1970).

35. Carmona, F., *Ann. Chim. Fr.,* 13, 395, (1988).

36. Derryaguin, B. V. and Landau, L. D., *Act. Physchem. SSSR,* 14, 375 (1941).

37. Verwey, E. J. W. and Overbeek, J. Th. G., *Theory of Stability of Lipophobic Colloids,* Elsevier, Amsterdam, 1948.

38. Miyasaka, K., Watanabe, K., Jojima, E., Aida, H., Sumita, M. and Ishikawa, K., *J. Material Sci.,* 17, 1610 (1982).

39. Geuskens, G., Gielens, J. L., Desheef, D. and Deltour, R., *Eur. Polym. J.,* 23, 12 (1987).

40. Dannenberg, E. M., *Ind. Eng. Sci.,* 21, 809 (1981).

41. Boonstra, B. B. and Medalia, A. I., *Rubber Chem. Technol.,* 36, 115 (1963).

42. Cembrola, R. J., *Polym. Eng. Sci.,* 21, 809 (1981).

43. Parris, D. R., Burton, L. C. and Siswanto, M. G., *Rubber Chem. Technol.,* 60, 705 (1987).

44. Broadent, S. P. and Hammersley, G. M., *Proc, Camb. Phil. Soc.,* 53, 629 (1956).

45. Kirkpatrick, S., *Rev. Mod. Phys.,* 45, 574 (1978).

46. Mouney, C., Thèse de 3ième cycle, Université de Bordeaux I, 1987.

47. Hsu, W. Y., Holtje, W. G. and Barkley, J. R., ACS meeting, Los Angeles, April 1985.

48. Song, Y., Noh, T. W., Lee, S. I. and Gaines, J. R., *Phys. Rev.* B. 33, 904 (1986).

49. Fug, G., Canet, R. and Delhaes, P., *C.R. Acad. Sci.,* Paris B 287, 5 (1978).

50. Balberg, I., and Bosowski, S., *Solid State Comm.,* 44, 551 (1982).

51. Chen, C. C. and Chou, Y. C., *Phys. Rev. Lett.,* 54, 2529 (1985).

52. Carmona, F., Prudhon, P. and Barreau, F., *Solid State Comm.,* 51, 255 (1984).

53. Hamaker, H. C., *Physica,* 4, 1058 (1937).

54. Kawamoto, H., in *Carbon Black-Polymer Composites,* E. K. Sichel ed., Marcel Dekker, N. Y., 1982.

55. Sichel, E. K., Gittelman, J. I. and Sheng, P., in *Carbon Black Polymer-Composites,* E. K. Sichel ed., Marcel Dekker, N. Y., 1982.

56. Sheng, P., Sichel, E. K. and Gittelman, J. I., *Phys. Rev. Letter,* 40, 699 (1978).

57. Sichel, E. K., Gittelman, J. I. and Sheng, P., *J. Elect. Mat.,* 11, 699, (1982).

58. Fug, G., Canet, R., Delhaes, P., *C. R. Acad. Sci.,* Paris, B 287, 5 (1978).

59. Issi, J. P., Poulart, B. and Herremans, J., *Measurement,* 1, 167 (1983).

60. Berman, R., *Thermal Conduction in Solids,* Clurendon Press, Oxford, 1976.

61. Anderson, A. C., *Amorphous Solids, Low Temperature Properties,* W. A. Phillips ed., Springer Verlag Berlin, 24, 6580.

62. Poulart, B. and Probst, N., *Kautsch. Gummi, Kunst.,* 37, 5 (1986).

Chapter 9
Carbon Black Reinforcement of Elastomers

Siegfried Wolff
and Meng-Jiao Wang
Degussa AG,
Hürth, Germany

Soon after carbon black was discovered to be an active filler in rubber at the beginning of this century, it became one of the most important components in the manufacture of rubber products, with a consumption second only to rubber itself. This situation will probably continue into the next century and there is no indication of carbon black being replaced completely by other materials. Carbon blacks have held their position mainly thanks to their unique ability to enhance the physical properties of elastomers. This well-documented phenomenon [1,2], termed reinforcement, has a profound effect on today's tire and rubber industry.

During the last 50 years, a vast amount of information on elastomer reinforcement by carbon blacks has been published. It is recognized that the main parameters of carbon blacks which govern their reinforcing ability in rubber are the following:

* The size and distribution of primary particles, sometime referred to as nodules, which are joined by fusion into aggregates arranged at random. The particle size and its distribution directly determine the surface area of the carbon blacks.

* The size, shape, and distribution of aggregates (aggregate

complexity), i.e., the degree of irregularity of the carbon black units or the development of branchings due to the aggregation of primary particles and the asymmetry of the aggregates. These parameters are generally termed carbon black structure.

* Surface activity which, in a chemical sense, is related to the reactivity of the chemical groups on the carbon black surface, and, in terms of physical chemistry, is referred to as adsorption capacity. This capacity is determined by carbon black surface energy, both its dispersive and specific components, and the energy distribution on the carbon black surface.

All these parameters play a role in rubber reinforcement through different mechanisms, such as interfacial interaction between rubber and carbon black, occlusion of the polymer in the internal voids of the aggregate, and the agglomeration of carbon black aggregates in the polymer matrix.

9.1. Effect of Carbon Blacks in Rubber

9.1.1. Interfacial Interaction between Carbon Black and Polymer

One of the consequences of the incorporation of carbon blacks into a polymer is the creation of an interface between a rigid solid phase and a soft solid phase. For rubber-grade carbon blacks, whose surfaces exhibit very little porosity, the total area of the interface depends on both filler loading and the specific surface area of the filler. In a unit volume of compound, the interfacial area, ψ, is given by

$$\psi = \phi \rho S \quad (1)$$

where ϕ is the volume fraction of the carbon black in the compound, and ρ and S are the density and specific surface area of the filler, respectively.

Due to the interaction between rubber and filler, the polymer molecules can be adsorbed onto the filler surface either chemically

or physically. This adsorption leads to two phenomena which are well documented, the formation of bound rubber and a rubber shell on the carbon black surface. Both are related to the restriction of the segmental movement of polymer molecules.

Bound Rubber

Bound rubber, sometimes termed carbon gel, is defined as the rubber portion in an uncured compound which cannot be extracted by a good solvent due to the adsorption of the rubber molecules onto the filler surface. This phenomenon has been studied extensively and is recognized as a typical feature of filler surface activity. Several reviews [16] have dealt with the mechanism and the factors affecting the formation of the bound rubber and its influence on rubber properties. A comprehensive survey of recent investigations on this subject was given by Dannenberg [7].

Generally speaking, bound rubber is a parameter which is simple to measure, but the factors which influence the test results are highly complicated. It was reported that the filler-polymer interaction leading to the formation

of bound rubber involves physical adsorption, chemisorption, and mechanical interaction. As far as the filler is concerned, bound rubber is not only affected by the physicochemical characteristics of the filler surface, but also by filler morphology. With regard to the polymer, both the chemical structure of the molecules (saturated *vs.* unsaturated, polar *vs.* nonpolar) and their microstructure (configuration, molecular weight and its distribution) influence the level of bound rubber. Moreover, bound rubber also shows a strong dependence on the processing conditions of the compound, such as mixing and storage time. Furthermore, there are important factors during the measurement itself which determine the bound rubber content, e.g., the nature of the solvent and the temperature of extraction. Results reported in publications are, therefore, sometimes contradictory, since they are affected by the compound composition, compound preparation, as well as by the test procedures. Bound rubber is thus a phenomenon which, although well-known and the subject of numerous publications, is still a matter of controversy.

Two arguments concerning bound rubber have been widely debated in the literature for many years. One is the nature of the polymer-filler interaction involved in bound rubber formation, and the other is the validity of bound rubber being considered a measure of filler surface activity.

It has been proposed that the chemisorptive mechanism of bound rubber formation is a free radical reaction between carbon black and polymer. The existence of unpaired spin electrons on carbon blacks has been demonstrated by electron spin resonance [8] and they were assumed to be free radicals [8,9]. If free polymer radicals

can be generated by chain scission during processing, the stabilization of the polymeric radical by carbon black may result in the grafting of rubber molecules onto the carbon black surface by means of covalent carbon-carbon bonds. Gessler [10,11] further postulated that the free radicals of carbon blacks, originating from the mechanical breakage of the carbon black aggregate structure during milling of rubber and carbon black, is a new source of free radicals and responsible for the higher bound rubber content when a high-structure carbon black, which is easily broken up, is used instead of a low-structure black. Although this conclusion was supported by the suppression of bound rubber formation by radical chain stoppers such as thiophenols, observations indicating the contrary were also reported. Donnet and coworkers [1214], with model free radicals, were able to show that the free radical activity of carbon blacks does not play a significant role with regard to chemical reactivity and that the reinforcement of natural rubber is not related to the free radical content of carbon blacks.

On the other hand, while the oxygen functional groups on the carbon black surface seem to lower the polymer-filler interaction for unsaturated rubbers [15,16], in the case of saturated or nearly saturated rubbers, such as butyl rubber, the oxygen functionality plays an important role in bound

rubber formation. The mechanism of this oxygen group functionality still remains unclear, even though Gessler [17] postulated a cationic interaction between polymer and carbon black. He believed that the active hydrogen on the surface of oxygenated black, especially of the carboxyl groups, is donated as a proton to the polymeric double bond in butyl rubber, and the carbonium ion formed on the polymer chain is proposed either to react directly with the anion left on the carbon black surface or to serve as an agent effecting electrophilic substitution at the crystal edges of the graphitic crystallites of the carbon black surface. However, this mechanism is doubtful for the simple reason that carbon blacks with a wide range of carboxyl group functionalities, resulting from ozonization for varying periods of time and at different temperatures, do not show any influence of the concentration of carboxyl groups on their reinforcing effect in butyl rubber. Similarly, no relationship was observed between the reinforcement in butyl rubber and the concentration of phenolic or quinonic groups [18].

The existence of physical adsorption resulting in bound rubber formation has been demonstrated by Ban, Hess and coworkers [19,20]. In a study of EM micrographs of microtome samples of N330-filled SBR compounds, in which the sol was extracted with benzene in a vapor extractor, they found that bound rubber is nearly totally absent on the greater part of the carbon black surface (especially in the convex region of the aggregates). The very small amount of rubber remaining in the concave region of the aggregates would be due to the retraction of the polymer during sample preparation, instead of a chemical reaction between polymer and carbon black surface, since it is hard to believe that

there should be a difference in chemical reactivity between concave and convex regions. Recently, Wolff, Wang, and Tan [21] reported that at an extraction temperature above 70°C in xylene, the bound rubber of SBR compounds filled with 50 phr N330 decreases very rapidly with increasing temperature and only about 3% of bound rubber is left on the carbon black surface at 100°C. Even this low level of bound rubber cannot be attributed to chemisorption from primary valence bonding because the measurement of bound rubber was carried out at room temperature after extraction. In this case, some molecules of rubber adsorbed physically on the carbon black surface from the solution at room temperature could not be fully removed by the solvent [1,22]. Wolff et al thus concluded that the polymer-filler interaction, involved in the formation of bound rubber in SBR-carbon black compounds, is essentially a physical phenomenon.

Regardless of the nature of the interaction between filler surface and polymer, bound rubber should be a measure of surface activity. At fixed and practical loadings, the bound rubber content increases with the surface area of the carbon black [7,21]. This is, obviously, related to the difference in interfacial area in the compound between different grades of carbon blacks. With

regard to the surface activity of carbon blacks, meaningful information can only be obtained by a comparison of the bound rubber per unit surface. By normalizing the bound rubber content with the interfacial area in the compound, Dannenberg [7] showed a decrease in bound rubber per unit surface with decreasing particle size of the carbon blacks for SBR compounds filled with 50 phr of carbon black. Wolff et al [21] reached the same conclusion with different loadings as shown in Fig. 1. This is in contrast to observations made in surface energy measurements where both the dispersive and specific components were higher for small-particle carbon blacks [59]. Since bound rubber is essentially a physical phenomenon for SBR-carbon black compounds and since the physical adsorption of a substance is related to the surface energy of the solid, these contradictory results were interpreted in terms of interaggregate multiattachment of rubber molecules and the agglomeration of carbon blacks [21]. It is understood that the rubber molecule may repeatedly attach onto the carbon black surface at different sites. This would reduce the effectiveness of the surface since only a single attachment would render the whole molecule inextractable in solvent. The multiattachment of single chains may occur on different aggregates close to each other, which, of course, depends on the distance between the aggregates. This distance decreases as the surface area of carbon blacks increases at constant loading (see Equations 8 and 9), which in turn reduces the efficiency of the surface for the formation of bound rubber. On the other hand, the agglomeration of the aggregates in the polymer matrix enhances interaggregate multiattachment, and/or decreases
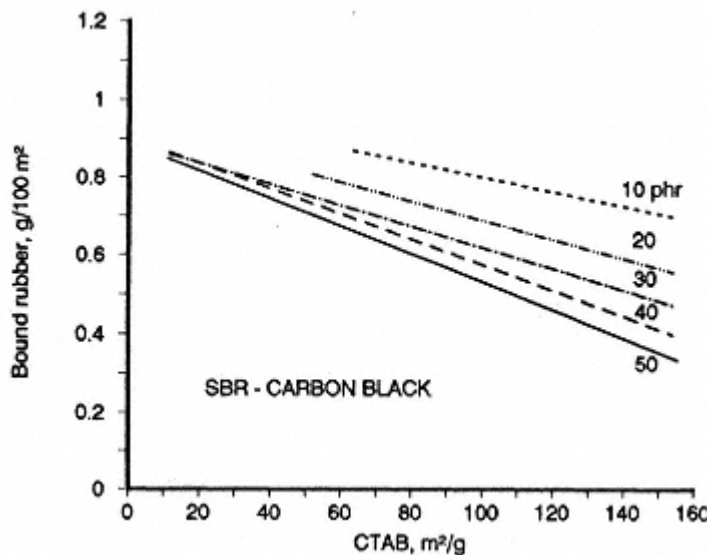
Fig. 1.
The bound rubber contents on unit surface of the carbon blacks as a function of CTAB surface area (from ref. [21]).

the interfacial area by direct contact between aggregates. This agglomeration also shows a strong dependence on aggregate distance [23]. The greater tendency of agglomeration of the smaller-particle carbon blacks would also result in a reduction of the effectiveness of the filler surface. It is thus understandable that the bound rubber per unit surface is underestimated when the normalization is based on the total area of interface calculated from filler loading and specific surface area of the carbon blacks. This has been confirmed by the loading dependence of the bound rubber content per unit surface, showing lower values for the higher loadings which is obviously related to greater interaggregate multiattachment and more developed agglomeration rather than to low surface activity [21]. The bound rubber per unit surface of black filled SBR compound at critical loading, i.e., the lowest loading at which a coherent gel can be formed, is approximately proportional to the surface energy of the carbon blacks (Fig. 2). It can be assumed that, at critical loading, the interaggregate multiattachments are similar and no significant agglomeration of the carbon blacks exists.

Therefore, when the specific surface activity is investigated with regard to bound rubber, the compounding parameters and conditions of measurement should be well defined. Nevertheless, the total bound rubber content in the compound may be an important parameter influencing rubber properties, especially compound processability.

Among the carbon blacks with similar surface area, high-structure products generally have a higher bound rubber content. Several explanations
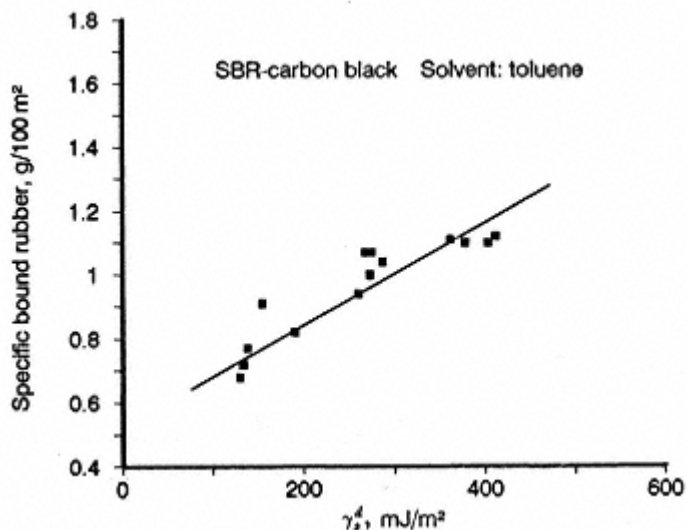
Fig. 2.
Bound rubber contents on unit surface area of carbon blacks at critical loadings as a function of dispersive components of surface energies (from ref. [21]).

have been proposed in this regard, including (i) a greater probability of multiple molecular segment adsorption [7]; (ii) a less ordered graphite layer structure, leading to higher surface activity; and (iii) easier breakdown of the aggregates during mixing [7,10] in the case of high-structure carbon blacks [24]. The latter explanation seems to be more reasonable because the aggregate breakdown could result in two things: an increase in filler-polymer interface and higher surface activity of freshly built surface [21,186].

Rubber Shell

Another result of filler-polymer interaction is the formation of a more or less immobilized layer or rubber shell surrounding the carbon black, in compounds as well as in vulcanizates, resulting from the restriction of the molecular motion of the rubber in the vicinity of the filler surface. This immobilization of rubber may also be related to increased entanglements due to filler-polymer attachments.

The existence of a rubber shell on the filler surface has well been demonstrated experimentally. Westlinning and coworkers [25,26], in their investigation of the freezing point depression of benzene in swollen networks, concluded that crosslink density is higher in the vicinity of carbon black surface. Westlinning [27] suggested that, at 20°C, molecular movement was hindered by the filler surface up to a depth of 35 nm. At 100°C, this layer would disappear. Schoon and Adler [28] reported that the thickness of this hindered layer is 3550 nm for SBR and 2530 nm for NR.

Following his investigations of rheological behavior of rubber

compounds and the dynamic properties of carbon-black-filled SBR and *cis*-BR vulcanizates, Smit [29 32] proposed a rubber shell of 25 nm on the carbon black surface to explain his results. This model was supported by the investigation of filled rubber by NMR [16,33 38], DSC [36], and DMTA [36]. Kaufman et al [33], using the nuclear spin relaxation time measurement to investigate carbon-black-filled *cis*-BR and EPDM, demonstrated the presence of three distinct regions, characterized by different mobility of the rubber chains, i.e., a unbounded, mobile rubber region like gum, a bonded rubber in an outer shell around the carbon black, suffering some loss in mobility, and an inner shell of tightly bonded rubber with very limited mobility.

More recently, Haidar [39,40], based on the study of the effect of static strain on the dynamic modulus, suggested that the segmental mobility of the polymer on the filler surface was diminished and that the polymer at this point had glassy characteristics.

Although there is sufficient evidence to show the existence of a rubber shell on filler surface, considerable disagreement exists with regard to the thickness or volume of this shell. Kraus and coworkers [41,42], for instance, concluded from their investigation of Tg and the coefficient of expansion of the filled rubber that the segmental motion of the rubber was not severely

restricted over a substantial distance from the filler surface.

Obviously, there is no boundary between the rubber shell and the unbonded mobile region. Since the force field of the filler decreases rapidly with increasing distance from the filler surface, the restriction of segmental motion of the rubber molecules should also decrease with increasing distance from the filler surface. The different values for the thickness of the rubber shell given in the literature are, therefore, related to the criterion applied for the mobility of the rubber segments, the precision of the test method, the physical chemistry of the filler surface and the polymer concerned.

Although bound rubber and rubber shell are both related to polymer-filler interaction, they represent different concepts. Bound rubber refers to the whole molecule in which one or several segments are in contact with the filler surface, and to the whole molecule entangled with other molecules which are attached to the filler. The pre-condition for the rubber molecule being bound rubber is that the adsorptive attachments cannot be separated and that entanglements cannot be solvated during solvation of the rubber compound. In the case of the rubber shell, the definition is related to the change of segmental mobility of the rubber molecules. The segments, rather than the molecules, whose motion is affected by the force field of the filler, constitute the rubber shell, whether they satisfy the necessary conditions for bound rubber formation (contact or entanglement) or not.

Since the rubber shell has its origin in the restriction of the segmental motion of rubber molecules near the filler surface, it should also show a strong dependence on the experimental

temperature and the rate of strain to which the rubber is subjected. At high frequencies of the dynamic strain, the rubber shell may be harder and decrease rapidly with increasing temperature. Therefore, when estimating the thickness of the rubber shell, the measurement conditions should be taken into consideration.

9.1.2. Occlusion of Rubber

The effect of filler structure on the rubber properties of filled rubber has been explained by the occlusion of rubber by filler aggregates. In 1970, Medalia [43] proposed that, when structured carbon blacks are dispersed in rubber, the polymer portion filling the internal void of the carbon black aggregates, or the polymer portion located within the irregular contours of the aggregates, is unable to participate fully in the macrodeformation. The partial immobilization in the form of occluded rubber causes this portion of rubber to behave like the filler rather than like the polymer matrix. Due to this phenomenon, the effective volume of the filler, with regard to the stress-strain behavior of the filled rubber, is increased considerably.

The occlusion of rubber is a geometrical concept. As pointed out by Medalia [43,44], its quantitative representation is quite difficult since most aggregates do not contain any significant volume of three-dimensional ink

bottle-like concavities. The definition of occluded rubber therefore depends on what is meant by within the aggregates. Conceptually, the occluded rubber could be defined as the rubber contained within the convex hull surrounding the aggregate, but it is difficult to estimate in three dimensions from electron micrographs. For practical purposes, Medalia defined the occluded rubber as the rubber within a sphere of the same projected area as the aggregate, i.e., the volume of occluded rubber within an aggregate, *Vocc,* was defined geometrically as the difference between the volume of this equivalent sphere, *Ves,* and the solid volume of the aggregate, *Va. Ves* can be measured directly on electron micrographs. *Va* can also be estimated from electron micrographs by means of floc simulation of the aggregate by primary particles. Based on the quantitative treatment of the so-called soft ball DBP absorption, in which the void volume filled almost completely with DBP consists of the void volume within equivalent spheres, related to the projected area of the aggregate as measured in electron microscope, and the void volume between the spheres in a closely-packed state, Medalia proposed the following equation to calculate the occluded rubber:

$$\phi' = \phi \left(\frac{1 + 0.02139 DBPA}{1.46} \right) \tag{2}$$

where ϕ' is the volume fraction of filler plus occluded rubber, and ϕ is the volume fraction of the filler. The volume ratio between occluded rubber and carbon black is given by

$$\frac{V_{occ}}{V_a} = \frac{\phi' - \phi}{\phi} = \frac{DBPA - 21.5}{68.26} \tag{3}$$

Using the occluded rubber concept, Kraus [45,46] investigated the effect of carbon black structure on modulus of SBR vulcanizates and proposed a so-called carbon black Structure-Concentration Equivalence principle. He applied it to the strength properties of vulcanizates filled with carbon blacks having the same surface areas, but different structure. Assuming that the effective filler concentration includes the internal void volume of the primary aggregate structure, and that this internal void volume in turn is proportional to the excess of the observed crushed DBPA (24M4 DBPA) value over the corresponding value of a structureless carbon black, Kraus proposed another equation to calculate the volume of occluded rubber:

$$\frac{V_{occ}}{V_a} = \frac{24M4DBPA - 31}{55} \qquad (4)$$

Simply by relating the endpoint of crushed DBP absorption to the void space within and between equivalent spheres of aggregates and assuming the

spheres to be packed at random, Wang, Wolff and Tan [23] obtained a similar equation but with different numerical constants:

$$\frac{V_{occ}}{V_a} = \frac{24M4DBPA - 33}{87.8} \quad (5)$$

The crushed DBPA values were used because they are more representative of the aggregate state in rubber.

Studies carried out by Medalia [47] and Sambrook [48] showed that the relative modulus, calculated by means of Guth-Gold equation, using ϕ' instead of ϕ, was higher than experimental values. Medalia believed that the occluded rubber was only partially immobilized and that its contribution was therefore only partially effective. In order to fit his experimental data, he introduced a so-called F factor, i.e., the occluded volume effectiveness factor. This factor is, of course, dependent on the basis used for the calculation of occluded rubber and on the rubber properties concerned which are related to different levels of strain and temperature.

9.1.3. Filler Networking

The filler aggregates in the polymer matrix have a tendency to associate to agglomerates, especially at high loadings, leading to chain-like filler structures or clusters. These are generally termed secondary structure or, in some cases, filler network, even though the latter is not comparable to the continuous polymer network structure. Although this phenomenon has been known for a long time, it was not until investigations of the dynamic properties of filled rubber were carried out that its role in rubber reinforcement was better understood. In 1950, Warring [49] observed that the

dynamic modulus E' decreases with increasing strain amplitude from a high plateau E'_o to a low plateau E'_∞ *. This phenomenon, later termed Payne effect, is unique to filled rubber, and the difference $(E'_o - E'_\infty)$, or $\Delta E'$, increases exponentially with increases in filler loading. A simple explanation for this phenomenon is that the network structure formed by carbon black aggregates is destroyed at high dynamic strain amplitude. Although a number of objections to this explanation were raised, there is no doubt that a secondary network structure of carbon blacks exists.

In their studies of the dynamic mechanical properties on carbon-black-filled vulcanizates, Gerspacher and coworkers [50,51] used a shift factor for the Cole-Cole plot to characterize the networking of carbon blacks. They

* In the literature of rubber science and technology, the elastic and viscous modulus are generally denoted with E' and E'' for extension and compression strain and G' and G'' for shear strain. The discussion of E' and E'' in this chapter is generally valid for G' and G'' and *vice versa*.

also used the same method as that Fritzgerald used [52] to measure network cohesion energy. The investigation of various carbon blacks showed that the network cohesion energy is related to the specific surface area of the carbon black, i.e., the higher the surface area of the carbon black, the higher is the cohesion energy.

Measuring the dynamic properties of filled rubber under static strain, Voet and Morawski [53] reported a decrease in elastic modulus for HAF loaded SBR, followed by a pronounced increase with increasing static strain. They attributed the decrease in E' with increasing strain at low deformations to the disintegration of the filler network.

Wolff and Donnet [54] studied the stress-strain behavior of vulcanizates filled with carbon blacks and silicas, respectively, and observed a decrease in the effective factor, which converts the actual volume fraction into the effective volume fraction, at low strain. This effect was also interpreted as being caused by a breakdown of the secondary filler network.

Based on their evaluation of the electrical properties of dynamically [55] and statically [56] strained carbon-black-filled vulcanizates, Voet and coworkers confirmed the formation of carbon black network in unstrained vulcanizates. These results were in agreement with mechanically dynamic and static properties, showing that carbon blacks with smaller particles and higher structure had a greater tendency to undergo filler networking.

There is still no experimental evidence which shows how the secondary filler network is constructed, i.e., whether it is formed by

direct contact between filler aggregates or via a layer of immobilized rubber on the filler surface.

For silicas, which are poorly compatible with hydrocarbon rubbers, it can be assumed that agglomeration between aggregates occurs through direct contact by means of hydrogen bonding [57]. In the case of filler well wetted by rubber, e.g., carbon blacks in hydrocarbon rubber systems, the filler network might be formed by a joint shell mechanism.

The formation of filler network is, of course, dependent on the intensity of interaggregate attractive potential and the distance between aggregates. Assuming that only van der Waals force exists between the particles and that the shape of a carbon black particle lies statistically between a cube and a sphere, Van den Tempel [58] proposed that average interaction energy between particles of various shapes and orientations, ΔF, is given by

$$\Delta F = \frac{AD^{1.5}}{12H^{1.5}} \quad (6)$$

and that the attractive force between consecutive particles in a chain is given by

$$Force = -\frac{AD^{1.5}}{8H^{2.5}} \quad (7)$$

where D is average particle diameter, H average distance between two particles, and A a constant which depends on the polarizabilities of the atoms present. The equations show that the smaller the distance between the particles and the greater the particle diameter, the higher is the attractive force.

It should be noted that the formation of filler network depends not only on interparticle interaction, but to a considerable extent also on polymer-filler interaction. In other words, if filler-filler interaction remains constant, the filler networking would be impeded as filler-polymer interaction increases. Therefore, taking both filler-filler and filler-polymer interaction into consideration, Wang, Wolff and Donnet [59] proposed a factor S to represent the tendency of the filler to undergo networking in hydrocarbon rubbers. This factor is related to the ratio between filler-filler interaction and filler-polymer interaction, and can be determined by means of inverse gas chromatography at infinite dilution (see Chapter 6). If the distance between aggregates is constant, a high value of S would be equivalent to easy formation of filler network in hydrocarbon rubbers. Wang et al [59] found that the values of S for the adsorption of acetonitrile on carbon blacks were mostly in the same range, with slightly higher values for large-particle carbon blacks.

Based on the arrangement of equivalent spheres and the concept of occluded rubber, Wang, Wolff and Tan [23] obtained an equation for the calculation of the interaggregate distance, $\delta aa,$ which is another important factor governing filler networking:

$$\delta aa = [k\phi_{-1/3}\beta_{-1/3} - 1]da \quad (8)$$

or

$$\delta_{aa} = \frac{6000}{\rho S}[k\phi^{-1/3}\beta^{-1/3} - 1]\beta^{1.43} \qquad (9)$$

where ϕ is the volume fraction of carbon black, da the projected equivalent of the aggregate diameter, ρ the density of the filler, S the specific surface area, and k a constant which is dependent on the arrangement of aggregates in the polymer matrix. For a cubic arrangement, k is 0.806, and for face-centered cubic arrangement, k is 0.905. In this equation, β is an expansion factor which is defined as the effective volume of the filler divided by the solid volume of the aggregates. It can be calculated from Equations 3, 4, or 5. Equation 9 shows that the distance between aggregates, at given loadings, decreases with decreasing aggregate size or increasing surface area. On the other hand, the filler structure influences the interaggregate distance through the factor β.

One of the consequences of filler networking is that the rubber trapped in the filler agglomerates, or secondary structure, is largely immobilized in the sense that this rubber portion is shielded from deformation under stress. Of course, the effect of networking is highly dependent on strain and temperature. At moderate and high strain, most of the agglomerates are broken down

and the rubber trapped in the agglomerates acts as the polymer matrix. On the other hand, rising temperature weakens interaggregate interaction and reduces the modulus of the rubber shell. Consequently, filler agglomeration would be expected to be low.

9.2 The Properties of Uncured Compounds

The properties of uncured rubber, especially their rheological behavior, are highly important from a manufacturer's point of view. They are associated with the visco-elastic response of the rubber compounds and are affected noticeably by the incorporation of carbon blacks.

9.2.1. Compound Viscosity

While the unfilled compounds generally undergo Newtonian flow at low shear rates, carbon blacks are known to alter the rheological behavior of the compounds, resulting not only in highly non-Newtonian flow, but also in comparatively high viscosity (Fig. 3) [60]. Several factors are responsible for this:

Firstly, the hydrodynamic effect of carbon black loading reduces the volume fraction of the flow medium and causes a shear strain amplification of the polymer matrix, thus increasing the viscosity of the filled compounds.

Secondly, the structure of the carbon blacks, which is associated with the anisometry of the filler aggregates and the occluded flow medium, plays a very important role in compound viscosity. In contrast to spherical particles, the anisometric aggregates increase the flow resistance [61]. The occlusion of
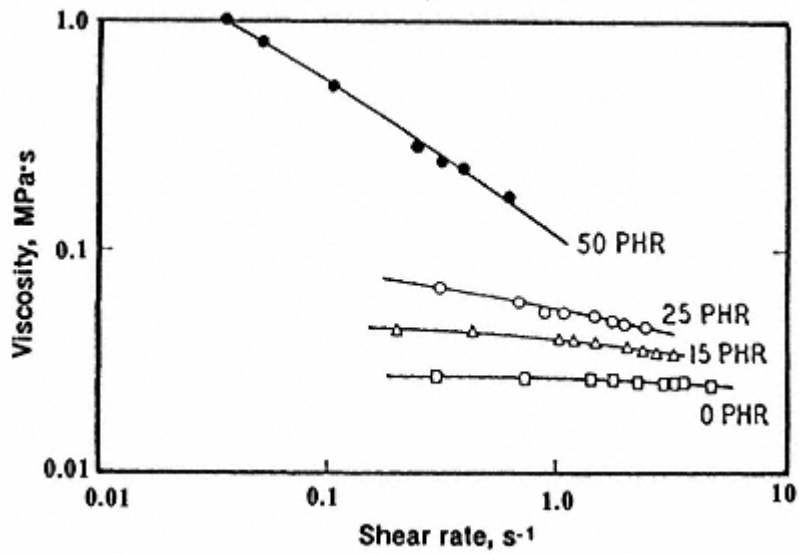
Fig. 3.
The viscosities vs. shear rates for SBR compounds filled with
different loadings of N220 (from ref. [60]).

rubber within the aggregates, in turn, greatly increases the effective hydrodynamic volume of the carbon blacks. Consequently, high-structure carbon blacks always lead to higher compound viscosity [62]. In fact, Kraus, using SBR filled with 50 phr of different carbon blacks with specific surface areas ranging from 14 to 164 m2/g, found an empirical correlation between Mooney viscosity and structure as measured by compressed DBP absorption [63].

Another factor which is related to the addition of carbon blacks and which influences compound viscosity is the adsorption of rubber molecules on the filler surface. This effect is quite complex. The adsorbed rubber surrounding the carbon black surface, which can either be treated as a shell of immobilized rubber [3032] or as bound rubber [64], was used as the filler volume in order to calculate compound viscosity. Irrespective of the details of molecular adsorption, this approach seems sensible since once a segment is anchored on the filler surface, the movement of the whole molecule in the flow field should be restricted. Although this reflection is rendered somewhat more complicated by the reduction in molecular weight of the free rubber phase in the matrix, as large molecules are adsorbed preferentially [65], this adsorption process may help to explain the increase in viscosity with decreasing particle size. At the same loading, the larger interfacial area per unit volume of compound and the strong polymer-filler interaction caused by the higher surface energy of small-particle carbon blacks should result in a greater amount of adsorbed rubber [21]. This can be confirmed by the deactivation of carbon blacks. Both the graphitization of blacks by heating [66,67] and their surface modification by alkylation [68] lead to a considerable reduction in their capacity for rubber adsorption, and hence to a drastic decrease

in compound viscosity. On the other hand, as indicated in the above discussion of bound rubber per unit surface (see Section 9.1.1.), the smaller distance between aggregates for the finer carbon blacks should lead to multi-attachment between aggregates. Such a three-dimensional structure could contribute to the higher viscosity of compounds filled with small-particle carbon blacks.

Moreover, networking of carbon blacks, i.e., the formation of an interaggregate structure, is one of the reasons for the high viscosity of the filled compounds and the major source of the highly non-Newtonian and thixotropic behavior. At increasing shear rates and/or shear strain, the interaggregate network is gradually destroyed and viscosity decreases (Fig. 3). This effect is more pronounced for higher loadings and finer particle blacks, both of which affect networking. With two model fillers, a carbon black and a silica having comparable surface areas and structures, Wolff and Wang [69] were able to demonstrate the effect of networking on the viscosity of filled NR. The much more rapid increase in Mooney viscosity and minimum rheometer torque with increasing loadings for the silica, in comparison to carbon-black-loaded rubber, was attributed to its more rapid development of a filler network. This is

due to greater tendency of filler networking in the case of the silicas, which is related to their higher value for *S*.

9.2.2. Die Swell

In practice, the elastic response of rubber compounds is reflected in their processing behavior in terms of die swell (extrusion shrinkage) and surface roughness of the extrudate.

Die swell is defined as the ratio between the area of the cross-section of the extrudate and that of the die and is generally greater than unity. This phenomenon, which is associated with elastic recovery, is caused by the incomplete release of long-chain molecules oriented by shear in the die (or capillary) and occurs in the rubber phase alone [70]. It is therefore obvious, that, besides the test conditions such as temperature, extrusion rate and geometrical features of the die, the primary factor influencing the die swell of unfilled elastomers is the entanglement of elastomer molecules, which, in turn, is determined by their molecular weight and molecular weight distribution. The die swell is improved by the addition of carbon blacks, due to the reduction of the elastic component of the compound and the decrease in effective relaxation time [71]. Fig. 4 illustrates the effect of HAF loading and naphthenic oil on the die swell of SBR compounds [72]. It shows that the filler concentration is much more important than the processing oil, particularly for highly loaded compounds. Simply by normalizing the die swell with the rubber volume fraction of SBR filled with MT black, Cotten [73] was able to superimpose all data at different shear stresses onto a single master curve
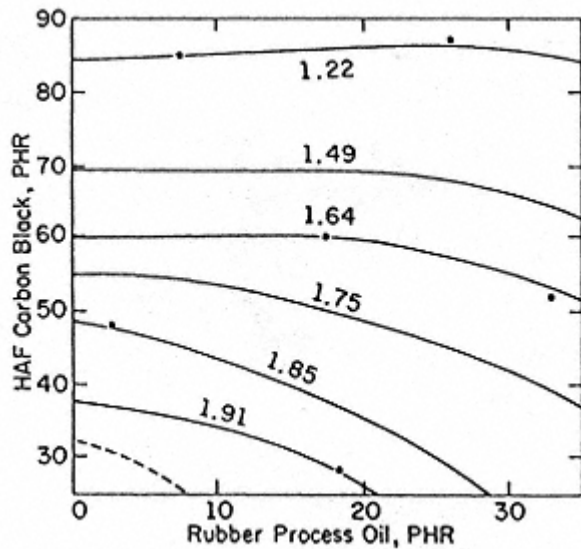
Fig. 4.
Effects of oil and black on extrudate
swelling at 100° C, 286.7 sec-1 and L/D of
22.41 (from ref [72]).
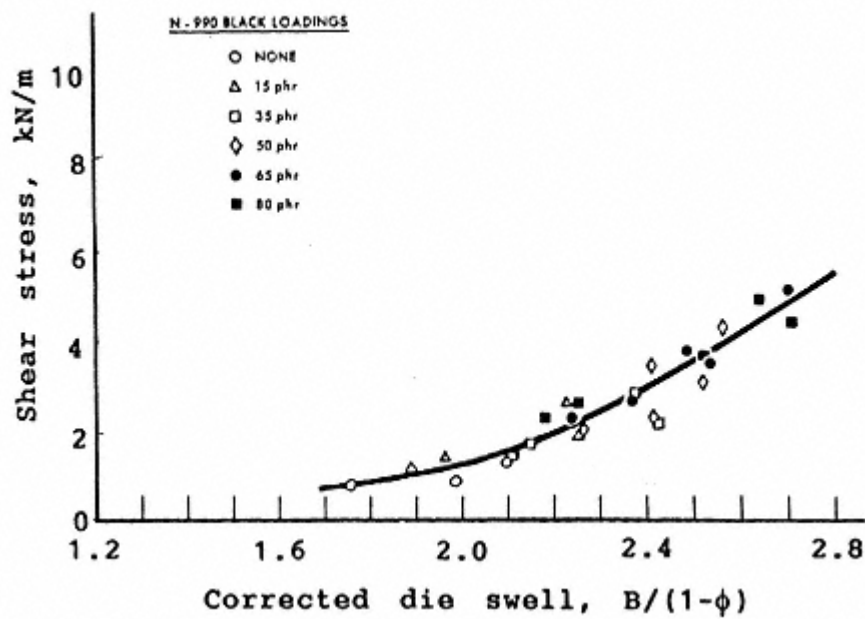
Fig. 5.
Die swell of SBR filled with MT black at 120°C, normalized
with the rubber volume fraction (from ref. [73]).

(Fig. 5). The die swell data of reinforcing blacks can also be
brought to coincide with a single master curve when the filler
volume is replaced by the effective volume calculated from rubber
occlusion for filler loadings up to 35 phr [43] (Fig. 6). This implies
that the rubber occluded within the aggregates
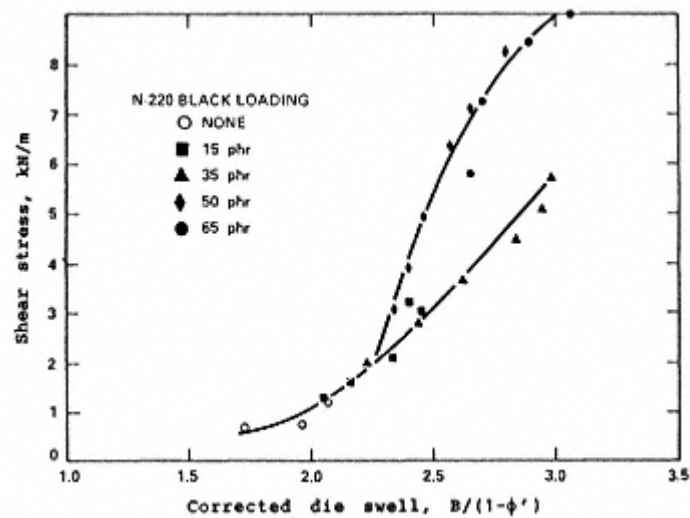
Fig. 6.
Die swell of SBR 1500 with N220 black at 120° C,
corrected for volume of equivalent spheres (from ref.
[43]).

is dead in terms of elastic memory. This correction is valid for carbon blacks with low-, normal-, and high-structure ranging from soft to hard grades [43]. Since the correction was only carried out with DBP absorption, it is apparent that, among the fundamental properties of carbon blacks, their structure is the main parameter contributing to die swell, and the effect of surface area seems to be insignificant. Indeed, the die swell of filled compounds has been adopted as a measure of carbon black structure [74]. The fact that the die swell is lower than expected from the correction for occluded rubber above loadings of 35 phr (Fig. 6) has been attributed to interaggregate interaction, in which the anisometry of the aggregates would be expected to play an important part and where the simple equivalent sphere model, from which the occluded rubber is calculated, would not be applicable, as pointed out by Medalia [43]. The occluded rubber not being totally dead, and hence not acting as a non-elastic filler, may be another reason for the small reduction in die swell, particularly at high shear stress.

Above a certain shear stress, termed critical stress, the extrudate will be distorted, resulting in a rough surface. This is another phenomenon which is related to the elastic behavior of the rubber compound. The distortion of the extrudate increases with increasing stress and may, in some cases, even lead to the complete fracture of the extrudate. The effect of the HAF carbon black and processing (naphthenic) oil on the melt fracture of SBR compounds is illustrated in Fig. 7 by a contour diagram [72]. The compound with the
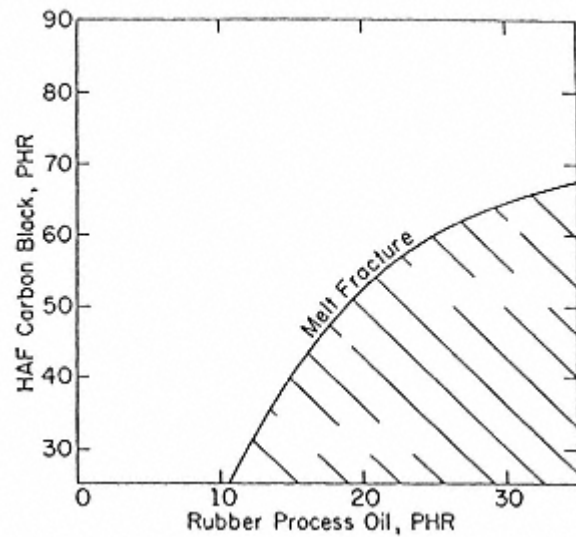
Fig. 7.
Effects of black and oil on extrudate surface
roughness of SBR compound at 100° C and
286.7 sec-1 (from ref. [72]).

highest carbon black loading and the least amount of oil yields the best appearance of the extrudate surface. As the shear rate increase, the boundary of the fracture region shifts toward the upper left-hand corner.

9.2.3. α

When a carbon black is incorporated into a compound, the maximum change in curometer torque during vulcanization increases. The ratio between the torque increase of the loaded compound, *Dmax - Dmin,* and that of the gum, $D^o_{max} - D^o_{min}$, was found to be directly proportional to filler loading. The slope of the linear plot showing the relative torque increase as a function of filler concentration was defined by Wolff [75,76] as α:

$$\frac{D_{max} - D_{min}}{D^o_{max} - D^o_{min}} - 1 = \alpha_f \frac{m_F}{m_P} \quad (10)$$

where *mP* is the mass of the polymer in the compound, and *mF* is the mass of the filler in the compound.

It was found that α of all furnace blacks is independent of the type of cure system used. Changes in primary particle size or surface area have no influence on α. Its value only depends on carbon black structure. It can therefore be concluded that α is a measure of the in-rubber structure of carbon blacks, i.e., the remaining structure after mixing. This was confirmed by graphitization of the carbon blacks. Boonstra [77] showed that α is one of the properties that change very little after deactivation of the carbon black surface by graphitization because the structure cannot change significantly during heat treatment.

More recently, Wolff and coworker [69] applied α to demonstrate the existence of a strong secondary structure in vulcanizates filled with precipitated silica. They found that a silica having almost the same surface area and structure as a reference carbon black showed a much higher value for α. Moreover, whereas α is independent of carbon black loading, it increases with silica concentration (Fig. 8). This suggests that, due to the high S value of the silica (3.58 and 1.64 for acetonitrile adsorption for Ultrasil VN2 and N110, respectively), the secondary structure formed by the silica is so strong that it cannot be destroyed by oscillating shear strain in the curometer. The increase in α with loading can, therefore, be attributed to the decrease in interaggregate distance, yielding a more developed secondary network. Evidence supporting this interpretation can be obtained by surface modification of silicas. When the high specific component of surface energy is shielded by long alkane chain grafts, α decreases drastically and no longer shows a concentration dependence [78]. This implies that the silica network no longer exists at this point.

The above discussion seems to suggest that no secondary network is
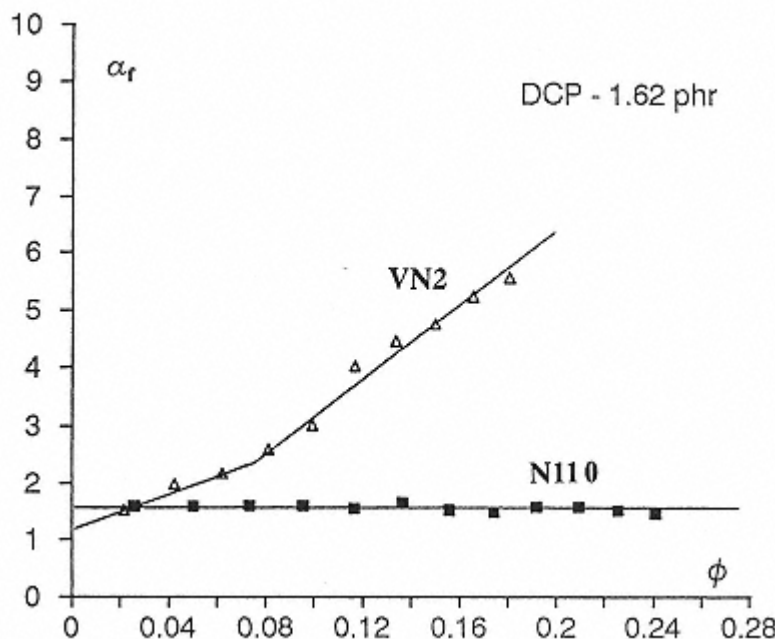
Fig. 8.
α of carbon black N110 and precipitated silica filled
compound vs. the filler loadings (from ref. [69]).

formed in carbon black filled materials. This contradicts a widely
accepted view which was discussed previously (see Section 9.1.3.).
Perhaps the carbon black network is so weak, as suggested by the
low values of S, that it is destroyed by shear deformation. This
would be understandable since an angular movement of the rotor in
the Oscillating Disc Rheometer of 3° is equivalent to
approximately 20% strain [74]. In this region of strain, most of the
carbon black agglomerates may no longer exist, especially when
comparatively high temperatures (150°C) are involved.

It is, therefore, obvious that α is indeed a measure of in-rubber
filler structure. In the case of a low S, i.e., a weak filler network,
such as that observed in carbon-black-filled rubber, it reflects the
structure of individual aggregates. When strong agglomerates are

formed, the existing secondary network should also affect the value of α. Investigations of the change in α thus yield information concerning the strength of the filler network.

9.3. The Properties of Filled Vulcanizates

It is necessary to discuss the effects of carbon blacks on individual rubber properties since each property of the filled rubber involves different molecular processes. The effects of the carbon blacks can, therefore, not be generalized.

9.3.1. Swelling

Whereas uncrosslinked rubber can be dissolved in a good solvent, vulcanized rubber can only be swollen in a solvent to an extent determined by crosslink density and the nature of the solvent. After incorporation of the filler, the volume fraction of the filled rubber in the swollen gel, Vrf (corrected for the filler volume, since the filler is assumed not to swell in the solvent), should differ from that of the pure gum, Vro. In the case of reinforcing fillers, the strong interaction caused by strong physical and/or chemical adsorption may have the same effect as crosslinks in the composites. The ratio Vro/Vrf should thus decrease with increases in filler loading. On the other hand, the addition of a filler may change the crosslink density in the polymer matrix, since it affects the vulcanization reaction. For cases where the crosslink density of the matrix is independent of the presence of a filler, e.g., peroxide-cured natural rubber [79,80], Kraus [81] derived the following expression relating the ratio Vro/Vrf to filler loading

$$\frac{V_{ro}}{V_{rf}} = \frac{1 - V_{ro}\phi}{1 - \phi} \quad \text{(for non-adhering filler)}$$

(for non-adhering filler) (11)

and

$$\frac{V_{ro}}{V_{rf}} = 1 - \frac{m\phi}{1 - \phi} \quad \text{(for adhering filler)}$$

(for adhering filler) (12)

with

$$m = 3C(1 - V_{ro}^{1/3}) + V_{ro} - 1 \quad (13)$$

where C is a characteristic parameter of the filler and related to filler-polymer interaction. Higher values of C suggest stronger

interaction between filler and rubber matrix.

In addition, the swelling of filled vulcanizates is also dependent on filler structure. In other words, C is a structure-related parameter. Rigbi and Boonstra [82] have shown that a high filler structure leads to a considerable restriction of swelling. Besides, the secondary structure of filler also exerts a considerable restraint on swelling. This has been demonstrated by a comparison of swelling of vulcanizates filled with carbon black and silica, respectively, both having comparable surface areas and structures. It was found that, although filler-polymer interaction was much higher for the carbon black, C was higher for the silica-filled vulcanizates. This suggests that the secondary structure formed by strong silica interaggregate interaction may still exist, at least partially, in swollen vulcanizates, and may play an important role in reducing swelling [69].

9.3.2. Stress-Strain Behavior

Low Strain

The main change in the stress-strain behavior of rubber due to the incorporation of carbon blacks is observed with regard to stiffness which is scaled with the modulus, i.e., the ratio between stress and strain. (In rubber technology, for the quasi-static measurement, it is customary to refer to the stress at a specified strain as modulus. This stress is always calculated on the basis of the original cross-sectional area.) The modulus of carbon-black-filled rubber, whether measured in shear, compression or extension, under static or dynamic conditions, is considerably higher than that of the pure gum. The first attempt at a theoretical description of the increase in modulus caused by the filler was made by Smallwood [83] and Guth [84]. Using Einstein's viscosity equation as modified by Guth and Gold [85,86], which takes into account the mutual disturbance caused by spheres at high concentration, they proposed the following equation for Young's modulus:

$$E = E_o(1 + 2.5\phi + 14.1\phi 2) \quad (14)$$

where E and E_o are Young's moduli of the filled rubber and of the gum, respectively. Several authors proposed different values for the coefficient of the second term [87]. Other analytical equations were also proposed [8891]. Kraus compared these equations for modulus and found that they deviated considerably from each other at high filler loadings.

However, all of the above equations are inadequate for reinforcing fillers, especially at filler loadings commonly used in practice, since they are based on the same assumptions as Einstein's

equation, i.e., spherical particles, well wetted particles, low strain, perfect dispersion, negligible particle-particle interaction, and no effect on the characteristics of the polymer.

In practice, it is extremely difficult to satisfy these conditions because (a) most carbon black aggregates depart considerably from the spherical shape, and (b) the mobility of the rubber matrix is not uniform due to different filler-polymer interaction. Furthermore, particle-particle interaction enables the particle to agglomerate, which affects the uniformity and continuity of the polymer matrix. So far, the applicability of Equation 14 has been limited to almost structure-less, very-large-particle carbon blacks (MT/FT) [92,93] and filler concentrations of ϕ smaller than 0.2.

Considering the asymmetry of fillers for the purpose of practical applications, Guth [94] later proposed another equation for rod-shaped particles:

$$E = Eo(1 + 0.67\phi + 1.622\phi2) \tag{15}$$

where is the shape factor. When Mullins and coworkers [93] applied this equation to calculate the strain amplification of the polymer matrix for an

HAF-filled compound, it was found that the best fit with the experimental data was obtained when had a value of 6.7. Meinecke [95] found a value for of 4.7 for HAF in SBR. Medalia [47], on the other hand, used electron microscopy in his investigation of HAF blacks and obtained values between 1.7 and 1.9. This was confirmed by Hess [96]. Ravey et al [97], in their investigations using light scattering, obtained values between 1.8 and 2.2 for the range of ultra-low-structure to high-structure HAF carbon blacks. The applicability of Equation 15 and the significance of the shape factor for reinforcing fillers are therefore doubtful.

Considering the effect of filler structure on modulus, Medalia [47] replaced ϕ in Equation 14 by the effective volume fraction of the filler, ϕe:

$$E = E_0(1 + 2.5\phi_{eff} + 14.1\phi_{eff}^2) \quad (16)$$

He believed that ϕe was related to the occlusion of rubber [98].

Wolff and Donnet [54,99] recently investigated the extension modulus of SBR compounds filled with a series of carbon blacks chosen at random. They also used the effective volume by introducing a factor which converts the filler volume fraction into an effective volume fraction, i.e.,

$$f\phi = \phi'_{eff} \quad (17)$$

They found that the experimental data could be fitted to the Guth-Gold equation for a wide range of quasi-static tensile strains and filler concentrations, even though this is not justified by the original theory. The original theory is limited to very low levels of strain where the stress-strain behavior is linear. When this concept

was applied to the dynamic storage modulus in extension, *E'*, at low strain, Tan and coworkers [23,100] found that, for filled SBR vulcanizates, a better fit can be achieved at medium loadings for most carbon blacks. Above a certain filler concentration, which is defined as the critical loading, $\phi_{crit.}^{E'}$, deviations occur, since the experimental data are higher than expected from the modified Guth-Gold equation. It was found that the factor and the critical loading $\phi_{crit.}^{E'}$ are characteristic parameters for each carbon black.

Since the factor is related to the effective volume of the carbon black in the rubber matrix, all factors which influence the strain of the polymer under stress will have a determining effect on the value of . As mentioned in Section 9.1.2, Medalia [47] related the effective volume to the occlusion of rubber and believed that only part of the occluded rubber calculated from Equation 3 could be effectively shielded from bulk deformation. For TMTD-cured SBR filled with different grades of carbon blacks, an effectiveness factor 0.5 was introduced empirically to fit the experimental data of low-strain equilibrium modulus. Another factor influencing the effective volume, as calculated on

the basis of rubber occlusion, is the breakdown of the aggregates during mixing, which reduces the volume of occluded rubber. It was found that the effectiveness factor achieving the best fit of the dynamic modulus to the volume of occluded rubber calculated from Equation 5 is higher than the value calculated from Equation 3 (0.70 *vs* 0.32) [23]. This is probably due to the fact that in the former equation the occluded rubber is calculated on the basis of compressed DBP absorption which may be more representative of the structure of carbon blacks in vulcanizates. In Fig. 9, the effective factor is plotted as a function of compressed DBPA, and the straight line represents the values calculated from Equation 5 with an effectiveness factor of 0.70. Although the effectiveness factors are, to a large extent, determined by the occlusion of rubber, significant deviations are observed. In contrast to the large-particle carbon blacks, the systematically higher -values of small-particle carbon blacks may be associated with their higher surface energies. This would result in stronger polymer-filler interaction or a more developed rubber shell, giving rise to an increased effective volume of the fillers.

The deviation of the low-strain modulus from the modified Guth-Gold equation above the critical loading suggests that, besides the factors taken into account by the modified Guth-Gold equation, such as hydrodynamic effects, the occlusion of rubber, and the immobilization of the rubber molecules on the filler surface, additional effects of the filler come into play. The critical loading is highly dependent on the carbon black grade, which suggests that
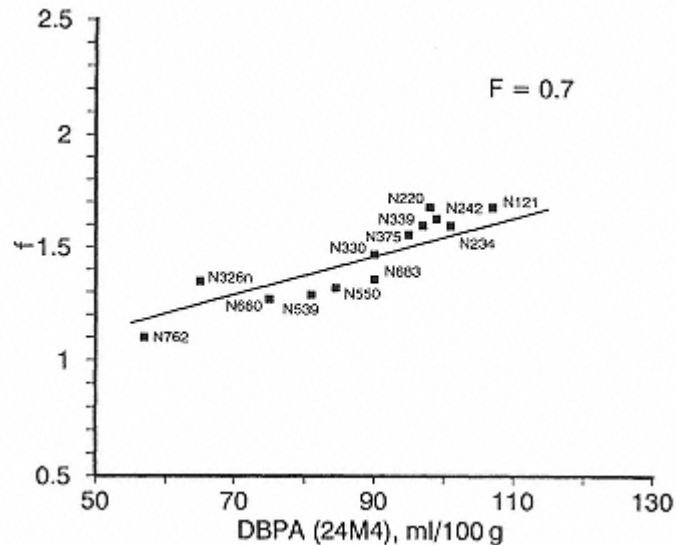
Fig. 9.
Effective factor vs. DBPA(24M4) for carbon
black filled SBR. The straight line is calculated
from Equation 5 with an effectiveness factor of
0.7 (from ref [23]).

small-particle blacks have a lower $\phi_{crit.}^{E'}$. It is believed that, in addition to the considerable strain amplification of the polymer matrix at high loading, resulting in non-affine deformation of the polymer chains, the high modulus is mainly related to filler networking and hence a greater amount of rubber trapped within agglomerates [23]. This leads to a marked increase in the effective volume. As indicated above, the formation of the secondary network is governed by the specific interaction and the distance between aggregates. Since S of all carbon blacks, i.e., the ability of the fillers to agglomerate, is almost constant, with a tendency toward slightly higher values for the soft carbon blacks, the interaggregate distance is the primary factor affecting networking. In fact, the interaggregate distance at $\phi_{crit.}^{E'}$ is, to a first approximation, the same for all rubber-grade carbon blacks, with slightly higher values for the soft grades [23].

Medium and High Strains - The Strain Dependence of Modulus

It is well known that a linear stress-strain behavior of unfilled vulcanizates can be achieved in a certain limitation of the strain. However, when carbon blacks are added, non-linearity occurs at very low strain. The decrease in modulus which occurs when the strain is increased from as little as 1% to intermediate level was studied extensively by Payne after whom the effect is often named [101,102]. It is generally believed that this effect is related to interaggregate interaction. The breakdown of an agglomerate network (or secondary structure) should release trapped rubber, thus reducing the apparent filler volume. The existence of such a mechanism has also been demonstrated by Wolff et al [69] for NR vulcanizates having the same crosslink density, but filled with

different fillers. Using the carbon black N110 and the silica ULTRASIL VN 2, both of which are comparable in particle size (or surface area) and structure, they were able to show in dynamic measurements that the silica-filled rubber, as compared to the one filled with carbon black, gave a much higher modulus at very low strain, and that the elastic modulus started to decrease at higher strain amplitudes. They attributed this to the existence of a more developed and stronger silica network in the vulcanizates. Moreover, once the modulus started to decrease with increasing strain, the decrease occurred more rapidly for the silica than for the carbon black, suggesting a more rapid destruction of the silica network beyond a certain level of deformation. The difference in Payne Effect for these two types of fillers was related to their surface energy characteristics which are illustrated schematically in Fig. 10.

In a systematic study of the effect of carbon blacks on stress-strain behavior, Wolff and Donnet [54] investigated the applicability of the Guth-Gold equation to the non-equilibrium tensile modulus for the first stretch of the stress/strain curve. For all carbon-black-loaded NR compounds, the factors, as defined by Equation 17, first decrease with increasing deformation
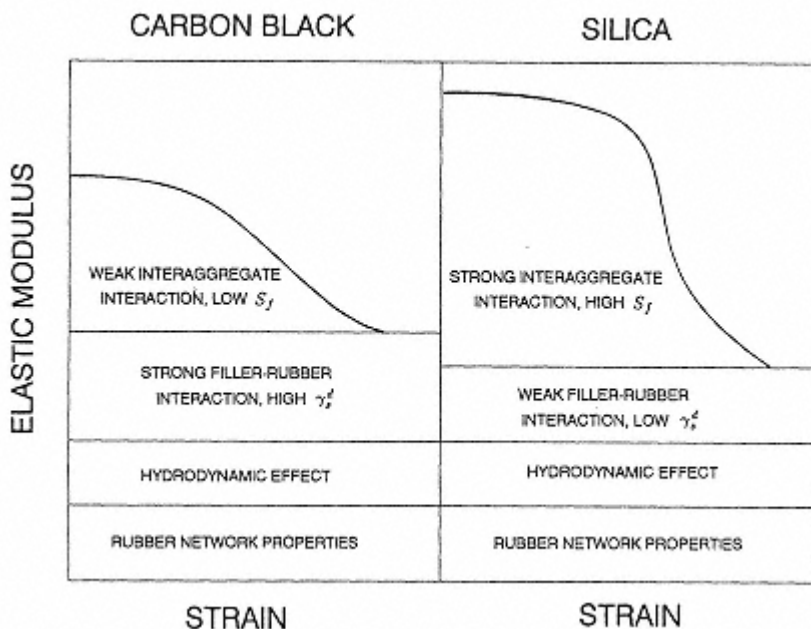
Fig. 10.
Schematic illustration of the effect of filler surface energy on
elastic modulus.

and then increase at high strain, with a minimum min typically at λ $\approx$ 1.75. Whereas the low-strain behavior, as discussed above, is explained mainly by the destruction of the filler network, non-affine deformation (non-Gaussian behavior) of polymer chains and crystallization would be involved at high strain. This leads to an increase in stress at a given deformation, which is equivalent to an apparent rise in filler loading. This effect would be reduced by slippage and/or deattachment of the rubber molecules on the filler surface and, hence, would be related to polymer-filler interaction. Therefore, the slope of the linear section of versus strain, λ, which is defined as γE, is closely related to the surface activity of the fillers, in particular to the dispersive components of filler surface energy, as far as hydrocarbon elastomers are concerned. This was

shown not only for carbon blacks, but also for other types of fillers. The very low γE of silica can definitely be attributed to poor poymer-filler interaction, resulting from its low γ_s^d.

Fig. 11 shows the rate of decrease in at low strain and its rate of increase at high strain which diminishes with rising temperature. Although the lack of crystallizability of natural rubber at high temperatures can be attributed to the low value of at high elongations, the main factors are polymer-filler and interaggregate interaction which are highly dependent on temperature. The decrease in the gradient of the linear sections with rising temperature is a characteristic feature of the different fillers. Moreover, the
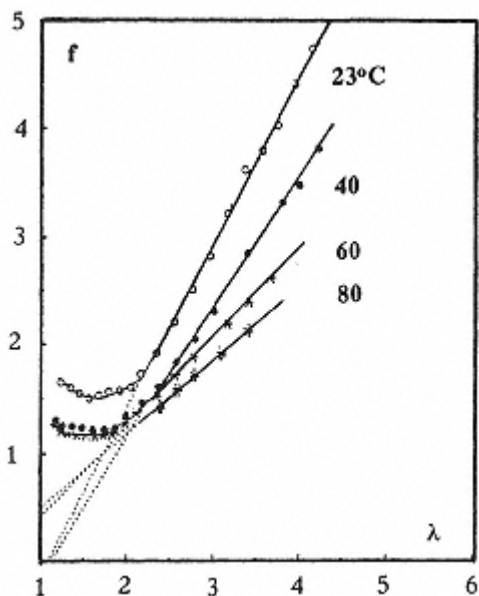
Fig. 11.
factor vs. extension strain at
different temperatures for N110 filled
NR (from ref. [99]).

pronounced decrease in *min* at elevated temperatures, where *min* tends to unity, suggests that all factors which increase the effective volume of the filler at medium strain, at which the secondary network is destroyed, have been eliminated. This is understandable since, on the one hand, the rubber shell would be drastically reduced, and on the other hand, the high mobility of the molecular chains and weak polymer-filler interaction, which is not strong enough to anchor the rubber on the filler surface, would noticeably diminish the occlusion of the rubber.

Recently, Kilian and coworkers [103,104] described the stress-strain behavior of filled vulcanizates using a new approach. They proposed that the filler aggregates are stabilized by filler-filler contacts and that the filler aggregates themselves are

multifunctionally bound to the polymer matrix. The filler-to-filler rubber chains are linked in parallel arrangement. When the filler aggregates are drawn apart, the strain energy is strongly dependent on the filler-to-filler chain length distribution. The shorter chains would store more strain energy. The filler-filler contacts operate as solid-body contacts which undergo yielding at the smallest strain. As illustrated by Dannenberg [105,106], they believed that at intermediate strain chain slippage is enforced. This filler-polymer yielding is controlled by the strength of filler-polymer adhesion. The slippage of filler-matrix contacts determines the slope of the stress-strain curve in the region of high strain. Combining this with the van der Waals model of a real network, they were able to describe the stress-strain curve quantitatively.

9.3.3. Effects of Carbon Blacks on Energy Loss in Vulcanizates

It is generally accepted that rubber reinforcement by fillers is closely related to processes of energy dissipation during deformation. The importance of energy dissipation in the fracturing of vulcanizates, such as ultimate strength, tearing, cracking, abrasion and fatigue, is also widely recognized. In practice, the energy loss in rubber products during dynamic strain is of great importance, as for instance in vibration mounts, springs, and particularly in automotive tires where it affects the service performance of the product with regard to heat generation, rolling resistance, traction, and skid.

Stress-Softening Effect

For all vulcanizates, whether filled or not, the stress required to attain a given elongation is less during the second cycle of deformation. This is the so-called Stress-Softening Effect or Mullins Effect [107,108] (Fig. 12). The incorporation of carbon black greatly enhances this effect. Several mechanisms have been proposed to address this phenomenon, including breakage of polymer network chains, and slippage of permanent entanglements along the chains toward crosslinking points. These occur in both filled and unfilled vulcanizates. As far as the filled rubber is concerned, the breakdown of the secondary filler network, and deattachment (dewetting) of rubber molecules from the filler surface, as well as the rupture of the short chains between filler particles have been considered to be responsible for the lower modulus of the successive stretches. Moreover, depending on strain rate and temperature, movement of the aggregate, rotationally and otherwise, would be another
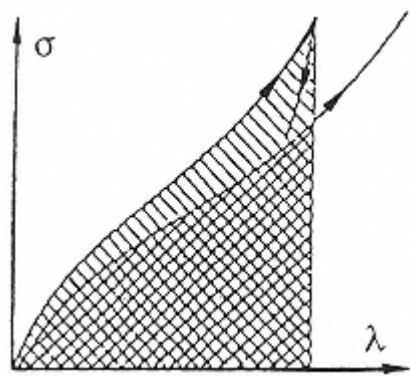
Fig. 12.
Stress-softening effect.

reason for the relief of excessive stress in localized areas. Since the second stress-strain curve coincides with the original one when the subsequent deformation exceeds the largest deformation of the first stretch, and since the stress of the softened vulcanizate can be recovered by heat treatment [109,110] or by swelling in a solvent [110], the breakage of the network chains seems to be of less importance in this regard. Therefore, the molecular slippage mechanism proposed by Dannenberg [105,106,110] and others [104,112] appears to be more appropriate. According to this concept, the sliding of elastomer segments across the filler interface is the major source of the softening, at least at medium and high strains. During the slippage process, the elastically stored energy is converted into heat (hysteresis) and the stress is redistributed to neighboring molecules, resulting in partial relief of most of the tension of highly stretched chains. A consequence of this mechanism is that the softening effect is dependent on interfacial area and polymer-filler interaction. The fact that, at the same loading, the small-particle carbon blacks show a more pronounced softening effect is clearly related to their large surface area, even though this should be more or less compensated by their higher polymer-carbon black interaction. When strong chemical linkages are introduced between polymer network and filler surface, the processes of molecular alignment, stress redistribution, and strain energy dissipation, which are caused by slippage, cannot occur, resulting in a lower softening effect. This has been demonstrated by the silica modified with a bifunctional silane. Compared to the nonmodified silica which exhibits weak filler-polymer interaction, the vulcanizates filled with modified silica and

containing covalent filler-polymer bonds show much lower stress softening [113].

Since molecular slippage is related to the dissipation of strain energy and to the stress uniformity of the polymer network, it is an important process which improves the fracture properties of the material. Polymer-filler interaction, in this regard, has to be strong enough to prevent dewetting from the filler surface, but should not be too strong either, so as to allow the adsorbed molecules a certain amount of mobility.

Energy Loss During Dynamic Strain

Mechanism of Energy Loss, Viscous Modulus, and tan δ: When an elastomer is subjected to periodically varying stress, strain will vary sinusoidally and out of phase, i.e., with the strain lagging behind the stress. Thus the strain, ε, and stress, σ, can be written as

$$\varepsilon = \varepsilon_o \sin wt \quad (18)$$

$$\sigma = \sigma_o \sin(wt + \delta) \quad (19)$$

where w is the radian frequency, t is time, δ is the delayed phase angle, and ε_o and σ_o are the maximum stress and maximum strain, respectively. The

strain can be subdivided further into different components, i.e., in phase and 90° out of phase, namely

$$\sigma = \sigma o \, sin \, wt \, cos\delta + \sigma o \, cos \, wt \, sin\delta \quad (20)$$

Therefore, the dynamic stress-strain behavior can be expressed by a modulus E', which is in phase with strain (or elastic modulus), and a modulus E'', which is 90° out of phase (or viscous modulus):

$$\sigma = \varepsilon o E' \, sin \, wt + \varepsilon o E'' \, cos \, wt \quad (21)$$

with

$$E' = (\sigma o/\varepsilon o) cos \, \delta \quad (22)$$

and

$$E'' = (\sigma o/\varepsilon o) sin \, \delta \quad (23)$$

These equations can be expressed by the complex modulus, E^*, as

$$E^* = \sigma o/\varepsilon o = E' + iE'' \quad (24)$$

and

$$\tan \delta = \frac{E''}{E'} \quad (25)$$

The imaginary part of the complex modulus, i.e., the viscous modulus, E'', is related to the lost energy and is also termed loss modulus. The energy loss during one cycle of strain, ΔE, is given by

$$\Delta E = \int \sigma \, d\epsilon = \int_0^{2\pi\omega} \frac{\sigma \, d\epsilon}{dt} dt \quad (26)$$

From Equations 18 and 21, one has

$$\Delta E = \omega \epsilon_o^2 \int_0^{2\pi/\omega} (E' \sin \omega t \cos \omega t + E'' \cos^2 \omega t) dt = \pi \epsilon_o^2 E''$$
(27)

and from the definitions of E'' and E^*, one has

$$\Delta E = \pi \sigma_o \epsilon_o \sin \delta \approx \pi \sigma_o \epsilon_o \tan \delta$$
(28)

or

$$\Delta E = \pi \sigma_o^2 E'' / (E'^2 + E''^2)$$
(29)

Equations 27, 28 and 29 are very useful for estimating the energy loss during dynamic strain, which, depending on whether $\varepsilon o, \sigma o$ or $\sigma o \varepsilon o$ is kept

constant during the dynamic deformation, corresponds to constant strain, constant stress or constant energy input, respectively. Thus, under constant strain, the energy loss is proportional to E'', while under conditions of constant energy input, the energy loss is related to tan δ.

It should be pointed out that, since the deformation of the vulcanizate during dynamic measurements usually does not exceed 25% and since the data are measured after several cycles of deformation or several preconditioning transients, the Mullins Effect, i.e., the difference between the first and second strain cycles, is of no consequence [114].

Fillers, when added, are known to cause a considerable increase not only in E', as discussed in the previous section, but also in E''. Since E'' is representative of the viscous component of the modulus, the Guth-Gold equation obtained from Einstein's viscosity equation can theoretically be applied to E''. On the other hand, both Einstein's and the Guth-Gold equation are based on hydrodynamic effects only, whereas E'' includes all processes of energy dissipation. It can therefore be argued that interaggregate interaction must be involved to a considerable extent in energy loss, which would be highly dependent on strain amplitude, filler concentration, and filler properties.
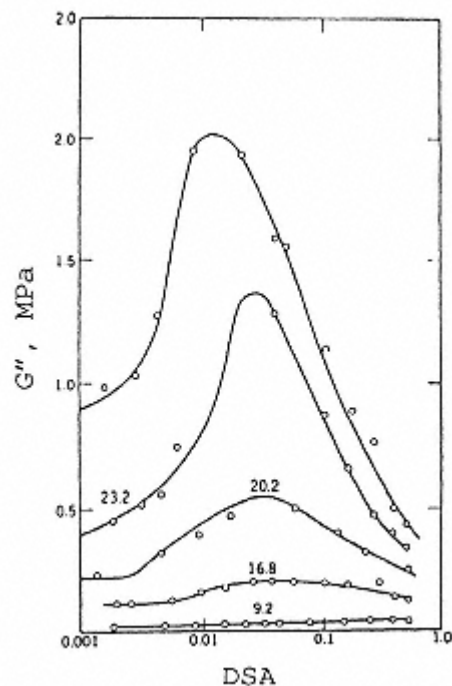
Fig. 13.
Loss shear modulus vs. double strain amplitude at 0.1 Hz for butyl rubber filled with various loading up to 28.8 vol.% HAF black (reproduced from ref. [102]).

Fig. 13 shows that the loss modulus of filled rubber, G'', measured under dynamic shear strain, passes through a maximum, G''_{max}, with increasing strain amplitude. This maximum is reached at a point where G'' changes rapidly (point of inflection) and increases with carbon black concentration. Payne [115], in his investigation of different polymers and carbon blacks at different loadings, found that G''_{max} is linearly related to G'_o, G'_∞, i.e., the maximum change in elastic modulus with increasing strain amplitude, and can be expressed as

$$G''_{max} = 0.17(G'_o - G'_\infty) \quad (30)$$

where G'_o and G'_∞ are the leveling values of G' at low and high amplitudes, respectively.

Several authors [116120] later investigated different polymers and polymer blends filled with various carbon blacks and arrived at similar equations with different slopes and intercepts.

Payne [115] believed that this type of energy loss was related to the breakdown and reformation of the filler network. At small amplitude, the disruption of the network structure is insignificant. G'' is therefore low, but increases rapidly at higher amplitudes where breakdown and reformation of the network are significant. High amplitudes will largely destroy the secondary filler structure, so that less energy is required for dynamic oscillation, thus leading to a reduction in G''. This suggests that internal friction is the dominant mechanism in energy dissipation during dynamic deformation. In a systematic study dealing with the effect of carbon blacks on rubber hysteresis, Ulmer et al [121] concluded that the

formation of three-dimensional carbon black-rubber network is one of the factors affecting E''.

Based on the assumption of the breakdown and reformation of secondary structure, Kraus [122] theoretically derived the following equations for loss modulus:

$$E'' = E''_\infty + \frac{C\epsilon_o^m(E'_o - E'_\infty)}{1 + (\epsilon_o/\epsilon_c)^{2m}} \quad (31)$$

and

$$E'' = E''_\infty + C'\epsilon_c^m(E'_o - E'_\infty) \quad (32)$$

where m, C, and C' are constants, and ϵc is the characteristic strain given by

$$\epsilon_c = \left(\frac{k_m}{k_b}\right)^{0.5m} \quad (33)$$

in which kb is the rate constant of breakage of interaggregate contacts, and km is the rate constant of reagglomeration.

It is obvious from Equation 31 that the loss modulus is not only dependent on $(E'_o - E'_\infty)$ and E''_∞ (i.e., E'' after total destruction of the secondary

structure), but also on the rates of network breakdown and reformation which are related to internal friction in the filled vulcanizates. This was confirmed by comparing the energy loss of a silica with that of a carbon black having almost identical surface area and structure. At low strain amplitude, as common in dynamic measurements, the strong secondary network of the silica cannot be destroyed. The energy loss is therefore much lower than that of carbon-black-filled rubber, even though $(E'_o - E'_\infty)$ is much greater for the silica [69].

Nevertheless, if the secondary structure is an important factor for the energy loss, which has also been demonstrated by Gerspacher et al [50,51], the process of energy loss would be affected by both filler loading and the morphology of carbon blacks.

Effect of Carbon Black Morphology on tan δ: According to Equation 25, tan δ is the ratio between E'' and E'. As discussed previously, both E' and E'' are determined by hydrodynamic effects and filler networking. However, whereas the hydrodynamic effects may be associated with the mechanisms for E' and E'' which are described by the effective volume, the effect of filler networking on E' and E'' involves different mechanisms. E' is related to the filler network which subsists during dynamic deformation, and E'' to the breakdown and reformation of the network. Therefore, with regard to tan δ, the hydrodynamic term, which is mainly determined by filler structure and loading, may be eliminated or reduced until it is negligible [23]. Consequently, the filler factor governing tan δ is the state of filler networking, or more precisely, the ratio between the network portion that is capable of being broken down and reconstituted and the one that remains unchanged during dynamic

strain. The greater the network portion that withstands dynamic deformation and the smaller the one that is broken down and reformed, the lower is tan δ. This suggests that the development of a secondary filler network and its strength have a major effect on tan δ. Again, since S is virtually identical for all furnace blacks, the distance between the aggregates should be the controlling parameter for the filler network, and thus determine the tan δ of carbon-black-filled hydrocarbon rubber.

On the other hand, numerous researchers have investigated the effect of filler morphology (surface area and structure) on the loss of mechanical energy of filled rubber during dynamic strain. These studies were extensively reviewed by Medalia [114]. Recently, Patel et al [123,124] and Gerspacher et al [50,51] also carried out investigations of this subject. Caruthers, Cohen and Medalia [125] studied the dynamic properties of SBR vulcanizates at various degrees of loading with different carbon blacks. They correlated tan δ with the interfacial area ψ (see Equation 1) and, by plotting the tan δ values for all carbon blacks and all loadings as a function of ψ, obtained a scatter of points along a single line. The plot was improved empirically by replacing ψ with

$\psi\phi$, a so-called loading-interfacial area parameter. No effect of carbon black structure on tan δ was observed. Using the data published by Ulmer et al [126], Caruthers et al also observed a good correlation between tan δ and $\psi\phi$ in oil-extended SBR filled with a wide range of carbon black grades ranging from low to high surface area. In their analysis of the dimension of the loading-interfacial area parameter, they found that its dimension was length-1 and that it might be related to the interaggregate distance. This would mean that, as discussed above, the interaggregate distance is the primary factor influencing tan δ: the shorter the distance between the aggregates, the higher is tan δ.

Recently, Wang, Wolff and Tan [23], in a systematic study of the dynamic properties of SBR vulcanizates filled with 17 carbon blacks with surface areas ranging from 30 to 139 m2/g, compressed DBPA values from 57 to 107 ml/100 g, and loadings from 0 to 50 phr for hard blacks and 0 to 70 phr for soft blacks, respectively, showed an excellent correlation between tan δ measured at very low strain and the interaggregate distance calculated from Equation 9 (Fig. 14). This result lends strong support to the above assumption.

With regard to the effect of basic carbon black parameters on tan δ, it is not surprising that tan δ correlates well with surface area, and not with DBPA [114,122,125,128], because the interaggregate distance depends primarily on the specific surface area. In addition, the structure-dependent hydrodynamic effect is eliminated, or at least greatly reduced, in the ratio *E″/E′*.
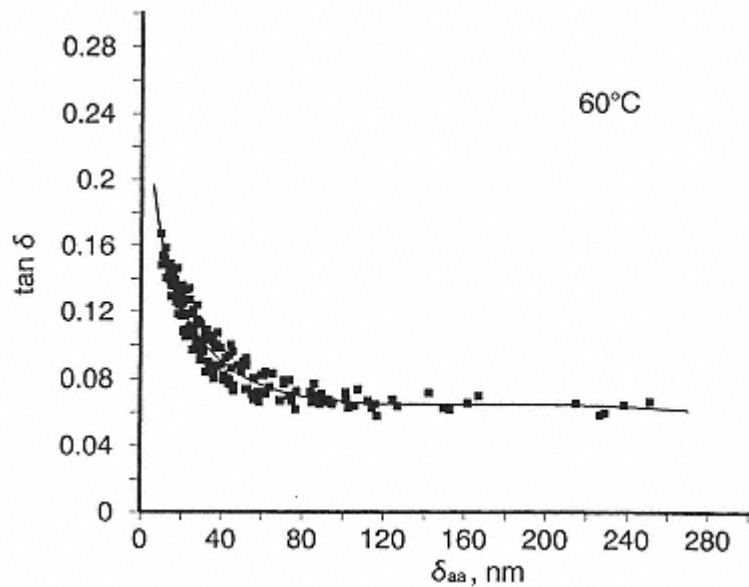
Fig. 14.
tan δ at 60° C as a function of interaggregate distance for
carbon black filled SBR (from ref. [23]).
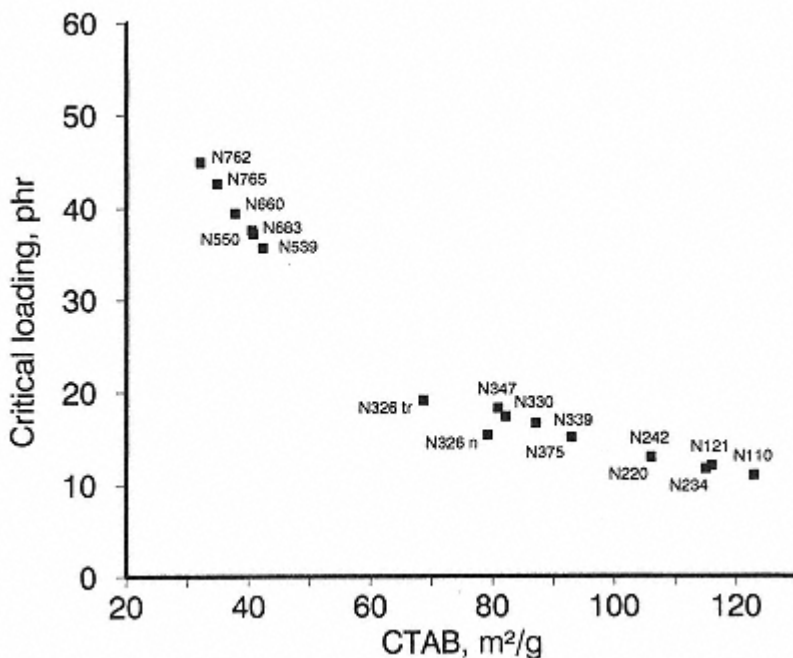
Fig. 15.
Critical loadings for tan δ as a function of CTAB surface
areas for variety of carbon blacks (from ref. [23]).

It is also evident from Fig. 14 that, when the aggregate distance reaches a certain value, defined as the critical distance $\delta^{tan\delta}_{aa,crit.}$, tan δ increases exponentially with decreasing δaa. It seems that below the critical distance, which is the same for all carbon blacks, network formation is enhanced considerably, giving rise to a marked increase in hysteresis. It is obvious that this critical distance corresponds to different degrees of loading, defined as the critical loading, $\phi^{tan\delta}_{crit}$. The critical loadings for tan δ showed an excellent correlation with CTAB surface area (Fig. 15). This had indeed been expected from the relationship between δaa and surface area, as expressed by Equation 9, where the structure of the carbon black plays a less important role.

The effect of the aggregate size distribution of carbon blacks on tan δ has been investigated extensively by Kraus and coworkers [118,129,130] and other researchers [23,127,131,132]. Using either experimental carbon blacks or blends of products with different aggregate sizes, they arrived at the following general conclusion: in contrast to conventional carbon blacks having the same surface area and DBPA, carbon blacks with a broad aggregate size distribution generally give lower tan δ values and high resilience. As suggested by Kraus [118], this may be due to differences in structure of the secondary agglomerates of the carbon blacks, but the increase in interaggregate distance, obtained by broadening the aggregate size distribution, should contribute to low tan δ values [23]. This is true, in particular, for hard carbon blacks and

practical levels of loading where a small reduction in interaggregate distance would entail a noticeable increase in loss tangent as shown in Fig. 14.

Effect of Surface Activity on tan δ: Surface activity is another factor which influences the processes of energy loss and has been widely studied with the aid of graphitized carbon blacks. The deactivation of the carbon black surface by graphitization has been demonstrated both by measurements of adsorption and of bound rubber. Payne [133], Voet and Cook [134], Medalia [135], and, more recently, Wolff et al [23] investigated the dynamic properties of rubber filled with graphitized blacks. They all reported an increase in tan δ upon graphitization, and most of the results showed that there was no significant change in elastic modulus at low strain. Payne [133] attributed the higher tan δ of graphitized carbon blacks to the loss of volatiles and increased aggregation during heat treatment, resulting in a reduction of rubber-carbon black association and in poor microdispersion. However, this does not seem to be the case, firstly because the heat treatment of carbon blacks in an inert atmosphere at temperatures of 420 as well as at 900°C, after which no volatiles were left on the surface, did not show any increase in tan δ [136], and secondly, because aggregation would increase the interaggregate distance, hence reduce tan δ. It, therefore, appears that a change in surface energies must be responsible for the higher tan δ of graphitized carbon blacks. Their lower γ_s^d [59], which results in poor polymer-filler interaction, would lead to molecular slippage of the rubber [135] and low apparent crosslink density of the vulcanizates. This, in turn, would give rise to a higher viscous component of the modulus, thus enhancing energy dissipation. On the other hand, the

lower specific component of surface energy (lower S [59]) will weaken the agglomerates, so that they are easily broken up and reformed, thereby increasing tan δ through internal friction.

Perhaps due to the improvement of the microdispersion of the carbon blacks in vulcanizates and the introduction of strong chemical linkages between the polymer and the filler surface, Wolff and Görl [137] were able to show that carbon blacks which had been modified with the bifunctional silane bis(3-triethoxy-silylpropyl)-tetrasulfane (Si69) gave a significantly lower loss tangent than nonmodified carbon blacks, particularly when the silane dosage was in the practical range. This is yet another confirmation of the mechanism discussed for graphitized carbon blacks.

Heat Build-Up: Heat build-up measured in the flexometer (e.g., a Goodrich Flexometer) is generally related to the energy loss under constant work input. The increase in temperature during the measurement, $\Delta T,$ would thus be linearly related to tan δ, as reported by Wolff and Panenka [138] for NR filled with a series of different carbon blacks. The factors influencing tan δ can, therefore, also be applied to heat generation. In some cases, especially when different types of fillers are compared, care should be taken because
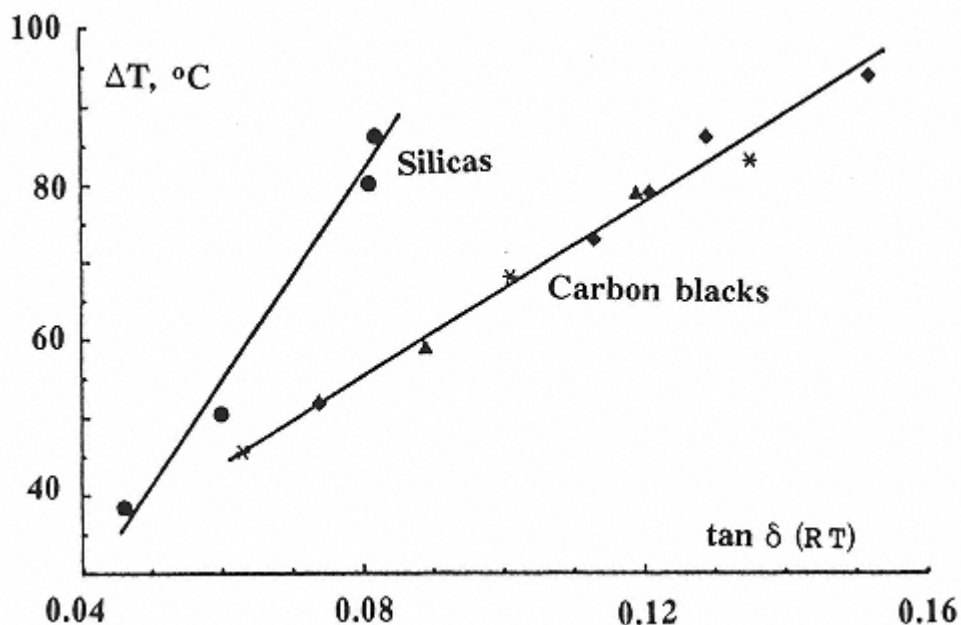
Fig. 16.
Heat build-up vs. tan δ at room temperature for silica and carbon
black filled NR (from ref. [139]).

different relationships may be obtained. This is shown in Fig. 16 [139] which highlights the differences between two types of fillers. At constant tan δ, the silica gives a high ΔT, which is certainly due to the different experimental conditions and, of course, reflects the structure of the vulcanizates. The stress or strain is usually lower in the standard tan δ measurement which is unable to destroy the strong filler network formed by silica, consequently leading to lower tan δ. In the case of the heat build-up measurement, the high static load and large stroke applied should largely destroy the secondary filler structure, giving rise to considerable energy dissipation in developed silica network. On the other hand, the low modulus of silica vulcanizates after stress softening during the first few cycles of compression under static load should lead to high

dynamic strain and, hence, to considerable heat generation. Moreover, while tan δ represents the hysteresis of one cycle of deformation at a constant temperature (even when measured after several cycles of deformation), ΔT constitutes a cumulative value for heat generation. It is determined not only by the hysteresis of the sample, but also by the heat exchange with the environment. The temperature of the sample at equilibrium could, therefore, be affected by the thermal conductivity of the filled vulcanizates.

Resilience: Resilience, or the rebound in single pendulum tests using a hemispherical striker or falling ball, also represents a measure of the hysteresis under conditions of constant energy input, although the deformation is

complex, involving extension, compression, and shear. Gehman [140] used a pendulum test and showed that tan δ was directly proportional to the logarithm of the fractional rebound, *R:*

$$tan \ \delta = -lnR/\pi \ (34)$$

Other authors [141143] also observed a good correlation between resilience and tan δ. It is therefore not surprising that the correlation between tan δ and the interaggregate distance, δ*aa,* can also be applied to resilience [23]. As illustrated in Fig. 17, a single curve may be used to represent the results for Firestone Ball Rebound as a function δ*aa* for SBR vulcanizates filled with the whole range of rubber-grade carbon blacks at various degrees of loading [23]. The ball rebound increases rapidly in the low δ*aa* region and reaches a maximum value which corresponds to that of the gum. The change in resilience with interaggregate distance follows the same mechanism which was discussed in the case of tan δ.

The Firestone Ball Rebound measurement showed empirically that the difference between the rebound of filled rubber, *R,* and that of the gum, *Ro,* increases linearly with increases in filler loading as [144]:

$$R_o - R = A\frac{m_F}{m_P} \ (35)$$

where m_F and m_P are the mass of the filler and the polymer, respectively. It
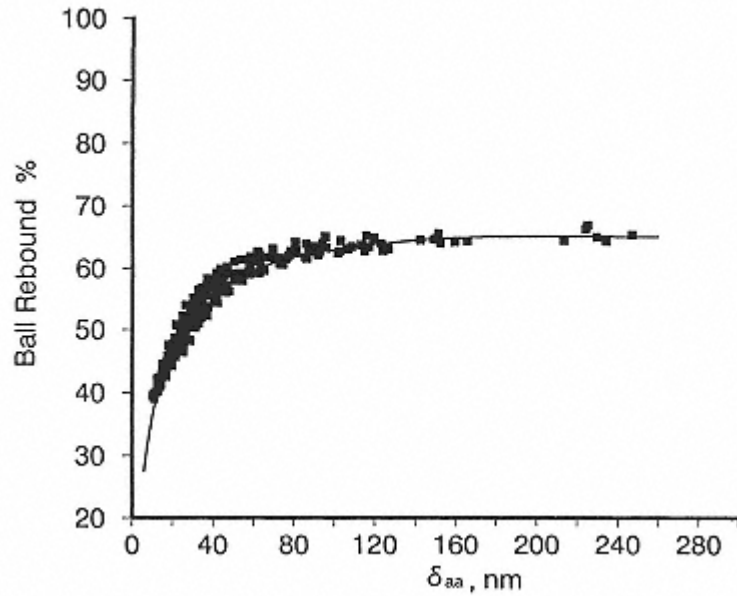
Fig. 17.
Firestone ball rebound as a function of interaggregate
distance (from ref. [23]).

was found that the constant *A,* i.e., the slope of the plot of (*Ro* - *R*) versus *mF/mP,* is independent of the crosslink density of the vulcanizates, of filler loading, and of filler structure, but that it depended on the type of elastomer and on carbon black surface area. This parameter is characteristic for each carbon black and was defined as a measure of the in-rubber surface area of furnace carbon blacks.

Temperature Dependence of tan δ and its Relationship with Tire Performance: The tan δ values of filled rubber are highly dependent on temperature, showing a maximum value at a temperature slightly above *Tg.* After passing through the maximum, tan δ decreases rapidly with further increases in temperature and then gradually reaches a low level plateau. This temperature dependence for filled rubber can, to a certain extent, be influenced by filler parameters. On the other hand, repeated movement of the rubber, as caused by rotating tires, traction, and skid, can be considered to constitute a process of constant energy input involving different temperatures and frequencies [145,146]. Rolling resistance, for instance, is related to the movement of the whole tire, corresponding to deformation at a frequency of 10100 Hz and a temperature of 6080°C [146]. In the case of skid or wet grip, the stress is generated by resistance from the road surface and movement of the rubber occurs at the surface, or near the surface, of the tire tread. The frequency of the movement, when related to skid and wet grip, depends on the roughness of the road surface, but should be very high, probably around 104 to 108 Hz at room temperature [145,146]. It is obvious that any change in tan δ at different frequencies will alter the performance of the tire. Since

certain tire properties involve frequencies which are too high to be measured, these frequencies
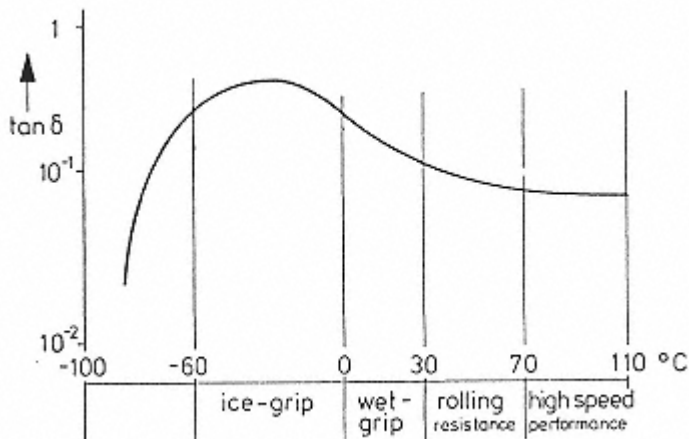
Fig. 18.
Reduced temperatures for different tire properties at
1 Hz (reproduced from ref. [147]).

are reduced to a measurable level (e.g., 1 Hz) at lower temperatures by applying the Time-Temperature Equivalence Principle (or WLF Temperature-Frequency Conversion). The reduced temperature for different tire properties at 1 Hz is shown in Fig. 18, which has been used as criterion for polymer development for tires [147]. An ideal material which is able to meet the requirements of a high-performance tire should give high tan δ values at about 0°C, in order to obtain high skid resistance and wet grip for safety, and low tan δ values at about 60°C, in order to reduce rolling resistance and save energy. The suitability of this principle for the purposes of filler development was confirmed in field tests of passenger tires [148]. Considerable efforts have been made in order to obtain the ideal tan δ curve by adjusting filler parameters, but only limited progress has been achieved during the past few years in breaking the interdependence between rolling resistance and skid, i.e., increasing one without sacrificing the other. It can nevertheless be expected that, as our knowledge of the mechanisms of energy loss increases and our understanding of elastomer reinforcement is deepened, we are steadily progressing on the road toward the optimum tire.

9.3.4. Effects of Carbon Blacks on the Fracture Properties of Vulcanizates

In theory, fracture is a process in which new free surface area of the material involved is created. The energy required for the creation of new surface area is usually considerably greater than the intrinsic fracture energy necessary to merely rupture the bond in this area. This suggests that other processes of energy dissipation are involved in rubber fracture. The addition of carbon blacks should

enhance energy dissipation by different mechanisms, as discussed previously, and improve the fracture properties of rubber materials. In practice, this effect should have a considerable influence on the service performance and service life of rubber products, which are dependent on different failure modes, such as cracking, fatigue, tensile failure, tearing, and abrasion.

Crack Initiation

It is generally believed that cracks frequently start at an inherent flaw, e.g., inclusions, microvoids, shortcomings of network chemistry, contamination, and other local inhomogeneities. When a vulcanizate undergoes stress, the local stress at the tip of the flaw is greatly magnified. Once the local stress at the tip of the flaw reaches a critical level, which is dependent on the radius of the tip and the rupture energy per unit volume of rubber, cracks will form, creating new surfaces. It is, therefore, understandable that an increase in the inherent strength by changing the network structure, and a reduction of the stress concentration at the tip by dissipating input energy as heat, both of

which help to distribute the stress uniformly to the molecular chains at the front of the flaw tip, should effectively delay crack expansion.

When vulcanizates containing rigid-particle fillers are subjected to tensile stress, this not only results in strain amplification in the polymer matrix, but also causes non-uniform stress distribution with the stress tensor including effective bi- and triaxial strain besides tensile and shear strains. Oberth and Bruenner [149] indicated that the maximum triaxial stress is generated at a short distance into the rubber matrix, above and below the filler particle. These regions may act as sites that favor the initiation and growth of internal voids and cracks (matrix cavitation mechanism) [150]. According to this mechanism, the rubber does not immediately detach itself from the filler particle, but undergoes internal rupture near the filler surface, nucleated by a precursor microvoid present within the rubber matrix. This microvoid is expanded by the triaxial stresses generated and, when the expansion of its walls reaches the breaking extension of the matrix, the original cavity will burst, and a crack is initiated at an applied critical stress σc. This critical stress is, of course, dependent on the aggregate size of the filler and the modulus of the vulcanizate. The higher the modulus, the higher is σc [149]. Moreover, as pointed out by Gent [151], if the radius of the precursor microvoids is less than $0.1 \mu m$, their surface energy will exert a significant additional restraint on expansion. Thus, when the rubber contains no microvoids with a radius greater than 10 nm, it will be more resistant against initiation of cracks by matrix cavitations.

On the other hand, the matrix cavitation mechanism can only take

effect if polymer-filler interaction is strong. When the dewetting stress at the direct interface between filler and polymer is lower than the nucleated failure stress of the polymer matrix or rubber shell, in other words, in vulcanizates with poor polymer-filler interaction, cavitation will occur at the filler surface (interfacial debonding or dewetting mechanism) [150,152,153] instead of matrix cavitation near the filler surface. Based on the analysis of an energy balance, Gent [152] proposed the following equation for the critical stress of dewetting, σc:

$$\sigma_c = \left(\frac{2\pi G_{if} E}{3 d_p}\right)^{1/2} \tag{36}$$

where Gi is the interfacial fracture energy, E is Young's modulus of the vulcanizate, and dp is the diameter of the spherical filler particle. This suggests that σc increases not only with increasing polymer-filler interaction, characterized by Gi, but also with decreasing particle size of the filler. In this regard, high-surface-area carbon blacks have a tendency to delay crack initiation via dewetting processes, due to the smaller radius of their aggregates and strong filler-polymer interaction [60]. This is consistent with electron microscope observations by Hess and coworkers [154] on strained supported microtome

sections of SBR vulcanizates filled with different grades of carbon blacks. While extensive cavitation was observed at the particle edges for nonreinforcing MT black, the number of vacuoles between filler surface and polymer matrix is greatly reduced in the case of small-particle blacks.

Crack propagation, or crack growth, is similar to the tearing process when static stress is applied, and to fatigue failure under dynamic deformation, both of which are affected considerably by carbon blacks.

Tearing

Once cracks have been initiated in a vulcanizate, they will propagate under stress. The basic process underlying crack growth is tearing. As mentioned previously, the tearing energy, i.e., the rate at which strain energy is released, is much greater than that required to create a new surface. It is thus obvious that the energy is dissipated irreversibly in a highly localized region around the tip of a growing tear. On the other hand, it is known that the tearing energy is a fundamental measure of the strength of macromolecular materials, irrespective of the shape of the test piece and of how force is applied to it [155,156]. It is thus an inherent strength property of rubber, in addition to other failure properties, such as tensile strength and fatigue which are initiated from small, naturally occurring flaws [157,158].

State of Tearing: Two types of tear phenomena are observed in tearing tests (in trouser tear, for instance), namely, stable tearing and unstable tearing. In the case of stable tearing, the tear force fluctuates only slightly and the rate of tear propagation is basically

continuous. The torn surface obtained by this type of tearing is rather smooth. Unstable tearing is often referred to as stick-slip tearing. Instead of the tear propagating at a steady rate, tear growth is arrested and reinitiated at fairly regular intervals. Correspondingly, the force necessary to propagate the tear varies widely, from a minimum at tear arrest to a maximum at tear initiation. This type of tearing leads to surface irregularities with periodic knots. This effect is viscoelastic since it depends on changes in both tearing rate and temperature. The commonly accepted unstable tear mechanism is based on the assumption of the existence of an anisotropically reinforced structure at the tear tip, involving an energy dissipation process [155,158]. As stress is applied, an orientated structure (crystallization for strain-crystallizing rubber like NR, or alignment of molecules for amorphous rubber such as SBR) is created in the region of the tear tip which is associated with large local deformations. This structure is oriented parallel to the direction of the applied stress and perpendicular to the direction of tear growth. Since much more energy is required to propagate a tear perpendicular to the orientation direction [159], the onset of tear rupture is retarded. As stress continues to increase, this force is exceeded at some point and catastrophic rupture occurs. After this point of initiation,

the crack advances rapidly (slip) around the reinforced region until the highly strained web is removed and the propagation rate of the tear drops to zero. After this process, a knot remains on the torn surface. When stress continues to be applied, this process is repeated. Since the minimum and the maximum of the tear force correspond to tear arrest and tear initiation, respectively, the difference in the recorded forces between peak and minimum was considered as a measure of the level of stick-slip. Quantitatively, several pairs of peaks and minima of the tear force are used to calculate the standard deviation, and the relative deviation is taken as a stick-slip index, *SSI* [160], which is a measure of unstable tearing. This parameter is determined by the formation of a reinforcing structure near the tear tip. The more developed the orientation of the polymer molecules, the higher is *SSI*.

For crystallizable elastomer such as NR, the presence of carbon blacks enhances rubber crystallization [161,163], and promotes stick-slip tearing. The enhancement of strain-induced crystallization of NR by carbon blacks was confirmed by X-ray study [162,164] and differential scanning calorimetry. Using NR vulcanizates filled with different amounts of HAF black, Lee et al [163] recently observed in X-ray analyses that the amount of crystallization of the rubber, and the size and energy density of the process zone near the crack tip, in which strain, stress, and the energy density are determined by the crack, increase considerably with carbon black loading. This effect is, in the first place, due to strain magnification by the filler as crystallization increases rapidly with increasing strain [165,167].

Even for amorphous elastomers, the presence of carbon black will

enhance the molecular orientation in a stress-strain field. This was demonstrated by investigations of the anisotropy of the amorphous peak of X-ray patterns for stretched carbon-black-loaded NR in which the molecular orientation factor increases with extension and carbon black content [163]. The fact that carbon black assists in the orientation could help explain the effect of carbon blacks on the reinforcement of amorphous polymers.

While no unstable tearing is observed for non-crystallizable gum, such as unfilled SBR, pronounced stick-slip tearing appears at certain levels of temperature and tear rates for the compounds filled with carbon blacks, particularly with the reinforcing grades (Fig. 19) [160]. This is, of course, due to the fact that the carbon blacks facilitate molecular alignment, perhaps due to slippage of the rubber segments along the filler surface and the orientation of filler aggregates in the stress field. This would lead to the development of an anisotropic structure over a large volume, causing the stress to be uniformly distributed to the network chains. This is certainly true at the crack tip where the polymer matrix is subjected to high tensile strain.

The unstable tearing has a viscoelastic character. At low temperature and/or high tear rates, the viscosity of the rubber is too high, or the segmental
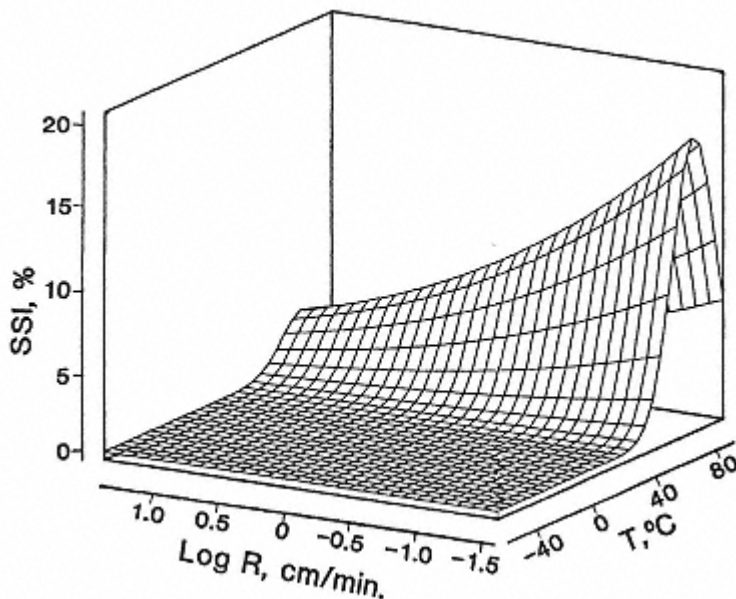
Fig. 19.
Stick-slip index of tearing as a function of tearing rate
and temperature for SBR filled with 50 phr N330 carbon
black (from ref. [160]).

movement too slow, for the anisotropic structure to be formed
within the short space of time during which the rubber is stretched
as the tear tip advances, thereby producing a smooth torn surface.
At high temperature, the high molecular movement and the rapid
relaxation would also result in less stick-slip tearing, as shown in
Fig. 19.

Tearing Energy: Experimentally, the energy required for tearing is
not only related to tear propagation, but also involves elastic strain
energy stored and dissipated in the legs of the test piece (trouser
tear). When the deformation of the legs can be eliminated, for
instance in the case of a trouser test piece with wide enough legs or
backed by undeformed materials, the tearing energy, *G,* can be

calculated from the force, Ft, required to propagate a tear in rubber [155]:

$$G = 2Ft/t \ (37)$$

where t is the thickness torn through. In the stable tearing region, the average force can be used for the calculation of tearing energy because the force varies only slightly with tear propagation. For unstable tearing, the force of tear initiation is much higher than that of arrest. In this case, as pointed out by Kelley and coworkers [158], the tearing energy at arrest is more representative of the inherent tear strength of the materials, even though the initiation value is an important feature of the rubber since cracks do not develop below this energy level. The presence of carbon black can significantly increase the tearing

energies of arrest and initiation. This effect is even more pronounced in amorphous rubber. Of course, as mentioned above, the increase in initiation tearing energy can be attributed to the easy formation of a reinforcing structure around the tear tip, but the enhancement of energy dissipation during tearing, by other molecular processes which are promoted by the carbon black (see section on *Stress-Softening Effect*), may also be considered as a major contribution to the high values of the tearing energies of both initiation and arrest.

The viscoelastic behavior of tearing energy has demonstrated that the equivalence between changes in the rate of tearing and in temperature follows the well-known William-Landel-Ferry (WLF) relationship [170] for unfilled amorphous vulcanizates [168,169]. With regard to amorphous rubber filled with carbon blacks, this can only be assumed to be true for the values of tearing energy at arrest in the unstable tearing region. Fig. 20 shows the arrested-tearing energy master curve referenced to 25°C for SBR sulfur-cured vulcanizates filled with 50 phr of N330 carbon black [160]. The temperature-related horizontal shift factors a_T, i.e., the factors by which the tear rate has to be multiplied to yield a master curve, were calculated from the WLF equation:

$$Log\, a_T = \frac{-C_1(T - T_s)}{C_2 + (T - T_s)} \quad (38)$$

where C_1 and C_2 are experimental constants for the reference temperature
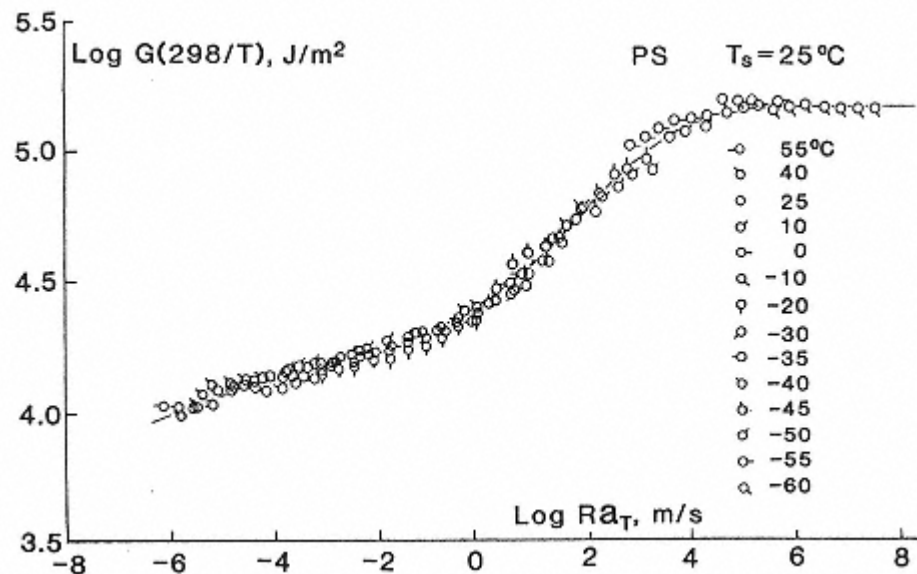
Fig. 20.
Master curve of tearing energy of SBR filled with 50 phr N330
carbon black (from ref. [160]).
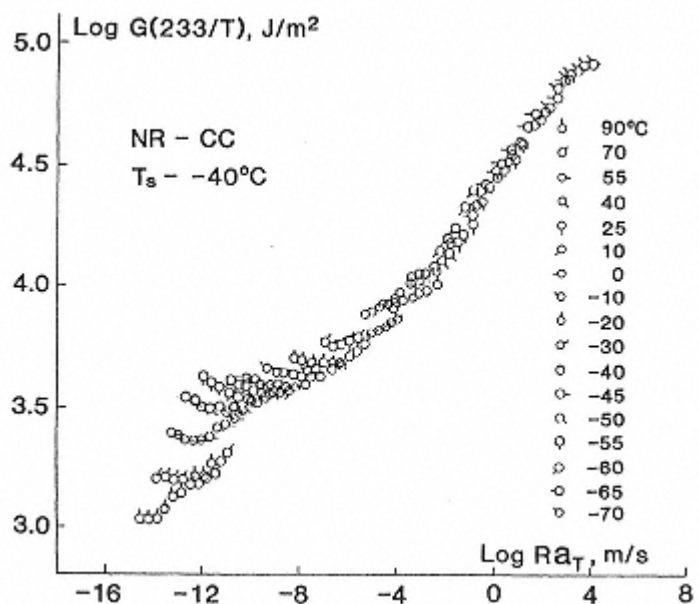
Fig. 21.
Master curve of tearing energy of NR filled with 50 phr
N330 carbon black (from ref. [160]).

Ts. Similar to the unfilled gum [169], the curves of N330-filled
SBR vulcanizates exhibit an S shape over a broad time scale. In the
short-time region, the curve displays a glassy plateau in the vicinity
of 120130 kJ/m2. In the long-time region, it has a tendency to drop
towards the threshold tearing energy, *Go,* predicted by the theory of
Lake and Thomas [171], which is the lower limit of the mechanical
strength of the rubber. This value is about the same as that of the
gum, showing that at high temperature and low tear rate the effect
of carbon black on the arrested-tearing energy can be eliminated.
For the initiation tearing energy in the unstable tearing region, the
experimental data cannot be shifted to a normalized master curve,
due to additional molecular processes, such as alignment of the
molecules in the front of the tear tip. This was confirmed for N330-
filled natural rubber (Fig. 21) [160]. At low temperature, where

tearing is stable or slightly unstable, the respective tearing energies at different temperatures and tear rates can be superimposed, forming a single master curve. However, at low tear rates or relatively high temperature, where stick-slip tear is marked, the data (even arrest values) cannot be shifted, due to the slow increase in tearing energy. One of the reasons for the impossibility of the values to be shifted to a master curve may be the stick-slip propagation of the tear, rendering the tear rate meaningless. Another reason may be that at low tear rates some strain-induced crystallization remains at the tear tip when the tear slip stops, thus increasing the arrest value.

For all rubber-grade carbon blacks, the tear energy increases with filler concentration, due to increasing energy dissipation, and then decreases for amorphous rubbers at high loadings. This is also true for crystallizable rubber such as NR. However, at very low concentrations (below 5 10 phr, depending on the type of carbon black), the tear resistance of NR is not improved by the addition of carbon blacks (the values are even lower than those of the gum) [172]. This may be associated with the interference of strain-induced crystallization.

Although the small-particle carbon blacks have a favorable effect on the tear energy, especially with regard to the initiation value, increases in structure are slightly detrimental because, as compared to low-structure carbon blacks, the high modulus will largely reduce the effective radius of the tear tip (the tip being sharpened), which is an important factor determining the tearing energy [173,174].

Tensile Strength

Although the mechanism of tensile failure of elastomers has not yet been fully established, it can be regarded as catastrophic tearing by growth of cracks initiated from accidental flaws, microvoids, dewetting or cavitation from the filler surface. If the elastomeric network is capable of dissipating input energy into heat through irreversible molecular processes in the bulk of the specimen (instead of near the crack tip in tearing), less elastic energy will be available to break the polymer network, thus increasing the fracture energy [175]. The strain-induced crystallization of elastomers is also one of the most effective processes of dissipation of stored energy. The formation of a filamentous structure prevents cracks

from growing until catastrophic rupture occurs, thus leading to high tensile strength of the crystallizable rubbers. As mentioned earlier, this process can be enhanced by the addition of carbon blacks. With regard to amorphous rubbers, lack of crystallization under strain has been attributed to inherent weakness of these materials. The incorporation of reinforcing carbon blacks has been considered a major source of energy dissipation, raising the strength to a level equivalent to that of crystallizable rubber. The relationship between tensile strength and energy dissipation during stretching was represented by Harwood and Payne [176] as:

$$U_b = B(H_b \varepsilon_b)^{\frac{1}{2}} \quad (39)$$

where U_b is the energy density to break, ε_b the elongation at break, H_b the energy dissipated in the deformation to break, and B a constant which is independent of filler loading and type of filler.

Several mechanisms have been proposed in order to interprete the function of carbon blacks in energy dissipation. Some are related to stress softening, i.e., the energy loss due to the breakdown of agglomeration, local

highly viscous flow due to the filler-frozen entanglements [162], and slippage of the rubber molecular chains along the filler surface [104106,110,112], which also results in uniform stress distribution to the network chains, etc. With regard to crack growth, the alignment of the network chains may have a similar function as crystallization in absorbing elastic energy as well as in strengthening and blunting the crack tip, thereby delaying the onset of catastrophic failure.

On the other hand, as in other materials, the presence of rigid filler particles plays a role in retarding cracks and dissipating energy by increasing the length of the required crackpath. Since the crack cannot occur through filler particles, it has to move around them, thus requiring more energy [162]. This effect is even more pronounced for a filler such as carbon black whose surface is covered by a strong rubber shell.

As suggested by Gent and Pulford [177], the filler particles may also act as stress risers by forming potential nucleating sites for secondary cracks, as will be discussed below, which are believed to increase energy dissipation considerably.

In order to prevent crack growth and increase hysteresis, loading and carbon black morphology may play an important role through interaggregate distance. As pointed out by Eirich [162], the interaggregate distance must not be so large as to allow the development of cracks of a critical size within the matrix before another aggregate is met. If the cracks, initiated by the filler aggregates via dewetting or matrix cavitation, are small enough to be harmless, but numerous enough to consume a large portion of the invested energy, the material will exhibit considerable strength.

At the same loading, the small-particle carbon blacks, having both small aggregate size and high surface area, will exhibit short interaggregate distance (Equation 9) and thus confer greater resistance against crack propagation.

Since small-particle carbon blacks with large surface areas are conducive to all these processes, such as greater rubber shell caused by higher polymer-filler interaction and large interfacial area, greater probability of molecular slippage, leading to developed molecular alignment, and short interaggregate distance, it is not surprising that the tensile strength increases with increasing surface area of the carbon blacks, especially for noncrystallizing elastomers, their structure being less important.

The degree of carbon black loading should have the same effect as surface area. In fact, tensile strengh increases with increasing filler loading up to a certain level and then drops at higher filler concentrations. The concentration at which maximum tensile strength is obtained varies with the carbon black. The maximum is attained earlier with small-particle blacks. Products with higher structure have the same effect, although its effect is not as evident as that of surface area. This phenomenon was interpreted in terms of

carbon black dispersion. At high loading, the carbon blacks may agglomerate into large clusters which furnish flaws that can easily create cracks and then develop into a catastrophic failure. This was confirmed by the fractographic observation of N330-filled and unfilled SBR vulcanizates [178], showing that the flaw size initiating tearing increases with filler concentration. Because agglomeration is dependent on interaggregate distance, the high-surface-area carbon blacks will form clusters at lower loadings (i.e., small-particle products are more difficult to disperse in rubber) and the maximum tensile strength will be expected to occur at lower concentrations.

The effects of carbon blacks on the strength of strain-crystallizing rubber, such as natural rubber, are rather complicated since strain-induced crystallization itself is an important source of energy dissipation and thus increases the fracture energy. The crystallites developed during extension of the unfilled rubber in bulk increase tensile strength to such an extent that most carbon blacks are unable to raise it much further. In comparison to amorphous rubber, the maximum tensile strength occurs much earlier as loading increases. In some cases, no maximum is observed at all [179]. It seems that the addition of carbon blacks may also interfere with the occurrence of strain crystallization in bulk rubber.

Since the strength and extensibility of the elastomer network depend on the test conditions, such as temperature and rate of extension, Smith [180,181] used a failure envelope to characterize the ultimate tensile properties of vulcanizates. He found that the stress at break, σ_b, and the ultimate strain,
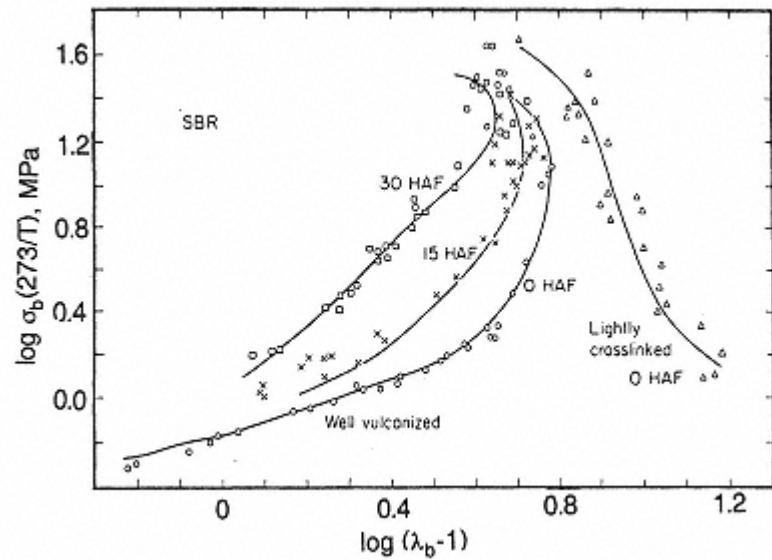
Fig. 22.
Effect of carbon black on failure envelopes of SBR
(from ref. [182]).
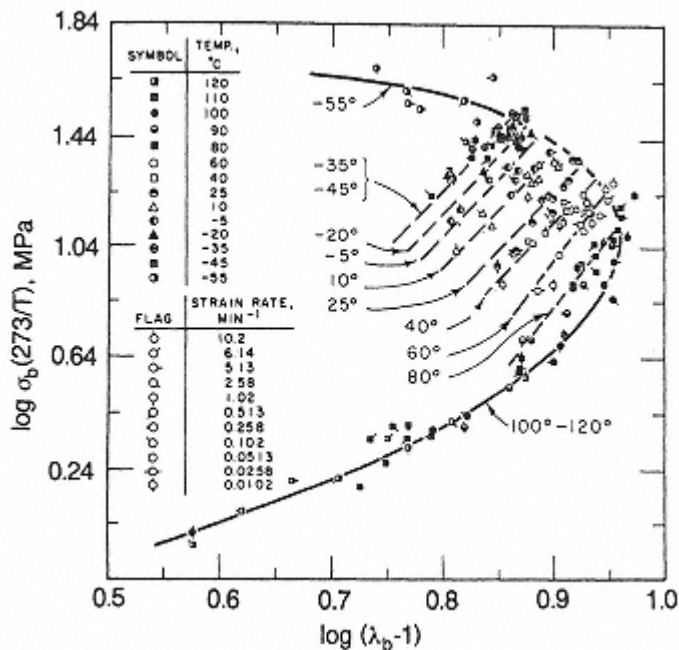
Fig. 23.
Failure envelopes of unfilled NR (from ref. [183]).

λb, measured over a wide range of temperatures and strain rates, yielded a single curve, the so-called failure envelope, when $\log(\sigma b T_0/T)$ was plotted against $\log(\lambda b - 1)$, where T and T_0 are the test and reference temperature, respectively. The failure envelope provides a basic characterization of the ultimate tensile properties because a change in strain rate or temperature results in the shift of a point along the curve. This suggests that the envelope is independent of the test conditions, and depends only on the structural characteristics of the vulcanizates. On the failure envelope, the fracture point moves clockwise around the envelope, either with rising temperature or with decreasing rate of extension. The extreme occurs at $\lambda b\text{-}max$, the largest extension ratio attainable.

Fig. 22 illustrates the effect of carbon blacks on the failure

envelopes of SBR vulcanizates [182]. When the filler concentration increases, the failure envelope moves toward higher tensile strength and lower elongation at break, while $\lambda_{b\text{-}max}$ decreases. This behavior is comparable to that of unfilled strain-crystallizing rubber (Fig. 23) [183]. The function of strain-induced rubber crystallites in tensile fracture is therefore similar to that of fillers, and *vice versa.*

Fatigue

As defined by Lake [184], fatigue refers, broadly speaking, to a progressive deterioration of one or several properties of the materials during

service life or test. In rubber technology specifically, it indicates the failure resulting from crack growth initiated by one or several naturally occurring flaws under repeated deformation (or stress) which is much smaller than that of a single extension to break. When the flaw is a small cut introduced deliberately, this process is sometimes termed cut growth. This vulcanizate property directly affects the service life of rubber products, as for instance of tires by groove and carcass cracking, tread and ply separation [185].

Once the force applied exceeds a certain level (critical stress or tear strength) in the case of static or monotonic tearing, the crack propagates continuously until rupture occurs (stable tearing) or travels rapidly for some distance before arresting (unstable tearing). In the case of fatigue, the crack (or cut) growth occurs under a repeated load which is less than the tear strength. During dynamic deformation, the crystallization or alignment of rubber molecules occurs in front of the crack tip in the loading cycle. This reorganization disappears in the unstrained cycle when the rubber is relaxed to zero strain. This causes the stress distribution around the crack tip to move forward, and further growth to occur during the next cycle [150]. If the strengthening structure does not totally disappear at zero strain, crack growth may be slowed down or prevented. It is, therefore, understandable that the rate of formation and disappearance of the alignment structure, as well as the test conditions, should have a considerable influence on rubber fatigue.

Lake et al [166,184,187189] found experimentally that four distinct regions exist in the relationship between crack (or cut) growth and maximum tearing energy, G, attained in each cycle (Fig. 24). Below G_o, cyclic crack growth is very low and the growth rate is

largely independent of tearing energy. This growth was attributed entirely to ozone attack. Above G_o, but below G_1 which is a distinctive value of G as defined in Fig. 24, the growth rate of the crack is proportional to $(G - G_o)$. Between G_1 and G_c, the static tearing energy, the crack growth rate increases exponentially with tearing energy. Above the static tearing energy, catastrophic tearing occurs.

When a long strip of rubber in the unstrained state is subjected to cyclic extension, the crack growth behavior over the whole range of tearing energies can be expressed approximately as:

$$\frac{dc}{dn} = BG^\beta \quad (40)$$

where c is the crack length, n is the number of cycles, and B and β are constants. β is mainly dependent on the rubber used and generally lies between 1 and 6. For natural rubber, β is about 2, and for amorphous SBR, it is about 4 [190192], i.e., the effect of the flaw size and strain on fatigue properties is much more pronounced for SBR than for NR. The tearing energy, G, of a
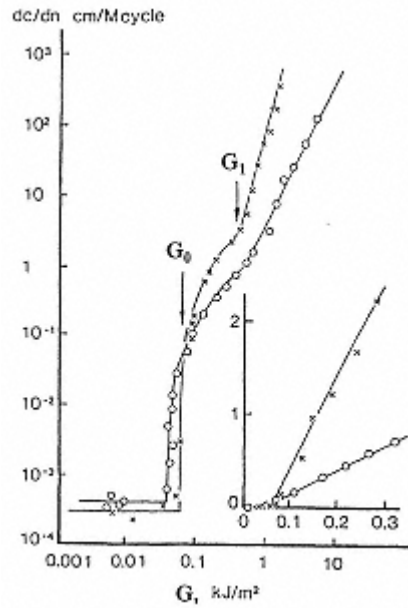
Fig. 24.
Relationship between crack
growth and maximum
tearing energy attained in
each cycle for NR and SBR
(from ref. [166]).

long strip of rubber with edge cracks of a length c is given by
[193]:

$$G = 2KcW \quad (41)$$

where W is the strain energy density in the bulk of the test piece,
and K is a constant which changes only slightly with strain. The
fatigue lifetime can thus be estimated by integration of Equation 40
and by substituting G from Equation 41:

$$n = \frac{1}{(\beta - 1)B(2KW)^\beta} \times \left(\frac{1}{c_o^{\beta-1}} - \frac{1}{c^{\beta-1}} \right) \quad (42)$$

where c_o is the effective initial flaw size. At fatigue failure, $c \gg$

co, the number of cycles to failure can be obtained from this equation by eliminating the *c* term. Satisfactory agreement with the experimental data was obtained for unfilled rubber at moderate and high strain, and the flaw size required to fit the experimental data is a few μm which is about the same order of magnitude as imperfections in the rubber caused by particulate impurities and test piece processing [184]. Another factor affecting fatigue is the atmosphere. Not only *Go,* but also the constant *B* are affected by the oxygen concentration through mechano-oxidative mechanisms [184,187,194].

With regard to the effect of carbon black on fatigue, very few investigations have been carried out systematically and under well controlled conditions.

In principle, as reviewed by Kraus [195], the presence of carbon black plays an important role through the effects of poor dispersion and agglomeration on c_o, the effect of rising strain energy, and its action as a mild thermal antioxidant in sulfur vulcanizates. Moreover, the value of β in Equation 42 for non-crystallizable SBR decreases upon incorporation of carbon black from 4 to about 2 in fully reinforced vulcanizates, which corresponds to the value for natural rubber. On the other hand, by increasing the energy dissipation, as discussed previously, the stress concentration at the tip of the growing crack and hence the rate of crack growth can be reduced by the addition of carbon blacks [197].

Recently, Goldberg et al [178], using SBR vulcanizates filled with different amounts of N330 carbon black, reported that the residual strength of the samples, subjected to 100 cycles of deformation at different cycling stresses, increased with increasing filler concentration. The stress, with which the samples were fatigued to failure within 100 cycles of deformation, also increased with filler loading.

Lake and Lindley [198] showed that 50 phr HAF in NR are able to reduce the rate of cut growth considerably at a tear energy above G_o. However, in fatigue, this improvement is cancelled out by the large size of the flaws created by this filler. This is in a good agreement with observations made by Wolff [199], who, using the DeMattia test, was able to show that the number of cycles n, enabling the cut to grow from 8 to 12 mm, first increases with carbon black loading, passes through a maximum, and then decreases (Fig.
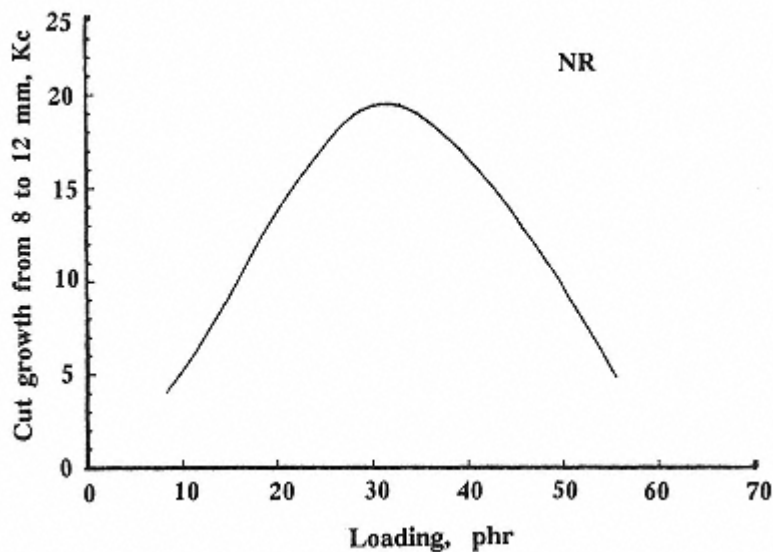
Fig. 25.
Effect of carbon black loading on DeMattia cut growth
for NR filled with N330 carbon black (from ref. [199]).

25). With increasing surface area, the maximum shifts towards lower filler concentrations. While the improvement of fatigue at low concentration is due to increase in tearing energy, the lower fatigue life at higher loading is related to the high value of c_o resulting from the agglomeration of the carbon black. It is thus apparent that the lower concentration of the maximum for small-particle blacks can be attributed to their difficulty of dispersion. In addition, when the comparison is carried out at constant stain, as is common in laboratory testing, and at practical loadings, the high fatigue resistance of rubber filled with large-particle and low-structure carbon black may also be caused by their lower stiffness which requires less energy input [195,196].

Abrasion

Abrasion is one of the rubber properties that are strongly affected by carbon blacks, and it has been the subject of extensive studies. It is generally recognized that the mechanism of rubber abrasion is highly complex, involving not only mechanical failure of the material, but also mechano-chemical and thermo-chemical processes.

During abrasion, the rubber surface generally develops patterns which are characterized by one ridge after the other perpendicular to the direction of abrasion. A cross section of the ridges shows an asymmetric shape with the steep side facing the direction of attack. This phenonenon was believed to play an important part in rubber loss and was described by Schallamach [200,201]. Southern and Thomas [202] treated the pattern abrasion process theoretically as a fatigue fracture process. When the ridged surface of the rubber moves on a track or road, the ridges are bent backward and the

friction stress causes shallow crack growth at the base of the re-entrant corner of the ridges (Fig. 26). Ultimately, the ridges break off and abrasion occurs. This process is characterized by the fact that it is self-perpetuating, by the crack propagation distance, *dc,* per pass of the abrader (per cycle), and by the shallow angle of the crack, θ. During each pass in a steady state, the ridge
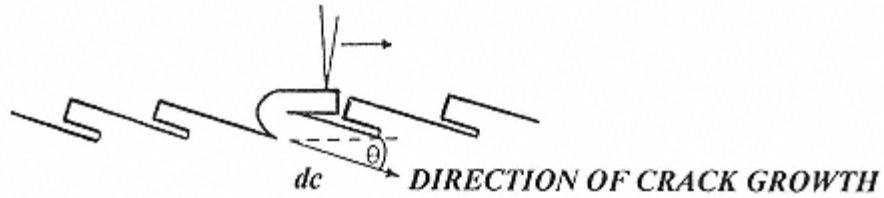
Fig. 26.
Schematic illustration of tire abrasion process (from ref. [203]).

advances by *dc cos* θ, and the height drops by *dc sin* θ. The volume loss, *A,* per pass is therefore

$$A = w \, dc \, sin \, \theta \quad (43)$$

where *w* is the width of the sample. From Equation 40, *dc* is given as

$$dc = BG\beta \quad (44)$$

and the tearing energy, *G,* is related to the frictional force *F* as

$$G = F(1 + cos \, \theta)/w \quad (45)$$

Thus

$$A = wB sin \, \theta[F(1 + cos \, \theta)/w]\beta \quad (46)$$

This suggests that the abrasion rate is related to the crack growth in fatigue, which is determined by the tearing energy, and the angle of the ridges, *θ.* This angle reflects the coarseness of the abrasion pattern. It is thus obvious that abrasion resistance can be improved by reducing fatigue crack growth under the prevailing conditions and by reducing the coarseness of the pattern. By comparing the plot of *dc versus G* obtained from fatigue measurements, and that calculated from Equation 43 with the measured abrasion loss, good agreement was found for various non-crystallizing rubber, but poor agreement for strain-crystallizing natural rubber [202]. This suggests that strain-induced crystallization does not occur or is ineffective during abrasion.

Although this model helps to understand the abrasion process, a number of significant discrepancies remain. As pointed out by Gent [204], the abrasion rate is not only faster than predicted from the

fatigue measurement, but carbon-black-filled rubber is also strikingly more resistant against abrasion, while being not so much more resistant against fatigue crack growth. Moreover, fatigue crack growth diminishes rapidly with increasing temperature, but abrasion resistance is less affected by the test temperature. Gent believed that not only the crack growth mechanism, but also abrasion initiation, plays an important role in the abrasion process. The formation of surface pits of a certain size, in the order of a few μm, by the detachment of rubber particles of this size under the influence of frictional force, should also be taken into consideration. When the creation of the initial cracks becomes more difficult, the whole abrasion process should be retarded. The overall rate of abrasion would be determined by the fatigue failure process, when the cracks form readily as in the case of unfilled amorphous rubber. Otherwise, the abrasion rate should depend largely on crack initiation. Gent further proposed that the creation of subsurface cracks during fraction sliding consists of the unbound elastic expansion of microscopic precursor voids until they burst open as cracks under the action of internal pressure or of triaxial tension in

the surrounding rubber. The critical inflation pressure for internal rupture is proportional to the elastic modulus and the mechanism by which a sufficiently large inflation pressure is most probably generated. This seems to be due to the thermal decomposition of rubber, generating a volatile product, basically a micro-scale blowout process. This is understandable since the surface temperature may reach 200°C or more due to frictional wear during abrasion [205].

The considerable improvement in the abrasion resistance of rubber by incorporation of carbon blacks may be explained by enhanced fatigue crack growth resistance, through dissipation of part of the friction energy via various processes, as discussed earlier, and the retardation of crack initiation by increasing stiffness without much loss of extensibility of the rubber. The latter is probably of greater importance because the elastic modulus is less dependent on temperature than crack growth, which is consistent with the low temperature-dependence of abrasion. In addition, carbon black is able to increase the thermal conductivity of rubber, thus influencing crack initiation on the rubber surface.

Irrespective of the complex mechanism of abrasion, which is not yet fully understood, an enormous amount of work was carried out on rubber abrasion with regard to the wear resistance of tires, and a wealth of knowledge concerning the effects of basic properties of carbon blacks on abrasion resistance has been accumulated [179,199,206211]. Particle size (surface area) is generally considered to be one of the most important parameters of carbon blacks contributing to abrasion reinforcement [179,199,212214]. Rubber filled with high-surface-area carbon black usually shows a

higher abrasion resistance. Shien et al [132] found that above a certain surface area limit, abrasion resistance cannot be increased further. On the contrary, poor abrasion resistance was observed for carbon blacks with very high surface areas. The optimum CTAB surface area for an SBR/BR blend system lies between 130 and 150 m2/g. The lower abrasion resistance of rubber filled with very fine carbon blacks may be attributed, firstly, to poor carbon black dispersion caused by very short interaggregate distance. This is confirmed by the increase in agglomerate size with increasing surface area and by the loading dependence of abrasion which is similar to that on surface area [132]. The rate of abrasion passes through a maximum as carbon black loading is increased to very high concentrations at which the dispersion of the carbon blacks in the polymer matrix becomes difficult, thus resulting in poor abrasion resistance. The higher abrasion rate of rubber filled with very fine carbon blacks may also be associated with their higher heat generation, causing high surface temperature which accelerates the thermo-oxidative degradation of the polymer. All these effects promote crack initiation and fatigue crack growth, thus lower abrasion resistance.

The response of abrasion to carbon black structure is dependent on test severity. While carbon black structure is less important at low severity, at higher severity, increases in structure lead to higher abrasion resistance. Furthermore, it was found [132] that abrasion is significantly affected by the detail morphology. For carbon blacks with comparable surface area and DBP absorption, broadening the aggregate size distribution, as measured with a Disc Centrifuge Photosedimentometer, does not change abrasion resistance significantly at high severity. However, at relatively low severity, the carbon blacks with a broad distribution exhibit a higher abrasion rate. On the other hand, for a given surface area, highly complex carbon blacks, as characterized by their aggregate size, their structure and the number of primary particles per aggregate, enhance abrasion resistance significantly, especially under conditions of high severity.

The effect of the surface activity of carbon blacks on abrasion has long been recognized. The obvious proof is that graphitization of the carbon blacks reduces abrasion resistance drastically [179,214]. Since surface area and structure do not change significantly, this effect has been considered to be the result of the deactivation of the surface, characterized by low bound rubber content, which is known to be related to low surface energy. The high abrasion resistance of small-particle carbon blacks can probably be attributed in part to their high surface activity, since their surface energy is approximately proportional to their surface area [23]. For the non-graphitized carbon blacks with similar surface area and aggregate morphology, rubber filled with carbon blacks having a high bound rubber content always shows a higher resistance against abrasion [132].

Even though the effect of carbon blacks on abrasion as measured in the laboratory is so difficult to analyze, their effect on tire treadwear, which is the prime reason for conducting abrasion experiments, is even more complicated [215,216]. Predictions of tire wear on the basis of laboratory abrasion tests have been successful only to a certain extent. More work will be required before reliable correlations are obtained. This is due to the fact that the conditions under which rubber abrasion is produced by laboratory test machines and those to which tires are subjected in practice differ considerably [206]. Firstly, the localized surface temperature during tire roadwear seems to be extremely high in some cases and may cause serious thermal decomposition of the polymer. Secondly, the localized strain rate involved in tire wear has been estimated at 100,000 to 1,000,000 % per second. In most cases, however, the surface temperature and localized strain will be lower than in abrasion testing. In addition, instead of usual pattern abrasion during accelerated abrasion testing, in which the conditions are well controlled, worn tire surfaces are sometimes rather smooth or exhibit multidirectional abrasion. This, as well as wear rate, is also associated with the complex tire service conditions,

including variations of road surface, types of vehicles, vehicle loads, weather etc. Even personal driving habits which are related to the speed of driving, braking, and cornering have a pronounced effect on tire wear. Several excellent reviews recently have dealt with treadwear under different aspects [203,206,215,216]. With regard to the effect of carbon blacks, contradictory results have sometimes been reported due to differences in test conditions. Nevertheless, it is generally accepted that the specific surface area of the carbon blacks is important at all severities, and that carbon black structure only has a marked effect on treadwear resistance when high severity is involved [132,210,216].

9.4 Property-Loading Master Curve

Considerable research work has demonstrated that the properties of filler-reinforced rubber are governed by the degree of filler loading as well as the basic filler parameters, such as particle size (specific surface area), structure, and surface activity.

In a series of investigations, mentioned in Section 9.1.2 in relation to the occlusion of rubber, Kraus [45,46] demonstrated a structure-loading equivalence which was first illustrated for the moduli of vulcanizates. He found that various modulus values of carbon-black-reinforced rubber were functions of the product of the actual black loading and a structure-dependent factor. This factor could be calculated from DBP absorption, a measure of carbon black structure. With a limited number of carbon blacks of constant specific surface area and surface characteristics, but differing in structure, Kraus was also able to show the applicability of the structure-loading equivalence principle to tensile strength, elongation at break, and rupture energy. The same concept was also

described by Sambrook [48] and Medalia [98]. While the former used an effective volume fraction of fillers in order to predict Young's modulus, the latter correlated the die swell of compounds and the shear modulus measured under compression at low strain and at 300% elongation to an effective filler volume deduced from carbon black structure (Equation 2).

Instead of calculating the effective filler volume on the basis of structure, Wolff [99] showed in a comprehensive study that the modulus-loading function at a given strain for a whole series of carbon blacks chosen at random could be superposed to a single master curve by introducing a shift factor '. This factor converted the filler volume fraction ϕ into the effective filler volume fraction ϕ_e referenced to the N330 black. The shift factor can be determined experimentally, i.e., visually, by successively adjusting ' for each carbon black until optimum superposition with the reference black is obtained. Wolff found that the shift factors obtained experimentally differ slightly from those calculated from the occlusion of rubber. It was believed that this factor reflects all effects of filler properties on modulus via the effective loading.

More recently, Wolff, Wang and Tan [217219] applied the same principle
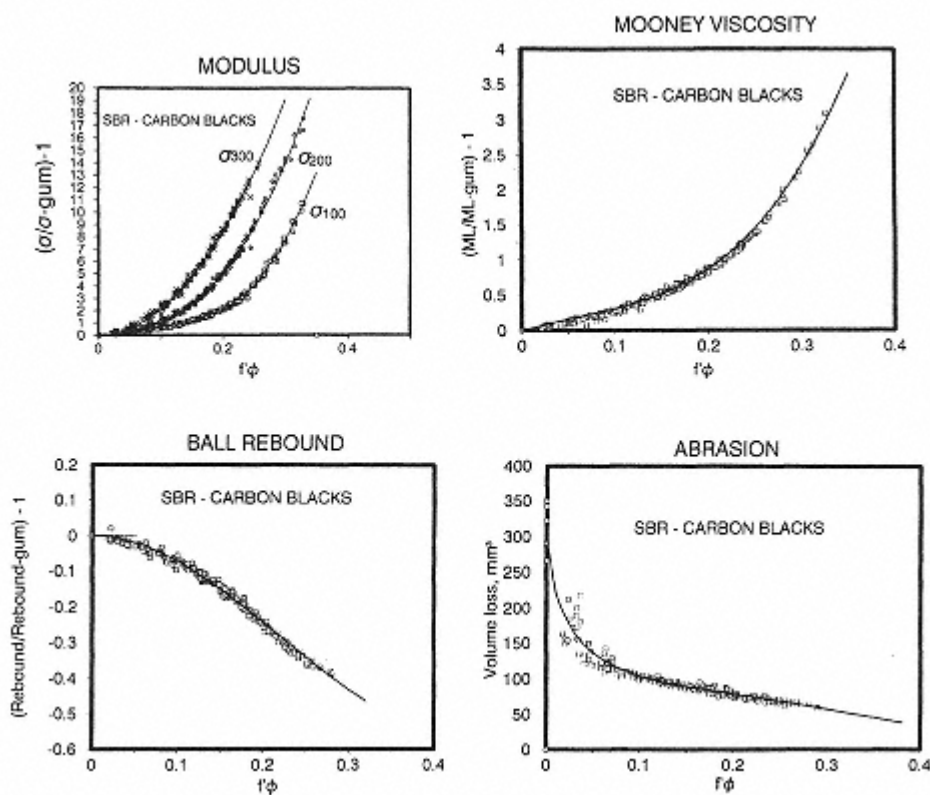
Fig. 27.
Property-loading master curves for SBR filled with various carbon
blacks and loadings (from ref. [217]).

to other rubber properties such as compound viscosity, mechanical
properties of vulcanizates, and swelling. Fig. 27 illustrates the
results for Mooney viscosity, modulus at 100%, 200% and 300%
elongation, respectively (σ100, σ200 and σ300), ball rebound, and
abrasion resistance. Regardless of the experimental error, all
superpositions are good for the properties considered. This implies
that the filled rubber properties are functions of the reduced filler
volume fraction 'ϕ alone:

$$Y = F('\phi) \quad (47)$$

or

$$\frac{Y_f}{Y_o} - 1 = F'(f'\phi) \tag{48}$$

where Y is the relevant property of rubber and the subscripts and o denote the filled and unfilled compounds and vulcanizates, respectively.

This immediately suggests that all carbon blacks, reinforcing and semireinforcing grades, are governed by the same principles for rubber reinforcement. In other words, the mechanism of rubber reinforcement is the same

for all carbon blacks. Since carbon blacks are classified by their particle size, structure and surface activity, all these parameters seem to play a role through their effect on the effective volume of filler in rubber.

According to the above discussion of the filler-polymer interfacial interaction, rubber occlusion, and filler networking, which are related to both the immobilization of rubber and filler properties, it is perhaps not too surprising that all in-rubber effects of the basic filler properties can be related to changes in the effective filler volume, or, in other words, every change in basic filler properties will result in a change of the shift factors.

Since the effect of individual filler parameters on the effective filler volume is associated with different mechanisms which, again, differ in their respective strain and temperature dependence, and since different properties of the rubber compounds are involved at different temperatures and strains, the shift factors should vary from property to property. Therefore, the investigation of the effect of filler parameters on rubber reinforcement may be facilitated by discussing the shift factors of the filler for the rubber properties concerned.

It should again be emphasized that the shift factor ' is the factor used to reduce the filler volume fraction to that of a reference black. It is a relative measure of the effective filler volume. The real effective filler volume is the product of ' and the effective volume of the reference filler.

References

1. Donnet, J. -B. and Voet, A., *Carbon Black, Physics, Chemistry,*

and Elastomer Reinforcement, Marcel Dekker, New York, 1976.

2. Kraus, G., in *Reinforcement of Elastomers,* G. Kraus ed., Wiley Intersci., New York, 1965.

3. Twiss, D. F., *J. Soc. Chem. Ind.,* 44, 1067 (1925).

4. Stickney, P. B. and Falb, R. D., *Rubber Chem. Technol.,* 37, 1299 (1964).

5. Kraus, G., *Adv. Polymer Sci.,* 8, 155 (1971).

6. Blow, C. M., *Polymer,* 14, 309 (1973).

7. Dannenberg, E. M., *Rubber Chem. Technol.,* 59, 512 (1986).

8. Collins, R. L., Bell, M. D. and Kraus, G., *Rubber World,* 139, 219 (1958).

9. Riess, G. and Donnet, J. -B., in *Physico-Chimie du Noir Carbone,* p. 61, Edition du CNRS, Paris, 1963.

10. Gessler, A. M., *Proc. Fifth Rubber Technol. Conf.,* p. 249, Maclaren and Sons, London, 1968.

11. Gessler, A. M., *Rubber Chem. Technol.,* 42, 858 (1969).

12. Donnet, J. -B. and Papirer, E., *Rev. Gen. Caout. Plast.,* 42, 729 (1965).

13. Donnet, J. -B. and Furstenberger, R., *J. Chim. Phys.,* 11/12, 1630, 1638 (1971).

14. Donnet, J. -B., Rigaut, M. and Furstenberger, R., *Carbon,* 11, 153 (1973).

15. Hess, W. M., Lyon, F. and Burgess, K. A., *Kautsch. Gummi Kunstst.,* 20, (3), 135 (1967).

16. Serizawa, H., Nakamura, T., Ito, M., Tanaka, K. and Nomura, N., *Polymer J.,* 15, 201 (1983).

17. Gessler, A. M., *Rubber Chem. Technol.,* 42, 850 (1969).

18. Voet, A., *Kautsch. Gummi Kunstst.,* 26, 254 (1973).

19. Ban, L. L., Hess, W. M. and Papazian, L. A., *Rubber Chem. Technol.,* 47, 858 (1974).

20. Ban, L. L. and Hess, W. M., in *Interaction Entre les Elastomeres et les Surfaces Solides Ayant une action Renforcante,* p. 81, Colloques Internationaux du CNRS, Paris, 1975.

21. Wolff, S., Wang, M. -J. and Tan, E. -H., presented at a meeting of the Rubber Division, ACS, Detroit, Oct. 811, 1991.

22. Kraus, G. and Dugone, J., *Ind. Eng. Chem.,* 47, 1809 (1955).

23. Wang, M. -J, Wolff, S. and Tan, E. -H, presented at a meeting of the Rubber Division, Louisville, Kentucky, May 1922, 1992.

24. Hess, W. M., Ban, L. L., Eckert, F. J. and Chirico, V. E., *Rubber Chem. Technol.,* 41, 356 (1968).

25. Westlinning, H. and Butenuth, G., *Makromol. Chem.,* 47, 215

(1961).

26. Westlinning, H., Butenuth, G. and Leine-Weber, G., *Makromal. Chem.,* 50, 253 (1961).

27. Westlinning, H., *Kautsch. Gummi Kunstst.,* 15, WT475 (1962).

28. Schoon, T. G. F. and Adler, K., *Kautsch. Gummi Kunstst.,* 19, 414 (1966).

29. Smit, P. P. A., *Rheol. Acta,* 5, 4 (1966).

30. Smit, P. P. A., *Rheol. Acta,* 8, 277 (1969).

31. Smit, P. P. A. and Van der Vegt, A. K., *Kautsch. Gummi Kunstst.,* 23, 4 (1970).

32. Smit, P. P. A., in *Interaction Entre les Elastomeres et les Surfaces solides Ayant une Action Renforcante,* p. 213, Colloques Internationaux du CNRS, Paris, 1975.

33. Kaufman, S., Schlichter, W. P. and Davis, D. P., *J., Polymor Sci.,* A-2, 9, 829 (1971).

34. O'Brien, J., Cashall, E., Wardell, E. G. and McBrierty, V. J., *Rubber Chem. Technol.,* 50, 747 (1977).

35. O'Brien, J., Cashall, E., Wardell, E. G. and McBrierty, V. J., *Macromolecules,* 9, 653 (1976).

36. Kenny, J. C., McBrierty, V. J., Rigbi, Z. and Douglass, D. C., *Macro-*

molecules, 24, 436 (1991).

37. Fujimoto, K., et. al., *Nippon Gomu Kyokaishi.,* 43, 54 (1970), 57, 23 (1984).

38. Fujiwara, S and Fujimoto, K., *Macromol. Sci. - Chem.,* A4, 5, 1119 (1970).

39. Haidar, B., presented at a meeting of the Rubber Division, ACS, Las Vegas, May 29-June 1, 1990.

40. Haidar, B., presented at IRC'90, Paris, June 1214, 1990.

41. Kraus, G. and Gruver, J. T., *J. Polymer Sci.,* 8, A2, 571 (1971).

42. Waldrop, G. and Kraus, G., *Rubber Chem. Technol.,* 42, 1155 (1969).

43. Medalia, A. I., *J. Colloid Interf. Sci.,* 32, 115 (1970).

44. Medalia, A. I. in *Les Interactions entre les Elastomeres et les Surfaces Solides Ayant une Action Renforcante,* P. 63, Colloques Internationaux du CNRS, Paris, 1975.

45. Kraus, G., *Polymer Letter,* 8, 601 (1970).

46. Kraus, G., *Rubber Chem. Technol.,* 44, 199 (1972).

47. Medalia, A. I., *Rubber Chem. Technol.,* 45, 1171 (1972).

48. Sambrook, R. W., *J. Inst. Rubber. Ind.,* 4, 210 (1970).

49. Warring, J. R. S., *Trans. Inst. Rubber. Ind.,* 26, 4 (1950).

50. Gerspacher, M., Yang, H. H. and Starita, J. M., presented at the IRC'90, Paris, June 1214, 1990.

51. Gerspacher, M., Yang, H. H. and O'Farrell, C. P., presented at a meeting of the Rubber Division, ACS, Washington D.C., October, 912, 1990.

52. Fitzgerald, E. R., *Rubber Chem. Technol.,* 55, 1547 (1982).

53. Voet, A. and Morawski, J. C., *Rubber Chem. Technol.,* 47, 765 (1974).

54. Wolff, S. and Donnet, J. -B., *Rubber Chem. Technol.,* 63, 32 (1990).

55. Voet, A. and Cook, F. R., *Rubber Chem. Technol.,* 41, 1208 (1968).

56. Voet, A., Sircar, A. K. and Mullens, T. J., *Rubber Chem. Technol.,* 42, 874 (1969).

57. Wolff, S., presented at the International Exhibition Tires' 91, Moscow, March, 14-12, 1991.

58. Van den Tempel, M., *J. Colloid Sci.,* 16, 284 (1961).

59. Wang, M. -J., Wolff, S. and Donnet, J. -B., *Rubber Chem. Technol.,* 64, 714 (1991).

60. Kraus, G., *Rubber Chem. Technol.,* 38, 1070 (1965).

61. Devries, Thesis, Leiden, Holland, 1952. Donnet, J. -B. and Voet, A., *Carbon Black, Physics, Chemistry, and Elastomer Reinforcement,* Ch. 7, Marcel Dekker, New York, 1976.

62. Degussa AG, unpublished work.

63. Kraus, G., *Reinforcement by Fillers,* unpublished.

64. Pliskin, I. and Tokita, N., *J. Appl. Polymer Sci.,* 16, 473 (1972).

65. Kraus, G. and Gruver, J. T., *Rubber Chem. Technol,* 41, 1256 (1968).

66. Kraus, G., *Rubber Chem. Technol.,* 51, 297 (1978).

67. Brennan, J. J., Jermyn, T. E. and Boonstra, B. B., *J. Appl. Polym. Sci.,* 8, 2687 (1964).

68. Shi, Z., Ph. D. dissertation, University of Haute Alsace, France, 1989.

69. Wolff, S. and Wang, M. -J., *Rubber Chem. Technol.,* 65, 329 (1992).

70. Spencer, R. S. and Dillon, R. E., *J. Colloid Sci.,* 3, 163, (1948).

71. Minagawa, N. and White, *J. L., Appl. Polymer Sci., 20, 501 (1976).*

72. Hopper, R. J., *Rubber Chem. Technol.,* 40, 463 (1967).

73. Cotten, G. R., *Rubber Age,* 100, (11), 51 (1968).

74, Dannenberg, E. M. and Stokes, C. A., *Eng. Chem.,* 41, 821 (1949).

75. Wolff, S., *Kautsch. Gummi Kunstst.,* 22, 367 (1969).

76. Wolff, S., *Kautsch. Gummi Kunstst.,* 23, 7 (1970).

77. Boonstra, B. B., in *Rubber Technology and Manufacture,* Ch. 7, Second edition, C. M. Blow and C. Hepburn eds., Butterworth Scientific, London, 1982.

78. Donnet, J. -B., Wang, M. -J., Papirer, E. and Vidal, A., *Kautsch. Gummi Kunstst.,* 39, 510 (1986)

79. Hummel, K., *Kautsch. Gummi Kunstst.,* 15, 1 (1962).

80. Wolff, S., *Kaut. Gummi Kunstst.,* 23, 7 (1970).

81. Kraus, G., *J. Appl. Polymer Sci.,* 7, 861 (1963).

82. Rigbi, Z. and Boonstra, B. B., presented at a meeting of the Rubber Division, ACS, Chicago, Ill., September, 1315, 1976.

83. Smallwood, H. M., *J. Appl. Phys.,* 15, 796 (1944).

84. Guth, E., *Rubber Chem. Technol.,* 18, 596 (1945).

85. Guth, E., Simha, R. and Gold, O., *Kolloid Z.,* 74, 266 (1936)

86. Guth, E. and Gold, O., *Phys. Rev.,* 53, 322 (1938).

87. Bachelor, G. K. and Green, J. T., *J. Fluid Mech.,* 56, 401 (1972).

88. Kener, E. H., *Proc. Phys. Soc.* (London), B69, 802 (1972).

89. Brinkman, H. C., *J. Chem. Phys.,* 20, 571 (1952).

90. Eilers, H., *Kolloid Z.,* 970, 313 (1941).

91. Van der Poel, C. *Rheol. Acta,* 1, 202 (1958).

92. Cohan, L. H., *India Rubber World,* 117, 343 (1947).

93. Mullins, L. and Tobin, N. R., *J. Appl. Polymer Sci.,* 9, 2993 (1965).

94. Guth, E., *J. Appl. Phys.,* 16, 20 (1945).

95. Meinecke, E. M. and Taftaf, M. I., *Rubber Chem. Technol.,* 61, 534 (1986).

96. Hess, W. M., Mcdonald, G. C. and Urban, E., *Rubber Chem. Technol.,* 46, 204 (1973).

97. Ravey, J. C., Premilat, S. and Horn, P., *Eur. Polymer J.,* 6, 1527 (1970).

98. Medalia, A. I., *J. Colloid Interf. Sci.,* 24, 393 (1967).

99. Wolff, S., Ph. D. dissertation, University of Haute Alsace, France, 1987.

100. Tan, E. -H, Ph. D. dissertation, University of Haute Alsace, France, 1992.

101. Payne, A. R., *J. Polymer Sci.,* 6, 57 (1962).

102. Payne, A. R. and Whittaker, R. E., *Rubber Chem. Technol.,* 44, 440 (1971).

103. Kilian, H. -G, Schenk, H. and Wolff, S., *Colloid Polymer Sci.,* 265, 410 (1987).

104. Ambacher, H., Strauss, M., Kilian, H. -G. and Wolff, S., *Kautsch. Gummi Kunstst.,* 44, 1111 (1991).

105. Dannenberg, E. M., *Trans. Inst. Rubber Ind.,* 42, T26 (1966).

106. Dannenberg, E. M., *Rubber Chem. Technol.,* 48, 410 (1975).

107. Mullins, L., *J. Rubber Res.,* 16, 275 (1947).

108. Mullins, L., *J. Phys. and Colloid Chem.,* 54, 239 (1950).

109. Bueche, F., *J. Appl. Polymer Sci.,* 5, 271 (1966).

110. Dannenberg, E. M. and Brennan, J. J., presented at a meeting of Rubber Division, ACS, Philadelphia, 1965.

111. Boonstra, B. B., in *Reinforcement of Elastomers,* G. Kraus ed., Wiley Intersci., New York, 1965.

112. Brennan, J. J., Jermyn, T. E. and Perdagio, M. F., presented at a meeting of Rubber Division, ACS, Detroit, 1964.

113. Wang, M. -J. and Kelley, F. N., unpublished work.

114. Medalia, A. I., *Rubber Chem. Technol.,* 51, 437 (1978).

115. Payne, A. R., *Rubber J.,* 146, 36 (1964).

116. Payne, A. R., Swift, P. M. and Wheelans, M. A., *J. Polymer Res. Inst. Malaya,* 22, 275 (1969).

117. Medalia, A. I. and Laube, S. G., *Rubber Chem. Technol.,* 51, 89 (1978).

118. Kraus, G., *Proc. Internat. Rubber Conf.,* Paper 21, Brighton, U. K., 1977.

119. Sircar, A. K. and Lamond, T. G., *Rubber Chem. Technol.,* 48, 79 (1975).

120. Sircar, A. K. and Lamond, T. G., *Rubber Chem. Technol.,* 48, 89 (1975).

121. Ulmer, J. D., Hess, W. M. and Chirico, V. E., *Rubber Chem. Technol.,* 47, 729 (1974).

122. Kraus, G., *J. Appl. Polymer Sci., Appl. Polymer Symposium,* 39, 75 (1984).

123. Patel, A. C. and Jackson, D. C., Poster presented at IRC'91, Essen, June 2427, 1991.

124. Patel, A. C. and Lee, K. W., *Elastomerics,* 122 (3), 14 (1990); 122 (4), 22 (1990).

125. Caruthers, J. M., Cohen, R. E. and Medalia, A. I., *Rubber Chem. Technol.,* 49, 1076 (1976).

126. Ulmer, J. D., Chirico, V. E. and Dizon, E. S., *Rubber Chem. Technol.,* 48, 592 (1975).

127. McDonald, G. C. and Hess, W. M., *Rubber, Chem. Technol.,* 50, 842 (1977).

128. Degussa AG, unpublished work.

129. Janzen, J. and Kraus, G., *Proc. Internat. Rubber Conf.,* G7-1, Brighton, U. K., 1972.

130. Stacy, C. J., Johnson, P. H. and Kraus, G., *Rubber Chem. Technol.,* 48, 538 (1975).

131. Hess, W. M. and Chirico, V. E., *Rubber Chem. Technol.,* 50, 301 (1977).

132. Shieh, C. -H., Mace, M. L., Ouyang, G. B., Branan, J. M., and Funt, J. M., presented at a meeting of the Rubber Division, ACS, Toronto, Canada, May 2124, 1991.

133. Payne, A. R., *J. Appl. Polymer Sci.,* 9, 3245 (1965).

134. Voet, A and Cook, F. R., *Rubber Chem. Technol.,* 40, 1364 (1967).

135. Medalia, A. I., *Rubber Chem. Technol.,* 46, 877 (1973).

136. Degussa AG. unpublished work.

137. Wolff, S. and Görl, U., *Kautsch. Gummi Kunstst.,* 44, 941 (1991).

138. Wolff, S. and Panenka, R., presented at IRC'85, Kyoto, 1985.

139. Wolff, S., presented at IRC'88, F-15, Sydney, 1988.

140. Gehman, S. D., *Rubber Chem. Technol.,* 30, 1202 (1957).

141. Medalia, A. I., *Rubber World,* 168 (5), 49 (1973).

142. Barker, L. R., Payne, A. R. and Smith, J. F., *J. Inst. Rubber Ind.,* 1, 206 (1967).

143. Ulmer, J. D., Chirico, V. E. and Scott, C. E., *Rubber Chem. Technol.,* 46, 897 (1973).

144. Wolff, S., *Kautsch. Gummi Kunstst.,* 32, 312 (1979).

145. Bulgin, D., Hubbard, G. D. and Walters, M. H., *Proc. Fourth Rubber Tech. Conf.,* p. 173, London, 1962.

146. Saito, Y., *Kautsch. Gummi Kunstst.,* 39, 30 1986.

147. Nordsiek, K. H., *Kautsch. Gummi Kunstst.,* 38, 178 (1985).

148. Degussa AG, unpublished work.

149. Oberth, A. E. and Bruenner, R. S., *Trans. Soc. Rheol.,* 9, 165 (1965).

150. Kinloch, A. J. and Young, R. J., *Fracture Behaviour of Polymers,* Ch. 10, Applied Science, London, 1983.

151. Gent, A. N., in *Science and Technology of Rubber,* Ch. 10, F. R. Eirich ed., Academic press, New York, 1978.

152. Gent, A. N., *J. Mater. Sci.,* 15, 2884 (1980).

153. Nicholson, D. W., *J. Adhesion,* 10, 255 (1979).

154. Hess, W. M., Lyon, F. and Burgess, K. A., *Kautsch. Gummi Kunstst.,* 20, 135 (1967).

155. Rivlin, R. S. and Thomas, A. G., *J. Polymer Sci.,* 10, 291 (1953).

156. Kainradle, P. and Handler, F., *Rubber Chem. Technol.,* 33, 1438 (1960).

157. Griffith, A. A., *Philos. Trans. R. Soc.,* (London), A221, 163 (1921).

158. Stacer, R. G., Yanyo, L. C. and Kelley, F. N., *Rubber Chem. Technol.,* 58, 421 (1985).

159. Gent, A. N. and Kim, H. J., *Rubber Chem. Technol.,* 51, 35 (1978).

160. Wang, M. -J. and Kelley, F. N., unpublished work.

161. Gehman, S. D., in *Reinforcement of Elastomers,* G. Kraus ed., Wiley Intersci., New York, 1965.

162. Eirich, F. R., in *Les Interactions entre les Elastomeres et les Surfaces Solides Ayant une Action Renforcante,* p. 15, Colloques Internationaux du CNRS, Paris, 1975.

163. Lee, D. J. and Donovan, J. A., *Rubber Chem. Technol.,* 60, 910 (1987).

164. Liu, H., Lee, R. F. and Donovan, J. A., *Rubber Chem. Technol.,* 60, 893 (1987).

165. Andrews, E. H. and Gent, A. N., in *The Chemistry and Physics of Rubber-like Substances,* Ch. 9, L. Bateman ed.,

Maclaren and Sons, London, 1963.

166. Lake, G. J. and Lindley, P. B., *J. Appl. Polymer Sci.,* 8, 707 (1964).

167. Mark, J. E. and Erman, B., Rubberlike Elasticity, John Wiley & Sons, New York, 1988.

168. Mullins, L., *Trans. Inst. Rubber Ind.,* 35, 213 (1959).

169. Stacer, R. G. and Kelley, F. N., presented at a meeting of the Rubber Division, ACS, Los Angeles, April 2326, 1985.

170. Williams, M. L., Landel, K. F. and Ferry, J. D., *J. Am. Chem. Soc.,* 77, 3701 (1955).

171. Lake, G. J. and Thomas, A. G., *Proc. R. Soc.,* (London) A300, 108 (1967).

172. Degussa AG, unpublished work.

173. Thomas, A. G., *J. Polymer Sci.,* 18, 177 (1955).

174. Greensmith, H. W., *J. Polymer Sci.,* 21, 175 (1956).

175. Hamed, G. R., *Rubber Chem. Technol.,* 64, 493 (1991).

176. Harwood, J. A. C. and Payne, A. R., *J.Appl. Polymer Sci.,* 12, 889 (1968).

177. Gent, A. N. and Pulford, C. T. R, *J. Mater. Sci.,* 19, 3612 (1984).

178. Goldberg, A., Lesuer, D. R. and Patt, J., *Rubber Chem. Technol.,* 62, 272 (1989)

179. Studebaker, M. L., in *Reinforcement of Elastomers,* G. Kraus ed., Ch. 12, Wiley Intersci., New York, 1965.

180. Smith, T. L., *J. Appl. Phys.,* 35, 27 (1966).

181. Smith, T. L., *Polymer Eng. Sci.,* 17, 129 (1977).

182. Halpin, J. C., *Rubber Chem. Technol.,* 38, 1007 (1965).

183. Smith, T. L., in *Rheology,* F. R. Eirich ed., 5, 127, Academic Press, New York, 1969.

184. Lake, G. J., *Progress of Rubber Technology,* p. 89, Applied Science, England, 1983.

185. Beatty, J. R., *Rubber Chem. Technol.,* 37, 1341 (1964).

186. Wang, W. D., Ph. D. dissertation, University of Haute Alsace, France, 1992.

187. Lake, G. J. and Lindley, P. B., *J. Appl. Polymer Sci.,* 9, 1233 (1965).

188. Lake, G. J. and Lindley, P. B., *J. Appl. Polymer Sci.,* 9, 2031 (1965).

189. Lake, G. J. and Lindley, P. B., *J. Appl. Polymer Sci.,* 10, 343 (1966).

190. Thomas, A. G., *J. Polymer Sci.,* 31, 467 (1958).

191. Gent, A. N., Lindley, P. B. and Thomas, A. G., *J. Appl. Polymer Sci.,* 8, 455 (1964).

192. Lake, G. J. and Lindley, P. B., *J. Appl. Polymer Sci.,* 8, 707 (1964).

193. Rivlin, R. S. and Thomas, A. G., *J. Polymer Sci.,* 10, 291 (1953).

194. Lake, G. J. and Thomas, A. G., *Kautsch. Gummi Kunstst.,* 20, 211 (1967).

195. Kraus, G., in *Advances in Polymer Science,* volume 8, P. 155, H. -J Cantow et al eds., Springer-Verlag, Berlin, 1975.

196. Mullins, L., in *The Chemistry and Physics of Rubber-like Substances,* Ch. 11, L. Bateman ed., Maclaren and Sons, London, 1963.

197. James, A. G., Dtsch. Kautsch. Ges. Conf., Wiesbaden, 1971.

198. Lake, G. J. and Lindley, P. B., *Rubber Chem. Technol.,* 39, 348 (1966).

199. Wolff, S., *Kautschukchemikalien und Füllstoffe in der Modernen Kautschuktechnologie,* Weiterbildungsstudium Kautschuktechnologie, Universität Hannover, 1989/1990.

200. Schallmach, A., *Trans. Inst. Rubber Ind.,* 28, 256 (1952).

201. Schallmach, A., *Wear,* 1, 384 (1958).

202. Southern, E. and Thomas, A. G., *Plast. Rubber, Mater. Appl.,* 3, 133 (1978).

203. Pulford, C. T. R., *Rubber Chem. Technol.,* 58, 653 (1985).

204. Gent, A. N., *Rubber Chem. Technol.,* 62, 750 (1989).

205. McC.Ettles, C. M. and Shen, J. H., *Rubber Chem. Technol.,* 61, 119 (1988).

206. Dannenberg, E. M., *Rubber Chem. Technol.,* 59, 497 (1986).

207. Studebaker, M. L., *Rubber Chem. Technol.,* 41, 1159 (1971).

208. Hess, W. M., Micek, E. and Lyon, F., *Rubber Chem. Technol.,* 41, 2171 (1968).

209. Hess, W. M., Ban, L. L. and Papazian, L., *Rubber Chem. Technol.*,

47, 858 (1974).

210. Janzen, J. and Kraus, G., *J. Elastomers Plast.,* 6, 142 (1974).

211. Veith, A. G. and Chirico, V. E., *Rubber Chem. Technol.,* 52, 748 (1979).

212. Bulgin, D., *Composites,* 2 (3), 165 (1971)

213. Dizon, E. S., *Rubber Chem. Technol.,* 49, 12 (1976).

214. Dannenberg, E. M., *Rubber Age,* 98, 82 (1966).

215. Muhr, A. H. and Robert, A. D., presented at a meeting of the Rubber Division, ACS, Toronto, Canada, May 2124, 1991.

216. Grosch, K. A., *Rubber Chem. Technol.,* 65, 78 (1992).

217. Wolff, S. and Wang, M. -J, to be published.

218. Wolff, S., Wang, M. -J. and Tan, E. -H, to be published.

219. Wolff, S., presented at IRC'92, Beijing, China, October, 1315, 1992.

Chapter 10
Fracture Of Carbon Black Filled Vulcanizates At High Temperature And Under Swollen Conditions

Anil K. Bhowmick
Rubber Technology Centre, Indian Institute of Technology, Kharagpur, India

Fillers are used in almost all rubber articles. Carbon black, silica, clay, calcium carbonate, etc., are used as filler in rubber compounding. The incorporation of filler changes the fracture behaviour of rubber. Reinforcing carbon black improves failure properties of gum rubber vulcanizates while many others are used as diluent to cheapen rubber compounds. Earlier studies on the subject describe carbon black morphology, surface characteristics, physical and chemical interaction with rubber and mechanical properties of unvulcanized and vulcanized rubber compounds [13]. These also clearly indicate that most of the studies in this field have been done earlier under room temperature conditions. However, rubber vulcanizates fail in many applications at high operating temperatures and under conditions when vulcanizates become weak. For example, the temperature of a running tire sometimes goes up to 150°C. The tank track pad shows a temperature of 140°C in the field service. This chapter will highlight tear, tensile and fatigue strength and abrasion of rubber at high temperature and under swollen condition.

Fracture of rubber starts from nicks, cuts, scratches, sharp corners and flaws where the local stress exceeds a critical value for

fracture. A criterion for onset of tearing can be conveniently described by fracture energy [4] defined as

$$-\left(\frac{\partial W}{\partial c}\right)_l = G_c w$$

(1)

where W is the stored elastic energy of a thin sheet of rubber vulcanizate of thickness w with a crack length of c. Gc is the fracture energy characteristic of the material. The parameter l is the overall length which is a constant indicating that the external forces do not work. As shown by Rivlin and Thomas [4], a suitable choice of the test piece (trouser tear) reduces Equation 1 to

$$Gcwdc = dW \quad (2)$$

Hence, Gc may be defined as the energy expended irreversibly per unit increase of length of tear and per unit increase of thickness. The fracture energy Gc is, however, dependent on temperature and rate of tear propagation [5]. Fig. 1 shows how Gc changes with temperature for typical gum vulcanizate of natural rubber (NR) and polychloroprene rubber (CR) [6]. The decrease of Gc with temperature is mainly due to increase in segmental mobility and lower viscoelastic energy losses. Andrews [7] described Gc as follows:

$$G_c = G_{co}\phi(\dot{c}, T, \epsilon_o) \quad (3)$$

where Gco is the threshold fracture energy which is defined as the lower bound
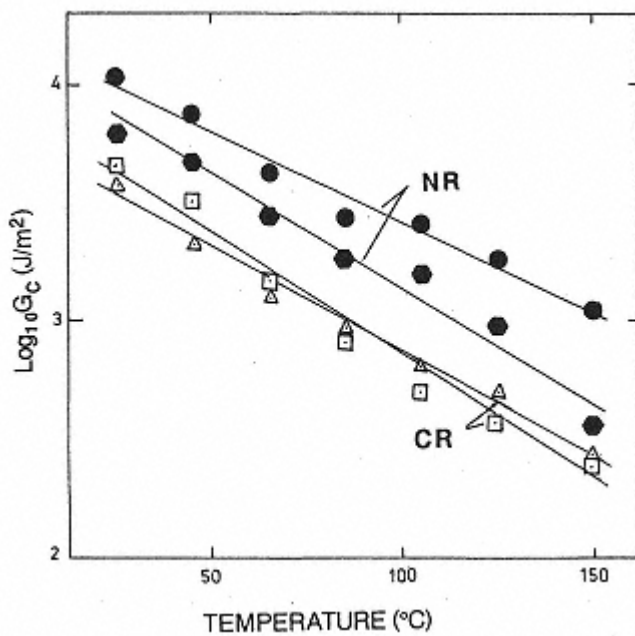
Fig. 1.
Change of Gc with change in temperature for
NR and CR of two different crosslink
densities. Tear rate 170μm/s (from ref. [6]).

on the fracture energy or the fracture energy of rubber when all dissipative processes are minimised. ϕ is a loss function dependent on the crack velocity $\dot{c}$, the temperature T and the applied strain ε_o. G_c increases with increase in the value of the loss function ϕ.

10.1. Contributions To Fracture Energy

Fracture energy, G_c, as discussed above comes from many contributions, which may not be additive. These different contributions involve the following types.

10.1.1. Minimum Fracture Energy

Every rubber vulcanizate shows a minimum value of fracture energy guided by network structure, chain flexibility, bond length, mass per main chain atom and bond dissociation energy [8]. Below this, crack does not propagate in the absence of chemical attack. This value is obtained only at high temperature and/or under swollen conditions. Thomas et al [8] and Gent et al [9,10] reported these minimum values to lie between 40200 J/m$_2$ depending on the factors mentioned above.

10.1.2. Energy Dissipation

The fracture energy of rubber determined under normal tearing experiments at room temperature is much higher (10$_2$ to 10$_5$ J/m$_2$) than the minimum value. This is because part of the energy supplied for crack propagation dissipates in the rubber matrix depending on the rate of tear propagation and temperature. The lower the temperature (but still above T$_g$), the higher would be the contribution of viscoelastic energy loss mechanism. As a result when the fracture takes place at a high temperature, the crack

propagates with little resistance through the matrix due to an increase in the mobility of molecular units with temperature. The magnitude of the viscous contribution to stresses also depends on the rate of deformation relative to the natural mobility of the molecular segments.

Hysteresis gives an idea about the contribution of energy loss in a rubber matrix. Fig. 2 shows the hysteresis of rubber vulcanizates measured at high temperature. The hysteresis is drastically reduced at high temperature. Also shown in the figure is the effect of filler on hysteresis. Carbon black increases the hysteresis of rubber vulcanizates quite significantly because of the various energy loss mechanisms through rubber filler debonding, breakdown of carbon black structure, etc. The same effect is however reduced at high temperature. (The highest temperature of measurement considered in this chapter is 150°C above which the polymer degrades.) Hysteresis is also reduced by swelling rubber vulcanizate in a good solvent. Measurement at high temperature and
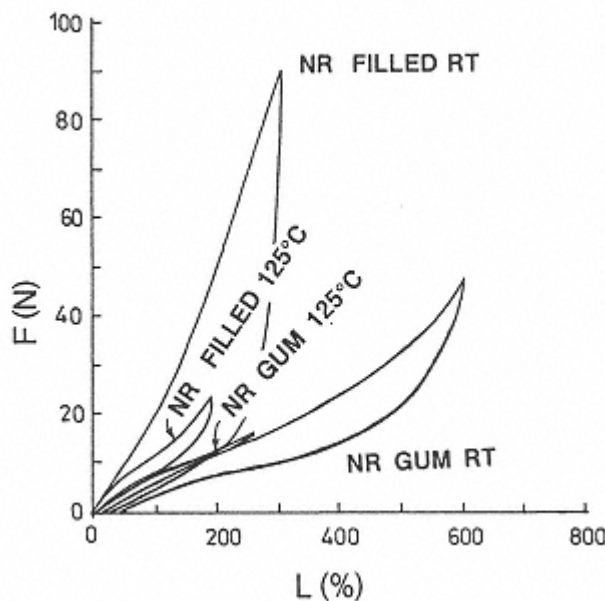
Fig. 2.
Hysteresis of gum and filled NR, measured
at room temperature and at 125°C
(formulation same as ref. [17]).

or under swelling conditions influences the value of loss function in Equation 3 causing a change in the fracture energy.

In fact, a general correlation between tear strength and the temperature interval T - Tg, where T is the test temperature and Tg is the glass transition temperature, has been known for many years [5]. Grosch et al [11] pointed out a relationship between energy dissipation on stretching and the energy per unit volume required to break for filled and unfilled elastomers. Mullins [12] discussed the role of viscoelastic process in the steady tearing of rubber from the relationship between tearing energy and the imaginary part of the complex shear modulus derived from torsion pendulum measurements. Fig. 3 shows a relationship between energy input and hysteresis loss for thermoplastic elastomers [13]. On swelling,

the hysteresis as well as the strength are lowered because of the smaller number of polymeric chains bearing the stress on the fracture plane [14].

10.1.3. Strain Induced Crystallization

Strength of gum natural rubber vulcanizate is higher than that of many synthetic rubber counterparts because of strain induced crystallization. X-rays and birefringence studies indicate that the strain induced crystallisation decreases with increase in temperature [15]. However, it is difficult to remove the effect of strain induced crystallization completely by a high temperature measurement, because threshold values of tear strength of natural rubber
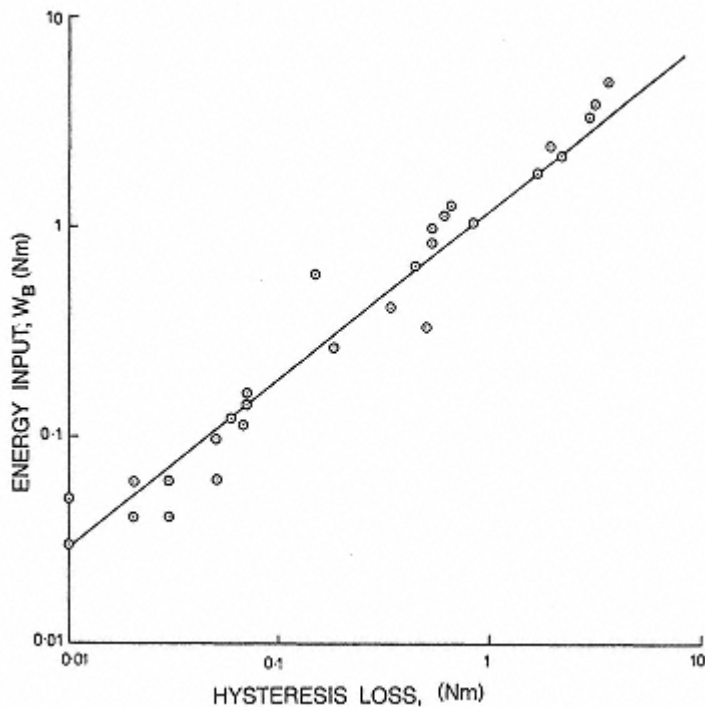
Fig. 3.
Relation between energy input and hysteresis loss
for thermoplastic NR (from ref. [13]).

could not be obtained from tearing experiments at high temperature [16].

10.1.4. Tear Deviation During Fracture

It has been observed that in the case of high strength rubber vulcanizates tear deviates from a straight path to a tortuous one and the character of the tear process changes from smooth tearing to a discontinuous stick-slip or knotty tearing. Carbon black filled vulcanizates reveal this phenomenon and their high strength is often ascribed to this reason. At high temperature or under swelling conditions, however, the magnitude of tear deviation is reduced [17]. Gent and Henry [18] demonstrated that the tear deviation in

carbon black filled rubber vulcanizate from its linear path could be partially prevented by closely spaced metal guide. They conclude that tear force is much smaller (only two to three times) than that for the corresponding unfilled material. If fracture energy is guided only by the segmental mobility and internal energy dissipation, the data points obtained from the measurement at different temperatures and rates should generate a master curve. However, this is not the case with the carbon black filled rubber vulcanizates as reported by Greensmith [19]. Using the restricted tear test, Bhowmick [14] and Stacer et al [20] observed that the tear strength data of the carbon black

filled rubber vulcanizates over a range of mearsurement conditions fall on a single master curve. With the increase in tearing energy, it displays a transition region followed by a plateau which is masked by the addition of filler [20]. Yanyo et al [21] described a relationship between angle of tear deviation and effective tear force for NR and SBR vulcanizates and concluded that the magnitude of the tear force oscillation might be predicted from constrained tear energy and simple tensile extension data.

Though the factors responsible for high strength of carbon black filled rubber vulcanizate are understood, the individual contribution of each of these factors to the fracture energy is yet to be established. Only with great care, various effects could be minimized to achieve a lower limit of fracture energy (threshold value). Fillers, especially the reinforcing ones, affect the contributions discussed above to different extents. The magnitude of these contributions will not only depend on the nature and type of filler and polymer but also on the mode of fracture, temperature, etc. Fracture can take place in various modes. This chapter will discuss fracture of rubber under tensile, tear, fatigue and abrasion modes.

10.2. Tear and Tensile Strength at High Temperature

The effect of nature and loading of carbon black on tear strength of natural rubber, HNBR and SBR vulcanizates at high temperature (125°C) is shown in Fig. 4. The tear strength increases with increase in loading of filler and also with increase in surface area of filler. Some of these values are much lower than that obtained at room temperature measurement. However, due to tear deviation, the data at room temperature could not be obtained for all the

samples under similar trouser tear measurement. The increase in tear strength of filled material may be due to increase in intrinsic strength, hysteresis and tear deviation while its decrease at high temperature is due to reduction of hysteresis and molecular friction and presumably also due to less tear deviation. Greensmith [19] concluded that the carbon black increased the tear strength of amorphous elastomers for a relatively narrow range of tearing rates and temperatures. He ascribed the enhancement of strength due to knotty tearing developed during fracture. Greensmith also obtained conditions of temperature and rate of tear propagation for knotty tearing. Bhowmick [14], however, obtained tearing energy spectrum with the help of restricted tear test for filled SBR using a WLF shift factor over a temperature range from -100 to 200°C. This indicates that the same viscoelastic energy loss mechanisms are operative over the whole range of temperatures even for the filled material if the tear deviation is controlled. Stacer et al [20] made detailed investigation on the tear strength of filled rubber from a low temperature to a high temperature using the same method as originally
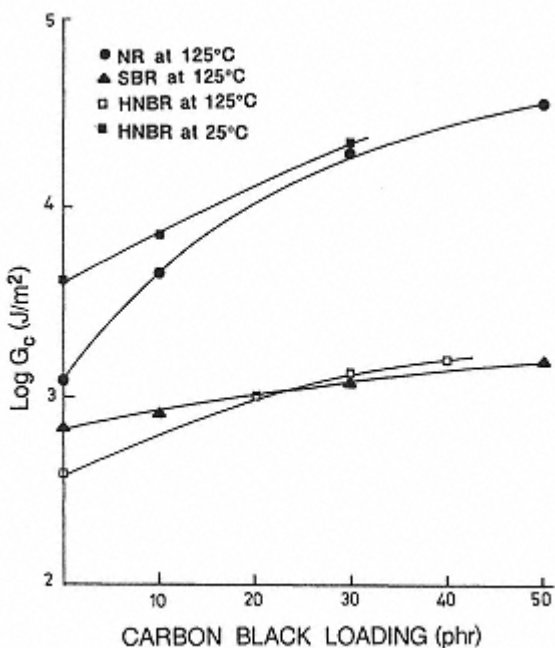
Fig. 4.
Influence of loading of carbon black on the
tear strength of NR, HNBR and SBR
tested at 125° C.

proposed by Gent and Henry [18]. Around the glassy state, the curves of reduced tearing energy against reduced rate meet, but at lower reduced rate (higher temperature), the curves remain well separated. The carbon black caused about a 63% increase in tearing energy in intermediate region.

A similar trend is obtained for tensile strength which increases with loading and surface area of carbon black. Table 1 shows the tensile strength obtained at different temperatures for natural rubber. As compared to room temperature data, these values are very low. It has been observed by Thomas and Whittle [22] and later Bhowmick et al [23] that there is a critical temperature above which the tensile strength drops suddenly. This critical point (θc) is

also dependent on the nature of the filler and the polymer, the crosslink density and the crosslinking system. The presence of carbon black (HAF) filler increases the strength above θ_c, but has little influence on the value of θ_c at a temperature below it. A dramatic drop was also observed for natural rubber when energy input to break was plotted against temperature [24]. The lower strength at high temperature may also be analysed using strain amplification factor which reduces at high temperature. The strain amplification increases with the surface area of carbon black even at high temperatures. Table 2 shows the strain amplification factor for several filled mixes [25]. This tends to attain a limiting value at higher temperatures. It has been reported that in the near absence of viscoelasticity and crystallization, the amplifica-

Table 1. Values of Tensile Strength (MPa) of Gum and Filled Unswollen Natural Rubber Vulcanizates at Different Temperatures

Sample code	25°C	75°C	100°C	125°C
Control	22.50	-	3.74	3.00
10 phr (N375) filled	23.30	10.81	7.61	3.49
20 phr (N375) filled	25.90	12.90	10.00	4.95
30 phr (N375) filled	26.60	15.90	13.60	6.68
40 phr (N375) filled	26.10	16.00	10.26	7.68
50 phr (N375) filled	24.60	16.90	14.29	7.86
10 phr (N330) filled	23.00	8.12	4.24	2.03
20 phr (N330) filled	24.80	12.80	7.76	4.52
30 phr (N330) filled	26.00	15.90	9.55	5.72
40 phr (N330) filled	25.70	16.00	9.26	7.13
50 phr (N330) filled	23.90	16.40	11.76	7.83

From ref. [36].

tion factor normalised with respect to surface area and loading at a particular strain gives a constant value. Neogi, Basu and Bhowmick [26] generated failure envelopes for filled NR and SBR vulcanizates from the data over a range of temperatures from 15 to 150°C. The observations are similar to those for gum vulcanizates. There are two extremes - one corresponds to an increase in strength with an increase in breaking extension and the other shows high breaking stress and low extensibility. The former data are obtained at high temperatures and low rates. The failure envelopes demonstrate the importance of the viscoelastic process during fracture. The authors also obtained proportionality between $\varepsilon_{b,max}$ (maximum elongation at break) with small strain modulus (E) of the filled vulcanizates. $\varepsilon_{b,max}$ decreases with an increase in E.

10.3. Fatigue Failure and Wear at High Temperature

The influence of carbon black on the fatigue strength is interesting. It is dependent on the nature of rubber, whether crystallizing or non-crystallizing, and the type of loading, whether constant stress or constant strain. Figs. 5(a) and 5(b) reveal the effect of carbon black (N375) on the growth of a crack in natural rubber and SBR vulcanizates at constant strain of 0.5 at 75°C and 125°C [27]. At a particular flexing cycle, the cut growth Δc increases with the increase in loading of carbon black in natural rubber whereas the same decreases up to 50 phr filler for SBR vulcanizates. At very high loading when the filler acts as a diluent, the cut growth in both NR and SBR vulcanizates

Table 2. Strain Amplification Factor for Different Black Filled Rubbers at Different Temperatures at Extension Ratio λ = 1.05

Sample code[a]	Temperature, °C	Strain amplification factor	Sample code[a]	Temperature, °C	Strain amplification factor
N5 (N220)	25	11.9	S5 (N220)	25	7.6
N5 (N375)	25	11.0	S5 (N375)	25	7.4
N5 (N550)	25	5.4	S5 (N550)	25	6.6
N5 (N660)	25	3.9	S5 (N660)	25	6.2
N5 (Clay)	25	1.4	S5 (Clay)	25	3.8
N5 (N220)	75	11.0	S5 (N220)	75	5.1
N5 (N375)	75	8.2	S5 (N375)	75	3.2
N5 (N550)	75	3.6	S5 (N550)	75	2.1
N5 (N660)	75	3.0	S5 (N660)	75	1.4
N5 (Clay)	75	0.8	S5 (Clay)	75	0.5
N5 (N220)	100	4.5	S5 (N220)	100	3.9
N5 (N375)	100	4.1	S5 (N375)	100	2.8
N5 (N550)	100	3.0	S5 (N550)	100	2.0
N5 (N660)	100	2.6	S5 (N660)	100	1.2

N5 (Clay)	100	0.4	S5 (Clay)	100	0.5
N5 (N220)	125	4.5	S5 (N220)	125	3.9
N5 (N375)	125	4.1	S5 (N375)	125	2.8
N5 (N550)	125	3.0	S5 (N550)	125	2.0
N5 (N660)	125	2.6	S5 (N660)	125	1.2
N5 (Clay)	125	0.4	S5 (Clay)	125	0.5

a N indicates NR and S indicates SBR. All the samples are loaded with 50 phr filler From ref. [25].

becomes very rapid. Neogi, Basu and Bhowmick [27] also studied the effect of N220, N375, N550 and N660 black at 50 phr loading on the cut growth process at high temperature. N220 filled NR sample shows fastest cut growth in the series. An opposite trend is observed with SBR. At still higher temperature, 125°C, the cut growth process becomes still faster (Fig. 5b). With constant stress of 5N, however, the authors observe that the cut growth becomes slower with the increase in filler loading. A plot of cut growth rate vs tearing energy (Fig. 6) shows that the value of the slope decreases for NR and SBR with the addition of filler. The same, however, increases with the increase in temperature.

Bhaumick, Gupta and Bhowmick [28] conducted experiments with filled EPDM, bromobutyl rubber and their blends. They noted an increase in the rate of cut growth by increasing the temperature from 25°C to 100°C. A representative figure illustrates this behaviour for a filled 50:50 EPDM - BIIR
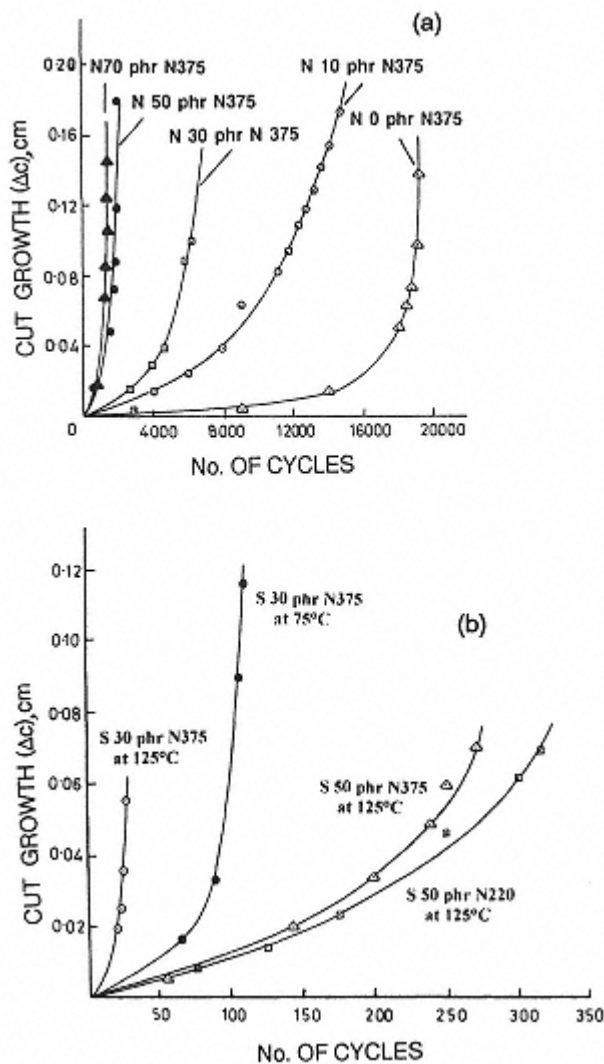
Fig. 5.
Effect of loading of carbon black on cut
growth. a: NR vulcanizates at 75°C and
at a strain of 0.5; b: SBR vulcanizates at
75 and 125°C and at a strain of 0.5 (from
ref. [27]).

vulcanizate (Fig. 7). It has been also observed from the
fractographs that the general features are similar to those reported

for samples fractured at room temperature. The crack lines are, however, more numerous.

All these results could be explained with the help of competing factors like strain energy density, flaw size, strength of the matrix and viscoelasticity. For example, addition of reinforcing filler raises the value of strain energy density (W') and flaw size (c_o) and at the same time enhances the tear strength and tensile strength as well as viscoelastic losses in rubber. In NR, the two
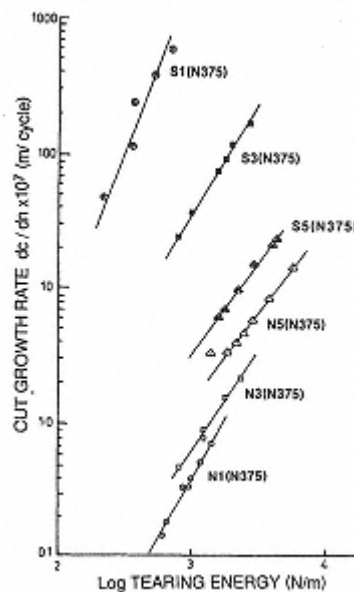
Fig. 6.
Relationship between rate
of cut growth and tearing
energy for carbon black
filled NR and SBR
vulcanizates at 75° C (from
ref. [27]).

factors W' and co seem to predominate at constant strain
experiment. SBR gum vulcanizate is, however, so weak that
reinforcing black helps in the crack growth resistance. The black
filler in SBR helps in distribution of stresses and the growth
process is always tortuous. Neogi, Basu and Bhowmick [27] also
calculated the critical number of cycles at which the growth
process becomes
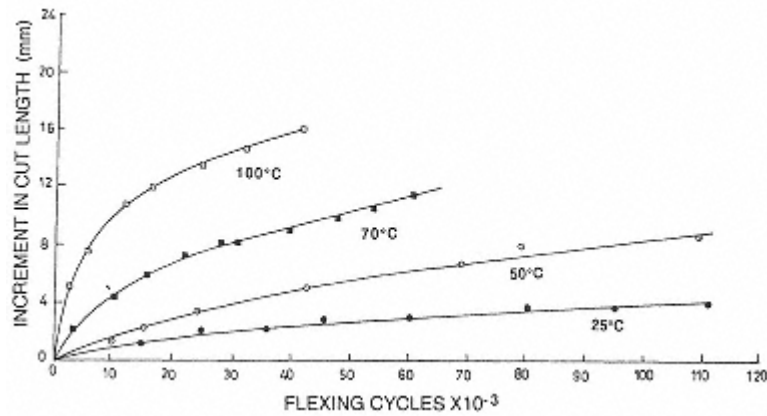
Fig. 7.
Increment in cut length as a function of flexing cycles of 50/50 EPDM/BIIR filled vulcanizates at different temperatures and at 3.15 mm precut (from ref. [28]).

Table 3. Critical Number of Cycles for Unswollen Vulcanizates at Which Catastrophic Failure States Occur (Strain=0.5)

Sample code[a]	No. of cycles, 75°C	No. of cycles, 125°C
S1 (N375)	8	-
S3 (N375)	90	22
S5 (N375)	600	180
S7 (N375)	5	-
S5 (N660)	30	-
S5 (N550)	50	-
S5 (N220)	840	220
N0	16600	-
N1 (N375)	8600	-
N3 (N375)	4000	230
N5 (N375)	1800	90
N7 (N375)	1100	50
N5 (N660)	13400	-
N5 (N550)	7000	110
N5 (N220)	1600	80

a S indicates SBR, N indicates NR; the numbers 1, 2, 3, 4, 5 and 7 indicate 10, 20, 30, 40, 50 and 70 phr filler loading respectively. From ref. [27].

suddenly rapid (Fig. 5). This also decreases with the increase in temperature (Table 3). Carbon black loading reduces this value for NR, and enhances the same for SBR upto 50 phr loading at constant strain.

Young [29] investigated the effects of temperature on the fatigue crack propagation (FCP) of chlorobutyl (CIIR), natural rubber and polybutadiene rubber (BR) at 20 s-1 strain rate at 0, 25, 50 and 75°C. The author observed an increase in FCP rates with an increase in temperature. Temperature affected the slope of the

fatigue function which was influenced by elastomer type. For example, BR showed the greatest effect which was opposite to the effect for the CIIR compound.

Goldberg et al [30] studied the fracture morphologies of carbon black loaded SBR subjected to low cycle, high stress fatigue at a series of temperatures ranging from 22 to 140°C. Increasing the test temperature decreases critical cyclic stress. The fine details of tear surfaces in regions contiguous with the flaws vary with temperature.

The mechanism of abrasion of rubber at high temperature is complicated. Gent and Pulford [31] examined the effect of temperature change from 25 to 100°C on the rates of wear of filled and unfilled NR, SBR, polybutadiene, *trans* - polypentanomer and NR/BR blend. At a particular frictional force, the rate of wear increases with temperature for SBR and NR/BR samples.

However, there is an overall smaller effect of large temperature rise on the wear rate. Gent and Pulford felt that their data were not consistent with a mechanical fatigue mechanism of abrasion. They observed various fracture surfaces (particulate debris, oily layer, or adhering rolls) during experiments at high temperature. In an interesting experiment on the wear of carbon black filled hydrogenated nitrile rubber (HNBR) at high temperature (up to 100°C), it has been observed that the addition of the carbon black decreases the abrasion loss, but increases the dynamic coefficient of friction and frictional force [32]. The abradibility, defined as the abrasion loss per unit frictional work, increases linearly with the reciprocal of breaking energy. The abraded surfaces of the vulcanizates does not show ridges at a testing temperature of 25°C. These are observed only above 50°C. The ridge spacing decreases with carbon black loading and varies inversely with dynamic shear modulus. The spacing increases with testing temperature.

10.4. Effect of Swelling on Tear, Tensile and Fatigue Strength and Abrasion

As discussed before, swelling reduced the viscoelastic losses considerably and minimised the barriers to tear propagation. Hence, the fracture energy of swollen samples is much lower than their unswollen counterpart. Measurement of tear strength of swollen urethane rubber was carried out by Muller and Knaus [33]. Ahagon and Gent investigated polybutadiene elastomers crosslinked to varying degrees [9]. They obtained threshold values of fracture energy which were in good accord with the values calculated on the basis of Lake and Thomas theory. However, practical difficulties arose for the determination of threshold tear

strength of carbon black reinforced rubber vulcanizates. This is because measurements at high temperature and under swelling conditions do not yield the same value. It was, however, felt that the vulcanizates could be swollen with various mobile liquids or good solvents (of high b.p.) and the tear strength of the swollen vulcanizates can be taken as threshold or minimum value, provided it is independent of the nature of the solvent and rate of testing.

Tear strength of filled elastomers under swollen conditions was reported first by Gent and coworkers [16]. Filled BR and EPDM vulcanizates swollen with paraffin oil show lower values of tear strength, which are 34 times more than the simplest unreinforced vulcanizate of the same elastomer. These values are again much smaller than the tear energies determined under normal tearing experiments. For example, they obtained threshold values of ~200 J/m2 for filled elastomers. Detailed studies were taken up later by Bhowmick et al [17].

The influence of loading and nature of carbon black on the tear strength of swollen rubber vulcanizates is shown in Figs. 8 and 9. Equilibrium swelling
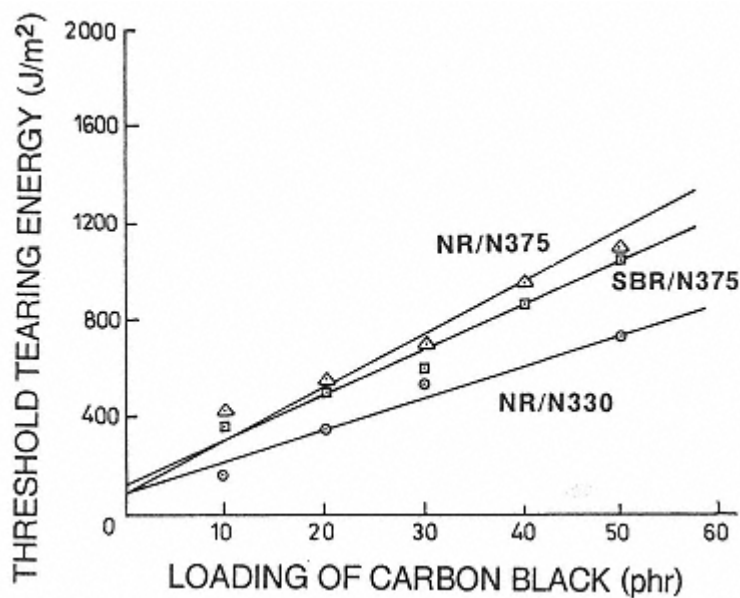
Fig. 8.
Effect of loading of carbon black on threshold tear
strength (from ref. [17]).

in xylene, toluene, heptane and benzene gives similar values of tear strength in each case. Bhowmick et al [17] observe that the tear strength increases with the increase in loading and surface area of carbon black. The values lie between 150 J/m_2 to 750 J/m_2 for N330 filled NR vulcanizates. N220 filled
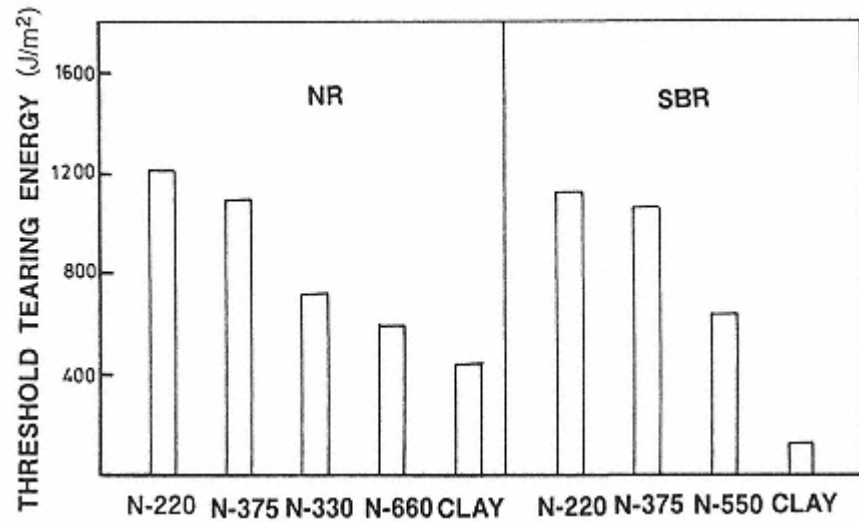
Fig. 9.
Threshold tear strength of rubber with different types of fillers
(from ref. [17]).

systems show higher values than N375 filled ones. SBR vulcanizates show marginally lower threshold tear strength than their NR counterpart. Gent et al [16], however, earlier reported much lower values of threshold tear strength of 50 phr filled EPDM and polybutadiene vulcanizates. The difference may be attributed to differences in crosslink density and modulus of the various rubbers. All these results indicate that there is approximately a two- to tenfold increase in strength with loading of carbon black filler up to 50 phr. A non-reinforcing filler like clay was shown to have minimum influence on threshold tear strength of NR and SBR vulcanizates.

The authors also derived relation between tearing energy Gco and loading of black as follows

$$Gco = Gco + m\phi Gco \quad (4)$$

were ϕ is the volume fraction of filler and m is a constant characteristics of the black.

According to Lake and Thomas [8], many bonds on a fracture plane are stressed in order to break one of them. They show a dependence of threshold fracture energy on the average molecular weight (Mc) of chains between points of crosslinking for gum vulcanizates. In filled vulcanizates, when the filler concentration is low, there will be a larger number of polymeric bonds in a plane which must be stressed to break a molecular chain. On the other hand, there will be a smaller number of them crossing a fracture plane. Similarly, when the filler is added in large quantity, the number of polymer chains on the fracture plane will be low and the filler aggregate will be present in higher quantity. These factors do

not cancel out each other - their net effect is a dependence of the fracture energy on the small strain elastic modulus E. Bhowmick et al has noted that as the value of small strain modulus increases, the threshold tear strength increases [17]. Lake and Lindley [34] reported that for accelerated sulfur vulcanizates, the threshold fracture energy obtained from fatigue experiments increased approximately in proportion to the Young's modulus. The results are, however, different from the results of gum vulcanizates where it varies with E-½ or $G_{cof} = G_{co} + m\phi_f G_{co}$ [8,35]. For filled systems it is apparent, then, that the filler overshadows the effect of factors like network structure, chain flexibility, bond length, mass per chain atoms, etc.

Tensile strength of various filled vulcanizates under swelling conditions was also determined. The strength decreases on swelling and ultimately threshold values are obtained under equilibrium swelling [36]. Threshold strength when plotted as a function of loading of carbon black reveals that the value increases rapidly with loading for SBR and NR up to a certain loading. The increase is slow after this point. Similarly, at 50 phr loading, the influence of surface area of the black was studied. The improvement in tensile strength for NR follows the order:

N220 > N375 > N330 > N660

For SBR vulcanizates also, N220 black displays the highest minimum tensile strength. It is important to note from these observations that the tensile strength is drastically reduced when the samples are swollen with mobile liquid, although the trend in tensile strength with reference to filler loading and nature of filler still remains the same even when the samples are weak.

Threshold values of tensile strength could be calculated using the values of threshold fracture energy and invoking the equation

$$\sigma_{b,o} = \left(\frac{G_{co}E}{\pi c_o}\right)^{1/2} \quad (5)$$

Taking a representative value of E as 2 MN/m2, G_{co} as 50 J/m2 and c_o=40µm, $\sigma_{b,o}$ is 0.9 MN/m2 and the corresponding value of $\varepsilon_{b,o}$ is 0.45. These values are indeed close to experimental fatigue limits. For filled vulcanizates, the value of E can be calculated from

$$E = E_o(1 + 2.5\phi' + 14.1\phi'2) \quad (6)$$

$$\frac{V_{occl}}{V_c} = \frac{\phi' - \phi_f}{\phi_f} \quad (7)$$

$$\phi' = \phi(1 + 0.02139DBPA)/1.46 \quad (8)$$

Voccl and *Vc* refer to the total volume of occluded rubber and of carbon black, respectively. ϕ' and ϕ are the volume fraction of filler plus occluded rubber and volume fraction of filler alone, respectively, and DBPA is the dibutyl phthalate number. Using the values of *Gco* for filled rubber and $c_o = 50$µm, the theoretical

values of threshold tensile strength reported in Table 4 are in good accord with the experimental values. This clearly indicates that the strengthening mechanism is similar for all the filled vulcanizates.

Cut growth experiments were also conducted on swollen filled vulcanizates by Neogi et al [27]. The samples fail catastrophically at a critical value of flaw which could not be accurately measured. The fatigue life goes through an optimum with the increase in loading of filler at constant strain experiment at 125°C (Table 5). At 50 phr loading, N660 filled vulcanizates show higher life than N220 counterpart.

Measurement of wear of vulcanizates under swollen conditions when the hysteresis is reduced reveals that the wear rate is drastically increased at similar frictional forces [32]. Comparison of wear data of filled and unfilled swollen vulcanizates indicates that the enhancement of abrasion resistance is only twofold due to addition of filler. The abrasion resistance, however, increases with loading and surface area of carbon black. The ridge patterns are observed only at lower normal load for NR and SBR, and extensive tearing

Table 4. Theoretical and Experimental Values of Tensile Strength

Sample code	Tensile strength (MPa) theor.	Tensile strength (MPa) exper.
SBR + 10 phr (N375)	1.14	0.62
SBR + 20 phr (N375)	1.43	1.12
SBR + 30 phr (N375)	1.93	1.61
SBR + 40 phr (N375)	2.64	2.10
SBR + 50 phr (N375)	3.34	2.24
SBR + 50 phr (N220)	3.36	2.96
SBR + 50 phr (N550)	3.30	2.59
SBR + 50 phr (N660)	2.15	2.98
NR + 10 phr (N375)	1.20	1.30
NR + 20 phr (N375)	1.51	1.76
NR + 30 phr (N375)	1.93	2.10
NR + 40 phr (N375)	2.50	2.46
NR + 50 phr (N375)	2.89	2.61
NR + 10 phr (N330)	0.68	0.76
NR + 20 phr (N330)	1.17	1.61

NR + 30 phr (N330)	1.64	1.95
NR + 40 phr (N330)	2.00	2.10
NR + 50 phr (N330)	2.31	2.44
NR + 50 phr (N220)	2.85	2.90
NR + 50 phr (N550)	2.15	3.18
NR + 50 phr (N660)	2.01	2.33

From ref. [36].

and ploughing are noted at higher normal load. It is interesting that ridges (which have not been observed at room temperature testing of HNBR) are generated during testing under swollen condition.

Fractography gives very useful information on the fracture mechanism. Our earlier studies indicated the role of carbon black filler and the inclusions on the fracture surface morphology [3739]. Tear fracture of swollen filled samples generates a large number of fissures separated by ridges that make an angle of 80 to 90° with the given cut [40]. Similarly, the tensile failed surfaces show tear lines separated by 50100 μm. Although qualitatively lower strength of swollen material is due to smaller tear deviation and larger cracks, it is difficult to put forward any quantitative correlation. Gent and Pulford [41], however, characterized stronger material with more closely spaced steps and greater height of the steps and weaker materials with smooth torn areas. It is clear from these studies that carbon black leads to tear deviation presumably by creating barriers in the path of the tear.

Table 5. Fatigue Life of Paraffin Oil Swollen Vulcanizates at Different Temperatures and at a Constant Strain of 0.2

Sample code[a]	No. of cycles, 75°C	No. of cycles, 125°C
N (0)	13000	35
N1 (N375)	5500	205
N3 (N375)	5380	315
N5 (N375)	205	54
N7 (N375)	42	15
N5 (N550)	250	55
N5 (N660)	325	60
S (0)	5	1
S1 (N375)	1800	55
S3 (N375)	1120	340
S5 (N375)	475	310
S7 (N375)	85	50
S5 (N660)	600	400
S5 (N220)	400	310

a N indicates NR; S indicates SBR; the numbers 1, 3, 5 and 7 indicate 10, 30, 50 and 70 phr filler loading respectively. From ref. [27].

The kinetic theory has been applied to crack propargation to describe the fracture of molecules at the tip of the crack [42]. This approach has certain limitations in that it ignores the predominant role of inelastic process. If, however, one accepts molecular fracture as an activated process, the rate constant for the net bond fracture suggests that there is an increase in bond breakage with increasing temperature. With the incorporation of carbon black or swelling of the vulcanizates, the activation energy barrier, G^*_{AB} will be modified. G^*_{AB} will presumably be lower on swelling and

increase with the loading of black. However, investigations are needed to prove these points.

References

1. Donnet, J.-B and Voet, A. *Carbon black, Physics, Chemistry and Elastomer Reinforcement,* Marcel Dekker, New York, 1976.

2. Kraus, G., *Reinforcement of Elastomers,* Wiley Interscience, New York, 1965.

3. Medalia, A. I., *Rubber Chem. Technol.,* 51, 437 (1978).

4. Rivlin, R. S. and Thomas, A. G., *J. Polym. Sci.,* 10, 291 (1953).

5. Gent, A. N., in *Science and Technology of Rubber,* F. R. Eirich, ed., Academic Press, New York, p. 419, 1978.

6. Bhowmick, A. K. and Gent, A. N., *Rubber Chem. Technol.,* 56, 845 (1983).

7. Andrews, E. H., *J. Materials Sci.,* 9, 887 (1974); Andrews, E. H. and Fukahori, Y., *J. Materials Sci.,* 12, 1307 (1977).

8. Lake, G. J. and Thomas, A. G., *Proc. Roy. Soc. London,* A. 300, 108 (1967).

9. Ahagon, A. and Gent, A. N., *J. Polym. Sci., Polym. Phys. Ed.,* 13, 1903 (1978).

10. Gent, A. N. and Tobias, R. H., *J. Polym. Sci., Polym. Phys. Ed.,* 20, 2051 (1982).

11. Grosch, K. A., Harwood, J. A. C. and Payne, A. R., *Nature* (London), 212, 497 (1966).

12. Mullins, L., *Trans. Inst. Rubber Ind.,* 35, 213 (1959).

13. Roy Choudhury, N. and Bhowmick, A. K., *Plastics & Rubber-Processing and Applications,* 11, 185 (1989).

14. Bhowmick, A. K., *J. Mater. Sci.,* 21, 3927 (1986).

15. Bhowmick A. K., Kuo C. C., Manzur A, MacArthur, A. and Mclntyre, D., *J. Macromol. Sci., Phys. Ed.* 25, 283 (1986).

16. Bhowmick, A. K., Gent, A. N. and Pulford, C. T. R., *Rubber Chem. Technol.,* 56, 226 (1983).

17. Bhowmick, A. K., Neogi, C. and Basu, S. P., *J. Appl. Polym.*

Sci., 41, 917 (1990).

18. Gent, A. N. and Henry, A. W., *Proc. Int. Rubber Conf.,* p. 193, 1967.

19. Greensmith, H. W., *J. Polym. Sci.,* XXI, 175 (1956).

20. Stacer, R., Von Meerwall, E. D. and Kelley, F. N., *Rubber Chem. Technol.,* 58, 913 (1985).

21. Yanyo, L. C., Stacer, R. G. and Kelley, F. N., *Rubber Chem. Technol.,* 58, 421 (1985).

22. Thomas, A. G. and Whittle, J. M., *Rubber Chem. Technol.,* 43, 222 (1970).

23. Saha Deuri, A. and Bhowmick, A. K., *J. Materials Sci.,* 22, 4299 (1987).

24. Harwood, J. A. C., Payne, A. R. and Whittaker R. E., *J. Appl. Polym. Sci.,* 14, 2183 (1970).

25. Neogi, C., Basu, S. P. and Bhowmick, A. K., *Plastics & Rubber-Processing and Application,* 12, 147 (1989).

26. Neogi, C., Basu, S. P. and Bhowmick, A. K., *J. Materials. Sci.,* 9, 1379 (1990).

27. Neogi, C., Basu, S. P. and Bhowmick, A. K., *J. Elastomers and Plastics,*

24, 96 (1992).

28. Bhaumick, T. K., Gupta, B. R. and Bhowmick, A. K., *J. Materials Sci.,* 22, 4336 (1987).

29. Young, D. G., *Rubber Chem. Technol.,* 59, 809 (1986).

30. Goldberg, A., Leuser, D. R. and Patt, J., *Rubber Chem. Technol.,* 62, 272 (1989).

31. Gent, A. N. and Pulford, C. T. R., *J. Appl. Polym. Sci.,* 28, 943 (1983).

32. Thavamani, P. and Bhowmick, A. K., *Plastics, Rubber and Composites-Processing & Applications,* 18, 35 (1992).

33. Mueller, H. K. and Knaus, W. G., *Trans. Soc. Rheol.,* 15, 217 (1971).

34. Lake, G. J. and Lindley, P. B., *J. Appl. Polym. Sci.,* 9, 1233 (1965).

35. Bhowmick, A. K., *J. Macromol. Sci., Rev. Macromol. Chem. Phys.,* C-28 (3 & 4), 339 (1988).

36. Neogi, C., Bhowmick, A. K. and Basu, S. P., *J. Materials Sci.,* 25, 3524 (1990).

37. Bhowmick, A. K., *Kautsch. Gummi Kunstst.,* 37, 191 (1984).

38. Bhowmick, A. K., *Rubber Chem. Technol.,* 55, 1055 (1982).

39. Bhowmick, A. K., *J. Materials Sci.,* L.5, 1042 (1986).

40. Neogi, C., Bhowmick, A. K. and Basu, S. P., *Kautsch. Gummi Kunstst.,* 43, 974 (1990).

41. Gent, A. N. and Pulford, C. T. R., *J. Materials Sci.,* 19, 3612 (1984).

42. Andrews E. H. and Reed P. E., in *Molecular Fracture in Polymers,* in *Advances in Polymer Science,* volume 27, p. 3, Springer-Verlag, Berlin, Heidelberg, 1978.

Chapter 11
Dynamic Viscoelastic Properties Of Loaded Elastomers

Michel Gerspacher
Sid Richardson Carbon & Gasoline Co.,
Fort Worth, Texas, U. S. A.

In the tire industry, which uses as much as 90% of the worldwide produced carbon black, the importance of the filler is essentially in the reinforcement of the end product: the vulcanized tire.

If the word reinforcement is sometimes used as a general statement it always refers to an increase of a parameter, the strengthening of properties, improvement of material characteristics, i.e., modulus increase, tear strengthening, wear improvement, etc. These enhanced qualities apply to an object whose utilization is characterized by dynamic and periodic deformations. These deformations can be defined using three essential parameters, which are: strain, frequency and temperature.

These three parameters are essential because of the viscoelastic nature of the rubbery phase of rubber goods. As mentioned later, a tremendous amount of work has been done for several decades to understand the role of these parameters on the performance of rubber based materials [1].

11.1. Background

A carbon black filled elastomer should be regarded as a composite

characterized by a rubbery continuous phase and a particulate rigid dispersed phase. The continuous phase is responsible for the rubbery behavior of the composite, while the filler plays a specific and important role in enhancing the various properties. In order to better define the rubbery behavior of the composite, it is necessary to refer to the theory of viscoelasticity.

A purely elastic material is characterized by a linear relationship between stress and strain (Hookean material); whereas, a purely viscous fluid exhibits a stress directly proportional to the strain rate but independent of strain itself (Newtonian). This description however characterizes ideal materials. In fact, many solids and liquids exhibit Hookean and Newtonian behavior for infinitesimal small strain or strain rate only. When larger strains or strain rates are applied, most of the materials depart from the ideal situations and lead to more complex relationships.

When bodies are subjected to periodic oscillatory stresses due to sinusoidal strains, the stress (σ) and the strain (γ) are out of phase by a quantity generally noted δ.

These materials generally, when strained, store part of the energy input while some of it is dissipated as heat. Both the heat dissipation and the phase angle between stress and strain are characteristics of viscoelastic materials.

It has been shown [2,3] that strain dependency is much more important than the influence of frequency or temperature in *distinguishing the reinforcing role of carbon black* in polymeric compounds. Two domains of strain, defined as low (< 10%) and high (> 10%), are characterized by different overall behavior of the polymer/carbon black composite.

Originally the distinction between these two strain domains occurred from technical constraints. Indeed, to measure low strain properties, the mechanical spectrometer has to be extremely accurate and have a very low compliance. An adequate instrument which was used is a Rheometrics S IV. This spectrometer is,

however, limited by its load cell capacity (10 Kg-cm torque max.). The measurements at strains higher than 10 to 12% at times exceed the limit of the load cell. To measure higher strain levels, a test in simple shear (sandwich shear) mode using a computer-driven servohydraulic tensile tester has been developed.

The sandwich shear test can also be used for low strain measurements and the results obtained are similar to those obtained in the rotational shear experiments. The slight discrepancy noted between the two testing procedures over the overlapping strain range (Fig. 1) may be explained by the difference in strain field in both specimens.

11.1.1. Low Strain Dynamic Properties: General Considerations

For many years the dynamic mechanical properties of carbon black reinforced systems have been studied, and an excellent review has been written by A. Medalia [3].

A viscoelastic body subjected to sinusoidal strain, the strain γ is given by

$$\gamma = \gamma o sin\ wt \quad (1)$$

where γo = max strain and $w/2\pi$ = frequency (Hz).
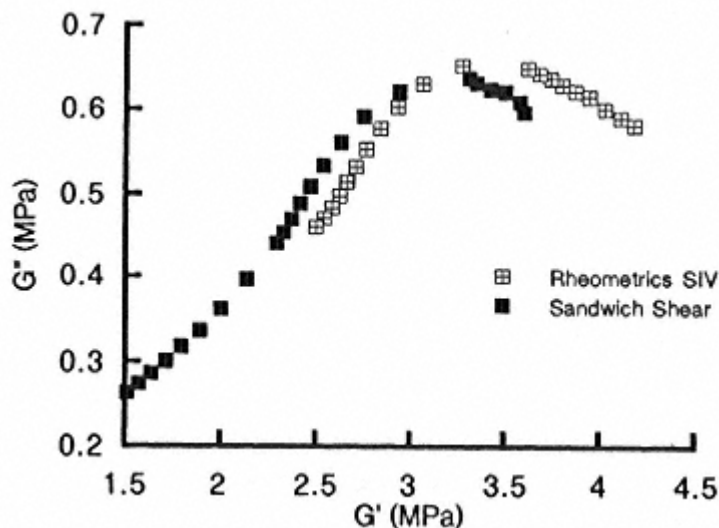
Fig. 1.
G" vs. G' for different measurements.

The body exhibits a sinusoidal stress of identical frequency but out of phase (δ) with the strain (linear viscoelasticity). In that case the stress can be expressed by

$$\sigma = \sigma o sin(wt + \delta) \quad (2)$$

It can be shown [1] that in the case of linear viscoelasticity the stress σ can be expressed as a function of two sinusoidal functions out of phase by $\pi/2$

$$\sigma = \gamma o [G'(w)sin(wt) + G''(w)cos(wt)] \quad (3)$$

thus defining two shear moduli, $G'(w)$ and $G''(w)$. The storage modulus $G'(w)$ measured from the signal in phase with a strain is a measure of energy (elastic) stored and recovered in cyclic deformation; while the loss modulus $G''(w)$ (measured from the $\pi/2$ out of phase component) is a measure of energy dissipated as heat. The ratio G''/G' is tan δ, the loss tangent.

It is worthwhile noting that in a prescribed strain cycle experiment where γo is the maximum strain amplitude, the energy lost per cycle (hysteresis) is given by the expression:

$$2\pi(\gamma o)2G''(w)$$

and not by tan δ, which in this case is related to the energy dissipated per unit energy stored and not per unit energy input [1].

Thus the above considerations show clearly that characterization of a material exhibiting viscoelastic behavior requires two parameters. Thus the parameters G' and G'' are used to fully define the fundamental behavior of

carbon black filled compounds at low strain. In the case of carbon black filled compounds, it has been shown [3] that G' and G'' are also functions of γ. In the studies reported here, the experiments are run at 30°C and 1 Hz, and the representation of G' and G'' as a function of strain is judicious.

It is also recognized that there exists a relationship between G' and G''. It was therefore interesting to consider $G' = 1(\gamma)$ and $G'' = 2(\gamma)$ as a parametric representation of a general equation:

$$G'' = 3(G') \quad (4)$$

The rotational shear experiment and the simple shear give essentially identical results (Fig. 1). These experiments highlight the existence of two energy dissipating processes which can be considered as responsible for the reinforcement by the filler of the elastomeric matrix.

This function exhibits below 7% strain similarities with the known Cole-Cole plots [4] established for complex dielectric permittivity. This G-Plot representation previously considered by Payne [5] allows better insightful understanding into the mechanism of carbon black reinforcement as discussed later in this chapter.

As mentioned in Chapter 7 of this book on *Fractal Geometry,* this behavior allows one to establish a comparison between a carbon loaded compound and an electrochemical system if in the first one the momentum transfer replaces the electron transfer of the later system.

11.1.2. High Strain Properties: General Considerations

Another high strain testing procedure was developed based on the

work reported by Rivlin and Thomas [6]. The principle of the test is based on energy calculated from a stress-strain curve. Indeed, the area between a stress-strain curve and the strain axis is an energy.

A cyclic stress-strain curve using rubber compounds exhibits a hysteretic loop. The area (ED) of the loop can be considered as proportional to the energy loss per cycle (hysteresis) and the area (ES) under the return curve as an indication of the energy elastically stored in the system due to the input strain energy, ET, which obviously is equal to the sum of the two above-mentioned energies.

$$ET = ES + ED \ (5)$$

A pure shear specimen, for which the tearing energy $T=(1/t)(\partial w/\partial c)_l$ is reduced to $T=W_o l_o$ where W_o is the stored elastic energy density and l_o the unstrained sample width was used because of its tendency to have a tear energy independent of any cut length (flaws, etc.) [6]. The experiment is run in order to obtain a closed hysteretic loop (steady regime) at five predetermined maximum strains.
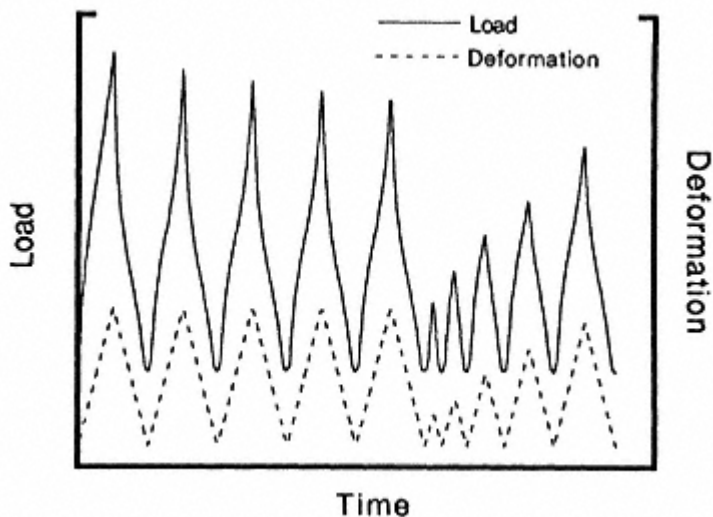
Fig. 2.
Load and deformation vs. time.

The sample previously broken-in is strained to the maximum strain, in five steps in ascending order, with no relaxation time between cycles (Fig. 2).

The strain energy stored, as well as the dissipated energy, is measured for all cycles and is plotted versus strain as in the case of low strain experiments.

As for the low strain G-Plots, ED plotted against ES gives E-Plot, which is a general relation obtained by eliminating the strain factor from the parametric representation (Fig. 3).
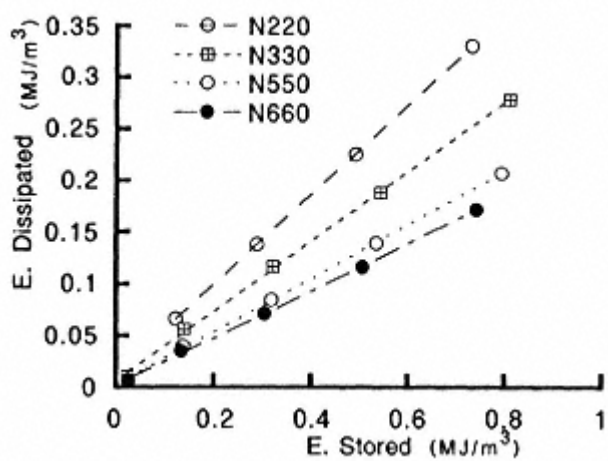
Fig. 3.
ED vs. ES for a variety of carbon blacks.

One characteristic of E-Plots obtained from this type of experiment is that for each compound *ED/ES* is strain independent. This indicates that:

$$ED/ES = k \ (6)$$

which implies that the energy dissipated per unit energy input is independent of the strain (within the studied strain range).

11.2. Experimental Results

The carbon blacks in these studies were compounded in the ASTM D3192 (NR) and D3191 (SBR) formulas at a 50 phr loading. The curing characteristics were determined using a Monsanto Rheometer, 1° arc, 100 cpm, 160°C, and the test specimens were cured to $t90$ at the same temperature.

The cured samples were tested for low and high strain properties according to the above-mentioned procedures.

11.2.1. Low Strain (< 10%) Results: G-Plot Similarity

As an example of the results obtained, Fig. 4 shows the G-Plots of 4 carbon blacks (N220, N330, N550, and N660) compounded in the SBR formula. Similar curves were obtained for all the 22 carbon blacks studied in both SBR and NR model formulations.

All these G-Plots are similar in shape, in spite of the inherent differences in moduli (G' and G'') values, which obviously depend on the type of carbon black (difference in reinforcing potential of the filler).

It was shown [7] that all G-Plots obtained with the different fillers in one type of compound can be shifted to a reference curve.

All the G-Plots obtained for a given polymer were shifted to the reference N110 G-Plot and the results can be summarized as follows [8].
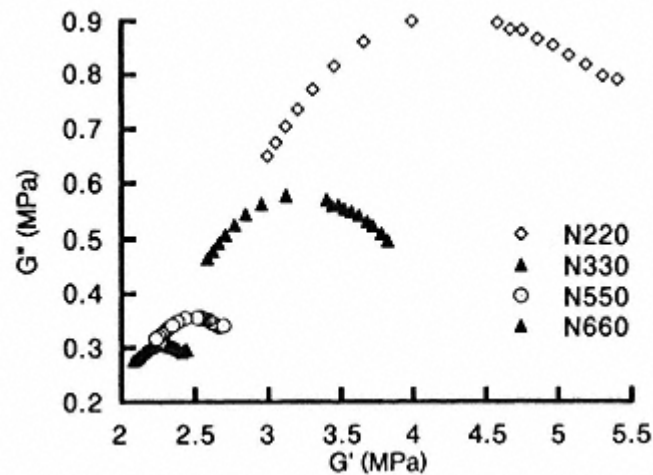
Fig. 4.
G" vs. G' for a variety of carbon blacks.

* *G′* and *G″* are not independent moduli.

* All shifts are remarkably good. The shiftability criterion [7] was generally met with a high degree of confidence.

11.2.2. High Strain Results

As described at the beginning of this chapter, the high strain (extension ratio between 1.2 and 2) properties of the same compounds, as used to measure low strain properties, were evaluated using a pure shear specimen. The E-Plot for four of the samples (*ED* vs. *ES*) (Fig. 3) exhibits a remarkably linear relationship between these two parameters, confirming that the energy dissipated per unit energy stored is a constant (*K*) independent of strain for a given temperature and strain rate. This linear behavior is true for all samples tested, and the constant *K* is carbon black dependent.

It is interesting to note that the *K* values in SBR and in NR, independent of the carbon black, are identical within experimental error.

$$KNR/KSBR = 1.04 \quad (7)$$

All the above indicates that the carbon black is responsible for the value of that constant *K;* whereas, the polymer effects, with the exception of strain crystallization, seem secondary. This might indicate that if an interaction between the polymer and the carbon black exists, it has a more limited effect on that fundamental property of the balance of energy dissipated per unit energy stored. The polymer obviously plays a key role when the amount of energy input into the system is concerned.

11.3. Interpretation Of The Results

The specific types of testing described have led to a set of results which enables one to better understand why and how the carbon black/polymer composite can produce the unique physical properties that allow its use in extremely demanding end-use applications.

11.3.1. Filler-Filler Interaction

Low Strain Behavior

It is theorized that at low strain, below 68% (depending on the carbon black grade), the filler is a main contributor to the reinforcement of the polymeric system. The carbon black agglomerates dispersed in the polymeric media form a network, held together by van der Waals type forces. This network is, therefore, extremely sensitive to strain, and upon straining is broken, diminishing the overall stiffness of the composite (G' decreases), whereas some of the network energy is dissipated as heat (G'' going through a maximum). The remarkable aspect of such a network is its reformation when the strain is removed, allowing the carbon black entities to be close enough

again to reform a filler network interpenetrating and therefore reinforcing the polymeric network.

All the obtained G-Plots are characterized by the fact that after a given strain the change $\Delta G''$ for a given $\Delta G'$ is constant, equal to S (Fig. 1). This clearly indicates that the filler network responsible for the variation of G' and G'' has vanished. These results are in very good agreement with the network energy measured using other techniques. Researchers [9] using conductivity measurements came to the same general conclusions regarding the role strain plays on the network integrity.

Other studies [2,10,11] have shown that by studying the variation of G'_o with temperatures at very low strain (0.1%), at which the filler network is the least affected by strain, it is feasible to quantify the network energy of the carbon black. Indeed, if one considers that the number of nodes N forming the network at temperature T can be calculated from the number of nodes No at a reference temperature $To,$ then N can be expressed using an Arrhenius type relationship:

$$N = N_o exp[E/R(1/T - 1/T_o)] \quad (8)$$

where E = network cohesion energy, R = gas constant, T = temperature (in K).

It is also reasonable to assume that the stiffness of the unstrained polymer/carbon black composite G'_o is proportional to the stiffness of the filler network, which should be proportional to the number N of nodes. Therefore, at very low strains the following expression holds:

$$G'_{o,T} = G'_{o,T_o} exp[E/R(1/T - 1/T_o)] \quad (9)$$
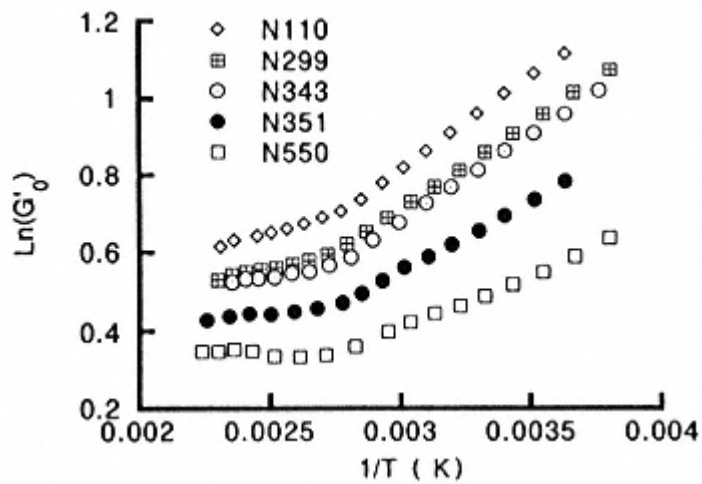
Fig. 5.
G'_o as a function of temperature for various carbon blacks.

Thus, by measuring G'_o as a function of temperature, and plotting the logarithm of G'_o versus $1/T$, it should be possible to determine the value of E which can be interpreted as being the network cohesion energy. Fig. 5 shows typical plots of ln G'_o vs. $1/T$, illustrating the linearity of the relation in the temperature range from 0 to 90°C, and confirming the hypothesis of the Arrhenius type relationship between the low strain dynamic modulus and the temperature.

An analysis of the total curve ln G'_o versus $1/T$ reveals that for T_o above 90°C in SBR, G'_o variations with temperature are much less pronounced with a well-defined transition point around 90°C. This transition point can be hypothesized as being the vanishing network threshold.

It was found that for all the studied carbon blacks mixed in both NR and SBR, as shown elsewhere [2,10,11], the value of E in both NR and SBR is small, validating the hypothesis of the van der Waals type network formed by the filler.

Summarizing the findings and the above-mentioned hypothesis, it is clear that the low strain dynamic properties of carbon black loaded compounds are reasonably well explained by a filler network whose cohesion depends mainly on the carbon black itself and the polymer being essentially the spatial support of that network.

High Strain Behavior

The G-Plot also indicates that the high strain properties can be predicted from dynamic measurements. As discussed earlier, the linear portion of the G-Plot is a characteristic of that representation.

After the carbon black network is completely disrupted, the carbon black/polymer composite exhibits what is referred to here as high strain behavior. Another way to express this fact is to consider that at higher strain the ratio of energy dissipated per unit energy stored in the sample or energy input is independent of strain, which is typical for a non-filled polymer. Therefore, in order to rationalize the observed data, it is proposed that the filler network is broken, in discontinuous sub-networks which interfere with the polymer matrix primarily by hindering the free movement of the polymer chains and/or perturbate the momentum transfer throughout the composite. Obviously the perturbation must be filler size, structure, etc., dependent.

11.3.2. Filler-Polymer Interaction

It is obvious that interactions between the filler and the polymer chains are necessary to keep the filler network spatially stable in a compound. Numerous studies have quantified this interaction mainly by inverse gas chromatography [12] using simple organic probes. However, it appears that these interactions do not govern, at least at low strain, the physical properties of filled compounds.

11.3.3. Predictability of Carbon Black Characteristics

Since carbon black is generally characterized by two parameters: specific surface area (N2SA) and structure (DBP, CDBP), it is interesting to evaluate the predictability of these characteristics on both the low and high strain behavior of carbon black reinforced rubber compounds.

At low strain the relationship between G'_o and N2SA is known to be significant, as is the networking energy E and N2SA (Fig. 6).

Since at low strain the physical properties are mainly due to the filler network, it is postulated that the higher the specific surface area, the higher the cohesion of the network due to stronger and/or more van der Waals type bonds. The crystallite size Lc which decreases [2] with increasing specific surface area might give an indication of the energy state of the conduction electrons which might play a key role in the network cohesion. However, no satisfactory relationship between structure and low strain properties was found from the results of these experiments.

The high strain constant K seems also linearly dependent on N2SA. It is to be noted that as for a lot of other properties, a relationship appears to exist only if the whole range of N2SA is taken into consideration. If only the tread blacks are considered (N2SA>70 m2/g), the relation is doubtful; even so, the tendency of increasing K with N2SA is still there. For the carcass grades, on the other hand, the specific surface area seems to be more predictive of high strain properties.

On the other hand, structure (as measured by DBP, CDBP) which does not correlate with low strain properties does begin to correlate

with strength properties measured at higher strains.
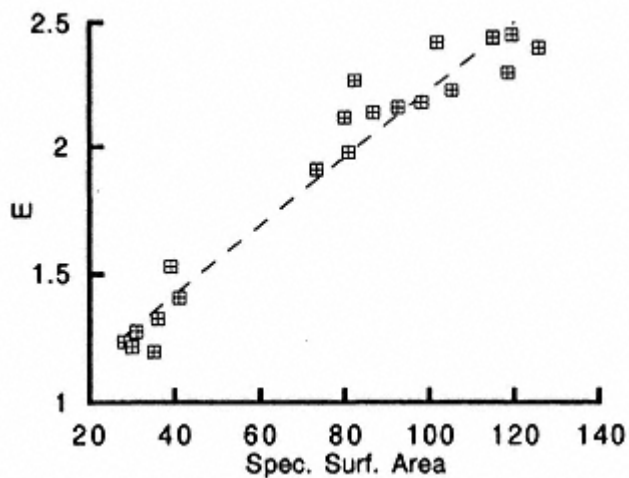
Fig. 6.
Network cohesion energy vs. nitrogen surface
area for various carbon blacks.

It is proposed that at low strain, below 67%, the carbon black network is mainly responsible for the observed enhanced physical properties of the carbon black-polymer composite and can be predicted by the specific surface area of the filler, while at higher strain, when the network has vanished, the carbon black subnetworks' primary contribution is to perturbate the flow of the polymeric chains when both the structure and the size (specific surface area) can play an influencing role.

References

1. Ferry, J. D., *Viscoelastic Properties of Polymers,* 3rd edition, J. Wiley & Sons, 1980.

2. Gerspacher, M. and Lansinger, C. M., presented at a meeting of the Rubber Division, ACS, April, 1989.

3. Medalia, A. I., *Rubber Chem. Technol.,* 51, 437 (1978).

4. Cole, K. S. and Cole, R. H., *J. Chem. Phys.,* 9, 341 (1941).

5. Payne, A. R. and Whittaker, R. E., *Rubber Chem. Technol.,* 44, 440 (1971).

6. Rivlin, R. S. and Thomas, A. G., *J. Polymer Sci.,* 10, 291 (1953).

7. Tricot, C., Private Communication.

8. Gerspacher, M. et al, presented at IRC, Paris, 1990.

9. Burton, L. C., Hwang, K. and Zhang, T., *Rubber Chem. Technol.,* 62, 838 (1989).

10. Gerspacher, M. and Donnet, J. -B., presented at a meeting of the Rubber Division, ACS, May, 1989.

11. Fitzgerald, E. R., *Rubber Chem. Technol.,* 55, 1597 (1982).

12. Lansinger, C. M., Ph.D. Thesis, The University of Haute Alsace, Mulhouse, 1991.

Chapter 12
Carbon Black in Plastics

John M. Funt,
William L. Sifleet
and Marcel Tommé
Cabot Corporation,
Billerica, Massachusetts, U. S. A.

Carbon black is used in plastics to alter key physical properties of the compound, which determines their applications in a given market segment. The characteristics of the carbon blacks used for each application are generally different. The most important applications of plastic-carbon black compounds are due to properties such as conductivity, color, aging (UV protection) and reinforcement. The relative volume and the relative value of the different market segments are different for each application (Table 1). Aging and reinforcement applications are lumped under regular color.

Carbon black in plastics can impart unique properties to the plastic compounds. Among these are:

* excellent UV protection,

* electrical conductance or resistance,

* range of blackness/jetness,

* opacity,

* reinforcement.

Compounding for each of these applications requires an optimization of the primary property of interest against other key physical properties that influence mechanical properties or processing characteristics of the compounds and the compound cost. The primary carbon black characteristics that affect these compound properties are particle size (surface area), structure, aggregate size (tint) and pellet properties. Particle size and structure are the more important properties which control performance. The general effects of these two carbon black attributes are summarized in Tables 2 and 3.

Table 1. Market Segments for Carbon Black in Plastics

Market segment	Relative size by volume, %	Relative price, utility=1.0	Relative size by revenue,%
Conductive	15	3.0	25
Medium color	5	6.0	20
Regular color	15	1.5	15
Utility	65	1.0	40

Table 2. Effect of Particle Size on Compound Properties

Property	Small particle size	Large particle size
Masstone jetness	Darker	Lighter
Viscosity	Higher	Lower
Dispersion	More difficult	Easier
Wetting	Slower	Faster
Tint strength	Higher	Lower
Conductivity	Higher	Lower
UV absorption	Better	Poorer
Cost	Higher	Lower

Table 3. Effect of Structure on Compound Properties

Property	High structure	Low structure
Dispersibility	Easier	More difficult
Wetting	Slower	Faster
Masstone jetness	Lower	Higher
Gloss	Lower	Higher
Conductivity	Higher	Lower
Viscosity	Higher	Lower
Loading capacity	Lower	Higher
Tint strength	Lower	Higher

Tint is strongly coupled to the particle size and structure. Pellet properties indirectly affect compound properties through their effect on processability and dispersion. Other carbon black properties can affect performance. Surface chemistry of the blacks, moisture adsorption and density can influence product performance.

The following chapter describes some of the key performance criteria for each of the major applications, typical carbon blacks used for the applications and some of the underlying physical theory related to the performance.

12.1. Conductive Applications

Carbon black is intrinsically a semi-conductor. It can impart good conductivity to normally high resistivity plastics compounds. The compound conductivity, however, depends upon the type and loading of the carbon black. Table 4 shows the typical range of conductivity for selected materials and applications. Table 5 summarizes the loading ranges for some typical formulations with different carbon blacks.

The resistivity of a compound depends strongly upon the carbon black loading (Fig. 1) [1,2]. At very low loadings of carbon black, such as used for tinting or color applications, the compound resistivity remains at the level of the unfilled polymer. As the carbon black loading is increased, the resistivity decreases rapidly by 810 orders of magnitude. This region of rapid resistivity decrease is called the percolation region. At sufficiently high loadings, the resistivity reaches a plateau that is often 12 orders of magnitude higher than that of dry carbon blacks.

Carbon black aggregates are on the average 10 nm or further apart in the low loading of the non-conductive range. In this range the electrical properties

Table 4. Volume Resistivity of Polymer Compounds and Reference Materials

Material	Volume resistivity (ohm-cm)
Uncompounded polymer	1×10^{12} and above
Anti-static	1×10^{4} to 1×10^{6}
Semi-conductive	1×10^{0} to 1×10^{2}
Dry carbon black	1×10^{-2} to 1×10^{-2}
Metal	1×10^{-4} to 1×10^{-4}

Table 5. Carbon Black Loadings for Typical Conductive Applications

Application	VULCAN Pc	VULCAN XC-72	BLACK PEARLS 2000
Anti-static, %	1825	1520	58
Semi-conductive, %	2538	2035	818
Conductive, %	over 35	over 33	over 18
Surface area$a$, m2/g	143	254	1475
Structure$b$, cm3/100 g	118	178	330

aSurface area - nitrogen surface area measured by BET method.
bStructure - DBPA adsorption.
cVULCAN and BLACK PEARLS are registered trademarks of Cabot Corporation.
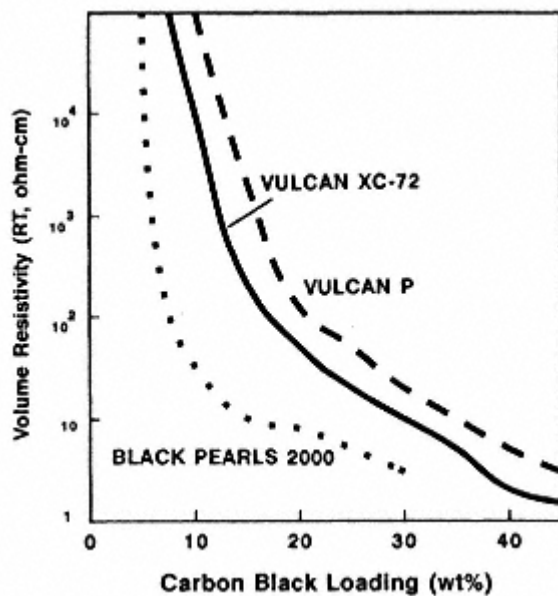
Fig. 1.
Dependence of volume resistivity on
loading.

are dominated by the polymer phase between the aggregates. As the carbon black loading is increased, the average distance between the aggregates decreases. If the carbon blacks were dispersed to the level of the individual aggregate, and the aggregates were uniformly spaced in the compound, then there would be no change in resistivity until the compound was so highly loaded that the aggregates would be in contact with one another. A small change in loading would then give a sharp step decrease in resistivity.

Two factors modify the compound behavior from the highly theoretical case just described. First, the carbon black is usually not dispersed to the extent where all aggregates are completely separated. In practice, the carbon black retains a significant degree of agglomeration on a microscopic level (<110 microns). In the region or interior of an agglomerate, the carbon black loading is

higher than the average, so that the local resistivity will be lower. Second, the aggregates and agglomerates are not uniformly distributed through the volume of the compound. The aggregates and agglomerates are randomly positioned in the compound.

The theory of the effect of agglomeration on conductivity in a carbon black filled compound has not yet been developed. The effect of agglomerate size is indirectly shown by the effect of mixing time on resistivity, where an increase in mixing time causes a reduction in the size and number of agglomerates (Fig. 2).

The gradual decrease in resistivity with increase in loading is a result of the random distribution of aggregates in the compound. Kirkpatrick [3]
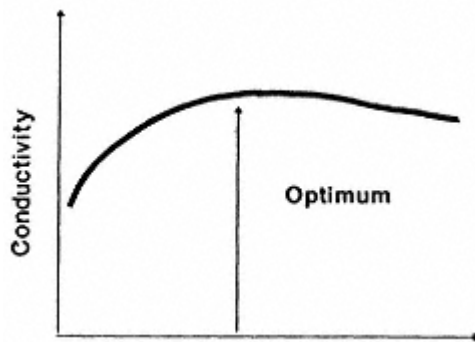
Fig. 2.
Dependence of resistivity on mixing time.

and Sichel [2] treated conduction in a composite of an insulator filled with conductive particles as a theoretical percolation problem. They assumed that conduction through the bulk of the compound is controlled by conduction over a number of paths of randomly formed chains of particles. As the number of particles increases, the number of continuous chains or conductive paths through the compound increases. The local effect is largest where the first chains have formed. The total resistance for any chain consists of the sum of individual resistances at each point of contact. If the resistance at each point of contact remains constant, the resistivity ρ of the composite at volume loading ϕ follows the form:

$$\rho = \rho_o(\phi - \phi_c)\text{-}t \ (1)$$

where ϕ_c is the volume fraction filler at the percolation point, ρ_o is a scale factor, and t is a geometric factor. The value of t commonly is 1.6 to 2. The percolation model usually describes compound performance well into the percolation region [4].

The percolation point for carbon black depends strongly on the

structure [5]. Janzen estimated the average number of contacts an aggregate would have with its neighbors (C_{av}) as:

$$C_{av} = \frac{\phi/(1-\phi)}{\phi_m/(1-\phi_m)} C \quad (2)$$

where C is the coordination number for close packing of spheres and ϕ_m is the maximum possible volumetric fraction of carbon black that the polymer can hold. ϕ_m depends upon the structure of carbon black, as measured by crushed DBPA:

$$\phi_m = (1 + \rho_c CDBP)^{-1} \quad (3)$$

where ρc is the density of carbon black. Based on simulations of network formation, Janzen estimated the critical number of contacts for first paths to occur as 1.5. Using the coordination number for random dense packing of spheres, $C=6$, the percolation point ϕp can be estimated by:

$$\phi p = (1 - 4\rho c CDBP)\text{-1} \quad (4)$$

The percolation factor in Equation 4 is related to the resistance between aggregates, the number of contacts between chains and the number of chains per unit volume. In practice, it is estimated from an empirical fit to the data.

Much of the experimental data in the literature and the theoretical developments to describe these effects have been based on measurements made at a single temperature. In many conductive applications, the compound operates at elevated temperatures that are frequently limited by the softening of the polymer. As the temperature rises, the resistivity of carbon black filled compounds increases (Fig. 3). This phenomenon is called a positive temperature coefficient (PTC). The coefficient of thermal expansion for most polymers is greater than that of carbon blacks. As the temperature rises, the gap between aggregates at the contact points tends to increase, thus increasing the resistance at the contacts. The shapes of the loading curves are essentially unchanged. The scale factor ρo is changed by temperature.

Another industry segment has developed to take advantage of PTC by using the change in resistivity to switch circuits on and off or to limit power in circuits. Two key performance measures are used to design compounds
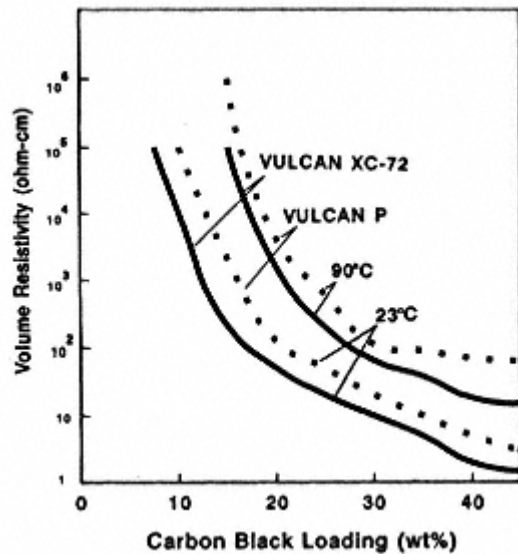
Fig. 3.
Temperature effect on resistivity.

for these applications. The first is the sharpness of the change in resistivity as temperature is increased. With a single carbon black at loadings in the percolation range, the transition in resistivity tends to be gradual as temperature is increased. The transition can be made sharper using blends of carbon blacks. Second, the resistivity at high and low temperatures can change as the compound cycles with temperature. The hysteresis in the resistivity with cycling depends upon the type and loading of carbon black as well as the degree of dispersion.

12.1.1. Wire and Cable Applications

The wire and cable market can be broken into several segments [6]:

* electronic,

* telephone,

* power,

* control and signal,

* building,

* apparatus and cordage,

* magnet,

* miscellaneous.

Carbon black usage prevails in the telephone, building and power segments. Carbon black is used in jacketing compounds for UV protection as well as to provide conductivity to the inner plastic layers.

Compounds for extruded dielectric power cables for distribution systems are one part of the conductive market for carbon black. These cables are used to transmit energy from the local sub-stations to neighborhoods and individual buildings. The construction of the cable assembly is complex (Fig. 4). The central conductive metal core is covered with the strand shield, a thin semi-conductive carbon black filled compound. The strand shield is
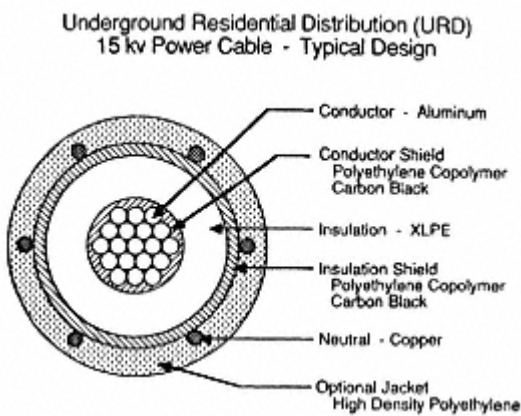
Fig. 4.
Composition of transmission cable.

used to prevent gaps from forming between the wire and the insulating layer that could lead to corona discharge. An insulating layer of non-conductive plastic surrounds the strand shield. The insulation shield compound covers this layer. Copper wires are frequently used outside the insulation shield to act as a neutral. Finally, a cable cover is applied. Details of the internal design depend upon the application and the manufacturer. A broad range of carbon blacks is used in these applications. Products include those based on acetylene blacks, byproduct blacks, low area blacks in the N700 series, carbon blacks in the N400500 series and some N300 series carbon blacks. VULCAN P and VULCAN XC-72 carbon blacks are typical of those used for insulation and strand shield formulations.

Cross-linkable polyethylene copolymers such as EVA and EEA are commonly used for these applications. The type of carbon black used and the performance requirements for the compound may be different for the strand shield compared to the insulation shield compound. An overwhelming requirement for all the compounds is long life after installation. The initial material costs are small compared to the labor and other costs involved in replacing cable once it has been installed. Underground cables are used in both urban and rural settings. Replacement of the cable entails location of the failed cable, excavation, exchanging the failed segment, and replacing the cable underground. Replacement costs can be many times higher than the cost of the cable and materials.

Two critical factors in the compound affect the life of the cable. The strand shield is a very thin layer of conductive polymer that surrounds a metal core that is at high voltage. The strand shield

layer works in conjunction with the neutral wires to contain the electric field inside the cable. The bulk of the voltage drop occurs across the insulation layer. Any protuberances on the strand shield can greatly increase the local field. These bumps on the surface can be caused by impurities in the compound and by undispersed carbon blacks. The local high voltage gradient can break down the polymer, leading to premature failure. The carbon black used in these compounds must be clean, free from contaminants, and easy to disperse. In addition, the compound must have low viscosity to enable easy extrusion of the strand shield onto the cable. Pellet properties are critical for this application. The smoothness of the strand shield is further improved by using more intensive dispersion techniques, such as the Buss Co-Kneader extruder, and screening the melt through fine screens on the extruder.

Moisture leaking through the protective cable jacket can cause premature cable failure through treeing. Treeing describes the dendritic structures that can form inside the cable as the polymer breaks down under high electrical stress. Cleanliness of the carbon black is critical in reducing this mode of failure.

Finally, the mechanical properties of the polymer compounds in the cable are important. The materials must withstand the cycles in temperature and the attack from ozone and other threats from the environment. The cable is finally assembled in the field, where lengths of cable must be joined physically to form the network. The material around the conductor is stripped away to get good contact with the connectors. The modulus and tear strength of each layer and the adhesion between polymer layers are important for field service. The mechanical properties are largely set by the choice of the polymer types, with some modification by processing conditions and the type and loading of carbon black.

12.1.2. Electromagnetic Interference Shielding (EMI)

The spread of small electrical machines that have high frequency components, particularly those with microprocessors, such as desktop computers, has caused an environmental problem. The high frequency electrical circuits in the equipment can generate radiation in the radio frequency range. The radiation can interfere with telecommunications and cause cross-talk between machines. Housings for the circuits can be made to shield the machines or computers from outside radiation and to contain the radiation generated inside the equipment.

The machine housings must meet a variety of mechanical, electrical and aesthetic requirements. The compounding problem is that additives to plastics, such as metal particles or carbon black, interfere with the properties that make the polymer attractive in the first place. As a consequence, carbon black has had a relatively limited use in this market segment. A primary limitation with carbon black in this application is that too much impact strength is

lost when sufficient carbon black is added to obtain the resistivity required to shield the electrical components. There is a direct relation between compound resistivity and EMI shielding (Fig. 5).

12.1.3. Anti-Static Shielding

Carbon black is widely used to impart anti-static properties to plastics compounds. Many different blacks could be used for these applications. Carbon blacks such as VULCAN XC-72, VULCAN P and BLACK PEARLS 2000 are widely used. These blacks can provide adequate resistivity for anti-static applications while minimizing the impact on other mechanical properties. A critical compounding effect is to obtain an appropriate level of resistivity that is not too difficult to control with process variations, such as small variations in loading or dispersion. The sharpness of the resistivity-loading curve will indicate which carbon black may be preferred.

The tensile strength at a fixed level of resistivity for the anti-static application can depend strongly on the choice of carbon black (Fig. 6). The tensile strength at break is higher for higher area blacks (smaller particles)
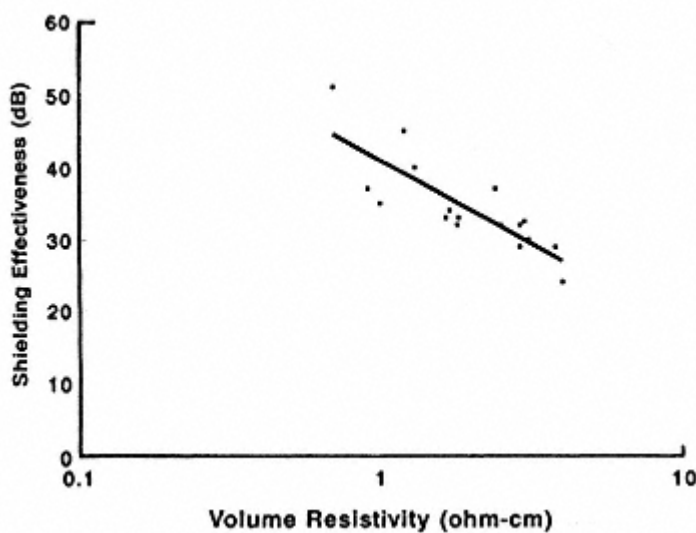
Fig. 5.
Compound resistivity and shielding effectiveness.

because less loading of carbon black is required to achieve the required resistivity level. The tensile yield strength of the compound depends explicitly on the loading and particle size (Fig. 7). Higher loading of smaller particles increases yield stress.

12.2. Ultraviolet Protection of Plastics

Many plastics suffer from photochemical degradation when subjected to
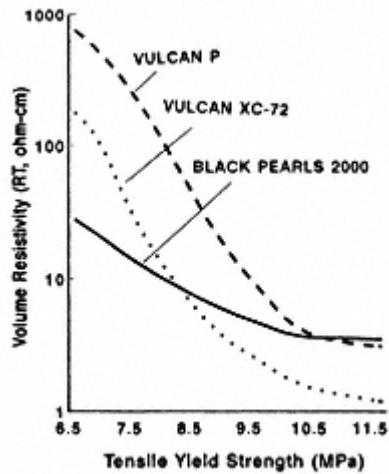
Fig. 6.
Balance of electrical and
mechanical property -
volume resistivity vs. tensile
strength in EVA.
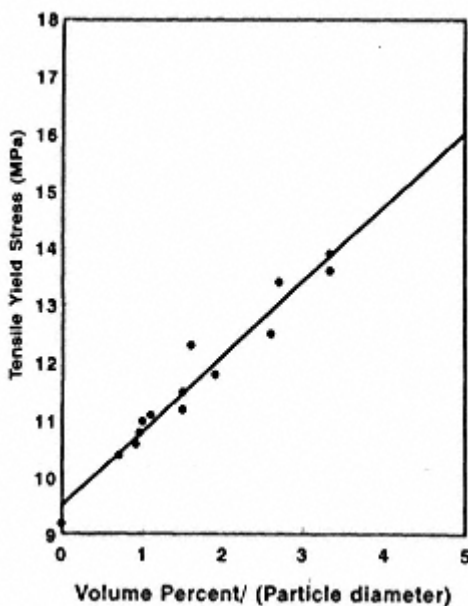
Fig. 7.
Effect of carbon black on tensile
yield stress in PE.

ultraviolet light, such as the components in sunlight. Exposure to ultraviolet light can significantly increase the rate of physical and chemical degradation, particularly when coupled with ozone or other aggressive environmental chemicals. Carbon black dispersed in plastic tends to absorb UV light and re-emit it as heat. This effect greatly reduces the harmful effects of the radiation. As a consequence, carbon black is widely used for this application (Table 6).

Bell Labs has conducted among the longest UV protection studies recorded. In 1950, Wallder and coworkers [7] found that polyethylene containing 12% carbon black with particle size less than 25 nm provided life expectancies long enough to be used for outdoor wire and cable applications. This study, which was

primarily based on accelerated testing, specifically found that UV protection improved with:

* carbon black loading - plateau at 2% with 10 nm carbon black,

* smaller particle sizes,

* dispersion quality.

In a follow-up report, Howard and Gilroy [8] reported the results of continued testing of similar compounds. They measured the results of exposure up to 22 years for polyethylene containing carbon blacks at four particle sizes (17, 28, 35 and 275 nm) and five concentrations (0.1, 0.2, 0.5, 1., 2. and 5%). They found similar results to the previous study. They related particle size and loading of the compound to the absorption coefficient of the compound. Consequently, the absorption coefficient at 375 nm for carbon black filled pla-

Table 6. Carbon Black Use for UV Stabilization

Application	Typical loading, %	End use	Performance requirements
Cable jacketing, PE, PVC	2.5	Commercial cable	Optimum UV Easy dispersing
Plastic pipe, XLPE, HDPE, PVC, ABS	2 or less	DWV industrial potable H_2O	Good to optimum UV stabilization Good dispersion
Film, PE	12	Agricultural mulch film	Good UV stability Good dispersion
Elastomeric film, HDPE	2.5	Industrial pond	Good UV stability Good dispersion
Metal pipe, (tape)PE	2.5	Protection of steel pipe from corrosion	Optimum UV Easy dispersing
Engineered plastics, ABS, PC, etc	2 or less	Automotive parts	Optimum UV Jetness Good dispersion
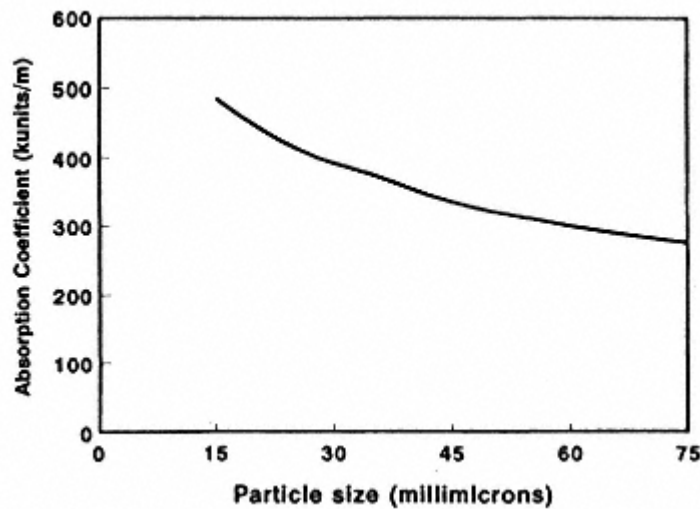
Fig. 8.
Effect of particle size on UV absorption. 2.5%
carbon black in LDPE measured at 375 nm.

stics has become generally accepted as a measure of its ability to withstand UV radiation. In 1985, Gilroy [9] reported again on the samples from the previous study. After 38 years of exposure, there was no noticeable deterioration in compounds that contained at least 2% carbon black with a particle size less than 35 nm. The particle size strongly affects the UV absorption coefficient at fixed loading (Fig. 8). Up to nearly 3% loading, the absorption is proportional to carbon black loading. Above 3%, the absorption is saturated.

The primary carbon black variables that affect UV stabilization are particle size, structure and surface chemistry. The surface chemistry is usually characterized by the volatile content of the carbon black.

For larger particles, with lower surface area, the increased stabilization with decreased particle and primary aggregate size is primarily due to the increase in surface area of carbon black that is available to intercept the light. However, the UV stabilization tends to level off for particles smaller than 2025 nm with the accompanying small primary aggregates. Light scattering becomes more important for these smaller primary aggregates. Finer primary aggregates exhibit less back scattering than coarser aggregates. This is why lower structure blacks tend to be darker in color than higher structure blacks with the same primary particle size. The reduced back scattering with finer aggregates works against further UV stabilization because forward scattering continues to threaten the stability of the polymer. UV stabilization by carbon black in polymers depends upon its ability to absorb and to backscatter light. While absorption increases with finer aggregates and

particles, the backscattering decreases. The combined effect is to give a leveling of UV stabilization.

The volatiles on carbon black can affect UV stabilization. The volatiles consist of a complex mixture of chemisorbed, oxygenated groups. These groups tend to act as radical scavengers. The groups may also be chromophores, contributing to the UV absorption as well.

Carbon black is used as a UV stabilizer in the wire and cable jacket market. Typically, 2.5% carbon black loading is used. The two most common

Table 7. Carbon Black Properties for UV Stabilization

Carbon black	VULCAN 9A32	VULCAN P
N_2SA, m2/g	140	140
DBPA, cm3/100 g	114	116
Tint, % IRB3	114	101
Volatiles, %	1.5	1.4
Absorption coefficient[a], kilounits	500	485

[a]ASTM procedure D3349-74.

grades used are Cabot Corporation's VULCAN 9A72 black, in the US, and VULCAN P black, in Europe (Table 7). Degussa, Columbian and other manufacturers offer similar grades.

12.3. Color Applications

Carbon black is used in plastics for two color applications. First, carbon black is used to make black plastics. Second, carbon black is used to modify the color imparted by other pigments. The two applications rely on different aspects of the ability of carbon black to interact with light.

The primary attribute of carbon black in color applications is its ability to impart a degree of blackness, or jetness, in its dispersed form. Jetness is a complex function of the primary particle size (surface area), the primary aggregate size (tint or Stokes diameter) and the degree of dispersion. Finer particles have more surface area for absorbing light and they are more efficient at forward scattering of light. A secondary attribute of carbon black in plastics is the undertone, or masstone, which is a complex function of the scattering and absorption efficiencies as a function of the wavelength of light. Two plastics can have equal jetness but differ in masstone. For carbon black in plastics, the masstone ranges from a blue tone to a brown/blue tone.

The second attribute of carbon black in color applications is its ability to modify the intensity of other pigment colors through tinting. Tinting effectiveness is measured by the tinting strength, which measures the ability of carbon black to modify the appearance of a white pigment. The tinting strength depends primarily on the aggregate size and size distribution. Tint tone,

which refers to the undertone imparted by the carbon black, is usually less blue due to increasingly preferential absorption of the blue end of the spectrum as the particle size decreases.
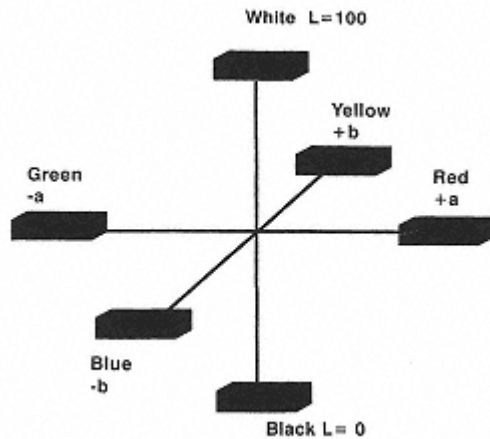
Fig. 9.
Three dimensional color space.
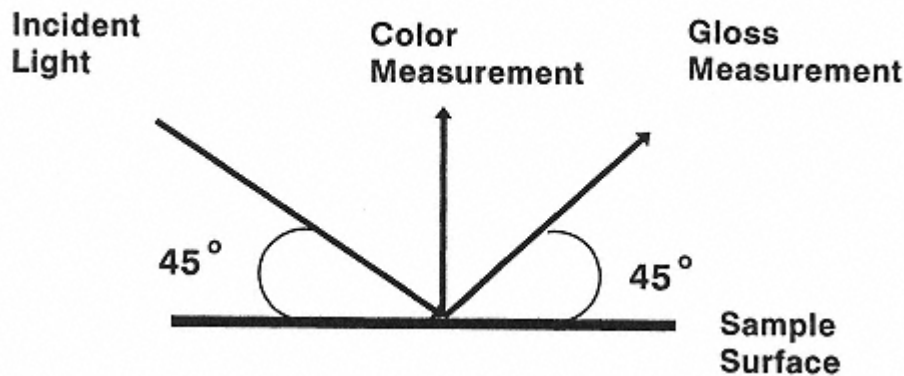
Fig. 10.
Angles of measurement.

The jetness and undertone, or masstone, can be measured quantitatively using instrumental analysis [10,11]. The primary analysis is made using calculations from primary measurements using the CIE color space (Fig. 9). The three dimensional color space splits the observations into three orthogonal components. The black/white dimension L measures the jetness of the compound. The red/green balance is calculated as $a*$ and the blue yellow balance is calculated as $b*$. The coordinates $L, a*, b*$ are calculated automatically with modern test instruments. The primary measurement is usually made by observing the intensity of light as a function of frequency that is reflected from the specimen at a non-specular angle to the angle of incidence. The intensity at the specular angle can be used to measure gloss (Fig. 10).

The relative jetness of a series of commercial carbon blacks has been measured as a function of the carbon black loading (Fig. 11). The carbon blacks were compounded in LDPE. The analytical properties of the carbon blacks are summarized in Table 8. In the $L, a*, b*$ coordinates, smaller values are darker (jetter) in appearance.

Typically the color is fully developed between 0.5 and 1% loading of carbon black. Higher loadings are used to obtain more opaque compounds. The precision of such measurements is typically

Table 8. Summary of Analytical Properties

Carbon black	N2SA, m2/g	DBPA, cm3/100 g	Tint, % IRB3
REGAL 660	112	60	116
MONARCH*a* 700	200	117	118
MONARCH 800	210	74	120
MONARCH 900	230	64	120

a MONARCH is a registered trademark of Cabot Corporation.
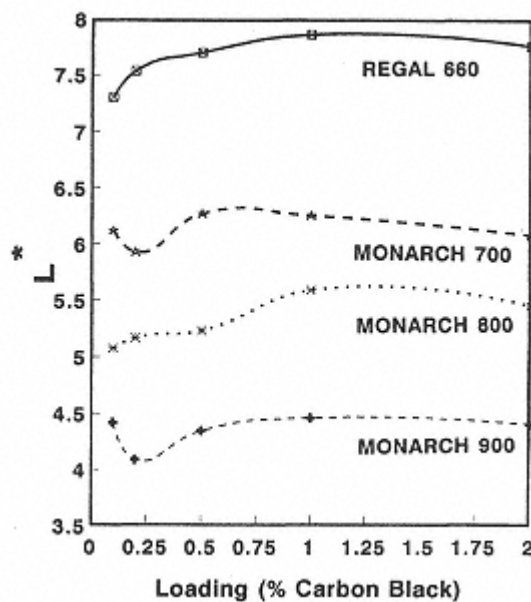
Fig. 11.
Loading effect on jetness.

12% or better [12]. Empirically, the CIE L value at a fixed loading can be related to the ratio of particle size to particle volume, where particle size is represented by the CTAB surface area and aggregate volume is measure by the mode Stokes diameter (Fig. 12). These measurements were made on compounds with 2% carbon black in LDPE. The ratio represents the balance between the ability of carbon black to absorb light compared to its light scattering properties.
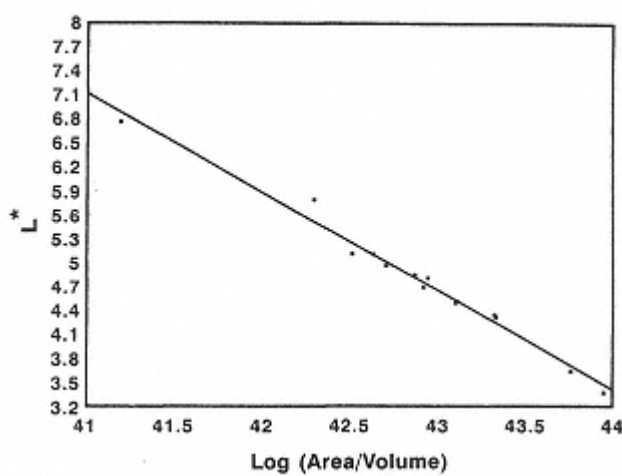
Fig. 12.
Jetness dependence on aggregate area/volume.
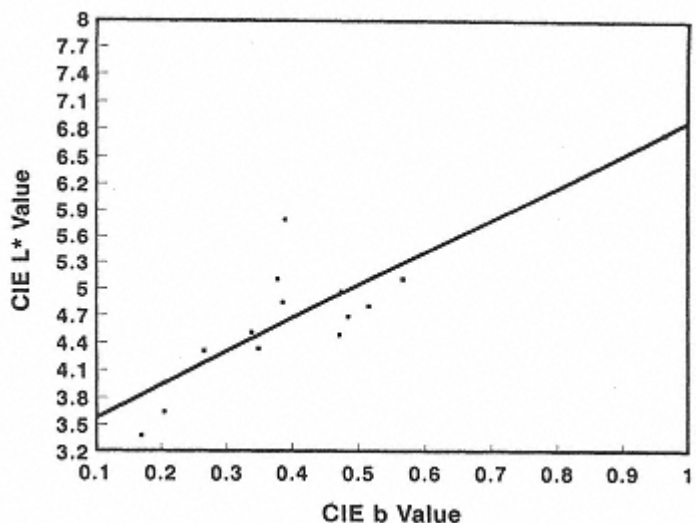
Fig. 13.
Tone-jetness relation for carbon black in PE.

The $b*$ value, or the blue/yellow balance, is strongly correlated to the jetness, or L value (Fig. 13). The $a*$ value is essentially constant over a broad range of blacks. The slightly positive values of b for carbon black combined with the positive $a*$ values gives carbon black filled plastics a blue/brown to slightly brown undertone with visual observation. The color of carbon black filled compounds depends weakly on dispersion. However, poorly dispersed blacks or other pigments can reduce the gloss of the plastic component when formed. Gloss depends upon the intensity of the light measured at the specular reflectance angle. Small imperfections on the surface can scatter light in directions away from the specular reflectance angle. This reduces the intensity of light reflected to the measuring point, reducing the gloss. Visually, a surface with many small imperfections appears duller rather than glossy. The undispersed pigments near the surface can cause surface imperfections.

12.4. Other Compound Properties

Carbon black can significantly affect compound properties other than the principle properties described in the previous sections.

12.4.1. Processability

Processability of filled compounds depends upon three factors. The importance of each factor depends specifically upon the processing equipment used.

First, the carbon black and other ingredients need to be dispersed effectively at minimum cost. Internal mixers, twin screw extruders and reciprocating screw mixers, such as the Buss Co-Kneader, are used to disperse

carbon blacks [13]. Internal mixers offer greater flexibility in mixing plants where compound changes are frequent. However, twin screw and reciprocating screw mixers frequently give more intensive mixing, resulting in better dispersion of carbon black. The primary carbon black variables affecting the ease of dispersion are the pellet strength and the aggregate and particle sizes. The aggregate and particle sizes affect the pellet strength. The rate of dispersion depends upon the tensile strength of the pellet and the ratio of the pellet strength to the energy intensity developed by the mixer [14]. Plastic melts at low loading frequently have too low a viscosity to develop the shear stresses required to disperse carbon black and other fine pigments. A masterbatch with high loadings of carbon black is frequently used to disperse the carbon black. The masterbatch is then let down to the final carbon black loading for the application.

Second, the compound viscosity affects the rate of extrusion or injection molding of the compound. Although there are good, complex models for predicting the effect of carbon black on viscosity, in practice the Mooney equation gives a satisfactory description of the data with a simple expression [15,16]:

$$ln\ \eta/\eta_o = k_e\phi(1 - \phi/\phi_m)\ (5)$$

where k_e is the Einstein coefficient, with a value near 2.5, and ϕ_m is the maximum volume packing of the carbon black. This equation fits a broad range of carbon blacks at loadings from 0.1% to 36% loading. The Guth-Gold equation, widely used in rubber technology, is based upon a different theoretical underpinning [17]. However, the equation can be approximated as the first few terms of the Taylor expansion of the Mooney equation:

$$\eta/\eta_o = 1 + a\phi + b\phi^2 \quad (6)$$

The increase in viscosity is usually not important for color and UV applications at the final loadings. The increase in viscosity is critical for conductive applications and for masterbatch for color applications.

Third, the propensity of the compound to plug screens is a key factor for critical compounds. For very thin extrudates, such as used for film coating applications and for strand shield applications in wire and cables, the presence of particulate contaminants can greatly reduce the utility of the compound. The impurities can come from the polymer, from carbon black or other additives, or from gel formation during processing. The particulate impurities are reduced or removed by extruding the compound through fine mesh screens. The pressure drop across a clean screen is usually small. The openings in the screen are reduced in size and number as the screened impurities collect on the screen. The constriction of flow paths raises the pressure ahead of the screen. At some point the constriction has become so great, and the pressure has increased so much, that the rate of extrusion is severely depressed.

At this point, the contaminated screen is replaced by a clean screen. Screen changes and reduced extrusion rates are costly to the polymer processor. Primary carbon black variables affecting the screen life of the compound are the dispersibility of the carbon black and the concentration of contaminants.

12.4.2. Mechanical Properties

Carbon black can affect the mechanical properties of compounds. The effects of loading on tensile properties have been described in Section 12.1. Carbon black can affect other properties such as impact strength, thermal conductivity and related physical properties. At the 0.52% concentration levels used for color and UV protection applications, the effect of carbon black is small. However, the effect can be large for highly loaded compounds, such as used in the wire and cable market. In practice, these other mechanical properties are secondary in the highly loaded applications. The resulting properties are significantly affected by the choice of polymer grade and other compounding ingredients. This area of the technology remains highly proprietary in users' technology.

References:

1. Medalia, A. I., *Rubber Chem. Technol.,* 59, 432 (1986).

2. Sichel, E. K., *Carbon Black-Polymer Composites: The Physics of Electrically Conducting Composites,* Marcel Dekker, Inc., New York, 1982.

3. Kirkpatrick, S., (1973). *Rev. Mod. Phys.,* 45, 574 (1982).

4. Bellamy, A., Robin, P. and Micheron, F., *Int. Rub. Conf.,* Paris,

III-3, 1982.

5. Janzen, J., *J. Appl. Phys.,* 46, 966 (1975).

6. Bluestein, A. C., *Elastomerics,* March, 10 (1987).

7. Wallder, V. T., Clarke, W. J., DeCoste, J. B. and Howard, J. B., *Ind. Eng. Chem.,* 42, 2320 (1950).

8. Howard, J. B. and Gilroy, H. M., *Poly. Eng. Sci.,* 9, 286 (1969).

9. Gilroy, H. M., *Proc. of Soc. Plas. Eng. 43rd ANTEC,* Washington, p. 258, 1985.

10. Hunt, R. W. G., *Measuring Colour,* Halsted Press, John Wiley and Sons, New York, 1987.

11. Billmeyer, F. W. Jr. and Saltzman, M., *Principles of Color Technology,* John Wiley and Sons, New York, Ch. 2, 3, 1981.

12. Murphy, L. J., Unpublished work, Cabot Corporation, 1991.

13. Bigg, D. M., *Principles of Polymer Mixing Technology, Developments in Plastics Technology,* Vol. 2, A. Whelan and J. L. Craft eds., Elsevier Applied Science Publishers, New York, Ch. 4, 1985.

14. Manas-Zloczower, I., Feke, D. L. and Rwei, S. P., *Polym. Eng. Sci.,* 30, 701 (1990).

15. Mooney, M., *J. Colloid Sci.,* 6, 162 (1951).

16. Nielsen, L. E., *Mechanical Properties of Polymers and Composites,* Marcel Dekker, Inc., New York, 1987.

17. Guth, E. and Gold, O., *Phys. Rev.,* 53, 322 (1958).

Chapter 13
Carbon Black In Xerographic Toners

Paul C. Julien
Webster Research Center, Xerox Corporation,
Webster, New York, U.S.A.

The last thirty years has seen rapid growth in the creation and duplication of documents through the use of a process called xerography, meaning dry writing. Several books are available on the technology of this process [13], while there are several articles on xerographic materials [46]. In brief, an electrostatic image is formed on a photoconductive drum through the selective neutralization of a uniform electric charge by light, either from an optical image of the document or from a laser controlled by computer code representing the document. This electrostatic image is then converted to a black and white (or colored) image by the neutralization of the remaining charge on the drum by small charged particles of pigmented plastic constituting the dry ink or toner used in the process. The particles are then transferred to paper and melted to bind them to the paper to form a permanent document.

Originally all the toner used in xerography was black. While there has been a growing interest in color inks in the last few years, carbon black has continued to be the most important pigment. In 1990 in the United States the copier industry consumed over 2000 metric tons of carbon black [7]. This was a relatively small market compared to the tire industry; however, it was a significant portion

of the market for specialty blacks. There is little in the literature about the colorimetric properties of different carbon blacks when used in toners. The toner particles are about 10 microns in diameter and are used at roughly 1 mg/cm2 to make a solid area. With a 10% carbon black loading there is little problem obtaining a black image. However, with other factors about equal a toner made from a black with a higher jetness, i.e., a

blacker black, can give a higher image density [8]. The major effects of a carbon black on toner are on the electrical charging and melt flow properties of the particles.

13.1. Electrical Charging Characteristics

13.1.1. Triboelectrification

The movement of toner particles is primarily controlled by means of their electrical charge [9]. This is typically generated by mixing 10 micron toner particles with carrier which may be 100 micron beads of either steel or ferrite used bare or coated with a suitable polymer. The mixing action generates equal and opposite charges on the toner and carrier and leads to an attractive force between them. The carrier beads are usually magnetic, allowing the use of magnets for stirring the mixture and brushing it across the electrostatic image to deposit toner on the charged areas representing the image. The sizes of the toner and carrier particles vary greatly among different machines; the above values are typical. Also, the toner can be either positively or negatively charged, depending on machine requirements.

The charge generated on the toner particles by mixing with carrier is measured by placing about 1 gram of the mixture of toner and carrier in a small metal cage which has screens with a mesh large enough to allow the passage of toner but not carrier. The charge on the toner is then measured by blowing it off the carrier while the device is connected to an electrometer. By weighing the cage before and after the toner was removed, the mass of the toner can be determined. The charge to mass ratio can then be calculated. If this is too large, it will be very difficult to remove sufficient toner

from the carrier, and the copy will be too light. If the charge level is too low, the toner will be uncontrolled and will end up at unintended places on the paper. This will result in high dirt levels on the copy. For negatively charged toners reasonable performance is typically found between -10 and -30 microcoulombs per gram (μc/g). In a given toner polymer against a given carrier different carbon blacks can make a difference in charge level of about 10 μc/g [9]. This is quite significant in toner charging. Thus it has been of considerable practical interest to understand the factors that determine the amount of charge transferred and of considerable fundamental interest to understand the nature of charge transfer in carbon black.

13.1.2. Electronegativity and Work Functions

The tendency for any material to gain electrons through contact with other materials is described as its electronegativity. Considerable work has gone into the development of experimental techniques and theoretical approaches for contact electrification in metals and insulators [10]. Since carbon blacks are conductive, the electronegativity of a black can be discussed on

the basis of its work function, i.e., the energy necessary to remove an electron from the material [9]. When two conductors are brought together, a contact potential difference will be generated equal to the difference in the work functions, with higher work function materials having more negative contact potentials compared to a standard reference material. The potential can be measured by the Kelvin vibrating capacitor method using wafers of compressed carbon black [9]. In repeated comparisons between blacks the internal error between black samples can be reduced to ±0.02 volt. When carbon black values are compared to gold reference electrodes, unoxidized blacks give values approximately equal to gold. Highly oxidized acidic (low *pH*) blacks typically give values 0.5 volt more negative than unoxidized relatively basic (high *pH*) blacks [9,11]. This difference leads to the 10 µc/g change in charge level noted above, where blacks with a more negative contact potential lead to more negative tribos. Table 1 gives manufacturer's values for the surface area, volatile content (a measure of surface functionality), and *pH* for various blacks, the measured contact potentials for the blacks and triboelectric charging for polyester toners made from the blacks [9]. Other studies also find that the triboelectric charge of toners containing carbon black is of the same order as the work function [12], or the acidity [13], of the blacks.

The general tendency of acidic blacks to have lower contact potentials implies that the surface chemical groups that determine acidity probably play a role. Also, peracetic acid oxidation of different carbon blacks has been

Table 1. Properties of Carbon Blacks

Type[a]	Surface area, m2/g	Volatile content, %	pH	Contact potential, V	Charge level[b], μc/g
Regal 330	94	1	8.5	+0.10	+4.0
Raven 1020	82	1	7.0	+0.10	+3.6
Raven 420	28	0.4	9.0	+0.10	NA
CSX99	520	5.1	8.3	+0.05	+0.2
Raven 8000	935	9.6	2.4	-0.15	-3.5
Black Pearls L	135	5.0	3.4	-0.30	-4.6
CSX137	290	9.5	3.2	-0.40	-9.3

[a]The Raven blacks are produced by the Columbian Chemicals Company. All the other blacks are produced by the Cabot Corporation. The CSX blacks are experimental. The values for surface area, volatile content, and pH are those given by the manufacturer as typical.

[b]The measured charge to mass ratio when toners made from different carbon blacks at a 10% loading in a polyester resin are blended for one hour against a carrier coated with the same resin.

found to lead to more negative contact potentials [14]. Considerable work has been done on the surface chemistry of carbon black [15]. More recently, Fourier transform infared spectroscopy has been used to characterize the surface functional groups [16,17]. However, none of these investigations studied the relationship between specific functional groups and contact potential.

13.1.3. Composite Morphology and Dielectric Measurements

While the chemical nature of the carbon black itself is important in triboelectric charging, it is also true that the morphology of the carbon black-polymer composite should play a role. In particular the amount of carbon black on the surface of a toner may not be simply related to the bulk percentage of carbon black. Low energy electron emission has been used to determine the amount of carbon black available at the surface of a toner particle [18]. It was found that at the weight loadings typically used in toner fabrication (5 to 10%) the amount on the surface could be calculated by assuming equal probabilities of fracturing along the polymer surface, the carbon black surface, or the carbon-polymer interface. At higher loadings significantly less carbon black was available than the calculation predicted. Using thin organic films on aluminum it was determined that the depth of detection in the emission experiment is 9 nm or less. The true penetration depth for charge exchange in toner charging has not been definitively determined.

Matsui and Oka [12] have combined both work function and pigment dispersion properties in a model of the role of carbon black in toner charging. The equation for the rate of change of the charge consists of a generation term and a leakage term. The

former is equal to the difference in work function between the toner and carrier (ϕTN - ϕCR) multiplied by a proportionality constant k which is determined by unspecified characteristics such as mixing dynamics and toner morphology. The second is equal to the charge on the toner q (measured by the charge to mass technique discussed above) divided by a time constant τ. Thus:

$$\frac{dq}{dt} = k(\phi_{TN} - \phi_{CR}) - q/\tau \quad (1)$$

For an initially uncharged toner, this leads to:

$$q = qmax[1 - exp(-t/\tau)] \quad (2)$$

where:

$$qmax = k\tau(\phi TN - \phi CR) \quad (3)$$

The time constant τ can be related to the amount and dispersion of the carbon black through the dielectric properties of the carbon black-polymer composite. The dielectric constant ε' is a measure of the capacity C of the composite,

while the dielectric loss ε'' is a measure of its conductivity, and hence $1/\varepsilon''$ is a measure of its resistivity R. The product RC should be proportional to the time constant τ for electrical processes including triboelectrification. The ratio of the dielectric loss to the dielectric constant, $\varepsilon''/\varepsilon'$, is referred to as the dielectric loss tangent, $\tan \delta$, and hence:

$$\tau \alpha \ (tan \ \delta)\text{-1} \quad (4)$$

When τ from charging studies is compared with $(\tan \delta)$-1 from toner dielectric measurements for different carbon black loadings, the agreement is quite good (Fig. 1). Typically, ε', ε'', and $\tan \delta$ (and hence $1/\tau$) all increase with increased carbon black loading and decrease with improved dispersion at a given loading. Matsui and Oka find q_{max} approximately proportional to t for carbon black loadings above 10% (Fig. 2), as expected if the carbon black is dominating the toner work function. Thus the charge level decreases with increasing carbon black loading in their experiments.

However, Daly et al [19] found q increasing with carbon black loading between 6 and 13%. In this case q was evaluated after 20 minutes, a length of time which was short compared with the time constants found by Matsui and Oka. Thus, q_{max} may not have been reached. It is also possible that the polymer alone had low charge level against the carrier used compared to the carbon black; an increasing work function difference would increase the charge levels. The polymer that Matsui and Oka used led to high charge
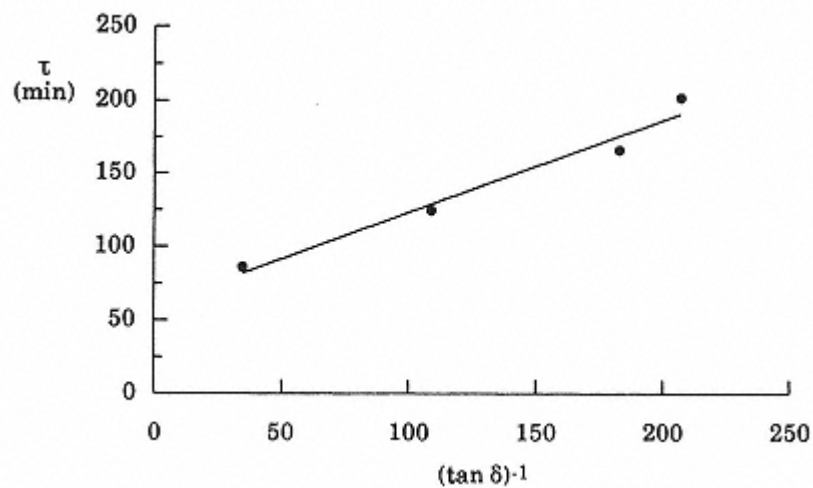
Fig. 1.
Relationship between τ and tan δ in case of varying
carbon black loadings (from ref. [12]).
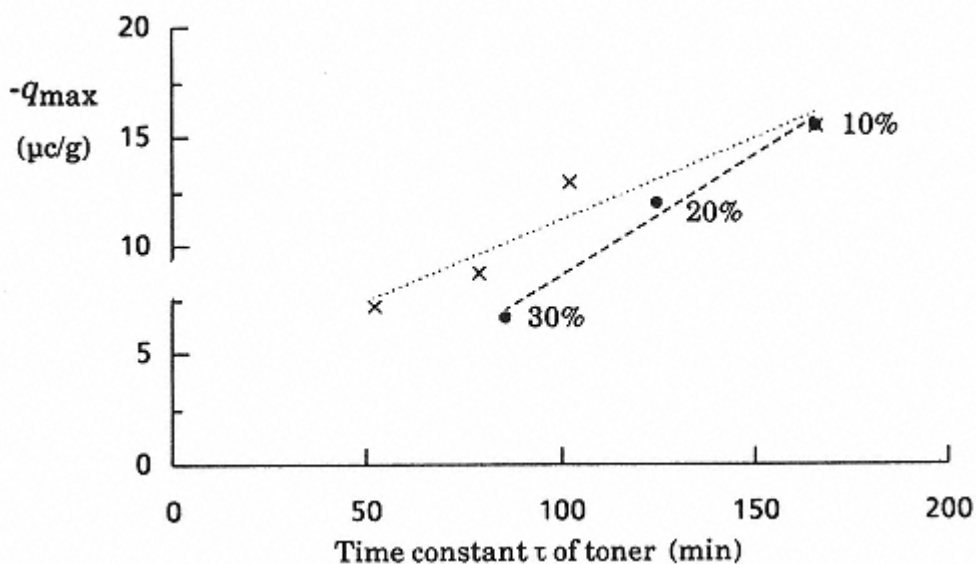
Fig. 2.
Relationship between qmax and τ in case of varying carbon black loadings () and melt-mixing conditions at 10 wt% loading ($\times$). Both plots use the same carbon black with surface area 138 m2/g and pH 3.0 (from ref. [12])

levels at very low carbon black loadings. Julien [9] found significant differences in charging with different toner polymers with the same carbon blacks at 10% loadings.

Daly et al also observed a decrease in q with longer rubber mill compounding times, which should correspond to a better dispersion. The dielectric constant ε' decreased with longer milling, consistent with better dispersion. Matsui and Oka found that $qmax$ is again approximately proportional to τ for different melt mixing conditions (Fig. 2), but they did not give dielectric measurements or rank the blends by mixing intensity. Transmission electron microscope (TEM) photomicrographs did not show clear differences in dispersion. The differences in the two plots in Fig. 2

could have been due to small changes in either the toner work function ϕ^{TN} or the proportionality constant k in Equation 3 as the toner is modified in the different ways.

Stubbe and Schumacher [8] also found both the chemistry and dispersion of the blacks important. Comparing different blacks at 7% loading in polyester resin, they found that an unoxidized black which gives the poorest dispersion has the highest value of tan δ in agreement with Matsui and Oka. The most acidic material with the highest volatile content, although not having the best dispersion in TEM analysis, had tan δ equal to the best dispersions and the highest charge level. Based on print tests they found that a moderate charging, well dispersed black was superior in tone rendition

and absence of copy background to the highest charging black, while the low charging, poorly dispersed black was unsatisfactory due to background on copy.

Other work has used a charge spectrograph to investigate the distribution of charge among toner particles of different size [20]. The spectrograph balances viscous and electrostatic forces on an airborne particle to determine the charge to diameter ratio of the particles. In combination with a computer controlled image analysis system it can independently determine the charge and size of a toner particle. While most theories of toner-carrier charging predict that the charge on a toner particle is proportional to its surface area, it was found that the presence of carbon black in the toner leads to increased charge on the smaller toner particles, possibly due to toner-toner charge exchange processes.

Contemporary toners typically contain more ingredients than simply carbon black and polymer. These are discussed in the articles on xerographic materials cited above [46]. In particular, positive toners usually have special chemicals to control the magnitude and speed of charging. Surface flow enhancers also have a dramatic effect on charge. These additives act to modify but not overwhelm the charging effects of the carbon black discussed above.

13.1.4. ESR and ENDOR Studies

The recognition of the role of carbon black in triboelectrification has led to a sequence of experiments using electron spin resonance (ESR) to investigate the nature of the charge carriers in the process

[14,2126], resulting in considerable evidence that there is charge exchanged through electron transfer to the black.

Both untreated and commercially oxidized versions of a high surface area (560 m2/g) black show only a broad ESR signal at room temperature [21]. This broad signal is temperature independent, indicating that it arises from conduction electrons. When the temperature is lowered, a narrow ESR signal is seen in both blacks with the magnitude of the signal roughly 4 times less intense in the untreated black [22]. A schematic representation of the broad and narrow signals is shown in Fig. 3. When treated with quinone the behavior of the initially unoxidized black closely resembles the oxidized case, while devolatilizing the oxidized black leads to behavior similar to the untreated case. This indicates that surface functional groups are playing a significant role in the generation of the narrow signal. Electrochemical reduction increases all the signal strengths, allowing the observation of the narrow signal at room temperature for all the cases except the untreated black. The signals due to electrochemical reduction also depend on the oxidation state of the carbon black and follow a $1/T$ temperature dependence, indicating localized spins (bound surface states). Another signal characteristic, the g-factor, also indicates that the localized states are associated with both carbon and
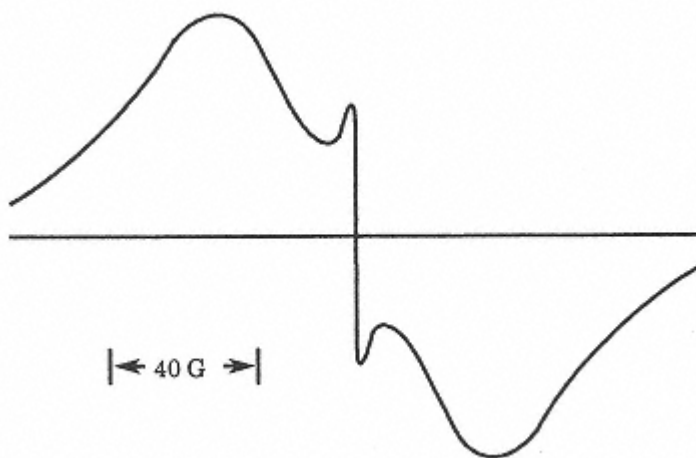
Fig. 3.
A simulated ESR spectrum which results from the
addition of broad and narrow ESR signals with
widths = 75 gauss and 2.5 gauss, respectively
(from ref. [23]).

oxygen atoms. The signal due to the reduction of the above oxidized black was later calculated to be sufficiently sensitive to allow the observation of the extremely small amounts of charge transferred during triboelectrification [23], but no experiment has been reported testing this in the mixing of toner and carrier.

When a low surface area (90 m2/g) black was examined, electrochemical reduction of both untreated and commercially oxidized versions produced a narrow signal that was independent of temperature, indicating that it originated from nonlocalized spins (mobile conduction electrons) [24]. As noted in the section on electronegativity, when the untreated black is oxidized to varying degrees with peracetic acid, the contact potential becomes more negative [14]. This correlates with an increase in the intensity of the narrow ESR signal and thus with an increase in the number of

electron accepting sites. In contrast to the commercial oxidation, the sites generated by the peracetic acid are localized.

When the untreated 90 m2/g black was blended with a styrene copolymer, a narrow signal was observed that is very similar to the reduction case, including the temperature independence [25]. The latter property indicates that it is also produced in conduction electrons and hence in the carbon black. When a high surface area oxidized black was blended with a styrene copolymer, it also gave rise to a narrow signal, but one showing the localized state characteristics seen in the electroreduced high surface area blacks [26]. In both cases melt blending apparently leads to electron transfer from the polymer to the blacks, either through triboelectrification or through reduction of the carbon blacks by polymer radicals generated during the blending process.

The above ESR work has been supplemented by electron-nuclear double

resonance (ENDOR) studies [2628]. These experiments look at the effect on the ESR signal in the carbon black during excitation of the nuclear spins of either hydrogen or fluorine. The observation of such a coupling between the electron and nucleus indicates that they must be in close proximity (less than about 1 nm). This coupling is observed only in the narrow ESR signals rather than in the broad signals. It occurs between electrons and hydrogen in the surface functional groups of the carbon black, but the signal is much stronger between the electrons and the hydrogen nuclei of the polymer in the blends discussed in the last paragraph. This coupling with the polymer is expected from the surface state origin of the high surface area black signal, but it also indicates that the conduction electron in the low surface area black must be spending time near the surface. The ENDOR signal in the composite falls rapidly as the temperature of the styrene copolymer was raised above the onset of molecular motion in the polymer chains, indicating a dipole coupling between electrons in the carbon black and polymer nuclei which can be averaged to zero by molecular motion [27]. When a composite is attrited to 10 μ by the processes used to make toner, the ENDOR signal is substantially increased, indicating that these processes force the carbon black and polymer into close proximity [28]. If partially fluorinated polymers are used, comparisons between the ENDOR signal ratios and the relative concentrations of fluorine and hydrogen indicate a changing degree of coupling between the fluorine and carbon black depending on the state of fluorination. This in turn is related to the orientation of the polymer on the carbon black surface.

13.2. Rheological Properties

In the great majority of cases, the fusing of toner to paper is accomplished by passing the toned sheet between two rolls under pressure. One or both of the rolls are heated to melt the toner. The critical time associated with fusing is the time during which the area to be fused is caught in the nip between the heated rollers. This will decrease as the speed of the copier increases and increase as the size and softness of the rolls increase. Values range from roughly 5 to 50 milliseconds [4].

There are three critical temperatures in toner rheology. The lowest is the blocking temperature at which the particles tack together after long exposure times and lose their flowability; this should be above those temperatures typically encountered in shipping and storage. The second is the temperature at which the particles flow sufficiently to melt into the paper and form a good bond; this should be as low as possible. The third is the temperature at which the toner is so fluid that it splits between the paper and the fuser roll, contaminating the latter; this should be as far as possible above the second temperature to provide the most fusing latitude.

Published papers typically do not directly examine the effect of carbon

black on these temperatures in actual fusers, but rather they give viscosity, the storage (or elastic) modulus (G') and the loss (or viscous) modulus (G'') versus sinusoidal shear rate at different temperatures [2931]. Time-temperature superposition can be used to create master curves for simple materials, but it is difficult to relate these to actual fusing situations. The correspondence of the temperature in the viscoelastic measurements to the temperature of the toner in the fusing zone and the correspondence of the shear rate to the inverse of the dwell time in the fuser are both very rough. Nonetheless, the data are useful to estimate the level of effect expected at different loadings and types of carbon black. The types of carbon black are primarily distinguished by surface area.

The addition of carbon black will raise the glass transition temperature of a carbon black polymer composite [32], and this in turn will raise the blocking temperature of the toner.

For several carbon blacks in styrene butyl methacrylate, the dependence of viscosity on shear rate at a given temperature can be represented by a universal curve showing a significant viscosity enhancement at low shear rate, dropping toward the unfilled value at high shear rate [29]. Fig. 4 shows this dependence for a 10% loading of 95 m2/g carbon black at 150°C. The plot would be shifted towards higher shear rates for higher carbon black loadings and for higher surface area carbon blacks at a given loading, corresponding to a larger effect on viscosity for these conditions. For the composition shown
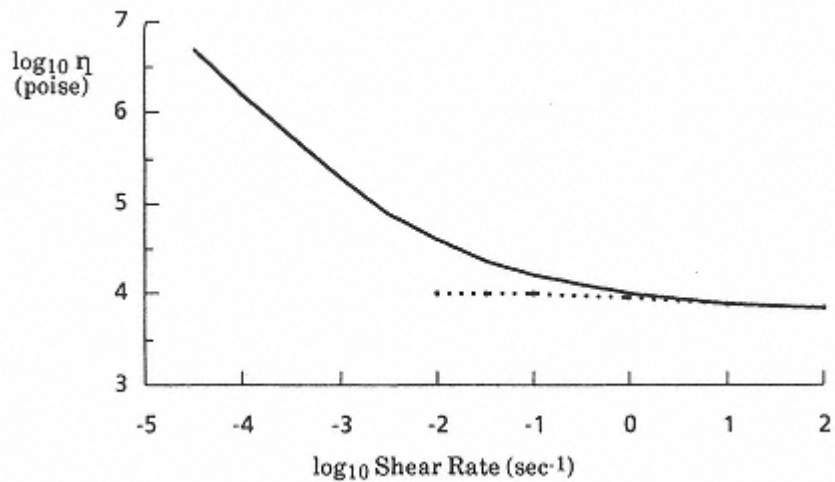
Fig. 4.
Master curve of the logarithm of the viscosity of carbon
black filled styrene butyl methacrylate at 150°C vs. the
logarithm of the shear rate using a reference concentration of
10% and a surface area of 95 m2/g. Dotted line is polymer
alone (from ref. [29]).

little effect is seen for the region above 10 sec-1 (log10>1) corresponding to typical fusing dwell times. Increasing the loading of the 95 m2/g black from 0 to 30% shifts the log of the shear rate about 1.5, which still gives little effect. A toner with 30% of a 625 m2/g black shifts the log of the shear rate by 3, leading to a significant rise in viscosity and requiring higher fusing temperatures to achieve adequate bonding to the paper. The viscosities shown in Fig. 4 will change with temperature and copolymer composition. Other work at 120°C in another styrene butyl methacrylate also shows little effect above 10 sec-1 for 10% carbon black but a significant rise in viscosity for 30% loadings [30].

There is some evidence from unpigmented systems that fusing latitude decreases as the rheological loss tangent (G''/G') increases [33]. The latter quantity plays the same role in viscous rheological behavior that the dielectric loss tangent plays in the resistive electrical behavior discussed above. Since G''/G' decreases with increased carbon black loading for both 24 and 625 m2/g blacks [31], the fusing latitude should increase as carbon black is added.

The effect of the carbon black on the rheological properties is likely to be quite small at the levels currently used in toner. However, a few degrees centigrade can be quite significant, so that the fusing performance is monitored closely as pigment loadings are changed.

13.3 Summary

Carbon black is an important pigment for use with xerographic toners. Maintaining a suitable level of electric charge on the toners

is essential for proper operation of electrophotographic copiers and printers, and carbon black has been found to play a significant role in modifying this charge. The surface acidity and dispersion properties of the various carbon blacks are the most important influences on the charging performance of toners made from them. ESR studies indicate that the mechanism of charging is most likely electron transfer into the carbon black. Carbon black at high loadings can act to raise the critical temperatures associated with proper fusing of the toner to paper, but at typical loadings the effect is generally small. However, even modifications of a few degrees may be significant.

References

1. Scharfe, M. E. *Electrophotography, Principles and Optimization,* Research Studies Press, Letchworth, England, 1984.

2. Schein, L. B., *Electrophotography and Development Physics,* Springer-Verlag, New York, 1988.

3. Williams, E. M., *The Physics and Technology of Xerographic Processes,* Wiley-Interscience, New York, 1984.

4. Gruber, R. J., Ahuja, S. K. and Seanor, D., in *Encyclopedia of Polymer Science and Engineering,* H. F. Mark, N. M. Bikales, C. G. Overberger and G. Menges eds., Wiley-Interscience, New York, 1989.

5. Scharfe, M. E., Pai, D. M. and Gruber, R. J., in *Imaging Processes and Materials: Neblettes's Eighth Edition,* J. M. Sturge, V. K. Walworth and A. Shepp eds., Van Nostrand Rienhold, New York.1989.

6. Gruber, R. J. and Julien, P. C., in *Handbook of Imaging Materials,* A. Diamond, ed., Marcel Dekker, New York, 1991.

7. Cooper, J. F., *Proceedings of the Seventh Annual Diamond Research Corporation Toner & Developer Industry Conference,* Santa Barbara, California, 1990.

8. Stubbe, A. and Schumacher, W., *American Ink Maker,* 65, 18 (1987).

9. Julien, P. C., *Carbon Black-Polymer Composites,* E. K. Sichel ed., Marcel Dekker, New York, 1982.

10. Lowell, J. and Rose-Innes, A. C. *Advances in Physics,* 29, 947 (1980).

11. Fabish, T. J. and Hair, M. L., *J. Colloid Interf. Sci.,* 62, 177 (1977).

12. Matsui, N. and Oka, K. *Denshi Shashin Gakkaishi (Japan),* 27, 307 (1988),

13. Bahkshaee, M., Daly, J. H., Hayward, D., Pethrick, R. A., Rashid, H. U. and Sherrington, D. C., *J. Electrostatics,* 19, 181 (1987).

14. Harbour, J. R., Walzak, M. J., Limburg, W. and Yanus, J., *Carbon,* 24, 725 (1986).

15. Medalia, A. I. and Rivin, D., in *Characterization of Powder Surfaces,* G. D. Parfitt and K. S. W. Sing, eds., Academic Press, New York, 1976.

16. Prest, W. M. and Mosher, R. A., in *Colloids and Surfaces in Reprographic Technology,* M. Hair and M. D. Croucher, eds., American Chemical Society, Washington, D. C., 1982.

17. O'Reilly, J. M., and Mosher, R. A., *Carbon,* 21, 47 (1983).

18. Matsui, N., Kim, S., Oka, K. and Pu, L., *Hyomen Kagaku (Japan),* 9, 608 (1988).

19. Daly, J. H., Hayward, D. and Pethrick, R. A., *J. Phys. C: Appl. Phys.,* 19, 885 (1986).

20. Julien, P. C., *Proceedings of the Sixth International Congress on Advances in Non-Impact Printing Technologies,* Orlando, Florida, 1990.

21. Harbour, J. R. and Walzak, M. J., *Carbon,* 22, 191 (1984).

22. Harbour, J. R., Walzak, M. J. and Julien, P. C., *Carbon,* 23, 185 (1985).

23. Harbour, J. R. and Walzak, M. J., *J. of Imaging Sci.,* 32, 141 (1988).

24. Harbour, J. R. and Walzak, M. J. *Carbon,* 24, 743 (1986).

25. Harbour, J. R. and Walzak, M. J., *J. Colloid Interf. Sci.,* 119, 150 (1987).

26. Harbour, J. R., Walzak, M. J. and Veregin, R. P., *J. Colloid Interf. Sci.,* 138, 380 (1990).

27. Veregin, R. P., Harbour, J. R., Kotake, Y. and Janzen, E. G., *Carbon,* 25, 541 (1987).

28. Veregin, R. P., Harbour, J. R., Kotake, Y. and Janzen, E. G., *J. Colloid Interf. Sci.,* 132, 542 (1989).

29. Lakdawala, K. and Salovey, R., *Polym. Eng. Sci.,* 25, 797 (1985).

30. Ahuja, S. K., in *Rheology,* Vol. 2, G. Astarita, G. Marrucci and L. Nicolais eds., Plenum Press, New York, 1980.

31. Gandhi, K. and Salovey. R., *Polym. Eng. Sci.,* 28, 1628 (1988).

32. Jachym, B. J., in *Carbon Black-Polymer Composites,* E. K. Sichel, ed., Marcel Dekker, New York, 1982.

33. Ekong, E. A., *Proceedings of the Seventh Annual Diamond Research Corporation Toner & Developer Industry Conference,* Santa Barbara, California, 1990.

Chapter 14
Health Effects Of Carbon Black

Donald Rivin
Department of the Army,
Natick Research, Development and Engineering Center,
Natick, Massachusetts, U. S. A.

14.1. Production and Product Characteristics

From the earliest lampblack manufacture in ancient Egypt and India to subsequent larger scale commercial production as a synthetic pigment in China 1500 years ago, carbon black has evolved into a major industrial material. Over six million metric tons are produced worldwide for use mainly as a rubber reinforcing agent, with smaller quantities used as a pigment, plastics additive, and for myriad specialized applications. Through the first half of this century carbon black was produced by five processes which involve the partial combustion and/or pyrolysis of gaseous or liquid hydrocarbons; channel or impingement, thermal, gas furnace, lampblack, and acetylene. However, since its introduction in 1943, the oil furnace process has become dominant, and now accounts for over 95% of carbon black production. In this process, a heavy aromatic hydrocarbon feedstock is sprayed into a flame where it vaporizes then cracks to small molecular fragments which recombine to form an aciniform carbon aerosol [1]. Polynuclear aromatic compounds (PNA) are inevitable by-products of this process in amounts ≤ 0.1 wt%, with two- and three-ring polynuclear aromatic hydrocarbons (PAH) predominating in the filtered

gaseous effluent, and $\geq$four-ring PAH comprising most of the extractable organic impurities adsorbed on the carbon product. Smaller amounts of nitrogen and sulfur heterocyclics are adsorbed on oil furnace carbon blacks, whereas oxygenated PNA are present on channel blacks and aftertreated (oxidized) furnace blacks. Inorganic impurities in carbon black, also present at

≤0.1 wt%, are derived mainly from dissolved salts in the quench water spray used to cool the aerosol prior to filtration, and in water added during wet pelletizing to convert the initial low density (fluffy) powder to a more easily handled densified pellet form. Additional trace metal impurities arise from the feedstock, reactor erosion, alkali metal compounds introduced to control aggregate morphology, and pelletizing aids. Sodium accounts for about 70% of the extractable inorganic cations on commercial oil furnace blacks but at least fifteen other elements are present in amounts ≥1 ppm [2]. These include: at 110 ppm: Ba, Cr, Cu, Mn, Ni, P, Sr, Ti and Z, at 1150 ppm: Al, Ca, Fe, Mg and K, at >50 ppm: Si and Na.

A clear distinction exists between carbon black, and environmental soots which are variable mixtures of carbonaceous particles with oils, tars, resins, and refractory inorganic salts and oxides [1,3]. Soot deposits consist mostly of inorganic ash and extractable organic compounds, with <1% aciniform carbon in the presence of fragments of coke, char, partially carbonized material, and carbon cenospheres. Aciniform carbon is prevalent in chimney smoke, and engine exhausts. For example, diesel soots are composed of aciniform carbon similar in size to carbon blacks, but with a large (usually 1080 wt%) extractable organic fraction rich in PNA.

14.2. Emissions And Occupational Exposure

Particulate emissions from the oil furnace process are usually below 0.1 g/kg product. Gaseous effluents vary with the feedstock and grade of carbon black although nitrogen, water, and carbon dioxide normally constitute ca. 90% of the gaseous emissions in the absence of recycle or combustion of process gas. A 1982 report of ambient dust levels in North American carbon black plants [4]

noted a time-weighted average (TWA) exposure for production workers of 0.5 mg/m3, with the highest dust level (1.5 mg/m3) in material handling areas where fluffy black is packaged. Earlier industrial hygiene studies of the major carbon black use industry, tire manufacture, found similar mean dust levels in most locations but ambient dust concentrations near 4 mg/m3 associated with carbon black compounding and mixing. Regulations limiting occupational exposure to carbon black at a TWA of 3.5 mg/m3 are found in many countries, although a few allow higher exposure, e.g., Germany - 6 mg/m3, and Switzerland - 8 mg/m3.

14.3. Extractable PAH

Organic solvent extracts of carbon black contain mainly four- to seven-ring PAH, among which are known animal mutagens, and carcinogens. However, PAH interact strongly with the carbon surface, and are not readily bioavailable when adsorbed on carbon black [68]. Observed ranges in concentration for the ten compounds which account for most of the PAH fraction

Table 1. PAH in Carbon Black Extract (ppm)

Carbon black type	Channel (3)a	Oil furnace (20)	Thermal (5)
Fluoranthene	0.20.5	0.182	1197
Pyrene	0.10.3	0.1400	1603
Benzofluoranthenes	-	<0.01102	0.0220
Cyclopenta(cd)pyrene	<0.2	0.1145	-
Benzo(a)pyrene	0.10.2	0.125	0.01186
Indeno(1,2,3-cd)pyrene	0.1	<0.335	-
Benzo(e)pyrene	0.00.2	0.140	0.1145
Benzo(ghi)perylene	0.50.7	0.6166	0.2217
Anthanthrene	-	<0.0126	0.2299
Coronene	0.40.6	0.1219	0.3800

aNumber of commercial grades analysed.

in solvent extracts of carbon black are shown in Table 1 [2]. Currently produced furnace and thermal blacks tend to have PAH contents near the low end of the observed range.

14.4. Acute Toxicity

Powdered carbon is well-established as a safe and effective adsorbent for ingested toxins. This is consistent with the low acute toxicity found for channel and furnace blacks in aqueous dispersion when administered orally (gavage) to mice [9]. No toxic effects were observed up to the maximum dose which corresponds to $LD_{50} > 10g/kg$ body weight.

In other animal studies [2], no inflammation was noted when aqueous dispersions of carbon black were injected intraperitoneally in mice or rats, or intravenously in mice, rats, or rabbits. No dermal irritation resulted when oil or water suspensions of carbon black were painted on the skin of mice, rabbits, or monkeys.

No evidence for acute toxicity is associated with occupational exposure to carbon black, although a high incidence of dermatoses such as hyperkeratosis was observed among workers in a Rumanian factory producing high-extract lampblack [10].

14.5. Inhalation Toxicology

Upon inhalation of carbon black dust, particles having aerodynamic diameters > 5µm deposit in the nose and head, those between 1 and 5 µm deposit primarily in the tracheobronchial region, while smaller particles deposit in the bronchioles and alveoli [11]. Particles in the nose, pharynx, and larynx are rapidly cleared with mucus and swallowed, whereas those deposited in the ciliated bronchi are transported to the larynx and ingested over a period of

days. Particles in the alveoli are quickly engulfed by scavenger cells (e.g., macrophages) and are cleared within several months, either by movement to the gastrointestinal tract via the larynx, or through the lymphatics to the regional lymph nodes where they enter the blood circulation to other organs and are eventually excreted.

A recent study of male Fischer rats exposed to a 0.2 μm furnace black aerosol at 7 mg/m3 for 20 h/day found an alveolar deposition efficiency (15%) typical of inert submicron particles [12]. Saturation effects were observed after several days, such that at accumulated lung burdens > 0.8 mg the rate of lung clearance decreased by half while lymphatic transport to the mediastinal lymph nodes accelerated. Particle retention at 1 year postexposure increased strongly with the lung burden attained during exposure, ranging from 9% (8% lung, 1% lymph nodes) for 1.1 mg after 1 week to 88% (61% lung, 27% lymph nodes) for 5.9 mg after 6 weeks. In spite of the significant alveolar particle loading no impairment in lung function was noted. Previous long-term studies of Rhesus monkeys, rabbits, and several rodent species exposed to channel and furnace black at dust levels of 53110 mg/m3 demonstrated the absence of major respiratory pathology including proliferative and fibrotic changes [2].

Enhanced production of scavenger cells is a primary reaction to the presence of exogenous material in the alveolar region; thus macrophage production increased ten-fold and no free particles remained in the alveoli, one day after intratracheal instillation of 4 mg of a carbon dispersion in mice [13]. Cytotoxicity is not associated with the presence of alveolar carbon particles in any

animal species, although a small reduction in immune response to inhaled influenza virus or bacteria (E. coli or K. pneumoniae) occurred in mice and guinea pigs [2].

Human subjects exposed to high concentrations (2550 mg/m3) of respirable carbon dust [14] or carbon-rich xerographic toner [15] exhibit only minor changes in mucociliary clearance rate, airway resistance, or respiratory function. Morbidity due to occupational exposure to carbon black has been studied extensively in the U.S.A. [16] and U.K. [17] via epidemiologic studies of carbon black production workers. There was no association between cumulative carbon black exposure and the incidence of respiratory disease (or, for that matter, circulatory system disease or malignant neoplasms), but a strong correlation was found between respiratory health and smoking history. A high incidence of simple pneumoconiosis, bronchitis, and other respiratory disease is reported in a number of small and poorly controlled epidemiology studies carried out in carbon black plants in Eastern Europe, and the former U.S.S.R. [18]. In addition to deficiencies in methodology and control of confounding factors (e.g., smoking and other exposures) these reports cite concentrations of dust, carbon monoxide, and hydrocarbon vapors well in

excess of occupational limits.

14.6. Genetic Toxicology

Enzymatic activation and detoxification of PAH in mammals is mediated by microsomal mixed function oxidases, particularly aryl hydrocarbon hydroxylase (AHH) which is present in macrophages and various mammalian tissues. No detectable increase in AHH levels was induced in the lungs and liver of rats after long-term inhalation of diesel exhaust (1.5 mg/m3) [19], or in mice fed a diet containing furnace black at 0.5 g/g body weight over 26 weeks [6]. Furthermore, a ten-fold increase in mucosal AHH was observed in rats following a 50 mg/kg body weight intragastric dose of benzo(a)pyrene (BaP) alone, but no induction was detected when BaP was administered with charcoal [20]. The consistent absence of AHH induction indicates that PAH strongly adsorbed on carbon are poorly eluted *in vitro,* and are not bioactive in their combined form. Experiments *in vitro* with BaP added to various particles support this interpretation, in that there was no transfer of adsorbed BaP from carbon black to phospholipid membranes [21] or rat liver microsomes [22], whereas most of the BaP was eluted from asbestos and other silicacious materials. Protein complexes from human serum or lung cytosol cause enhanced elution of PAH from aciniform carbon but are associated with a low level of PAH bioactivity due to strong binding between PAH and protein molecules [23].

Bacterial mutagenicity assays, such as the Ames test employing Salmonella typhimurium, are a convenient means to assess genotoxicity, although not necessarily carcinogenicity. Solvent extracts of carbon black are mutagenic in the Ames assay [18], but

the only study of whole carbon black (N339 furnace black containing 0.03% PAH) found slight cell toxicity at high doses with no evidence of mutagenicity in a battery of five short-term assays: the Ames test, mouse lymphoma and cell transformation tests, sister chromatid exchange in hamsters, and detection of chromosome damage in fruit flies [24].

Solvent extracts of carbon black are carcinogenic to several species of animals when administered by skin painting, ingestion, or subcutaneous injection, although tumor incidence is reduced significantly, presumably due to readsorption of free PAH, when the extract is coadministered with carbon black [18,25]. On the other hand, no tumors are produced in animals when whole carbon black is administered by: skin painting, ingestion, intratracheal instillation, and intraperitoneal, subcutaneous and intramuscular injection [18,25].

14.7. Epidemiology

In addition to the morbidity study previously cited [16], retrospective cohort studies spanning a period of forty years have examined mortality of North American carbon black workers [26,27]. The observed incidence of cancer,

Table 2. Maximum Allowed Metallic Impurity Content of Carbon Black[a]

Country/Metal	Sb	As	Ba	Cd	Cr	Pb	Hg	Se	Zn
Austria	2000	200	4000	4000	-	2000	400	-	4000
Belgium	2000	50	100	2000	1000	100	50	100	-
Czechoslovakia	-	50	100	100	100	1000	50	100	2000
France	-	50	100	1000	-	100	50	100	2000
Germany[b]	50	100	100	1000	-	100	50	100	-
Italy	-	50	100	2000	-	100	50	100	2000
The Netherlands	2000	100	100	1000	1000	100	50	100	-
Spain	2000	100	1000	2000	1000	100	50	100	2000
U.K.[c]	250	250	500	100	250	2500	100	-	-
Europe(EN71)-paper/plastics	250	100	500	100	100	250	100	-	-
EN71-paints	250	100	500	100	250	-	100	-	-
U.S.A.[d]	-	100	2000	20	100	100	4	20	-

[a]Extracted by 0.1N acid, ppm.

[b]DIN Method 53770.

[c]Colour Manufacturers Association.

[d] RCRA EP toxicity limit at pH 5.

major respiratory disease, or cardiovascular disease did not differ significantly from that expected based on age-adjusted regional death rates. A total of only 70,000 person-years at risk was appraised due to the relatively small work force of the carbon black industry. Many more workers are occupationally exposed to mixtures containing carbon black in user industries, such as rubber tire manufacture which is the subject of numerous epidemiologic investigations [5]. Tire workers exposed to solvents and a few identified curing additives appeared to experience excess chronic respiratory disease and several types of cancer, but for all workers

the incidence of respiratory and cardiovascular mortality was significantly less than expected. Tire manufacturing operations associated with high exposure to carbon black and inorganic dusts produced no pneumoconiosis, and relatively little respiratory disease.

14.8. Food Contact Regulations

As normally produced, carbon black is not suitable for use as a direct food additive but is generally approved for food contact applications. Detailed governmental regulations setting requirements for food-related use of carbon black in Western Europe and North America are compiled [2,18]. Many countries approve specific food, drug, or cosmetic applications of carbon black on an individual basis rather than rely on generic regulations. Restrictions on

carbon loading and organic extract content are common, as are limits on the quantity of trace metal impurities. Maximum metal content for carbon black allowed in the U.S.A. and in Europe (ten countries) is listed in Table 2 [28]. In addition to the limits shown in the table, ≤4000 ppm of copper, tin, and uranium are allowed in Austria, ≤100 ppm nickel in Spain, and ≤100 ppm silver in the U.S.A. Sweden allows no detectable amount of the listed elements in acid extracts.

References

1. Medalia, A. I. and Rivin, D., *Carbon,* 20, 481 (1982).

2. Rivin, D., chapter on Carbon Black in *The Handbook of Environmental Chemistry,* Vol. 3D, O. Hutzinger, ed., Springer Verlag, Berlin, 1986.

3. Medalia, A. I., Rivin, D. and Sanders, D., *Sci. Total Environ.,* 31, 1 (1983).

4. Smith, R. G. and Musch, D., *Am. Ind. Hyg. Assoc. J.,* 43, 925 (1982).

5. Rivin, D., *Dangerous Props. Ind. Mat. Rep.,* 5, 2 (1985).

6. Buddingh, F., Bailey, M. J., Wells, B. and Haesemeyer, J., *Am. Ind. Hyg. Assoc. J.,* 42, 503 (1981).

7. Bevan, D. R. and Worrell, W. J., in *Polynuclear Aromatic Hydrocarbons,* M. Cooke, and A. J. Dennis, eds., Battelle Press, Columbus, 1984.

8. Rivin, D. and Atkins, J. H., *Carbon,* 25, 135 (1987).

9. Leuschner, F., *Rept. Hamburg,* 1984.

10. Capusan, I., and Mauksch, J., *Berufsdermatosen,* 17, 28 (1969).

11. Heyder, J., Gebhart, J., Rudolf, G. and Stahlohfen, W., *J. Aerosol Sci.,* 11, 505 (1980).

12. Strom, K. A., Johnson, J. T. and Chan, T. L., *J. Toxicol. Environ. Health,* 26, 183 (1989).

13. Adamson, I. Y. R. and Bowden, K. H., *Lab. Invest.,* 38, 430 (1978).

14. Camner, P., Helstrom, P. A. and Philipson, K., *Arch. Environ. Health,* 26, 294 (1976).

15. Andersen, I. B., Lundqvist, G. R., Proctor, D. F. and Swift, D. L., *Am. Rev. Resp. Dis.,* 119, 619 (1979).

16. Robertson, J. McD. and Ingalls, T. H., *Am. Ind. Hyg. Assoc. J.,* 50, 510 (1989).

17. Crosbie, W. A., *Arch. Environ. Health,* 41, 346 (1986).

18. Rivin, D. and Smith, R. G., *Rubber Chem. Technol.,* 55, 707 (1982).

19. Chen, K. C. and Vostal, J. J., *J. Appl. Toxicol.,* 1, 127 (1981).

20. Kivela-Ikenon, P., Hanninen, O., Kalliokoski, P. and Koivusaari, U., *Environ. Res.,* 32, 1 (1983).

21. Lakowicz, J. R., Bevan, D. R. and Riemer, S. C., *Biochim. Biophys. Acta,* 629, 243 (1980).

22. Lakowicz, J. R. and Bevan, D. R., *Chem. Biol. Interact.,* 29, 129 (1980).

23. King, L. C., Kohan, M. J., Austin, A. C., Claxton, L. D. and Huisingh, J. L., *Environ. Mut.,* 3, 109 (1981).

24. Kirwin, C. J., Leblanc, J. V., Thomas, W. C., Haworth, S. R., Kirby, P. E. and Thilager, A., Bowman, J. T. and Brusick, D. J., *J. Toxicol. Environ. Health,* 7, 973 (1981).

25. *IARC Monographs on the Evaluation of the Carcinogenic Risk of Chemicals to Humans,* Vol. 33, Part 2, Lyon, 1984.

26. Ingalls, T. H. and Risquez-Iribarren, R., *Arch. Environ. Health,* 2, 429 (1961).

27. Robertson, J. M. and Ingalls, T. H., *Arch. Environ. Health,* 35, 181 (1980).

28. *Bulletin No. 3,* published by The European Committee for Biological Effects of Carbon Black, October, 1984.

Author Index

Numbers in parentheses are reference numbers and indicate that an author's work is referred to although his name is not cited in the text. Italic numbers refer to pages containing full bibliographic listings.

A

B

Kumer, A., 183(67), *218*

Kuo, C. C., 360(15), *375*

Kuwabara, H., 126, *169*

L

Ladd, M. W., 94, 121(49), *164*

Ladd, W. A., 90, 94, 107, 108, 121(49), 139(22), *164*

Lafleur, A. L., 83(91), *88,* 227(13), *227*

Lahaye, J., 71(25, 26), 74(53, 54), 77(62), 78(62), 79(25, 62), 80(25), 81(62, 72), 83(62, 84), *85-88,* 258(41), *269,* 272(10), *286,*

Lakdawala, K., 418(29), *421*

Lake, G. J., 333(171), 337, 338(166, 184, 187-189, 192), 339(166, 184, 194), 340, *353, 354,* 359(8), 371, *375, 376*

Lakowicz, J. R., 427(21, 22), *429, 430*

Lamb, L. D., 83(90), *88*

Lamond, T. G., 123, 125(155), *168,* 319(119, 120), *351*

Landau, L. D., 278(36), 282(36), *287*

Landel, K. F., 332, *353*

Lang, F. M., 181(94), 182(94), 192(94), *218*

Langella, C., 81(79), *87*

Langmuir, I., 117, *167*

Reitzer, C., 177(17), *216*

Wallace, D. R., 178(32a), *216*

Wallder, V. T., 399, *407*

Walters, M. H., 326(145), *352*

Walzak, M. J., 412(14), 415(14, 21-26), 416(14, 23-26), 417(26), *420, 421*

Wang, M. -J., 230(8, 9, 12), 231, 232(9), 233-235(12), 236(9, 12, 23), 237(12), 238(12), 239(14, 34), 240(12, 14), 241(14), *242, 243,* 292(21), 293(21), 293(59), 294(21, 23), 295(21), 298, 300, 302(21), 306(69, 78), 307(69), 308(69), 310(23), 311(23), 312(23, 69), 316(113), 320(23, 69), 321, 322(23), 323(23, 59), 325(23), 330-333(160), 344(23), 345, 346(217), *348-351, 353, 355*

Wang, W. D., 295(186), *354*

Wardell, E. G., 295(34, 35), *348*

Warren, B. E., 90, 91(29), 92(46), *164*

Warring, J. R. S., 298, *349*

Watanabe, K., 278(38), 282(38), *287*

Subject Index

A